

NOTICE: When government or other drawings, specifications or other data are used for any purpose other than in connection with a definitely related government procurement operation, the U. S. Government thereby incurs no responsibility, nor any obligation whatsoever; and the fact that the Government may have formulated, furnished, or in any way supplied the said drawings, specifications, or other data is not to be regarded by implication or otherwise as in any manner licensing the holder or any other person or corporation, or conveying any rights or permission to manufacture, use or sell any patented invention that may in any way be related thereto.

426714

64-5

7

RTD-TDR-63-1123

DEVELOPMENT AND DEMONSTRATION OF
MAIN TANK INJECTION (MTI) PRESSURIZATION
SYSTEM, FINAL REPORT

TECHNICAL DOCUMENTARY REPORT NO. RTD-TDR-63-1123

DECEMBER 1963

AD NO.

AIR FORCE FLIGHT TEST CENTER
AIR FORCE SYSTEMS COMMAND
UNITED STATES AIR FORCE
EDWARDS AIR FORCE BASE, CALIFORNIA

AIR FORCE PROGRAM STRUCTURE NO. 750G
PROJECT NO. 6753 TASK NO. 30304

426714

(PREPARED UNDER CONTRACT NO. AF01(611)-8198 BY THE MARTIN
COMPANY, DENVER DIVISION, DENVER, COLORADO, AUTHORS:
R. J. KENNY, P. FREEDMAN, A. P. LANE, AND P. BINGHAM)

Best Available Copy

FOREWORD

This is a final report on the Main Tank Injection (MTI) Pressurization System Program sponsored by the Air Force Rocket Propulsion Laboratory, Edwards Air Force Base, California, under Contract AF04(611)-8198. Mr. Charles H. Allen (DGRPT) of the Rocket Research Laboratories, AFFTC, Edwards Air Force Base was the Project Officer and Mr. Thomas R. Heaton of the Martin Company, Program Manager. The technical effort was primarily under the direction of Mr. Franklyn L. Roberts, Assistant Manager and Richard J. Kenny, Project Engineer.

In addition to the primary authors, technical contributions were also made by Messrs. T. Pharo, T. F. Morey, A. Joslin, and T. Blum who worked on specific areas of the investigation on a part time basis. Acknowledgement is also given to Messrs. D. Cary and T. Ward who conducted the Phase I and III test program, respectively, and Mr. R. Yarrow who programmed the MTI Mathematical Model on the IBM 7094 digital computer.

The research and development work was performed at, the Martin-Denver Hazardous Materials and Cold Flow Laboratories, while the major portion of the chemical analysis was conducted by the National Bureau of Standards Laboratory in Boulder, Colorado. The theoretical studies and engineering effort was the responsibility of the Advanced Technology Unit, Propulsion Section. This report covers the work performed during the 15-month period commencing 1 June 1962.

The Martin Company report number for this document is FTC-CR-63-23.

CONTENTS

	<u>Page</u>
Foreword	ii
Contents	iii
Abstract	xxiii
List of Symbols	xxiv
I. Introduction	I-1
II. Phase I Program	II-1
A. Preliminary Investigation	II-1
B. Research Testing	II-72
C. Chemical Analysis	II-189
D. Conclusions	II-217 thru II-221
III. Phase II Program	III-1
A. Theoretical Studies	III-1
B. System Design	III-46
C. Prototype Fabrication	III-71 thru III-77
IV. Phase III Program	IV-1
A. System Configuration	IV-1
B. Demonstration Test Series	IV-7 thru IV-46

V.	Phase IV Program	V-1
	A. Correlation of Test Data	V-1
	B. MTI System Design Handbook	V-17
	C. Application Study	V-45
	D. Reliability	V-83 thru V-96
VI.	Conclusions and Recommendations	VI-1 and VI-2
VII.	Future Studies	VII-1
	A. Hydrogen Pressurization of an Oxidizer Tank	VII-1
	B. Investigation of Other Reagents	VII-2
	C. MTI with Other Propellant Combinations	VII-2
	D. MTI Thermal Gradient Study	VII-3
	E. MTI with Thixotropic Propellants	VII-3
	F. MTI Zero Gravity Pressurization Analysis	VII-4
VIII.	Bibliography	VIII-1 thru VIII-6
	Appendix A -- Propulsion System Optimization Program	A-1 and A-2
	Appendix B -- Computer Program Description for MTI Application Study	B-1 thru B-8
	Appendix C -- MTI Pressurization System Program	C-1 thru C-6

Appendix D -- Propellant Tank Ullage Gas Dilution Computer Program	D-1 thru D-5
Appendix E -- MTI Pressurization System Thermodynamic Analysis	E-1 thru E-9
Appendix F -- IBM 7094 MTI Mathematical Model	F-1 thru F-75

Distribution

Figure

II-1	Relation of Performance to Composition of Fuel for the N_2O_4/N_2H_4 -UDMH Propellant Combination .	II-6
II-2	Effect on I_{sp} of Water in N_2O_4/N_2H_4 -UDMH . . .	II-7
II-3	Random Vibration Design Criteria for an MTI Pressurization System, Flight Environment . . .	II-8
II-4	Typical Start Transient Range for a Pump- Pressurized Propulsion System	II-10
II-5	Common Ullage MTI Pressurization System with Pneumatically Pressurized Remote Reagent Storage, Pressure-Fed Engine	II-13
II-6	Common Ullage MTI Pressurization System with Main Propellant Tank Reagent Supply, Pump-Fed Engine	II-14
II-7	Hybrid MTI Pressurization System with Pneumatically Pressurized Remote Reagent Storage and Evaporated Propellant, Pressure-Fed Engine .	II-16
II-8	Pump-Fed Injection System with Ullage Elimination	II-17

II-9	Turbopump Bleed-Crossfeed Injection System . . .	II-18
II-10	Common Ullage Feasibility Test Fixture	II-29
II-11	MTI Common Ullage Feasibility "Open Container" Test, Surface Impingement	II-30
II-12	MTI Common Ullage Feasibility "Open Container" Test, Submerged Impingement	II-31
II-13	MTI "Open Container" NTO Surface Injection Tests	II-33
II-14	MTI "Bomb" Test, Run 1	II-35
II-15	MTI "Bomb" Tests, Runs 2 and 3	II-36
II-16	Molecular Weight of Combustion Products (N_2O_4 /Aerozine 50)	II-41
II-17	Gas Temperature of Combustion Products (N_2O_4 /Aerozine 50)	II-42
II-18	Combustion Gas Density vs Reaction Mixture Ratio (N_2O_4 /Aerozine 50)	II-43
II-19	Constant Pressure Specific Heat Combustion Products (N_2O_4/N_2H_4 -UDMH)	II-44
II-20	Specific Heat Ratio Combustion Products (N_2O_4/N_2H_4 -UDMH)	II-45
II-21	Theoretical Combustion Products Thermodynamic Properties for a Mixture Ratio of 0.1 and Pressure of 35 psia	II-46
II-22	Actual Combustion Products Thermodynamic Properties for a Mixture Ratio of 0.1 and Pressure of 600 psia	II-47
II-23	Thermodynamic Properties of N_2O_4 - NH_3 Combustion Products at 36 psia	II-48
II-24	Theoretical Phase I Operating Pressure Effects on the Fuel Tank Injection Process	II-49

II-25	Phase I Fuel Tank Test Results	II-50
II-26	Theoretical Phase I System Performance for the Fuel or Oxidizer Tank	II-51
II-27	Phase I Fuel Tank Predicted Performance for a Mixture Ratio of 0.1 and Pressure of 36 psia .	II-52
II-28	Theoretical Phase III System Performance for the Fuel and Oxidizer Tank	II-53
II-29	Phase III Fuel Tank Predicted Performance for Mixture Ratio of 0.1 and Pressure of 36 psia .	II-54
II-30	Optimum Chamber Pressure for a Gimbaled Pressure-Fed Engine	II-57
II-31	Propellant Feed System Optimization	II-58
II-32	MTI vs Gas Generator Pressurization Systems, Case I, Booster Vehicle	II-63
II-33	MTI vs Gas Generator Pressurization Systems, Case II, Sustainer Vehicle	II-64
II-34	MTI vs Gas Generator Pressurization Systems, Case III, Upper Stage Vehicle	II-65
II-35	MTI vs Gas Generator Pressurization Systems, Case IV, Limited Space Vehicle, 1 Month Storage	II-66
II-36	MTI vs Gas Generator Pressurization Systems, Case V, Limited Space Vehicle, 1 Month Storage	II-67
II-37	MTI vs Gas Generator Pressurization Systems, Case VI, Space Vehicle, Indefinite Storage . .	II-68
II-38	Comparison of MTI and Heated Stored Helium Pressurization System Weights, Cases I, II, and III, Boosters and Upper Stage Vehicles . .	II-69
II-39	Comparison of MTI and Heated Stored Helium Pressurization System Weights, Cases IV and V, Limited Space Vehicles, 1- to 30-Day Space Storage	II-70

II-40	Comparison of MTI and Stored Helium Pressurization System Weights, Case VI, Space Vehicles, 1- to 30-Day Space Storage . .	II-71
II-41	Research Fixture Outside Upper Dome	II-75
II-42	Research Fixture Inside Upper Dome	II-76
II-43	Research Fixture Inside Lower Dome	II-76
II-44	Research Fixture Assembled	II-77
II-45	Phase I Primary Tank with Injector Installed .	II-77
II-46	Injector System Electrical Schematic	II-78
II-47	MTI Phase I Test System Schematic	II-80
II-48	Phase I Dual Tank Test Configuration	II-81
II-49	Research Fixture Control Console	II-82
II-50	Research Fixture Instrumentation System . . .	II-84
II-51	Phase I MTI Test Instrumentation Locations . .	II-85
II-52	Phase I Fuel Tank Test Schematic	II-87
II-53	Phase I Injector Orifice Tips	II-93
II-54	Typical Single Tank Pressurization System Performance with Solid Stream Surface Injection	II-95
II-55	Fuel Tank Internal Temperature Profile	II-96
II-56	Fuel Tank Wall Temperature Profile	II-97
II-57	Phase I Fuel Tank Pressurization System Performance Evaluation (N_2O_4 Solid Stream Surface Injection, Single Tank Test)	II-99
II-58	Theoretical Molecular Weight and Water Content of Gaseous Combustion Products vs Reaction Mixture Ratio	II-100

II-59	MTI Gaseous Combustion Products Total Weight vs Molecular Weight for the Small-Scale Single-Tank System	II-102
II-60	Injector Orifice Size Effects on Fuel Combustion	II-106
II-61	Orifice Size Effect on Ullage Gas Temperature and Reagent Consumption	II-107
II-62	Fuel Tank Wall Temperature vs Ullage Gas Temperature	II-108
II-63	Injection Penetration Rate Comparison	II-112
II-64	Fuel Tank Combustion Photographs	II-114
II-65	Single Tank MTI Pressure Transient	II-116
II-66	Pressurization System Performance Curves with Solid-Stream Surface Injection in Primary Tank	II-119
II-67	Primary Tank Internal Temperature Profiles with Solid-Stream Surface Reagent Injection	II-120
II-68	Primary Tank External Temperatures for Solid-Stream Surface Reagent Injection	II-120
II-69	Pressurization System Performance Curves with 15-deg Fan Spray Surface Injection in Primary Tank	II-122
II-70	Primary Tank Internal Temperature Profiles with 15-deg Fan Spray Surface Reagent Injection	II-123
II-71	Primary Tank External Temperatures for 15-deg Fan Spray Surface Reagent Injection	II-123
II-72	Pressurization System Performance Curves with Solid-Stream Subsurface Injection in Primary Tank	II-125

II-73	Primary Tank Internal Temperature Profiles with Solid-Stream Subsurface Reagent Injection	II-126
II-74	Primary Tank External Temperatures for Solid-Stream Subsurface Reagent Injection	II-126
II-75	Pressurization System Performance Curves with 15-deg Fan Spray Subsurface Injection in Primary Tank	II-127
II-76	Primary Tank Internal Temperature Profiles with 15-deg Fan Spray Subsurface Reagent Injection	II-128
II-77	Primary Tank External Temperature for 15-deg Fan Spray Subsurface Reagent Injection	II-128
II-78	Combustion Photographs - MFI of N_2O_4 into a 50-50 Mixture of UDMH and N_2H_4	II-130
II-79	Pressurization System Performance Curves with Surface Gas Impingement in Oxidizer Tank	II-135
II-80	Secondary Tank Gas Temperature Profile with Surface Gas Impingement on Oxidizer	II-136
II-81	Secondary Tank Pressure Profile with Surface Gas Impingement on Oxidizer	II-136
II-82	Primary Tank Internal Temperature Profile with Surface Gas Impingement in Oxidizer Tank	II-137
II-83	Primary Tank External Temperature Profile with Surface Gas Impingement in Oxidizer-Filled Secondary Tank	II-137
II-84	Temperatures in Oxidizer Tank with Surface Gas Impingement and Gunk Condenser	II-138
II-85	Pressurization System Performance Curves with Subsurface Gas Impingement in Oxidizer Tank	II-143

II-86	Primary Tank Internal Temperatures with Subsurface Gas Impingement in Oxidizer Tank	II-144
II-87	Oxidizer Tank Temperatures with Subsurface Gas Impingement	II-144
II-88	Restart Test Pressurization System Performance Curves with Uncontrolled Secondary Reaction	II-146
II-89	Restart Test Pressurization System Performance with Controlled Secondary Reaction, Subsurface Gas Impingement	II-148
II-90	Restart Test System Vibration with Controlled Secondary Reaction, Subsurface Gas Impingement	II-150
II-91	Restart Test Common Ullage Pressurization System Performance, Subsurface Gas Impingement	II-152
II-92	Restart Test Common Ullage Pressurization System Vibration, Subsurface Gas Impingement	II-155
II-93	Restart Test Common Ullage Pressurization Actual Data	II-157
II-94	Secondary Tank Common Ullage "S" Shaped Subsurface Gas Diffuser	II-159
II-95	Restart Test Common Ullage Pressurization System Performance with Secondary Reaction Reduction, Surface Gas Impingement	II-162
II-96	Restart Test Common Ullage Pressurization System Performance, Subsurface Gas Impingement	II-163
II-97	Failed Solid Stream 0.012 Diameter Injector Orifice	II-164
II-98	Check - Diffuser Poppet	II-164

II-99	Failed Demister Parts Resulting from Faulty Injector	II-165
II-100	Phase I Fuel Tank Gas Temperature vs Reagent Consumption	II-168
II-101	Phase I Fuel Tank Wall Temperature Increase vs Gas Temperature Increase	II-169
II-102	Parametric Test Common Ullage System Performance at 36 psia	II-174
II-103	Parametric Test Common Ullage System Performance at 100 psia	II-175
II-104	Subsurface Gas Diffuser	II-176
II-105	Parametric Test Fuel Tank System Performance at 36 psia	II-178
II-106	Parametric Test Fuel Tank System Performance at 100 psia	II-179
II-107	Parametric Test Fuel Tank System Performance at 200 psia	II-180
II-108	Parametric Test Oxidizer Tank Performance at 36 psia with Partial Spray Injector	II-181
II-109	Parametric Test Oxidizer System Performance at 36 psia	II-182
II-110	Oxidizer Tank Gas Temperature Profiles at 36 psia for Two Runs	II-183
II-111	Parametric Test Oxidizer Tank System Performance at 100 psia	II-186
II-112	Parametric Test Oxidizer Tank System Performance at 200 psia	II-187
II-113	Parametric Test Data Summary	II-188
II-114	Ullage Gas Dilution for the Small Scale Single Tank System	II-193

II-115	Fuel Tank Ullage Gas Molecular Weight vs Time, Single Tank Test N ₂ Initial Pressurization	II-194
II-116	Phase I Predicted Pressurizing Gas Dilution	II-195
II-117	Phase I Pressurizing Gas Requirements vs Molecular Weight	II-196
II-118	Combustion Product vs Residual Pressurizing Gas	II-197
II-119	Fuel Tank Ullage Saturation with UDMH Vapors	II-200
II-120	Oxidizer Tank Ullage Saturation with NO ₂ for Common Ullage System	II-202
II-121	Verification of Hydrogen Reaction in Oxidizer Tank	II-203
II-122	Oxidizer Tank Ullage Saturation with NO ₂	II-205
II-123	Theoretical Maximum Water Concentration vs Reagent Consumption	II-211
II-124	Propellant Temperature at Tank Outlet vs Time	II-213
II-125	Equivalent Ullage Gas Weight as a Function of Changes in Molecular Weight	II-216
III-1	Research Test Tank Correlation of Fuel Tank Ullage Gas Thermodynamics	III-7
III-2	Predicted Tank Wall Heating	III-11
III-3	Phase III Fuel Tank Temperature Change vs Heat Transferred	III-13
III-4	Phase III Fuel Tank Ullage Heat Transfer vs Final Pressurant Temperature	III-14
III-5	Phase III Energy Balance	III-19

III-6	Phase III Heat Balance Flow Diagram Inert Oxidizer	III-20
III-7	Phase III Predicted Performance Range . . .	III-21
III-8	Phase III System Propellant Tank Operating Pressure Histories	III-22
III-9	Phase I Mass Balance Schematical Representation for the Common Ullage Configuration . .	III-26
III-10	MTI Phase I Fuel Tank Performance	III-33
III-11	MTI Phase I Oxidizer Tank Performance . . .	III-34
III-12	MTI Phase I Common Ullage System Performance	III-35
III-13	Phase III MTI Fuel Tank Performance, Predicted	III-36
III-14	Phase III MTI Oxidizer Tank Performance, Predicted	III-37
III-15	Phase III Common Ullage System Performance (Deleted)	III-38
III-16	Theoretical Reaction Temperature Based on Actual Combustion Products at 36 psia . . .	III-39
III-17	Properties of Combustion Gases, Fuel Tank Reaction, N_2O_4 Injection	III-40
III-18	Properties of Combustion Gases, Secondary Tank Reaction, Common Ullage	III-41
III-19	Properties of Combustion Gases, Oxidizer Tank Reaction, Fuel Injection	III-42
III-20	Analytical Model of a Main Tank Injection Propellant Pressurization System	III-43
III-21	Main Tank Injection Phase III Test Schematic (Preliminary)	III-47
III-22	Main Tank Injection Phase III Separate Reagent Injection System	III-51

III-23	Phase III MTI Reagent Supply System	III-54
III-24	Phase III Reagent Injection and Pressure Relief Systems	III-55
III-25	MTI Injector	III-56
III-26	MTI Phase III Injector Orifice	III-57
III-27	Phase III Injector Flow Capacity	III-58
III-28	Phase III Secondary Tank Common Ullage Line Installation in Propellant Outflow System	III-60
III-29	MTI Phase III Secondary Tank Common Ullage Subsurface Gas Diffuser	III-61
III-30	Phase III MTI Fuel Catch Tank	III-67
III-31	Calculated Pressure Drop MTI Phase III Oxidizer System	III-68
III-32	Phase III MTI Test Article	III-69
III-33	Phase III MTI Fuel Tank System and Catch Basin	III-70
III-34	Phase III Tankage	III-74
IV-1	Phase III MTI Pressurization System Control Console	IV-3
IV-2	Instrumentation Location Phase III Tank Plan (Top) View	IV-5
IV-3	Instrumentation Locations, Phase III Fuel Tank - Side View	IV-6
IV-4	Run 2 Phase III Fuel Tank System Temperatures	IV-16
IV-5	Run 2 Phase III Fuel Tank Injector Performance	IV-17
IV-6	Run 2 Phase III Fuel Tank Pressurization and Propellant Flowrates	IV-18

IV-7	Run 3 Phase III Fuel Tank System Temperatures	IV-19
IV-8	Run 3 Phase III Fuel Tank Injector Performance	IV-20
IV-9	Run 3 Phase III Fuel Tank Pressurization and Propellant Flowrates	IV-21
IV-10	Run 4 Phase III Fuel Tank System Temperatures	IV-22
IV-11	Run 4 Phase III Fuel Tank Injector Performance	IV-23
IV-12	Run 4 Phase III Fuel Tank Pressurization and Propellant Flowrates	IV-24
IV-13	Typical Pressure Cycle at 5% Ullage	IV-26
IV-14	Actual Phase III Pressure Trace with 5% Initial Ullage, Fuel Tank	IV-27
IV-15	Run 5 Phase III Fuel Tank Injector Performance	IV-30
IV-16	Run 5 Phase III Fuel Tank MTI System Performance	IV-31
IV-17	Run 5 Actual Phase III Fuel Tank Pressure Trace, Restart Test.	IV-33
IV-18	Run 6 Phase III Oxidizer Tank System Temperatures	IV-35
IV-19	Run 6 Phase III Oxidizer Tank Injector Performance	IV-36
IV-20	Run 6 Phase III Oxidizer Tank Pressurization and Propellant Flowrates	IV-37
IV-21	Actual Phase III Pressure Trace with 5% Initial Ullage, Oxidizer Tank	IV-39
IV-22	Run 7 Phase III Oxidizer Tank Injector Performance	IV-43
IV-23	Run 7 Phase III Oxidizer Tank MTI System Performance	IV-44

IV-24	Run 7 Actual Phase III Oxidizer Tank Pressure Trace, Restart Test	IV-45
V-1	Molecular Weight Correlation, MTI in Oxidizer Tank	V-3
V-2	Molecular Weight Correlation, MTI in Fuel Tank	V-4
V-3	Reaction Mixture Ratio - MTI Oxidizer Tank	V-7
V-4	Reaction Mixture Ratio - MTI Fuel Tank	V-8
V-5	MTI Final Gas Temperature Comparisons, Small-Scale Systems	V-11
V-6	MTI Pressurant Weight, Oxidizer Tank	V-12
V-7	MTI Pressurant Weight, Fuel Tank	V-13
V-8	MTI Common Ullage Pressurant Weight	V-14
V-9	Phase III MTI Fuel Tank Performance	V-15
V-10	Phase III MTI Oxidizer Tank Performance	V-16
V-11	Combustion Product Molecular Weight for MTI Pressurization Systems	V-23
V-12	Vaporized N_2O_4 Propellant	V-25
V-13	Gaseous Nitrogen Tetroxide Thermodynamic Properties at 12 psia	V-26
V-14	Tank Wall Thermal Capacity	V-27
V-15	Initial Internal Energy of Prepressurants	V-34
V-16	Correction Factors, Wall Heat Transfer Coefficient	V-35
V-17	Existing Titan II Pressurization System, Stage I	V-47
V-18	Existing Titan II Pressurization System, Stage II	V-47

V-19	Flight Tank Pressure, Stage I Fuel Tank	V-48
V-20	Flight Tank Pressure, Stage I Oxidizer Tank	V-48
V-21	Flight Tank Pressure, Stage II Fuel Tank	V-49
V-22	Flight Tank Pressure, Stage II Oxidizer Tank	V-49
V-23	Pulse-Type MTI with Turbopump Bleed	V-54
V-24	Pulse-Type MTI Turbopump Bleed Fuel Tank and Separate Reagent Supply Oxidizer	V-55
V-25	Constant Flow-Type MTI, Turbopump, Bleed Fuel Tank Pressurization, Evaporated Propellant Oxidizer Pressurization	V-56
V-26	Pulse-Type MTI with Turbopump Bleed, Common Ullage System	V-59
V-27	MTI Titan II Stage I Predicted Performance	V-65
V-28	MTI Titan II Stage II Predicted Performance	V-66
V-29	Titan II, Stage I Fuel Tank, MTI Pressurization System	V-68
V-30	Titan II MTI Pressurization System Development Schedule	V-70
V-31	Titan III Transtage Helium Pressurization System	V-72
V-32	MTI Dual-Injection, Titan III Transtage, Gas- Pressurized Reagent Supply	V-76
V-33	MTI Dual-Injection, Titan III Transtage, Nitrogen-Pressurized Reagent Supply	V-77
V-34	MTI Dual-Injection, Titan III Transtage, Pump- Fed, Main Tank Reagent Supply	V-78
V-35	MTI Dual-Injection, Titan III Transtage, Me- chanically Pressurized Reagent Supply	V-79
V-36	MTI Single-Tank Injection, Common Ullage	V-80

V-37	Comparative Pressurization System Weight, Titan III Transtage	V-81
V-38	Titan III Transtage MTI Predicted Performance, Oxidizer Tank	V-87
V-39	Titan III Transtage MTI Predicted Performance, Fuel Tank	V-88
V-40	Titan III Transtage MTI Performance, Restart Mission, Oxidizer Tank	V-91
V-41	Titan III Transtage MTI Performance, Restart Mission, Fuel Tank	V-92
V-42	Titan III Transtage MTI Pressurization System Development Schedule	V-93

Table

II-1	Propellant Tank Internal Insulation Materials	II-23
II-2	Characteristics of Structural Materials Used in Tank Construction	II-24
II-3	Possible Storable Propellant MTI Systems	II-25
II-4	Main Tank Reaction Reagents	II-26
II-5	Liquid Pressurants	II-27
II-6	Instrumentation Nomenclature	II-86
II-7	Summary MTI Injector Development Tests	II-94
II-8	Single Tank Solid-Stream Surface Injection Sys- tem Mass Balance	II-101
II-9	Nonreaction Injection Penetration Test Data	II-109
II-10	Penetration Rate Comparison for a Reacting and Nonreacting Process	II-111
II-11	MTI Injection System Evaluation	II-131
II-12	Effects of Reagent Injection Technique on Fuel Composition	II-131

II-13	MTI Common Ullage System Evaluation-Continuous Test	II-167
II-14	Propellant Analysis - Common Ullage Test Series	II-167
II-15	MTI Common Ullage System Evaluation - Restart Test	II-170
II-16	Summary Phase I Parametric Data	II-184
II-17	MTI Fuel Tank Combustion Product Composition at 36 psia with Variations in N ₂ O ₄ Injection Technique	II-199
II-18	MTI Oxidizer Tank Combustion Product Composition of Various Common Ullage Systems at 36 psia	II-201
II-19	MTI Oxidizer Tank Combustion, Products Composition at 36 psia for Various Pressurization Techniques	II-204
II-20	MTI Combustion Product Composition Parametric Data	II-206
II-21	Propellant Analysis for Two-Tank Test with Water-Filled Second Tank	II-210
II-22	Typical Propellant Analysis for Two-Tank Test Series with Oxidizer-Filled Second Tank	II-210
III-1	Phase I Research Test Tank Correlation of Ullage Gas Thermodynamics, Twin Tank Expulsion (Water in Oxidizer Tank)	III-3
III-2	Estimated Phase III Pressurization System Performance	III-4
III-3	Phase I Heat Balance	III-16
III-4	Phase III Heat Balance	III-18
III-5	MTI Combustion Product Mass Balance Summary	III-23

III-6	Phase III MTI Pressurization System Components	III-72
IV-1	Phase III Instrumentation List	IV-4
IV-2	Phase III Vent and Relief Valve Test Results	IV-8
IV-3	Phase III Pressure Switch Test Results	IV-9
IV-4	Phase III Demonstration System Test Results	IV-42
V-1	MTI Combustion Product Composition	V-5
V-2	Propellant Tank Pressurizing Gas Composition, Volume Percent	V-9
V-3	Titan II Fuel and Oxidizer Tank Pressurization System Weights	V-50
V-4	Titan II, Stage I, Total Pressurization System Weights	V-62
V-5	Titan II, Stage II, Fuel Tank Pressurization System Weights	V-62
V-6	Titan II Candidate MTI Pressurization Systems Reliabilities	V-63
V-7	Basis for Cost Estimate, Titan II, MTI	V-67
V-8	Summary of Titan III Transtage Pressurization System Weights	V-82
V-9	Pressurization System Reliability Comparison	V-83
V-10	Summary of Pressurization System Reliability, Titan III Transtage	V-86
V-11	Basis for Cost Estimate - Titan III Transtage	V-96
B-1	Propellant Tank Sizing Factors	B-4
B-2	Inputs for MTI Pressurization	B-6
B-3	Inputs for Gas Generator Pressurization	B-7

RTD-TDR-63-1123

E-1	Phase I Research Tests ($MW_{cp} = 14$)	E-2
E-2	Phase III System ($MW_{cp} = 16$)	E-2
F-1	Sample Data Sheet	F-20
F-2	Locations of Input Parameters for Primary Tank	F-23
F-3	Locations of Input Parameters for Secondary Tank	F-26
F-4	Locations for Additional Input	F-28
F-5	Input Parameters Primary Tank	F-29
F-6	Input Parameters Secondary Tank	F-33

RTD-TDR-63-1123

ABSTRACT

This report describes the analytical and experimental effort expended in the development of a flight type ground demonstration test article employing a Main Tank Injection (MTI) Pressurization System. The overall program was conducted in four phases; (1) Preliminary investigations including the basic research and development of a small-scale system; (2) design and fabrication of a flight-type test article; (3) full-scale system development and demonstration test; and (4) system analysis resulting in the formulation of a design handbook and study of specific vehicle applications.

Several theoretical studies were performed to establish system requirements and determine possible system configurations. A brief investigation of materials required in the design of a chemical pressurization system was also performed. Based on an analysis of current vehicle requirements and information gained in the small-scale test program, an MTI pressurization system design criteria was compiled to direct the full-scale demonstration system design. An abbreviated version of the IBM-7094 MTI mathematical model was used in the early performance studies while a general description of the final version is contained with a comparison made of experimental and theoretical data.

A considerable amount of experimental data were accumulated during the course of the program and were analyzed to identify pertinent effects resulting from the chemical pressurization process. Composition and properties of the pressurizing gas and rate of ullage saturation with propellant vapors are reported based on extensive mass spectrometer gas analysis. An investigation of propellant degradation due to the reaction process and dilution by condensate is also included. Determining reaction process characteristics was a major consideration in this program to establish reagent consumption and system thermodynamics. Theoretical heat and mass balances are described, based on the reaction mixture ratio determination and combustion zone definition.

LIST OF SYMBOLS

a	Vehicle acceleration (g)
A_g	Heat transfer area, exposed gas surface (ft^2)
A_w, \bar{A}_w	Wall heat transfer surface, average (sq ft)
b	Perimeter of cross section surface of tank wall for longitudinal conduction (ft)
C_d	Orifice discharge coefficient
C_p	Specific heat of gas (Btu/lb °R)
C_m	Specific heat of wall material (Btu/lb °R)
C_v	Specific heat of constant volume (Btu/lb °R)
d	Orifice diameter (in.)
D_m	Diameter, mean (ft)
F	Thrust (lb_f)
g_c	Gravitational constant: 32.2 ft/sec^2
ΔH	Enthalpy difference (Btu)
H_c	Total enthalpy of combustion products in fuel tank (Btu)
H_o	Total enthalpy of gas leaving fuel tank (Btu)
$h_{g,L}$	Convective coefficient of heat transfer ($\text{Btu/sec ft}^2 \text{ °R}$)
h	Height of fluid above pump suction (ft)
I_{sp}	Specific impulse ($lb_f\text{-sec}/lb_m$)

J	Conversion factor (778 ft-lb/Btu)
k	Thermal conductivity (Btu/sec ft °R)
k_w	Ullage factor (V_i/V_{total})
MW	Molecular weight of gas (lb _m /mol)
MF or \bar{M}	Mole fraction
N_{Nu}	Nusselt modulus (hD/k)
N_{Gr}	Grashof modulus $\left(\rho^2 g_c \beta \frac{D^3 \Delta T}{\mu^2} \right)$
N_{Pr}	Prandtl modulus $\left(\frac{C_p \mu}{k} \right)$
n	Time interval
P	Tank pressure (psia)
Δp	Pressure drop (psi)
P_c	Chamber pressure (psia)
Q	Heat transferred by convection (Btu)
\dot{Q}_v	Volume outflow rate (ft ³ /sec)
$Q_{w,L}$	Heat transfer (to wall, to liquid) (Btu)
$(Q/A)_{ext}$	External environment wall heat rate (Btu/sec ft ²)
S	Cross section surface area of tank wall for longitudinal conduction (ft ²)
T	Temperature (°R)
\dot{T}	Temperature rate change (°R/sec)

t	Temperature (°F) or wall thickness (in.)
Δt	Temperature difference (°F)
T_a	Ambient temperature (°F)
U	Total gas internal energy (Btu)
U	Overall film coefficient (Btu/hr ft ² °R)
V	Volume (cu ft)
V_w	Volume of wall material (cu in.)
v	Velocity (fps)
W	Gas weight (lb _m)
w	Reagent weight (lb _m)
$\dot{w}_{f,o}$	Weight flow rate (lb _m /sec) fuel or oxidizer
\bar{w}	Weight fraction of gas

GREEK SYMBOLS

α	$\sqrt{h_{gw} k t} \left(\frac{D_m}{A_w} \right) \text{Btu/sec in.}^2 \text{ (}^\circ\text{R) or degree of } N_2O_4 \text{ dissociation}$
β	Coefficient of volumetric expansion $\left(\frac{1}{^\circ\text{F}} \right)$
ρ	$\frac{\rho c t}{\tau} \text{Btu/in.}^2 \text{ (}^\circ\text{R sec)}$
γ	Ratio of specific heats, C_p/C_v
τ	Time (sec)

RTD-TDR-63-1123

τ_b	Burning time (sec)
$\Delta\tau_r$	Response time (sec)
μ	Viscosity (lb/ft-sec)
ρ	Density (lb _m /cu ft) or (lb _m /cu in.) wall calculations
λ	Reaction mixture ratio, weight of oxidizer/weight of fuel
ξ	Constant for relative wall heat transfer
ω	Frequency, cycles per second

SUBSCRIPTS

b	Bleed
c	Condensable
cp	Combustion products
f	Final or fuel
g	Gas
i	Initial
int	Inert
m	Material
o	Oxidizer
v	Vaporized propellant
w	Wall

I. INTRODUCTION

The Main Tank Injection (MTI) Pressurization System is a chemical method of propellant tank pressurization. The process is initiated by injecting a small quantity of hypergolic reagent into the main propellant tank. Subsequent pressurization of the other tank may be accomplished either by direct reagent injection or in the case of the oxidizer tank, may be pressurized by the combustion products generated in the fuel tank. This system is desirable because of the high density and low-pressure storage of the reagent, and the capability for generation of a relatively low density pressurant without the use of a heat exchanger. This study concerns the adaptation of an MTI pressurization system to a flight-type test article and to specific current propulsion systems using the propellants nitrogen tetroxide and a 50/50 blend of hydrazine and unsymmetrical dimethylhydrazine.

The technical approach has been to study the important factors influencing the pressurization process by laboratory experiments and analytically determine system operating characteristics to evaluate various possible designs. Several engineering studies were completed initially to establish the pertinent design requirements of such a system, identify desirable configurations, and determine the most promising applications. Verification of the theoretical performance and development of a practical system was accomplished by a considerable amount of testing on 5 1/3-cu ft thick wall spherical tanks and subsequent demonstration in a 2,000-gal. full-scale flight-type ground test article. The research fixture was fabricated to investigate the actual reaction process and develop components and operating procedures on a small-scale basis at pressures up to 200 psia. Full-scale system design recommendations were established from this program, which involved approximately 80 tests.

Based on the full-scale system testing and correlation with the performance predicted by a mathematical model, the pertinent system characteristics were compiled in the form of a design handbook. By using the knowledge gained from the entire program, a study of two Air Force-designated vehicles was performed to evaluate the possible adoption of an MTI Pressurization System to those designated vehicles.

II. PHASE I PROGRAM

The primary objective of the Phase I program was to develop a small-scale MTI Pressurization System and obtain sufficient data to identify full-scale system design requirements. Several preliminary studies were performed to enable small-scale system design and provide guidelines for research testing. These studies included an identification of system requirements, an evaluation of possible configurations and applications, a materials investigation, and the development of small computer program for determining approximate system performance for separate tank pressurization. The major portion of the Phase I effort was devoted to closed system testing of the small-scale research fixture with a small amount of qualitative laboratory experimentation.

A. PRELIMINARY INVESTIGATION

A thorough search of the literature concerning similar processes and a review of previous experimentation on the chemical pressurizations of liquid propellant rocket propulsion system was performed initially to acquire a knowledge of the process and identification of anticipated problems. The feasibility of the process was established by the smooth combustion reported by Lockheed (SSD-TR-61-21). Thus, emphasis was placed on adapting the process to a flight weight system, and obtaining further information on process characteristics in view of the high combustion temperatures involved.

Further identification of the combustion phenomena or identification of influence parameters was not described in the literature, and only a very small portion of the information acquired was applicable to the type process involved. Using experimental data from the literature search and established techniques for equilibrium-type combustion reactions, estimates of expected operating characteristics were made. In addition, the general requirements, construction, and application of the MTI Pressurization System were studied and pertinent results are summarized in this chapter.

1. Requirements Study

The general requirements for adaption of the MTI pressurization process for any particular rocket vehicle application were studied to provide basic design and performance data. A specific attempt was made to identify pertinent operating conditions or environments

that would impose unique design considerations on the various injection techniques and system configurations. Where absolute values could not be established due to the general nature of the study, the important factors influencing the requirements were identified. The significant design requirements affecting the MTI pressurization techniques were studied for three basic applications, large boosters, sustainer vehicles, and space exploration systems. These requirements are discussed with respect to the pressurization system, propellant feed system, engine system, and structural characteristics.

Pressurization System - The primary advantage of the chemical pressurization system lies in its capability for high-density storage at low pressures, and low-density pressurization of the propellant tank ullage. The resultant overall system weight, however, has to be determined for the particular application, since the optimum design will be a function of pressurization system configuration and capacity. Therefore, a particular weight limit cannot be established as a general requirement. Pressurization system weight, however, can be computed from the sum of the weights of the pressurizing gas and components required. In the case of any pressurization system, the residual pressurant remaining in the storage container should be included. In the gas generator and MTI systems any condensate formed must be identified. If extra capacity turbo-pumps or gas generators are required to effect pressurization a proportional share of the weight of these systems should be included. For comparison, comparable pressurant storage density and final density of a stored gas in a helium system and an MTI pressurization system are shown in the following tabulation:

Type Design	Storage Density (lb/ft ³)	Pressurant Density (lb/ft ³)
Helium System	1.937 (525°R and 3000 psia)	0.018 (750°R and 36 psia)
MTI System	67* (525°R and 36 psia)	0.067* (750°R and 36 psia)
*Based on a reaction mixture ratio of 0.7 and molecular weight of 15.		

The final gas density of an MTI system operating at comparable temperatures is 3.7 times heavier than the helium density. However, the heat exchanger and large storage container required in the helium system imposes a severe weight penalty. Although the MTI system is penalized by condensing products of reaction, the elimination of a

heat exchanger and the lighter storage system required (due to the low storage pressure and 34.6 times higher initial density) makes this system appear attractive for many applications.

A study of pressure control requirements has indicated that separate characteristics are required for pump- and pressure-fed engines. The propellant tank ullage pressure requirement would be a function of the trajectory and vapor pressure (for pump systems). In general, a tolerance of 3% is mandatory for most applications for the pressure profile required during the mission. The pressurization system to be developed must maintain the desired tank pressure under variable propellant outflow to demonstrate system versatility, even though it may not be required for some future applications. Changes in ambient conditions as a result of a particular flight pattern or mission must not affect tank pressure control. That is, propellant slosh or inertia forces exerted on the reagent injected should not adversely affect the process. Based on possible future application, the pressure range for system operation would be from 20 to 300 psia. Special applications requiring higher operating pressures will cause unique problems in tank and insulation material requirements due to the inherent high temperatures encountered.

The system operating temperature limits have been established considering propellant, component, and tank materials. Although the effects of propellant vaporization cannot be identified for general application, an upper temperature limit of 1000°F at low pressure (20 to 60 psia) has been established for the storable propellants under consideration. This limit is based on possible rapid decomposition of the hydrazine-unsymmetrical dimethyl hydrazine mix. Similarly, a 1000°F hot gas temperature limit has been imposed due to current component design. The following tabulation identifies maximum system operating temperatures based on allowable tank wall temperatures.

Material	Maximum Material Temperature (°F)	Estimated Maximum Ullage Gas Temperature (°F)
Aluminum Alloy	300	500
Titanium	700	1000
Stainless Steel	1000	1400
High Temperature Steel Alloy	1300	1800

A gas temperature tolerance of $\pm 4\%$ in the 300 to 500°F range and $\pm 5\%$ tolerance in the 500 to 1000°F range has been established to verify system performance repeatability. This temperature control must be inherent in the MTI pressurization process to establish reagent loading quantities and minimum insulation requirements.

Other miscellaneous general requirements identified include:

- 1) Previous pressurization system experience has established a 5% maximum initial propellant tank ullage volume for efficient system design;
- 2) For certain space missions requiring a rendezvous and refueling operation, the absence of a facility gas supply for prepressurization of the initial ullage volume imposes a need for adequate MTI system response for pressure control with this minimum ullage;
- 3) Continuous pressurization during long-term storage in space may be required for an instant response engine re-start capability. However, pressurization after long coast periods should be demonstrated to establish time requirements since proper propellant orientation may be required before and during pressurization;
- 4) Hazardous conditions imposed by zero-gravity operation of an MTI common ullage system require that a suitable system design be developed.

Detailed MTI system and component requirements are presented in Chap. III.B for the small-scale system development program. The design parameters for full size applications are given in Chap. V.B.

Propellant System - MTI system design requirements resulting from propellant system characteristics were considered in view of rocket engine, flight control, and structural requirements. These requirements can generally be classified as functional and compatibility problems resulting directly from the condition of the liquid.

Functional requirements indirectly concern engine performance, component operation, residual propellant, and overall system and vehicle performance. Propellant vaporization resulting from the MTI pressurization process will directly contribute to the overall weight penalty imposed and must be minimized for any given propellant combination. The engine and component function requirements dictate the condition of the propellant must insure less than 5% soluble inerts and viscosity increase for the fuel and 1% limit for the oxidizer, based on available data. The following tabulation itemizes maximum particulate contamination.

Solids			Fibers	
Maximum Diameter (μ)	No. Allowed	Length (μ)	Maximum Diameter (μ)	No. Allowed
0 to 300	Not limited by count	0 to 750	25	Not limited by count
300 to 500	6/1000 ml of liquid	750 to 2000	25	21/100 ml of liquid
500 to 1000	2/100 ml of liquid	2000 to 6000	40	3/100 ml of liquid
Over 1000	1/100 ml of liquid			

In addition, the allowable entrained vapor in the propellant must be less than 3% for the turbopump pressurized systems to keep within the allowable thrust variation established by current propulsion system specifications. This specific requirement will be a function of pump design, and will have to be assessed on an individual basis. For gas pressurized systems as much as 10% or more entrained vapor may be allowed. The allowable moisture content should be less than 2% by volume to insure a reduction in specific impulse of less than 1/2%. A typical more specific description of this requirement is shown in Fig. II-1 with some performance predictions of a specific rocket systems shown in Fig. II-2.

The effect on vehicle stability due to slosh induced by the sub-surface pressurization process will require an analysis of the specific application. Vehicle-induced slosh, however, will create a design requirement to prevent splashing propellants into the common ullage manifold and to maintain stable pressure control with the surface reagent injection system. Vehicle pitch rates have been established from a review of nominal booster trajectories to insure MFI process control. The design pitch rates are 15 deg/sec for roll and 5 deg/sec for pitch and yaw; a frequency of <5 cps applies to all three maneuvers.

The random vibration design criteria are presented in Fig. II-3. Propellant surface effects created by this criteria were used to establish MFI capability under simulated flight conditions.

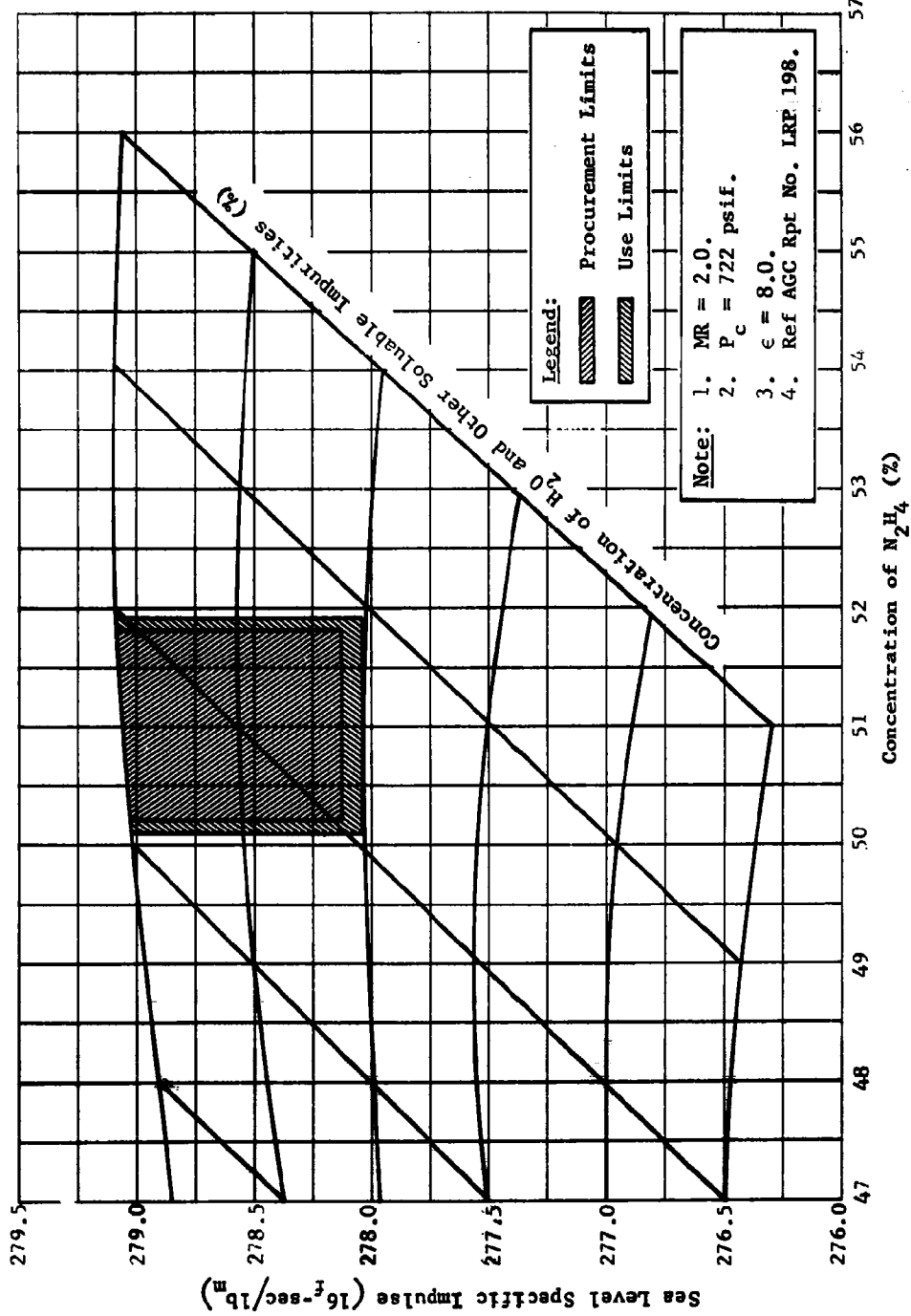


Fig. II-1 Relation of Performance to Composition of Fuel for the N₂O/N₂H₄-UDMH Propellant Combination

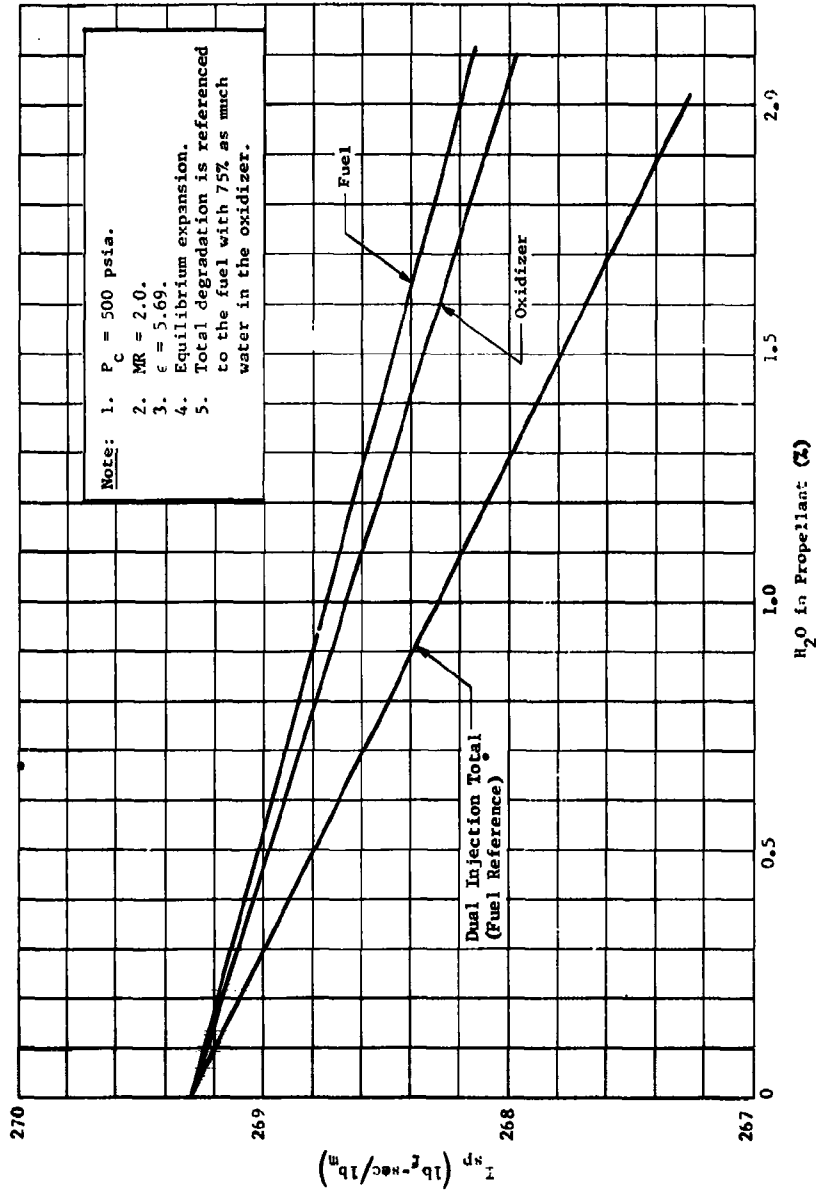


Fig. II-2 Effect on I_{sp} of Water in N_2O_4/N_2H_4 -UDMH

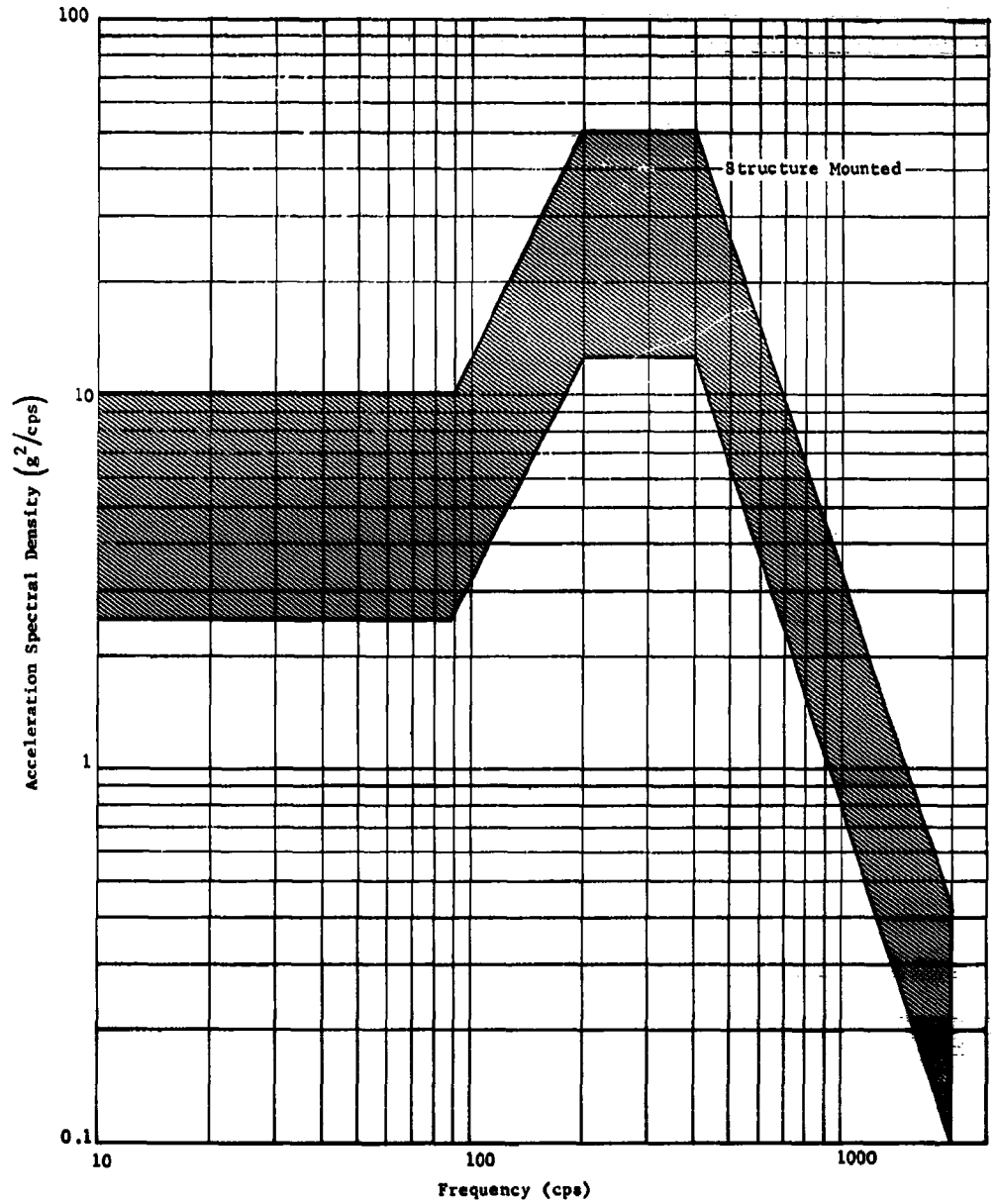


Fig. II-3 Random Vibration Design Criteria for an MTI Pressurization System, Flight Environment

Engine System - A survey of engine propellant feed requirements was made to identify significant requirements for an MTI pressurization system design. Two general engine types were investigated and categorized according to the type of propellant feed (pump or gas pressurized). The requirements established for each system considered engine performance degradation due to propellant or pressurization system effects that are induced by the MTI process. The required pressure range for tank pressurization has been established from a survey of current engine requirements at 20 to 50 psia for pump-pressurized systems and 50 to 200 psia for gas-pressurized system. The allowable pressure fluctuation of $\pm 3\%$ has been dictated by allowable mixture ratio shift and thrust variation. MTI system requirements include maintaining the desired tank pressure within tolerance during the engine start transient as well as during steady-state engine operation. An interpretation of existing booster engine model specifications has shown that the pressurization system response must be adequate to supply sufficient gas for a maximum propellant flow increase of 10% maximum/millisecond up to 60 to 70% rated thrust, and 0.75%/millisecond from 50% to full thrust. Steady-state propellant flow variations are not critical and amount to $\pm 1.25\%$. Figure II-4 shows a typical start transient for a pump-pressurized propulsion system.

Current engine design using density compensators requires that propellant density be defined for accurate engine calibration. An additional requirement is also apparent for turbopump systems since propellant vapor pressure must be considered. The following fluid bulk density variations have been established at the tank outlet with a maximum temperature variation rate of $4^\circ\text{F}/\text{min}$.

Propellant	Density (lb/cu ft)	Bulk Temperature ($^\circ\text{F}$)
N_2O_4	89.3 to 92.4	40 to 80
0.5 UDMH/0.5 N_2H_4	56.0 to 57.2	40 to 80

Additional pressurization system requirements occur when the design must adapt to changing propellant flow rates encountered with variable thrust engine designs. A review of current available engines established a requirement for adequate pressure control over a 100% to 10% range in propellant flow rate with a maximum rate of change of 10%/sec. This operating characteristic was established for evaluating the various injection techniques used in the small-scale MTI system and demonstrated in the full-scale system for the final configuration.

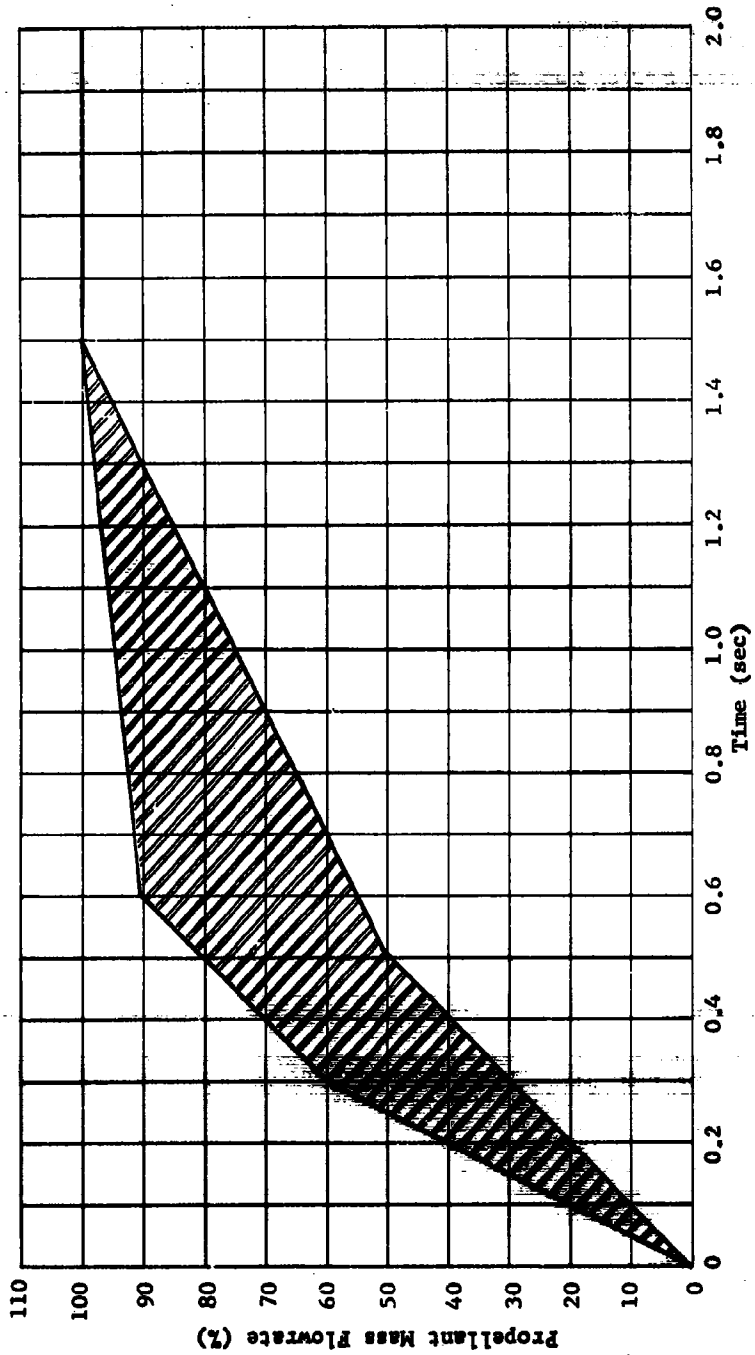


Fig. II-4 Typical Start Transient Range for a Pump-Pressurized Propulsion System

Structures - The design and construction of an MFI propellant tank will be influenced by both the characteristic pressure and thermal effects resulting from this pressurization process. Pressure pulsations due to an on-off injection system or unstable combustion encountered during continuous modulation will affect the selection of propellant tank material and construction techniques. Although the pressure cycling of the propellant tank is also a consideration with other pulse-type pressurization systems, the transmission of shock waves through the propellant may increase the design pressures somewhat due to 5 psi pressure surges detected at the lower dome with a submersed cross flow gas injection system to require special baffles for eliminating these effects. However, no special structural requirements were identified with the solid stream surface direct injection process. The fatigue strength of the tank material, as well as the quality of welds, will influence the amount of damping required.

The desirability of certain propellant tank designs will be determined to some extent by the particular characteristics of the injection process. A survey of current design philosophy has established a range of length-to-diameter ratios of 2.5 to 7 with a maximum tank length of 140 ft. Tank length will influence the pressurization process since the time required for a reaction to occur with a surface injection system will change with the propellant height variation. A submersed injection process would also be affected since the time required for the vapor bubble to reach the propellant surface would vary. With either injection process, combustion zone control and common ullage manifold requirements must be considered.

Temperature considerations will be significant when selecting the optimum tank design. Because of the manufacturing considerations and the moderate system operating temperatures associated with the MFI process, more efficient use can be made of existing aluminum tankage for low-pressure applications. For high-pressure designs an evaluation of insulation requirements versus available lightweight temperature resistant materials will be required. A practical temperature limit, however, can be established for each application for any given material based on tank volume. The increase in tank weight associated with high temperature operation will usually be greater than the amount of pressurization system weight saving achieved by lowering the pressurant density. Due to the reduction in strength of materials at high temperatures, a limit of 300°F has been established for the maximum aluminum tank wall temperature for efficient system design.

The incorporation of suitable baffles in the propellant tank will be required for some configurations to assure thermal protection and vapor bubble control. In the common ullage design, a suitable flow control valve will be required to prevent the hypergolic propellants from mixing. The submersed injection techniques will require careful attention to propellant flow control and bubble dispersion to eliminate entrained vapor and liquid agitation. Approximate requirements established during the research test program and incorporated in the Phase II design criteria were successfully demonstrated in the full-scale system test program.

2. Configuration Analysis

Various MTI system configurations were studied to determine the more practical design for the Phase III full-scale demonstration test program and possible future vehicle applications. Systems design considered both booster and sustainer propulsion systems as well as space vehicles. A quantitative comparison was made based on system cost, weight, reliability and development difficulty. Performance evaluation of the most promising systems were made for general applications discussed in Chap. II.A.6. A more detailed summary is contained in Chap. V.C. The oxidizer and fuel tank pressurization process was analyzed for several injection techniques, including various common ullage configurations. Based on the results of experimental small-scale system testing the solid stream surface reagent injection process or the common ullage configurations with suitable gas conditioning are the most promising for future applications.

Figure II-5 is a common ullage MTI Pressurization System with pneumatically pressurized reagent storage for a pressure-fed engine. This system has been tested without success when N_2O_4 was used as the reagent because the reactive constituents in the pressurizing gas could not be eliminated. The use of other reagents may eliminate this problem. Note the fuel is used to regeneratively cool the pressurizing gas.

Figure II-6 is also a common ullage MTI Pressurization System, however, the reagent supply is contained in the main propellant tank and supplied by turbopump bleed. This system shows the common ullage pressurization technique that was successfully demonstrated; however, subsurface injection is used for additional pressurizing gas cooling in the fuel tank. Inherent vibration associated with this process would require a development effort to suppress the vibration.

RTD-TDR-63-1123

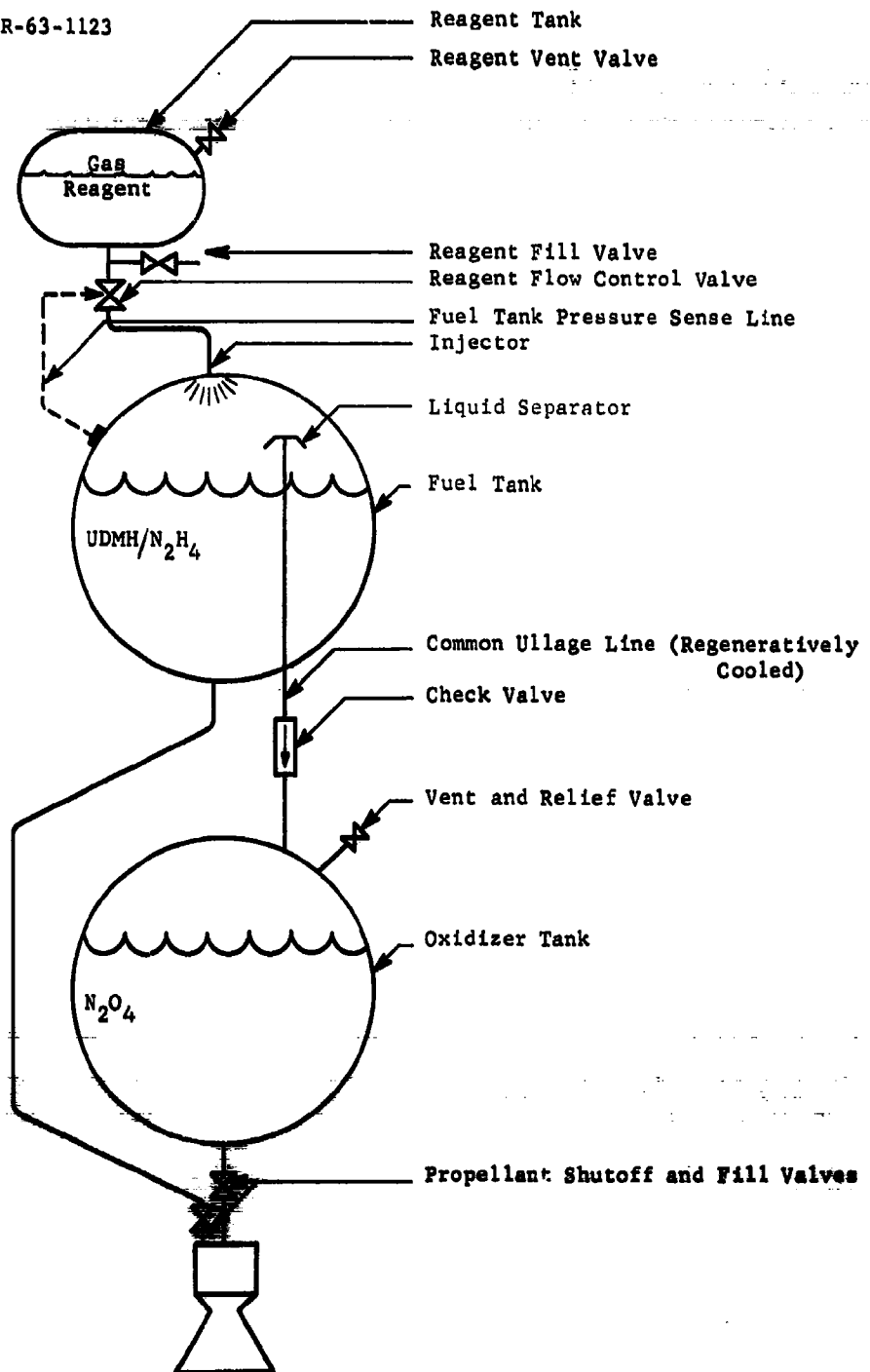


Fig. II-5 Common Ullage MTI Pressurization System with Pneumatically Pressurized Remote Reagent Storage, Pressure-Fed Engine

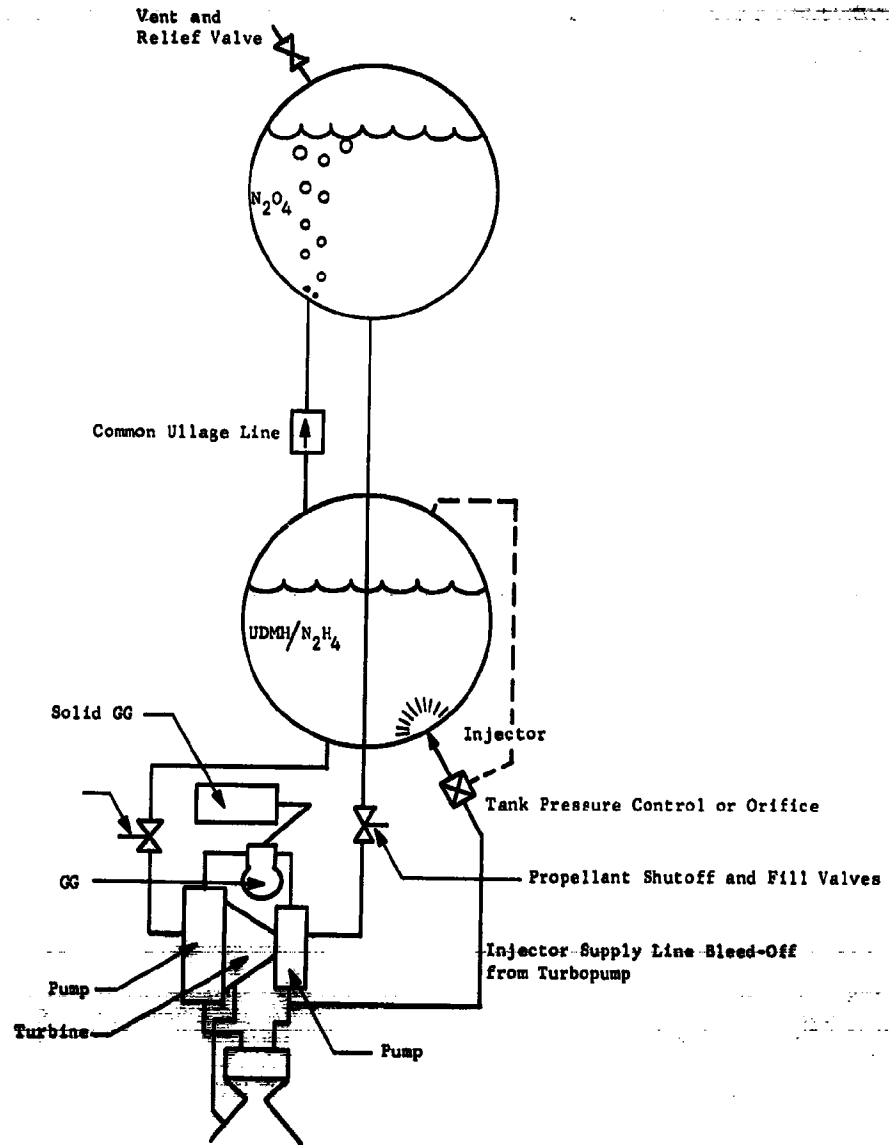


Fig. II-6 Common Ullage MTI Pressurisation System with Main Propellant Tank Reagent Supply, Pump-Fed Engine

Figure II-7 is a hybrid MFI Pressurization System with pneumatic pressurized remote reagent storage and evaporated propellant for a pressure-fed engine. Another version of this system could use stored gas for pressurization of the oxidizer tank. However, for most applications the weight penalty would be excessive unless the ullage could be prepressurized without additional pressurization during flight.

Figure II-8 shows a pump-fed injection system with an ullage elimination technique to reduce vaporized N_2O_4 . This system would require development of a satisfactory flexible diaphragm compatible with both propellants.

Figure II-9 is a schematic of a dual injection MFI Pressurization System for a turbopump-fed engine. This system takes advantage of the available high-pressure reagent supply by crossfeed. In the simplest form this system could employ burst discs for reagent isolation before start and a fixed orifice for flow control.

Pressurization Process Selection - Three basic MFI pressurization processes and the design requirements of each were evaluated. These processes are identified by the location of the reaction fuel tank, oxidizer tank, or both tanks. The significant advantages of initiating gas generation in the fuel tank rather than in the oxidizer tank with a common ullage manifold are summarized:

- 1) Process gas flow direction is more desirable;
- 2) Regenerative cooling capability is available;
- 3) Propellant contamination is less critical;
- 4) Propellant tank volumes are equalized.

The process gas flow direction is important in a common ullage configuration to eliminate possible hazardous reactions. Since the oxidizer vapor pressure is 15 psia higher than the fuel vapor pressure, there will be a tendency for N_2O_4 to flow in the direction of the fuel tank with the possibility of an undesirable reaction. If the normal pressurization process is in the direction of the oxidizer tank, this situation can be avoided with a check valve or isolation valve. The possibility of using a single tank vent and relief valve in the common ullage configuration for overpressure protection also depends on the gas flow direction. An overpressure condition can only occur in the fuel tank, if secondary reactions are eliminated in the oxidizer tank. Consequently safe venting can be accomplished by a single fuel tank vent valve. Double protection can be provided if oxidizer and fuel tank vents are incorporated in a system designed with sufficient flow capacity through the common ullage manifold.

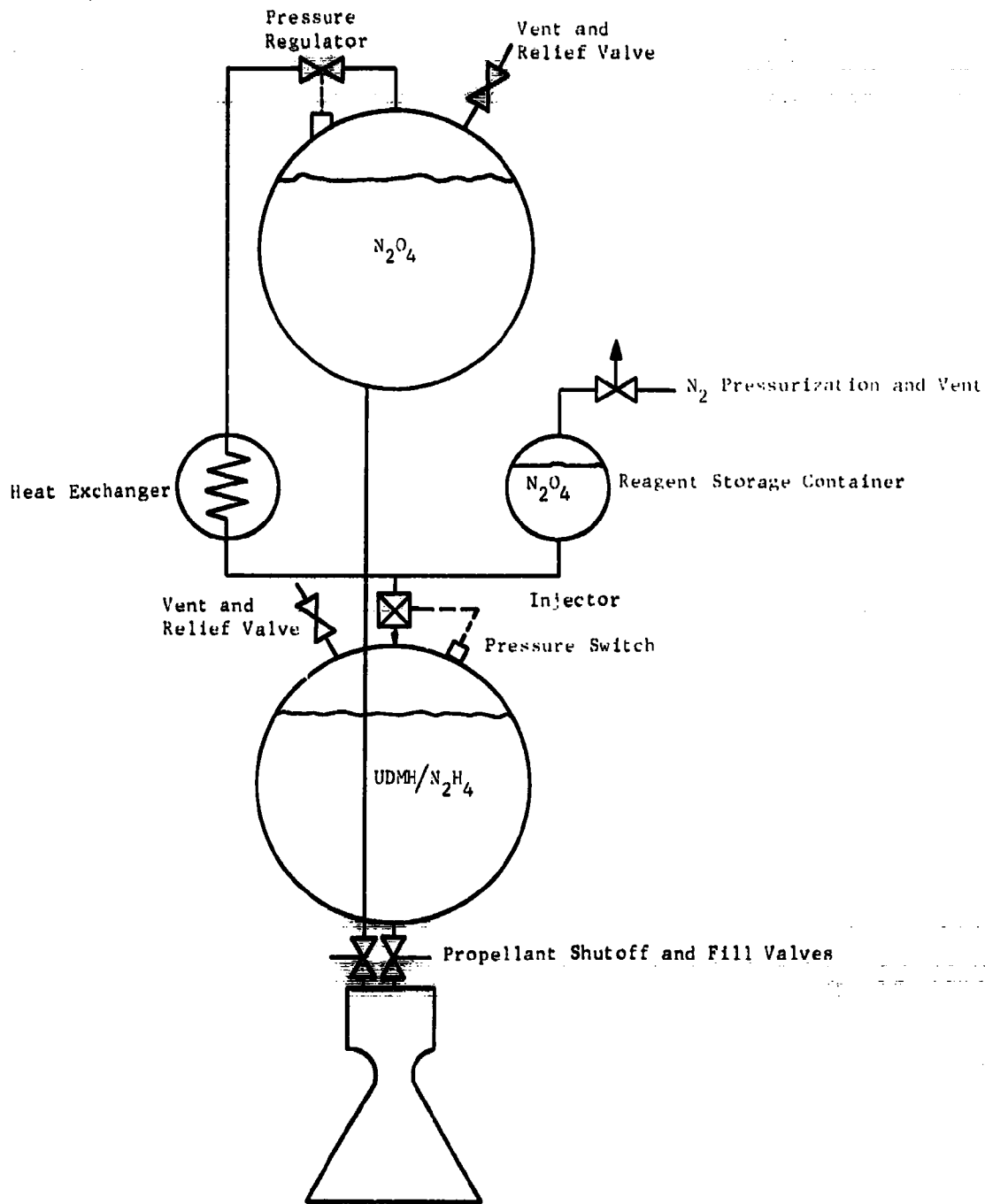


Fig. II-7 Hybrid MTI Pressurization System with Pneumatically Pressurized Remote Reagent Storage and Evaporated Propellant, Pressure-Fed Engine

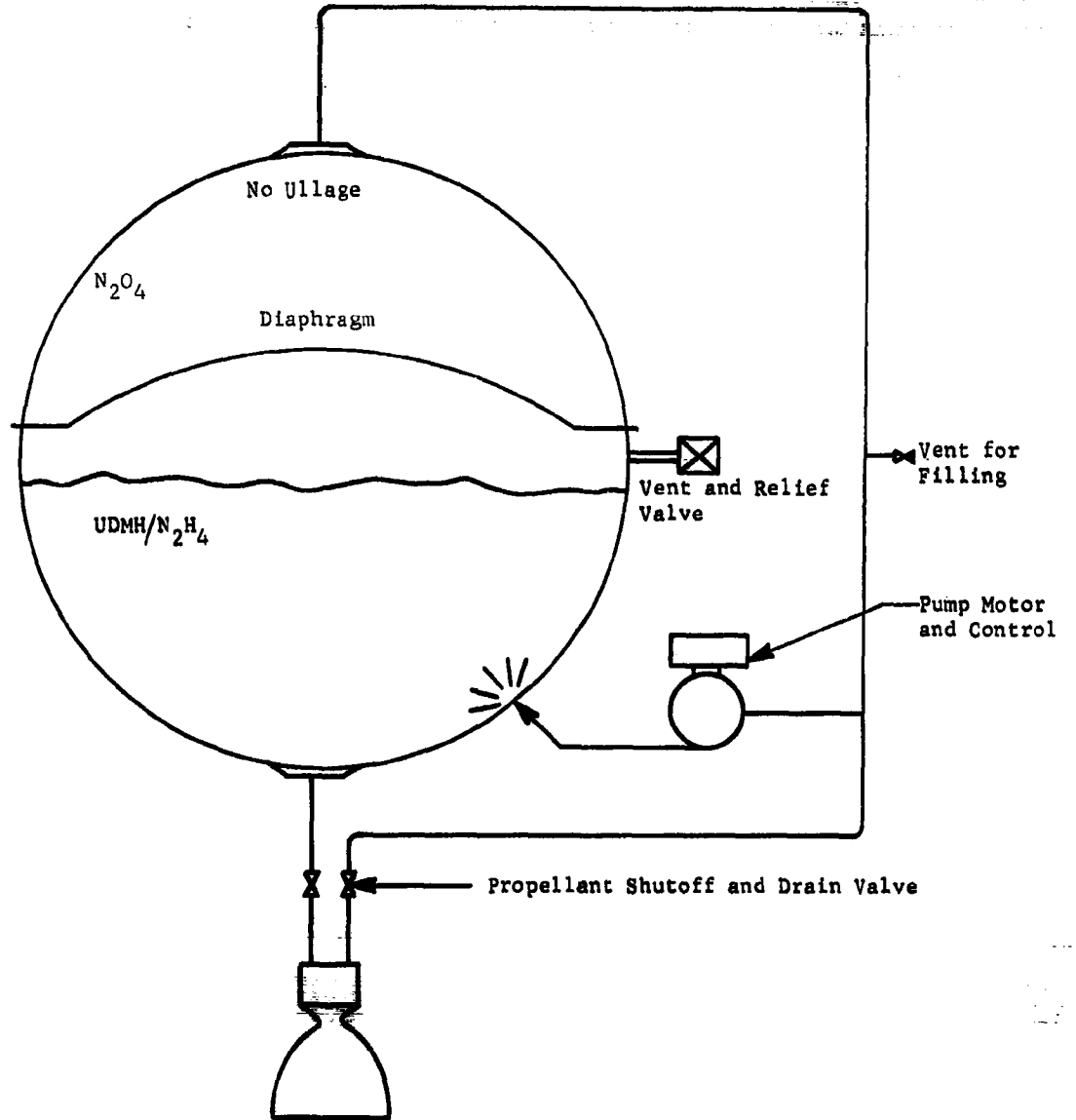


Fig. II-8 Pump-Fed Injection System with Ullage Elimination

RTD-TDR-63-1123

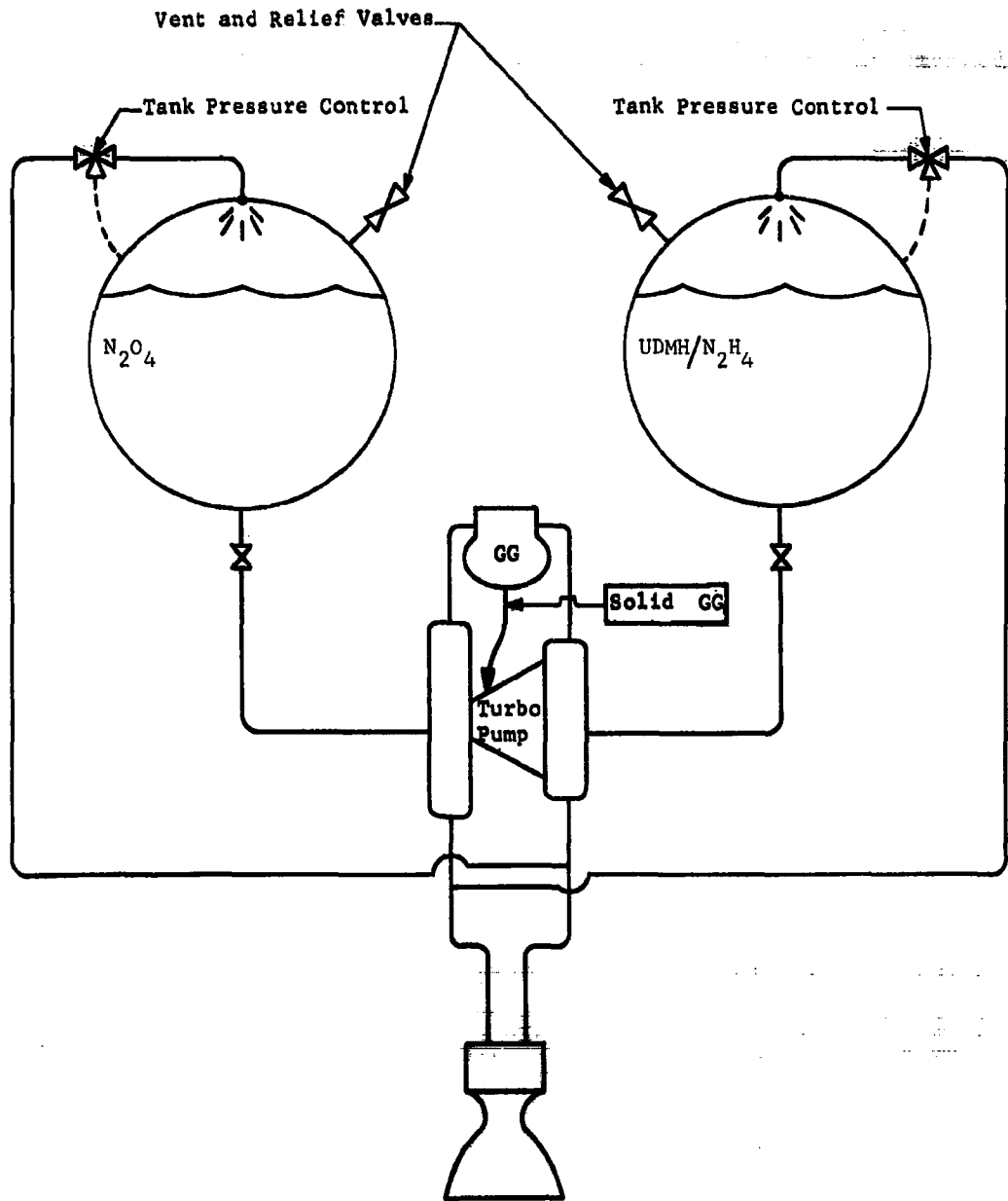


Fig. II-9 Turbopump Bleed-Crossfeed Injection System

Two regenerative cooling techniques were considered for ullage gas temperature control. The common ullage line passing through the fuel would give a simple, desirable temperature control method for a process initiated in either tank. The submersed injection process in the fuel tank, however, would be more advantageous from both a cooling and gas composition standpoint due to the condensation of certain reactive constituents. Since oxidizer vaporization is undesirable from a molecular weight point of view, its regenerative cooling capability would not be exploited. The increase in oxidizer temperature would also require a comparable increase in propellant tank pressure to achieve the same NPSH for a turbopump-pressurized propellant feed system. By initiating the reaction process in the fuel tank, the formation of hydrocarbons and water may be less critical. A review of possible biproducts resulting from the combustion processes indicates that many are fuel soluble and nonreacting biproducts. Water in the fuel system will not form corrosive fluids as it would in the oxidizer tank. Since a large ullage volume may be necessary to accommodate initial pressure response requirements, an increase in fuel tank volume would tend to equalize both propellant tanks. This is advantageous in that manufacturing costs would be reduced.

Initiation of the reaction process in the oxidizer tank does not appear attractive, primarily because of the anticipated difficulty in controlling the secondary reaction of oxidizer vapor with fuel vapors for a common ullage system. Some reaction of ammonia with nitrogen tetroxide is anticipated in the oxidizer tank with a fuel tank common ullage system, but to a lesser degree. If the secondary reactions cannot be controlled, a cross feed injection system could be developed. This system has been considered less desirable due to the increased complexity inherent in a dual injection system and resultant higher pressurizing gas molecular weight.

MTI Pressurization System Evaluation - In the injection system evaluation ten techniques for process initiation and continuation were considered. A figure of merit was established for each system for the three applications under consideration (booster, sustainer, and space vehicle) by the following empirical formulas:

$$\text{Booster } E_B = 0.2 C + 0.25 W + 0.3 D + 0.25 R$$

$$\text{Sustainer } E_S = 0.1 C + 0.35 W + 0.25 D + 0.3 R$$

$$\text{Space Vehicle } E_{SV} = 0.05 C + 0.4 W + 0.15 D + 0.4 R,$$

where

C = relative manufacturing cost

W = relative weight

D = relative development difficulty

R = relative reliability

The results of this study indicated the systems shown in Fig. II-5 and II-6 to be the most promising based on the particular common ullage applications considered. The optimum system for any particular application would depend primarily on available energy for reagent supply. In its simplest form, for booster vehicle, the MTI Pressurization System would consist of the reagent stored in the propellant tank and metered by a fixed orifice under constant turbopump discharge pressure. The gas pressurized propellant feed system may require an external pressure supply for reagent injection. Since the turbopump function in an MTI system can be simulated by a high-pressure gas source, both systems would then be identical except for the injection technique. The configuration has been simulated in the Phase III demonstration system for individual tank reagent injection corresponding to the system shown in Fig. II-9.

MTI Pressurization System Design - A primary consideration in the initiation of an MTI Pressurization System design is the location of the injector in the propellant tank. Surface, submersed, and floating injector configurations have been evaluated with distinct performance advantages inherent in each design. In high pressure applications the submersed injector offers the most promise since greater capability for regenerative cooling of the combustion process is available. The surface injector system avoids the disadvantages of propellant vapor entrainment and vibration of the submersed injector, but the increasing distance to the propellant surface and higher temperatures associated with this technique may be undesirable in some cases. The floating injector avoids both of these problems but presents more difficult servicing problems and increases the complexity of the design. A comprehensive investigation of the problems of each system indicated any of the three techniques could be developed. An injector adjacent to the propellant tank wall (surface or submersed) would lend itself to easiest development and was selected for evaluation in the research test program.

For efficient vehicle design precise propellant tank pressure control may be achieved by a modulating reagent flow system. However, in applications where reliability is a primary requirement an orifice system would generally be selected. If positive shutoff and/or restart is required with good pressure control, and on-off pulse- or modulating-type injector should be used. Only the pulse- or modulating-type injector may be considered for variable thrust applications. Regardless of the type of injector, it must be sized for the maximum reagent flow capacity to maintain an adequate propellant tank pressure. Maximum orifice size and design of the injector will be influenced by response requirements dictated by the complete system. From the research testing performed, proper control of the reaction process was influenced greatly by the ability to obtain a good solid stream of injected reagent, particularly in the surface injection system.

The detailed design of the injector requires reagent control at the injector nozzle to eliminate the possibility of an internal or delayed reaction. Specific characteristics desired would be a function of the technique used in reagent supply and depend on the quantity of reagent required. System response requirements will influence the method of actuation in a pulse-type system with solenoid motivation probably yielding the best results. A review of possible configurations indicated that an external gas pressurized reagent supply would be most desirable with control by a pressure switch that senses propellant tank internal pressure. Additional reagent supply systems included motor driven pumps, spring or gas loaded bellows, and tubropump bleed.

Safe operation of the common ullage configuration was found to be particularly difficult due to the presence of combustible gases in the oxidizer tank when N_2O_4 was used as the reagent in the fuel tank. Although the cross flow gas was found to be hypergolic with the oxidizer vapors, the injection below the oxidizer surface provided good pressure control. Primary difficulties inherent in this configuration are vibrations caused by this subsurface reaction, and preventive measures required to eliminate the possibility of the reaction progressing to the hydrogen/oxygen atmosphere in the tank ullage. Satisfactory process control was achieved with the small-scale system by using check valves with the hypergolic propellant combination. However, for larger systems a differential pressure switch controlled isolation valve is recommended. Detailed design requirements are presented in Chap. III.B.2.

3. Materials Study

A study of various materials pertinent to the MTI Pressurization System was made to establish the feasibility of the conceived systems. The area of investigation concerned not only the applicable propellants and possible reactants, but unique methods for pressurizing the reagents and withstanding the anticipated high temperature environment due to the reaction process.

Tank Insulation Materials - Reaction temperatures and heat transfer characteristics in the surface injection process at high pressures may create a problem in certain tank configurations. One solution to this problem is the use of an insulating liner within the tank. For optimum performance the liner should be light, temperature resistant, have a low heat transfer coefficient, and be compatible and nonabsorbent to the fuel or oxidizer. The latter requirement eliminates all brush, spray, or trowel-on insulations, unless protected by a suitable coating. Aluminum foil coating is suggested for this application.

Optimum design for such a system would be a sandwich of aluminum foil insulation and structural aluminum. As an alternate, the insulation could be brushed or bonded on with foil bonded over it. Lack of a suitable bonding agent presents some difficulty, although bond line attack by the fuel blend on fluorosilicone and butylphenolic adhesives is such that several months of exposure could be tolerated without excessive permeation or loss of adhesion.

The properties of three of the more promising insulation materials are shown in Table II-1. Many other materials are available in the same categories with roughly comparable properties. Note that Foam-Sil, a closed cell foamed silica, represents the only type of insulation that will not absorb fuel when uncoated. The physical characteristics of this material, i.e., brittle, possibility of dusting or flaking, and the necessity of bonding it in place, are major disadvantages.

Aluminum foil clad cork has been used extensively as an insulation, and is acceptable for use in splash exposure. No attack is expected during longer exposure, although lab data are not yet available to verify this. However, successful application here depends on no absorption of the fuel, and hence on the effectivity on the bond line at joints in the foil.

Table II-1. Propellant Tank Internal Insulation Materials

Materials	Thermal Conductivity (Btu/hr/sq ft/°F/ft)	Density (lb/cu ft)	Application
Chem-Seal 3810 (Silica filled silicone resin) Al foil clad	0.09	62.8	Brush-on, bond aluminum foil directly onto uncured surface.
Al foil clad cork	0.047	30.7	Bond-on in segments, bond aluminum foil over cork.
Foam-Sil (Closed cell silica foam)	0.04	13.6	Bond-on in segments, no cover required.

The most promising of the three types of insulation is the filled silicone. The representative material, Chem-Seal 3810, has a lower density than comparable materials due to the use of the silica microballoons as a filler. A further weight advantage accrues in that the material itself bonds to the aluminum, avoiding the use of a separate adhesive. When covered with aluminum foil, this material should exhibit very little fuel absorption through the foil joint bond lines.

Temperature Resistant Light Metals - An alternate solution to the problem of excessive tank temperature is the use of a tank material capable of withstanding the expected temperatures. The choice of construction materials is limited by compatibility as well as weight and structural requirements.

Properties of the most promising structural materials are shown in Table II-2. Of these, the titanium alloys offer the best strength/weight ratio in the applicable temperature range, thus negating the need for insulation.

Titanium also exhibits satisfactory compatibility characteristics with the fuel and oxidizer. Past reports concerning the vigorous reaction of nitrogen tetroxide with titanium are based on the reaction of titanium with tetroxide containing appreciable quantities of water. At the water content level of propellant grade tetroxide, less than 0.1%, the compatibility is very good.

Stainless steel alloys have a slight disadvantage in the strength/weight ratio, although they are completely acceptable in other respects.

Table II-2 Characteristics of Structural Materials
Used in Tank Construction

Material	Density (lb/in. ³)	Modulus (tension) (10 ⁶ psi)	Compatibility		Fabricability	
			UDMH/N ₂ H ₄	N ₂ O ₄	Form	Weld
301 Stainless	0.286	29.0	G	G	F	G
321 Stainless	0.290	29.0	G	G	F	G
316 Stainless	0.290	29.0	G	G	F	G
410 Stainless	0.280	29.0	G	NR	F	G
420 Stainless	0.280	30.0	G	G	F	G
17-7 PH Stainless	0.276	29.0	NR	NR	G	F
15-7 Mo (RH 950)	0.277	30.0	NR	G	G	F
Ti-6Al-4V	0.160	15.8	G	G	F	F
Ti-5Al-2.5Sn	0.161	16.5	G	G	G	G
Ti-13Al-11V-3Al	0.175	14.8	G	NR	E	E
Beryllium	0.063	37.0	G	G	P	VP
Tantalum	0.600	29.0	G	G	E	FG

Legend:

E	Excellent	P	Poor
G	Good	VP	Very Poor
F	Fair	NR	Not Recommended

The other materials discussed, beryllium and tantalum, suffer from a tremendous cost disadvantage. In addition, beryllium is difficult to form and weld. These two materials are still in a developmental stage.

One further approach was investigated. A composite tank wall constructed of a thin metal liner with a plastic outer wrap reinforced with glass fiber offers high strength, low weight, and good temperature resistance. The glass-reinforced plastic component exhibits a tensile modulus of around 150,000 psi at a density of 0.06 lb/in.³. An aluminum liner might possibly be used for this application. Although aluminum is not sufficiently heat resistant to withstand excessive operating temperatures, loss of the liner through local melting during operation would not result in leakage since the plastic vessel itself resists propellants for a short time. Stainless steel or titanium liners would, of course, avoid this possibility, although at a slight weight penalty.

Even with a steel or titanium liner a composite density of about 0.1 lb/in.³ can be expected. However, a low modulus in flexure (7×10^6 psi) results in an inherent lack of stiffness, requiring additional material to provide resistance to compressive loads. Composite tanks, therefore, are less advantageous in the lower pressure ranges. At 100 to 200 psig this approach should have considerable advantage.

Applicable Propellants - The literature survey revealed that the concept of propellant tank pressurization by an in-tank reaction is also applicable to other than the nitrogen tetroxide/UDMH-hydrazine combination specifically tested under this contract. For example, the combustion of RP-1 in the lox tank with an igniter has been considered as a method of pressurization the lox-RP-1 system. The disadvantage of nonhypergolic propellants is that they require an ignition system. They can however, be reacted by adding small quantities of pyrophorics, such as pentaborane, to the fuel or oxygen, or adding difluoride to the oxidizer. Hypergolic systems, such as the nitrogen tetroxide and hydrazine-based fuel, are ideally suited to MTI pressurization because they are storable, smooth in ignition and burning, and stable in the temperature range imposed by the reaction. Table II-3 lists some of the more common storable propellants to which the MTI pressurization system is applicable.

Table II-3 Possible Storable Propellant MTI Systems

Fuel	Oxidizer	Remarks
Hydrazine based fuels	N ₂ O ₄	Hypergolic
(including mixed amines)	ClF ₃	Hypergolic
(including mixed amines)	H ₂ O ₂	Hypergolic
(including mixed amines)	RFNA	Hypergolic
(including mixed amines)	BrF ₅	Hypergolic
(including mixed amines)	B ₅ H ₉	Hypergolic
(including mixed amines)	Cl O ₃ F	Hypergolic (semi-storable)
Pentaborane	H ₂ O ₂	Hypergolic
Hydrocarbon Fuels	N ₂ O ₄	Ignitor or pyrophoric additive required
Hydrocarbon Fuels	H ₂ O ₂	Ignitor or pyrophoric additive required
Hydrocarbon Fuels	ClF ₃	Hypergolic

Additional Reagents - An alternative to the injection of one propellant into the other for pressurization is the use of a reactant other than a hypergolic propellant. Advantages that may accrue from this approach are an increase in the quantity of gas produced per pound of reactant, the possibility of selecting reaction products (by choice of reactants) with more desirable properties, the possibility of operating at lower temperature and an increase in safety.

Examples of potential main tank reactant pressurization systems are shown in Table II-4. Three of the reactants shown are nonhypergolic, acetaldehyde, ammonium carbonate, and ammonium azide solution. Reaction rates of these three, however, are sufficient to accomplish the desired pressurization. Should a more rapid response, or high temperature, be desirable in these cases, the addition of small quantities of a hydrazine-based fuel to these reactants would result in a hypergolic reaction. In addition to the listed common reactants the new high-energy propellants triethylamine, airborne, and hybaline are also suitable for MTI pressurization process.

Table II-4 Main Tank Reaction Reagents

Propellant	Reagent	Density (lb/ft ³)	Products	Gas Generation		Reaction Temperature (°F)	Gas Average Molecular Weight
				lb gas/ lb reagent	cu ft gas/ lb reagent		
N ₂ O ₄	Acetaldehyde	85.5	CO ₂ /NO/H ₂ O	6.9	8.3	250 to 300	30
N ₂ O ₄	Dimethylamine	42.3	CO ₂ /N ₂ /NO ₂ / H ₂ O	6.4	6.75	300 to 500	34
N ₂ O ₄	Ammonium carbonate	99.6	CO ₂ /N ₂ /H ₂ O/NO	1.9	2.74	200 to 250	25
N ₂ O ₄	Ammonium azide in water 20% solution	79.1	N ₂ /H ₂ O/H ₂	0.32	1.14	250 to 300	21
UDMH/N ₂ H ₄	Sodium Peroxide	97.0	H ₂ O/H ₂ /NH ₃ /CO ₂	0.8	1.07	50 to 300	27
UDMH/N ₂ H ₄	Hydrogen 30%	72.0	CO ₂ /H ₂ O/N ₂	0.75	1.12	150 to 250	24
UDMH/N ₂ H ₄	Pentaborane	39.8	BN (solid) + H ₂	0.39	7.0	2100	2
UDMH/N ₂ H ₄	Nitrogen tetroxide	89.34	2CO ₂ /CH ₄ /3N ₂ / H ₂ /2NH ₂	2.0	3.43	1300 to 2000	21

The injection of acetaldehyde or dimethylamine into the oxidizer tank offers the best in theoretical reaction performance. The pentaborane fuel system, with hydrogen produced as a pressurizing gas, has the unique advantage of extremely low residual weight at mission termination. The presence of solid BN in the fuel is, at present, an unknown quantity. Other advantages of this system make it worthy of investigation.

Liquid Pressurants - Aside from stored gas pressurization systems, the use of liquid pressurants can be considered for pressurization technique has the advantage of high-density storage and self pressurization. Since the pressure achieved is a function of the liquid temperature, the selection of such an additive would depend on the pressure required and expected operating temperatures. Several candidate materials are shown in Table II-5. This list by no means exhausts the potential of the liquid pressurant additive system.

Table II-5 Liquid Pressurants

Material	Vapor Pressure at 70°F (psig)	Liquid Density (lb/cu ft)	Gas Molecular Weight	Compatibility
Cyanogen	73.5	55.3	52	Useful in both oxidizer and fuel; has fuel properties
Chlorine Trifluoride	21	115	92.5	Oxidizer only
Dimethylene	72	51.4	48	Fuel only
2 Methylpropane	61	38.1	58	Fuel only
Methylamine	53	48.6	31	Fuel only
Ammonia	132	51.6	17	Fuel only
Sulfur Dioxide	56	90.4	64	Oxidizer only
Chlorine	103	200.3	70.9	Oxidizer only

A significant advantage of the additive system over conventional stored gas systems is the solubility of the additive in the propellant. The desired pressure level can be maintained throughout the expulsion cycle without over-pressure at the start. An excellent example of this is the ammonia-in-hydrazine system. Similar systems, such as chlorine trifluoride, are proposed for the oxidizer, although the solubility and vapor pressure parameters have not yet been thoroughly investigated.

4. Laboratory Experimentation

Several small-scale experiments were performed to obtain a better understanding of the anticipated MTI reactions. This information was required to establish basic research fixture design and identify possible operating difficulties. Two basic areas were investigated; the hypergolic reaction process when liquids are mixed, and the interaction of propellant vapors with combustion products. Although most of the information acquired was of a qualitative nature, some of the tests where performance was measured have been included.

The availability of a gas generator test fixture at the Cold Flow Laboratory permitted an early investigation of possible common ullage manifold problems. A photograph of the test setup is shown in Fig. II-10. Test data are plotted in Fig. II-11 and II-12. The fuel-rich combustion products from the gas generator were passed through a cooler and gunk trap to simulate the anticipated conditions of the gas entering a propellant tank. The gases were then injected into a container filled with nitrogen tetroxide which was located inside of the horizontal barrel in the foreground of Fig. II-10. Two 30-sec tests were performed with surface and submersed impingement. In both cases a considerable amount of reddish-brown smoke was generated, indicating that a fair amount of reaction occurred. A white precipitate was noticed in the first test. There was no evidence of a high temperature reaction during either test.

Since a substantial portion of the pressurizing gas formed in the fuel tank was expected to contain fuel vapors, several additional experiments were performed with laboratory apparatus. The reaction of the propellant vapors was first studied by joining two glass flasks with a tube to observe common ullage reactions without isolation of the two hypergolic propellants. As the vapors were allowed to mix a reaction did occur and a substantial quantity of a white gas formed. Although the reaction did not destroy the test system, further definition of the magnitude was not warranted due to the uncertainty involved in a practical application. Therefore, the requirement for an isolation valve in the system was established.

RTD-TDR-63-1123

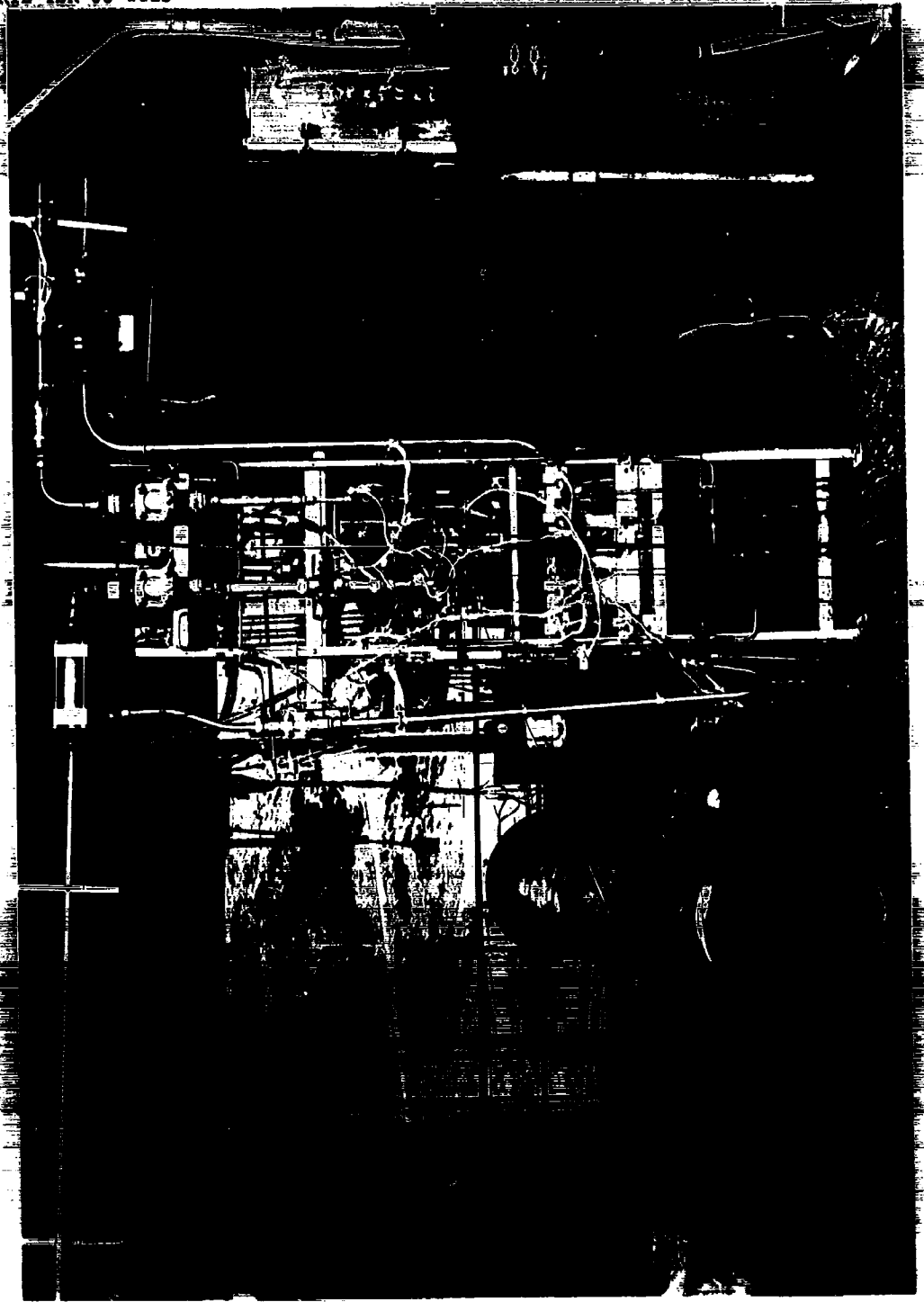


Fig II-10 Common Ullage Feasibility Test Fixture

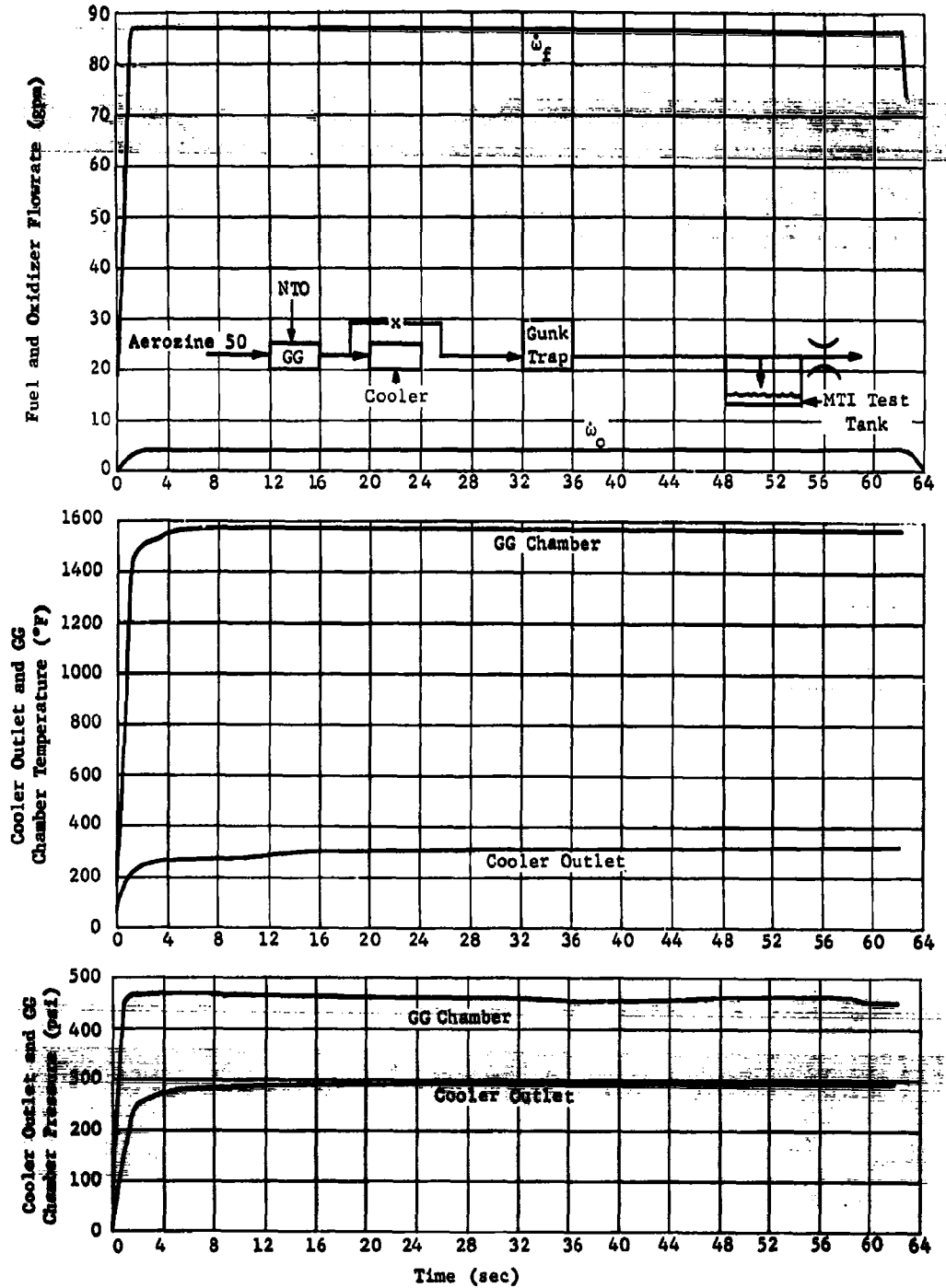


Fig. II-11 MTI Common Ullage Feasibility "Open Container" Test, Surface Impingement

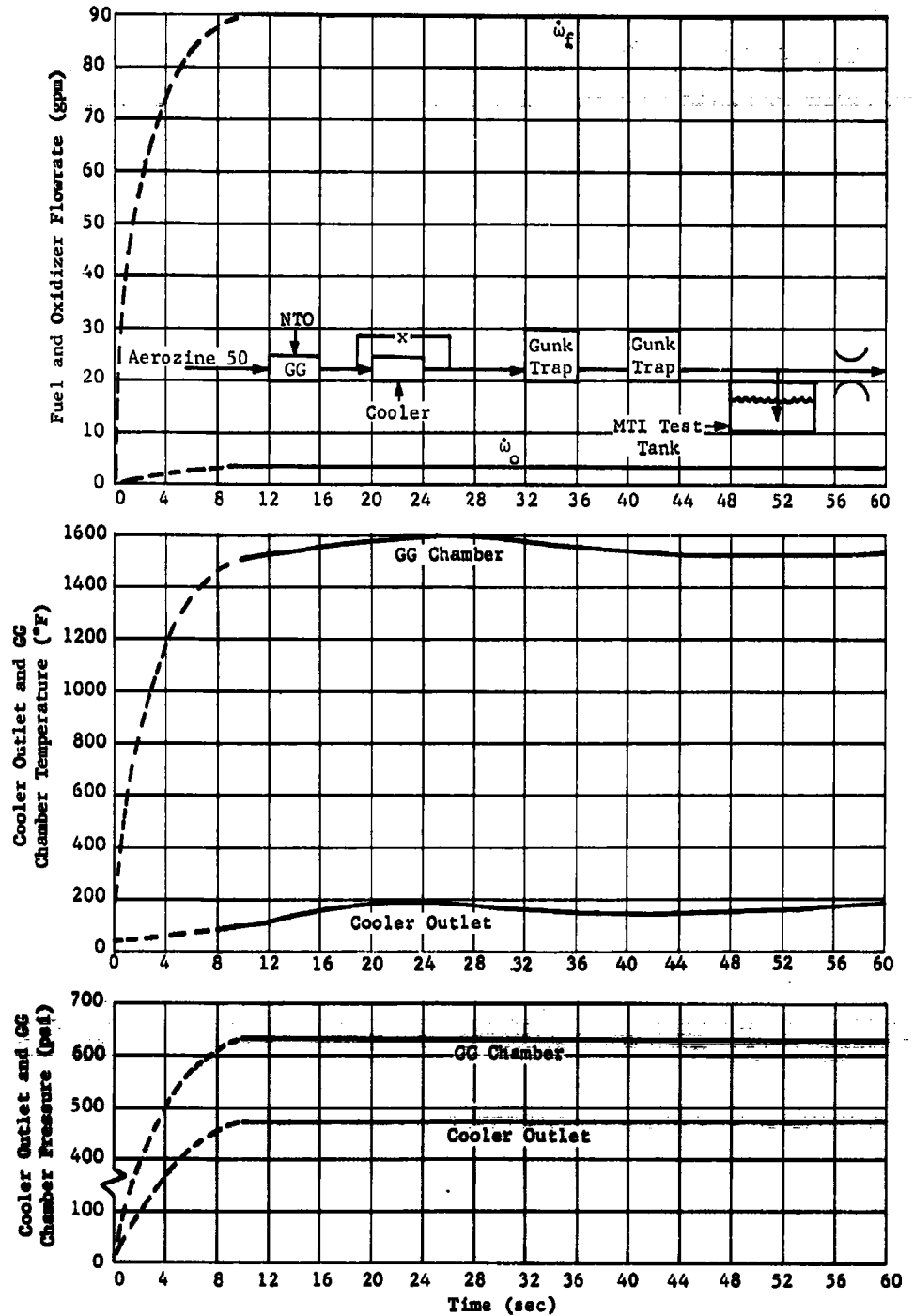
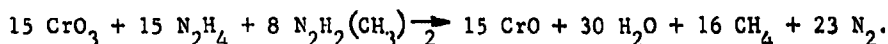


Fig. II-12 MII Common Ullage Feasibility "Open Container" Test, Submerged Impingement

Additional experiments were performed to determine if the propellant vapors could be conditioned to eliminate the reactive constituents. This testing was performed by heating a flask filled with the 50/50 blend of UDMH and hydrazine and discharging the vapors through a filter into a beaker containing nitrogen tetroxide. The various test filters consisted of the following materials:

- 1) $\text{CrO}_3 + \text{CaCO}_3 + \text{C}$ activated;
- 2) $\text{CuO} + \text{glass wool} + \text{zeolite 4-A}$;
- 3) $\text{CrO}_3 + \text{CaCO}_3 + \text{zeolite 4-A}$;
- 4) $\text{CrO}_3 + \text{CaCO}_3 + \text{zeolite} + \text{KMNO}_4$.

The calcium carbonate (CaCO_3) was primarily used to absorb any condensed fuel and also provide a gas flow path through the powdered chromium trioxide (CrO_3). The activated carbon and zeolite filters were used to absorb the reactive vapors. Zeolite 4-A is a molecular sieve commonly used for ammonia absorption while CuO acts as a catalyst to decompose hydrocarbons to nonreactive elements. Chromium trioxide was found to be readily reactive with the propellant vapors, but a substantial quantity would be required to obtain satisfactory neutralization of the pressurizing gas based on the following anticipated reaction:



When potassium permanganate was added to the filter system the reaction was sufficiently violent to produce a flame that would be undesirable due to the possibility of detonating hydrogen in the oxidizer-rich atmosphere. Filters (1) and a combination of (2) and (3) were subsequently tested in the research fixture with only moderate success as a result of this experimentation.

Several open beaker laboratory experiments were also performed to study the reaction of the hypergolic liquids. This experiment was primarily qualitative in nature. Some of the test data are shown in Fig. II-13 for the reaction of nitrogen tetroxide injected into a beaker of fuel. Stable combustion was obtained with fairly low liquid bulk temperatures. A slight increase in fuel temperature occurred when the injection velocity or mass flow was increased. The nature of the reaction process was determined to be a function of the injection technique for the surface injection process. From the investigation performed a need for adequate reagent filtration and inert blanket pressurization became apparent. Additional liquid

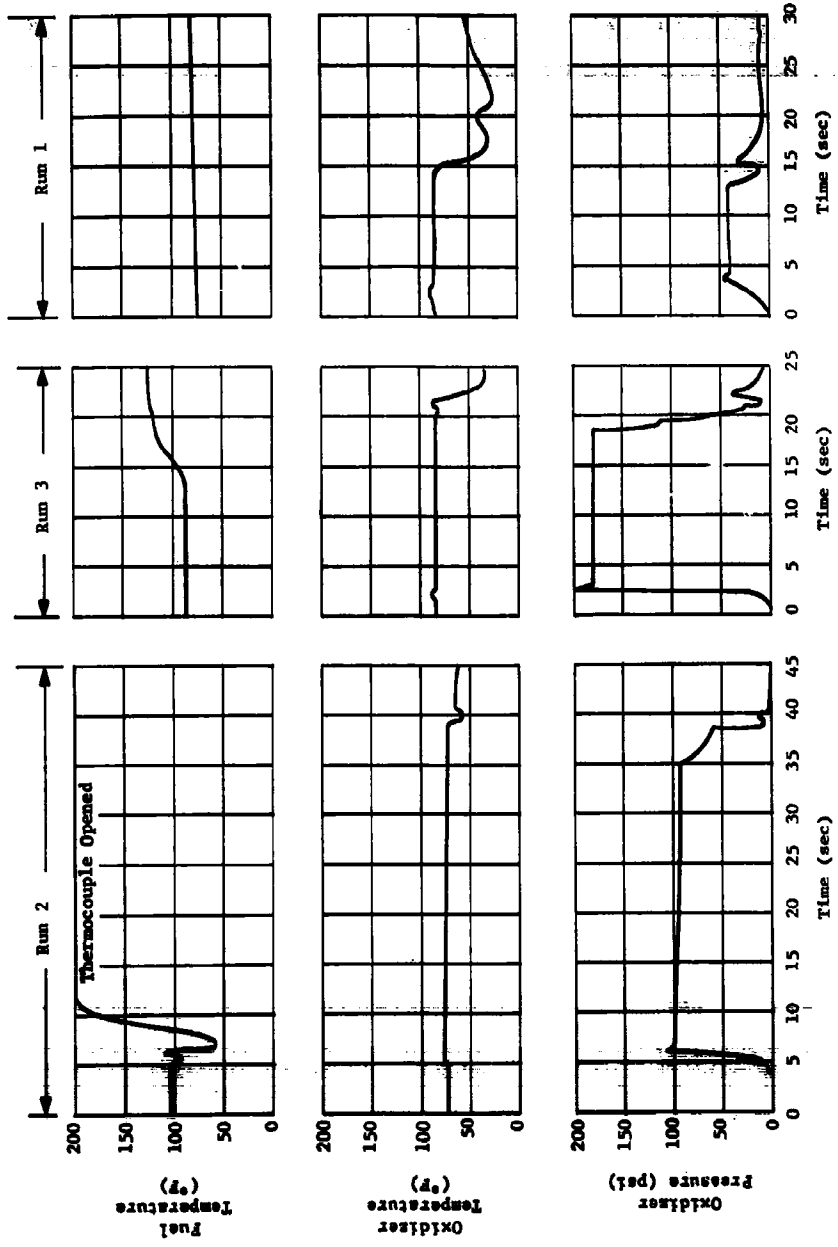


Fig. II-13 MTI "Open Container" NTO Surface Injection Tests

reaction tests were performed in a closed system to determine reaction rates. A small-scale $\frac{1}{2}$ cu ft spherical tank was used for this purpose with various quantities of oxidizer injected into a fixed volume of fuel. The results shown in Fig. II-14 and II-15 provided basic thermal data and requirements for overpressure protection.

5. Theoretical Studies

An early investigation of previous methods of predicting pressurization system performance indicated a thorough description of the MTI process could not be obtained with existing computer programs. Primary factors involved were the lack of a combustion zone in the primary tank (the reaction process was assumed external to the tank), and the gas entering the tank was at the combustion temperature for any given pressure and reaction mixture ratio. The entering gas characteristics were determined by a separate thermochemical computer program based on a shifting equilibrium calculation for complete combustion. Since a better definition of the reaction process and internal heat transfer were required, in addition to common ullage capability, a new computer program was desired. The initial attempt at a process description was programed on the IBM 1620 computer, based on the results of early investigations of the pressurization phenomena. To identify the most significant factors involved in the process an investigation of reaction kinetics, combustion products, physical properties, and secondary reactions was made.

A survey of existing literature concerning the physical aspects of the hypergolic reaction inherent in the MTI process indicated only a very small amount of information was available. To identify the process characteristics in the analytical model the knowledge gained from the laboratory experimentation was used. One of the basic difficulties in defining the reaction process is in determining or establishing the reaction mixture ratio. Early experiments showed that the reaction depended on the mixing technique, thus early theoretical studies were performed over a range of reaction mixture ratios. Later test data identified the apparent reaction mixture ratio for several injection techniques. The capability for altering the reaction, and hence the combustion product composition, was a major consideration of the early research testing to obtain a lightweight pressurizing gas compatible with the hypergolic propellants. In addition to identifying chemical composition and quantity of the resultant biproducts, the high temperature zone was undefined. Approximations were, consequently, based on the results of the laboratory experiments performed and later described by derived empirical relationships.

RTD-TDR-63-1123

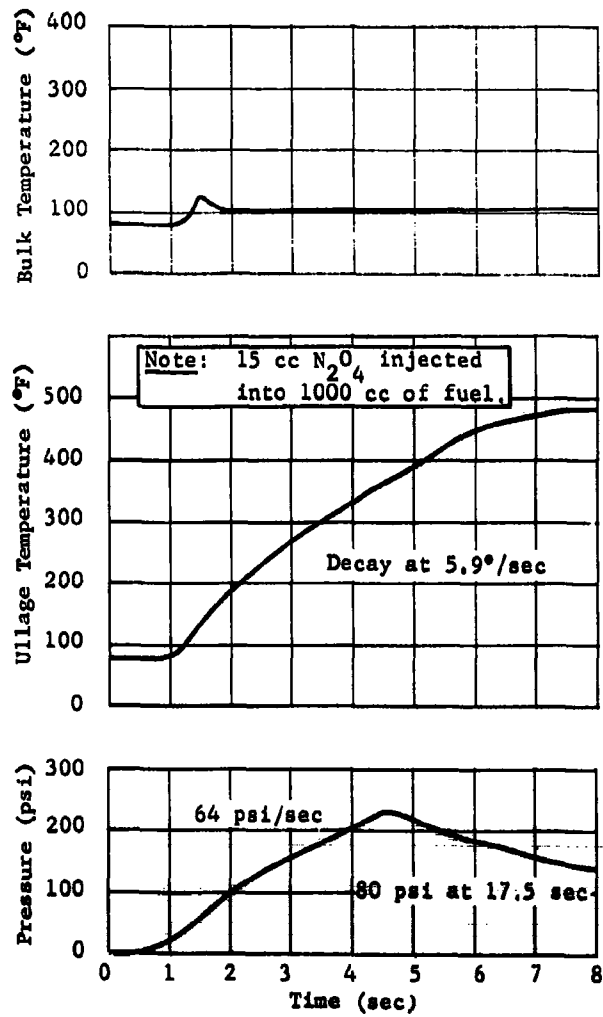


Fig. II-14 MTI "Bomb" Test, Run 1

RTD-TDR-63-1123

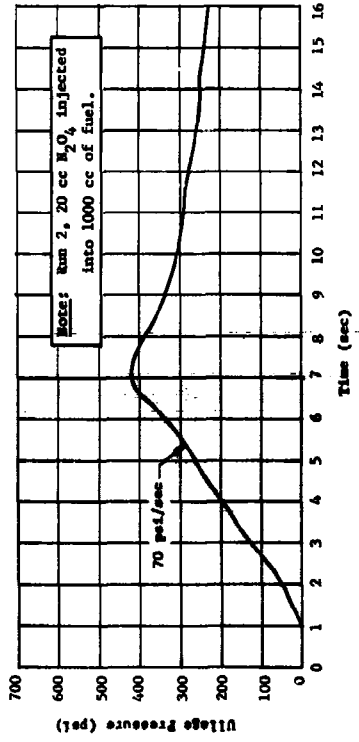
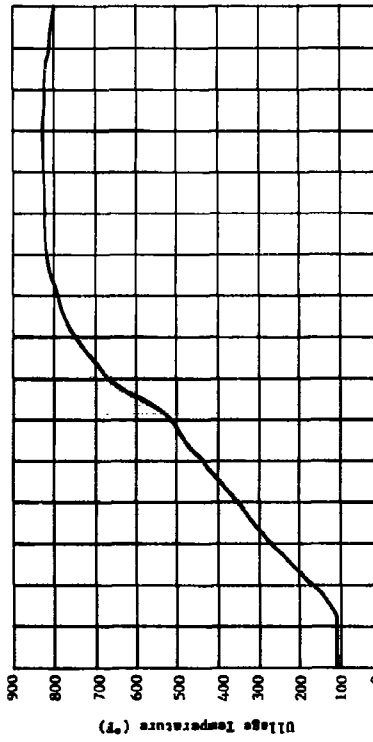
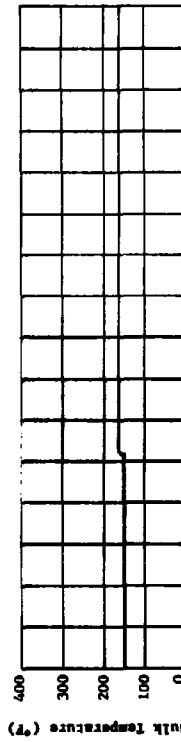
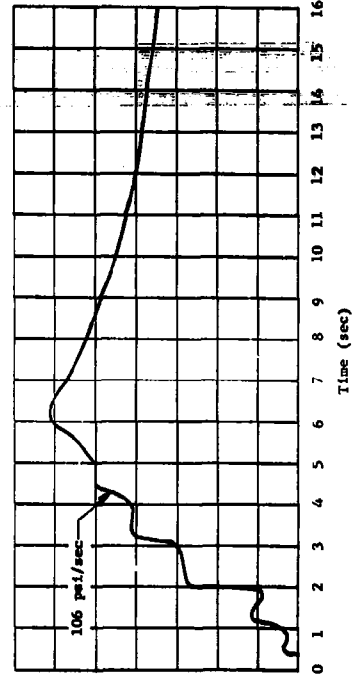
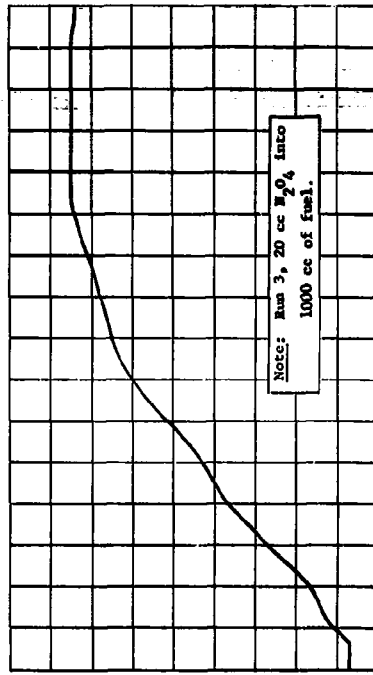
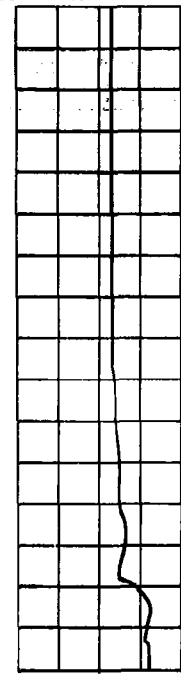


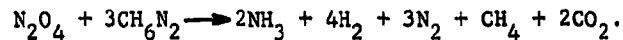
Fig. 11-15 HYI "Bomb" Tests, Run 2 and 3

Theoretical Combustion Products - The calculation of system operating characteristics first required a definition of the pressurizing gas. In lieu of any actual gas analysis data the theoretical composition and thermodynamic properties of the combustion products resulting from the reaction of nitrogen tetroxide and a 50-50 blend of UDMH and hydrogen were computed by an existing rocket engine performance program. Due to the unknown reaction mixture ratio, data were accumulated over the entire anticipated range. From this information the physical properties of the gas mixture were determined for the expected range in operating temperature based on no additional reactions occurring. These early data plus literature references have shown that combustion product composition cannot be predicted accurately for extreme reaction mixture ratios or for cases of incomplete combustion. The results, however, are included to show expected trends and provide a comparison with the actual test data compiled.

The molecular weight of the combustion products is shown as a function of mixture ratio and pressure in Fig. II-16. At 35 psia a reaction mixture ratio of approximately 0.7 is required for a gas molecular weight of 15, with a minimum of 11.4 occurring at a mixture ratio of 0.1. The expected reaction temperatures are plotted in Fig. II-17. Due to the increase in temperature associated with oxidizer-rich reactions, the resultant gas density becomes a minimum at a mixture ratio of approximately 1.2 even though a higher molecular weight gas is generated. This trend is shown in Fig. II-18. The specific heat and specific heat ratio are shown in Fig. II-19 and II-20, respectively. Based on a reaction mixture of 0.1 the physical properties of the gas were computed for a temperature range of 100 to 2,000°F and are shown in Fig. II-21. A comparison can be made with the physical properties of a liquid propellant gas generator included in Fig. II-22. The molecular weight of the combustion products of a gas generator operating at an apparent mixture ratio of 0.1 has been determined by test to be approximately 16.0. From the theoretical data a molecular weight of approximately 14 was expected. The possibility of incomplete combustion or an actual higher reaction mixture ratio may explain this slight discrepancy. The physical property data were based on the theoretical gas composition data shown in the following tabulation.

Constituent	Mole Fraction	
	Mixture Ratio = 0.1	Mixture Ratio = 2.0
N ₂	0.2595	0.3286
H ₂	0.5577	0.0753
H ₂ O	0.01	0.3608
CH ₄	0.0508	-
CO	0.0339	-
CO ₂	-	0.0472
OH	-	0.0419

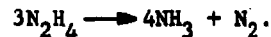
The values in the tabulation are based on complete combustion. Actual gas analyses conducted during gas generator testing have indicated the actual process is represented more closely by the following equation:



The presence of ammonia in the above reaction is a significant factor, since an additional reaction with nitrogen tetroxide is possible.



This reaction was studied and the results are shown in Fig. II-23. The result of this secondary reaction would be a small increase in the gas temperature in the oxidizer tank and reduction in the amount of combustion products required. Some additional ammonia will also be formed by the local decomposition of hydrazine as follows:



Although the decomposition of hydrazine and dimazine (UDMH) was established, little information is available on the 50/50 mix. The presence of UDMH, however, tends to stabilize the hydrazine with a resultant decrease in decomposition and increase in autoignition temperature. The limiting temperature of the ullage gas is approximately 1400°F with less than a 1% decomposition of hydrazine expected. A liquid temperature of 1400°F is also the autoignition

temperature of the fuel. The additional propellant and vapor properties required for the thermodynamic analysis of the MTI system were obtained from documents listed in the bibliography.

Predicted Performance - MTI pressurization system performance was predicted by a special program formulated for the IBM 1620 computer. Because of the limited storage space available with this machine, only a single tank mathematical model could be developed. This program provided for gas generation by a combustion process occurring in the tank liquid when a hypergolic reagent is injected on pressure demand. A detailed description of the analytical technique is contained in Appendix C. Because of the initial lack of information on the primary reaction the predicted performance was not representative of the actual process since a significantly greater amount of reagent was used. The increase in reagent consumption resulted from a decrease in gaseous combustion products due to the quantity of condensibles formed. More precise theoretical performance was obtained with a larger IBM 7094 MTI mathematical model and is discussed in Chap. III.A.3. The data generated with the abbreviated version is presented to show the original basis for system design and expected influence of heat capacity and volume of various systems.

A parametric study of theoretical MTI pressurization system performance was made for the range of press conditions anticipated. Since the small computer program could not analyze the common ullage system configuration, primary tank conditions were established by incorporating a conservative 60% gas bleed estimate to simulate the additional gas required for the pressurization of the second tank. A prediction of reagent used, tank wall temperature, and ullage gas temperatures for a single tank Phase I research fixture test are shown in Fig. II-24. These results indicate relatively moderate temperatures were expected over the planned range in test pressures. This tank has the 30% ullage volume initially pressurized with nitrogen and no gas bleed. Figure II-25 compares pressurized with actual data and the 5% initial ullage pressurized with helium. Figure II-26 shows the expected temperature increase due to a 60% gas bleed with a comparison of a fuel tank reaction and oxidizer tank reaction for 36 psia at the assumed reaction mixture ratios. The total weight of pressurizing gas obtained shows that approximately a 50% weight saving can be obtained by a fuel tank MTI pressurization system if the amount of condensibles formed is neglected. A prediction of the expected temperature and pressure during a 150-sec propellant expulsion is shown in Fig. II-27 for a reaction mixture ratio of 0.1 at 36 psia. The actual gas temperature and reagent consumption were significantly higher due to the amount of condensed combustion products formed and higher reaction mixture ratio experienced.

The Phase III 279 cu ft tankage was also thermodynamically analyzed. The results are shown in Fig. II-28 and II-29, as determined by the abbreviated mathematical model. The 30% ullage volume in the fuel tank was initially pressurized with helium. Calculations were also performed with nitrogen initial pressurization. However, the ullage gas temperature did not reduce significantly as a result of the higher heat capacity of the gas. The lower heat capacity of the full-scale system is seen by comparing the tank wall temperatures in Fig. II-26 and II-28. The high fuel tank wall temperatures predicted with a 60% gas bleed gave rise to a study of possible temperature control techniques. Further analysis of actual operating characteristics of the system operating at low pressures indicated adequate capability of the thin wall full-scale aluminum tankage. Figure II-29 shows the moderate temperatures and reagent consumption originally predicted during a 150-sec run at 36 psia with a reaction mixture ratio of 0.1 for a single tank and no gas bleed. No comparison with actual data obtained was attempted since a more detailed examination was accomplished later with the IBM 7094 computer program.

Since the early studies performed with the single tank computer program gave no indication of secondary tank requirements, the effect on the primary tank with an increase in gas flow could only be estimated. As further definition of the primary reaction was established and confidence gained in the theoretical technique, the effort was directed at expanding the program to analyze the common ullage two-tank system. Since each tank could not be thoroughly analyzed because of the limited capacity of the IBM 1620 computer an abbreviated version was attempted. Effort on a larger capacity IBM 7094 program was not considered feasible at this time because of unknown secondary reaction characteristics. In the abbreviated two-tank program, the primary tank process description is reduced to accommodate a more thorough examination of the thermodynamic characteristics of the secondary tank. To reduce the size of the program and minimize the number of single tank computer runs required, the computation of secondary tank conditions was based on anticipated conditions in the primary tank. After several revisions to the program, the data generated by this simplified technique were still unsatisfactory and further effort was cancelled. From the experience gained from the formulation of the first two small computer programs a larger version was prepared on the IBM 7094 computer. Using the additional capacity available with this machine, most of the basic equations from the early programs were used with additional detail added.

RTD-TDR-63-1123

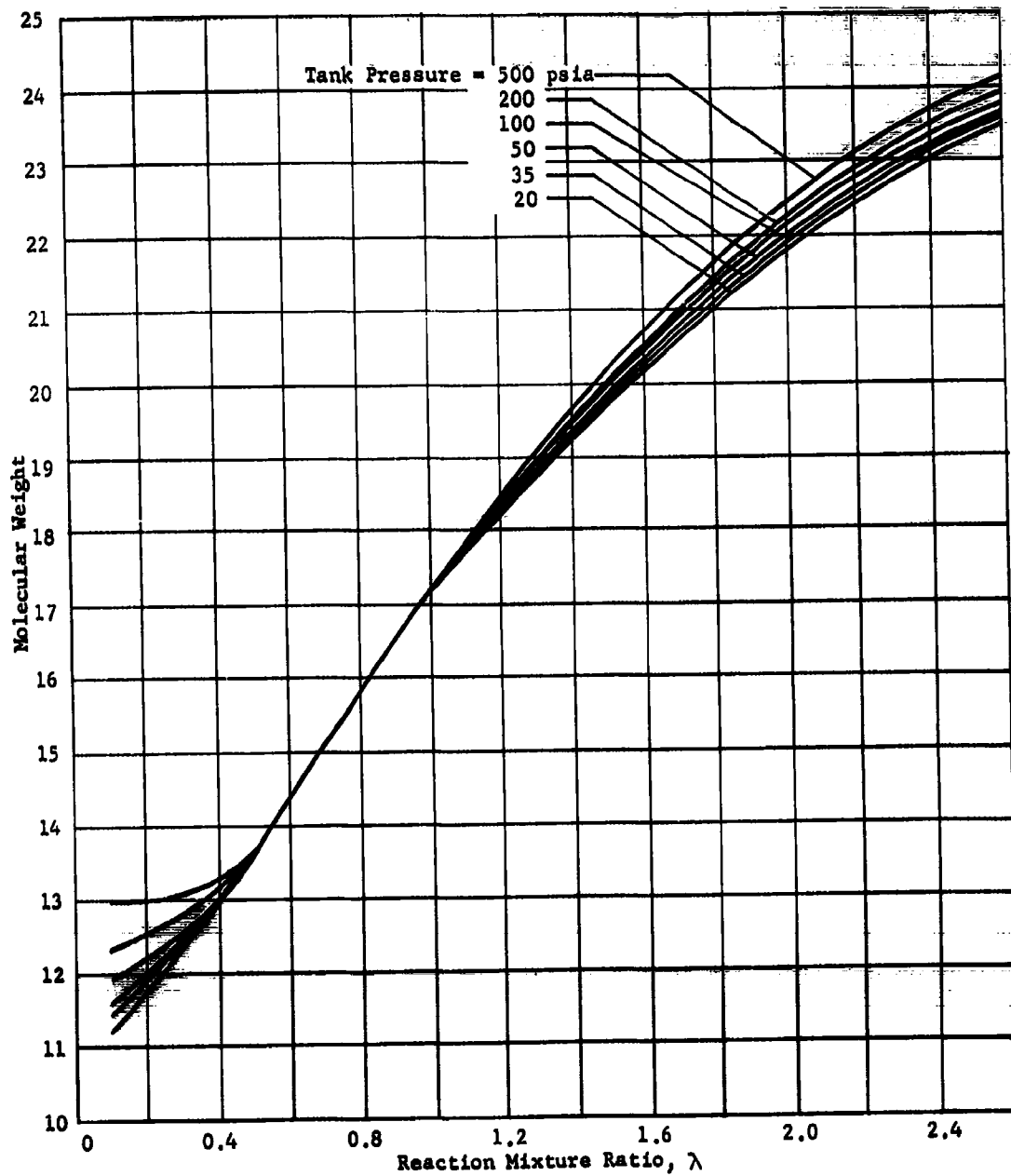


Fig. II-16 Molecular Weight of Combustion Products (N_2O_4 /Aerozine 50)

RTD-TDR-63-1123

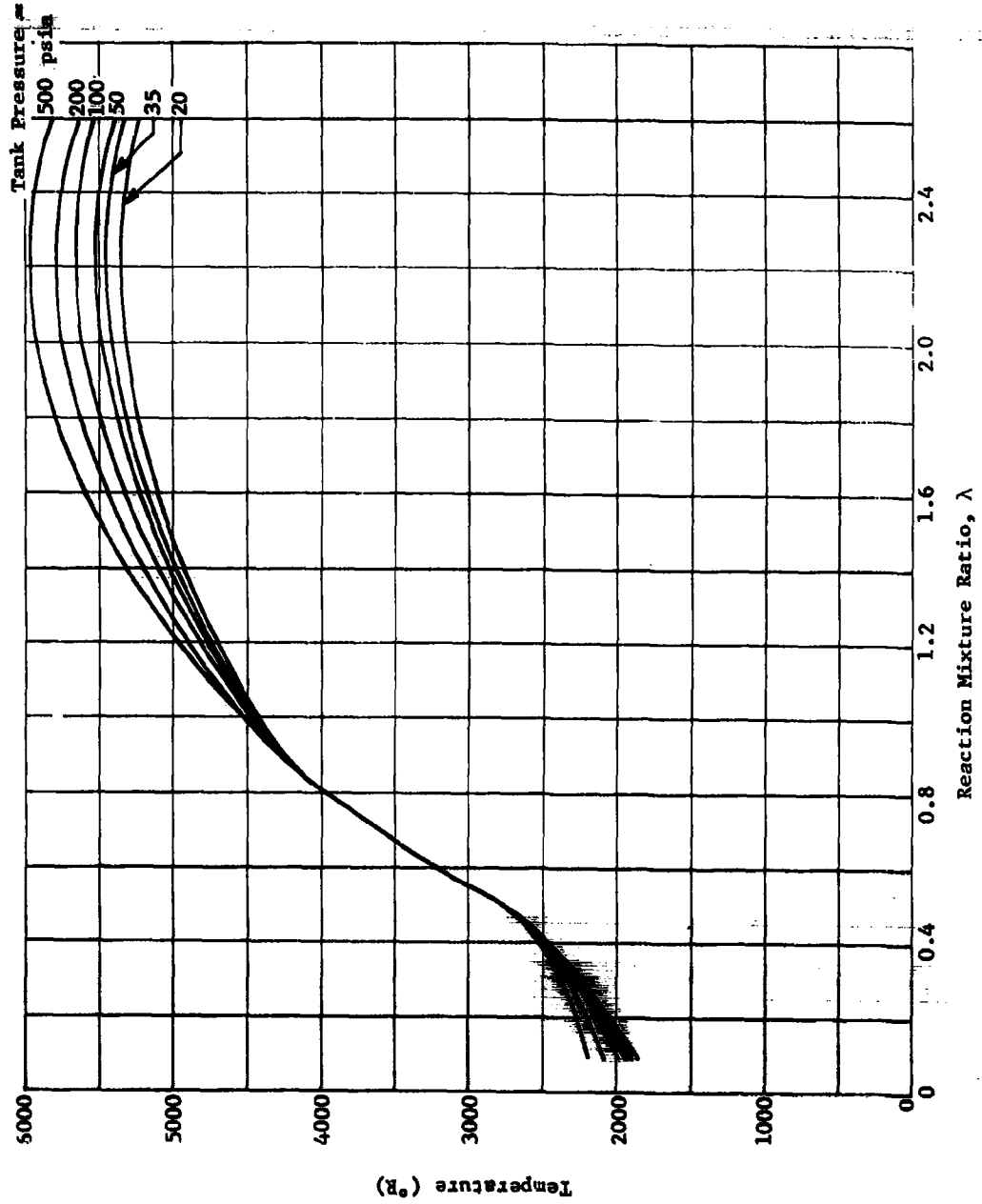


Fig. II-17 Gas Temperature of Combustion Products (N_2O_4 /Aerozine 50)

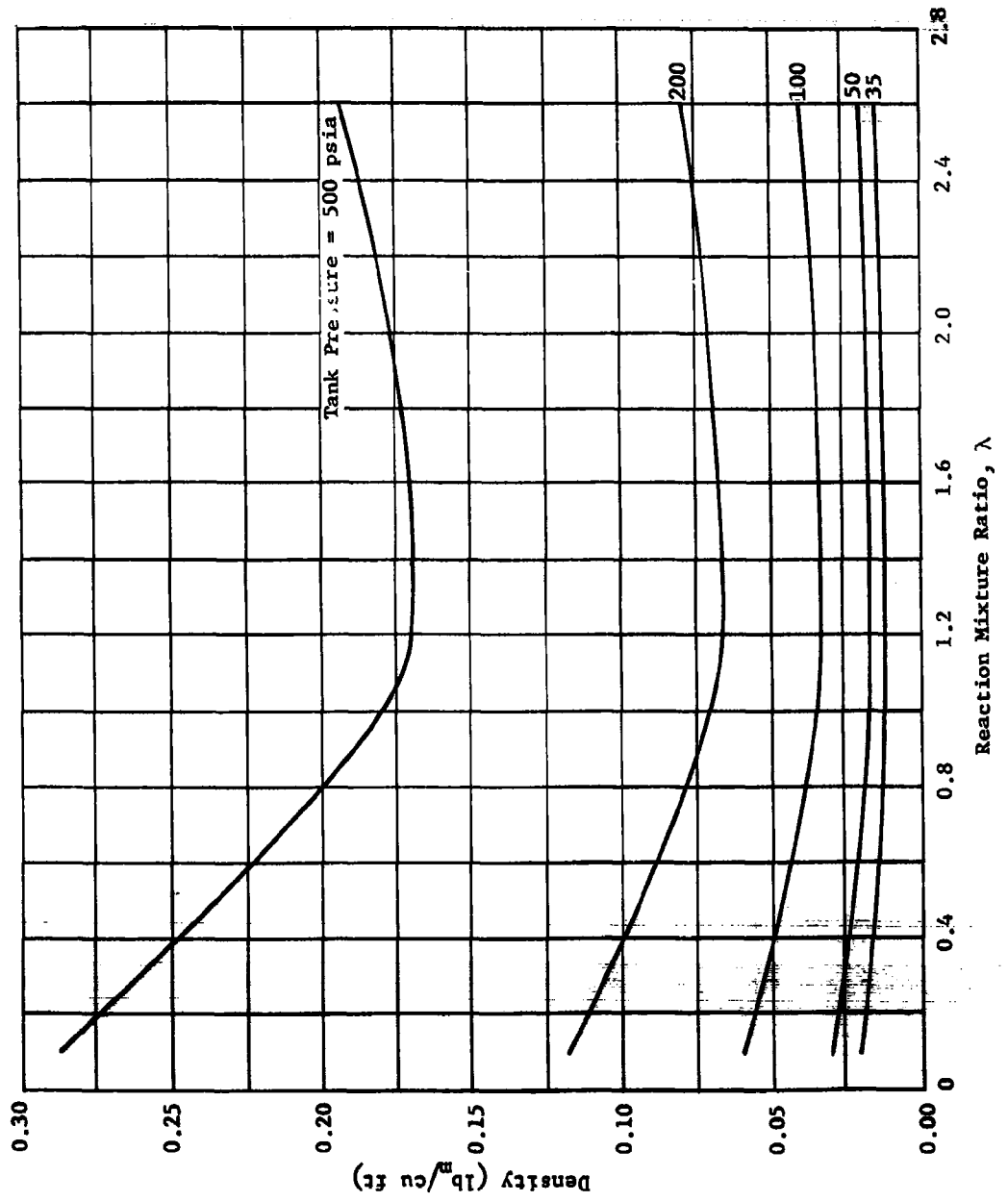


Fig. II-18 Combustion Gas Density vs Reaction Mixture Ratio (N_2O_4 /Aerozine 50)

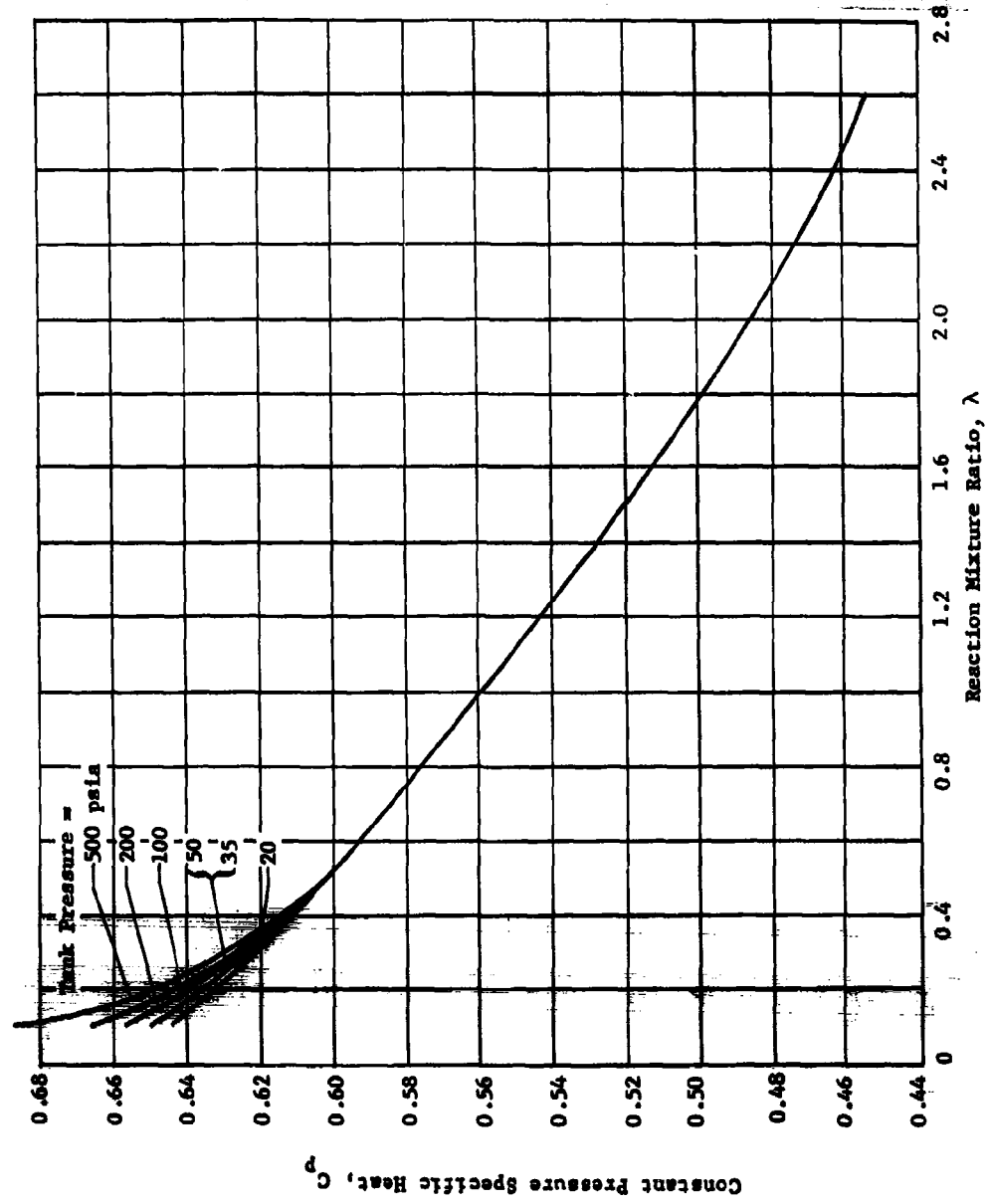


Fig. II-19 Constant Pressure Specific Heat Combustion Products (N_2O_4/NH_2UDMH)

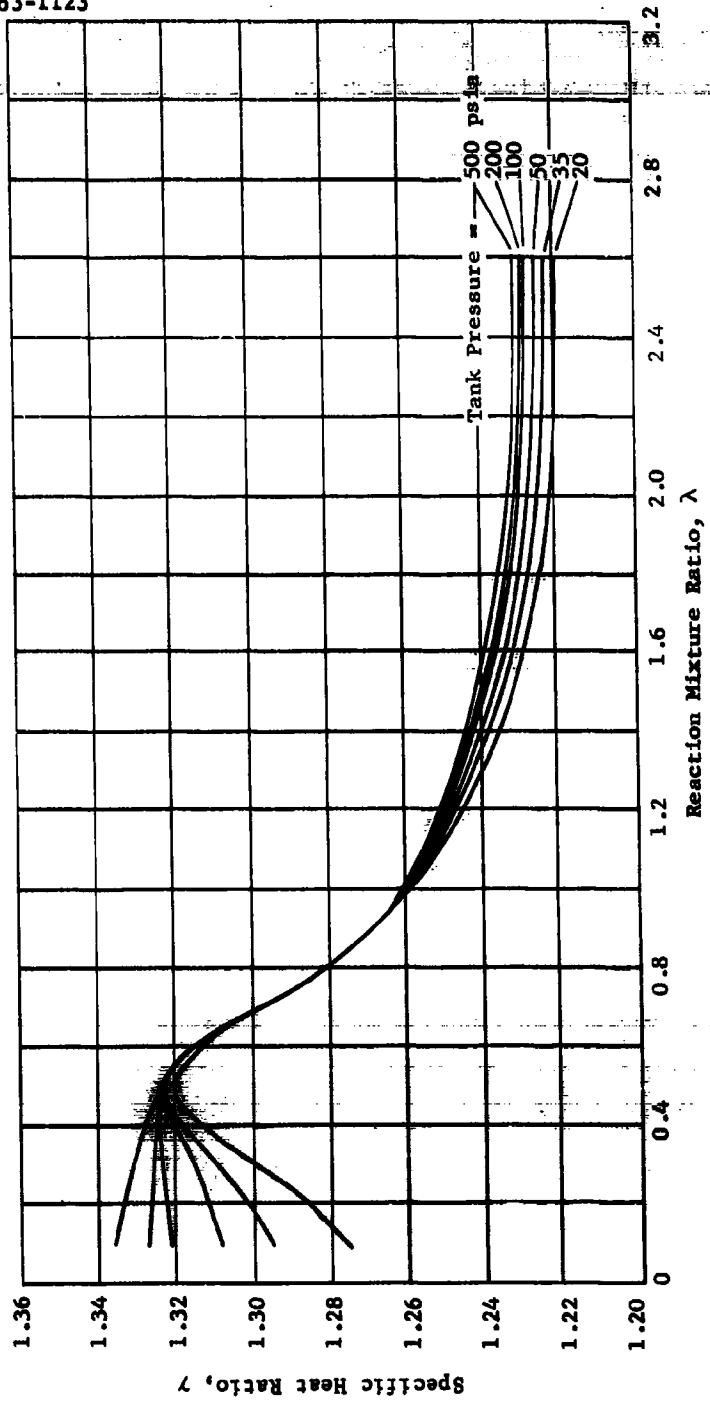


Fig. II-20 Specific Heat Ratio Combustion Products (N_2O/N_2H_2UDMH)

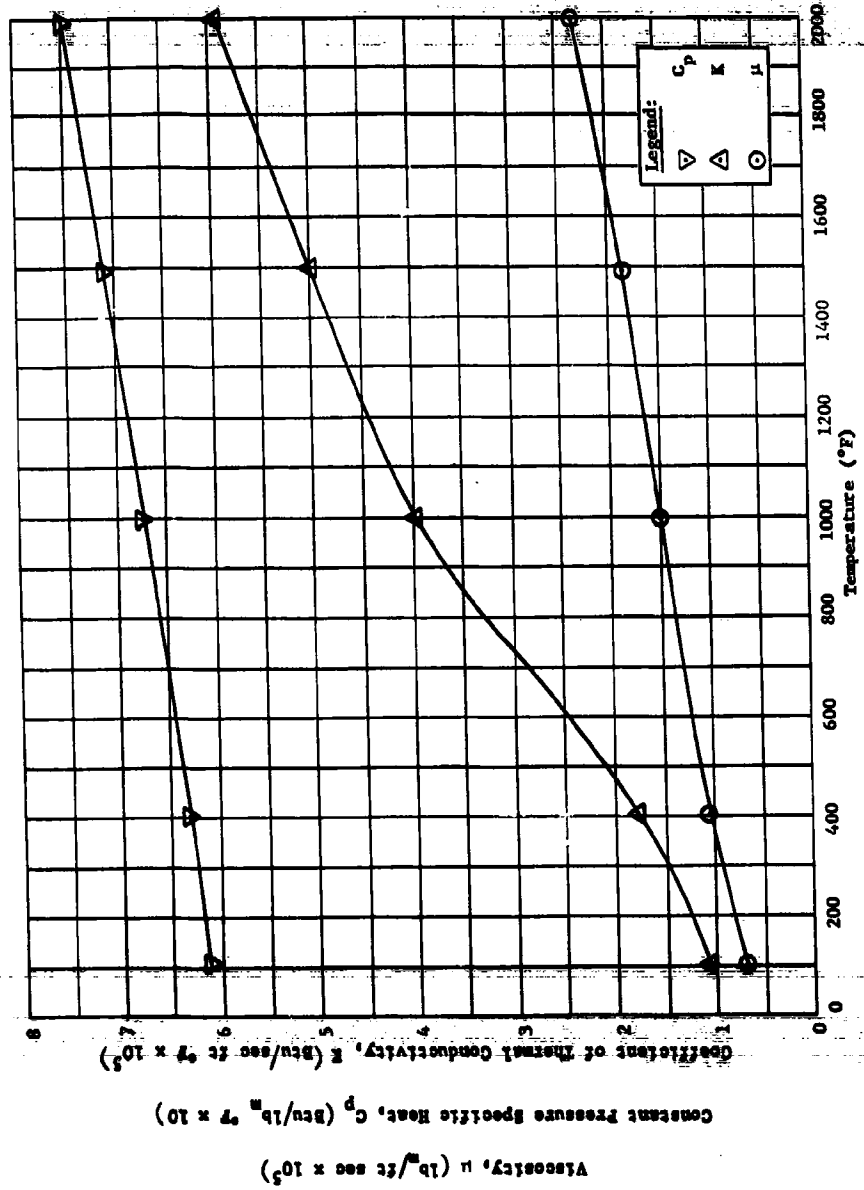


Fig. II-21 Theoretical Combustion Products Thermodynamic Properties for a Mixture Ratio of 0.1 and Pressure of 35 psia

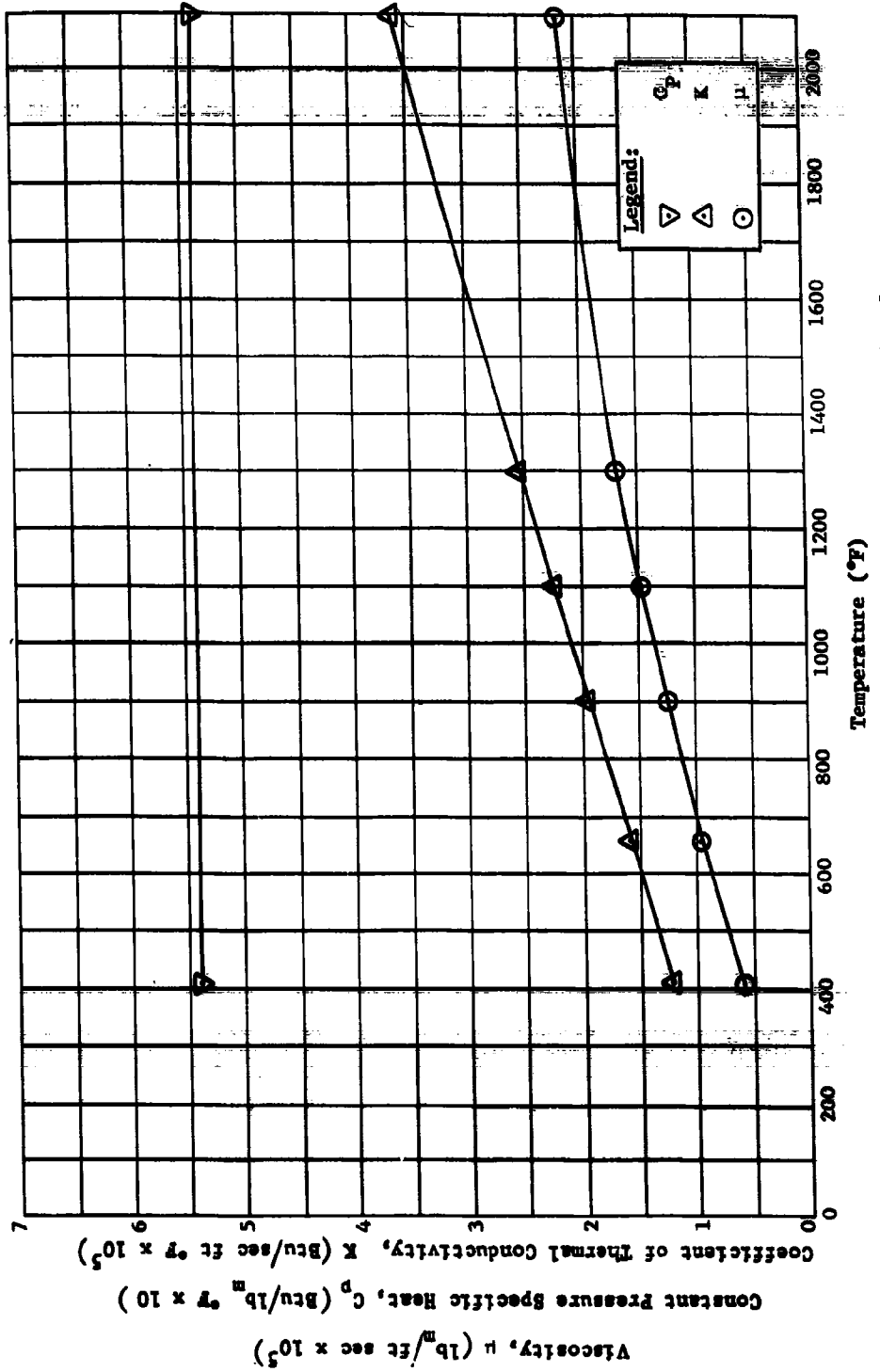


Fig. II-22 Actual Combustion Products Thermodynamic Properties for a Mixture Ratio of 0.1 and Pressure of 600 psia

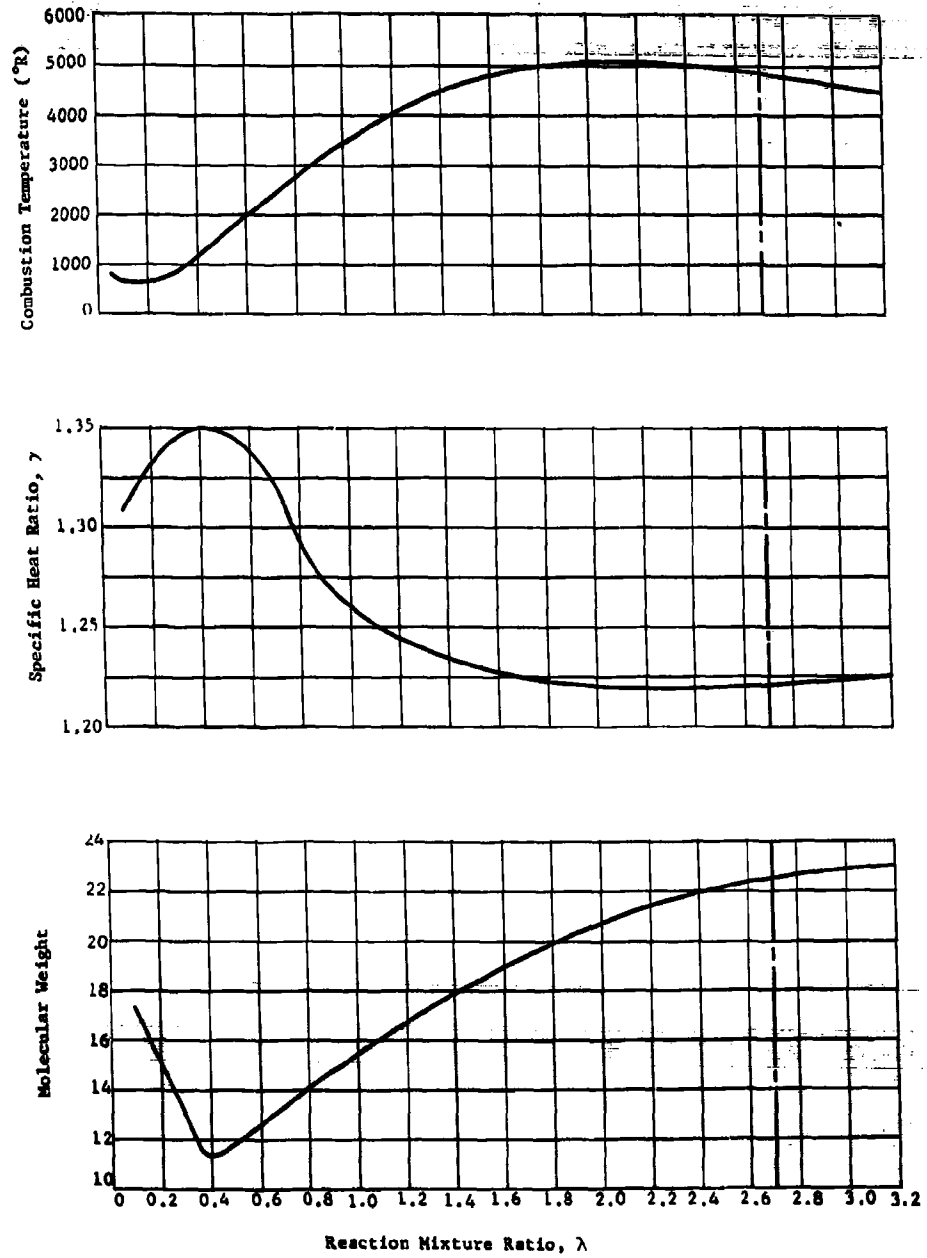


Fig. II-23 Thermodynamic Properties of $N_2O_4-NH_3$ Combustion Products at 36 psia

RTD-TDR-63-1123

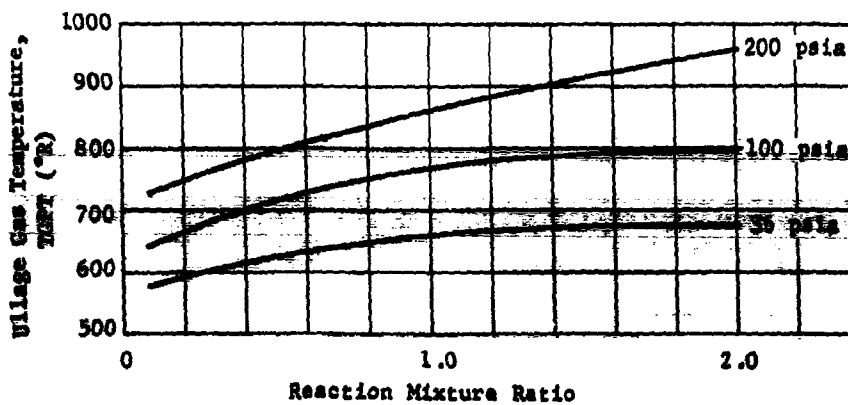
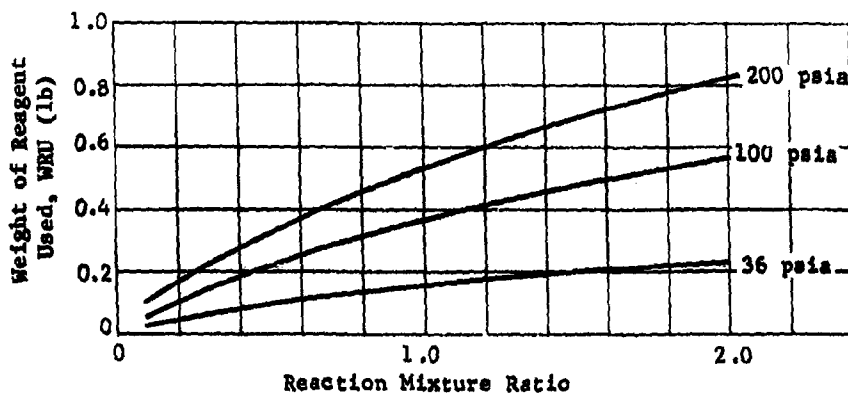
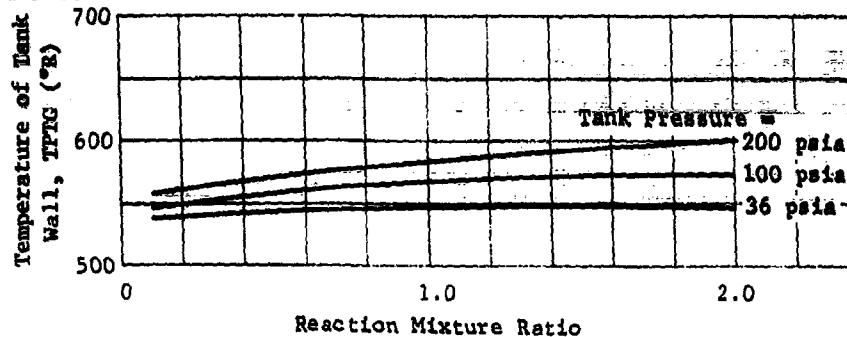


Fig. II-24 Theoretical Phase I Operating Pressure Effects on the Fuel Tank Injection Process

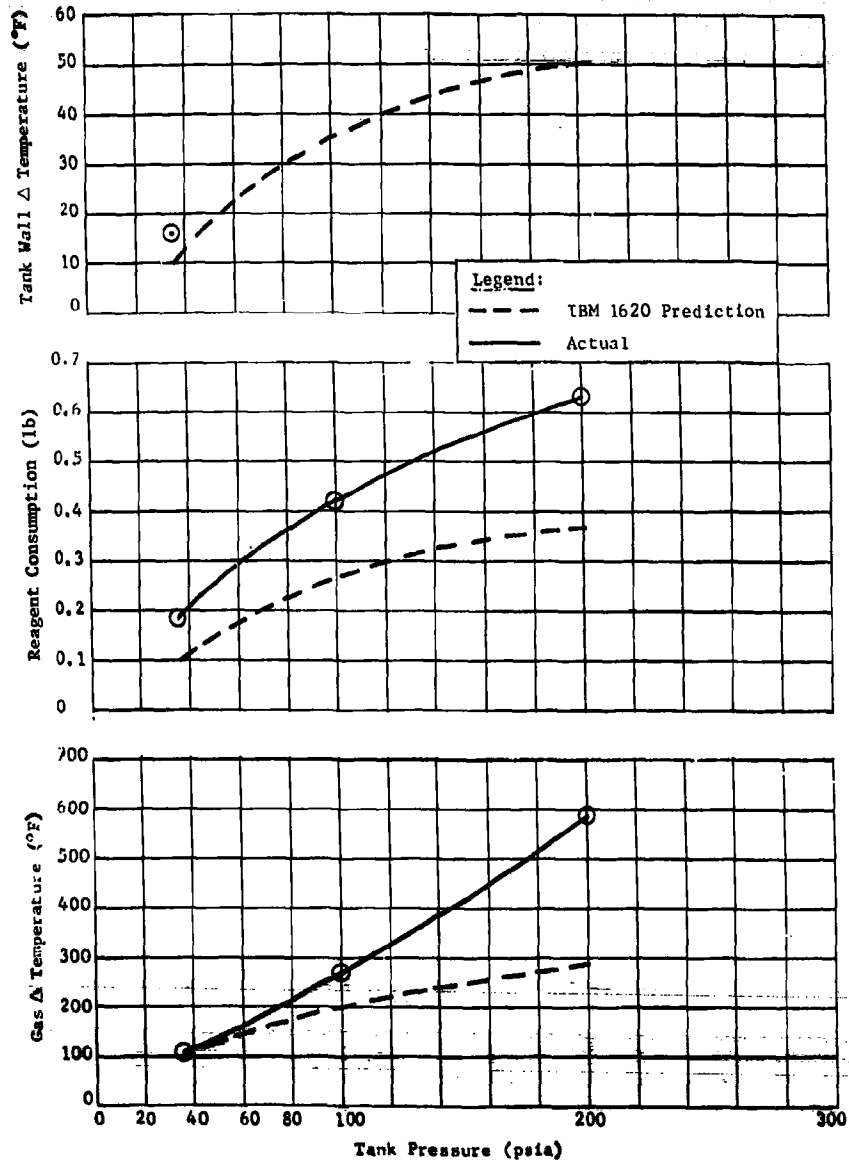


Fig. II-25 Phase I Fuel Tank Test Results

RTD-TDR-63-1123

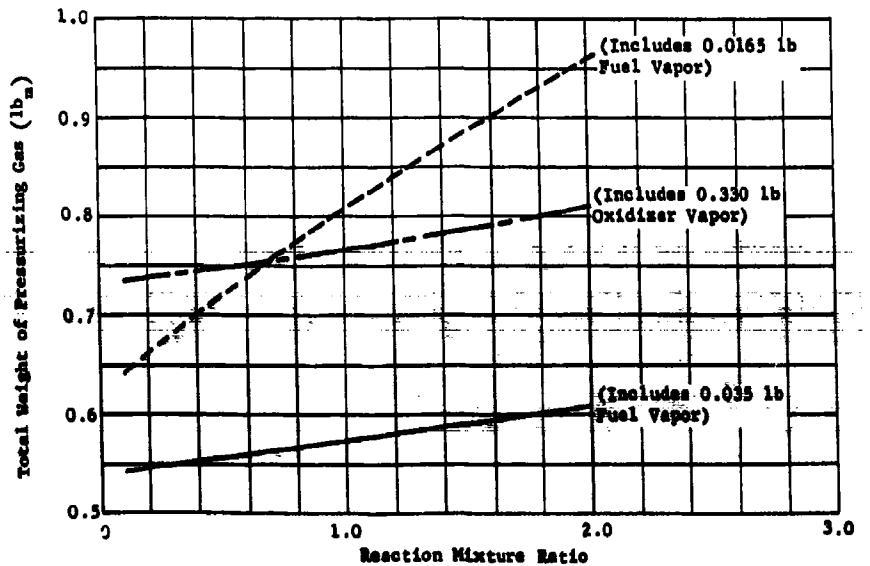
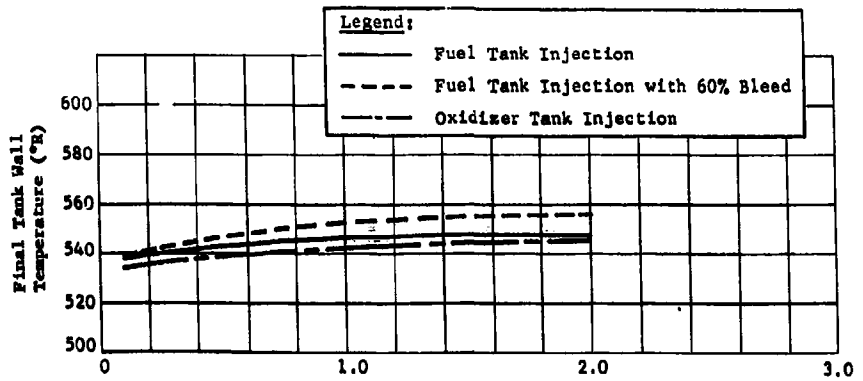
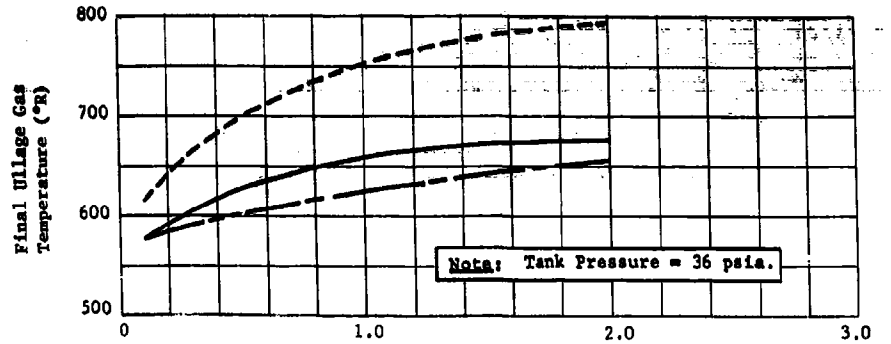


Fig. II-26 Theoretical Phase I System Performance for the Fuel or Oxidizer Tank

RTD-FDR-63-1123

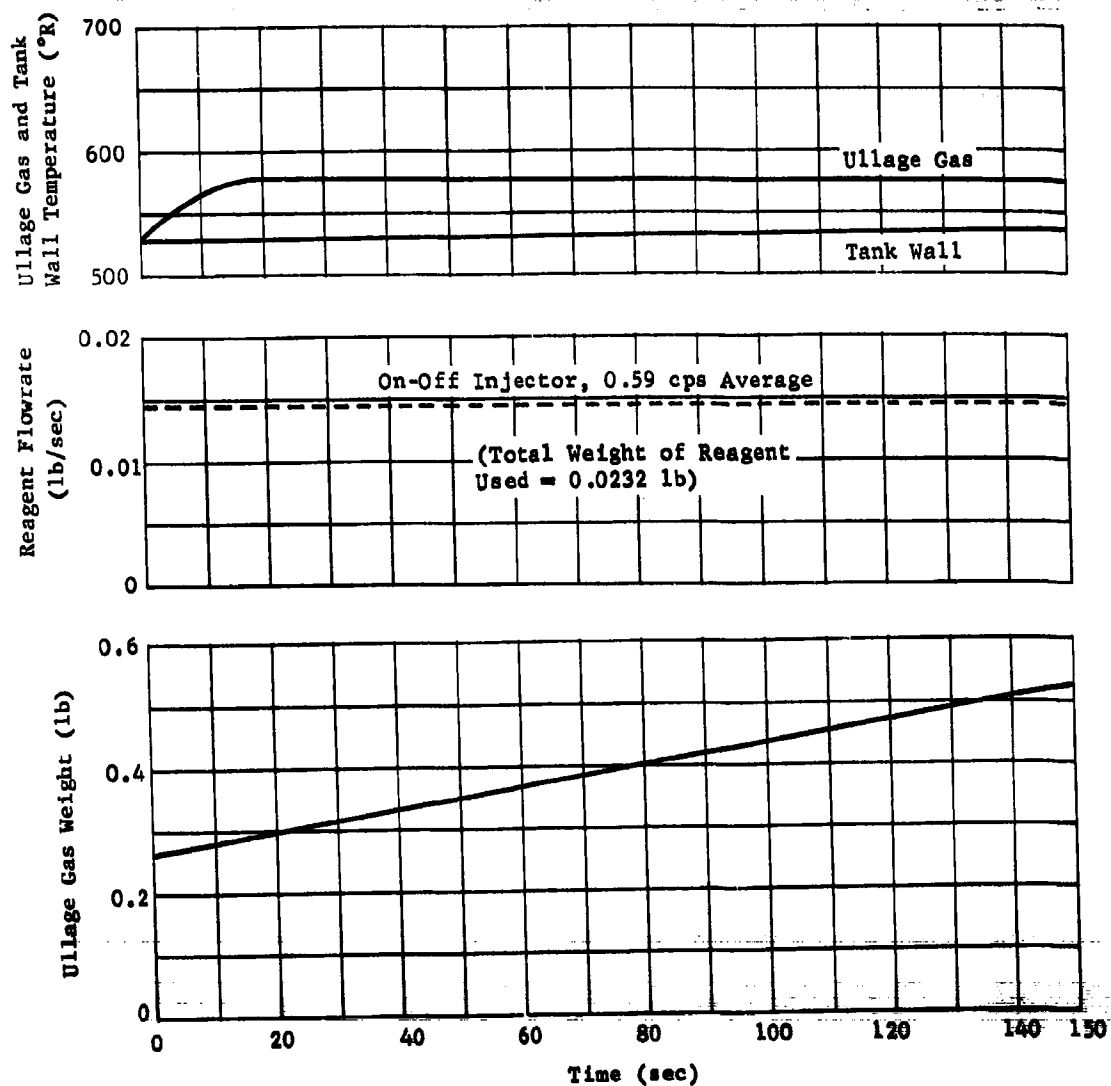


Fig. II-27 Phase I Fuel Tank Predicted Performance for a Mixture Ratio of 0.1 and Pressure of 36 psia

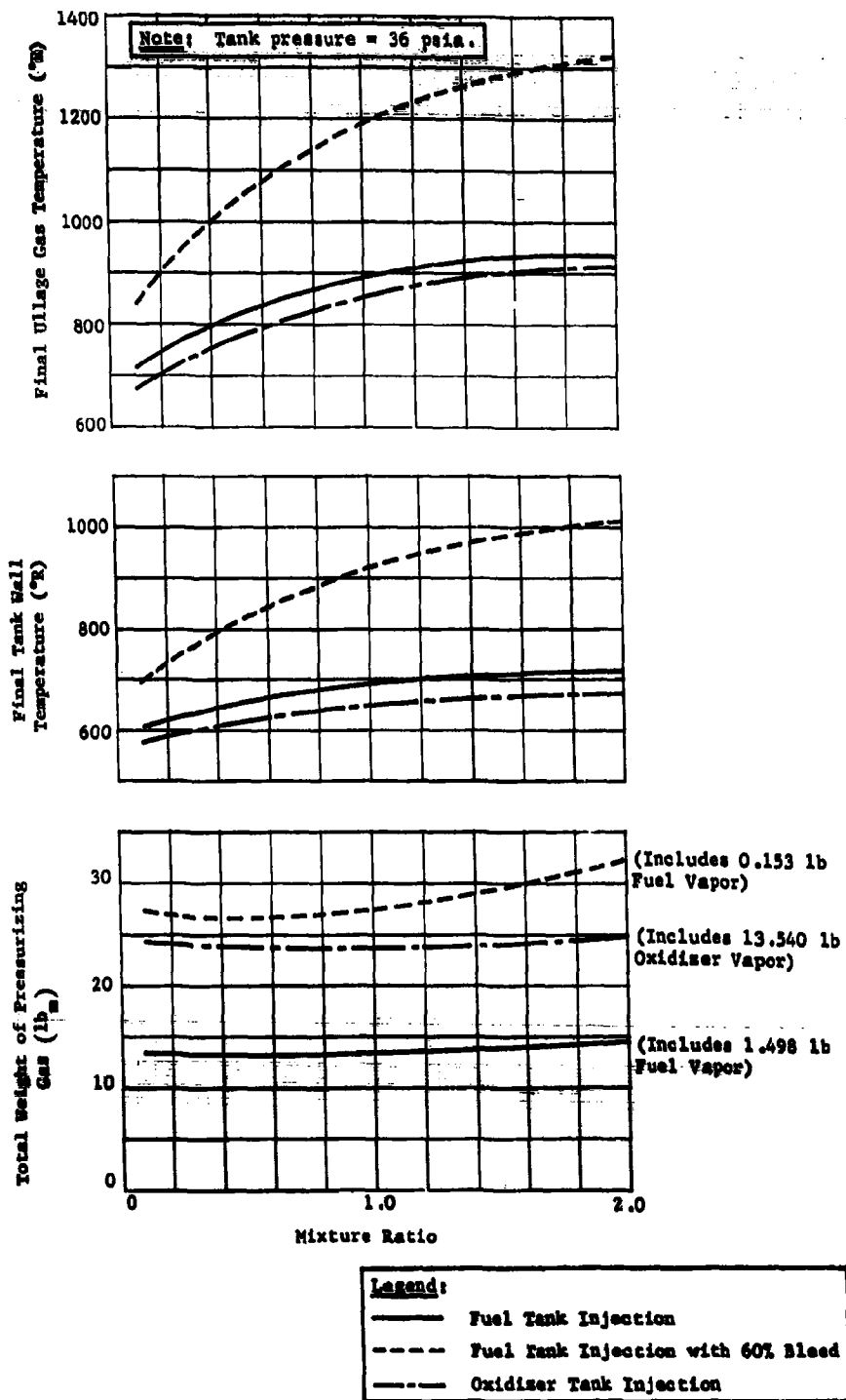


Fig. II-28 Theoretical Phase III System Performance for the Fuel and Oxidiser Tank

RTD-TDR-63-1123

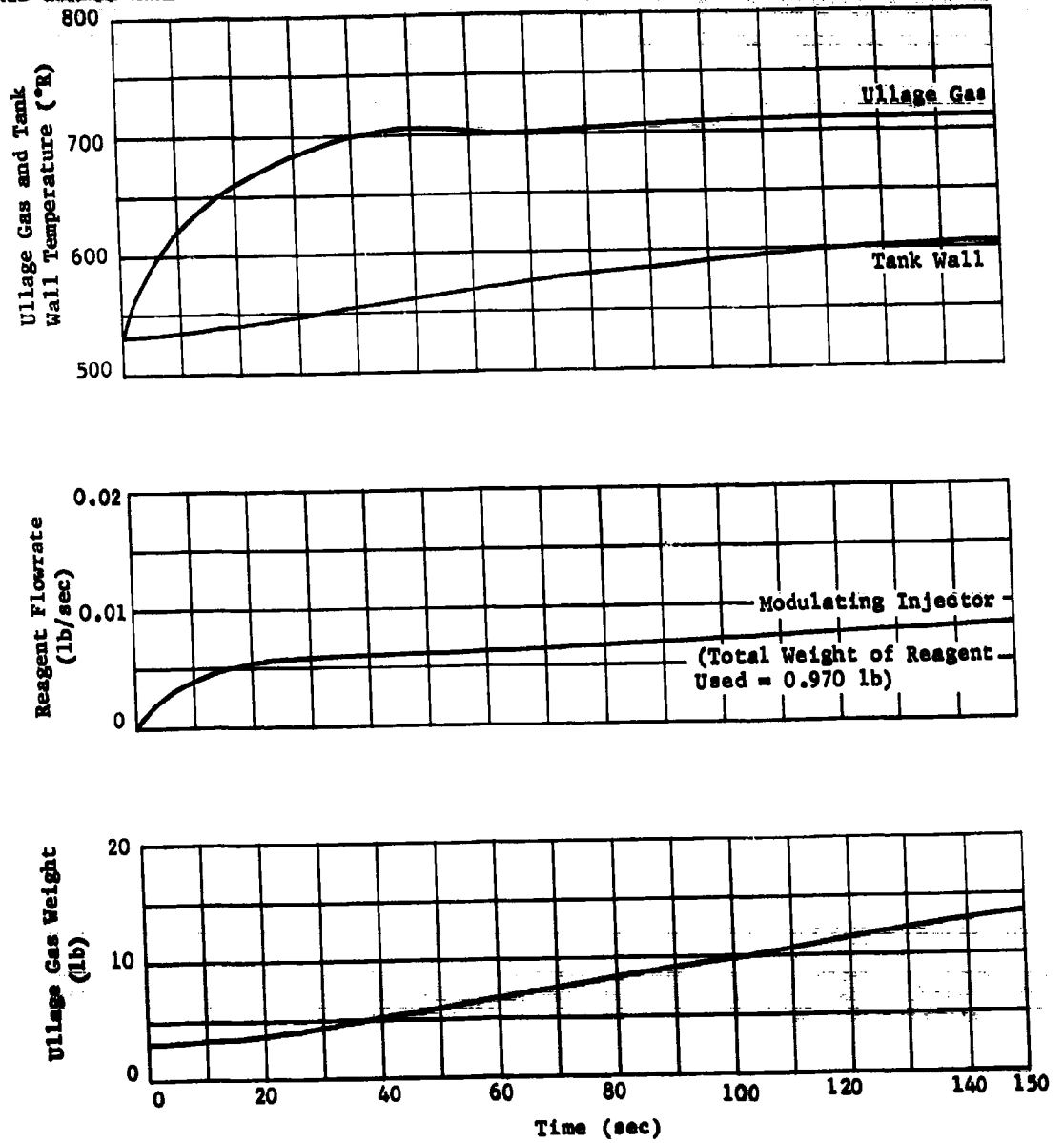


Fig. II-29 Phase III Fuel Tank Predicted Performance for Mixture Ratio of 0.1 and Pressure of 36 psia

6. Applications Study

The identification of the most promising MTI pressurization system applications has been achieved by a combination of two theoretical studies. The purpose of the first study was to establish optimum propellant system operating pressures for turbopump or gas-pressurized systems, based on total propulsion system weight. The second study is a weight analysis of stored gas, gas generator, and MTI pressurization systems to determine the most efficient use of each system as a function of pressurizing capacity. Both studies investigate a range in total impulse and thrust for various propellant tank pressures.

Propulsion System Optimization - A propulsion system weight analysis was made to determine optimum propellant tank pressures for various size missiles over a range of engine thrust. This study was required to establish the probable operating pressures of future MTI pressurization systems. A small computer program, described in App A, was developed for this purpose.

This program calculates the propulsion system weight for a storable bipropellant system with spherical aluminum tankage and a regeneratively-cooled gimbaled engine. A stored-gas helium pressurization system was selected for this study because actual hardware weight information was readily available. Since the pressurization system weight is generally less than 10% of the vehicle dry weight, the effects of propellant tank weight vs engine weight are the most important factors in establishing optimum tank pressures. (The selection of the lowest weight pressurization system was determined by a separate study.)

This study showed that for the large tank booster applications, a low propellant tank pressure (35 psia) is required to reduce tank weight. The engine size is then reduced by using a turbopump to increase combustion chamber pressure. For smaller systems, as required by space missions, analysis of both turbopump and gas pressurized propellant feed systems is required to determine the lowest propulsion system weight. The region of most efficient use of each system has been identified as a function of thrust and mission duration. The long-duration low-thrust

missions are most efficiently accomplished by gas-pressurized propellant feed systems in the 100 to 200 psia range, while higher thrust applications require use of a turbopump. This study was accomplished by comparing weights of a turbopump-pressurized engine ($P_c = 500$ psia) and an optimum gas pressurized propulsion system.

The optimum gas-pressurized propellant feed system was determined from plots of engine chamber pressures vs total propellant system weight for a thrust range of 1,000 to 50,000 lb_f , and total impulse of 2×10^5 to 5×10^6 lb_f -sec. The optimum engine chamber pressure was determined for each application and the results are summarized in Fig. II-30. The figure shows that the optimum engine chamber pressure decreases with an increase in vehicle size and thrust. The weight of each system corresponding to the optimum chamber pressure was compared to the turbopump system. The data show that the turbopump system becomes more competitive as the tankage becomes larger. The break-even size occurred at a total impulse of 1×10^6 lb_f sec where the pressure-feed system is better at low thrusts due to the small engine size (less than 3000 lb_f). However, at intermediate thrust levels the turbopump system is lighter since the engine requires a high chamber pressure for minimum weight. The gas-pressurized system again appears more attractive for the high-thrust applications, since the size of the turbopump becomes excessively large due to the high mass flowrates. The latter application is, however, unrealistic since it represents a region of operation not commonly encountered (less than 35 set).

As the vehicle increases in size beyond a total impulse of 2×10^6 lb_f -sec, the turbopump system becomes even more efficient. Figure II-31 shows the regions of most efficient application of pump pressurized propulsion systems. The use of a gas pressurization system is limited to a fairly narrow region where low-pressure operation is predominant. Since a greater range in missions can be efficiently accomplished by using a pump-pressurized propellant feed system, the importance of developing high-performance low-pressure pressurization systems is evident.

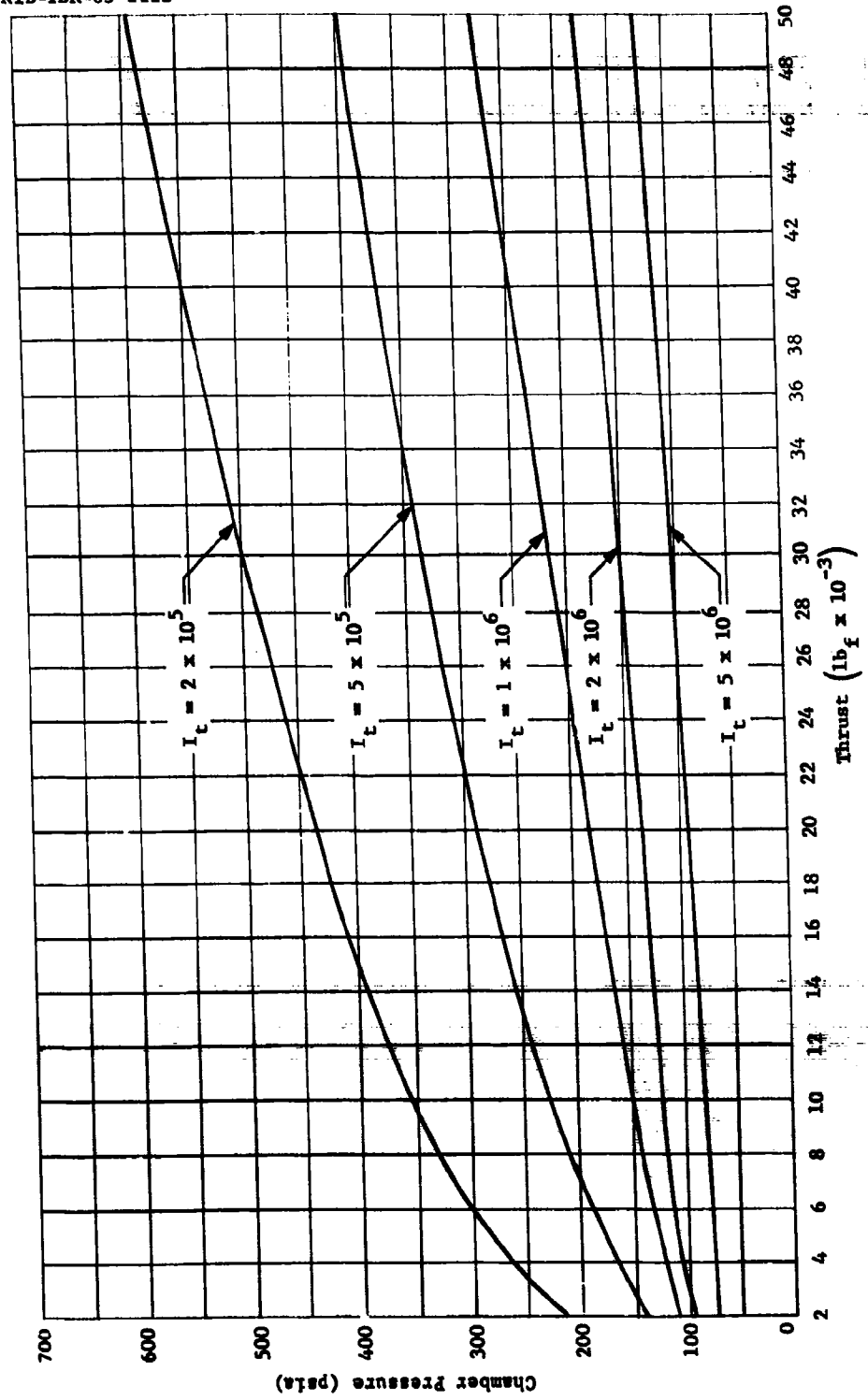


Fig. II-30 Optimum Chamber Pressure for a Gimbeled Pressure-Fed Engine

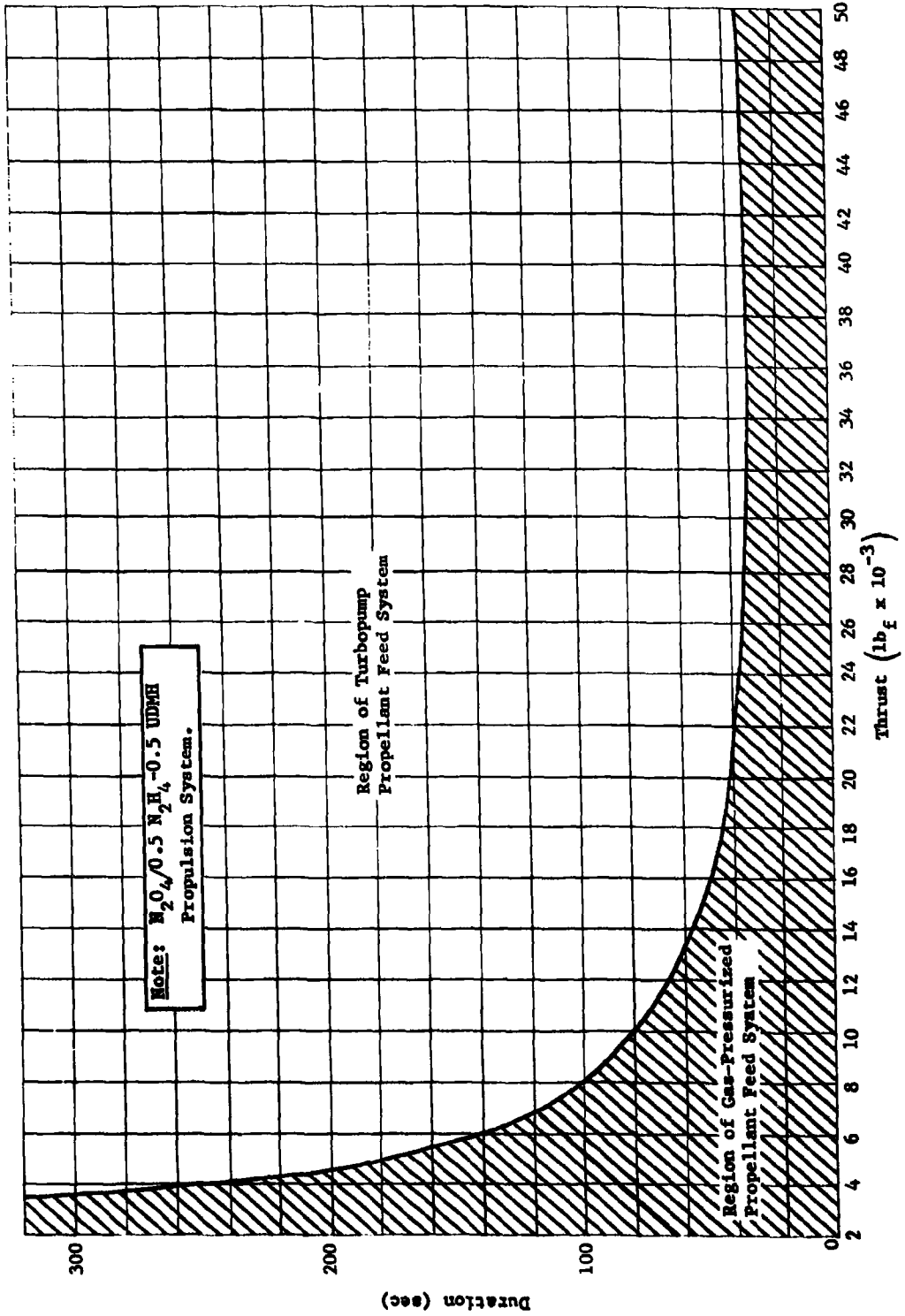


Fig. II-31 Propellant Feed System Optimization

Pressurization System Optimization - The spectrum of liquid rocket vehicle missions was explored to determine the appropriate region(s) where an MTI propellant tank pressurization system becomes desirable. Pressurization systems considered representative of current practice include:

- 1) Stored gas system (heated and unheated);
- 2) Gas generator system (precooled fuel rich gas products);
- 3) MTI (primary reaction in the fuel tank).

The three systems were evaluated on a weight basis with other factors, such as reliability, compatibility, complexity, and cost. The various applications considered are:

- 1) Case I -- boost vehicles;
- 2) Cases II and III -- sustainer or upper stage vehicles;
- 3) Cases IV and V -- limited space vehicles (1 to 30 days in space);
- 4) Cases VI and VII -- deep space vehicles (30 and 730 days in space).

The following tabulation shows the range of important parameters investigated.

	Case						
	I	II	III	IV	V	VI	VII
Total Impulse ($lb_f/sec \times 10^{-7}$)	5 to 10	2 to 5	2 to 5	2 to 5	2 to 5	0.1 to 2	0.1 to 2
Thrust ($lb_f \times 10^{-5}$)	1 to 10	0.1 to 1	0.1 to 1	0.1 to 1	0.1 to 1	0.005 to 0.5	0.005 to 0.5
Engine Feed System	Pump	Pump	Pressure	Pump	Pressure	Pressure	Pressure
Tank Pressure (psia)	20 to 50	20 to 50	100 to 300	20 to 50	100 to 300	100 to 300	100 to 300
Engine Nozzle Area Ratio	8	12	12	12	12	40	40
Engine Combustion Pressure (psia)	750	750	$P_t - 50$	750	$P_t - 50$	$P_t - 50$	$P_t - 50$
Engine Discharge Pressure (psia)	4	1.5	1.0	1	1	Vacuum	Vacuum
Engine Mixture Ratio	1.9	2	2	2	2	2	2
Space Storage (days)	0	0	0	1 to 30	1 to 30	30	730

A generalized digital computer program was specifically constructed to compute pertinent weight data. Separate programs were formulated for the stored gas and the MTI and gas generator pressurization systems. These programs have been simplified to facilitate a direct comparison of the various pressurization systems under investigation. Some of the basic assumptions are included in the general program description contained in App B. The heat transfer that affects tank wall temperatures is assumed comparable for each system with ullage gas temperatures coincident with propellant bulk temperature for space applications.

The weights of various stored gas pressurization systems were determined for heated and unheated helium or nitrogen gases. This study indicates that the storage container volume required for unheated large systems (I_t greater than 10×10^5 lb_f-sec) imposes a severe weight penalty for both pressurants. This is due primarily to the inefficient ambient storage assumed and gas cooling resulting from large expansion ratios. The heated systems reduce this weight penalty significantly for large vehicles, but can only be used efficiently for space-type applications. The amount of heat added for this application is just sufficient for cancellation of the temperature reduction due to gas expansion from the storage container.

An important consideration for gas storage pressurization systems is system leakage because of the high initial storage pressures. However, for the relatively leaktight systems investigated, the net leakage occurring during the space storage times up to 24 months has an insignificant effect on the total weight penalty. This results from the superior leakproof designs accepted for this study. To consider the effects of valve leakage degradation, from the operating life cycle, space environment influences, or contamination, accelerated system leakages of 10 and 20 times normal were examined. These, too, had a negligible effect for the large size vehicle (20×10^6 lb_f-sec). However, for the smaller size vehicle (1×10^6 lb_f-sec), an approximate 8-lb weight penalty per tenfold leakage increase was observed for the 24-month space storage time, with a negligible effect for the one-month period.

The weights of the MTI and gas generator pressurization systems were also investigated for the same applications. Figures II-32 and II-33 compare the weights of MTI with gas generator systems, for pump-feed systems of relatively large total impulse capacity (Cases I and II). These figures show that the MTI system has some weight advantages (20 to 150 lb, or 16 to 22%) over the gas generator system. It is highly probable, however, that factors other than weight considerations will govern system selection since the weight influences on vehicle performance are less severe for the lower stages. The results for upper stage vehicles (Fig. II-34, Case III) show a greater weight advantage for the MTI system, 100 to 800 lb, or 30 to 45%. This is because for the pressure-feed systems, a greater influence of the somewhat lighter MTI gas products is exhibited due to the larger amount of gas required. For space storage applications, the weight differences between both systems again become less significant because gas temperatures cool to 530°R in both systems. Consequently the major weight variations result from minor differences in hardware and accessories, and from the oxidizer tank pressurant gas consumption. The MTI system has weight advantages of 5 to 20% for this application (Fig. II-35 thru II-37).

The weight advantages of MTI over the gas generator system is primarily a function of the specific application; only for pressure-feed upper stage vehicles do these specific advantages become significant (over 25%). Large total impulse, pressure-feed space vehicles also benefit from the use of MTI pressurization. Although less than 25%, savings exceed 500 lb at the maximum tank pressurization.

The stored gas pressurization system has also been compared with the MTI system over the three basic operating regions to determine quantitatively the region of applicability of MTI pressurization. The first region investigated was booster and sustainer vehicles, both pump and pressure feed engines. This region is characteristic of a nonenvironment cooled operating system, and consequently the maximum advantages of the hot gas products of the MTI (and for that matter the gas generator system) is achieved. As expected the MTI system reflected significant weight advantages. This is illustrated in Fig. II-38 where weight penalty savings from 70 to 1100 lb or 40% to 60% are involved. These savings are based on a fuel tank molecular weight of 15, and a varying fuel tank gas temperature of 850 to 1000°R. Obviously this advantage will be reduced if the resultant molecular weight increases or gas temperature decreases. To evaluate the influence of molecular weight, successive molecular weight increases to 22 were examined, and the change in total weight penalty was small.

The second region examined was limited space vehicles, characterized by an environment-cooled system. For this condition, the heat advantage of the MTI system cannot be used due to the eventual cooling of the gas. Similarly, the fuel tank molecular weight is expected to increase because of condensation of the lightweight gas products. As a consequence, there is no weight savings from MTI pressurization. This is illustrated in Fig. II-39 which shows that the "heated" stored helium system is in fact lighter by up to 12%. The addition of heat in the stored gas system merely compensates for the temperature reduction due to gas expansion. The break-even point, where both systems have equivalent weight penalties, occurs at a molecular weight of approximately 14 to 15 for cool fuel tank gas products. Unheated stored helium systems and both types of stored nitrogen systems compare less favorably with MTI, being approximately 60% to 270% heavier. Consequently, these are not to be considered for limited space vehicles.

The last region investigated covered space vehicles. This region differed from the previous case in that vehicle size is reduced and only pressure-feed, maximum-expansion ratio rockets are considered. Figure II-40 indicates that for small size vehicles (1×10^6 lb_F-sec), unheated stored helium systems become weight competitive with MTI pressurization systems. As vehicle size increases, heated stored helium systems should be used to avoid substantial weight penalties. This is illustrated for the 20×10^6 lb_F-sec total impulse curve in Figure II-40. Obviously the storage tank weight penalties of stored gas systems have less influence as vehicle total impulse decreases, and thus gas pressurant demand is less.

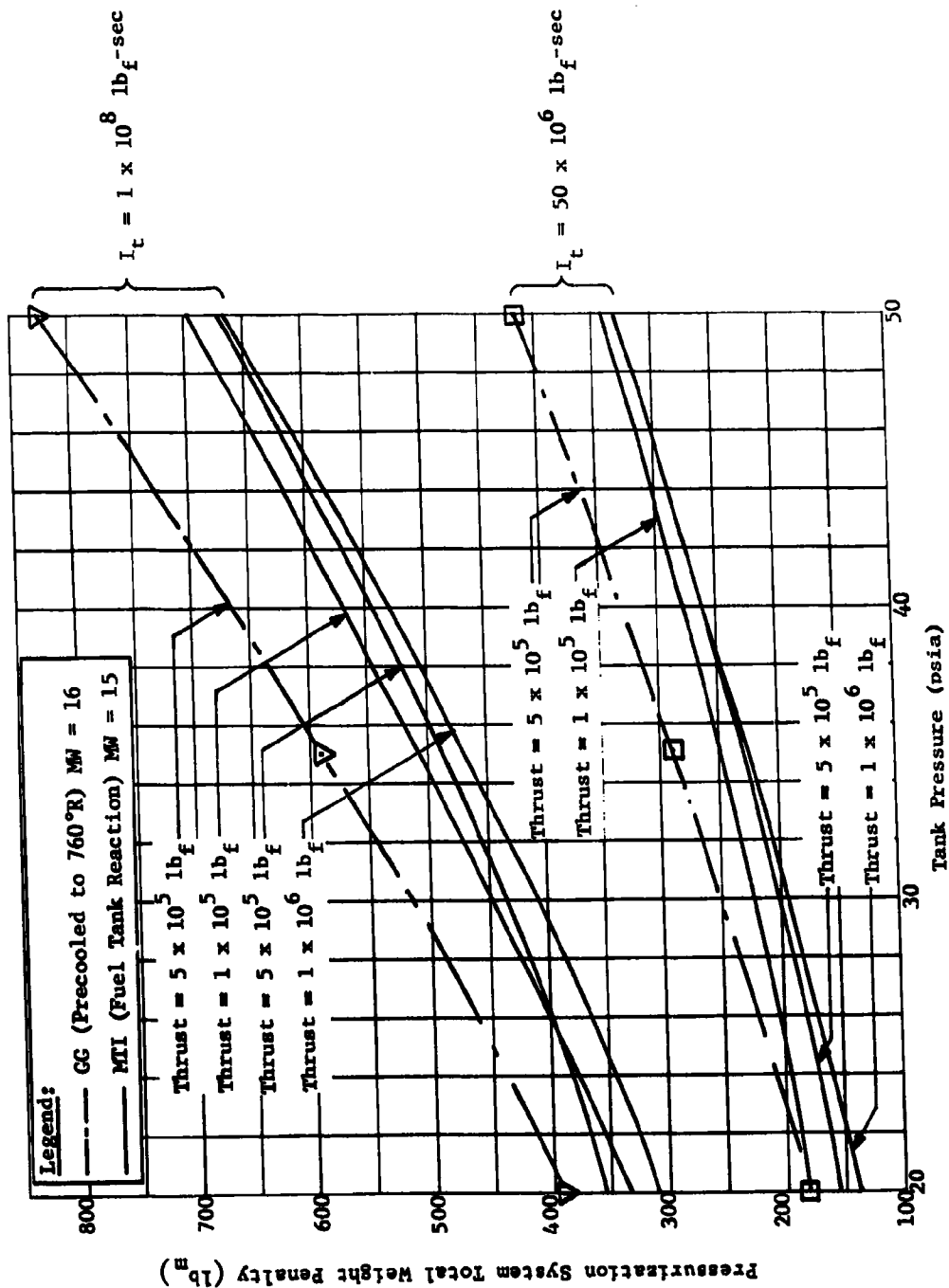


Fig. II-32 MTI vs Gas Generator Pressurization Systems, Case I, Booster Vehicle

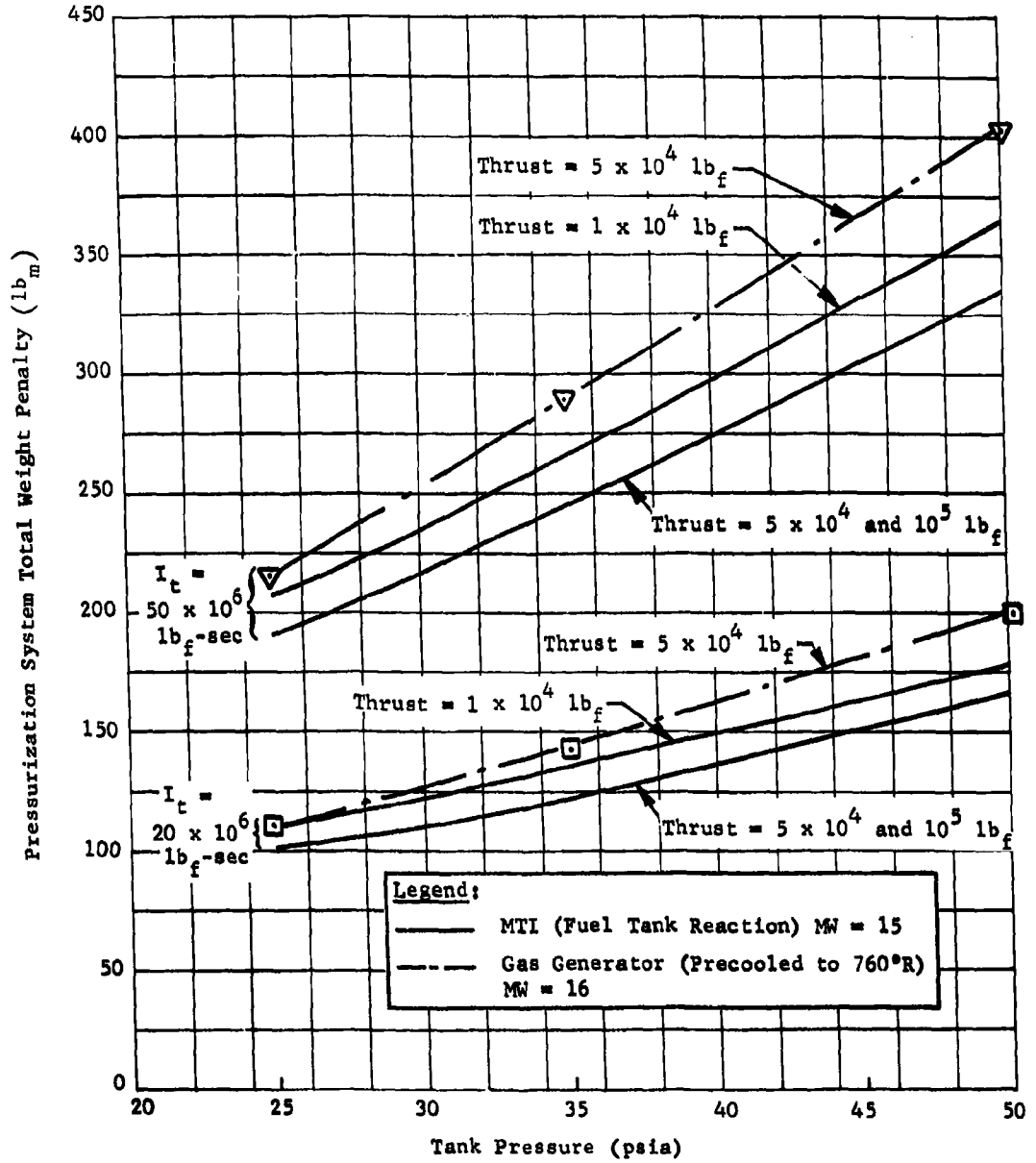


Fig. II-33 MTI vs Gas Generator Pressurization System, Case II, Sustainer Vehicle

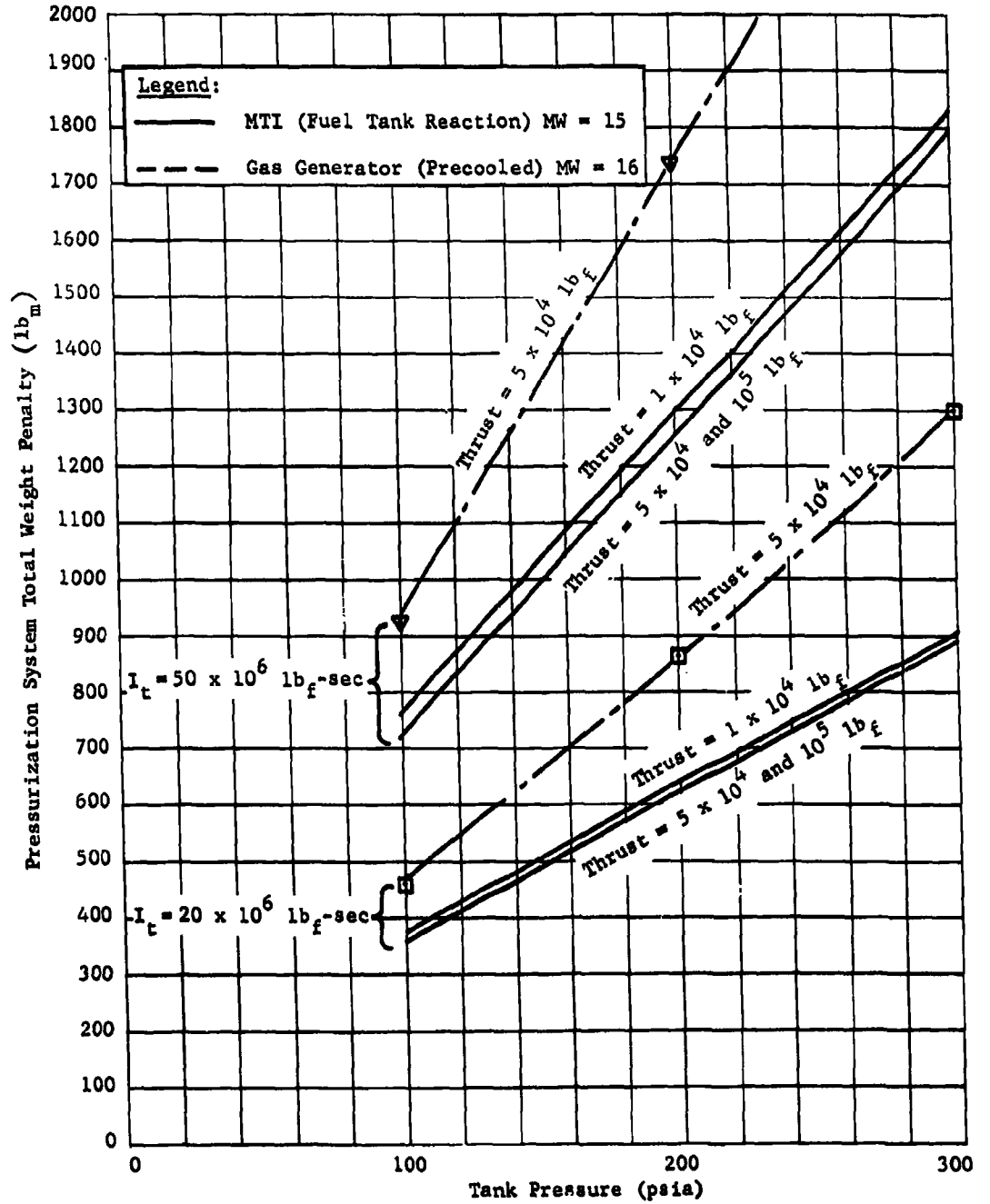


Fig. II-34 MTI vs Gas Generator Pressurization Systems, Case III, Upper Stage Vehicle

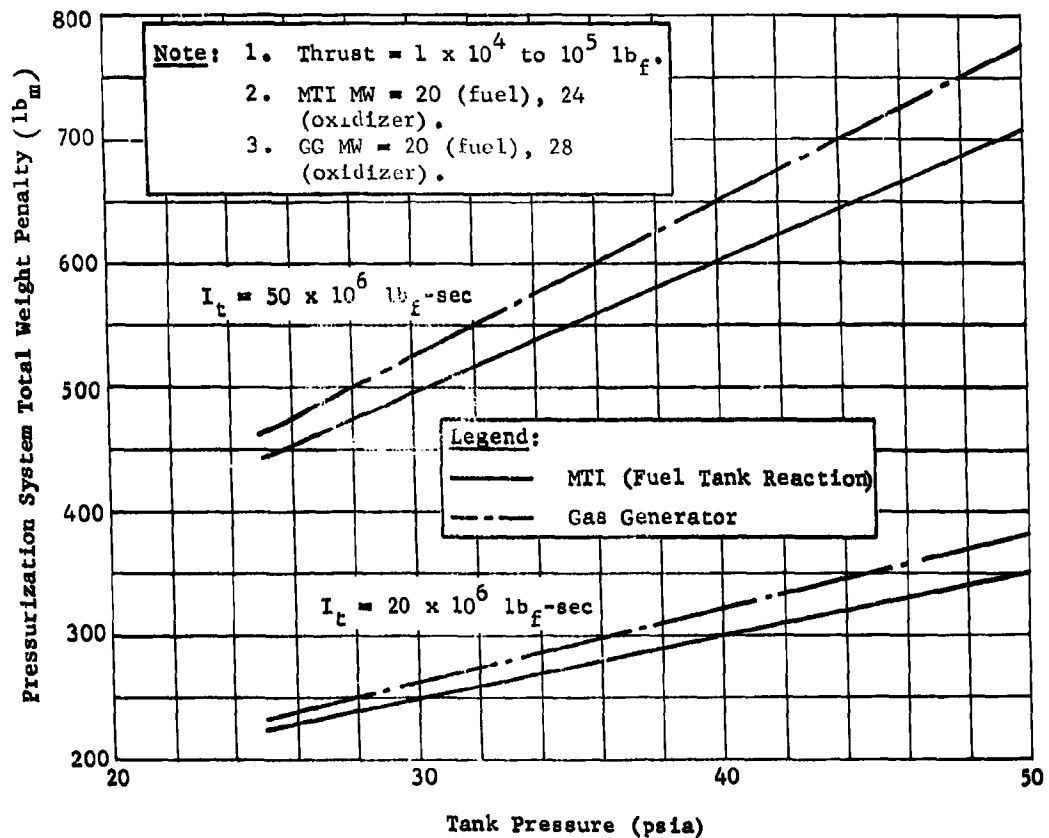


Fig. II-35 MTI vs Gas Generator Pressurization Systems, Case IV, Limited Space Vehicle, 1 Month Storage

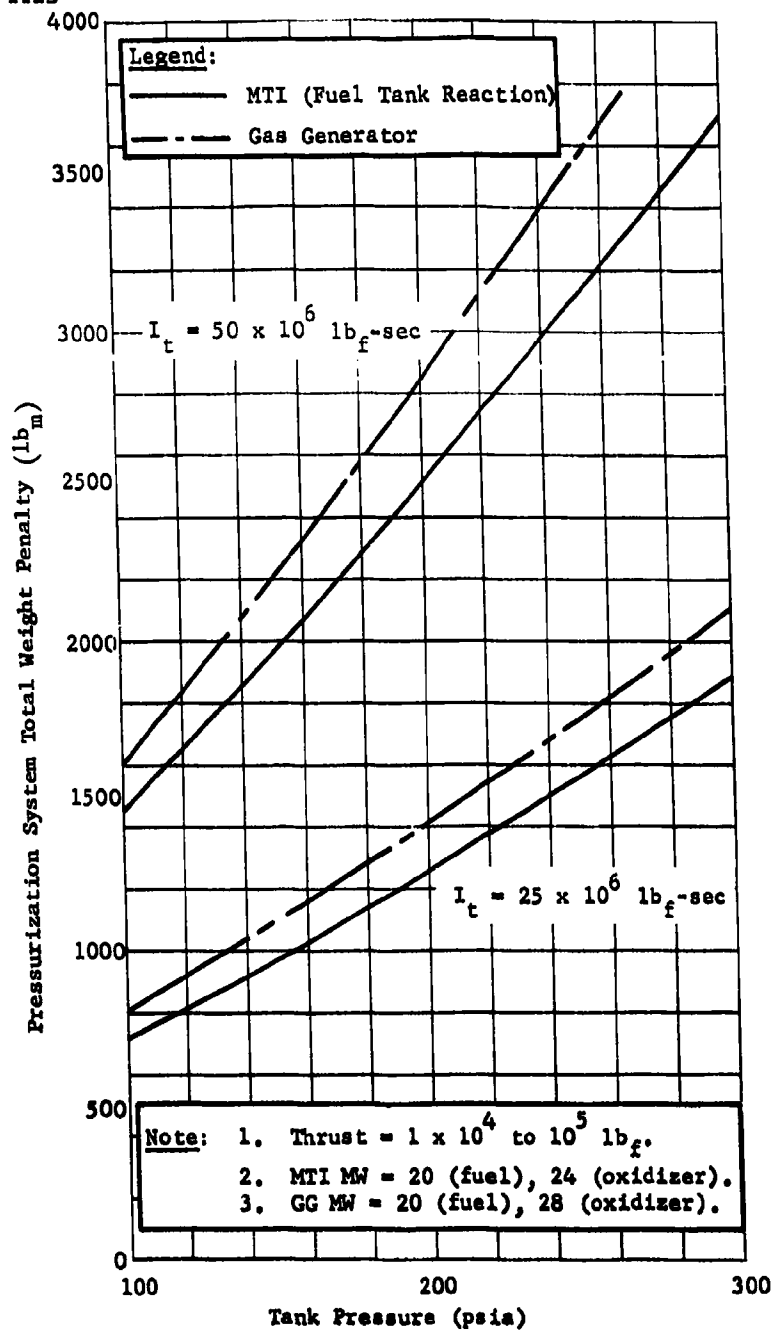


Fig. II-36 MTI vs Gas Generator Pressurization Systems, Case V, Limited Space Vehicle, 1 Month Storage

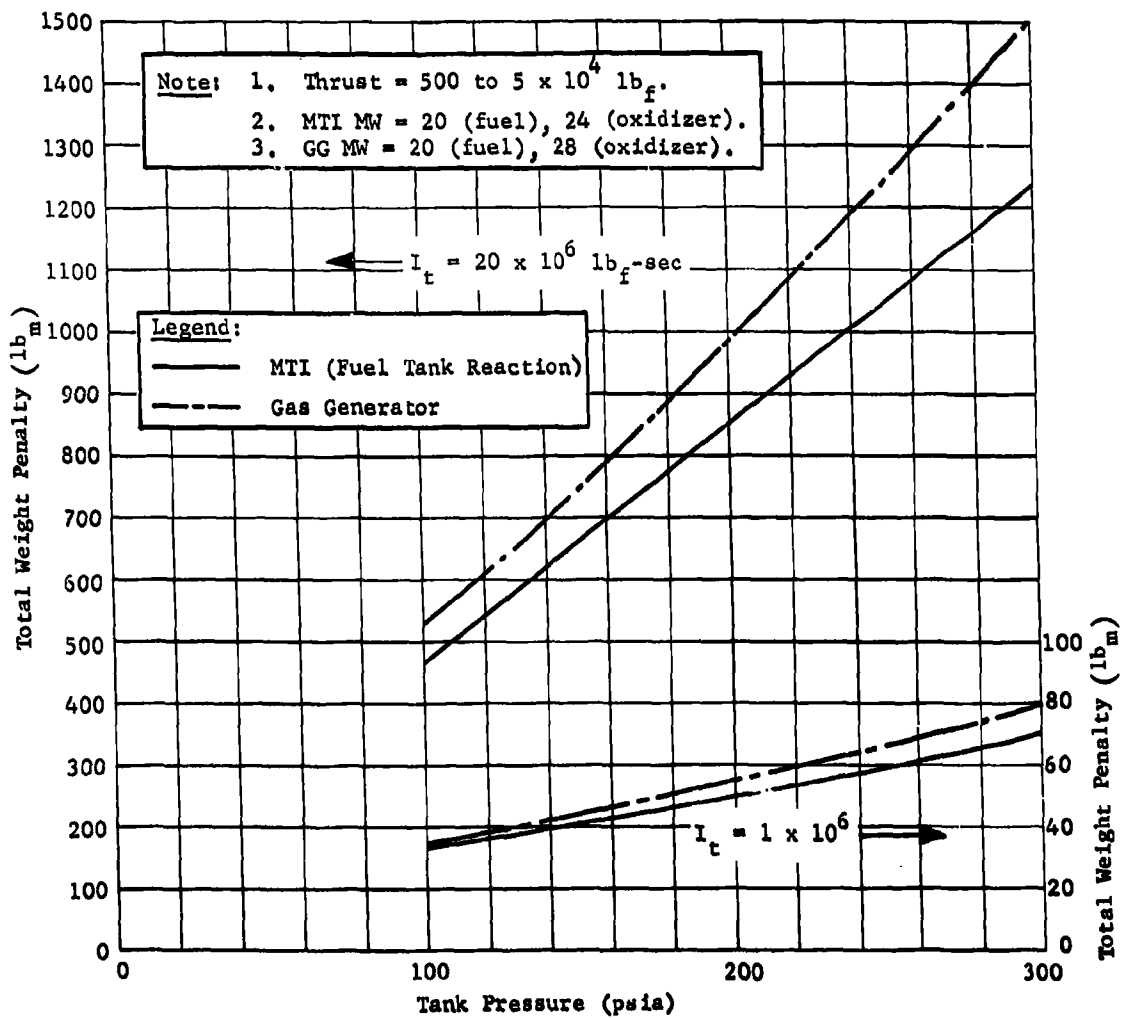


Fig. II-37 MTI vs Gas Generator Pressurization Systems, Case VI, Space Vehicle, Indefinite Storage

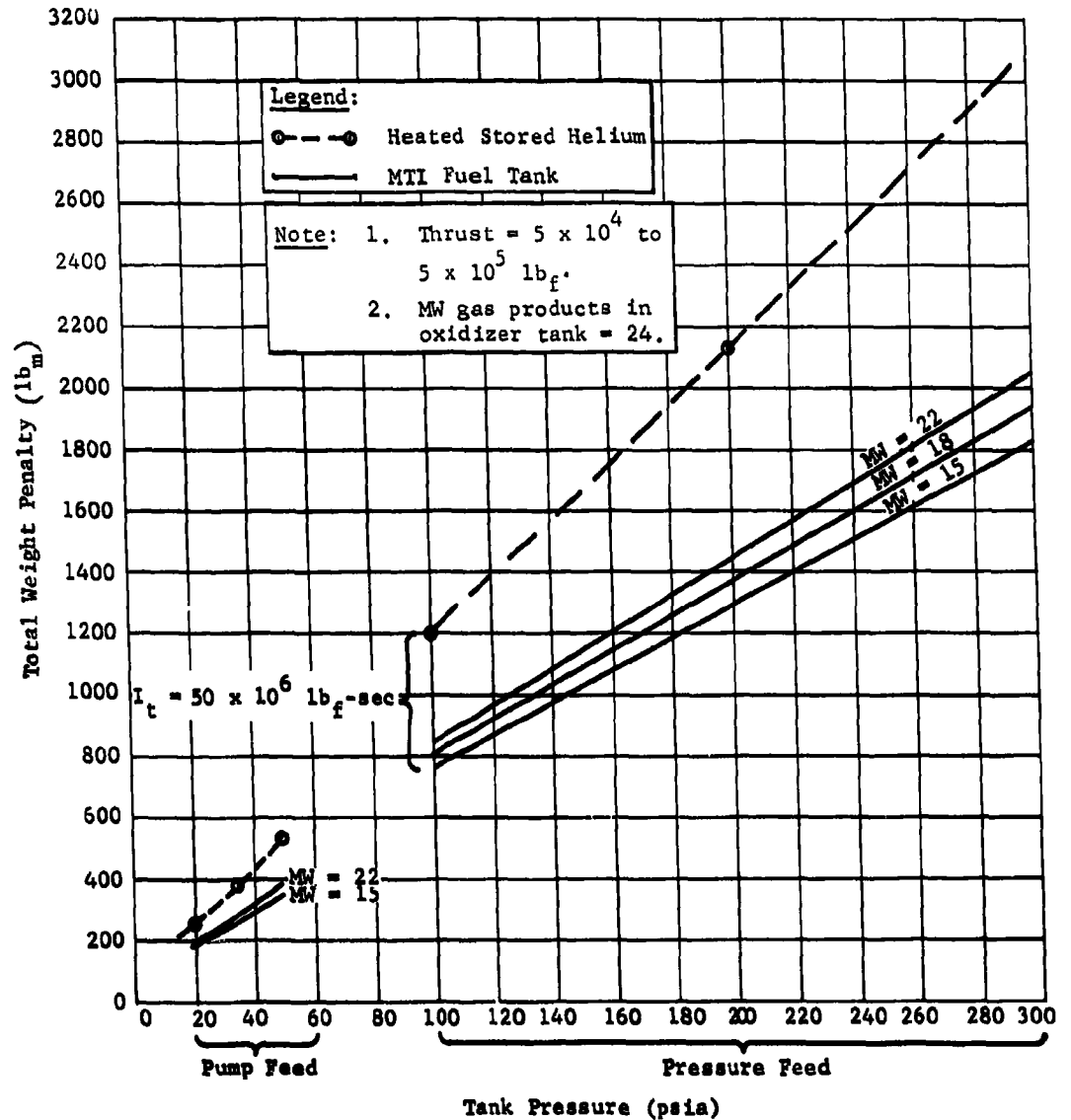


Fig. II-38 Comparison of MTI and Heated Stored Helium Pressurization System Weights, Cases I, II, and III, Boosters and Upper Stage Vehicles

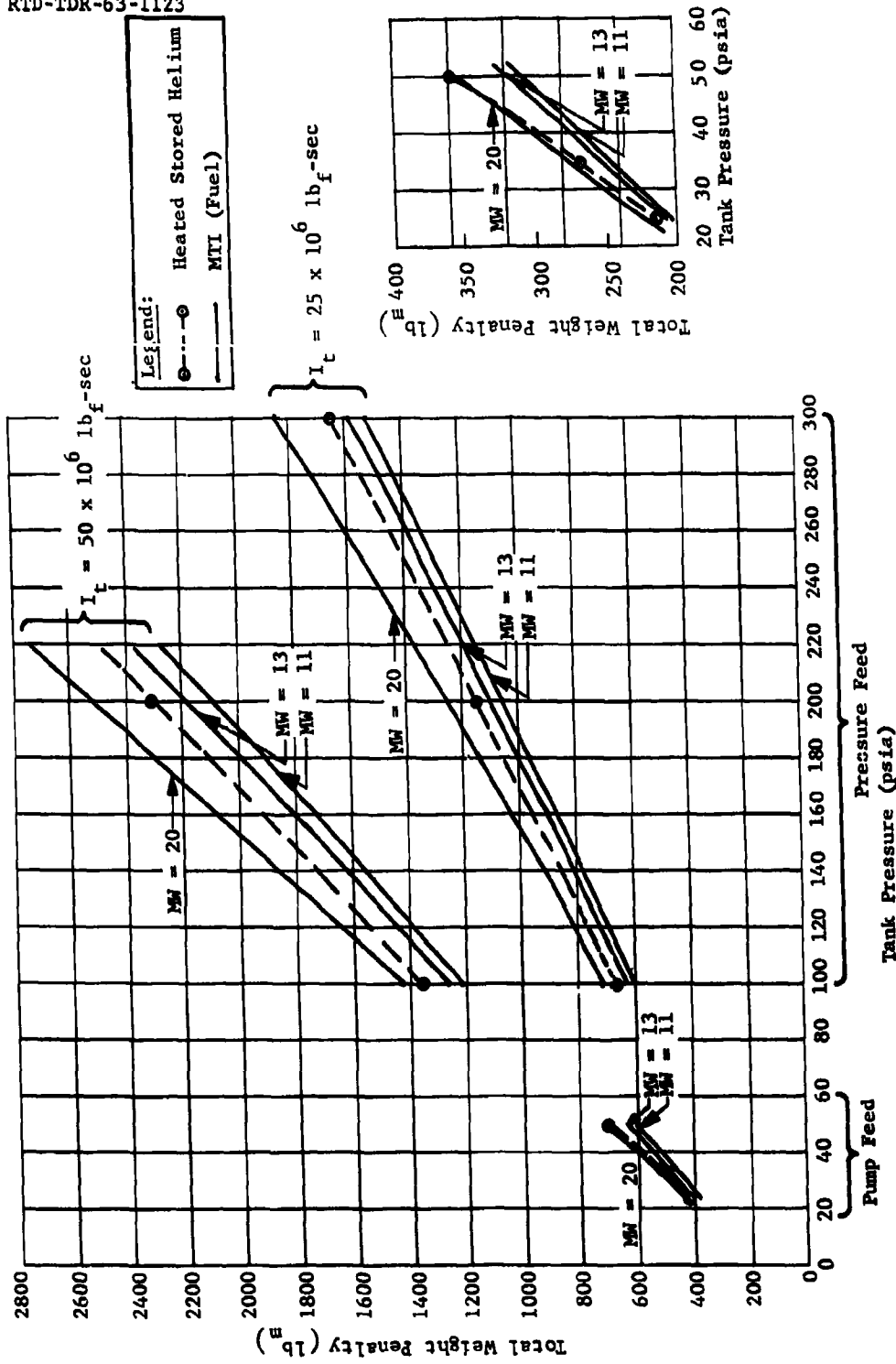


Fig. II-39 Comparison of MTI and Heated Stored Helium Pressurization System Weights, Cases IV and V, Limited Space Vehicles, 1- to 30-day Space Storage

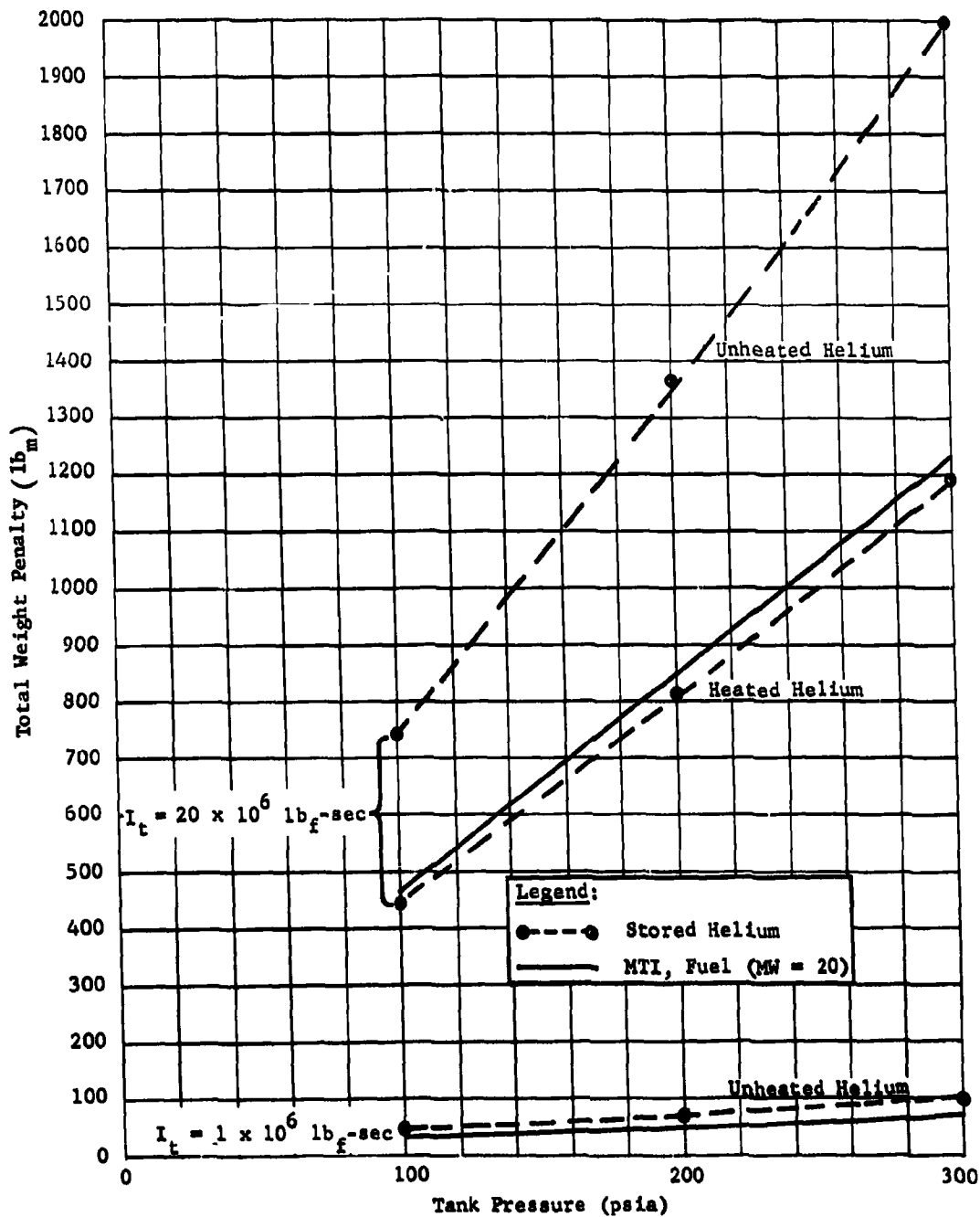


Fig. II-40 Comparison of MTI and Stored Helium Pressurization System Weights, Case VI, Space Vehicles, 1- to 30-day Space Storage

B. RESEARCH TESTING

The Phase I research test program enabled the investigation of the reaction process and development of a chemical pressurization system on a small-scale basis. Information gained from this program established the optimum injection technique and methods for generating desirable pressurizing gases in either the fuel or oxidizer tank with both the dual injection and common ullage configuration. A reagent injection device with adequate response and performance was successfully developed and provided important data concerning the combustion process and system thermodynamics to allow development of an MTI mathematical model. Since approximately 100 fully instrumented tests were performed, and approximately 75 of these tests underwent ullage gas analysis, substantial information was acquired to verify the MTI concept and aid in full-scale system design.

The basis research program was divided into four parts:

- 1) Fuel tank injection system development;
- 2) Fuel tank injection method evaluation;
- 3) Common ullage system development;
- 4) Parametric testing.

The injection system development program involved tests with a single tank to aid in modifying a commercial-type chemical spraying device used as the injector and verify the pressure control and reagent supply systems. In this series, nitrogen tetroxide was injected through a solid-stream orifice into the surface of the fuel at sufficient velocity to penetrate the surface and provide significant regenerative cooling of the resultant combustion gases. A pulse mode pressure-demand-type system was used, maintaining tank pressure within the pressure switch deadband. The injection method evaluation test series used the same basic pressurization system for the fuel tank with a common ullage manifold connecting the water-filled oxidizer tank. Two spray patterns (solid-stream and 15° fan spray) were investigated both above and below the liquid surface. For the common ullage system development program, the secondary tank was filled with oxidizer while surface and sub-surface gas impingement techniques were evaluated with various gas-conditioning methods. The parametric tests were performed by separately pressurizing each tank with solid-stream surface reagent injection at pressures of 36, 100, and 200 psia. Satisfactory system operation was achieved with MTI initial pressurization, variable outflow, restart, and induced random vibration.

1. Test Fixture Design

One primary consideration in designing the small-scale system was to provide maximum test safety and sufficient ability for process investigation with a variety of configurations. The availability of surplus 5.33-cu-ft aluminum (6061-0) spheres with 5/8-in. wall thicknesses permitted tests on an appropriate scale with maximum safety and a minimum amount of modification and cost. The spheres were cut in half and modified to provide a noncavitating non-dropout propellant outlet, propellant antivortex baffles, pressurization ports, pressure relief ports, instrumentation ports, and camera ports. Figure II-41 shows a top view of the upper dome, and Fig. II-42 shows the inside of the upper dome with the demister element used for common ullage gas filtration displayed outside the canister. Figure II-43 shows the inside of the lower dome and the baffle installation for propellant flow direction and combustion zone control. A satisfactory seal at the separation flange was obtained by filing the seal groove with RTV silicone rubber (MMS-M-138), which is compatible with storable propellants for only a limited time.

The total tank weight is approximately 212 lb, with an additional maximum propellant load of 286 lb of fuel or 455 lb of oxidizer when filled to the 5% ullage level sensor. The propellant load for each test was a function of the desired ullage since tests at 5 or 30% ullage in each tank were provided to permit operation at an outflow mixture ratio of approximately 2 to 1 and allow initial tests under less severe response requirements. A maximum 150-sec test duration was selected, based on current booster engine burning duration. Consequently, the nominal propellant flowrates of 2.5 lb/sec oxidizer and 1.25 lb/sec fuel were established, based on a residual 0.42 cu ft of fuel at injector shutoff. Low-level sensors were used to provide sufficient propellant for baffle regenerative cooling, and the remaining outflow was accomplished by ullage gas expansion.

The assembled tank is shown in Fig. II-44. A closeup permits observation of the injector installation contained in Fig. II-45. The hemispheres were joined with tension bolts designed for a 700-psig burst pressure with the upper dome restrained and counterbalanced to prevent facility or system damage in the event of catastrophic failure. Lower range overpressure protection was also provided with a 250-psig relief valve and two (300-psig rupture at 100°F) burst discs made of 6061 T-6 aluminum. The 1-in.-diameter propellant sight glass, incorporated for detecting entrained vapors, and the 3-in.-diameter x 3/4-in.-thick Tuf-flex camera ports, used for photographic and television observation of the reaction process, provided additional overpressure protection at

higher pressure levels. Vent stacks were provided to control any discharged fluids. The initial and final propellant levels were indicated by Powerton ultrasonic liquid detectors with propellant flow control accomplished by Annin Domotor and a Swartout remote control unit. The discharged fluid was stored in a catch tank shown in the lower left corner of Fig. II-44.

The injection system design was based on pulse mode operation with anticipated use in the full-scale system. The basic injector is a modified Spraying Systems Co. (Model 24 AUA-8980) chemical spray gun. This component uses a solid-stream injector orifice tip for flow control and is pneumatically actuated and pressure-switch controlled. Sufficient versatility is inherent in the basic design to allow spray pattern or injector location variations. The 100-psig nitrogen actuation was controlled by a 1/4-in. three-way solenoid valve. Reagent was supplied under pressure from a sight glass with dump capability in the event of abnormal conditions. An injector differential pressure of 75 psi was used in all of the tests. Sufficient capacity was provided to permit common ullage testing at pressures to 200 psia. The injector orifice diameter was originally based on an assumed reaction mixture ratio of 0.1 and a 300°F operating temperature in the fuel tank. For these conditions, the two-tank system only attained marginal flow capacity due to the amount of condensibles formed and the higher reaction mixture ratio. System response was determined by a method similar to that explained in Chapter V Section B, based on nominal component operation characteristics. Subsequent tests with a 0.014-in.-diameter orifice verified system capability for ± 1.0 psi pressure control and minimum ullage.

Although the injection system is comprised of several elements that limit the overall system response, excellent pressure control was achieved in all tests. Figure II-46 is a schematic of the injection system electrical circuit. This design uses a normally closed single-contact 36 ± 0.25 -psia Belleville-type pressure switch to control tank pressure and a manual override to prevent injection before the test starts. The electrical signal activates a relay that controls operation of a solenoid valve that supplies 100 psig pneumatic pressure for opening the normally closed injector. Injector response primarily depends on the pneumatic flow capacity of the activation system for opening and depressurization for closing. An additional time lag was detected due to the reagent stream above the liquid surface when the injector was signaled closed, so a slight tank overpressure was experienced. Since this phenomenon is a function of injection mass velocity and distance from the injector to the liquid surface, suitable allowances must be made.

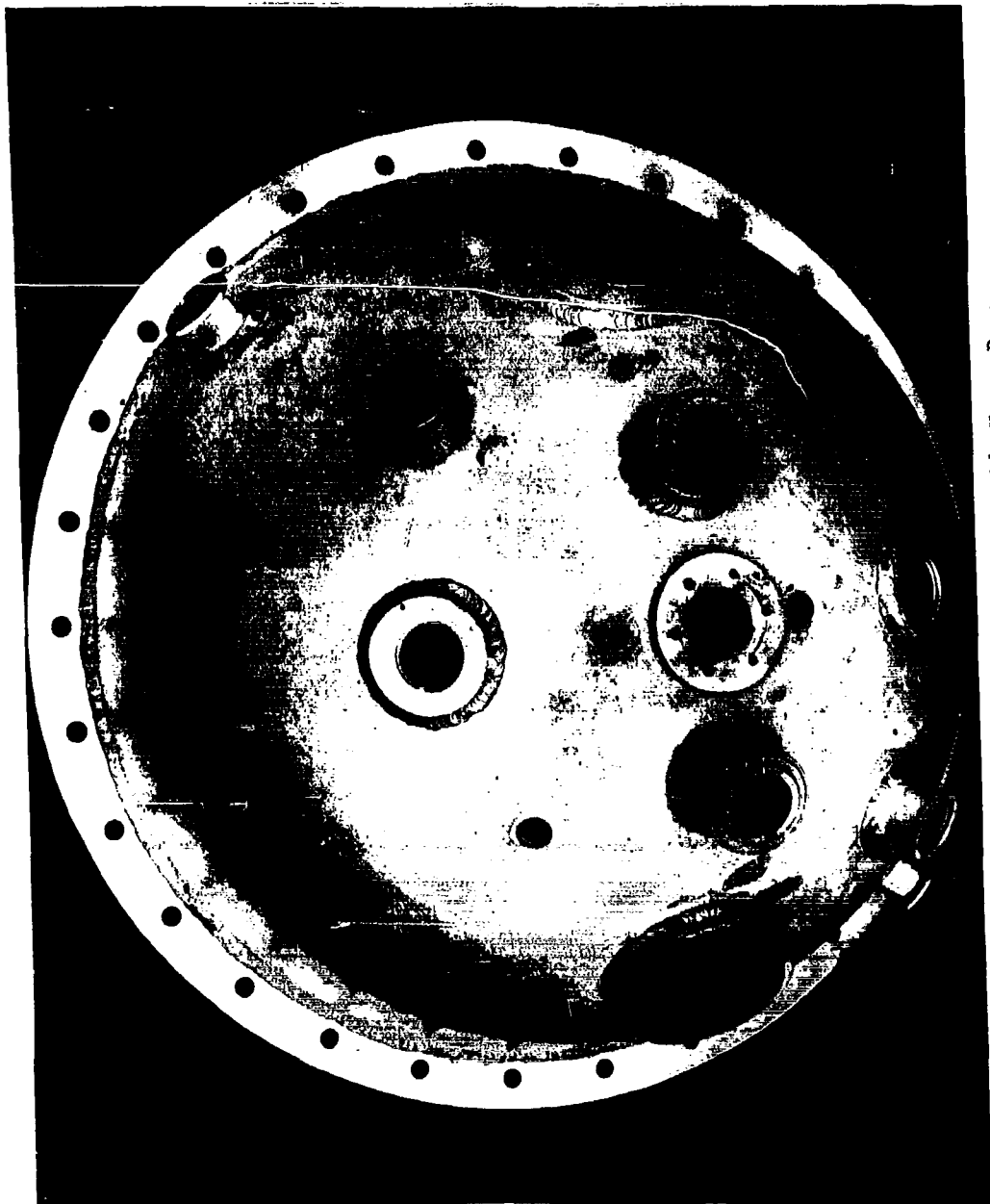


Fig. II-41 Research Fixture Outside Upper Dome

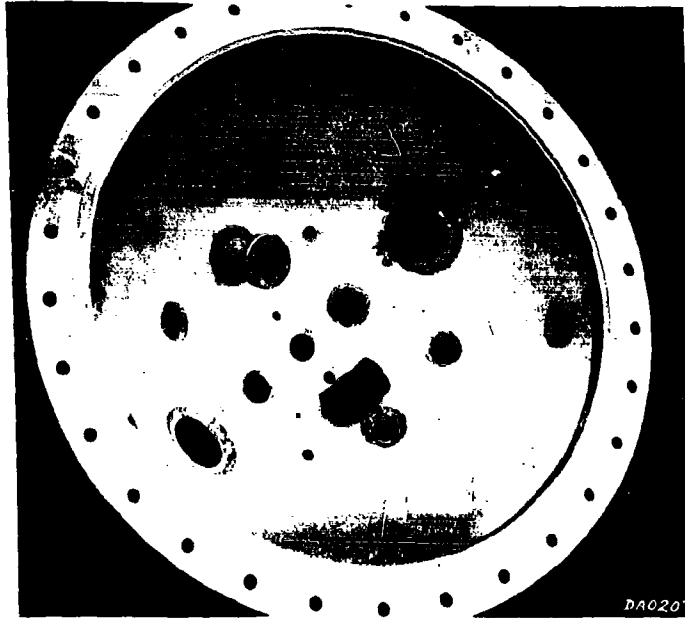


Fig. II-42 Research Fixture Inside Upper Dome

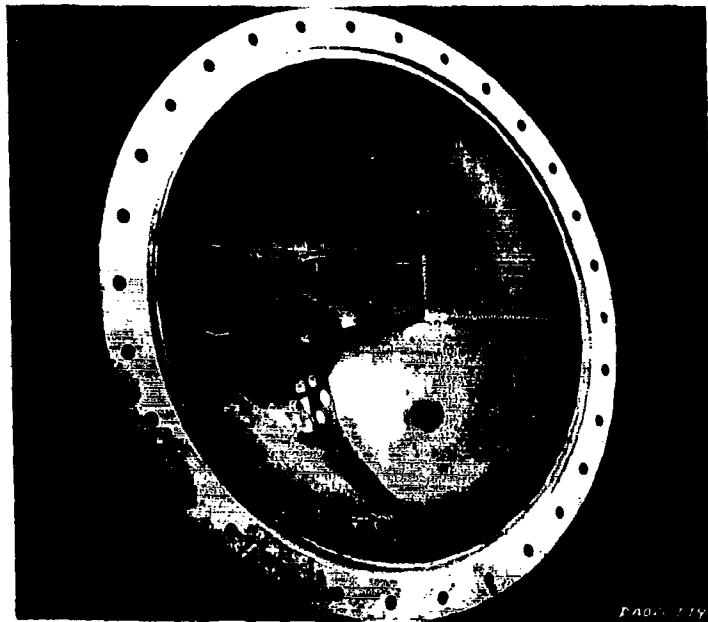


Fig. II-43 Research Fixture Inside Lower Dome

RTD-TDR-63-1123

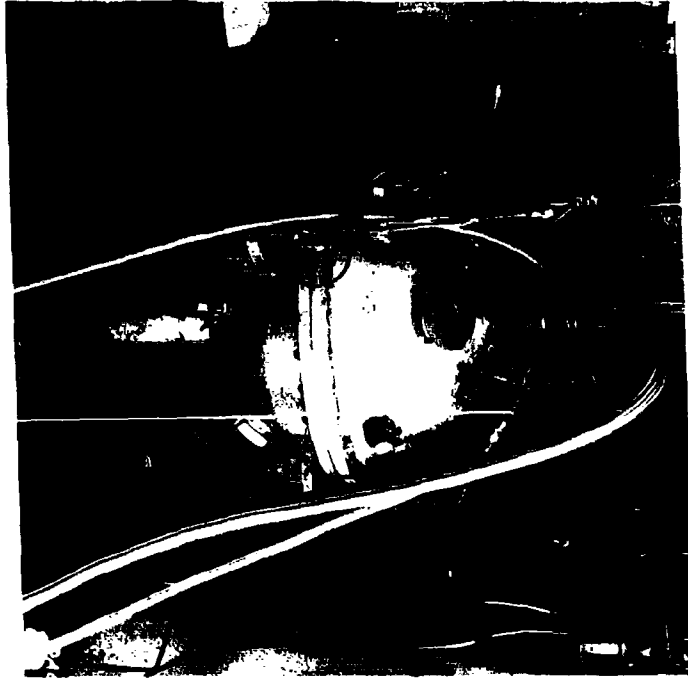


Fig. II-44 Research Fixture Assembled



Fig. II-45 Phase I Primary Tank with
Injector Installed

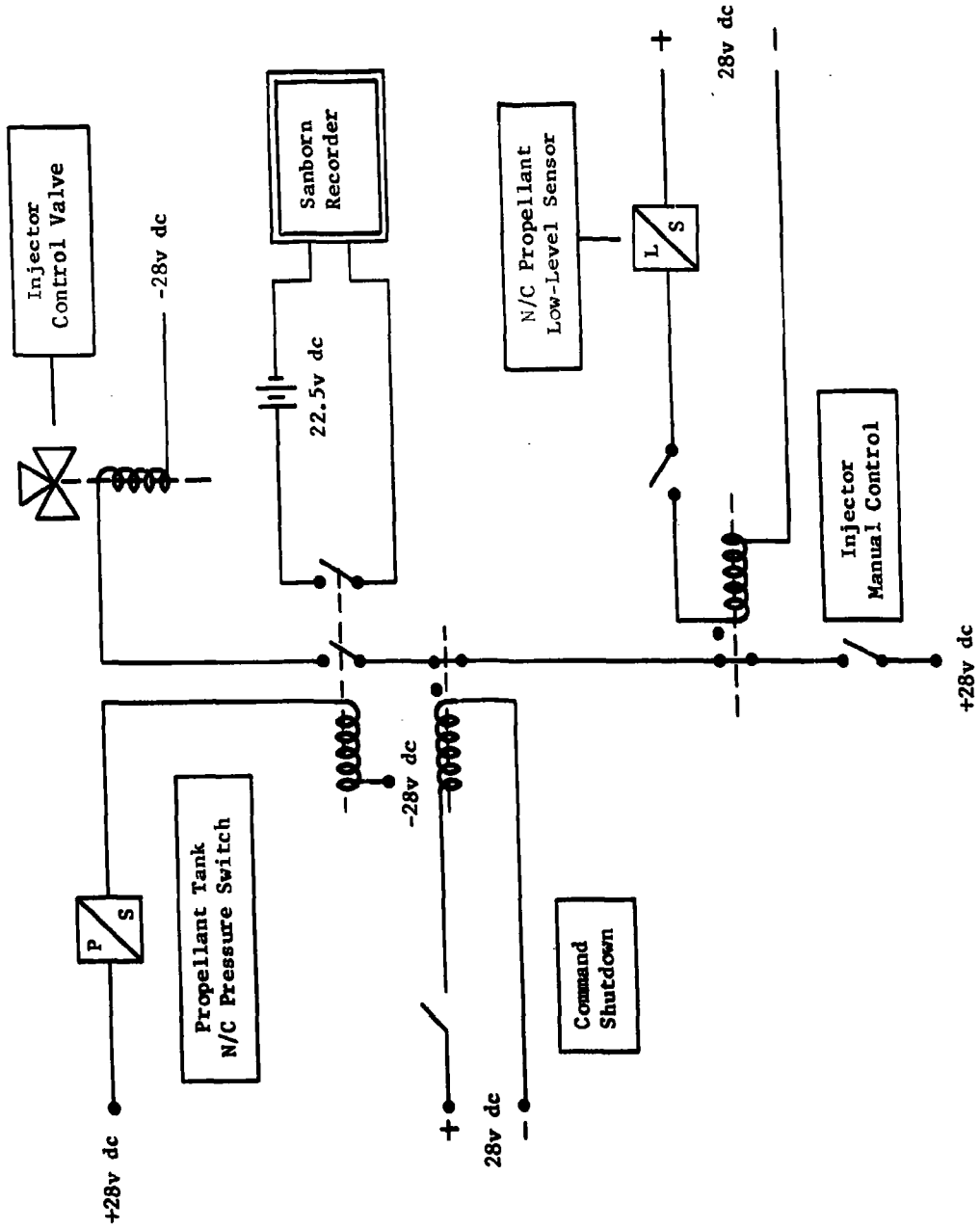


Fig. II-46 Injector System Electrical Schematic

2. System Description

The Phase I test system consisted of the control console, the research fixture, and the necessary instruments for data acquisition. The research test system consisted of two side-by-side spherical propellant tanks to permit common ullage pressurization experiments with simultaneous propellant outflow. Identical propellant expulsion systems were used for both the primary and secondary tanks, except an injector was installed in the primary tank. Figure II-47 shows a schematic of the complete system and Fig. II-48 shows a photo of the arrangement. Propellants were supplied to the main propellant tanks from the facility 55-gal storage drums under 10 psig nitrogen pressurization. Propellant expelled from the main test tanks was then stored in the catch tanks to permit rapid recycling for additional tests. The expelled propellants were observed through the sight glass at the tank outlets, and propellant flow was manually remotely controlled. Propellant loading and shutdown was controlled by liquid-level sensors to permit identical expelled volumes for test duplication.

Initial propellant tank pressurization can be provided by either helium or nitrogen through the dome loader pressure regulators. Nitrogen can also be used for relief valve and injector actuation in addition to pressurization of the reagent supply system. The reagent was supplied from a pressurized reservoir to the injector sight glass and then isolated from the facility system. A high-point bleed allowed entrained vapor to be vented for accurate measurement of reagent consumption. Each tank was separately pressurized with an isolation valve and a 1/4-psi differential pressure check valve installed in the common ullage line. All functions were observed by using appropriate instruments on the control console.

The MTI Phase I test console shown in Fig. II-49 provided remote control for all test phases including propellant and reagent loading, pretest pressurization, and automatic test sequencing. Important control and operating pressures were monitored by gages, while lights indicated all valve positions. In simultaneous common ullage propellant expulsion, an adjustable timer was used to give up to 1.3-sec oxidizer lead for simulating a typical engine start transient. The console provided malfunction detection with automatic shutdown in case of overpressurization, and normal shutdown in the event of visual or mechanical irregularities. The entire system was designed for fail-safe conditions during any part of the test operations.

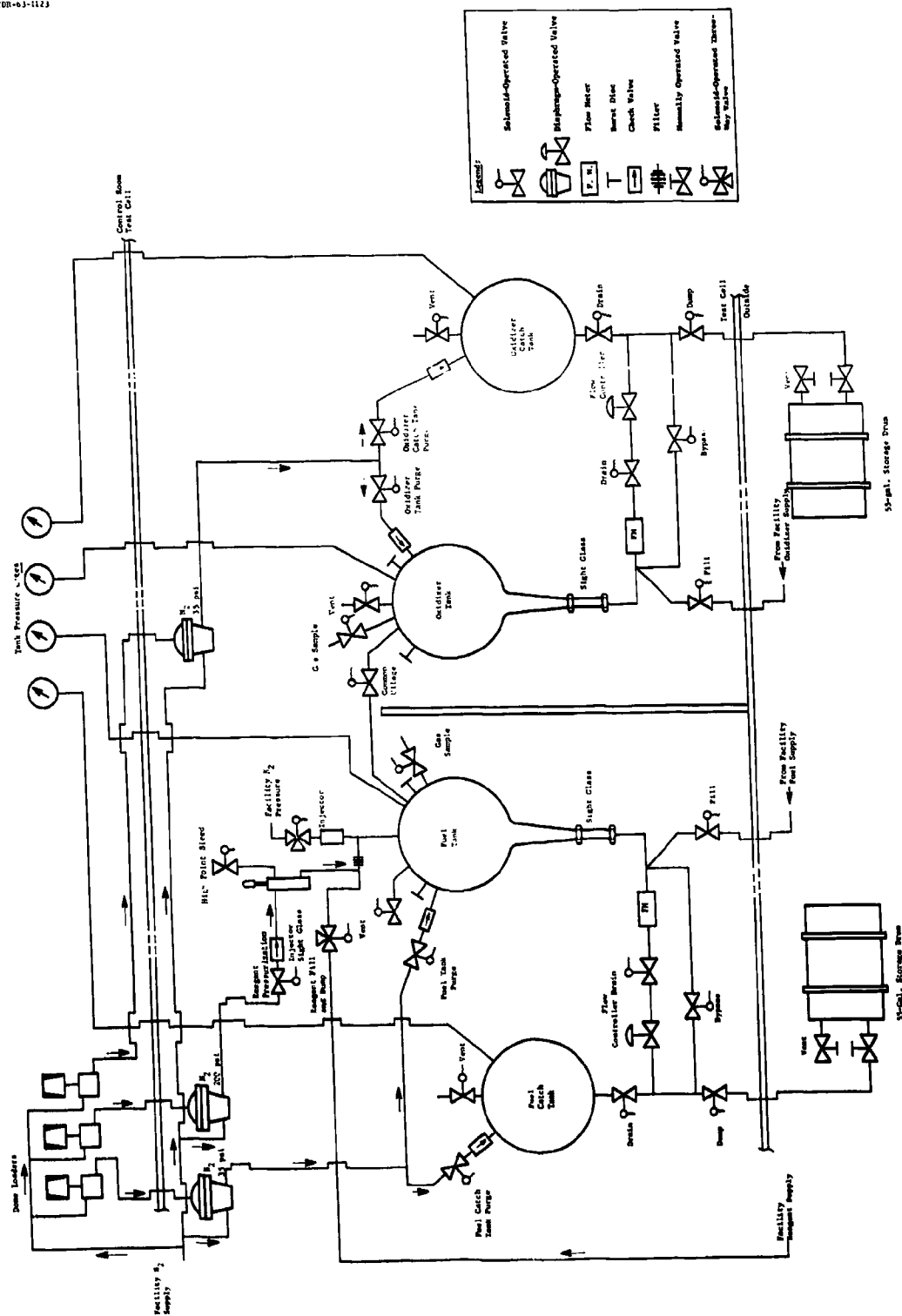


Fig. II-67. IRI Phase I Test System Schematic

RTD-TDR-63-1123

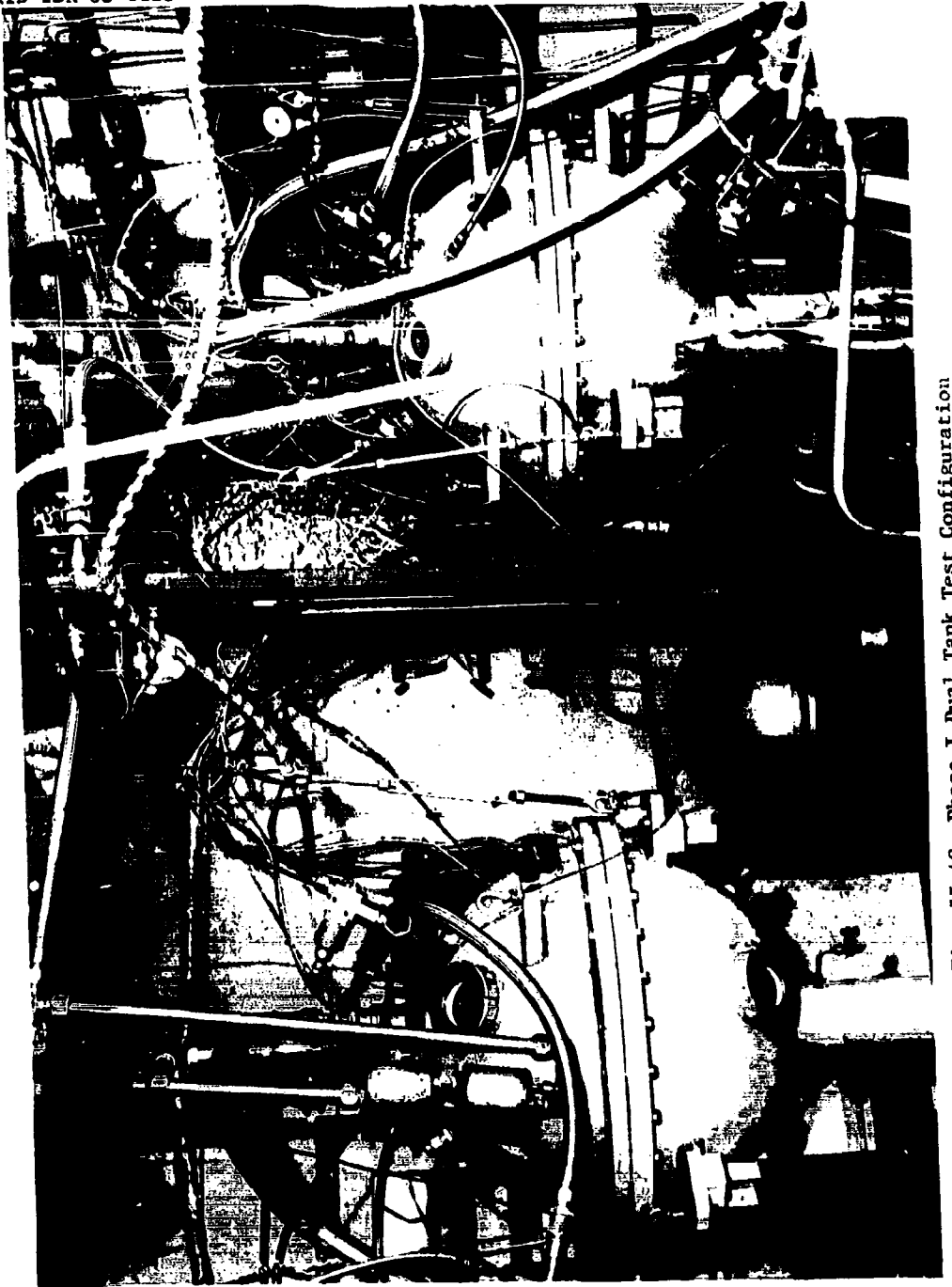


Fig. II-48 Phase I Dual Tank Test Configuration

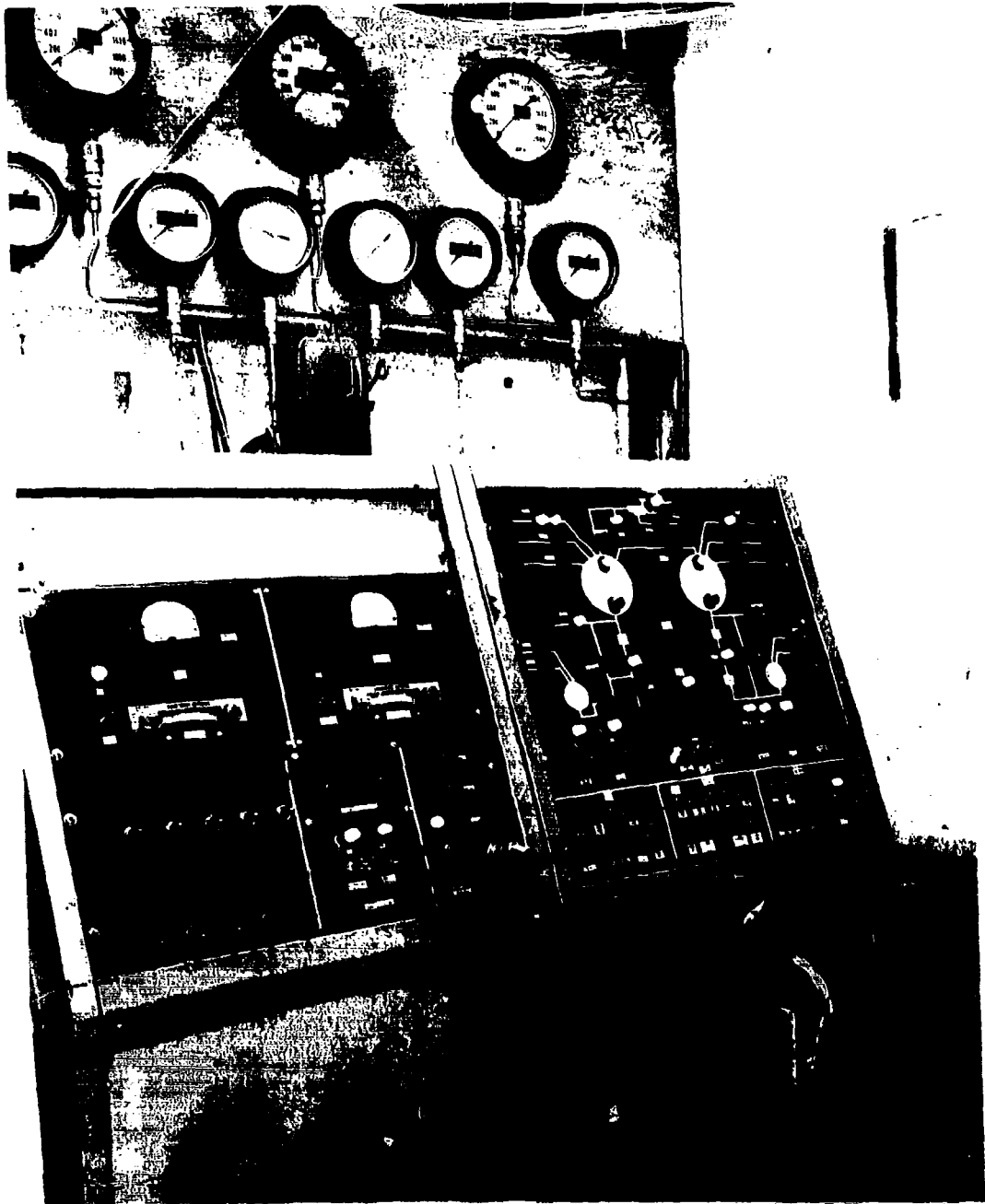


Fig. II-49 Research Fixture Control Console

The instrumentation monitoring system for the MTI Phase I program is shown in Fig. II-50. This system can process 42 data channels simultaneously with a 36-channel CEC oscillograph and a six-channel direct-writing Sanborn recorder. The Sanborn recorder was used exclusively for recording the critical test parameter required for quick-look data analysis. High-response parameters or those required for less urgent engineering analysis were handled by the CEC. Twenty-eight signal conditioning equipment channels, including 12 channels for bridge-type circuits, 12 for thermocouples, and four for flow-type measurements, were provided. All systems included calibration units to ensure 1% data accuracy.

Pressures were measured by CEC unbonded strain-gage bridge-type transducers and were temperature compensated. Principal measurements were propellant tank ullage and reagent supply pressures. Both shielded and unshielded chromel alumel type K thermocouples were used for measuring all liquid temperatures and the ullage gas temperature profile inside the tank. Tank wall temperatures were measured by copper-constantan type T thermocouples. Propellant flow measurements were obtained from Cox turbine-type flowmeters. Reagent mass flow was determined by a displacement technique due to the small quantities involved. A calibrated 1-in. diameter sight glass 18-in. long was found to have adequate capacity for all low-pressure tests; however, a parallel system was required for the higher operating pressures. Instrument locations are shown in Fig. II-51 for the common ullage tank arrangement and the measurement symbols are described in Table II-6.

A temperature rake was installed in the propellant tank to determine temperature distribution in the ullage and the extent of stratification in the fuel. Figure II-52 details the locations of the internal thermocouples as well as the tank wall measurements and gas sampling system used for the single-tank system.

Liquid temperature was also monitored at the tank outlet to establish the condition of the discharged propellant. Tank wall thermocouples were mounted on the external surface in three locations. Temperature profiles obtained by the internal instrumentation were augmented by photographic and television observation of the combustion process. In addition to the pressure, temperature, and flow histories recorded, four gas samples were also taken periodically during the run to provide additional performance data. The gas sampling system shown schematically in Fig. II-52 is detailed in Section C of this chapter. A chemical analysis of the propellant was also made on specimens acquired before and after each test to determine the extent of degradation and contamination. The sampling procedure is also described in Section C of this chapter.

RTD-TDR-63-1123

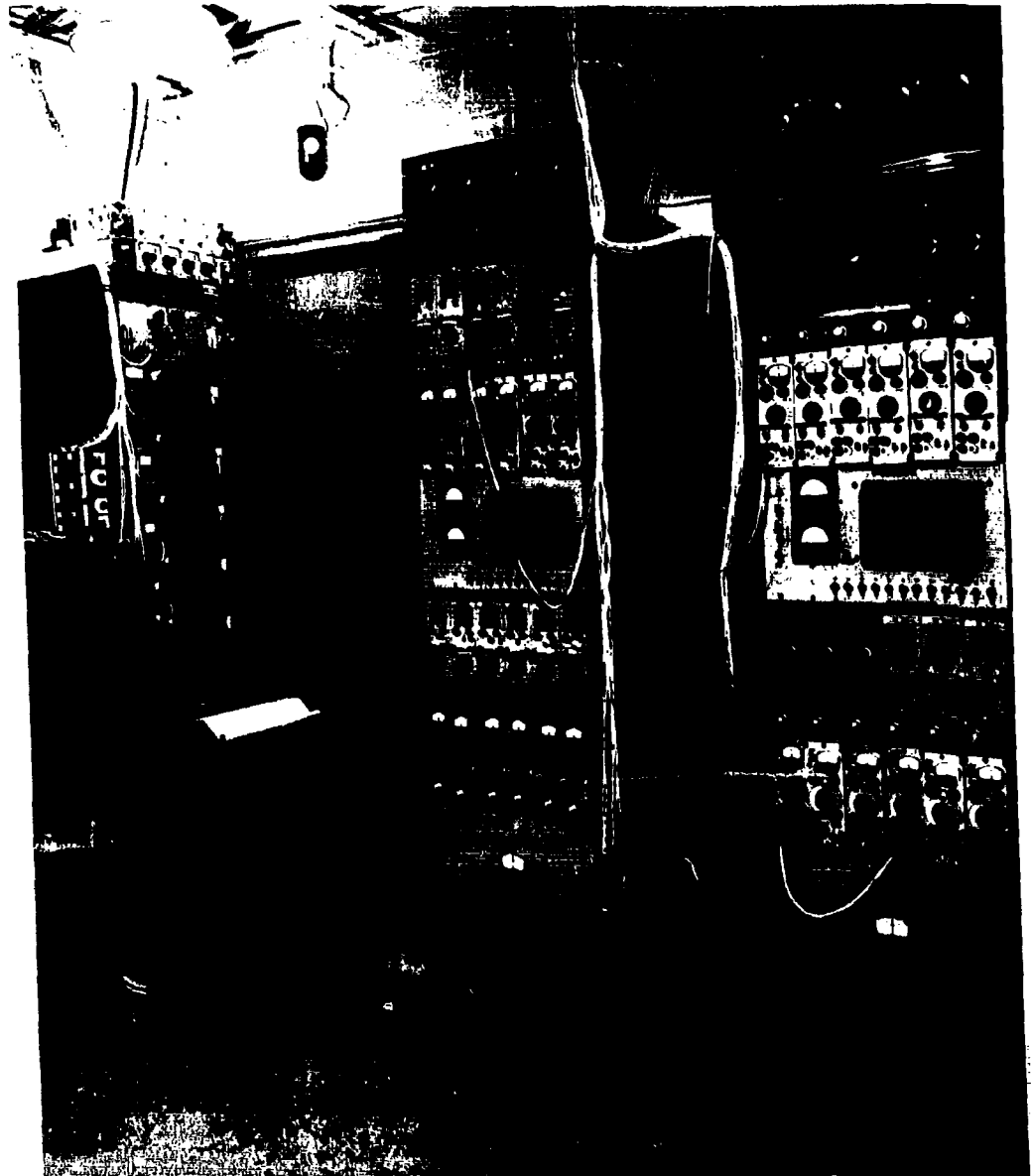


Fig. II-50 Research Fixture Instrumentation System

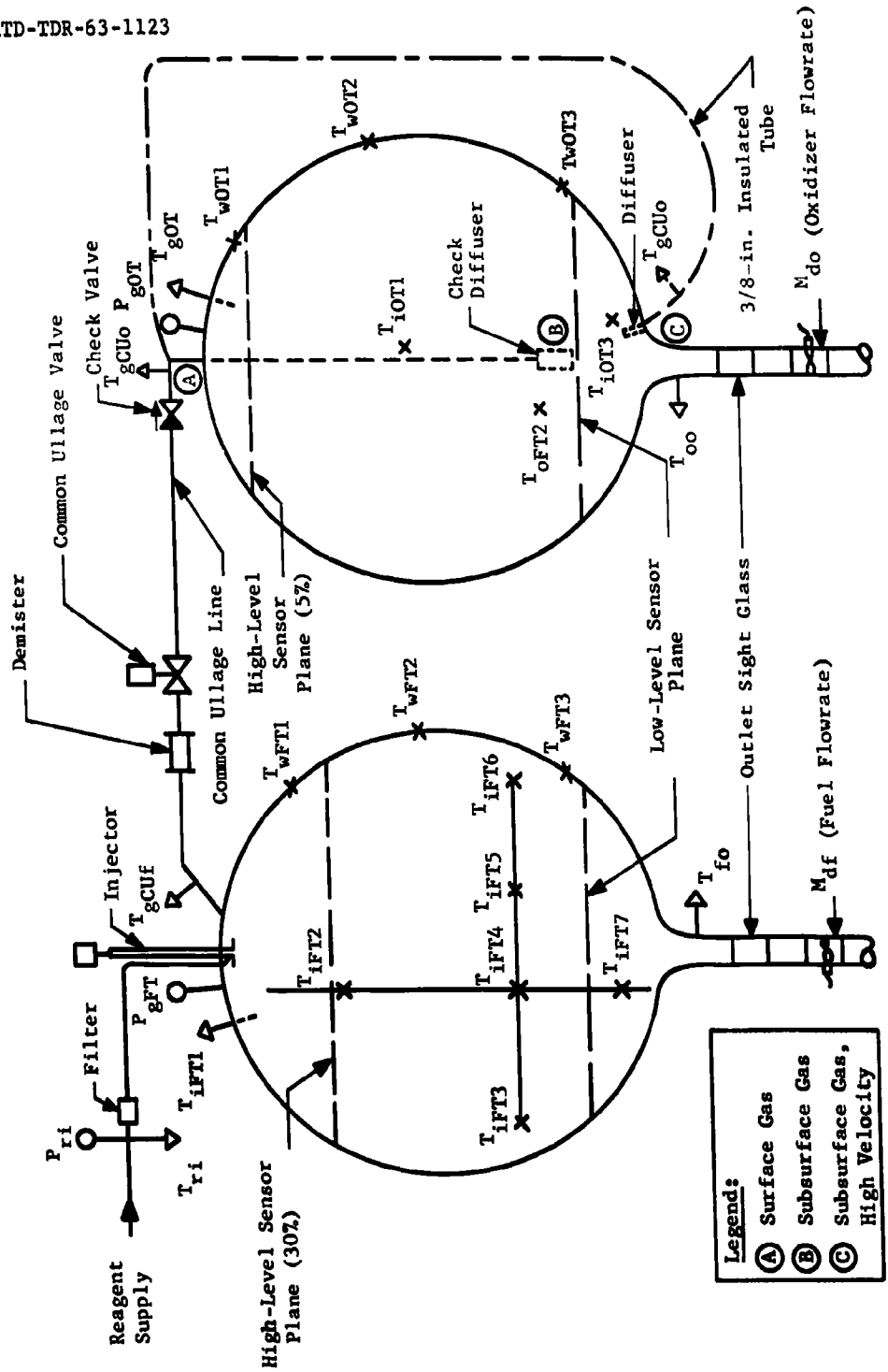
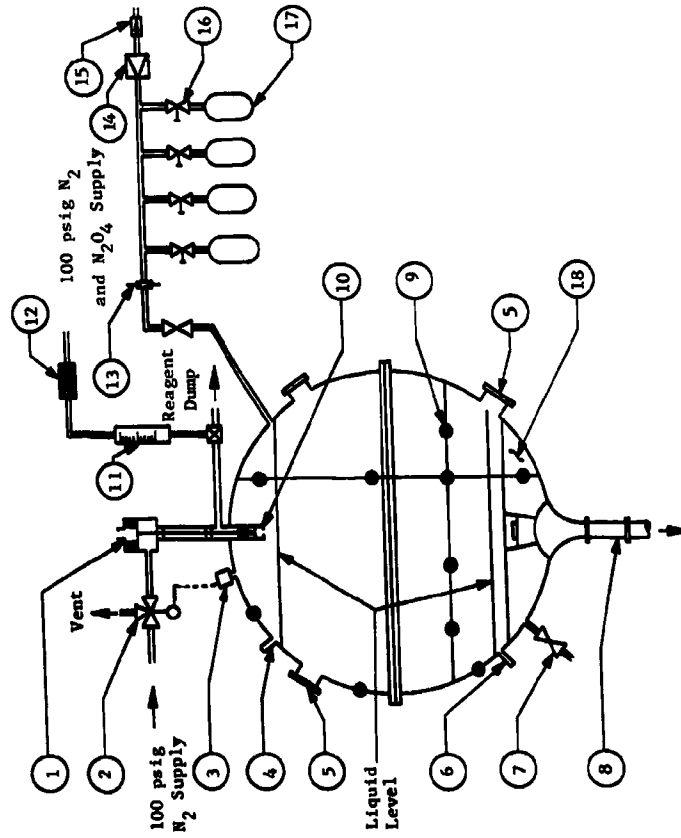


Fig. II-51 Phase I MTI Test Instrument Locations

Table II-6 Instrumentation Nomenclature

Symbol	Nomenclature
P_{gFT}	Gas pressure in fuel tank ullage
P_{gOT}	Gas pressure in oxidizer tank ullage
P_{ri}	Reagent injector supply pressure
M_{df}	Fuel mass flowrate
M_{do}	Oxidizer mass flowrate
T_{ri}	Reagent injector supply temperature
T_{iFT1}	Fuel tank rake temperature
T_{iFT2}	Fuel tank rake temperature
T_{iFT3}	Fuel tank rake temperature
T_{iFT4}	Fuel tank rake temperature
T_{iFT5}	Fuel tank rake temperature
T_{iFT6}	Fuel tank rake temperature
T_{iFT7}	Fuel tank rake temperature
T_{wFT1}	Fuel tank wall temperature
T_{wFT2}	Fuel tank wall temperature
T_{wFT3}	Fuel tank wall temperature
T_{fo}	Fuel outflow temperature
T_{gOT}	Gas temperature in oxidizer tank ullage
T_{gCUf}	Gas temperature in common ullage line, fuel tank outlet
T_{gCUo}	Gas temperature in common ullage line, oxidizer tank inlet



Component	
No.	Title
1	Injector
2	Three-Way Valve
3	Pressure Switch
4	High-Level Liquid Sensor
5	Photographic or TV Camera Ports
6	Low-Level Liquid Sensors
7	Propellant Sample Valve
8	Sight Glass
9	Thermocouples
10	Orifice Spray Tip
11	Reagent Measuring Device
12	Filter
13	Orifice
14	2-psig Back Press Regulator
15	Check Valve
16	Bottle Stop Cocks
17	Gas Sample Bottles
18	Propellant Baffles and Combustion Container

Fig. II-52 Phase I Fuel Tank Test Schematic

3. Test Description

The Phase I MTI research test program was conducted at the Martin-Denver Hazardous Materials Laboratory in an explosion-proof cell. Since the cell is open to atmosphere on the east side, the test system was fairly well isolated from afternoon solar heating effects or adverse wind conditions. Consequently, environmental factors did not appreciably effect the test results except for a few early development tests performed in 32°F weather. Primary system control as well as the recording equipment were in the block-house under controlled environmental conditions with a few operations performed outside to the complex. Although several series of tests were performed with single- and dual-propellant expulsion systems, the 150-sec test duration and operating procedures were maintained for all tests.

Before starting an MTI pressurization test, all instruments were calibrated in addition to a complete control system functional test. After the propellant specimens were procured and the gas sampling system readied, the reagent was loaded and a pressure decay check made to verify no injector leakage. Entrained vapor was bled from the system and the reagent level noted after the supply pressure was adjusted to provide a 75-psi injector differential pressure. Fuel was then loaded from the catch tanks since spillage could result in a fire that would be less hazardous with the oxidizer still in the storage system. Propellant levels were established by liquid-level sensors. In a common ullage test, oxidizer is loaded after the fuel and the tanks are pressurized either individually or through the fuel tank and common ullage system to approximately 40 psia by the facility gas supply. Nitrogen was initially selected for prepressurization, but helium was later used to better identify the combustion products generated. Initial pressurization of the ullage volume was originally established to provide a margin of safety if the injection system did not respond adequately to prevent overpressurization under conditions of minimum ullage and no propellant outflow (later tests indicated this precaution is unnecessary; however, prepressurization with helium may be desired to reduce total pressure weight).

The control console starts the test by automatically sequencing the propellant flow control valves. An 8-sec time delay was incorporated in the outflow system to provide final adjustment of the desired propellant flowrates. As the tank pressure decreased to within the injector pressure switch operating range, a reagent injection began to maintain the desired pressure within the pressure switch deadband by intermittent combustion. System operation was

monitored by both the control console instruments and Sanborn recording of critical pressures and temperatures in addition to TV observation of the reaction process. When required, gas samples were periodically taken during a test and a propellant specimen was acquired after test completion. Injection termination was signaled by the propellant low-level sensor, but outflow was continued in some tests to verify theoretical computations of residual propellant expulsion by ullage gas expansion. In some tests, additional system versatility was demonstrated by incorporating a 10-min coast period where propellant flow was discontinued, with and without continuous pressurization of the tank ullage. After a final reagent level reading, the system was purged and secured. In early tests, the injector was usually inspected for wear and contamination but later experience indicated satisfactory operation without cleaning or repair for five or more full-duration tests.

Fuel Tank Injection System Development - The injection system was initially developed on a single tank to avoid the possibility of undesirable secondary reactions in a common ullage bipropellant system. This enabled proper identification of the primary combustion products and permitted a more thorough examination of the basic process with nitrogen tetroxide solid-stream surface injection. From this experiment, the feasibility of this process for pressurizing the fuel tank was established. All tests completed were accomplished on the 5.33-cu-ft aluminum fuel tank with 30% initial ullage volume pressurized to 30 psig with nitrogen. A schematic of the test system is shown in Fig. II-52. The initial propellant load and expelled volume were identical for each run, established by the electronic liquid-level sensors providing duplication of the pressurized ullage volume for each test. Constant propellant flowrate was maintained during the 36-psia injector development tests.

Test Configuration - During the injector development process, it became apparent that adequate pressure control could be achieved by an on/off injection system; consequently, the effort was concentrated on improving this design. Since the injector was fabricated from a chemical spraying device, the initial tests indicated various mechanical deficiencies. In addition to material compatibility problems, the rapid cycling rate and severe environment inside the propellant tank presented additional difficulties. The first series of tests using a surface injection process was primarily hampered by injector plugging.

Several early tests with a 0.006-in. injector orifice were unsuccessful due to the presence of fine particles in the system. At this time, it was detected that some of the gaskets that appeared to be Teflon were actually nylon and had to be replaced with Teflon in addition to adding a 10-micron filter between the injector seat and orifice. These modifications did not prevent the injector from clogging. The filter was then installed further downstream in the system. Testing was resumed and plugging of the injector was again experienced. Since the injector had performed satisfactorily outside of the tank during pretest experiments, the formation of reaction products inside of the injector orifice was suspected. Also reactions had been observed in this area and gunk (unidentified fuel-rich compound) found on close examination of the injector after completion of a test. In order to minimize this condition, the volume between the injector seat and orifice was reduced. In addition, the original assembly was constructed with a tungsten carbide seat that had cracked sometime during service and was leaking. The decision was made to incorporate an aluminum seat to avoid these problems. The soft aluminum seat required that a guide be installed to align the injector rod with the seat. Excellent sealing was obtained at the seat with this design. Sealing rings had to be machined on the seat and orifice body to allow metal to metal contact for gasket elimination.

To alleviate the design problems associated with this commercial-type spraying injector, the assembly was revised so standard tubing connections could be used and to permit testing of two improved injector shutoff rods. The first design was a conventional 60-deg sharp tip valve that provided good sealing, but plugging of the orifice was again experienced. The second design employed a cleaning tip 0.004-in. in dia by 0.25-in. long. It was felt that this design would prevent reaction products from plugging the 0.006-in.-dia orifice; however, after several solid particles were found in the system, this theory was abandoned.

Since solid contamination was still present in the system, the design of the system was thoroughly checked. The particles were too small to be identified, so it was not possible to establish their origin. Chafing of the upper Teflon packing was later confirmed. The rod was polished and the packing replaced. The last remaining Teflon gasket between the injector seat and guide was also removed and a 10-micron cup filter installed in the swedge lock fitting. The filter was later removed since its effectiveness was limited by the clearance required for the injector rod passing through the center of the filter. Subsequently, a large capacity 20-micron filter was installed further upstream in the system that permitted several tests to be made.

At this point, it was discovered that the 0.006-in. sapphire orifice was somewhat marginal due to the greater-than-expected quantity of reagent required for propellant tank pressurization and the additional amount required for the generation of sample gas. An 0.008-in. stainless steel orifice was installed in the system and no pressure overshoot was experienced even though the injectant flowrate was increased 55%. Subsequent tests with a 0.009-in. dia aluminum solid-stream orifice indicated that adequate pressure control could still be obtained, and plugging was minimized. A test made with a 0.007-in.-dia 15-deg fan spray stainless steel orifice indicated that contamination was still present. This nozzle had to be modified to eliminate a noncompatible gasket that also hampered its use. Further testing with both the modified fan spray and solid-stream orifices indicated that additional development was still required to achieve the desired degree of reliability.

The injector was again modified to its present configuration (Fig. II-1), which has provided trouble-free operation in the last six tests. This design isolates the upper part of the injector by an aluminum injector rod guide. The reagent now enters the injector through a 0.125-in. OD (0.020-in. wall thickness) tube at the lower end, thus preventing particles originating in the upper portion of the assembly from entering the critical areas of the seat and orifice. The large-capacity 20-micron filter was installed at the inlet of the tube and the injector instrumentation was relocated to an upstream position. Since adequate pressure control was previously demonstrated by large diameter aluminum orifices an integral stainless steel orifice and seat design was evolved to eliminate sealing and alignment problems. This seat proved to be more durable than the aluminum, yet provided good sealing when lapped to the valve. The increase in orifice size to 0.012 in. posed no machining problems in the harder stainless steel. A subsequent test run with a 0.015-in. solid-stream orifice still permitted pressure control within ± 0.6 psi. The stream penetration into the fuel with the larger orifice was significantly greater than with the smaller orifice.

Some of the various injector orifice tips are shown in Fig. II-53. The 0.006-in. dia sapphire orifice fitting is shown as Item A in Fig. II-53. The sapphire is press fit into the back side of the stainless steel fitting and not visible in this photograph. Item B is an 0.008-in.-dia stainless steel orifice tip that was used in conjunction with the specially designed aluminum Seat C. The sealing rings machined on the face were required to eliminate external leakage. The tapered section on the discharge end was constructed to minimize injector ullage between the seat and orifice to avoid reaction products being formed. The included angle of the seat is 1 deg greater than the injector needle valve to provide efficient internal sealing. The 0.007-in.-dia 15-deg fan spray injector is shown as Item D in Fig. II-53. This is a commercially available design constructed of stainless steel with a tungsten carbide orifice insert. Item E is an experimental aluminum seat that was used in the orifice assemblies without integral seats. Item F is a 0.009-in.-dia aluminum orifice shown from the back with its integral 60-deg included angle seat. A similar 0.015-in.-dia solid-stream aluminum orifice and seat is shown as Item G. The final orifice configuration (Item H) evolved is a stainless steel design with a 0.009-in.-dia orifice and integral seat.

Test Results - The test effort completed during this test series was primarily concerned with injector development and securing ullage gas composition data. To establish a dependable pressurization system, 18 single-tank tests were performed with various injector configurations. Of the 18 tests performed, seven were only partially successful and the data were not reduced. In three of the remaining tests, system operating conditions were not controlled with sufficient accuracy for performance evaluation because of injector operating problems and a faulty gas sampling technique. The injector operating problems have been attributed to contamination by solid impurities and have been alleviated by the improved design.

Of the successful tests, five were performed with a 0.006-in.-dia solid-stream orifice with one each using a 0.009-, 0.012-, and 0.015-in.-dia orifice. The results are summarized in Table II-7 for the average data obtained. Each test was run under identical conditions except for ambient temperature that was approximately 50°F for the 0.006- and 0.009-in.-dia orifices and 35°F for the 0.012- and 0.015-in.-dia orifices. Approximately 185 lb of fuel were discharged in each 150-sec test.

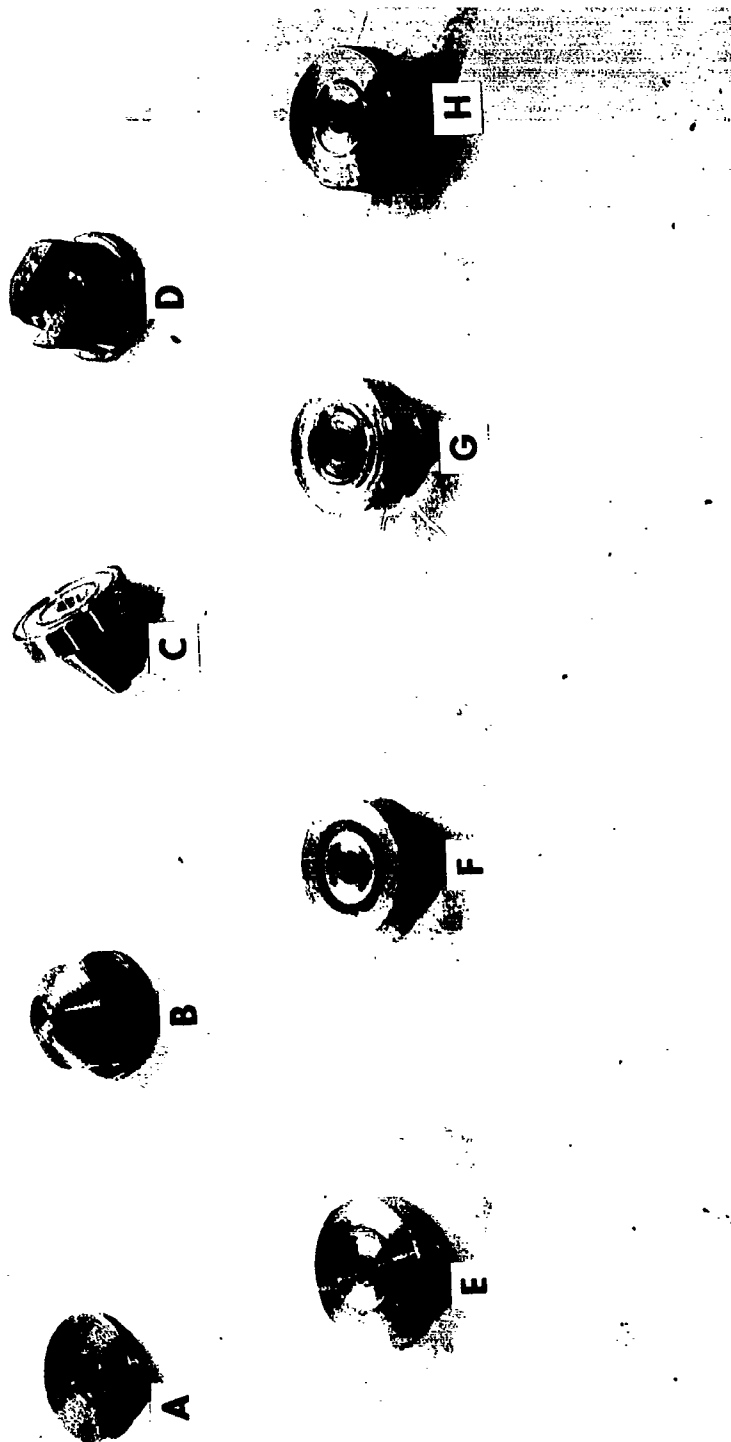


Fig. II-53 Phase I Injector Orifice Tips

Table II-7 Summary MFI Injector Development Tests

Injector Orifice	T _{Gas} (°F)	ΔT _{Fuel} (°F)	ΔT _{Wall} (°F)	N ₂ O ₄ Used (lb)
0.006-in.-dia Sapphire	247	6	18	0.185
0.009-in.-dia Aluminum	211	9	7	0.177
0.012-in.-dia Stainless Steel	180	17	13	0.207
0.015-in.-dia Aluminum	176	12	17	0.174

Test conditions were:

- 1) Single tank with N₂O₄ solid-stream surface injection at 100 psig;
- 2) 30% initial ullage volume pressurized with nitrogen to 41.7 psia;
- 3) Fuel tank pressure 36 psia and expulsion at 1.26 lb/sec.

Nitrogen initial pressurization was used to avoid system over-pressurization with initial small ullage volume and no propellant outflow. Pressure control was within ±0.25 psi for all tests during propellant expulsion. The gas temperatures, obtained 2 in. from the upper dome, are maximum values. Final fuel temperature was obtained by a probe in the propellant tank outlet with a residual 0.42 cu ft of liquid remaining in the tank at the end of the run. Propellant tank wall temperatures were measured externally at three locations with the highest reading reported. The quantity of reagent consumed was determined by actual measurement. Typical pressurization system performance curves are presented in Fig. II-54 thru II-56 to show the actual conditions during a 150-sec test. These data were compiled for solid-stream surface injection with a 0.012-in.-dia injector. Tank pressure was maintained within ±0.25 psi throughout the run while the injection frequency varied from 2.6 cps at the start of the run to 2.1 cps near the end. The gas sample valve was opened 10 sec after test initiation, allowing continuous gas bleed through a 0.025-in. orifice. A total of 0.206 lb of reagent was used, which was slightly higher than the average test. This was attributed to the low, ambient 39°F temperature. Figure II-54 shows basic pressurization system performance for the small-scale test fixture during a typical fuel expulsion. The internal and external temperature distributions in the propellant tank are shown in Fig. II-55 and II-56, and thermocouple locations are identified. In all tests conducted to date, a precise definition of the temperature profile in the combustion zone has not been possible, so the anticipated 1600°F flame temperature has not been verified.

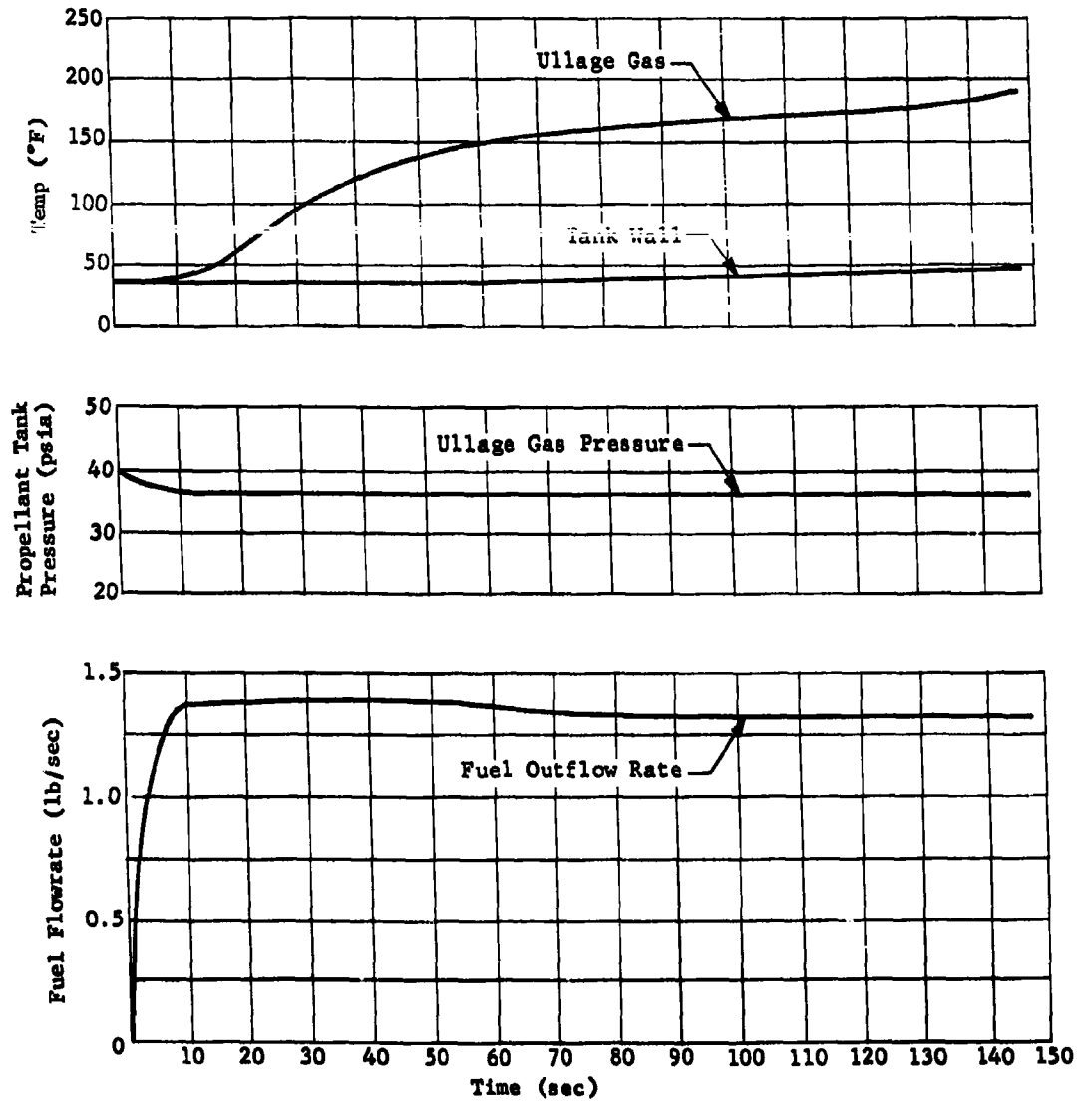


Fig. II-54 Typical Single Tank Pressurization System Performance with Solid-Stream Surface Injection

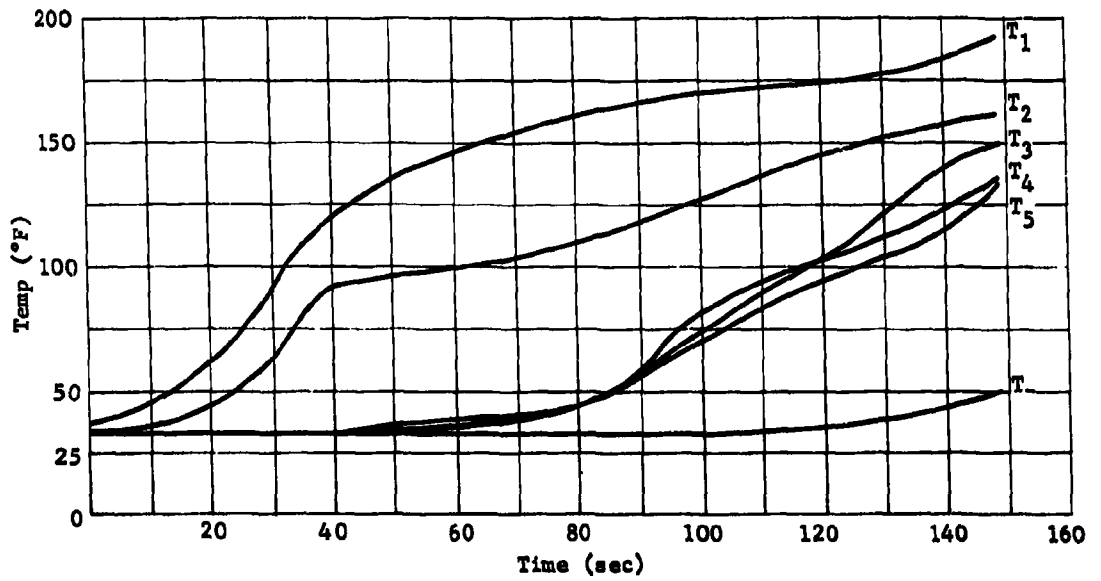
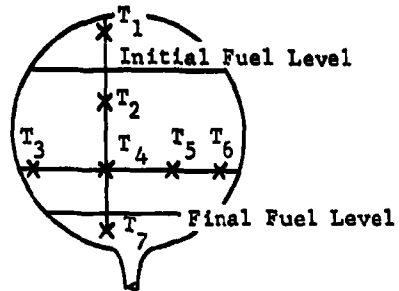


Fig. II-55 Fuel Tank Internal Temperature Profile

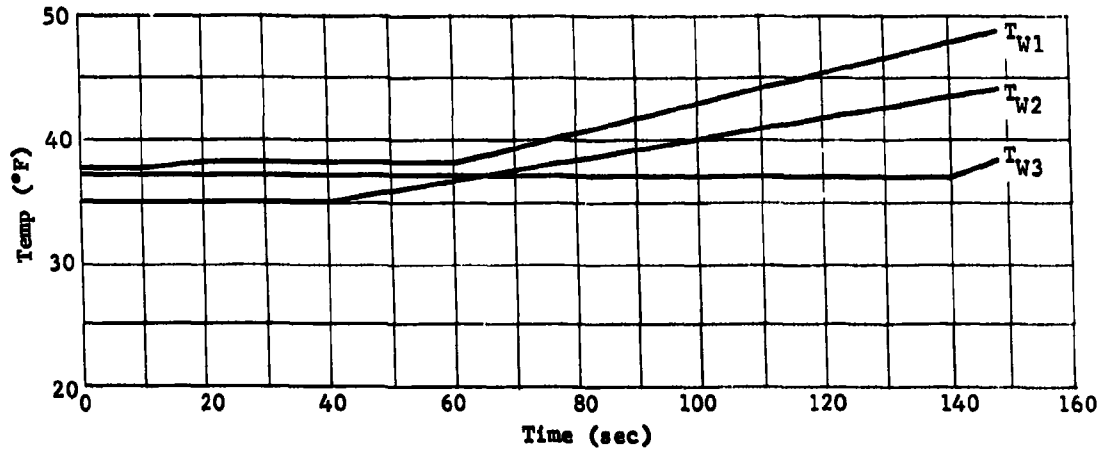
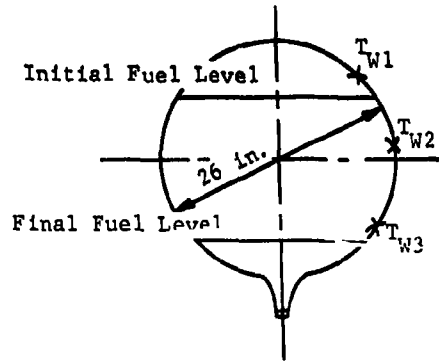


Fig. II-56 Fuel Tank Wall Temperature Profile

System Performance Analysis - The fuel tank solid-stream surface injection system was evaluated to determine the validity of the early version of the analytical model. In Fig. II-57, actual data are compared with predicted performance as functions of reaction mixture ratio (reaction mixture ratio is defined as the ratio of oxidizer to fuel mass consumed in the reaction process). Both the variation and average data are presented to show the degree of correlation with predicted values. Although minor modifications are required to adjust the heat balance, the quantity of reagent used is approximately twice that predicted for the reaction mixture ratio of 0.42 obtained due to the amount of condensibles formed. The apparent reagent consumption correlation in Fig. II-57 at a reaction mixture ratio of 1.25 has no significance since the theoretical computation was based on an assumed gas molecular weight of 19.5 and the actual molecular weight obtained was 13.

The theoretical quantity of reagent used was originally based on the quantity of combustion products formed and predicted range of reaction mixture ratios assuming no condensation occurs. In this computation, a combustion gas molecular weight and composition was determined from the theoretical equilibrium calculation for the assumed mixture ratio. The results of this computation are shown in Fig. II-58. For the combustion product molecular weight of 13, the theoretical reaction mixture ratio of 0.57 from Fig. II-58 is slightly higher than the actual 0.42 reaction mixture ratio determined from a mass balance. The actual reaction mixture ratio was based on the measured quantity of reagent consumed and total amount of products produced, as described by the following relation:

Reaction Mixture Ratio =

$$\frac{\text{Mass Oxidizer Consumed}}{(\text{Total Mass Products Produced}) - (\text{Mass Oxidizer Consumed})}$$

where the total mass of products produced includes condensed water and any other identified condensed products found in addition to the mass of combustion gas generated.

The mass balance performed required that the total quantity of combustion products generated be determined, including the part that condensed in the system and was consequently not included in the gas analysis. Since the actual amount of fuel consumed in the reaction could not be determined from test data, the unidentified products of reaction were assumed negligible so a probable reaction mixture ratio could be established.

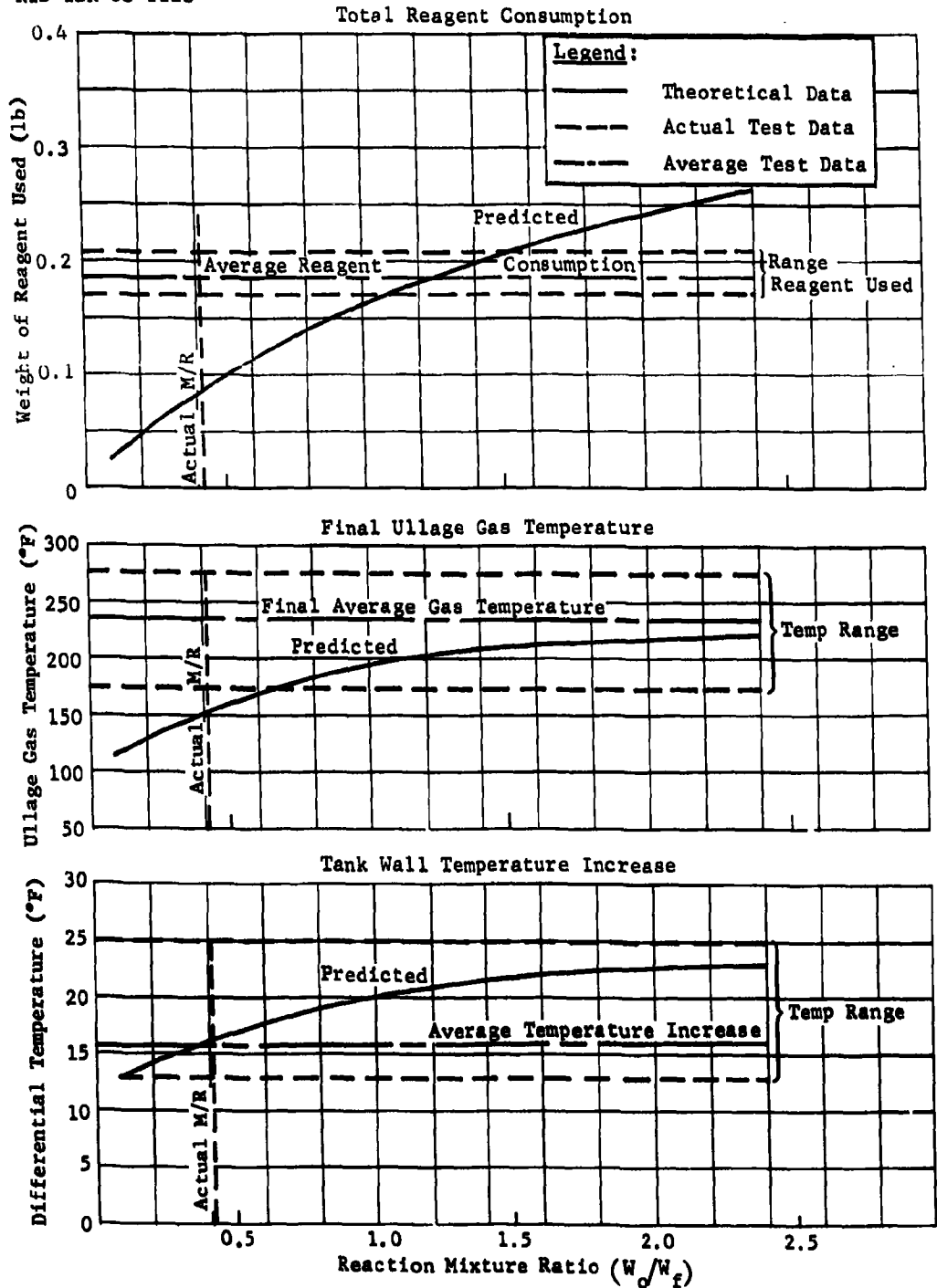


Fig. II-57 Phase I Fuel Tank Pressurization System Performance Evaluation (N_2O_4 Solid-Stream Surface Injection, Single Tank Test)

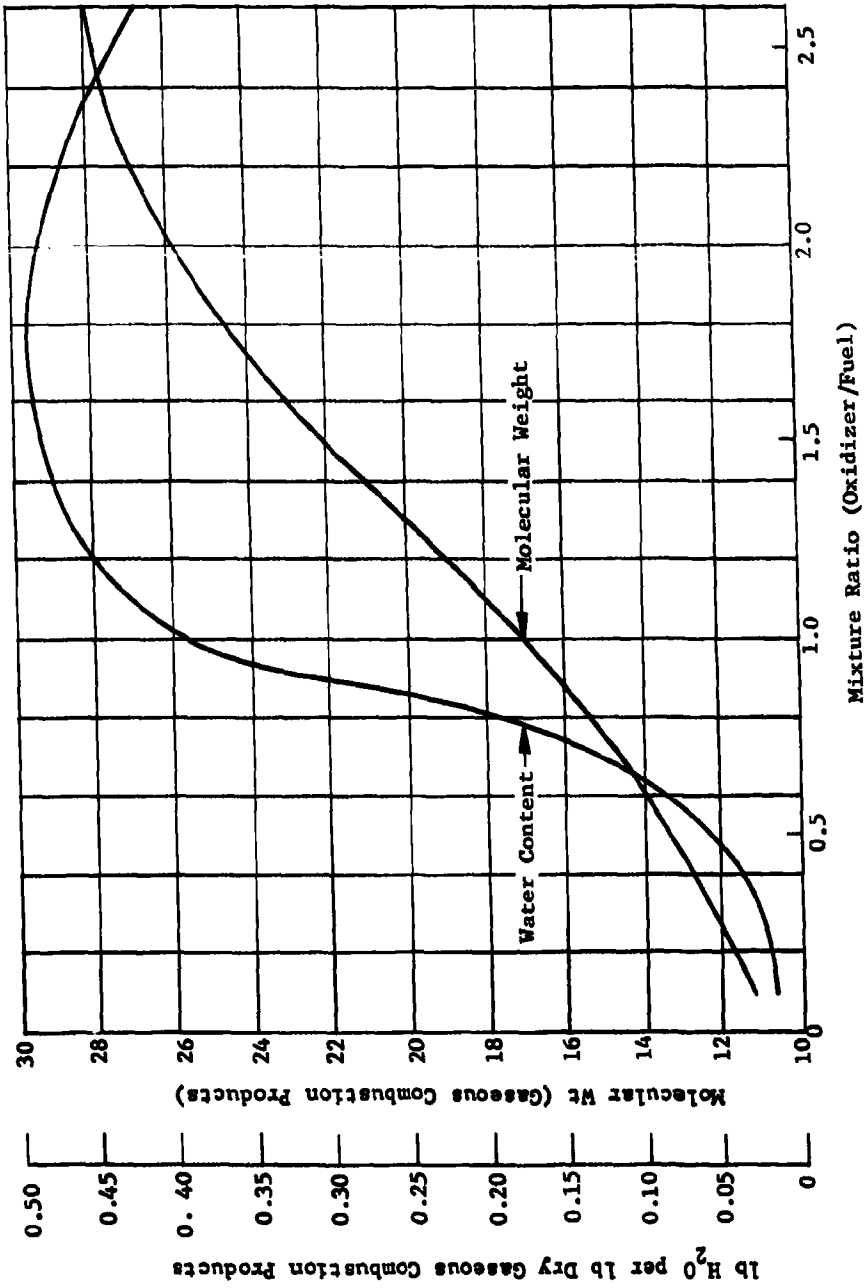


Fig. II-58 Theoretical Molecular Weight and Water Content of Gaseous Combustion Products vs Reaction Mixture Ratio

An attempt was made to further define the condensible products of reaction so the actual reaction mixture ratio could be verified; however, due to the complexity of the problem, an accurate identification was not possible. The actual quantity of gaseous combustion products generated was calculated from the physical characteristics of the system as a function of gas molecular weight for the actual final average ullage gas temperature, and is plotted in Fig. II-59, including a small part that was bled from the system continuously for gas analysis. A small computer program was formulated for this purpose and is described in Appendix A. The actual amount of condensible products formed was established from the increase in water content of the fuel. The 1.75 lb water/lb of combustion products estimated from the percentage of water in the final fuel specimen is substantially greater than predicted (Fig. II-58). Although the maximum quantity of water produced, based on a material balance (0.78 lb/lb of reagent consumed), is significantly lower than the estimated amount of 2.16 lb/lb of reagent determined from test data, the resultant error in apparent mixture ratio will be reduced since other condensibles formed are not included. Table II-8 summarizes the mass balance for the solid-stream surface injection system.

Table II-8 Single Tank Solid-Stream Surface Injection System Mass Balance

Reagent Consumed (N_2O_4) (lb)	Gas		Water		Reaction Mixture Ratio W_o/W_f
	Molecular Wt	Actual Wt (lb)	Fuel (%)	Est Wt (lb)	
0.185	13	0.227	0.2	0.4	0.42

From the actual composition of the reactants, a material balance was attempted to determine the exact quantities of reactants required to produce the various constituents of the combustion gas. Although the primary objective was to determine the quantity of fuel going into the reaction, this analysis was also required to identify the condensed products of reaction.

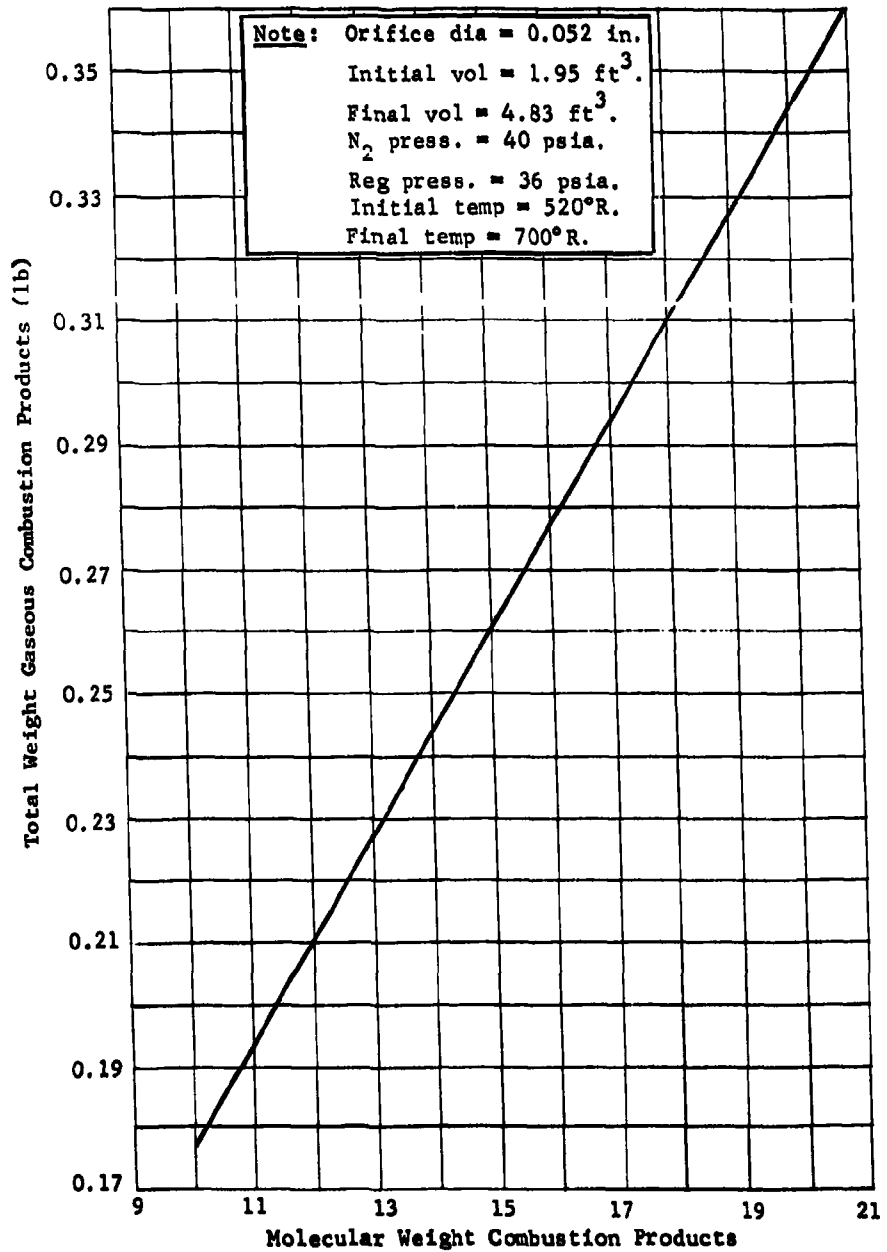


Fig. II-59 MTI Gaseous Combustion Products Total Weight vs Molecular Weight for the Small-Scale Single-Tank System

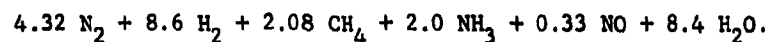
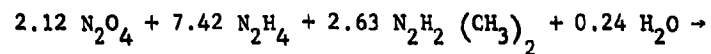
In this computation a particular test was selected with the following combustion gas composition:

<u>Constituent</u>	<u>Volume (%)</u>
N ₂	0.249
H ₂	0.497
CH ₄	0.120
NH ₃	0.115
NO	0.019

Due to the absence of water in the combustion products, the material balance was made assuming that all the available oxygen from the nitrogen tetroxide went into the formation of water. For this particular test, 0.195 lb of reagent was consumed to form 0.215 lb of combustion products with an estimated 0.32-lb increase in water content detected in the fuel. The fuel analysis before test showed the following composition:

<u>Constituent</u>	<u>Volume (%)</u>
N ₂ H ₄	0.544
N ₂ H ₂ (CH ₃) ₂	0.395
H ₂ O	0.011

Based on an assumed reacted fuel quantity of 0.4 lb, the following material balance was established:



By analyzing the above equation it is apparent that an exact material balance has not been achieved, primarily due to a shortage of nitrogen (0.187 lb) in the combustion products. Since a small quantity of both hydrogen and carbon is also absent from the analysis of combustion products, the resultant material missing may be the unidentified material condensed in the system. From the oxygen balance performed, the resultant mass of water formed

was 0.15 lb compared with 0.32 lb present in the fuel. The additional product of reaction required to balance the equation is 0.227 lb. In establishing the quantity of fuel going into the reaction, the hydrogen balance was considered to be the best approach. The large quantity of water produced was considered excessive in view of the quantity of reagent consumed. From the results of this material balance the reaction mixture ratio for this particular test was 0.487 compared with the average of 0.42 obtained by a pure mass balance.

In an attempt to resolve the nitrogen discrepancy in the material balance, helium was used in future tests to permit direct identification of the composition of the combustion products. Since small quantities of a viscous brown liquid were detected in the pressurization system in addition to a slight discoloration of the fuel, additional analysis, required to determine the composition of the unidentified substance referred to as gunk, is described in Chap. II.A.3. The high water content of the fuel can be explained by the hygroscopic nature of the fuel and inadequate storage of the specimen before analysis.

The injector development tests performed at 36 psia under a variety of conditions with various injector designs have furnished considerable data for determining the effects of orifice size on the reaction process and system thermodynamics. A study of the shape and size of the combustion zone identified by photographic observation has been made to correlate the theory employed in the analytical model. The amount of penetration of the reaction process into the fuel during this series of tests has been related to the mass flowrate change introduced through a variation in orifice size. The injection velocity was an independent variable for all tests since the injector differential pressure was held constant at 75 psi. An examination of the basic flow equations shows the influencing factors. Assuming a constant orifice discharge coefficient for the variation in test conditions, the reagent mass flowrate is:

$$\dot{m}_R = C_d A_o \sqrt{2g_c \rho_R \Delta P}, \text{ lb}_m / \text{sec} \quad [1]$$

where

C_d = discharge coefficient, 0.70

A_o = orifice area, sq ft

ρ_R = reagent density, 90 lb_m/cu ft

ΔP = orifice differential pressure, lb_f/sq ft

g_c = gravitational constant, 32.17 ft/sec².

By substituting Eq [1] in the continuity equation, the injection velocity is:

$$V = \frac{C_d \sqrt{2g_c \rho_R \Delta P}}{\rho_R} \text{ ft/sec.} \quad [2]$$

As can be seen from Eq [2], the injection velocity is independent of the orifice size for a given fluid and differential pressure. The mass flow is directly proportional to the square of the orifice diameter. The variation in penetration obtained from the injection process and consequently the amount of heat transferred to the propellant during the completed series of tests are therefore due to the change in mass flowrate resulting from the variation in orifice diameter.

Propellant penetration into the fuel as well as the temperature increase in the fuel vs orifice diameter are plotted in Fig. II-60. These results were obtained from photographs of the combustion process and liquid temperature measurements. The heat transfer to the fuel appears to be proportional to the surface area of the combustion zone for the range in orifice sizes tested. Since the amount of temperature stratification in the residual fuel is not known, an accurate account of the total amount of heat transferred cannot be determined. A heat balance to correlate the test results and further identify process characteristics is contained in Chap. III.A.

The ullage gas temperature increase due to the solid-stream surface injection process has been moderate (200°F) since approximately 75% of the available energy is transferred to the propellant. The reduction in gas temperature resulting from the increase in quantity of heat dissipated to the fuel with the larger orifice diameters is shown in Fig. II-61. The decrease in gas temperature is smaller than anticipated, due to the relatively large gain in propellant temperatures, since the heat capacity and quantity of fuel are much greater than those of the gas. The resultant 10% decrease in ullage gas temperature contributes to the slight increase in reagent consumption.

The wall temperature data compiled showed little effects other than being functions of the temperature and time exposed to the ullage gas. The tests that gave a higher gas temperature resulted in a slightly higher wall temperature. The increase was only 1°F for every 25°F change in ullage gas temperature over the test range. The wall temperature data shown in Fig. II-62 are corrected for the initial ambient conditions by showing the relative change.

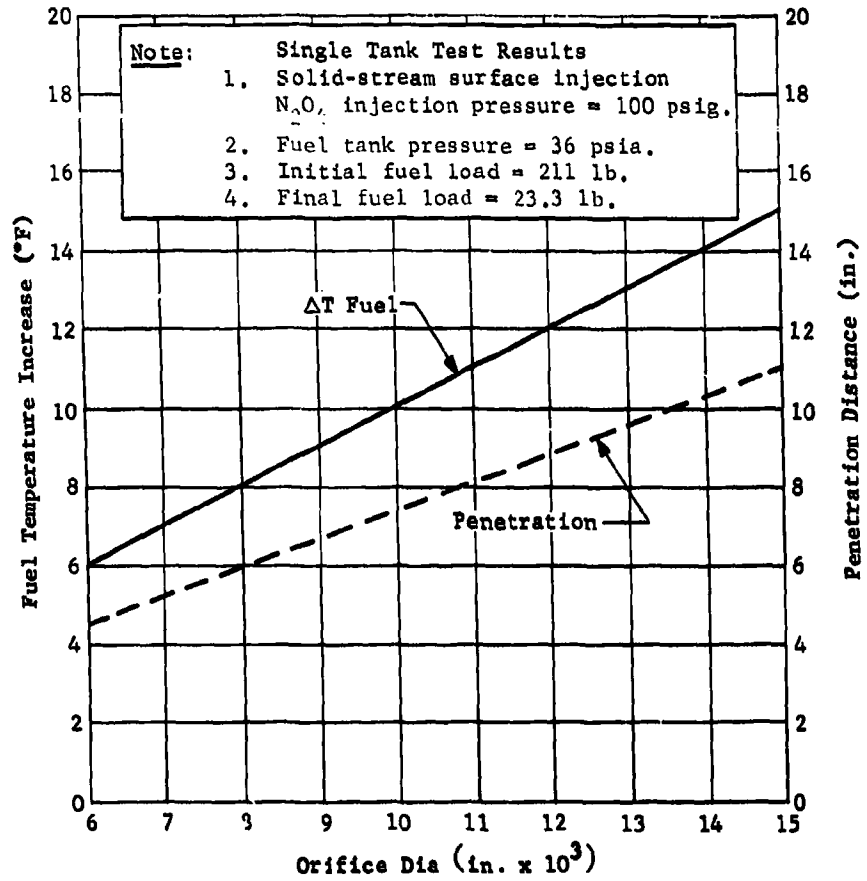


Fig. II-60 Injector Orifice Size Effects on Fuel Combustion

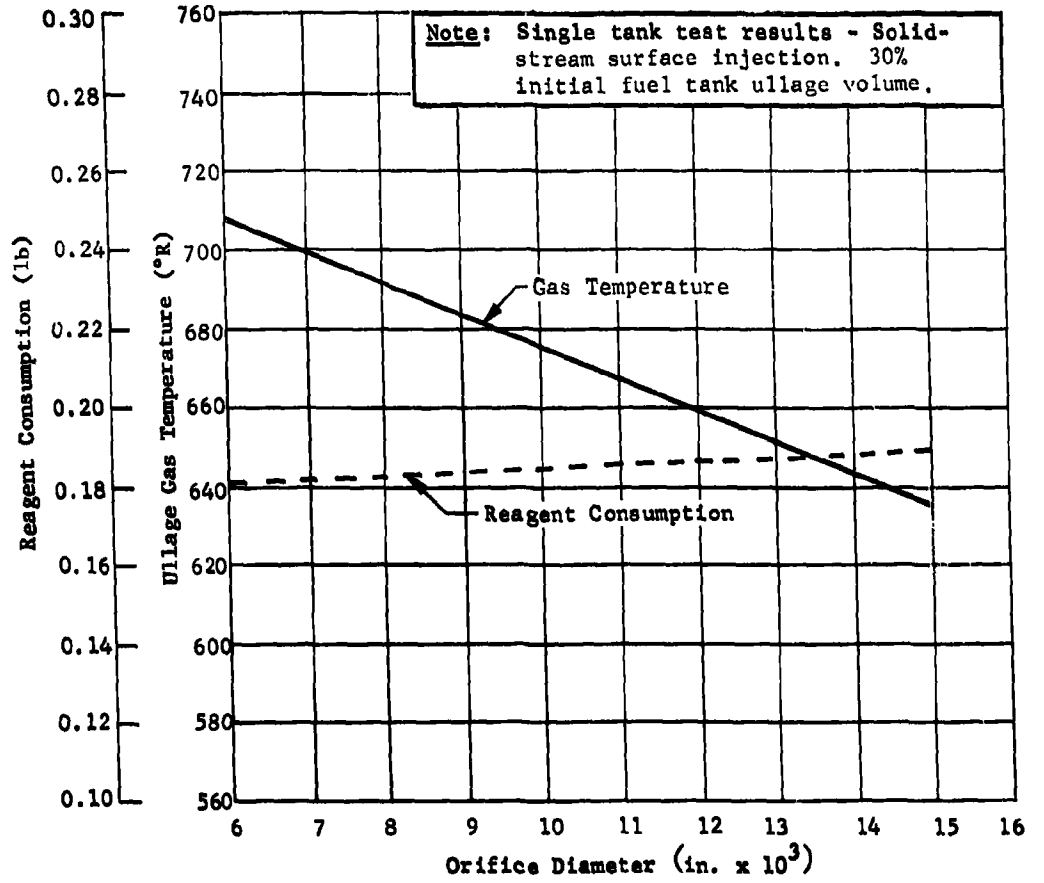


Fig. II-61 Orifice Size Effect on Ullage Gas Temperature and Reagent Consumption

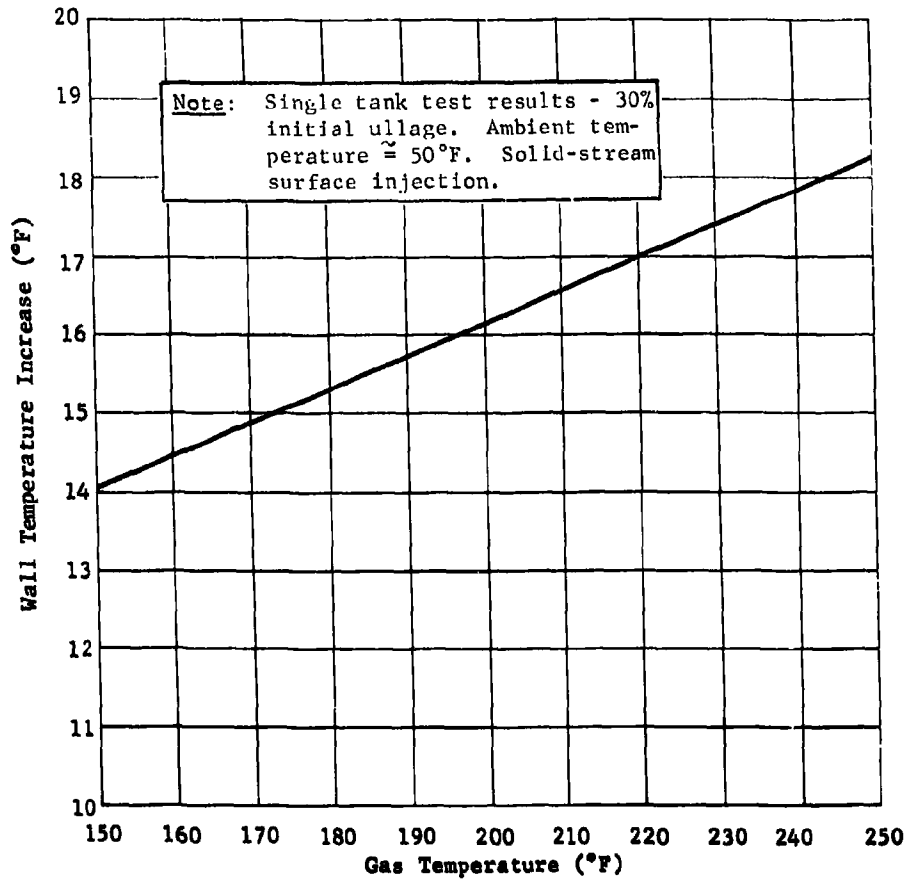


Fig. II-62 Fuel Tank Wall Temperature vs Ullage Gas Temperature

Since the amount of heat dissipation to the liquid propellant, hence penetration distance of the injected reagent, are particularly important to reduce ullage gas and tank wall temperatures, additional study of this phenomenon was performed in an attempt to establish the influencing factors. To assess the relative importance of injection velocity and injector orifice size, both a theoretical and an experimental program were undertaken. Based on a nonreaction process, an attempt was made to correlate this theory with the actual combustion data obtained from the research test fixture. The nonreacting process study was performed by the downward injection of colored water into a water-filled 5-gal. cylindrical glass container calibrated with a 1/2-in. grid. The process was analyzed by inspecting motion pictures taken at 200 fps. Water was injected through orifices of 0.006, 0.135, 0.015, and 0.040 in. in dia at differential pressures of 75 and 150 psia (higher differential pressures caused the solid stream to break up and were not considered in this investigation). The data obtained are summarized in Table II-9. Particularly interesting was the fact that a maximum penetration distance was reached in each nonreacting test, conversely to a reacting-type process that appears to be limited only by the injection duration or the physical boundary of the system.

Table II-9 Nonreaction Injection Penetration Test Data

Orifice Dia (in.)	Injector ΔP (psi)	Penetration (in.)	Time to Max Penetration (sec)	Penetration Rate Average (in./sec)	Injection Velocity (in./sec)
0.006	75	3.5			945
0.015	75	6.0	0.030	222	945
0.0135	75	6.0	0.030	222	945
0.0135	150	8.0	0.025	320	1340
0.040	75	13.0	0.053	244	945
0.040	150	15 (est)	0.048 (est)	315	1340

All data reported were determined from the photoanalysis except the injection velocity, which was computed. Particularly significant was the penetration distance, which increased linearly with the orifice diameter for a given injection velocity and was proportional to the square root of the differential pressure across the orifice. The average penetration rate was approximately 50% of the theoretical maximum and independent of orifice size, as expected from an inspection of the influencing parameters.

Based on an energy balance relating pressures at the stagnation point of a jet impinging on a target, it can be shown that

$$1/2 \rho_j (v_j - U)^2 = 1/2 \rho U^2 \quad [3]$$

where ρ_j and ρ are the densities of the injected and penetrated fluid,

v_j = injection velocity,

and

U = penetration rate.

If $\rho_j = \rho$, Eq [3] reduces to,

$$U = \frac{v_j}{2}. \quad [4]$$

If $\rho_j/\rho \neq 1$, Eq [3] can be expanded and solved for U_A , the average penetration rate giving

$$U_A = \frac{v_j \rho_j \pm \sqrt{v_j^2 \rho_j^2 - \rho_j v_j^2 (\rho_j - \rho)}}{2 (\rho_j - \rho)} \quad [5]$$

where v_j can be determined from the well known modified orifice flow equation

$$v_j = C_d \sqrt{\frac{288 g_c \Delta P}{\rho_j}} \text{ ft/sec} \quad [6]$$

and

 C_d = orifice discharge coefficient g_c = gravitational constant - 32.17 ft/sec² ΔP = injector differential pressure, lb_f/sq in. ρ_j = fluid density, lb_m/cu ft.

Table II-10 compares the expected velocities computed from Eq [5] and [6] for water, a 50/50 blend of hydrazine and unsymmetrical dimethylhydrazine, and nitrogen tetroxide for a 75-psi differential pressure.

Table II-10 Penetration Rate Comparison for a Reacting and Nonreacting Process

Injected Fluid	Penetrated Fluid	Density Ratio (ρ_j/ρ)	Theoretical Injection Velocity (ft/sec)	Theoretical Average Penetration Rate (in./sec)	Actual Penetration Rate (in./sec)
Water	Water	1	78.8	472	222
Fuel	Oxidizer	0.628	82.8	438	100
Oxidizer	Fuel	1.59	66.0	442	N/A

Since the combustion process was not photographed in the oxidizer tank, there is no identification of the actual penetration rate or distance. However, since the theoretical nonreaction penetration rates in the fuel tank are similar to those in the oxidizer tank, the penetration phenomena were assumed identical for design purposes, although additional investigation is required in this area. The actual penetration rate of 100 in./sec was primarily obtained from an analysis of two films, one with the 0.006-in.-dia injector orifice and the other with a 0.0135-in.-dia orifice. Although the penetration processes are significantly different, the actual penetration rate for the combustion process appears to be 50% of the theoretical average for a nonreacting process. The penetration test is summarized in curve form in Fig. II-63 for an injector differential pressure of 75 psi.

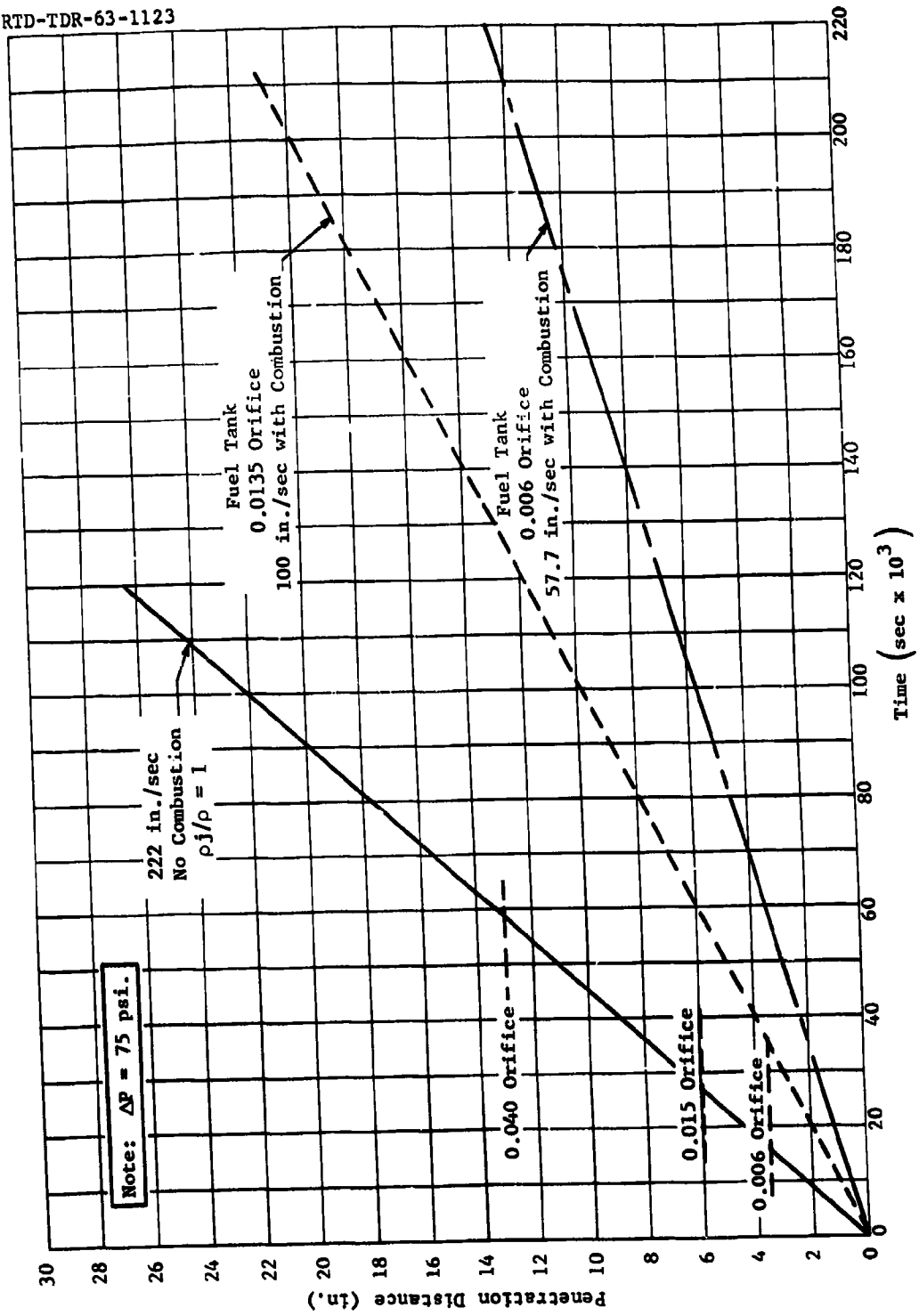


Fig. II-63 Injection Penetration Rate Comparison

Since the actual penetration distance was computed from the optics of the system, attempts were later made to measure the penetration and rate by a calibrated illuminated scale mounted inside the tank. However, diffraction and distortion incurred in the research test fixture prevented a more accurate determination. Reruns were made at 50, 75, and 100 psi and indicated the depth primarily increased with injection duration. It was therefore concluded, from the amount of testing performed on the penetration process, that additional studies should be conducted with high-speed photography and a specially designed system so the reaction can be investigated under a variety of conditions without optical interference. In the absence of further knowledge in this area, the primary emphasis for future MTI system design should be to ensure that a good solid stream is obtained from the injector for maximum penetration into the propellant. The orifice diameter will be controlled by the physical characteristics of the system and differential pressure limited to $200 \text{ lb}_f/\text{sq in.}$ based on current injector technology. A detailed analysis of injector sizing is contained in Chap. V.B.

Photographic observation of the reaction process provided valuable information in determining the size of the reaction zone and variation in spray pattern and penetration to aid in the study of heat transfer to the propellant and surroundings. Additional television observation of the process on many of the tests provided quick information for system analysis and development. A sequence of photos is provided in Fig. II-64 to show the shape and development of the combustion zone with nitrogen tetroxide solid-stream surface injection at 100 psig through a 0.006-in.-dia orifice. The photographs were taken through the fuel from the lower camera port at a 45° angle to the liquid surface, and represent a typical reaction for the pressurization process occurring at an average frequency of 2 cps.

RTD-TDR-63-1123

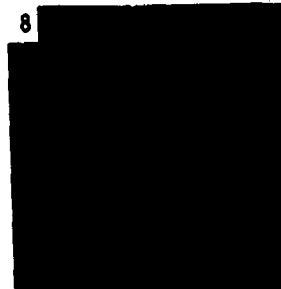
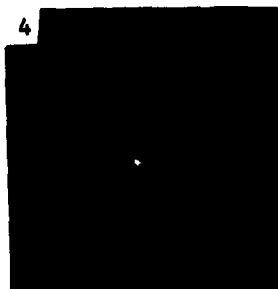
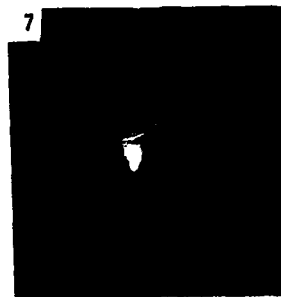
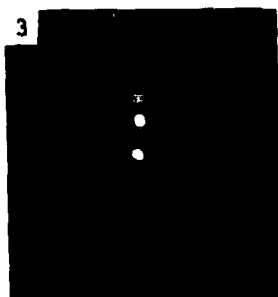
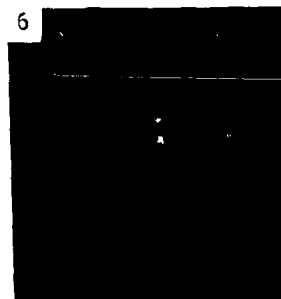
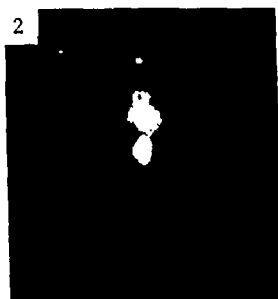
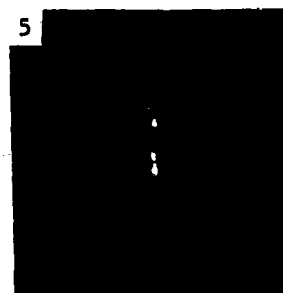
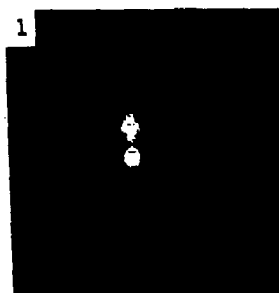


Fig. II-64 Fuel Tank Combustion Photographs

The dimensions of the combustion zone are approximately 4.5 by 0.75 in. dia. The area of the combustion zone shows correlation with the 0.1 sq ft assumed in the analytical model. In this computation, pressurization system performance is based on the theoretical reaction flame temperature for the anticipated reaction mixture ratio. The photographs were taken at 128 fps with a 10 mm lens at an aperture of f/1.8 on Ektachrome film. Attempts to photograph the reaction from the top of the tank with infrared film were unsuccessful. The average duration of the reaction process as determined from film speed was approximately 0.140 sec. Frame 4 shows the reaction fully developed with a slight reflection at the upper end of the combustion region indicating minor surface ripple. At this time, the reaction appears to break into several small balls of fire. The photographs of the reaction process with larger diameter solid-stream orifices show better concentration of the reaction and the penetration into the fuel is greater. As a result, the amount of heat transfer to the liquid increased. Injection system response was also measured from the time the electrical signal was initiated until a pressure increase was noted in the propellant tank. The average opening response of 0.120 sec also included the response of the measuring and recording system estimated to be less than 0.020 sec. The shutoff response was considerably faster at approximately 0.020 sec. Rapid pressurization termination after the injector signaled closed verified an absence of fuel autoignition; however, some pressure rise resulted due to the combustion of reagent unreacted after injector shutoff. Part of a typical propellant tank pressure trace is shown in Fig. II-65. The nominal combustion duration from the pressure trace confirmed the time of 0.140 sec determined from photographic observation. The high initial pressure was due to the nitrogen prepressurization. In this case, using a 0.006-in.-dia injector orifice, a slight pressure under and overshoot was experienced at the start of the test due to the small ullage volume. Excellent pressure control of ± 0.25 psi was achieved with 5 psi/sec pressure rise rate. With the 0.015-in.-dia injector orifice, the maximum width of the pressure band increased to 1.2 psi because of the relatively high 30 psi/sec pressure rise rate. The pressure decay rate increased slightly with time due to an increase in heat transfer resulting from the greater tank surface area exposed while the pressure rise rate decreased at a higher rate due to the increase in ullage volume. The result was a maximum injector frequency at the start of the test and lower frequency at the end. The frequency was reduced in tests with pressure overshoot. The nominal frequency for all tests ranged from 1 to 3 cps.

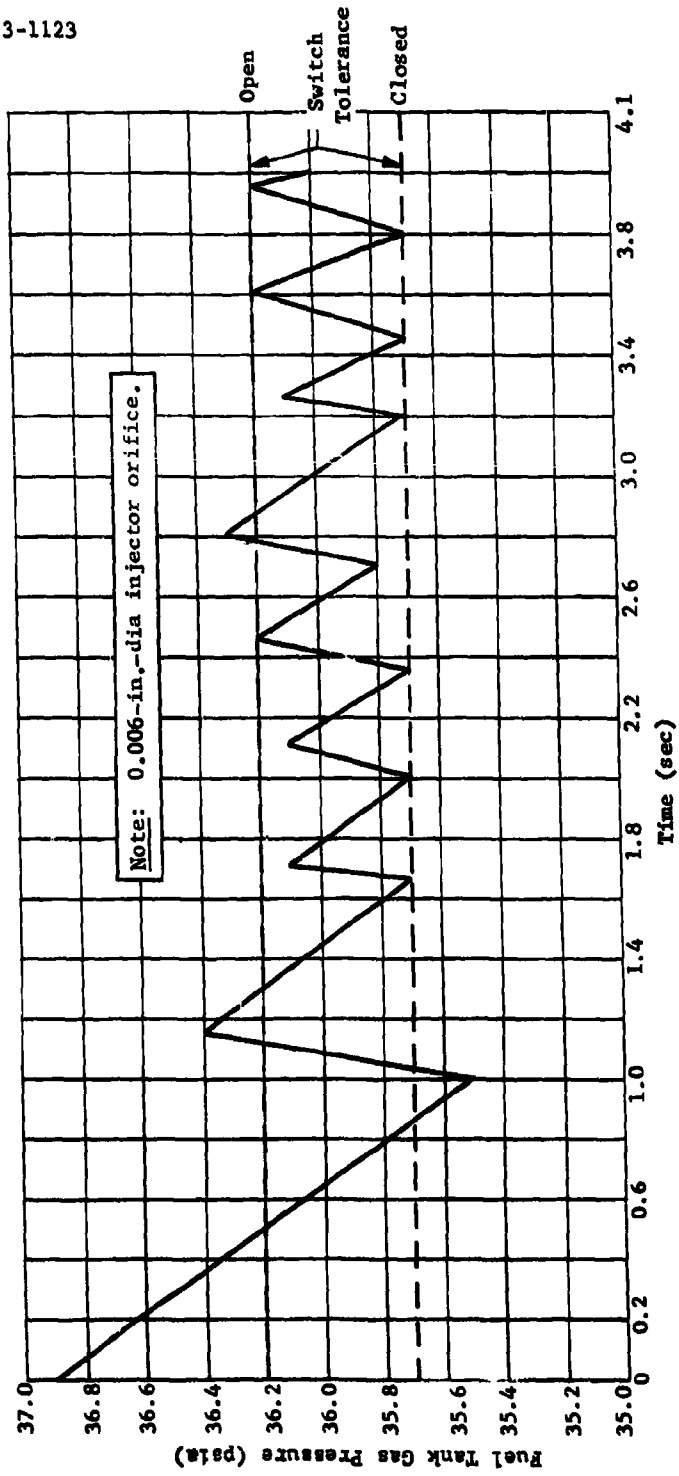


Fig. II-65 Single Tank MTI Pressure Transient

Fuel Tank Injection Method Evaluation - The primary objective of the injection system development test series was to determine if a significant change in gas composition and molecular weight could be achieved by varying the primary tank injection process. Other pertinent factors included reagent consumption, propellant contamination, entrained vapor, system vibration, and temperature distribution in the propellant, tank wall, and ullage. To investigate the reaction phenomena, the following four methods, which were considered to be representative of the variety of possible reactions, were selected for evaluation:

- 1) Solid stream surface injection;
- 2) Solid stream subsurface injection;
- 3) 15-degree fan spray surface injection;
- 4) 15-degree fan spray subsurface injection.

All of the injection system development tests were performed by injecting nitrogen tetroxide in the fuel-filled primary tank, and subsequently pressurizing the water-filled secondary tank through a common ullage manifold. Two tanks were tested to verify satisfactory performance of the common ullage system with a non-volatile inert secondary fluid. The absence of the secondary liquid vaporization or reaction permitted a detailed study of the primary gas composition without complications of a secondary reaction while providing a maximum quantity pressurizing gas generation. The inherent flexibility of the small-scale research test fixture and versatility of reagent injection provided sufficient capability for system changes with only minor adjustments. From an analysis of system performance obtained with the various methods of reagent injection, the most desirable system was established.

Test Configuration - A general description of the test configuration for this test series is contained in Chap. II.B.2 with an identification of system instrumentation location and nomenclature. Propellants were loaded to the 30% level in the primary (fuel) tank and to the 5% level in the secondary (oxidizer) tank. Initial pressurization of the system was adjusted to 40 psia by the facility helium supply. Subsequent pressurization during propellant expulsion was accomplished by the combustion process and interconnection of the primary and secondary tank ullages by a 1-in.-dia line. A 1/4-psi differential check valve in the line assured proper flow direction, and a mist eliminator was installed at the primary tank end reduced entrained

liquids. Reagent flow was maintained by a 100 psig pressurized 1-in. dia calibrated glass tube containing nitrogen tetroxide with the on-off injector controlled by a 36 ± 0.25 psia pressure switch. Liquid flow rates were individually maintained during the 150-sec test by remote adjustment of the flow control valves. Flow was terminated automatically by the propellant tank liquid low-level sensors. A visual determination of entrained vapor in the expelled propellant was provided by a sight glass in the tank outlet. The combustion process was televised and photographed through a lower camera port in the propellant tank.

Except for slight variations in ambient conditions, each test was run under identical conditions. The actual pressurized volume was controlled to close tolerances by the liquid level sensors so that small variations in average propellant expulsion rates could not significantly affect test data. System parameters monitored during each test include propellant tank gas, liquid, and wall temperatures, as well as ullage pressure and reagent temperature and pressure. All parameters except reagent consumption, which is determined from the volumetric change in the calibrated supply system, were recorded along with propellant flow rates. Process gas specimens taken from a continuous bleed manifold were chemically analyzed and are described in detail in Chap. II.C.3.

Test Results - A summary of the basic tests performed and injector systems used is presented in the following paragraphs, with the significant observations and system characteristics identified. Table II-6 explaining the instrumentation nomenclature, and Fig. II-51 showing the location of each parameter are contained in Chap. II.B.2.

Solid Stream Surface Injection - Two test runs were conducted using a 0.012-in. dia stainless steel orifice to inject a solid stream of reagent into the fuel tank on pressure demand. Pictures of the reaction process indicated a penetration depth of approximately 6 in. below the fuel surface. The combustion zone was confined to a small area around the penetrating reagent and combustion stopped when reagent injection was terminated.

Figures II-66 thru II-68 represent typical performance curves for this type of injection. Primary tank gas temperature (310°F maximum) and pressure (36 ± 0.25 psia) control was satisfactory. Total reagent consumption during the run was 0.412 lb. Visual observation detected no tank vibration or entrained vapors in the expelled propellant. Gas analysis indicated an average combustion product molecular weight of 13.4 for this type of injection.

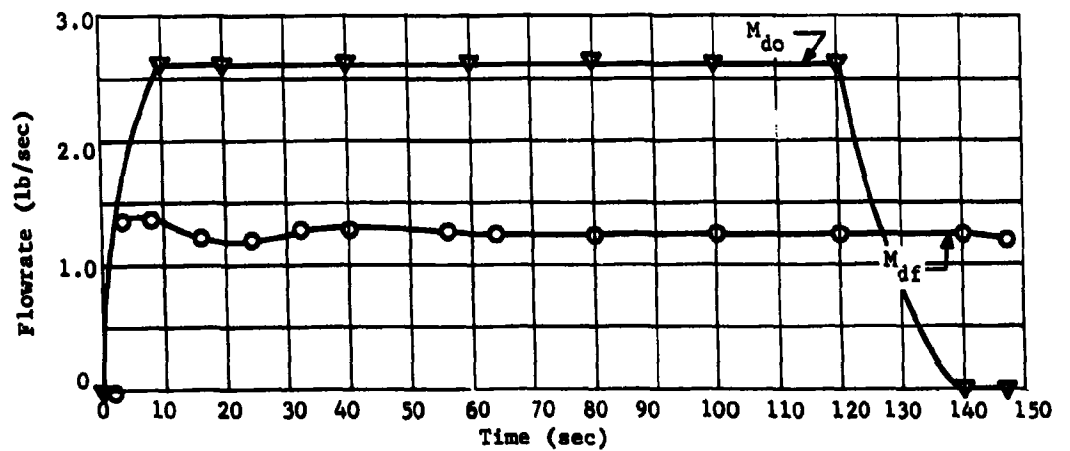
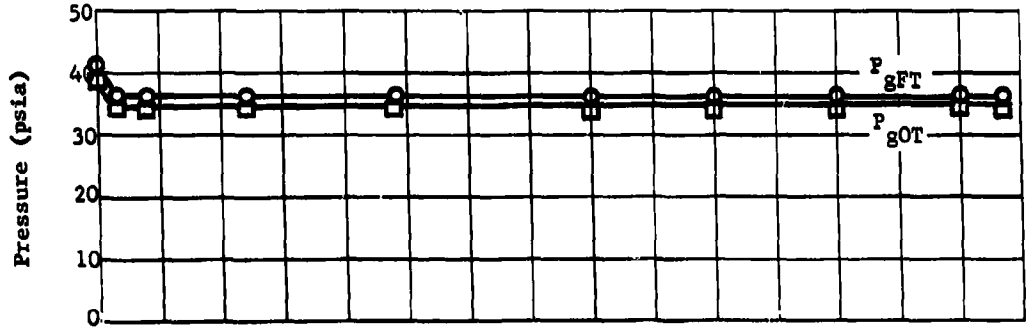
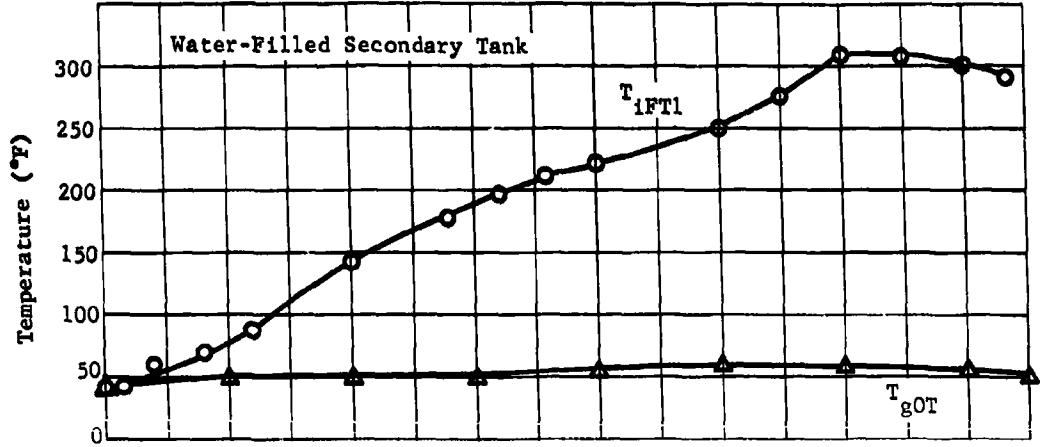


Fig. II-66 Pressurization System Performance Curves with Solid-Stream Surface Injection in Primary Tank

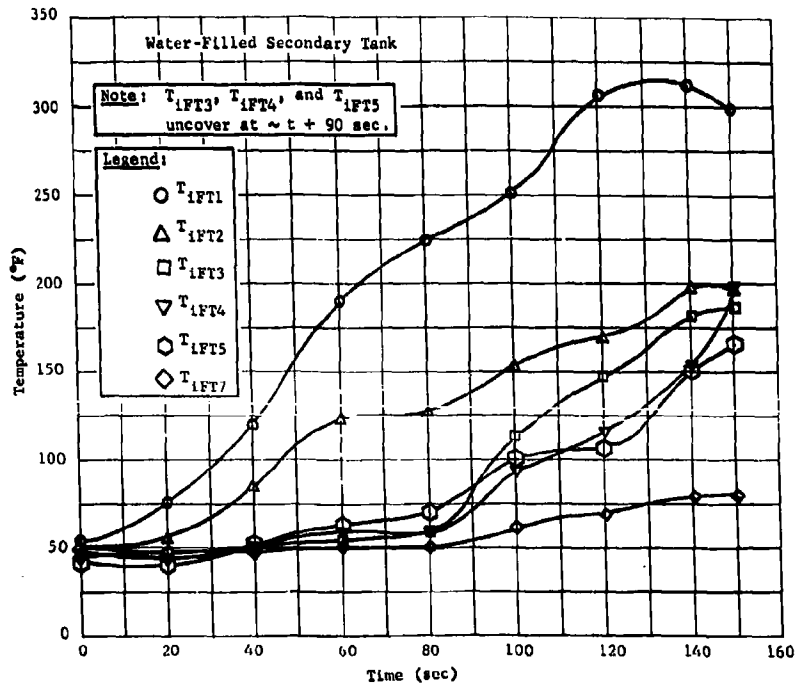


Fig. II-67 Primary Tank Internal Temperature Profiles with Solid-Stream Surface Reagent Injection

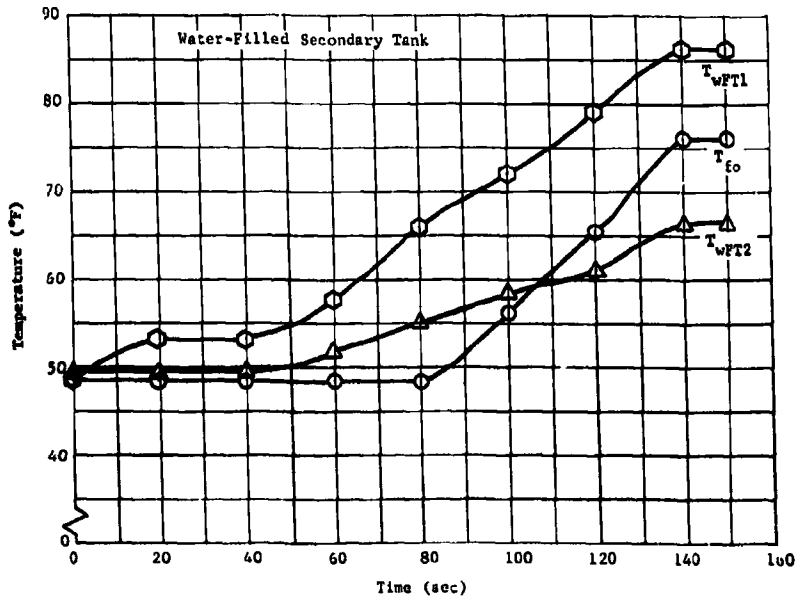


Fig. II-68 Primary Tank External Temperatures for Solid-Stream Surface Reagent Injection

15-deg Flat Spray Surface Injection - Three test runs were conducted using a 0.013-in.-diameter carbide orifice to inject a 15-deg flat spray pattern on the fuel surface on pressure demand. The spray pattern was used in an attempt to alter the gas composition and determine the effects on tank temperature and pressure control. Film coverage of the reaction process indicated little or no reagent penetration below the fuel surface. The reaction appeared to be the combustion of small reagent droplets on the fuel surface. As in the previous tests, the reaction stopped when reagent injection was stopped.

Figures II-69 thru II-71 represent typical performance curves for this type of injection. Primary tank pressure control was within ± 1.0 psi, which is greater than the required ± 0.5 -psi pressure range. Primary tank gas temperature was approximately 755°F for all test runs, which is substantially higher than the 300°F desired. Figure II-70 illustrates temperature changes from liquid to gas as the temperature rake thermocouples T_{iFT3} , T_{iFT4} , and T_{iFT5} uncover at approximately 85 sec. Average reagent consumption for the three runs was 0.634 lb.

Visual observation indicated no primary tank vibration or entrained vapors in the propellant outflow. Gas analysis indicated a combustion product average molecular weight of 22.7 for this type of injection.

Solid-Stream Subsurface Injection - Three test runs were conducted using the 0.012-in.-diameter solid stream orifice located 2 in. above the outflow baffle splash plate and directed toward the tank outlet. This technique was tested to determine the effects of combustion product regenerative cooling on the tank temperature, tank pressure, and combustion product molecular weight. One of the test runs yielded only limited test data due to clogging of the injector orifice after 50 sec of outflow. Film coverage of the reaction process indicated a controlled combustion zone approximately 4 in. in diameter around the injector orifice resulting in violent agitation of the fuel. The combustion zone flame color was yellow. As noticed in the other injection techniques, the reaction stopped when reagent injection was stopped.

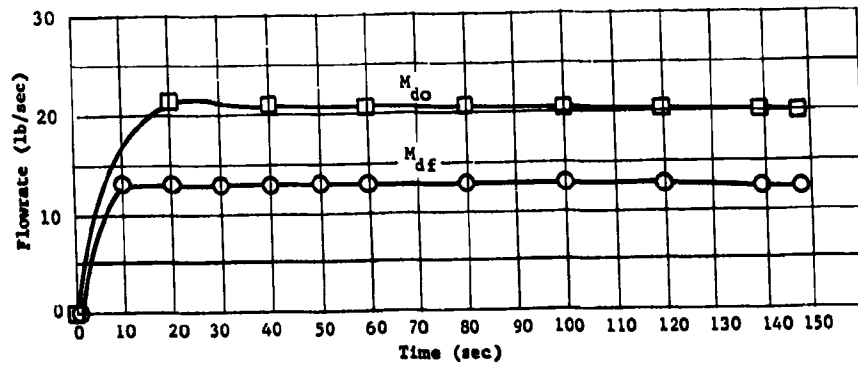
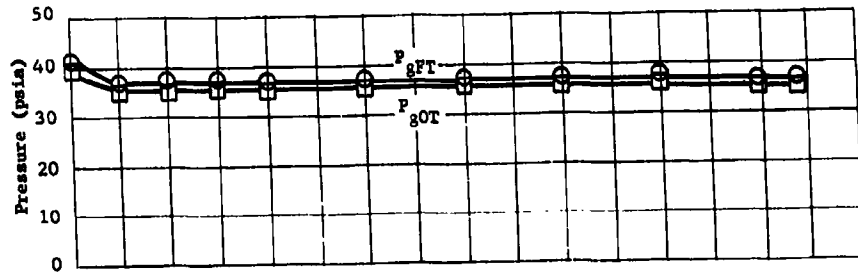
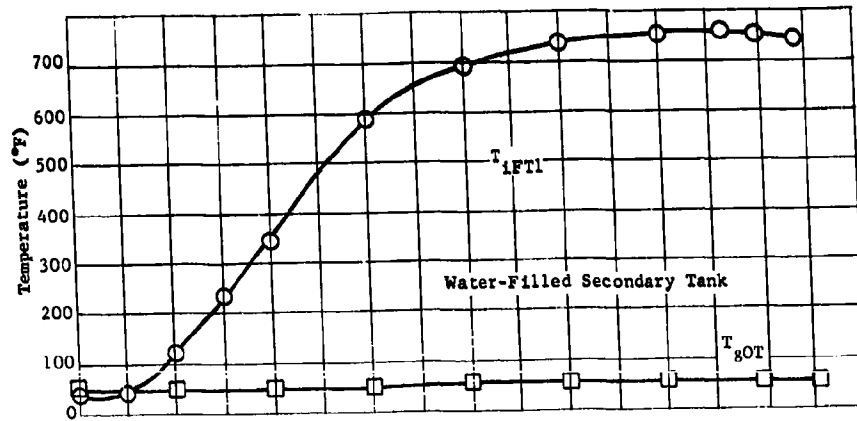


Fig. II-69 Pressurisation System Performance Curves with 15-deg Fan Spray Surface Injection in Primary Tank

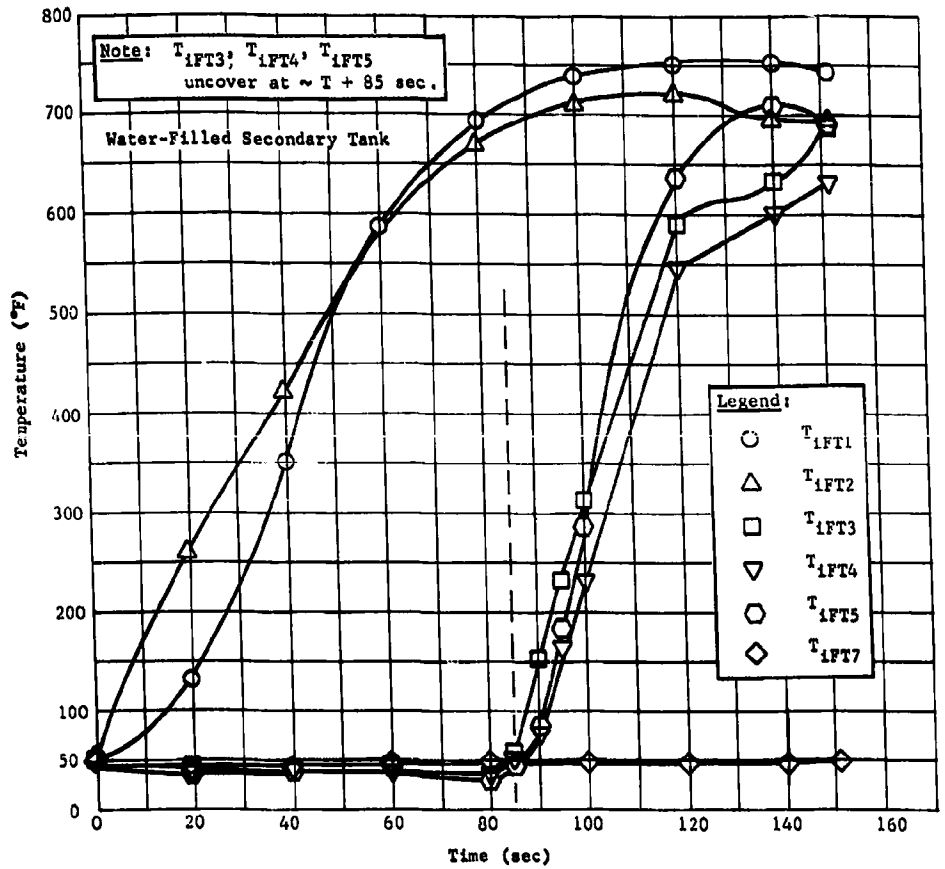


Fig. II-70 Primary Tank Internal Temperature Profiles with 15-deg Fan Spray Surface Reagent Injection

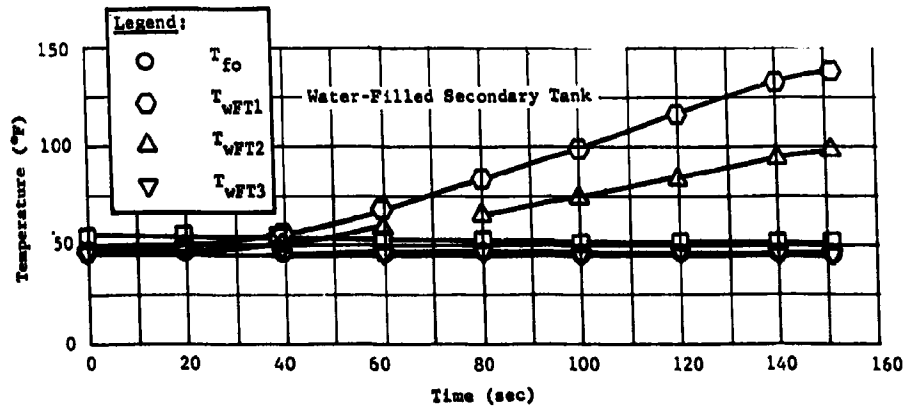
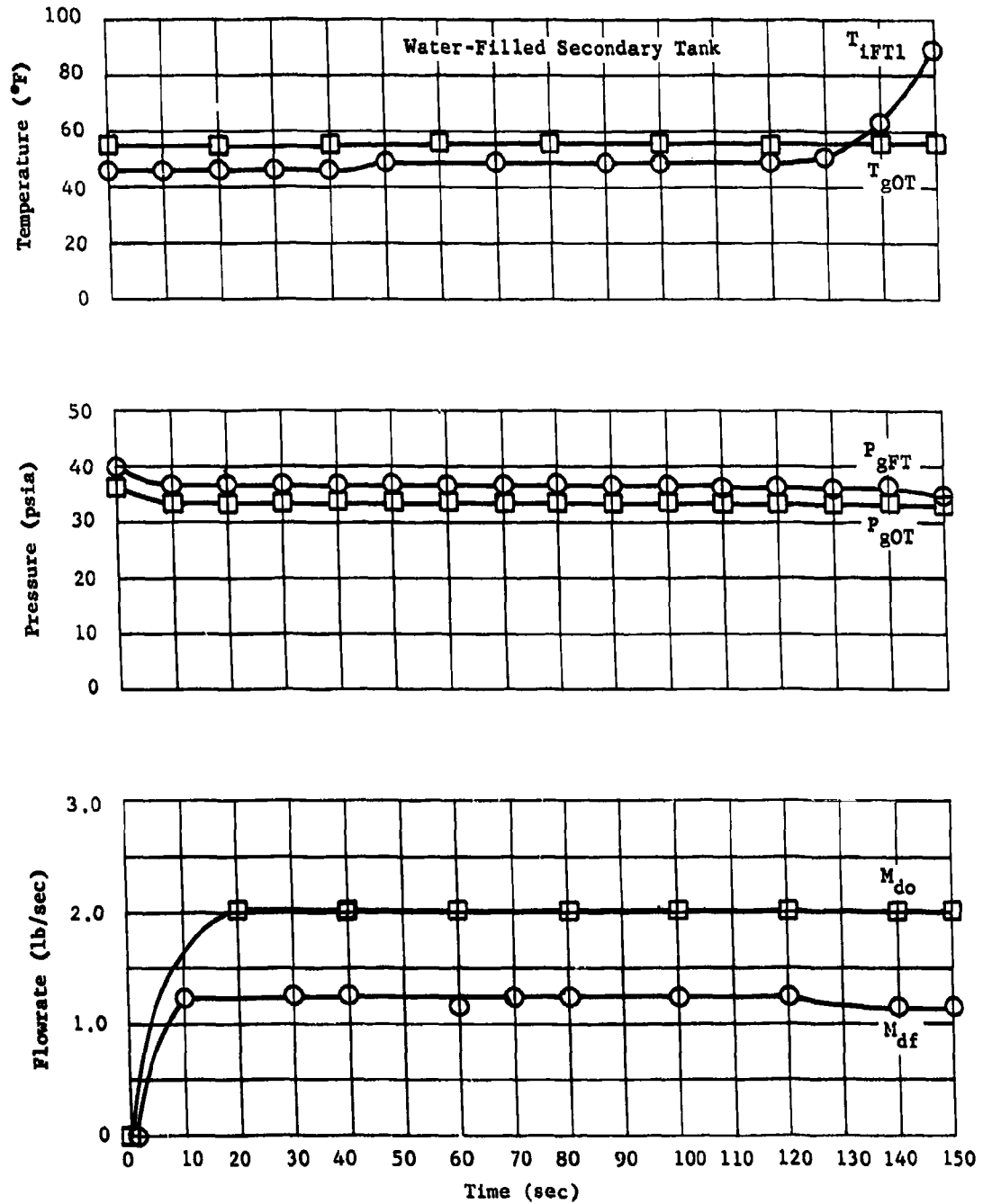


Fig. II-71 Primary Tank External Temperatures for 15-deg Fan Spray Surface Reagent Injection

Figures II-72 thru II-74 represent typical performance curves for this type of injection technique. Tank pressure control in both tanks was within a 0.5-psi pressure band. Figure II-72 shows that the fuel ullage temperature (T_{IFT1}) started a steady increase only after the fuel level fell below the injector orifice. Visual observation indicated a definite tank vibration caused by the subsurface reagent reaction. The average reagent consumption for the two complete test runs was 0.468 lb. No entrained vapors were noted in the propellant outflow. The combustion product average molecular weight was 15.6 for this injection technique. Inspection of the outflow baffle splash plate showed no damage due to subsurface reagent impingement and reaction.

15-deg Flat Spray Subsurface Injection - Two test runs were conducted using the 0.013-in. diameter 15-deg flat spray orifice located 2 in. above the outflow baffle splash plate and directed toward the tank outlet. This technique was tested to determine the effect of combustion product regenerative cooling and reaction mixture ratio change on tank temperature and pressure control and combustion product molecular weight. Film coverage of the reaction process indicated a combustion zone similar to that of subsurface solid-stream injection except that the combustion flame color was white. The reaction process again created violent agitation of the fuel. As noted in previous runs, the combustion stopped when reagent injection was stopped.

Figures II-75 thru II-77 represent typical performance curves for this type of injection. Tank temperature and pressure control was satisfactory using this technique. Pressure control was within a 0.5-psi pressure band. Tank ullage temperature remained near ambient until the fuel liquid level fell below the injector orifice. Average reagent consumption for these test runs was 0.412 lb. Visual observation indicated a definite tank vibration due to subsurface spray reagent injection. During the test runs, many very small vapor bubbles were entrained in the propellant outflow. The combustion product average molecular weight for this injection technique was 17.5. Inspection of the outflow baffle splash plate indicated no damage from direct impingement of the injected reagent.



(Fig. II-72 Pressurization System Performance Curves with Solid-Stream Subsurface Injection in Primary Tank

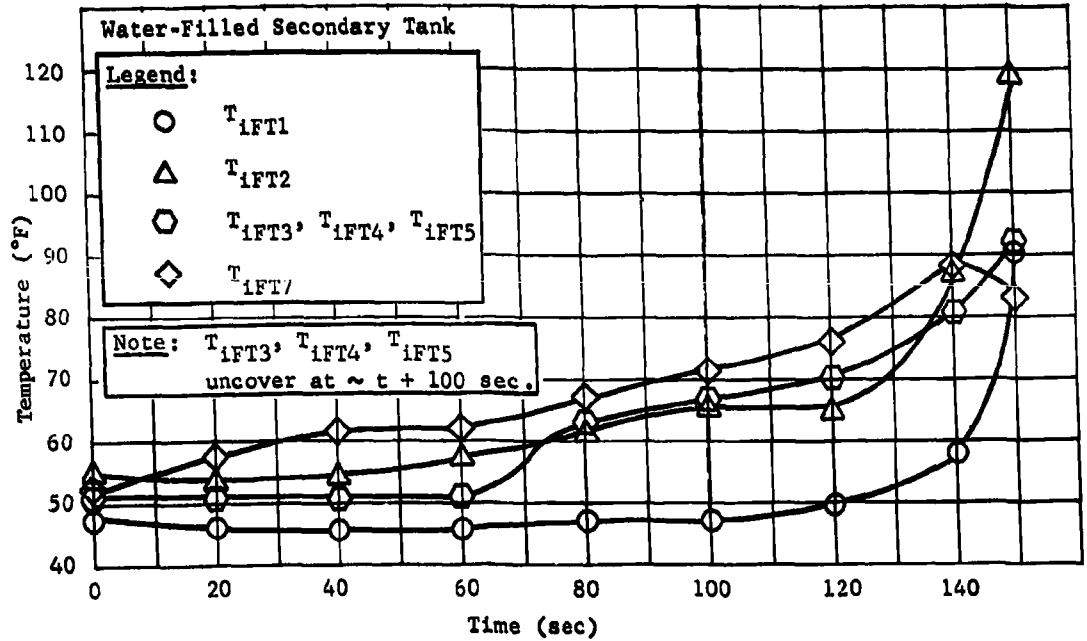


Fig. II-73 Primary Tank Internal Temperature Profiles with Solid-Stream Subsurface Reagent Injection

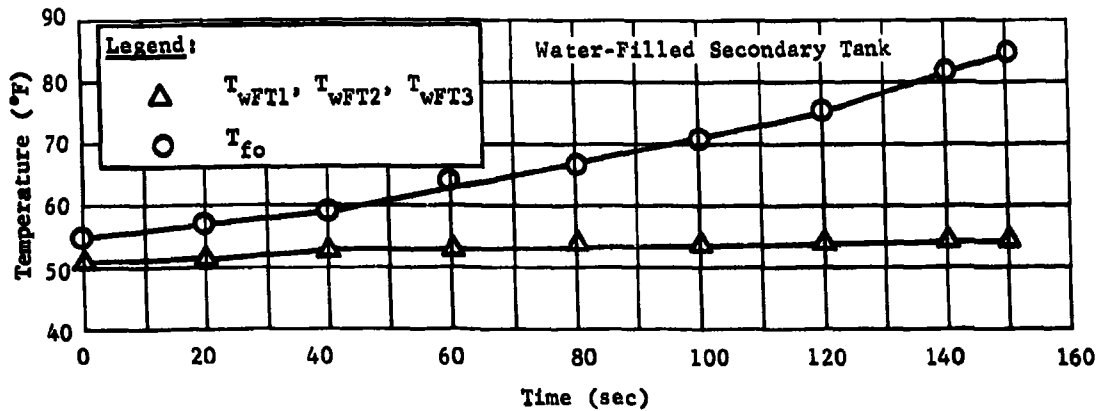


Fig. II-74 Primary Tank External Temperatures for Solid-Stream Subsurface Reagent Injection

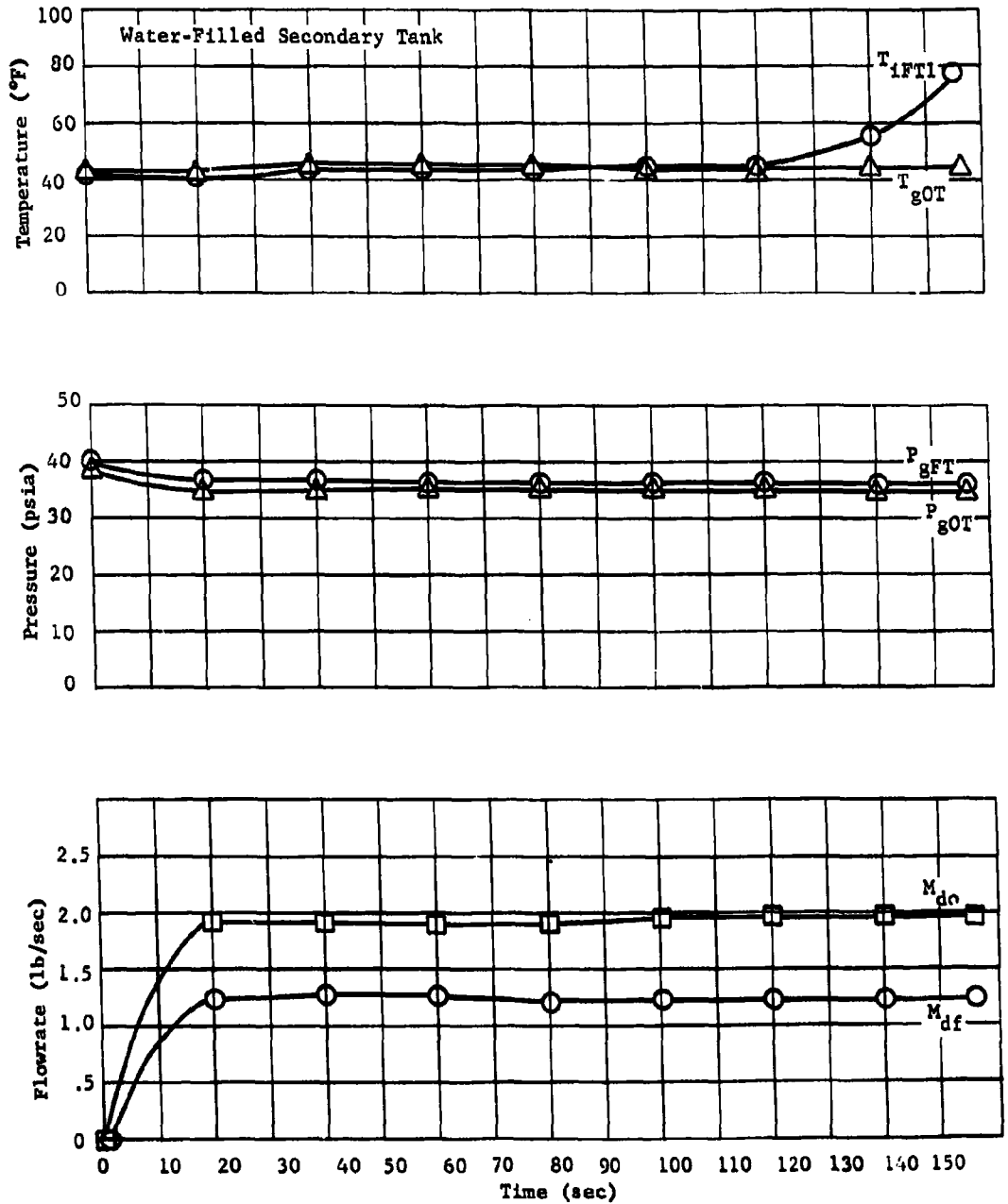


Fig. II-75 Pressurization System Performance Curves with 15-deg Fan Spray Subsurface Injection in Primary Tank

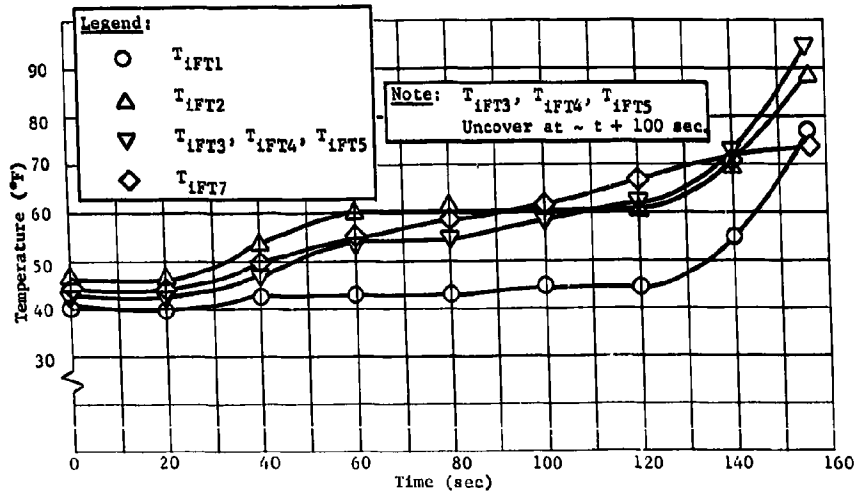


Fig. II-76 Primary Tank Internal Temperature Profiles with 15-deg Fan Spray Subsurface Reagent Injection

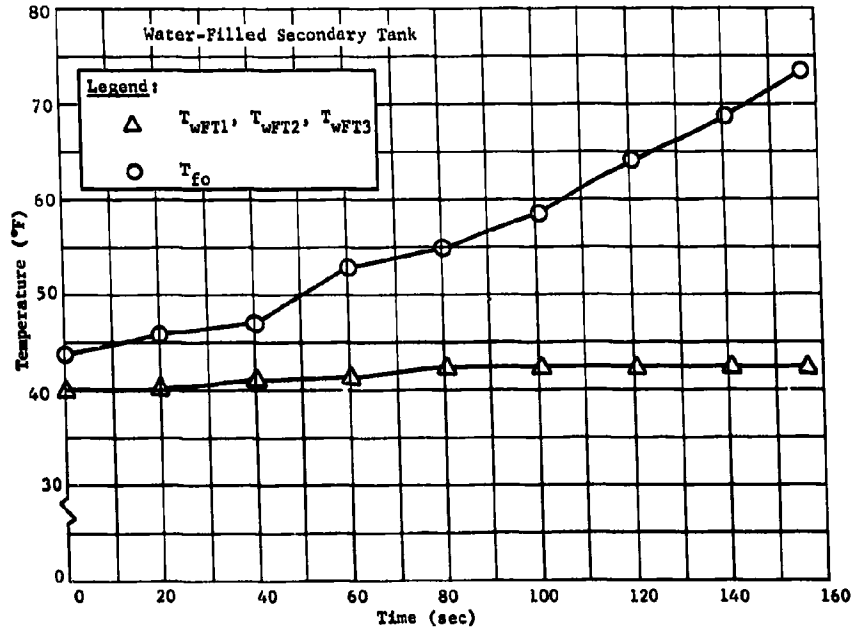


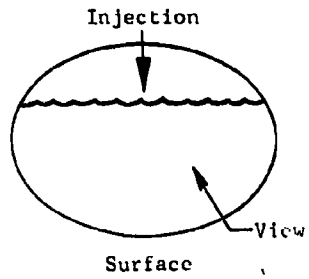
Fig. II-77 Primary Tank External Temperature for 15-deg Fan Spray Subsurface Reagent Injection

Performance Analysis - The functional operation of the four injection systems investigated were considered feasible for full-scale system application except for the surface spray technique, which incurred a minor explosion in a retest. This event resulted from a partially plugged injector, which allowed a high concentration of NO_2 in the fuel tank. The presence of an unreacted oxidizer in a hydrogen-rich atmosphere apparently caused an additional reaction to be initiated by the normal combustion of N_2O_4 and the fuel. Although no damage resulted from this occurrence, vaporized oxidizer must be avoided in the primary tank.

The location of the injector (either in the tank ullage or below the liquid surface) did not impose any significant operating problems. Elimination of tendencies to entrain vapors in the liquid or create excessive fluid agitation would, however, require additional consideration in a full-scale system.

In all the tests performed, the temperature of the gas in the water-filled secondary tank was moderate (60°F) and pressure control was excellent. Due to the large amount of heat absorbed by the common ullage line, a noticeable amount of condensate was detected after each test. The quantity and composition of this unidentified material is discussed in Chap. II.C.3.

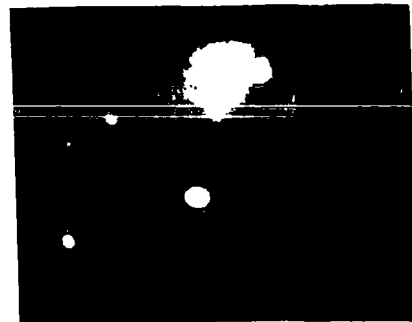
The results of the injection system development test series are based on the twelve tests performed by the injection of nitrogen tetroxide into the fuel tank, with subsequent pressurization of the water-filled secondary tank by means of a common ullage manifold. All the tests performed were successful except one that was only partially successful because of its early termination as a result of a plugged injector. Injection was effected in the fuel tank by both the surface and submersed systems, employing either a solid-stream or a 15-deg fan spray injector. Photographs of the combustion process are shown in Fig. II-78 for the four injection techniques investigated. The variation in injection technique has been determined to affect the reaction process and alter the gas composition in addition to influencing the heat transfer characteristics in the fuel tank. A summary of the average performance of each system is presented in Tables II-11 and II-12.



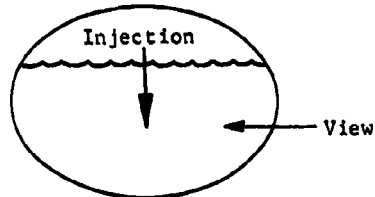
Surface



Surface Solid Stream



Surface Spray



Subsurface



Subsurface Solid Stream



Subsurface Spray

Fig. II-78 Combustion Photographs - MTI of N_2O_4 into a 50-50 Mixture of UDMH and N_2H_4

Table II-11 MFI Injection System Evaluation

Type Run	ΔT Gas (°F)	ΔT Fuel (°F)	ΔT Wall (°F)	Mole. Wt, Gaseous Comb Prod	Theo. Reaction Mix Ratio	Wt., Gaseous Comb Prod (lb)	N_2O_4 Used (lb)
Surface Solid	266	27	37	13.4	0.6	0.579	0.412
Surface Spray	707	2	82	22.7	2.6	0.755	0.634
Submersed Solid	45	33	4	15.6	0.8	0.778	0.468
Submersed Spray	37	29	2	17.5	1.0	0.900	0.412

Table II-12 Effects of Reagent Injection Technique on Fuel Composition

Type Test	Percent Change in Concentration during a 150-sec Test		
	UDMH	N_2H_4	H_2O
Surface Solid	-1.3	+0.9	+0.40
Surface Spray	-3.7	+0.1	+1.58
Subsurface Solid	-1.2	+0.7	+0.29
Subsurface Spray	-1.1	+0.6	+0.25
			Unknowns
			+0.2
			+3.0
			+0.2
			+0.25

Note: These data represent the condition of the propellant that would enter an engine before shutdown.

Since the gas molecular weight reported does not include the condensed products of reaction, the absolute value would be slightly higher than these figures. Although the relative variation in molecular weight has been definitely established, the reaction mixture ratio cannot be determined by test measurements, and consequently was based on the theoretical equilibrium calculation for the combustion product molecular weight obtained. A theoretical technique is also employed in obtaining the weight of combustion products produced; however, the computation is based on the actual physical characteristics of the system for the particular test run and the corresponding combustion product molecular weight. From the results of this test series, the solid-stream surface injection system was selected for further development in the live oxidizer test series, based on the following observations:

- 1) Low ullage gas molecular weight;
- 2) Desirable operating temperatures;
- 3) Low reagent consumption;
- 4) Low system vibration;
- 5) Moderate amount of condensibles formed.

Common Ullage System Development - After selecting the most desirable injection technique, the next phase of the research test program was to develop the common ullage pressurization technique using live oxidizer (N_2O_4) in the secondary tank. The development of a common ullage pressurization system for the hypergolic propellant combination was primarily concerned with the design of a system that would ensure safe and reliable system operation. Additional effort was also expended to improve system operating characteristics and efficiency. To avoid pressure or temperature control problems in the secondary tank and provide stable system operation, the common ullage development program was centered on two basic techniques, surface and subsurface gas impingement. Several variations to each design were tested to investigate the influence of entering gas velocity and uniform distribution with and without cross flow gas conditioning. A primary objective of this test series was to determine the nature and control of the secondary reaction in view of the reactive and potentially reactive constituents of the pressurizing gases. To verify safe system operation and potential capability, several tests were performed with MTI initial pressurization and a 10-min coast period before restart of propellant outflow. Because of the complexity of the problem, the evolved common ullage configuration was not recommended for full-scale demonstration testing.

Test Configuration - The test configuration for the common ullage development test series was basically the same as the injection system development test series and is described in Chap. II.B.2. Primary changes to the system involved the various modifications to the common ullage line and gas impingement technique in the oxidizer-filled secondary tank. The common ullage line configuration for the initial tests was the same as for the tests with a water-filled secondary tank. This system employed a demister inside the primary tank at the entrance to the upper dome. An isolation valve was installed in the line for additional flexibility and safety, but was maintained in the open position throughout the test series. Back flow of gas was satisfactorily controlled by the 1/4-psi check valve in the surface gas impingement tests, thereby preventing any undesirable reactions in the primary tank. The primary tank reagent injection system was unchanged for the initial series of tests.

Since considerable primary tank gas composition data were accumulated by the original multiple sampling system, a single specimen sampling technique was used to minimize the amount of gas generated. With the revised system, samples of the primary tank pressurizing gas were taken directly from the ullage in an evacuated bottle immediately after the termination of the test. Secondary gas samples were procured with the sampling system previously used for the primary tank. This system enabled specimens to be taken remotely at 20, 60, 120, and 160 sec during the test by a continuous-bleed heated system.

Test Results - The common ullage system development program required the major portion of the Phase I effort. The test results are contained in four parts:

- 1) Secondary tank surface gas impingement test series;
- 2) Secondary tank subsurface gas impingement test series;
- 3) Restart test series;
- 4) Secondary tank conditioned surface gas impingement test series.

The first two test series were 150-sec continuous tests; however, for thorough system development a restart demonstration was required. In the restart test series the primary development item, after pressure control was obtained, was a reduction in secondary tank vibration inherent in the subsurface gas injection process. Since the vibration level could not be reduced below a 3 g double amplitude level, attention was directed at the surface gas impingement process in a restart test plan with cross flow gas conditioning.

Secondary Tank Surface Gas Impingement Test Series - This series of tests initially required five full-duration (150 sec) continuous runs with one additional test performed during the subsurface gas impingement test series to investigate the possibility of total condensate removal from the cross flow gas. The first three tests were performed with solid-stream surface reagent injection in the primary tank and with direct impingement of the cross flow gas into the secondary tank. Figures II-79 thru II-84 represent typical pressurization system performance curves for the particular configuration.

RTD-TDR-63-1123

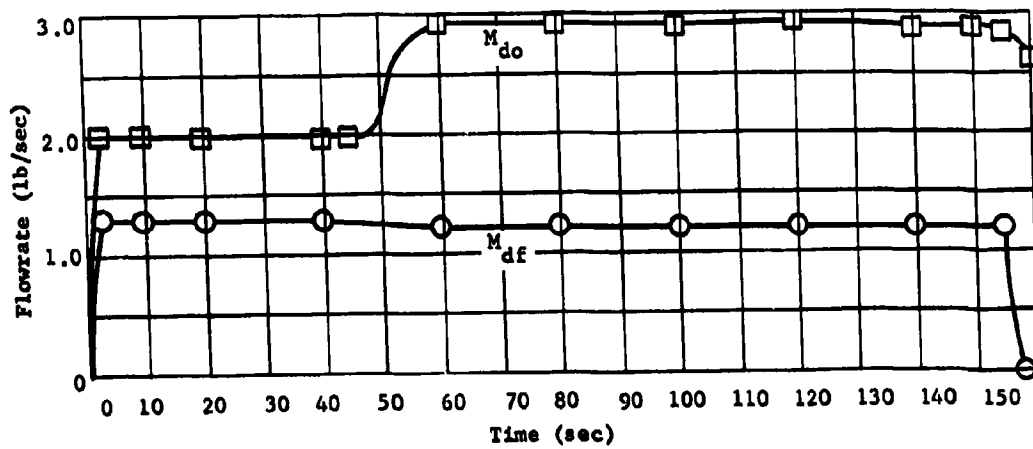
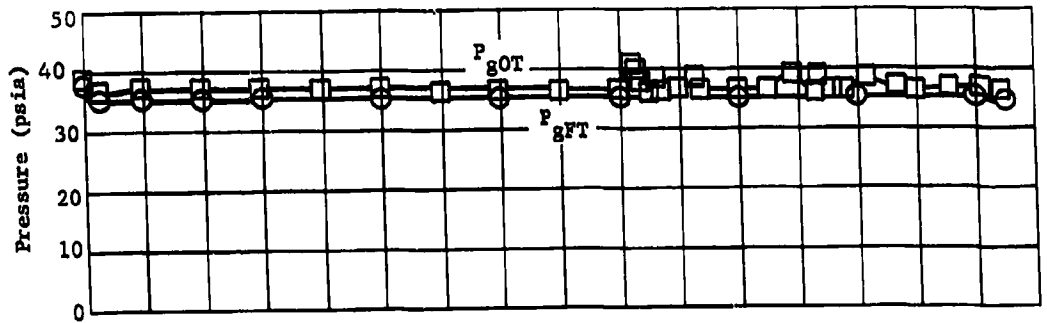
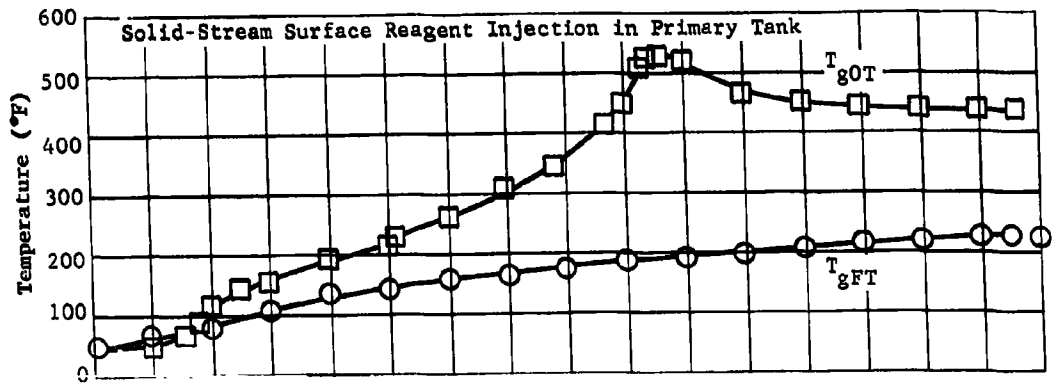


Fig. II-79 Pressurization System Performance Curves with Surface Gas Impingement in Oxidizer Tank

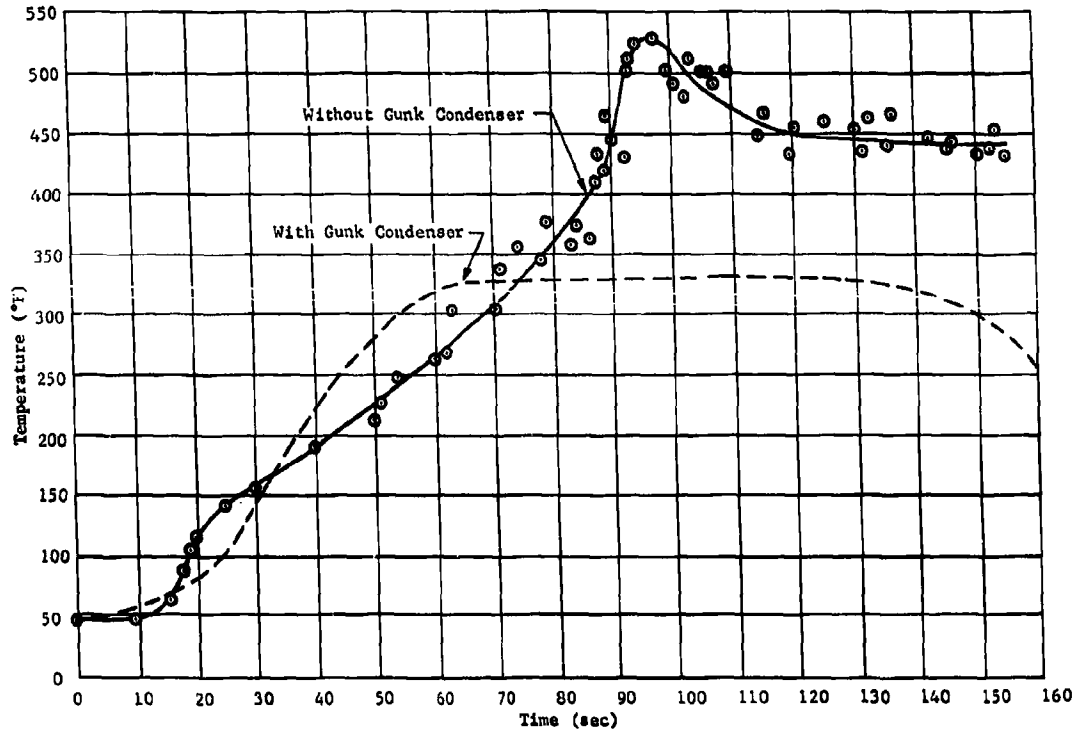


Fig. II-80 Secondary Tank Gas Temperature Profile with Surface Gas Impingement on Oxidizer

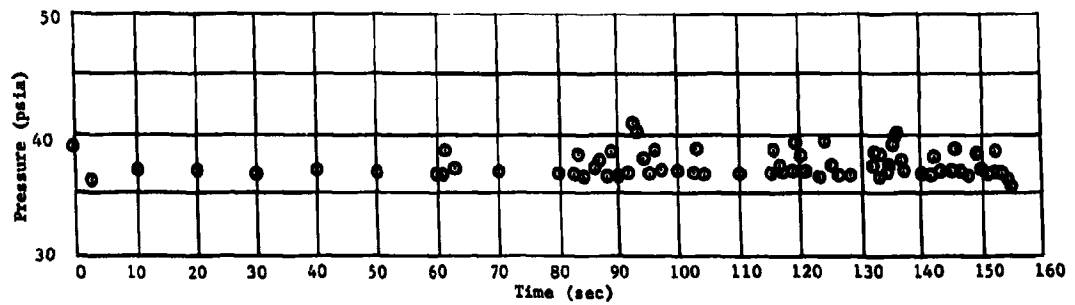


Fig. II-81 Secondary Tank Pressure Profile with Surface Gas Impingement on Oxidizer

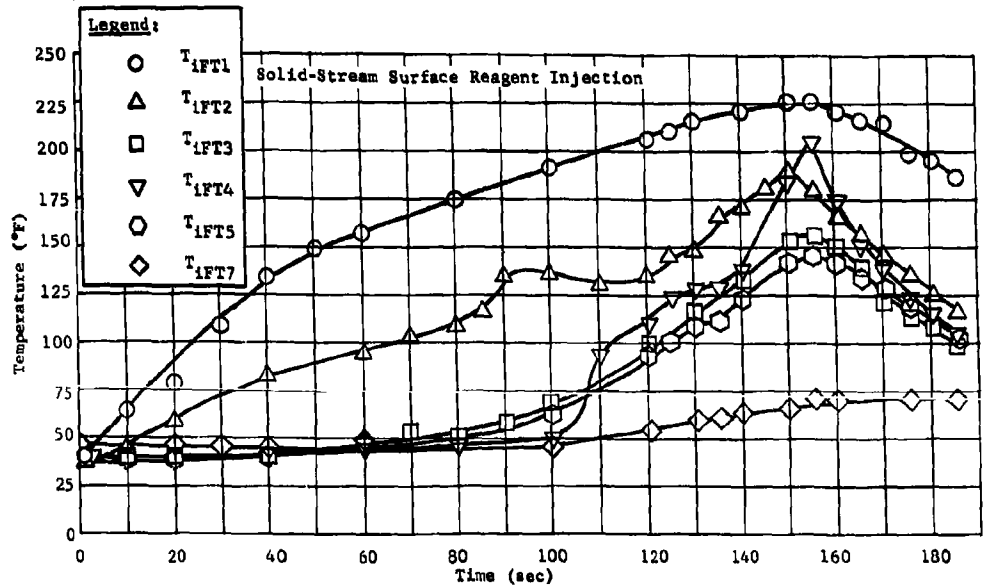


Fig. II-82 Primary Tank Internal Temperature Profile with Surface Gas Impingement in Oxidizer Tank

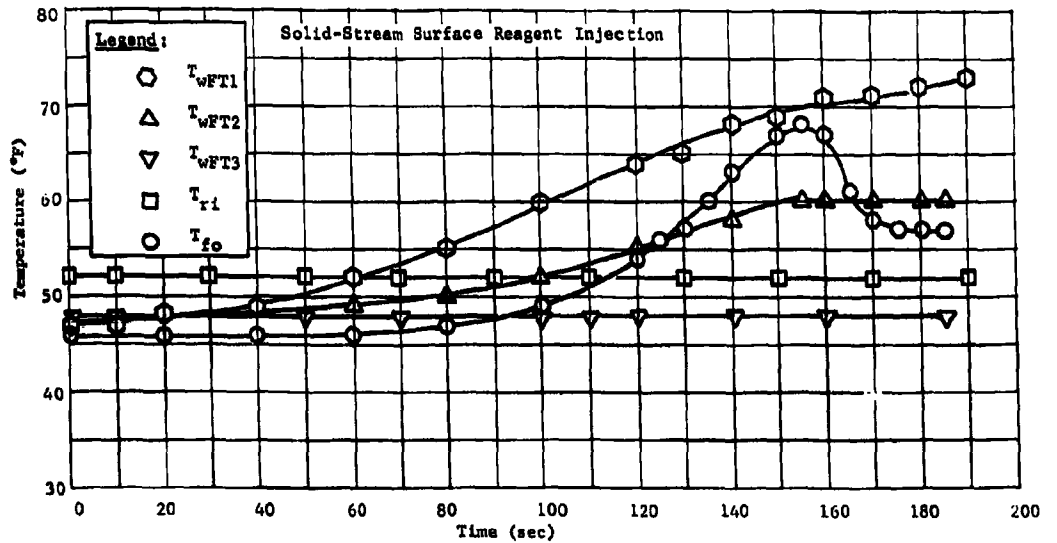


Fig. II-83 Primary Tank External Temperature Profile with Surface Gas Impingement in Oxidizer-Filled Secondary Tank

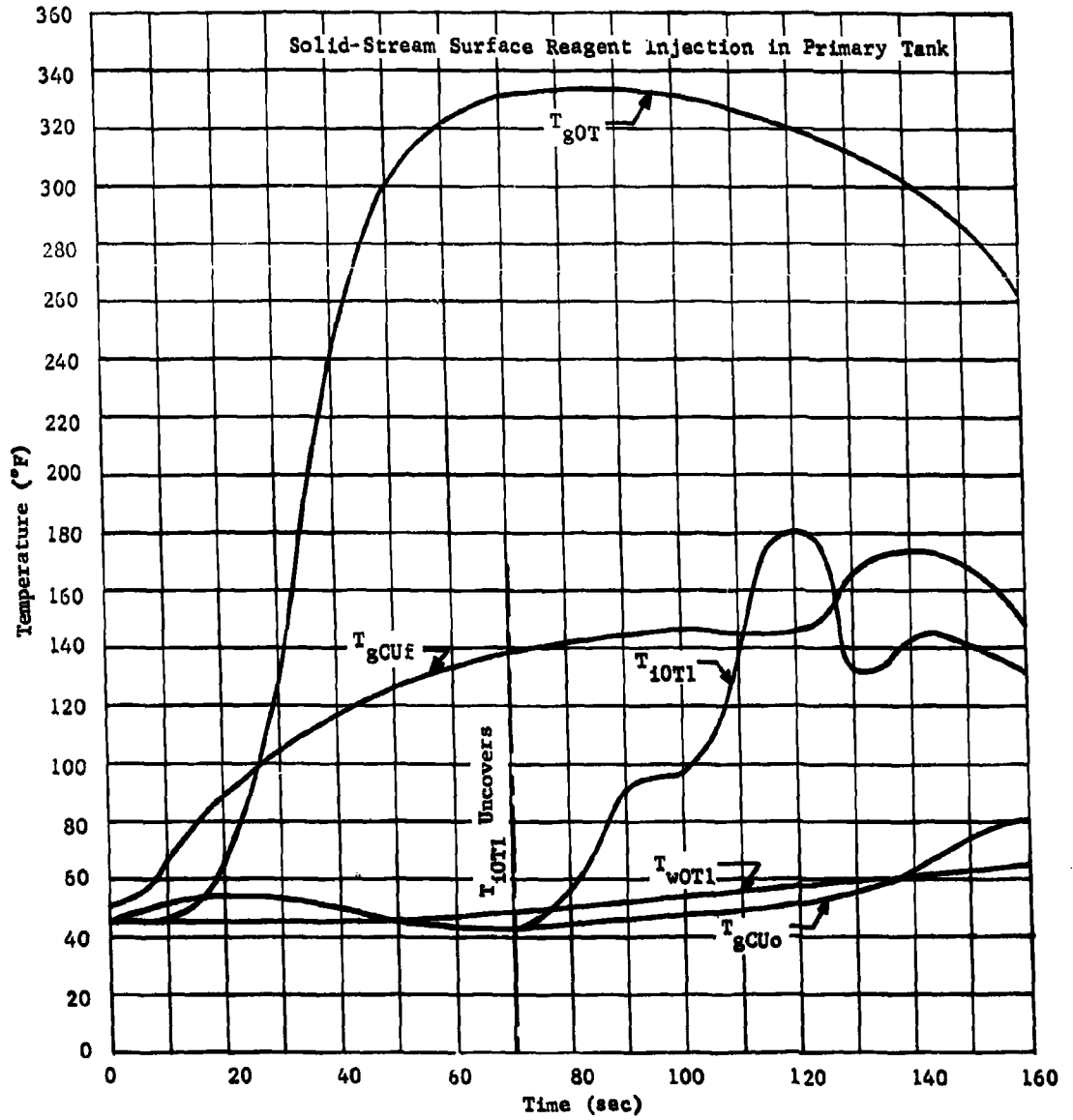


Fig. II-84 Temperatures in Oxidizer Tank with Surface Gas Impingement and Gunk Condenser

Primary tank pressure and temperature control was satisfactory, and no entrained vapors were noted in the fuel outflow. Acceleration measurement in the fuel tank X-axis showed a double amplitude vibration level of 0.13 g in the fuel tank. The average reagent consumption for the two good runs was 0.311 lb.

Secondary tank pressure control was erratic with pressure variations reaching ± 2.5 psi. The maximum temperature in the secondary tank ullage was well above the 300°F desired temperature. Figure II-79 shows the comparison between primary and secondary pressure and temperature control. The oxidizer flow rate change seen in Fig. II-79 was caused by remote flow control valve adjustment to obtain the desired outflow rate. A more detailed secondary tank temperature and pressure data plot showing the maximum fluctuation is presented in Fig. II-80 and II-81, respectively. Injection shutdown occurred at T - 155 sec, accounting for the decreasing temperatures noted after this time in Fig. II-82 and II-83. Secondary tank combustion product molecular weight was 23.3 with an average ullage molecular weight of 27.8 including the NO₂ but not the helium used for pressurization. The secondary tank erratic pressure and temperature control was believed to be caused by liquid condensate intermittently being injected onto the oxidizer liquid surface, causing secondary reactions between the oxidizer vapors and the combustible constituents of the combustion products formed in the primary tank.

The next test performed was identical to the previous tests except that subsurface spray injection was used in the primary tank. This test was made to determine if this injection technique would decrease the secondary tank reactions by altering the combustion product composition or condensing some of the reactive constituents of the combustion gas in the fuel.

The results of this test were: primary tank temperature and pressure control was satisfactory, and no entrained vapors were noted in the propellant outflow; acceleration measurements showed a double amplitude vibration level of 7 g along the fuel tank X-axis. This acceleration measurement confirmed visual observations of tank vibration made during injection technique development tests. Reagent consumption was 0.456 lb.

Secondary tank pressure and temperature control was again unsatisfactory. Secondary tank pressure variations were ± 2.0 psi. The maximum tank ullage temperature was 320°F, which was 200° lower than previous tests but still above the desired maximum temperature. Temperature changes were erratic and corresponded to the pressure variations, indicating the secondary reaction had not been appreciably reduced. Secondary tank combustion product molecular weight was 22.7.

A subsequent test run was performed using the subsurface spray injection technique identical to the previous run except that the common ullage line was extended into the oxidizer tank until the outlet was approximately 2 in. above the oxidizer surface at test start (5% ullage). In addition, the common ullage line outlet was reduced from a 1-in. dia to a 1/2-in. dia to increase the velocity of the gas impinging on the oxidizer surface. This test was performed to determine the effect of high velocity (31 fps as opposed to 7 fps previously used) surface gas impingement in the secondary tank.

The results of this test were primary tank temperature and pressure control was satisfactory; fuel tank X-axis vibration level was 6 g (double amplitude).

Secondary tank temperature and pressure control was satisfactory to T + 60 sec, at which time a sudden temperature and pressure rise occurred in the secondary tank. Secondary tank temperature spiked off scale (greater than 500°F) and the tank pressure was sufficient to rupture a 300 ± 50 psi burst disc on the secondary tank. The cause of this explosion was due to the high velocity of the combustion product condensate (gunk) impinging on the oxidizer surface igniting the explosive ullage gas. This conclusion is based on subsequent determination that liquid condensate (gunk) is hypergolic with liquid N_2O_4 , which in turn detonating the combustible constituents of the pressurizing gas.

Because of the vibration in subsequent tests associated with subsurface gas impingement in the secondary tank, another test run was made using surface gas impingement and a condensate trap to reduce secondary tank reactions previously seen with surface gas impingement. The test configuration was the same as the first surface gas impingement test except that the external demister was used in place of the internal demister. A trap designed to separate liquid particles from the common ullage gas was installed in the common ullage line and submerged in an ice water bath.

The results of the test are summarized below and the pertinent data are shown in Fig. II-84.

The primary tank temperature and pressure control was satisfactory and similar to tests without the condenser installed. No tank vibration or entrained vapor in the propellant outflow was noted. Reagent consumption was 0.298 lb. The primary tank gas sample was taken downstream of the condenser for this test and was determined to have a molecular weight of 14.07.

Secondary tank pressure was satisfactory, with pressure variations within a 0.5-psi band. Secondary tank temperature control was fair (maximum of 328°F), but maximum tank temperature was reached within the first 60 sec and remained at the high level throughout the remaining 102 sec of the test run. Molecular weight of the combustion products was 18.4. No vibration was noted in the secondary tank. No entrained vapors were noted in the oxidizer outflow. This test met all system requirements except for the moderately high temperature in the secondary tank. Inspection of the condensate trap showed that between 15 and 20 grams of gunk was collected; however, inspection of the common ullage line showed additional condensate in various areas, indicating complete gunk separation had not been achieved.

Secondary Tank Subsurface Gas Impingement Test Series - The next test sequence was made to determine the effects of subsurface gas impingement in the secondary tank, since the surface gas impingement had demonstrated poor temperature and pressure control in the secondary tank. The first two tests of this sequence had the following test configuration. Prepressurization, fuel outflow rate, and test conduction were identical to the previous surface gas impingement runs. The oxidizer ullage was increased to 30% and the oxidizer flow rate was decreased to 10 gpm for these runs. Surface solid-stream reagent injection was used in the primary tank. The common ullage line configuration was the same except the line was extended below the surface of the oxidizer and a check valve incorporated at the end of the line. The condensate trap was removed for this test and the demister was located inside the fuel tank. The line was reduced in size to 1/2-in. diameter for the entire extension. The outlet of the check valve was plugged and forty-eight 3/32-in. diameter holes were drilled in the valve body to direct the common ullage gas in a symmetrical radial pattern from the end of the line. The plugged outlet of the check valve was approximately 1/2 in. above the second tank outflow baffle splash plate. The results of these tests are given in the following paragraphs.

Primary tank temperature and pressure control was satisfactory and no entrained vapor was noted in the fuel outflow. Average reagent consumption for the two runs was 0.377 lb. The combustion products average molecular weight was 17.2 for these runs.

Secondary tank pressure and temperature control was satisfactory. Secondary tank pressure variation was within a 0.5-psi band on both runs. The maximum ullage temperature attained (second run) was 118°F. Acceleration measurements showed a vibration level of 0.65 g (double amplitude) for the secondary tank X-axis on both runs. Average combustion product molecular weight for the runs was 22.8.

Based on these test results, two more runs were made using the identical test configuration except that the oxidizer tank was loaded to a 5% ullage and oxidizer flow rate was increased to 14 gpm. An external stainless steel mesh demister was incorporated in the common ullage line between the fuel tank and the isolation valve to replace the internal demister, which had been ineffective.

Figures II-85 thru II-87 represent typical performance curves for these test runs. The general results of the runs are given in the following paragraphs.

Primary tank temperature and pressure control was satisfactory for both runs. The injector clogged after 110 sec of the second run, but data from this run were very similar to the first run up to the point of injector clogging. Visual observation indicated no entrained vapor in the fuel outflow and no fuel tank vibration. Reagent usage for the first run was 0.246 lb (140 sec), and 0.204 lb (110 sec) for the second run. Combustion product molecular weight was 17.0.

Secondary tank temperature and pressure control was good for both runs. Pressure control was within a 0.5-psi band, while the maximum tank ullage temperature was 64°F. The outlet plug was left out of the check diffuser for the first run, resulting in a 5.6 g (double amplitude) vibration level for the secondary tank X-axis. The plug was installed for the second run and the vibration level dropped to 3.3 g (double amplitude) in the X-axis. No entrained vapor was noted in the oxidizer outflow. Gas analysis showed an average combustion product molecular weight of 26.5 and ullage gas molecular weight of 31.5 on a helium-free basis.

Restart Test Series - The test series following the surface and subsurface gas impingement evaluation incorporated no helium prepressurization. It included a simulated coast period and a polytropic gas expansion process to expel the residual propellants.

The test sequence followed in all the test runs of this series was:

- 1) The common ullage valve was opened and both tanks were pressurized by injecting reagent into the fuel tank;
- 2) After the tanks were pressurized, the propellant outflow was initiated with a 1-sec oxidizer lead. The outflow was continued for 65 to 75 sec;

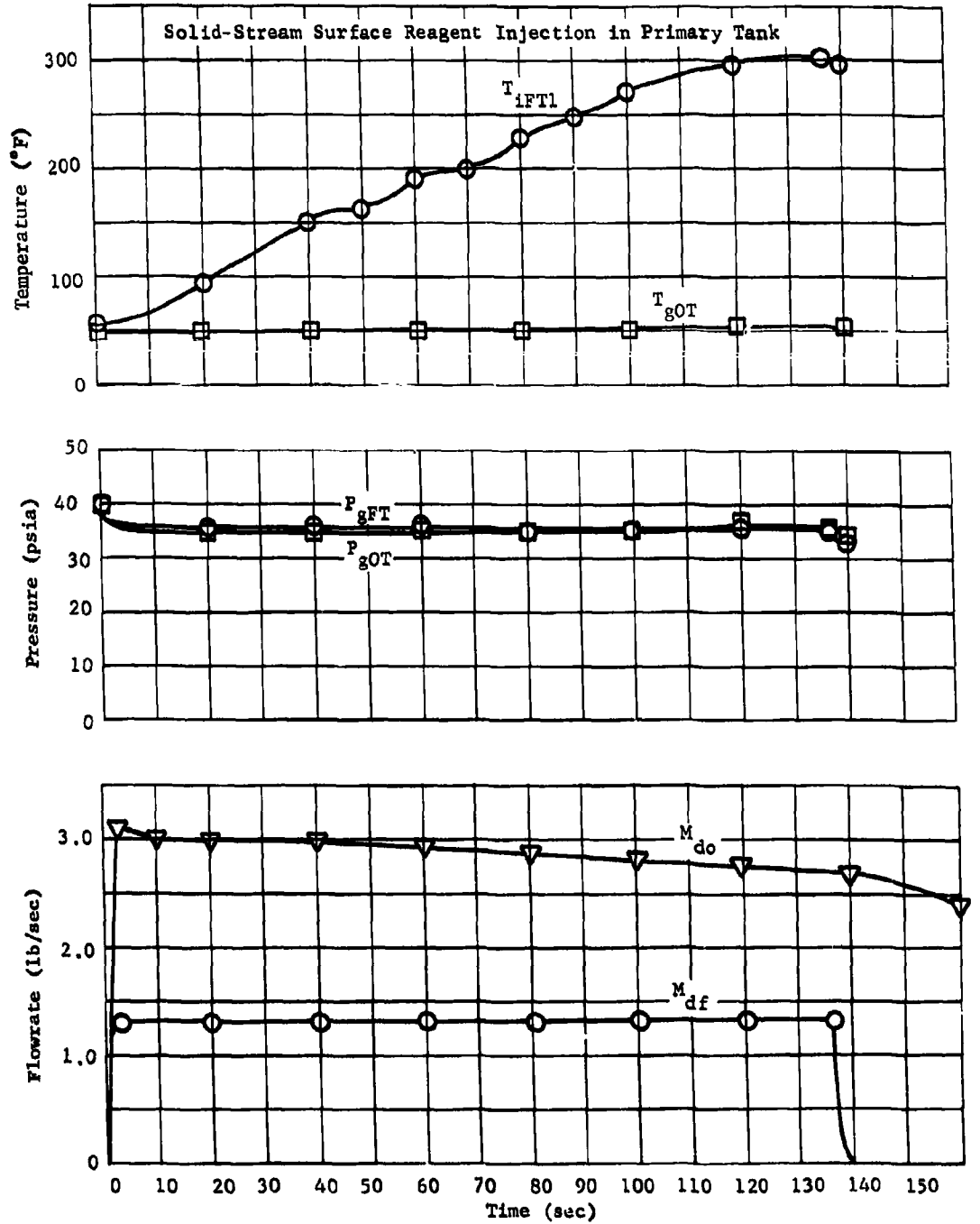


Fig. II-85 Pressurization System Performance Curves with Subsurface Gas Impingement in Oxidizer Tank

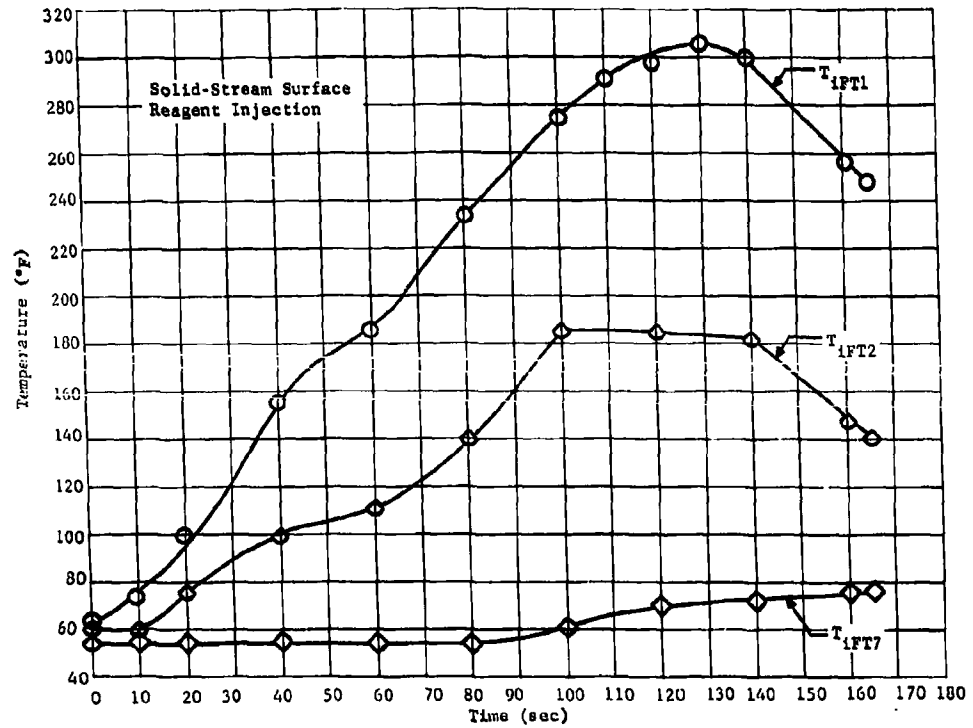


Fig. II-86 Primary Tank Internal Temperatures with Subsurface Gas Impingement in Oxidizer Tank

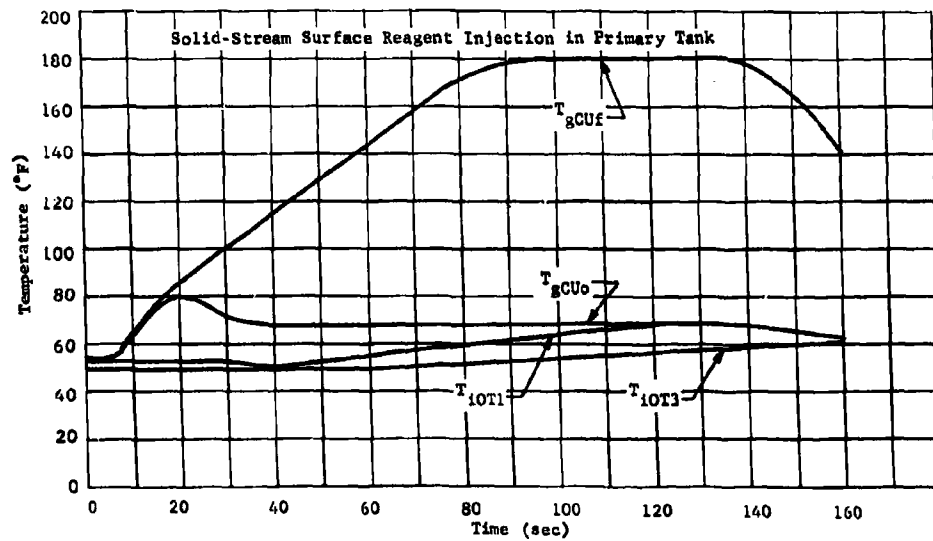


Fig. II-87 Oxidizer Tank Temperatures with Subsurface Gas Impingement

- 3) Throttle then outflowed to zero flow and a 10-min. coast period was started keeping the injector energized and common ullage open;
- 4) After the 10-min coast period, restart was initiated by opening propellant outflow valves;
- 5) The injector was de-energized when the fuel tank low-level sensor was uncovered;
- 6) Propellant outflows were continued with polytropic expansion until all propellant had been expelled from the tanks.

The first test configuration in this series was identical to the first test conducted using subsurface gas impingement. The fuel and oxidizer tanks were loaded to 30% and 5% ullages, respectively. The common ullage system consisted of a 1-in. flexline incorporating the external demister, isolation valve, and check valve. The subsurface gas impingement systems used the check diffuser at the end of a 1/2-in. tube (located 1/2 in. above the secondary tank outflow baffle).

Figure II-88 represents the primary performance curves for this test. The results of the test are given in the following paragraphs.

Primary tank temperature and pressure control was satisfactory. No tank vibration or outflow entrained vapors were noted during the test. The injection technique used was surface solid-stream, resulting in a reagent consumption 0.459 lb during the test run. Combustion product molecular weight was 17.0.

Secondary tank temperature and pressure control was satisfactory during the test until 12 sec after restart, when a sudden overpressure and high temperature occurred. The pressure returned to normal after 6 sec and the temperature was normal after 25 sec. The test run was continued satisfactorily. The overpressure and temperature rise was later determined to be due to a hydrogen reaction in the ullage, triggered by combustion product condensate still reacting when it reached the liquid surface. No entrained vapors were noted in the oxidizer outflow. The vibration level was similar to that in previous testing using the check diffuser gas injector in the secondary tank. The molecular weight of the combustion products was 25.5. A significant decrease in hydrogen was noticed after the uncontrolled secondary reaction.

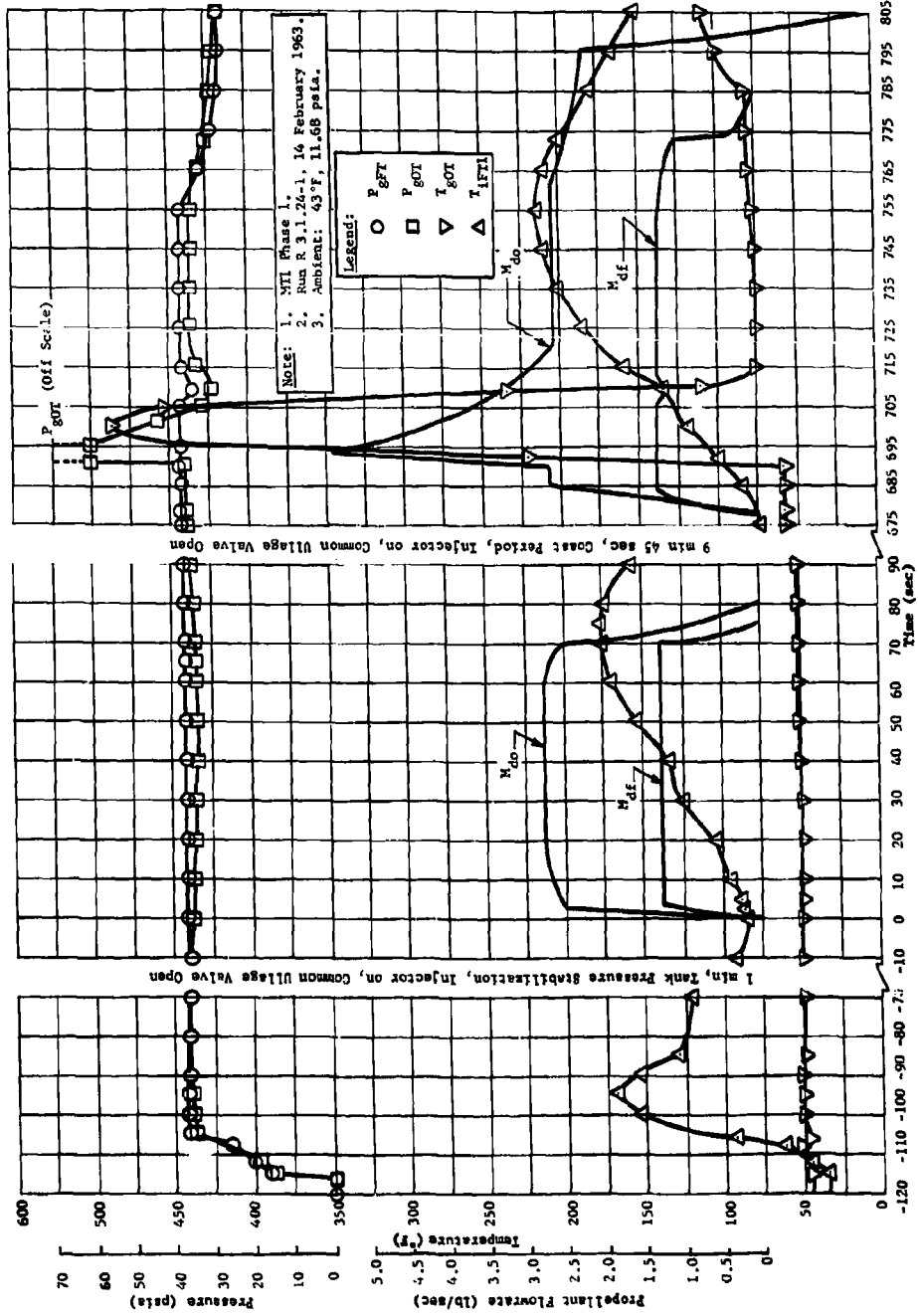


Fig. II-88 Instant Test Pressurization System Performance Curves with Uncontrolled Secondary Reaction

The next test in the series was identical to the first test except that two condensate (gunk) traps were installed in series in the common ullage line to minimize the condensate entering the secondary tank. The results of this test, up to the restart sequence, were almost identical to the first run. Twenty seconds after restart the oxidizer tank again experienced a rapid temperature and pressure rise. The pressure rise was sufficient to rupture one oxidizer tank burst disc (300 ± 50 psi). The maximum secondary tank temperature was greater than 500°F . Reagent usage was 0.415 lb at shutdown, because of the ruptured burst disc. The probable cause of the rapid temperature and pressure rise was the same as in the previous test. Figure II-48 is a photograph of the test configuration for this test run.

The third test in this series incorporated a different common ullage line configuration. The common ullage line was reduced in size to a 1/4-in. stainless steel line with a 0.035-in. wall thickness. The entire line was insulated to prevent cooling of the common ullage gases. The purpose of this configuration was to increase the gas velocity and decrease the heat transfer surface, to keep the gunk entrained in the common ullage gases and prevent it from condensing in large quantities. The common ullage line entered the second tank through a port on the tank bottom. A gas diffuser, a short tube with three 3/32-in. dia holes, was used as a gas injector. The isolation valve was a 1/4-in. solenoid valve. Two check valves were incorporated in the common ullage line to prevent back flow from the oxidizer tank to the fuel tank. The remaining test configuration was identical to the previous test run. Figures II-89 and II-90 show typical performance curves for this type of test run.

Primary tank temperature and pressure control was satisfactory. No entrained vapors were noted in the fuel outflow. Visual observation indicated slight primary tank vibration during this run. This vibration was probably transmitted from the secondary tank through the solid common ullage line. Reagent consumption was 0.434 lb. Combustion products molecular weight was 17.7.

Secondary tank temperature and pressure control was satisfactory. The pressure drop of 8 psid through the common ullage line was later found to be due to an undersized isolation valve. No entrained vapors were noted in the oxidizer outflow. Secondary tank vibration level was 3 g double amplitude during this run. The molecular weight of the combustion products was 24.7, giving a total molecular weight of 33.4 for the secondary tank gas.

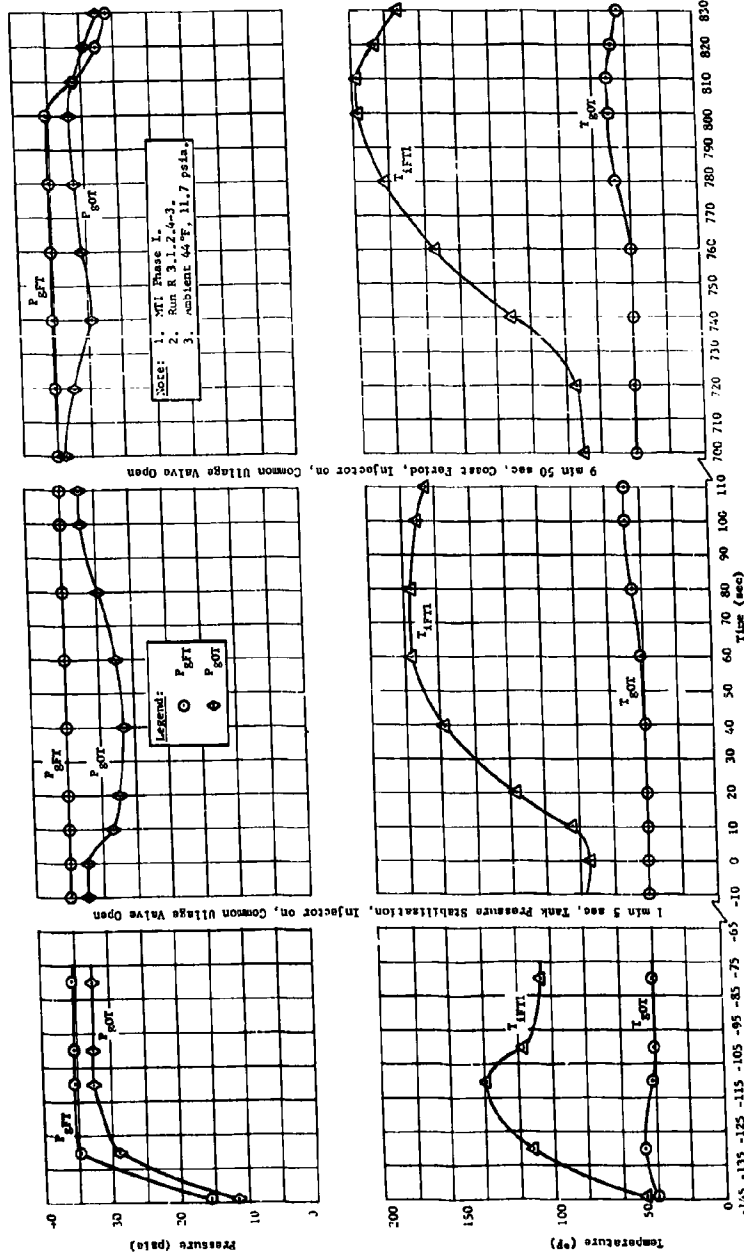


Fig. 11-89 Restart Test Pressurization System Performance with Controlled Secondary Reaction, Subsurface Gas Impingement

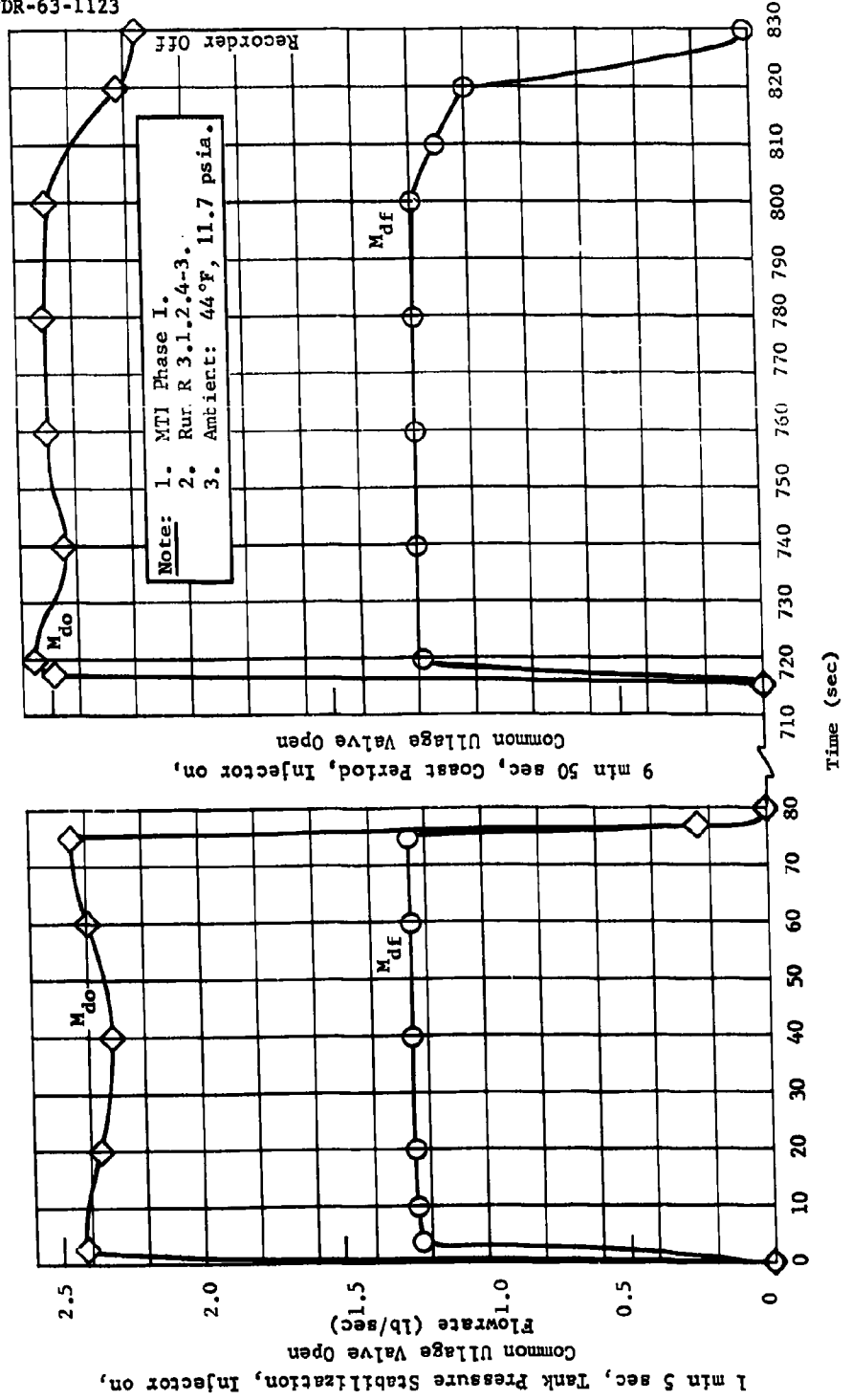


Fig. II-89 (concl)

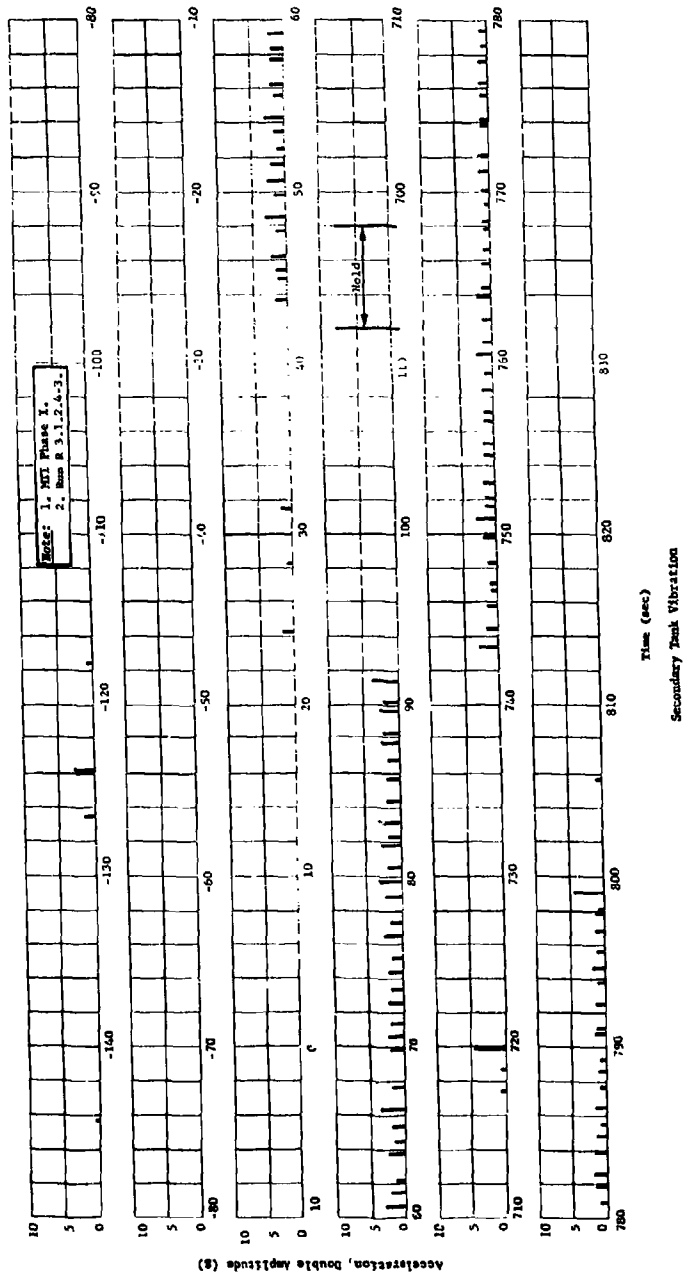


Fig. II-30 Restart Test System Vibration with Controlled Secondary Reaction - Subsurface Gas Impingement

The fourth test run was the same as the previous run except that the 1/4-in. common ullage valve was replaced with a 1/2-in. valve to decrease pressure drop, and the gas injection diffuser was replaced by a diffuser with twenty 0.040-in. dia holes. The results of the test were similar to those of the previous run. Temperature and pressure control was satisfactory in both tanks. No entrained vapors were noted in the propellant outflows. Tank vibration was the same as that described in the previous run. Reagent consumption was 0.626 lb. Erosion of the injector orifice resulted in a combination solid-stream spray injection pattern that caused the high reagent consumption typical of surface spray injection techniques. Molecular weights of primary and secondary tank combustion products were 19.3 and 20.5, respectively. Common ullage line pressure drop was again high, and a 1-in. isolation valve was later installed to reduce the pressure drop to 0.5 psid.

Three runs were then made to obtain the desired secondary tank pressurization performance. In addition to replacing the common ullage isolation valve and eliminating the lower check valve, the 3/8-in. dia gas diffuser was modified by increasing the number of holes to sixty. Additional tests were performed to improve system operation, however, the performance obtained is representative of the final configuration evolved. Detailed data are included in Fig. II-91 and II-92. An actual data history of a run with a 5-min coast is presented in Fig. II-93. Pressure and temperature control were good in both tanks. There was no evidence of entrained vapor in the expelled propellant. Oxidizer tank vibration was again 3 g double amplitude at an average frequency of 1 cps. Typical performance for this type test indicated a maximum primary tank gas temperature of 156°F and 51°F in the secondary tank with an average reagent consumption of 0.436 lb. The 650°F temperature rise detected periodically in the common ullage line was attributed to a gunk reaction with nitrogen tetroxide.

To reduce the vibrations in the secondary tank, uniform gunk injection was provided by a horizontal S-shaped subsurface gas diffuser with outlet ports designed to eject gunk, forced to the tube wall by centrifugal force, at predetermined distances. This system is shown in Fig. II-94. This test resulted in a sudden secondary reaction 32 sec after the coast period. No reduction in vibration was noticeable before the test ended.

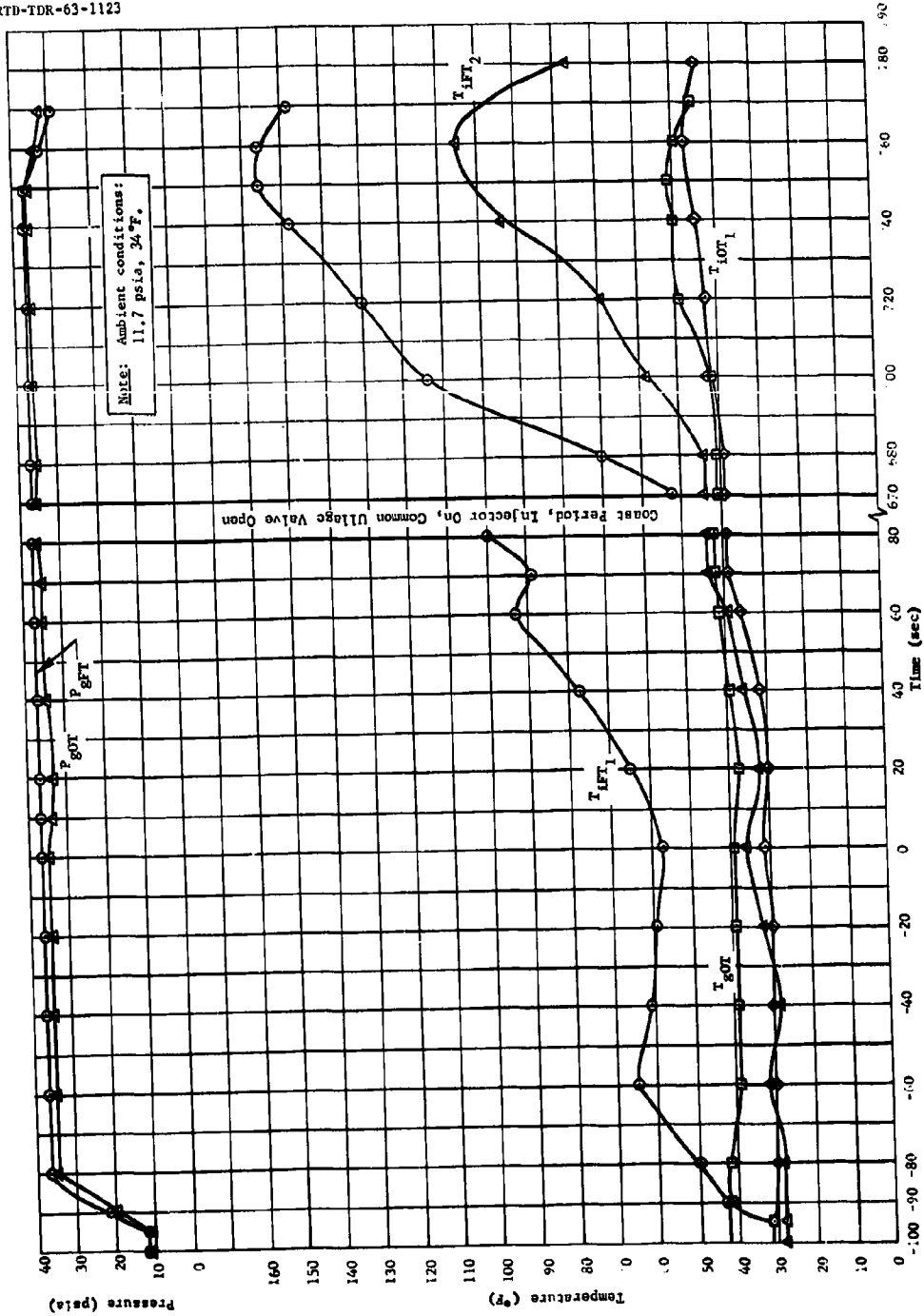


Fig. II-91 Restart Test Common Ullage Pressurization System Performance, Subsurface Gas Impingement

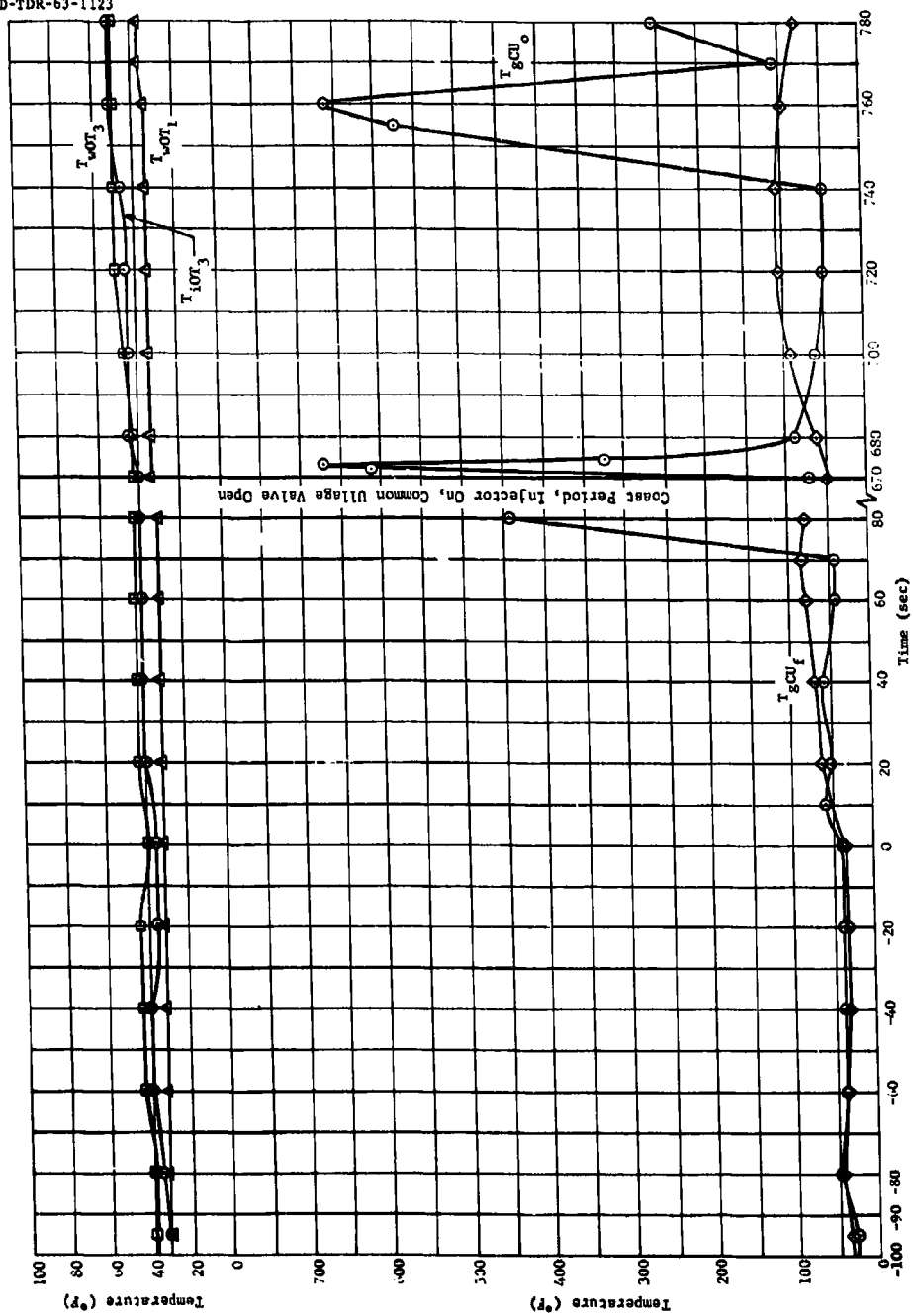


Fig. II-91 (cont)

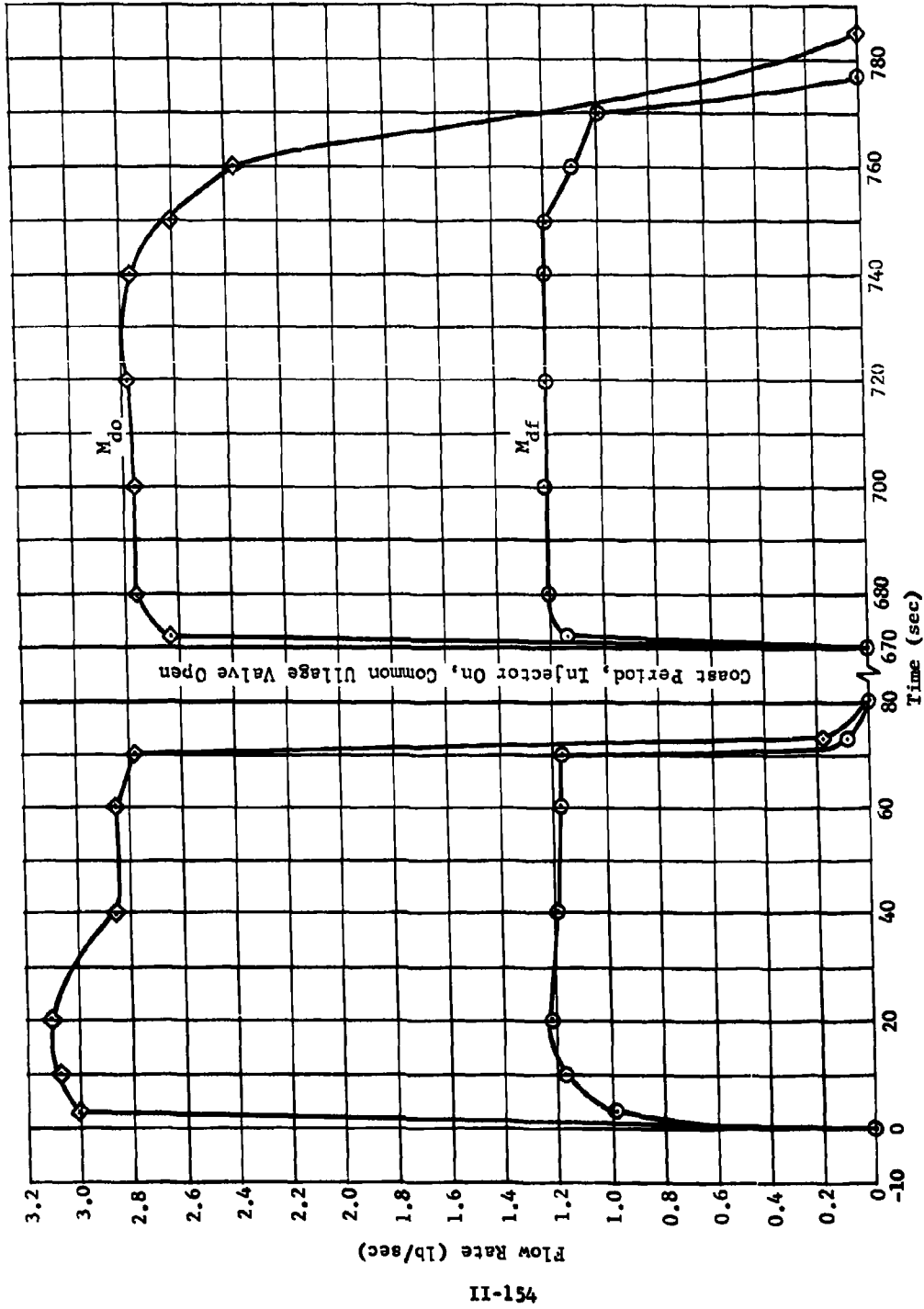
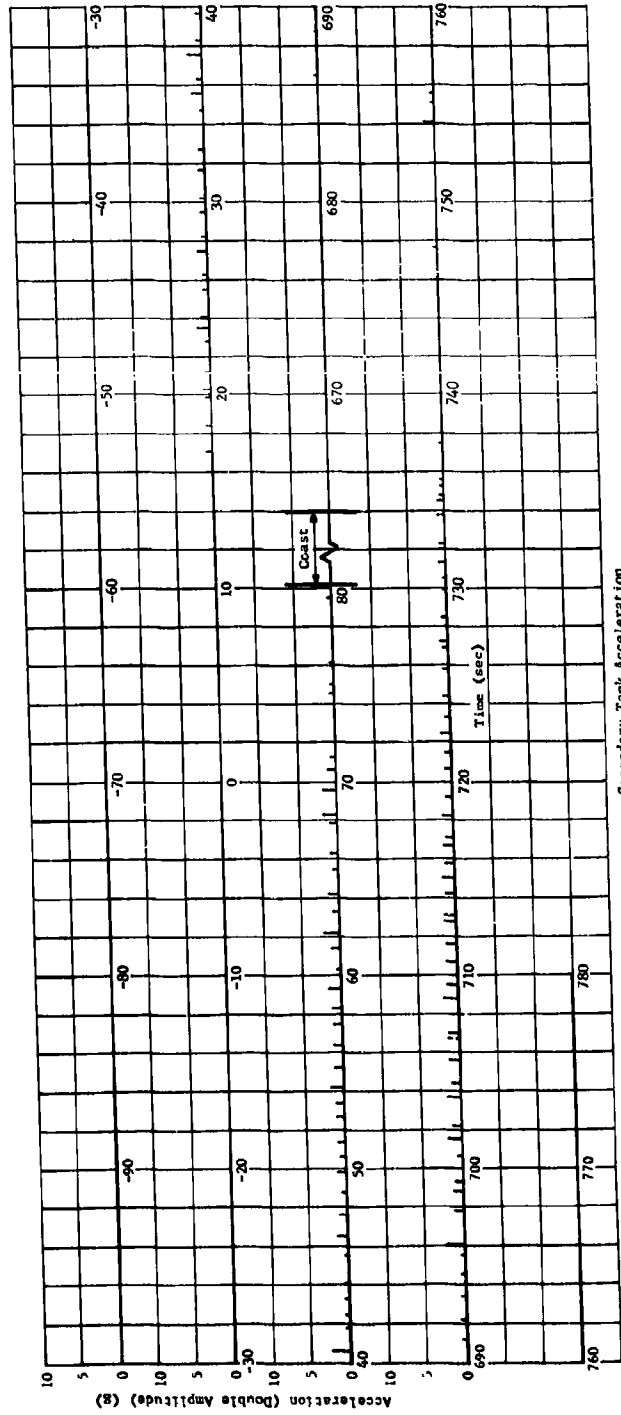


Fig. II-91 (concl)

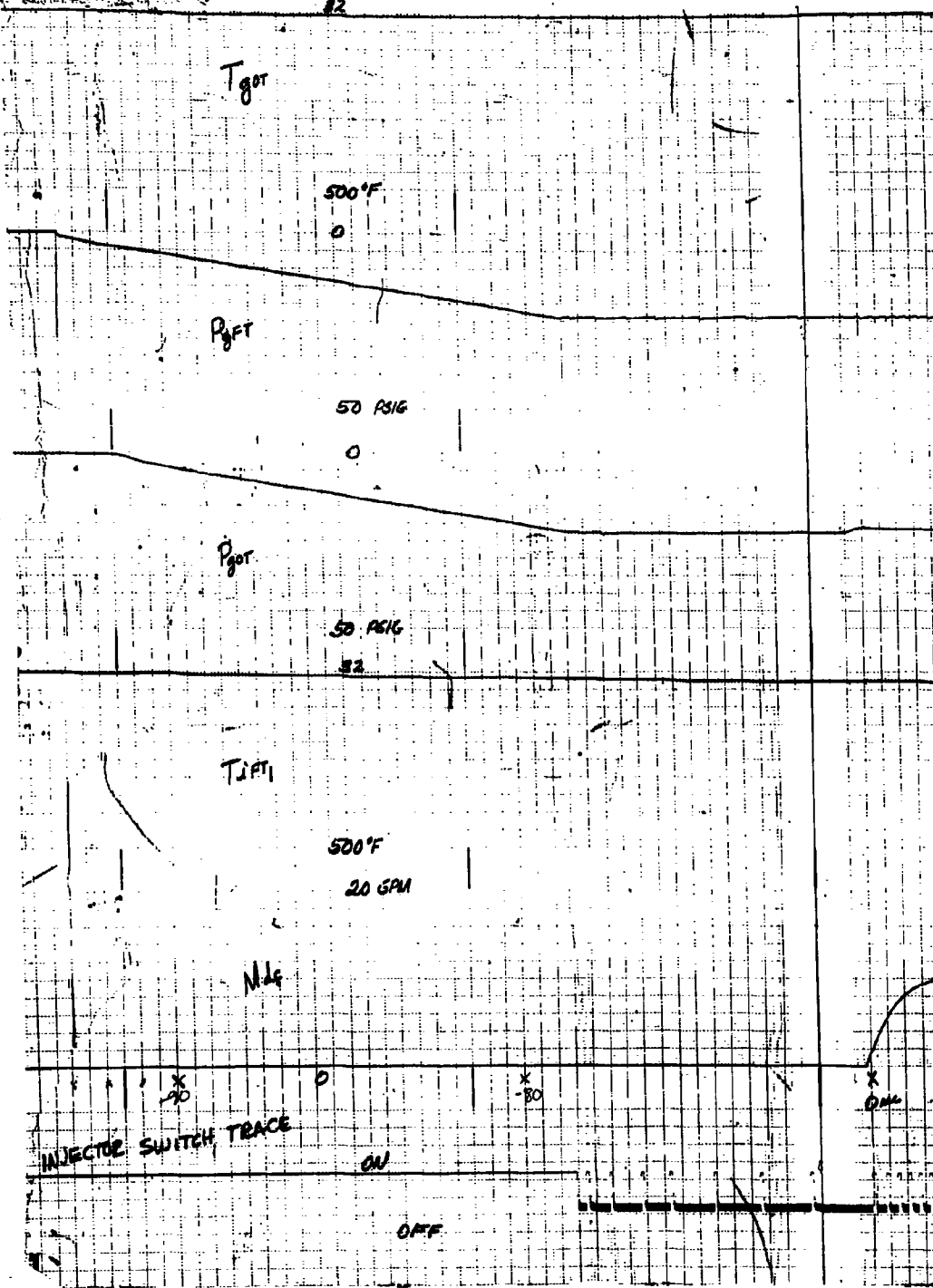


Secondary Tank Acceleration

Fig. II-92 Restart Test Common Illage Pressurization System Vibration, Subsurface Gas Impingement

RTD-TDR-63-1123

Text resumes on page II-157.



T_{gOT}

P_{gFT}

P_{gOT}

T_{gFT}

M_{dt}

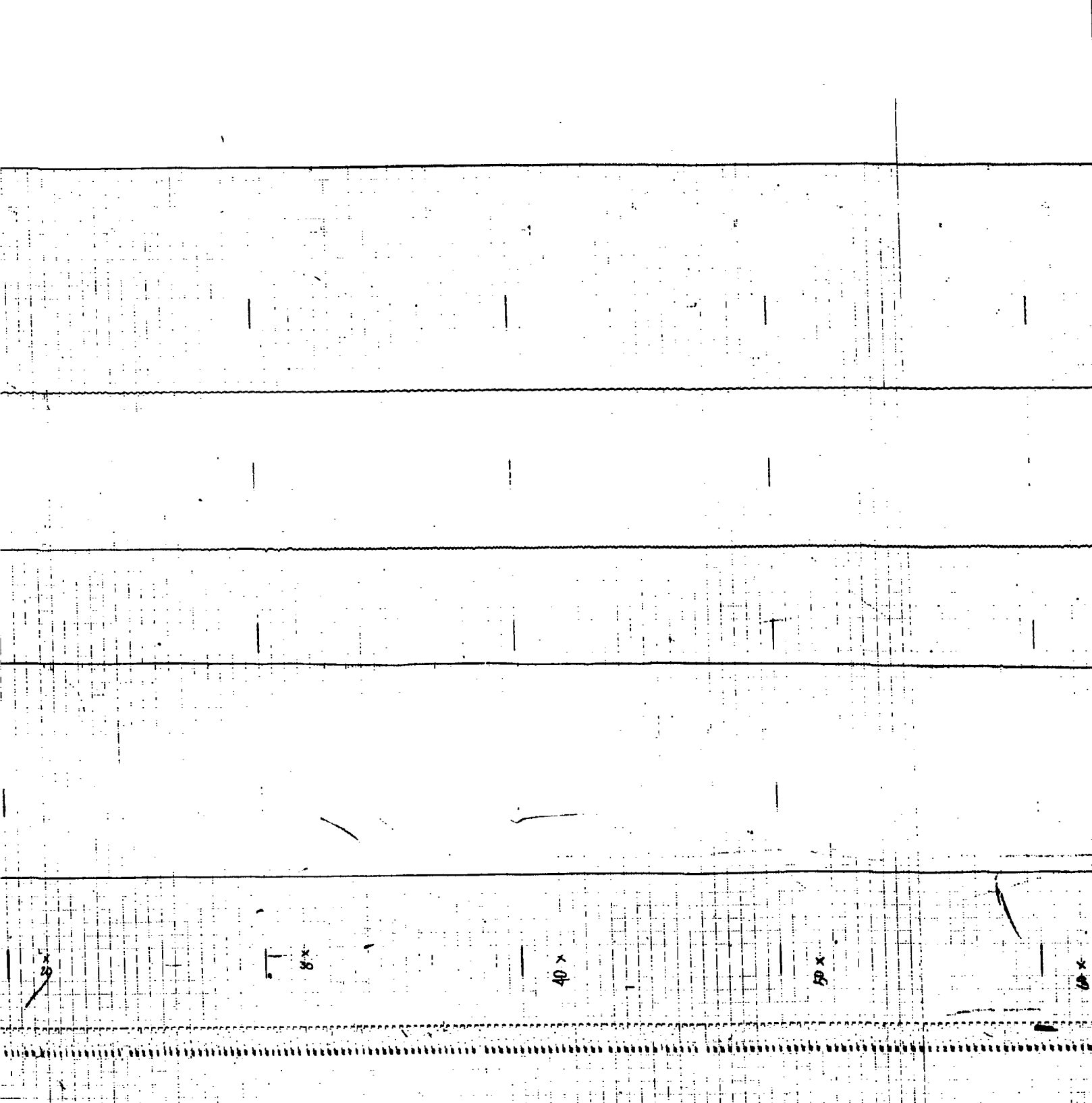
x
-30

x
0m

x
10

x
20





20 x

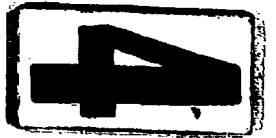
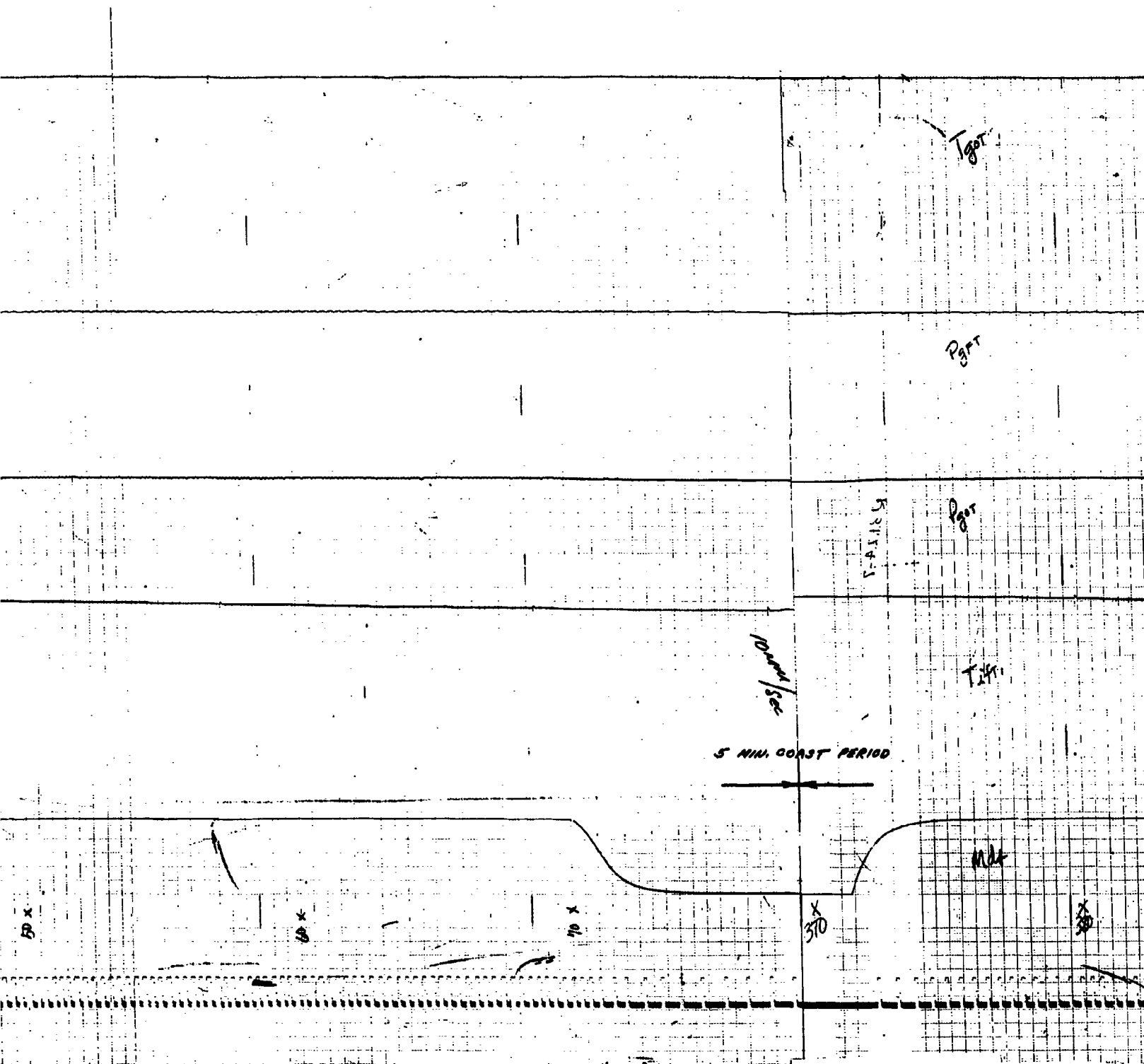
8 x

40 x

50 x

10 x

3



T_{got}

P_{got}

RAISE

P_{got}

T_{got}

PERIOD

ndt

X
70

X
30

X
390

X
410

X
410



X
410

X
420

X
430

X
440

9

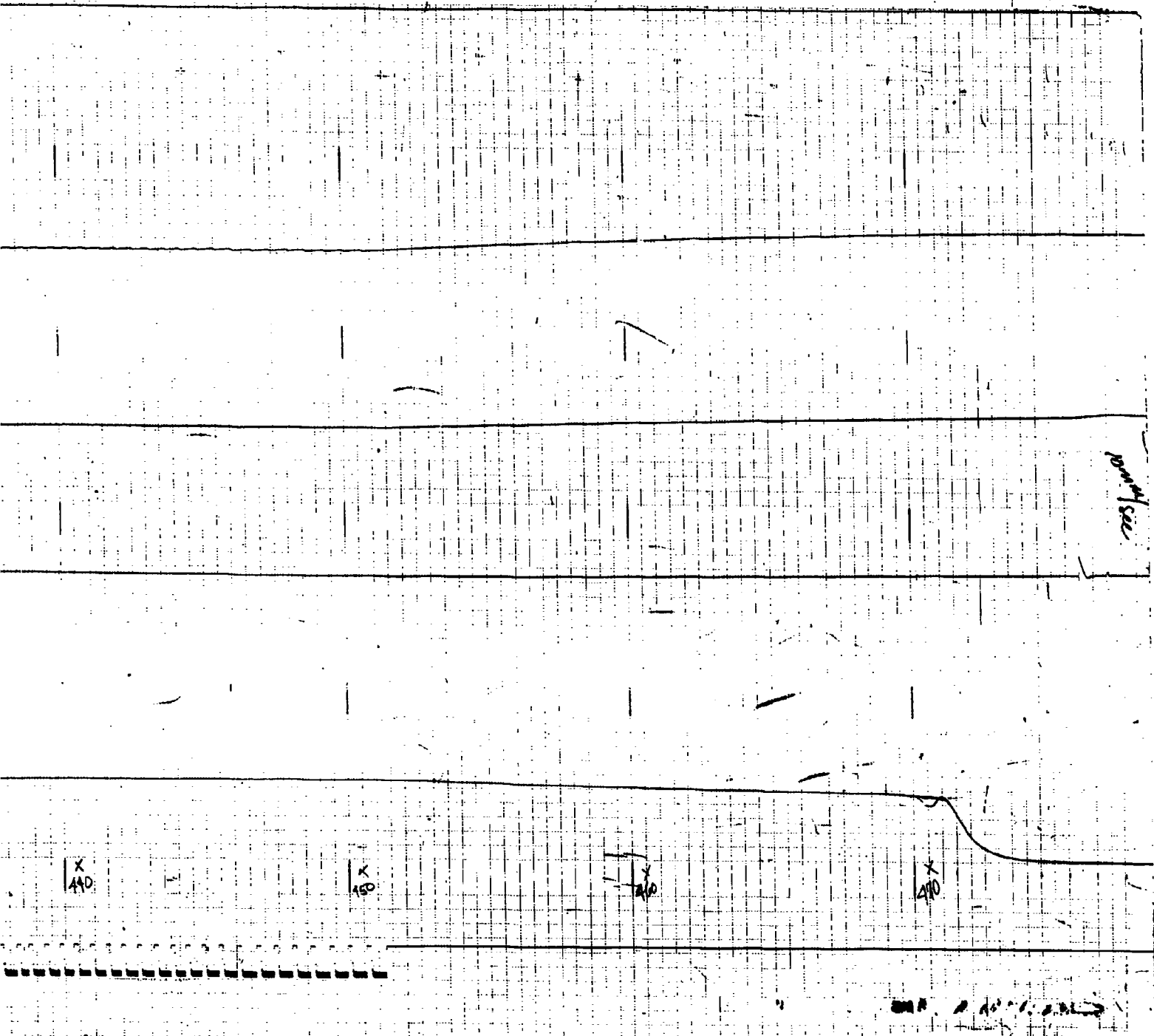


Fig. II-93 Restart Test Common Ullege Pressurization Actual Data



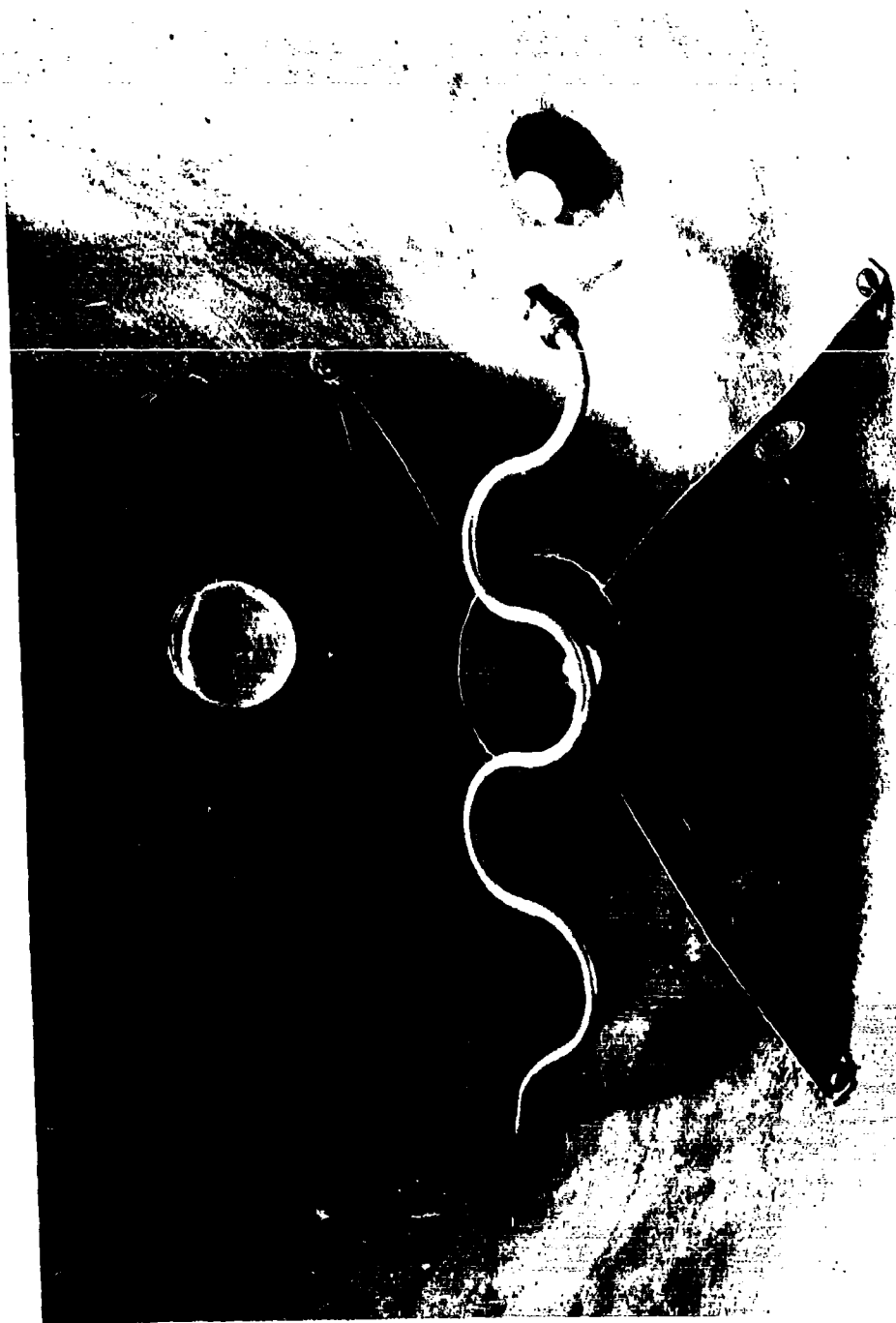


Fig. II-94 Secondary Tank Common Ullage "S" Shaped Subsurface Gas Diffuser

A second test was performed with a vortex separator installed in the gas crossflow line to reduce gunk injection. However, the amount that gunk injection was reduced (approximately 20 grams) was insufficient to noticeably reduce the secondary reaction or vibration levels. This configuration prolonged the detonation to 50 sec after the coast period. The cause of the previous explosions was attributed to insufficient stay time of the burning gunk below the liquid surface. This resulted in ignition of the hydrogen in the oxidizer tank ullage. A 20-in. long straight horizontal diffuser was then installed in the tank with downward gas diffusion provided by 65 0.040-in.-dia holes. The test was completed satisfactorily until a drop of gunk apparently dripped from the gas diffuser after it was uncovered by the oxidizer. This caused a minor explosion at shutdown. Since vibration was not reduced in any of the tests, attention was then directed to developing a surface gas impingement system.

Secondary Tank Conditioned Surface Gas Impingement Test Series -

The investigation of secondary tank pressurization by conditioned common ullage surface gas impingement was primarily initiated when attempting to reduce the vibration caused by the secondary reaction. A noticeable reduction in oxidizer tank ullage gas molecular weight was also realized in the successful tests. A lack of consistent performance discouraged development and a successful system was not conceived. Because of the complex nature of reactive constituent and elaborate gas conditioning equipment required to eliminate undesirable secondary reactions, additional investigation of gunk elimination techniques appears unwarranted. The research test effort was primarily concerned with investigating three basic oxidizer pressurization techniques for using surface cross-flow gas impingement:

- 1) Gas filtration by chemical or mechanical means;
- 2) Gas neutralization by chemical reaction;
- 3) Gas decomposition by catalysis.

All of the systems were based on eliminating the reactive constituent rather than hydrogen since a low molecular weight pressurizing gas was desired. Although hydrogen pressurization of an oxidizer tank is not the present missile pressurization method, an investigation of this technique demonstrated safe operation if the ignition source is eliminated.

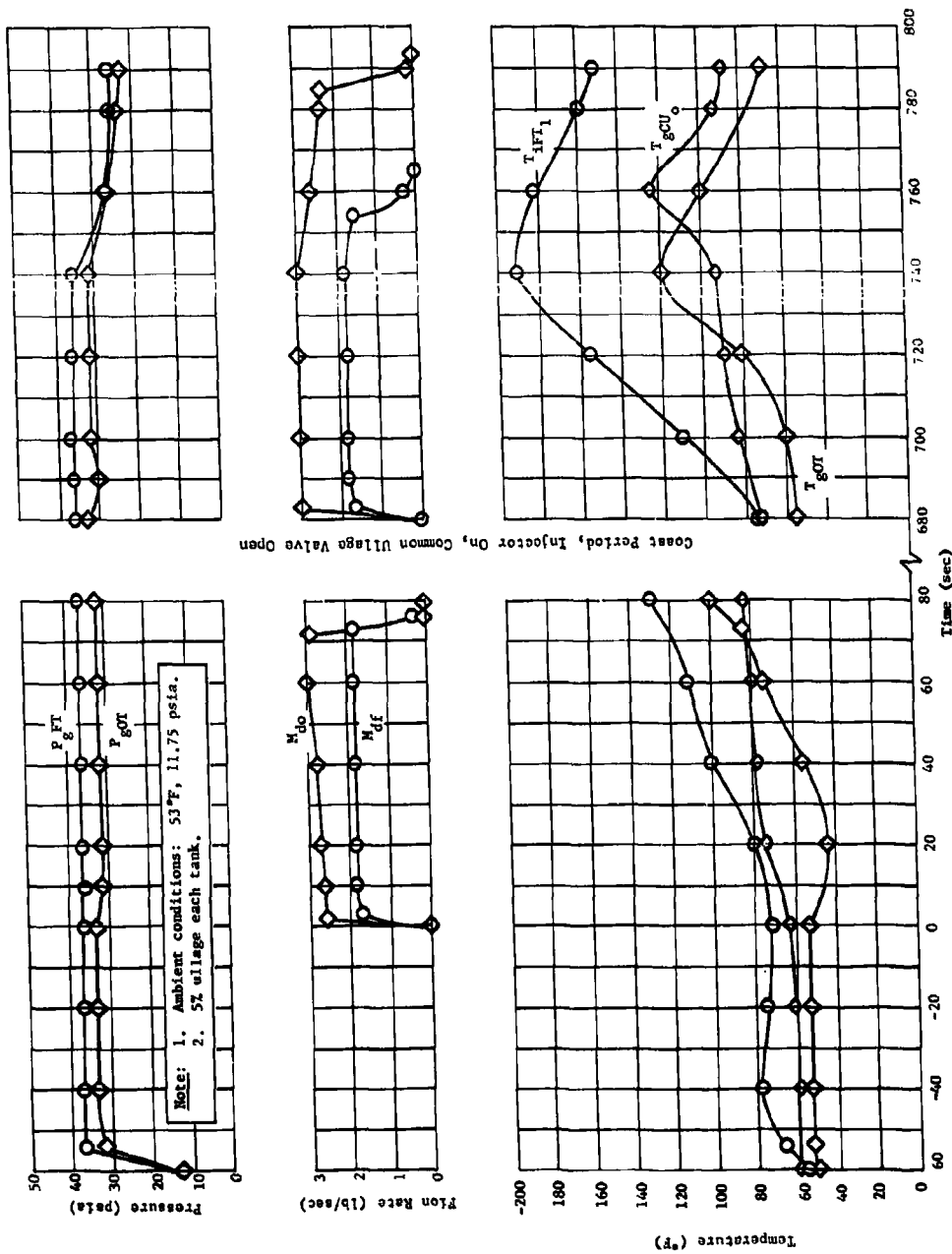
Initial tests were performed with a cross-flow gas filter consisting of a vortex separator and a filter containing spun glass, calcium carbonate, and activated carbon. Two tests were performed with both tanks loaded to 5% ullage and prepressurized with the MTI system. Although the first test, a 10 minute coast and restart, was performed satisfactorily with good pressure and temperature

control, a small amount of gunk was evident in the line downstream of the filter. Figure II-95 shows typical performance for this run, which is considered representative for common ullage oxidizer tank pressurization with gunk elimination. A comparable subsurface gas impingement test is presented in Fig. II-96. The accumulation of gunk, however, apparently caused an oxidizer tank overpressurization in a subsequent test.

Performance Analysis - Relatively consistent performance was obtained during the common ullage development test series with both the surface and subsurface gas injection process in the secondary tank for a continuous test. Only two mechanical failures were noted. The first problem occurred in the primary tank with solid-stream surface reagent injection when the orifice was damaged by erosion, causing a spray injection pattern (see Fig. II-97). No serious consequence occurred and the test was continued for the planned 150-sec duration. Subsequent analysis of the test data indicated the high gas molecular weight and temperature characteristic of this type process. However, the secondary tank temperature was somewhat lower (310°F) than was experienced with the undamaged injector for the surface gas impingement tests (500°F).

The second problem occurred in the secondary tank after test termination, when the oxidizer was being recycled for propellant sampling. While the main tank was being reloaded, oxidizer leakage past the check valve diffuser reacted with condensed gunk upstream of the check valve poppet. The reaction caused severe damage to the check valve poppet (see Fig. II-98), but no other damage from the reaction was noted. In the subsequent repair of the common ullage line, the internal demister showed signs of excessive fuel tank temperatures, which probably resulted from the failed injector. Figure II-99 shows the demister element and the end caps partially melted by the reaction process. A 1/2-in. dia by 2-in. tubular extension was welded to the injector orifice to provide proper direction to the stream in future cases of injector stream distortion.

Either subsurface or surface gas injection in the secondary tank can be employed in continuous-type tests with proper gunk control. Gunk elimination is mandatory for surface gas impingement in the oxidizer tank to provide stable pressure control and moderate temperatures. Proper gunk injection is required for subsurface gas impingement. The principal technique used in either method is to eliminate the combustion of large concentrations of hydrogen by maintaining the gunk reaction below the liquid surface or eliminating the gunk reaction entirely.



Coast Period, Injector On, Common Ullage Valve Open

Fig. II-95 Restart Test Common Ullage Pressurization System Performance With Secondary Reaction Reduction, Surface Gas Impingement

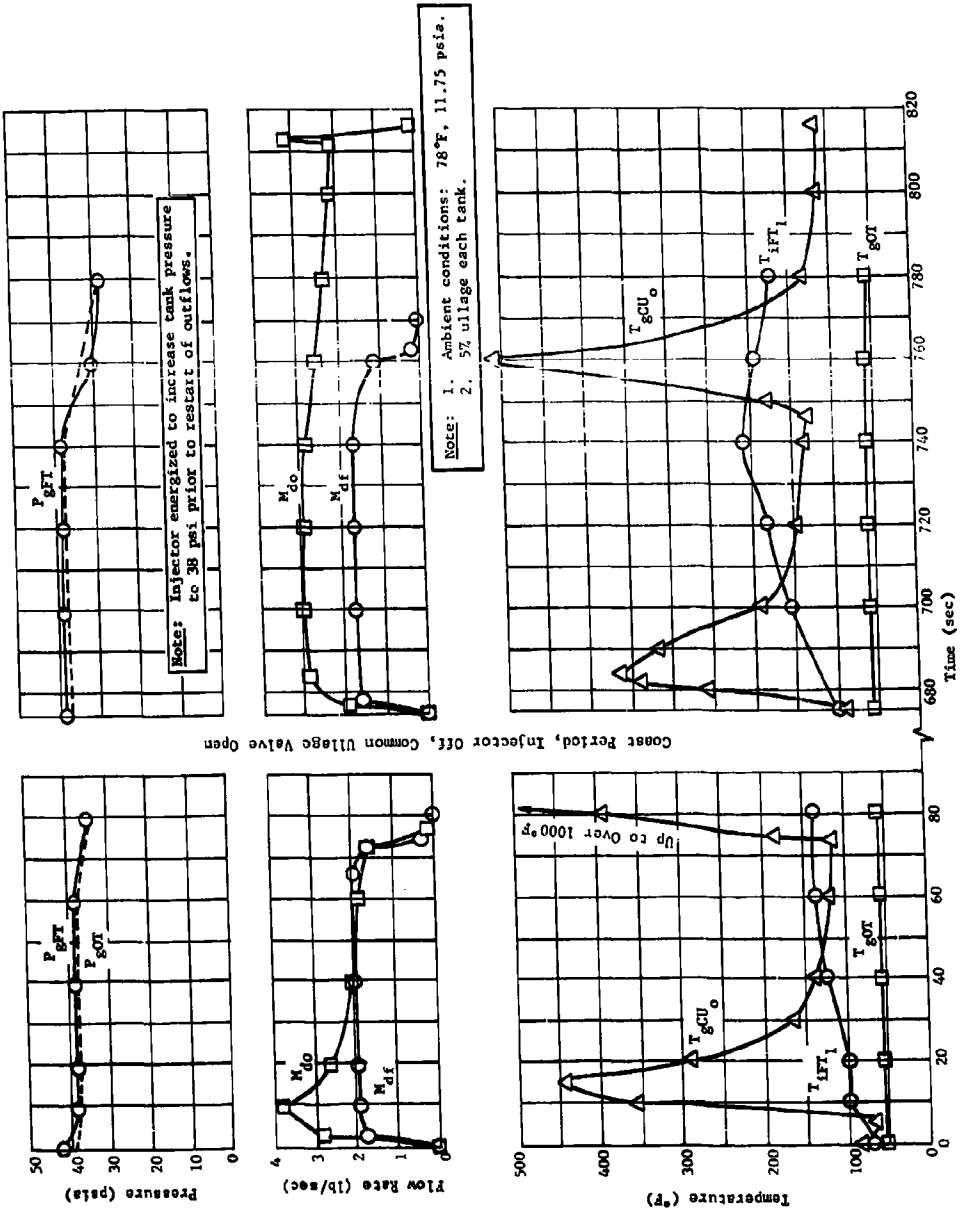


Fig. II-96 Restart Test Common Ullage Pressurization System Performance, Subsurface Gas Impingement



Fig. II-97 Failed Solid Stream 0.012 Diameter Injector Orifice



Fig. II-98 Check - Diffuser Poppet

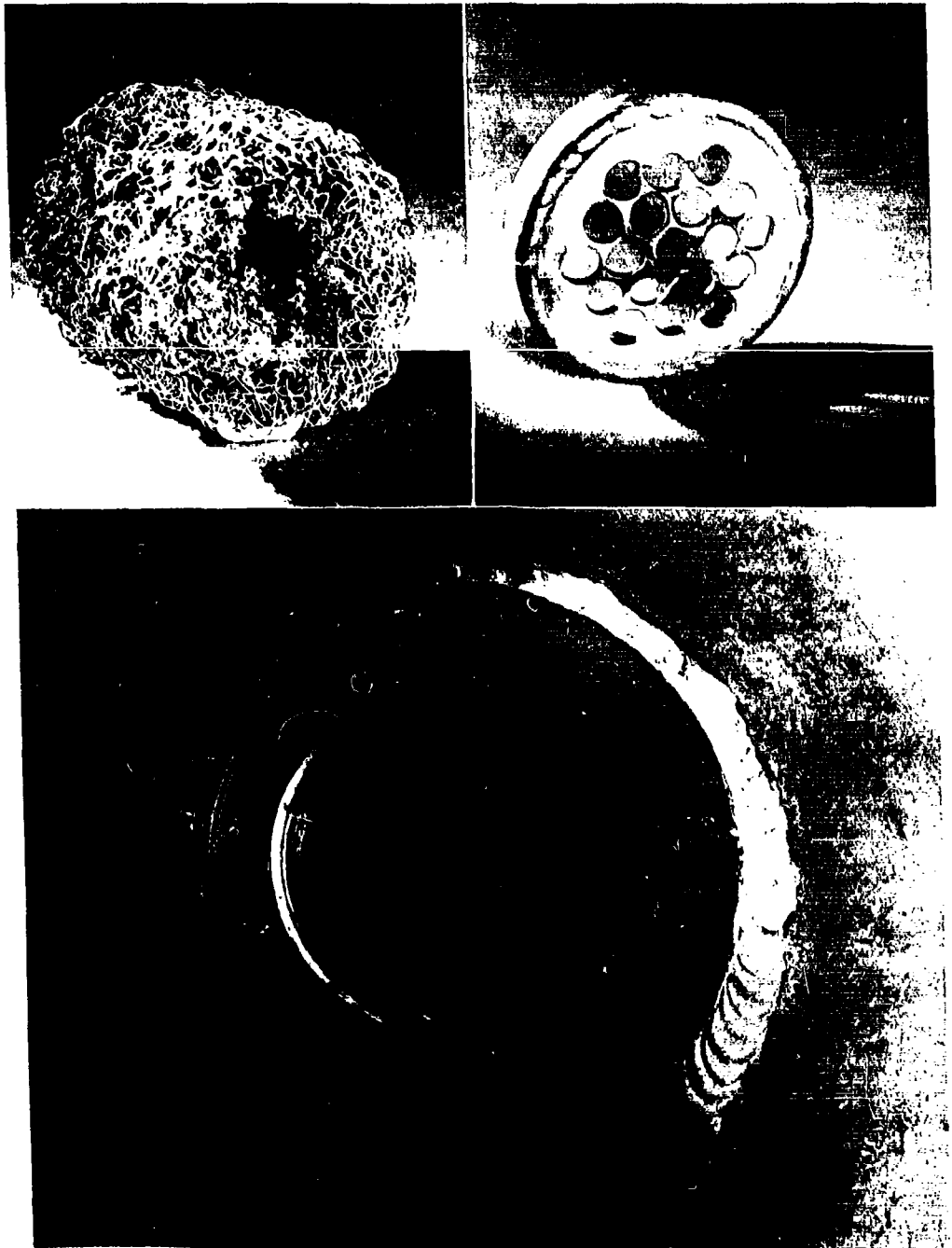


Fig. II-99 Failed Demister Parts Resulting from Faulty Injector

The reactive constituents can be isolated before test by readily available check valves or compatible solenoid valves of moderate response. During propellant outflow with subsurface gas impingement, reactions were observed in the cross flow line, but temperatures recorded were generally less than 500°F. A 25°F rise in the common ullage line (T_{gCuo}) at $T + 20$ sec was due to the presence of N_2O_4 when the reactive constituents entered this area (Fig. II-87). In most cases the reaction occurred at the gas diffuser, and a high reaction temperature was evident from the discoloration of the stainless steel part.

The common ullage development test series was primarily concerned with two basic methods of achieving satisfactory system performance:

- 1) Proper gas impingement to stabilize the secondary reaction;
- 2) Elimination of the secondary reaction.

A variation in the type of gas impingement technique (subsurface or surface) had indicated that the primary problem encountered was the difficulty in controlling the secondary reaction. Initial tests with the secondary reaction at the oxidizer surface resulted in unstable pressure control and excessive temperatures. Subsequent tests with the secondary reaction below the oxidizer surface demonstrated adequate pressure and temperature control. However, the safety hazard and propellant tank vibrations warrant additional study. Attempts to eliminate the reaction by various means were only moderately successful, and the subsurface gas injection common ullage technique was considered unsafe for future development.

Table II-13 summarizes the common ullage development test data for a continuous test with solid-stream surface reagent injection in the primary tank. A more detailed analysis of system operating temperature, based on data acquired during the entire Phase I program, is presented in Fig. II-100 and II-101. Additional information concerning gas composition can be found in Chap. II.C.1. Typical propellant analysis data for the selected process are shown in Table II-14. Table II-15 summarizes the common ullage development test data for a restart test with solid stream surface reagent injection in the primary tank.

Table II-13 MTI Common Ullage System Evaluation-Continuous Test

Type Run	Gas Molecular Weight			N ₂ O ₄ Used (lb)	Gunk Trapped (lb)
	ΔT_{gas} (°f)	Combustion Product	Combustion Product and Propellant Vapor		
(P) Surface Solid - 30% Ullage	212	17.0	17	0.258	None
(S) Subsurface - 5% Ullage	8	26.5	31.6		
(P) Surface Solid-30% Ullage	180	18.2	18.2	0.271	None
(S) Surface - 5% Ullage	480	22	27.8		
(P) Surface Solid	202	14.07	14.07	0.298	0.04
(S) Surface with Gunk Condenser - 5% Ullage	292	18.33	21.65		

Note: (P) Primary Tank (fuel), (S) Secondary Tank (oxidizer)

Table II-14 Propellant Analysis - Common Ullage Test Series

Propellant Condition	% Change in Concentration, 150-sec Test				
	Fuel				Oxidizer H ₂ O
	UDMH	N ₂ H ₄	H ₂ O	Unknown	
Maximum Change	-0.3	-0.6	+0.32	+0.58	+0.27
Average Change	-0.8	+0.3	+0.2	+0.2	+0.1

Note: 1. Primary Tank - Solid-Stream Surface Reagent Injection
 2. Secondary Tank - Subsurface Gas Impingement
 3. Maximum change represents change in propellant composition entered on engine.
 4. Average change represents actual change in total propellant composition.

Note: 1. 36 psia Tank Pressure.
2. Primary Tank, Solid Stream Surface Reagent Injection.
3. Secondary Tank, Subsurface Gas Impingement.

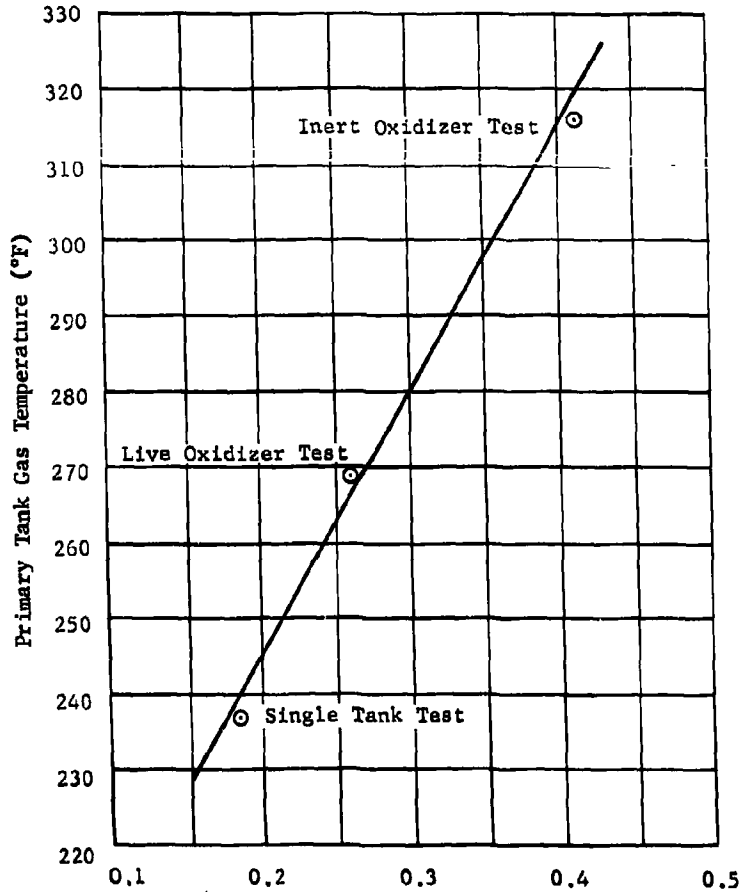


Fig. II-100 Phase I Fuel Tank Gas Temperature vs Reagent Consumption

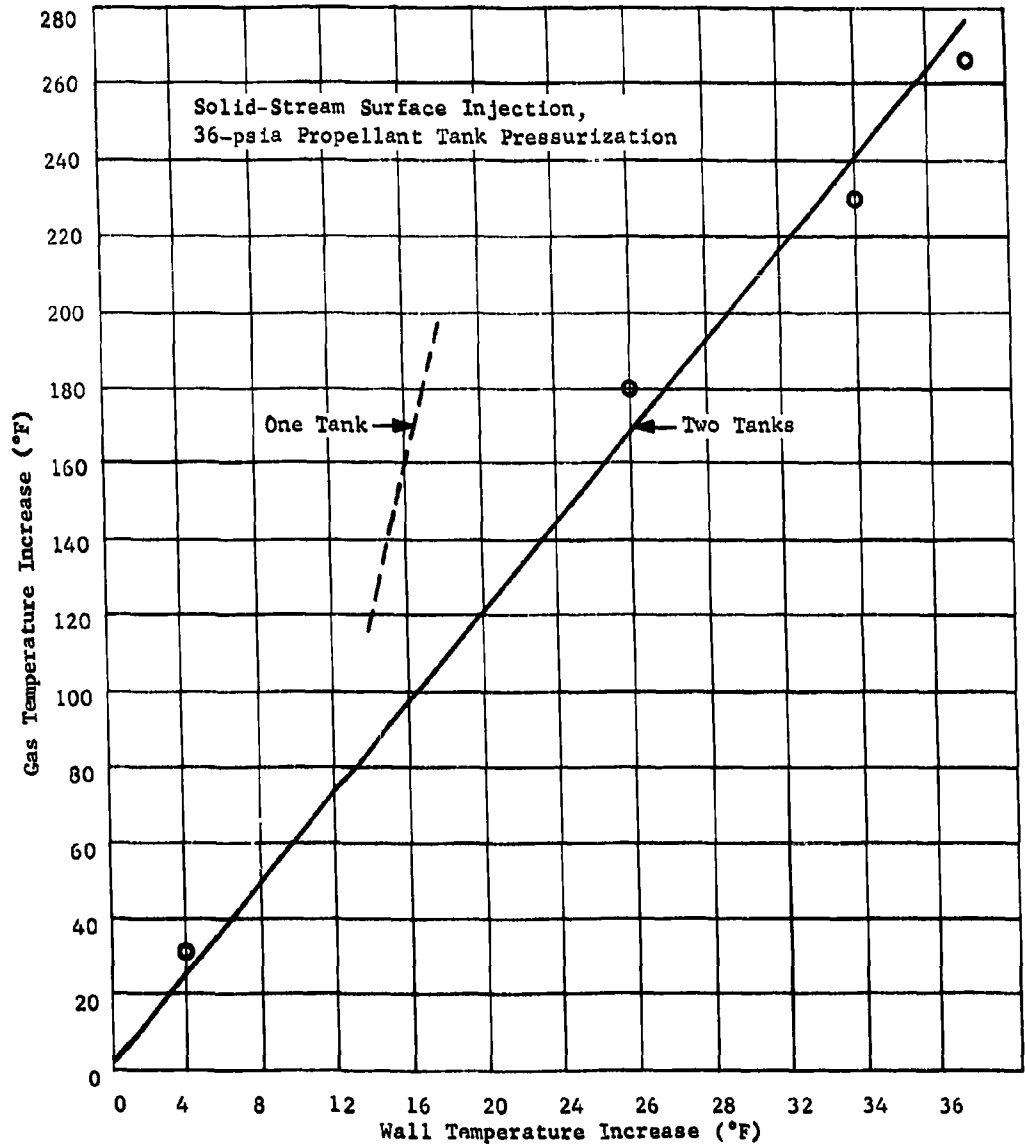


Fig. II-101 Phase I Fuel Tank Wall Temperature Increase vs Gas Temperature Increase

Table II-15 MII Common Ullage System Evaluation-Restart Test

Type Run	Gas Temperature (°F)	Molecular Weight		N ₂ O ₄ Used (lb)	Gunk Trapped (lb)
		Combustion Product	Combustion Products and Propellant Vapor		
(P) Surface Solid - 30% Ullage	122	17.16	17.16	0.440	None
(S) Subsurface - 5% Ullage	19	25.57	30.85		
(P) Surface Solid - 5% Ullage	138	13.77	13.77	0.258	None
(S) Surface - 5% Ullage	5	23.61	29.9		
(P) Surface Solid - 5% Ullage	337	16.0*	16.0*	0.318	Unknown
(S) Subsurface - 5% Ullage with CrO ₃ Reactor	260	20.43	27.0		
(P) Surface Solid - 5% Ullage	135	16.0*	16.0*	0.402	0.06
(S) Subsurface with Filter and Separator - 5% Ullage	70	17.0	24.0		

*Assumed average molecular weight.

The high molecular weight of the primary tank combustion products was apparently due to vaporized gunk increasing the nitrogen content of the specimen. Variations in molecular weight of the secondary tank combustion products were due to the change in gas impingement technique. A change in total secondary tank gas molecular weight was also evident from variations in NO_2 concentration resulting from the method of gas impingement. The reagent consumption reported included only that portion that was injected into the fuel tank. Any additional oxidizer consumed in the secondary gunk reaction was not identified. Since the actual reaction of the mass of gunk could not be directly measured, a material balance was conducted to determine the quantity of products generated based on the propellant and gas analysis performed. Chapter III.A includes a detailed presentation that can be used to assess the weight of the MII system for the particular process selected.

Subsequent testing with the subsurface gas impingement common ullage system was primarily designed to evaluate full system capability and investigate several vibration reduction techniques. During this portion of the test series, two minor explosions in the secondary tank occurred on separate tests after the system was shut down for 10 min and then restarted. One explosion generated pressures sufficiently lower than the relief features to provide ullage gas analysis both before and after the unexpected reaction. From the reduction in hydrogen noted in the gas samples taken after the explosion, it became apparent that there should be additional development effort with the subsurface gas impingement process.

The test results and additional gas composition data indicate that the hydrogen is ignited in the NO_2 atmosphere by hypergolic fuel-rich gunk reaction with N_2O_4 . Variations in the gas injector design showed hydrogen concentration reductions due to subsurface combustion. High hydrogen concentrations in the pressurizing gas did not always result in any significant reaction. By controlling the gunk reaction below the surface of the liquid, the hydrogen reaction was avoided, and secondary tank vibrations were reduced from approximately 8 g to 3 g.

The ability to pressurize the tank initially by the reaction process was not as significant as the stability obtained after restart. However, the increased concentration of hydrogen provided verification of system performance under adverse conditions. The polytropic decay used for residual propellant expulsion is particularly important to reduce residual propellants. It is also important to demonstrate adequate system capability with the gas diffuser above the oxidizer surface, where a gunk reaction could possibly initiate a violent hydrogen reaction.

Parametric Testing - The parametric test series was performed with two basic MTI pressurization concepts; the common ullage technique and the dual reagent injection method. Consequently the test effort during this portion of the research program involved pressurization of the oxidizer tank by fuel injection. From the experience gained during the development of a fuel tank pressurization system, only the surface solid stream reagent injection system was tested to obtain the desired regenerative cooling with minimum system vibration. During this test series the effects of system vibration on pressurization performance was investigated at the 36 psia operating pressure. Subsequent tests were performed at 36 and 100 psia on the common ullage configuration and at 36, 100, and 200 psia on both the fuel and oxidizer tank individual pressurized by identical reagent injection systems. Satisfactory performance was obtained for the dual reagent injection pressurization system over the operating pressure range investigated.

Test Configuration - The system configuration for the common ullage tests was identical to the optimum system developed previously that incorporated a 2½ in. long, 3/8 in. dia vertical sub-surface impingement gas injector tube with 60 0.040-in. dia holes. A single check valve was incorporated in the 3/8 in. by 0.035 in. stainless steel uninsulated common ullage line without a demister in the fuel tank exit. A parallel sight glass was used in the reagent supply system for the 100 psia tests to provide the additional pressurization capacity. The 0.014-in. injector orifice was satisfactory for all the parametric tests performed. An injector differential pressure of approximately 75 psia was maintained during each test. Since the injector orifice was optimally sized for a larger ullage, pressure control was not as precise with the initial 5% ullage volume single tank tests. To provide a direct comparison of all data accumulated, identical propellant loads and expulsion rates were maintained to achieve a 150-sec test duration. Helium prepressurization of the 5% initial ullage volume was adjusted to approximately 1% greater than operating pressure before each test. Since the time span between tests was relatively small and an ambient temperature of approximately 75°F prevailed during this test series, the data compiled were representative.

Test Results - The common ullage parametric tests were performed first, followed by the fuel and oxidizer separate reagents injection tests. A detailed description of the tests performed is included in the following paragraphs.

Common Ullage Parametric Tests - Since the common ullage system operated at 36 psia several times previously, additional performance data were desired under conditions of primary tank vibration to determine the extent of process alteration due to slosh. Satisfactory pressure control and negligible process effects were verified by imparting a horizontal random vibration of ± 0.25 in. displacement at an average frequency between 1 and 3 cps. Test performance is shown in Fig. II-102

Pressure control in both tanks was good. The following maximum variations occurred in the fuel tank: $1\frac{1}{2}$ psi up to 10 sec, 1 psi at 10 to 60 sec, and $\frac{1}{2}$ psi after 60 sec. The oxidizer pressure fluctuations were less than 1 psi. Maximum ullage gas temperature was 208°F in the fuel tank and 67°F in the oxidizer tank. An increase in common ullage temperature occurred at the start and end of test because of the oxidizer reaction with gunk. A pressure pickup was installed in the oxidizer tank lower dome to verify the absence of severe detonation. Maximum pressure surges detected were less than 5 psi, although 8 g double amplitude vibration levels were detected when the system was supported by wire ropes. There was no significant effect on the reagent consumption of 0.277 lb for the 187-sec test. A gas sample was not taken, however, an average combustion product molecular weight of 23.75 is expected in the oxidizer tank with primary combustion products of 16.0.

A second test was performed at 100 psia. The only change to the configuration consisted of an increased reagent supply capacity. Reagent consumption increased to 0.705 lb for the 147-sec test. Since propellant tank pressure was controlled by a facility-type instrument, the pressure control tolerance was wider than in the 36 psia pressure tests. Figure II-103 presents the performance of this run. The figure indicates that marginal flow capacity of the injector resulted in a low tank pressure during the latter portion of the test.

Maximum ullage gas temperatures were 596°F in the fuel tank and 89°F in the oxidizer tank. Common ullage line temperature was not monitored for this test. However, a slight detonation at 100 sec was detected and later determined to have occurred from a burst gas diffuser. With the gas diffuser damaged (Fig. II-104), there was not sufficient time to run the common ullage system at 200 psia.

Combustion product molecular weight was 21.5 in the fuel tank (indicating a definite increase at the higher pressure) and 28.0 in the oxidizer tank. Although vibration measurements were not taken for this test, the level appeared to be approximately the same as the previous test.

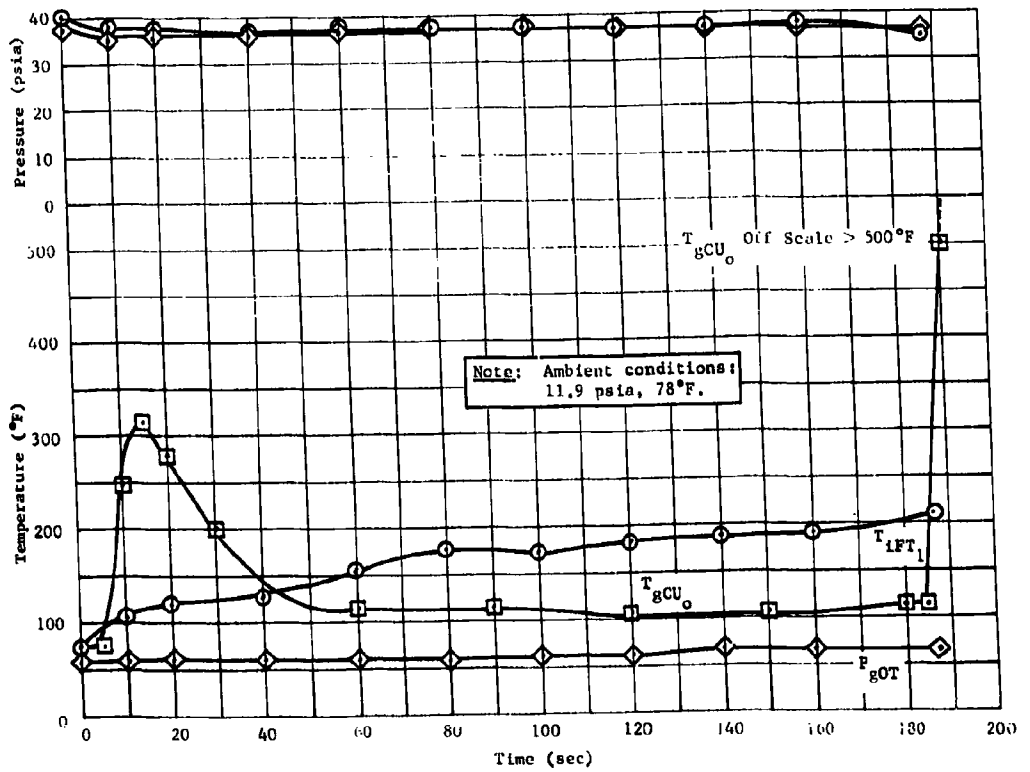
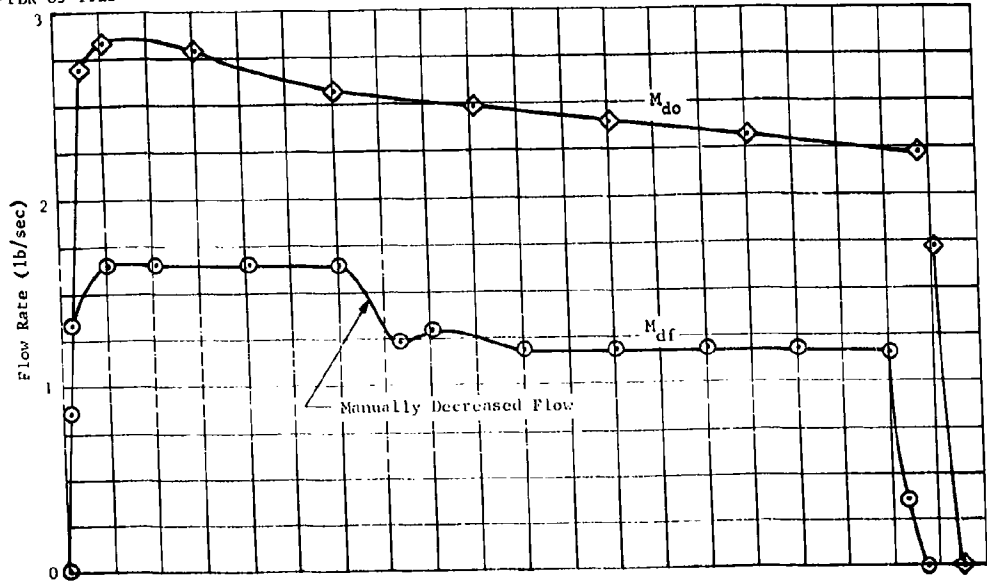


Fig. II-102 Parametric Test Common Ullage System Performance at 36 psia

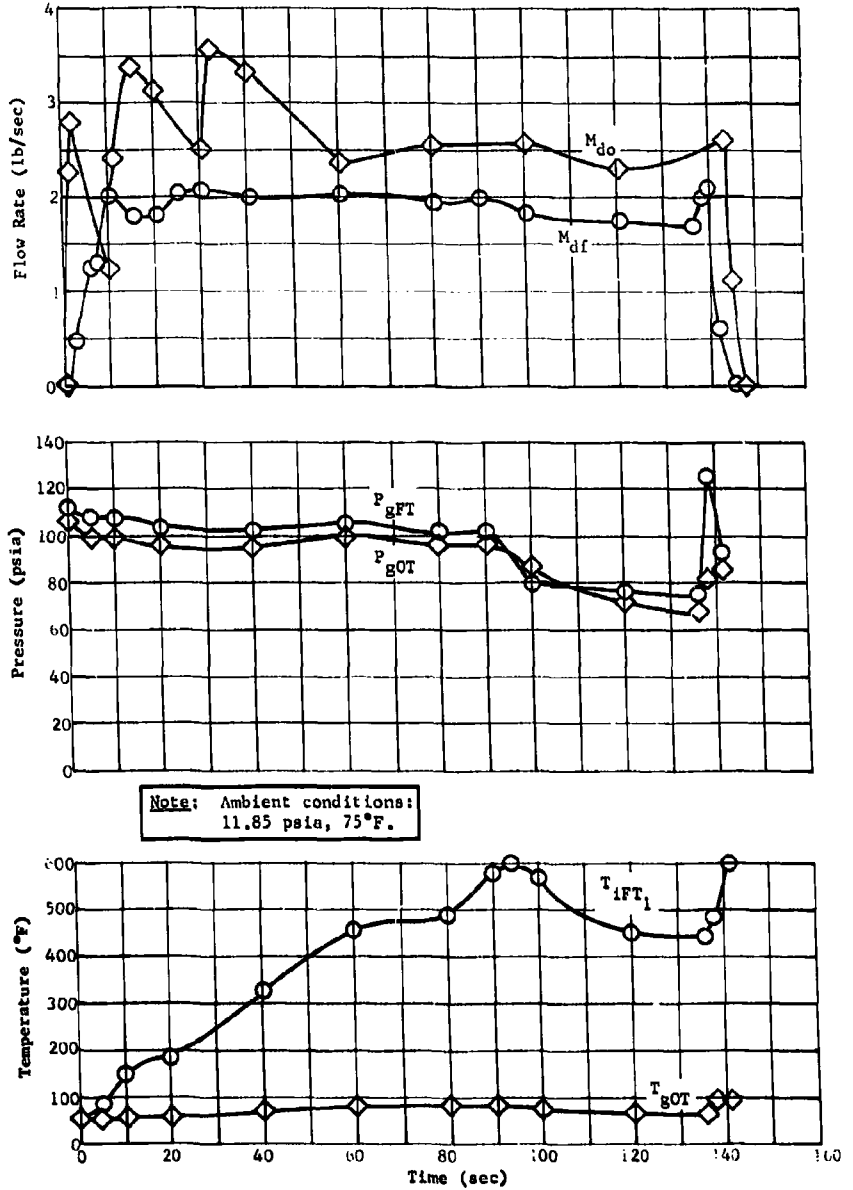


Fig. II-103 Parametric Test Common Ullage System Performance at 100 psia

RTD-TDR-63-1123



Fig. II-104 Subsurface Gas Diffuser

Fuel Tank Parametric Tests - The 36-psia fuel tank pressurization test was rerun during this test series to correlate the data with the subsequent higher pressure tests. Figure II-105 is a plot of the data obtained. The data are in agreement with previous low-pressure tests. Maximum pressure variation at the start of the test was 2 psi diminishing to $\frac{1}{2}$ psi after 20 sec. The wide pressure control tolerance was due to the oversized injector. Maximum ullage temperature was 136°F with 0.188 lb of reagent consumed during the 140-sec test.

Second and Third tests were later run on the same day at 100 and 200 psia. The data are shown in Fig. II-106 and II-107. Pressure control in each test was between 1 and 2% due to a less sensitive pressure switch than used during the low-pressure test. Injector flow capacity was adequate for the 100-psia test, but only marginal during the 200 psia test. Reagent consumption was 0.421 lb for the 100 psia test with a maximum ullage gas temperature of 349°F for the 131-sec test. Combustion product molecular weight was 21.5 compared to 20.5 for the 200 psia test. This discrepancy in molecular weight is within the normal distribution and implies an increase in molecular weight over a 36-psia test. For the 200 psia test, reagent consumption was 0.629 lb with a maximum ullage gas temperature of 660°F for the 100-sec test.

Oxidizer Tank Parametric Tests - The first attempts at pressurization of the oxidizer tank by solid stream surface fuel injection resulted in an excessively high ullage gas temperature of 560°F at the 36 psia test pressure. Figure II-108 shows the undesirable performance that was caused by a partial spray injection pattern. Reagent consumption for this 170-sec test was 0.161 lb. Pressure control was within 4 to 5 psi during the initial 10% of the test due to the rapidly varying ullage gas temperature. Combustion product molecular weight was 28.52. A retest was made with a good 0.014-in. dia injector orifice. The data, presented in Fig. II-109, indicate a significant reduction in reagent consumption and gas temperature. A comparison of the ullage gas temperature profiles of identical tests is shown in Fig. II-110. Reagent consumption was 0.148 lb and maximum ullage gas temperature 153°F for the 204-sec test. Tank pressure maximum variation was 2 psi, decreasing to $\frac{1}{2}$ psi later in the test. In general, the performance of the oxidizer system was similar to the fuel tank system with a somewhat lower operating temperature and reagent consumption due to the high mole fraction of vaporized main propellant. At higher operating pressures, however, the reagent consumption for oxidizer tank pressurization was higher than the fuel tank due to the correspondingly lower mole fraction of vaporized propellant.

RTD-TDR-63-1123

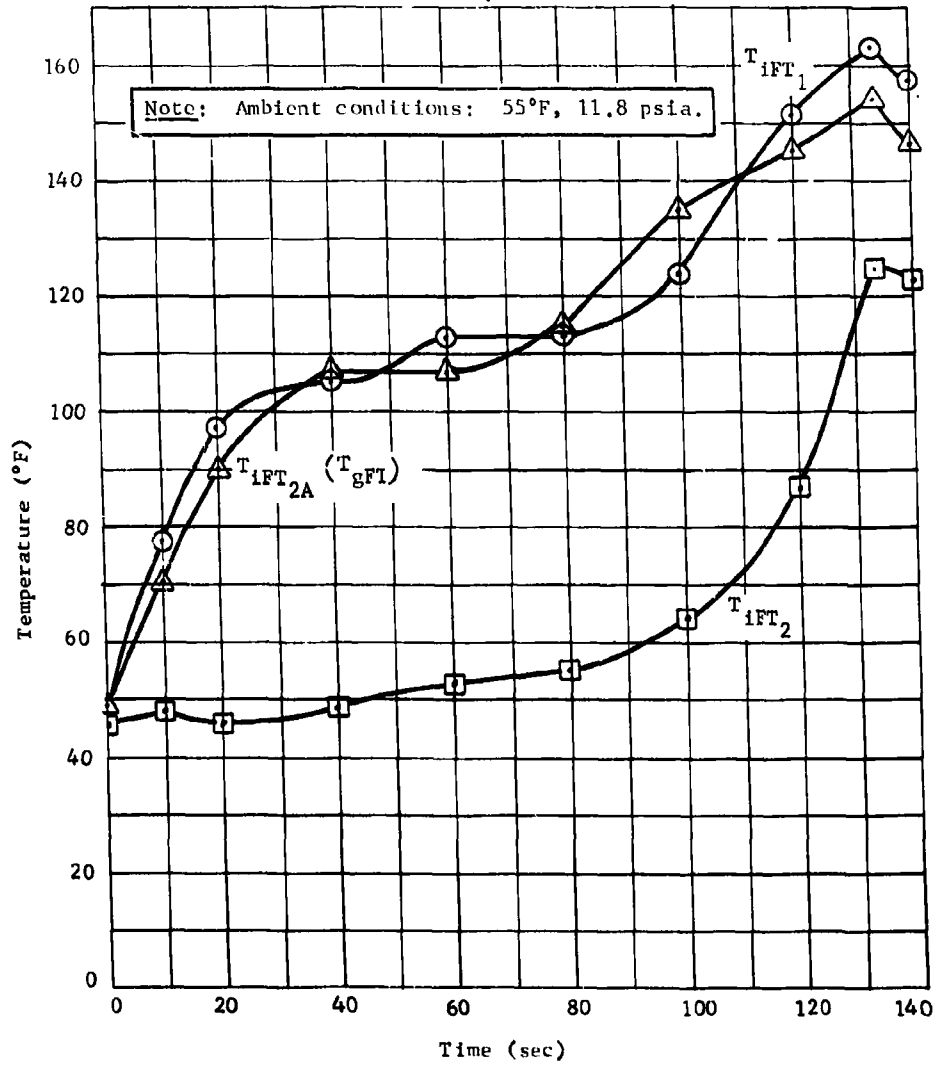
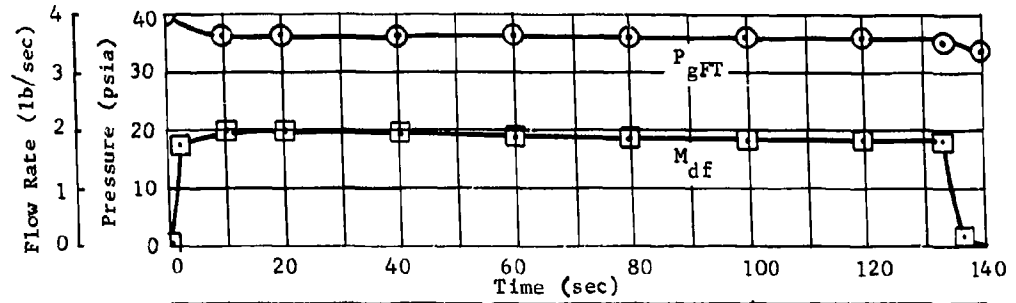


Fig. II-105 Parametric Test Fuel Tank System Performance at 36 psia

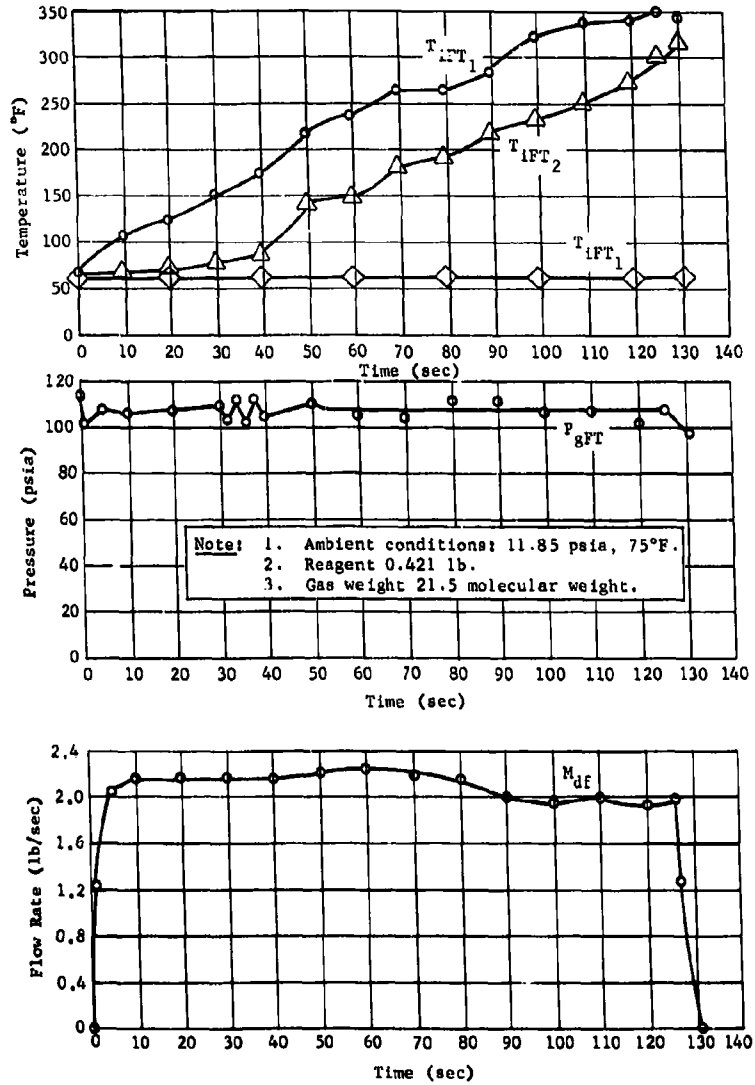


Fig. II-106 Parametric Test Fuel Tank System Performance at 100 psia

RTD-TDR-63-1123

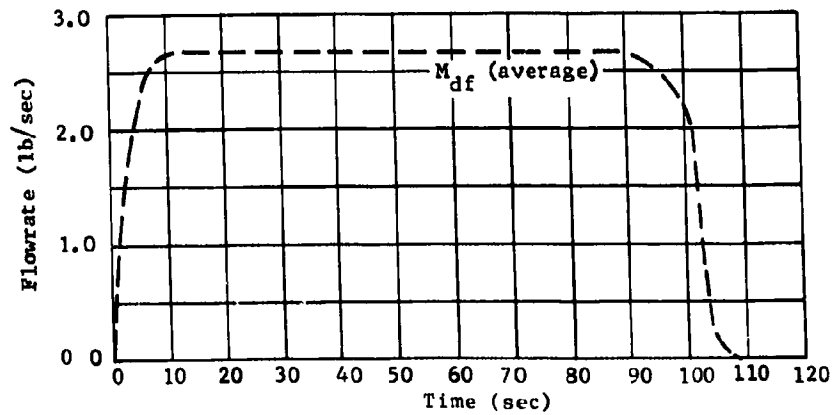
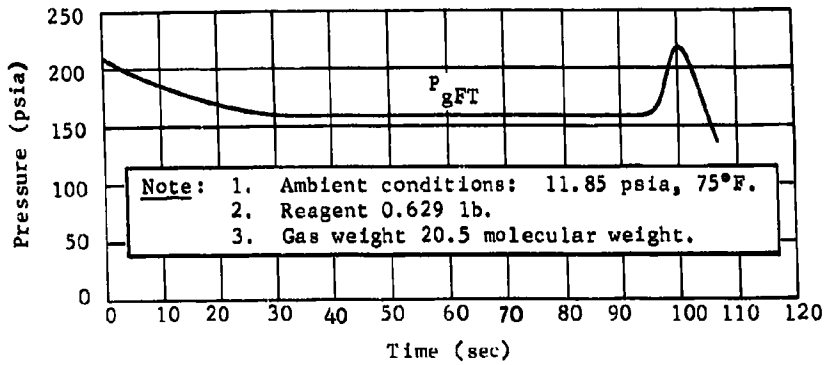
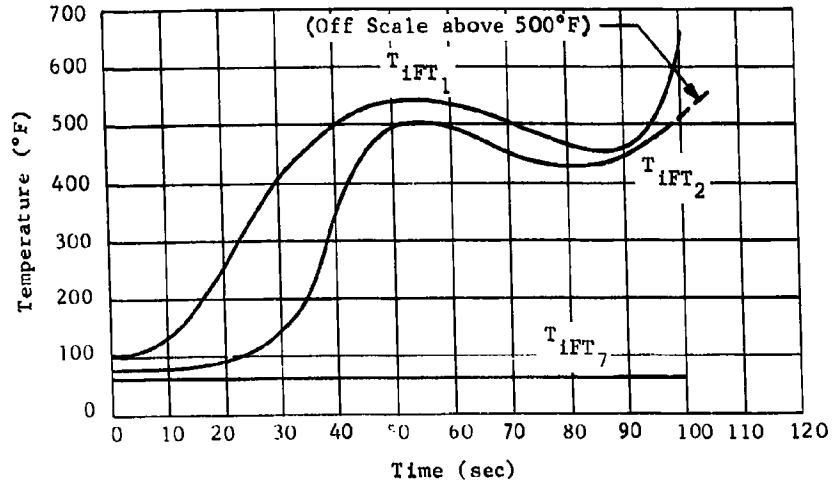


Fig. II-107 Parametric Test Fuel Tank System Performance at 200 psia

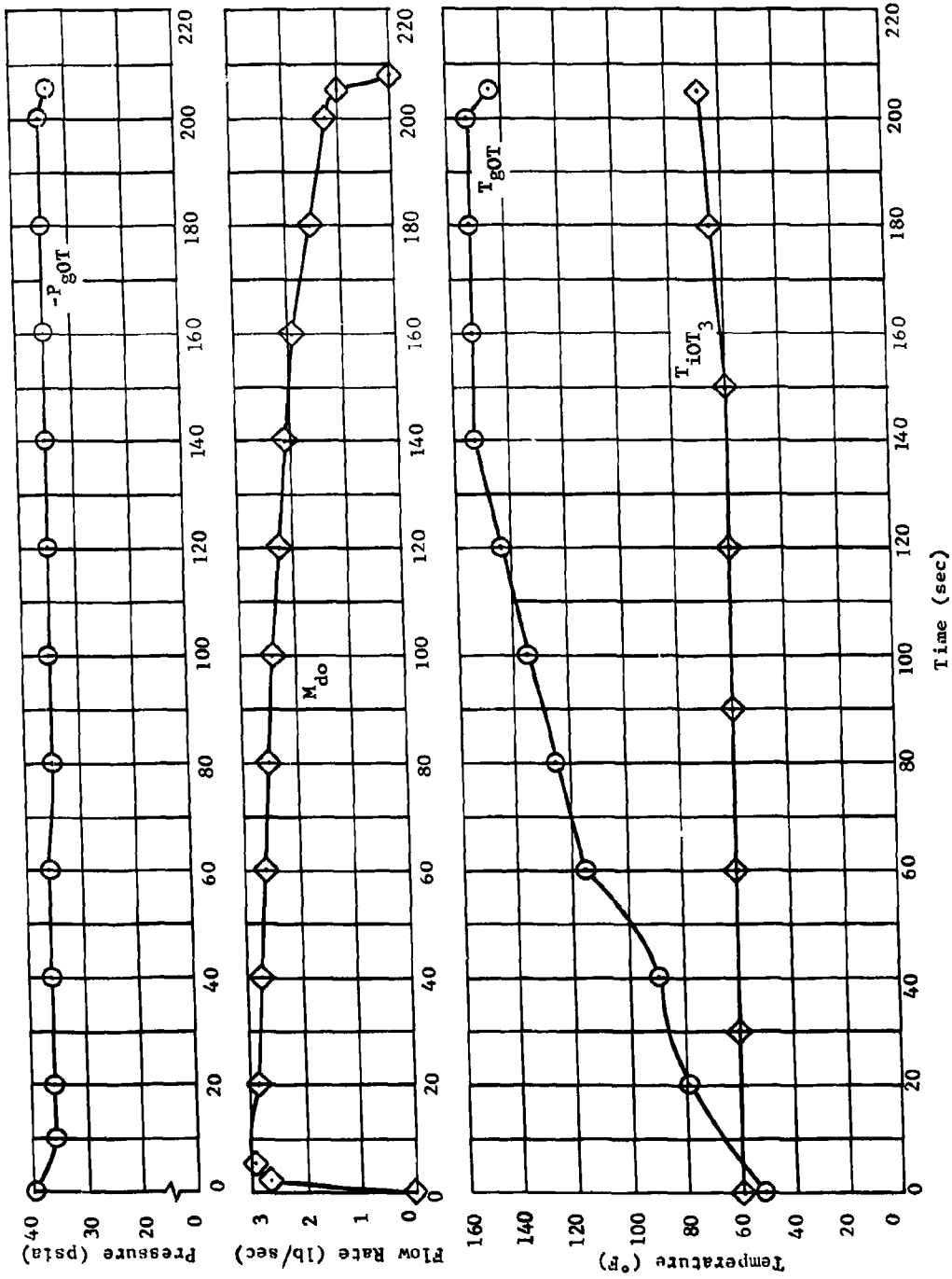


Fig. II-109 Parametric Test Oxidizer System Performance at 36 psia

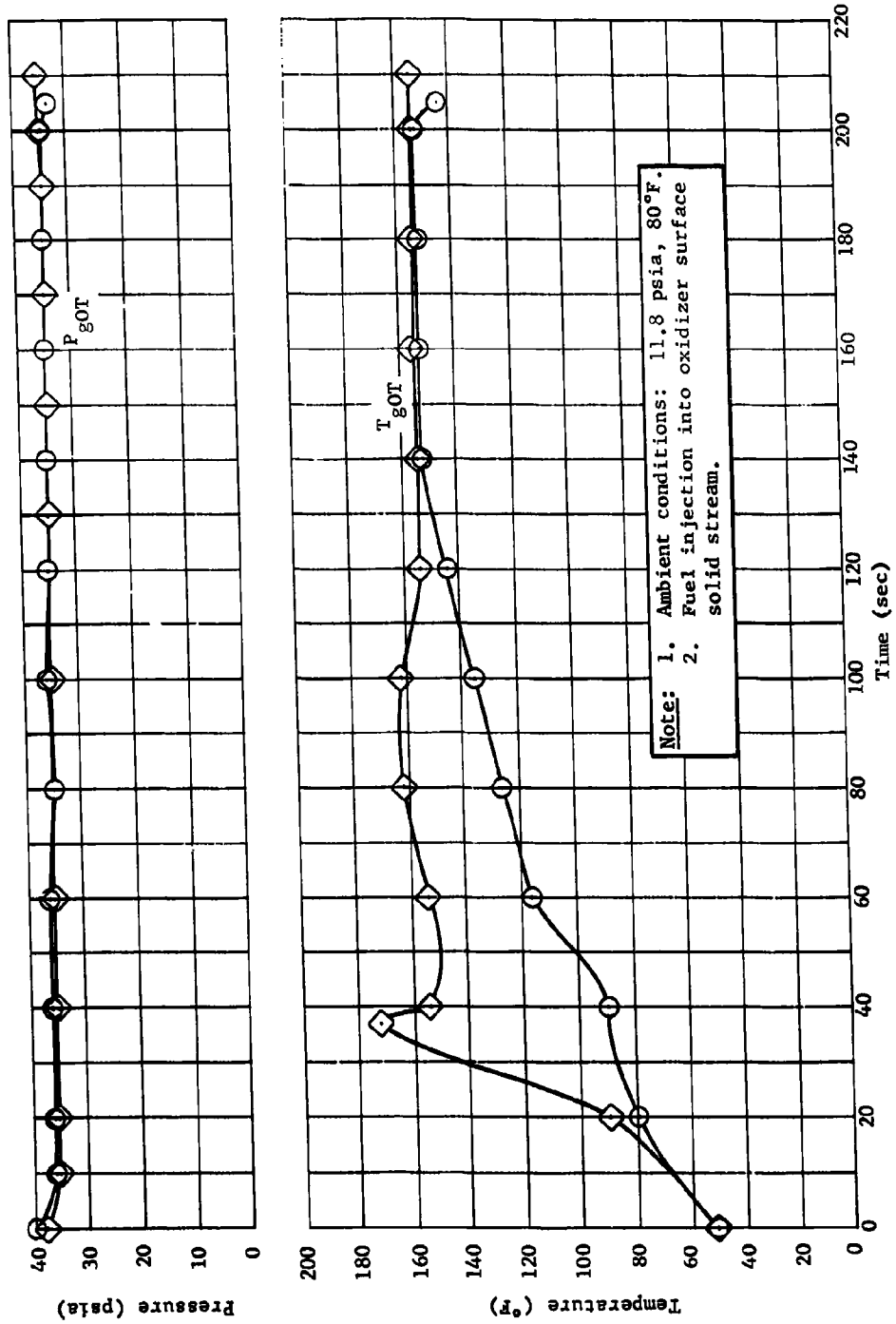


Fig. II-110 Oxidizer Tank Gas Temperature Profiles at 36 psia for Two Runs

Subsequent oxidizer tank pressurization runs were made at 100 and 200 psia. The satisfactory performance of the 100-psia test is shown in Fig. II-111. Reagent consumption was 0.448 lb for the 100-psia test of 200-sec duration. Pressure control was within ± 2 psi with a maximum ullage gas temperature of 302°F. Combustion product molecular weight reported to be 29.9 for the 100 psia test compares with the 29.5 obtained in the 200 psia test. Figure II-112 presents the 200 psia test data. Maximum ullage gas pressure variation was 10 psi with a 581°F maximum temperature indicated. Reagent consumption was 0.655 lb for the 180 sec operation. Variations in propellant flow control for the 100 and 200 psia tests was due to facility mechanical difficulties, while the temperature increase (T_{T01}) shown in Fig. II-112 was apparently due to the proximity of the combustion zone.

Performance Analysis - Results from the parametric test series show that satisfactory performance was achieved with the MTI dual injection pressurization system for operating pressures of 36 to 200 psia. There were negligible effects resulting from slosh or vibration. Summarized data are presented in Table II-16 for both the dual injection and common ullage pressurization systems. All of the data were accumulated with a 0.0135-in.-dia solid stream injector orifice at a 75 psi injector differential pressure.

Table II-16 Summary Phase I Parametric Data

Tank	Pressure (psia)	Max Gas Temp (°F)	Reagent Used (lb)	Gas Molecular Weight	
				Comb Prod	Ullage
Individual Tank Reagent Injection					
Fuel	36	163	0.188	16.0	16.0
Oxidizer	36	154	0.151	29.5	36.53
Fuel	100	349	0.421	21.5*	21.5*
Oxidizer	100	300	0.448	29.87	35.79
Fuel	200	660	0.629	20.46	20.46
Oxidizer	200	580	0.665	29.54	35.30
Common Ullage Pressurization					
Fuel	36	208	0.273	16.0	16.0
Oxidizer	36	67		23.75	30.63
Fuel	100	596	0.704	21.5	21.5
Oxidizer	100	89		28.0	32.8
*Based on common ullage test.					

The influence of tank pressure on pertinent operating parameters is shown in Fig. II-113 for the dual injection system. Although the trends are representative of a particular system with a definite size and heat capacity, several less desirable characteristics are encountered at the higher operating pressures:

- 1) Ullage gas differential temperature increases proportional to the tank pressure;
- 2) Fuel tank combustion product molecular weight appears to increase with pressure;
- 3) Partial pressure of propellant vapor in the oxidizer tank increases proportional to the operating pressure (equivalent to approximately 30%).

The increase in ullage gas temperature with propellant tank operating pressure may not be a particular disadvantage in some systems with stainless steel or titanium tankage, since tank wall temperatures limits probably would not be exceeded and a lower gas density would be achieved. Pressure control would, however, be more critical due to rapid temperature changes. The increase in combustion product molecular weight (also shown in Fig. V-11 of Chap. V.B.) is based on somewhat limited data but appears to be a definite disadvantage for ambient-cooled space vehicles. For uncooled systems, such as in booster applications or continuous-type missions, the high gas molecular weight is offset by the high operating temperature. This gives a lower gas density than might be expected from the extrapolation of low pressure fuel tank data. In the oxidizer tank, however, a significant increase in vaporized propellant (due to combustion zone liquid heating) has a detrimental effect on total pressurant weight for all high pressure applications even though a small decrease in reagent consumption is realized. Fortunately, this increase in system weight is not proportional to the operating pressure. A detailed presentation of actual Phase I test results concerning oxidizer vaporization is shown in Fig. V-12 of Chap. V.B.

RTD-TDR-63-1123

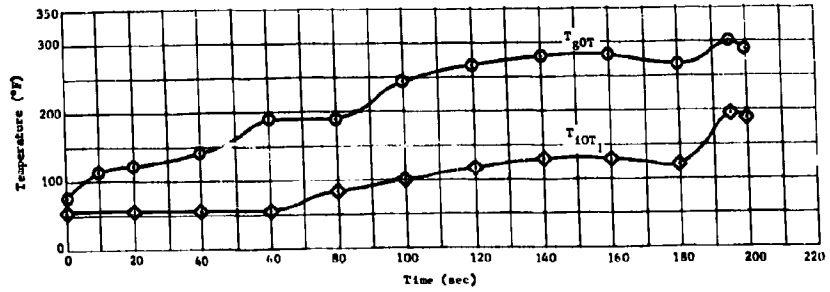
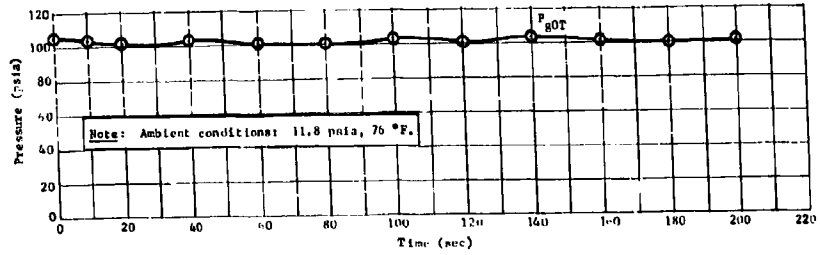
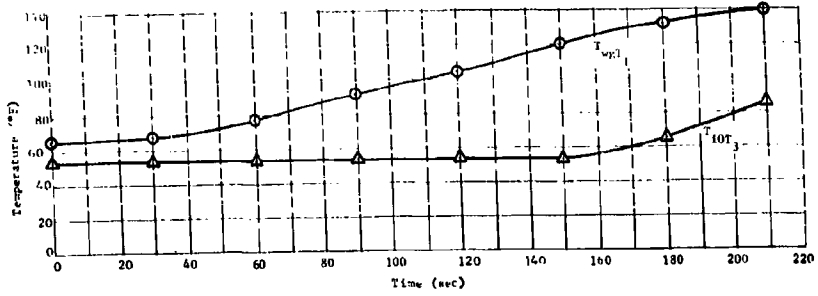
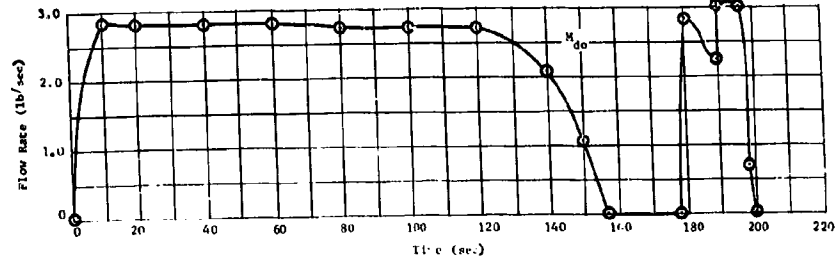


Fig. II-111 Parametric Test Oxidizer Tank System Performance at 100 psia

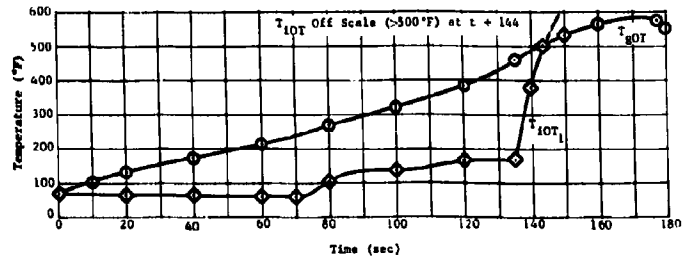
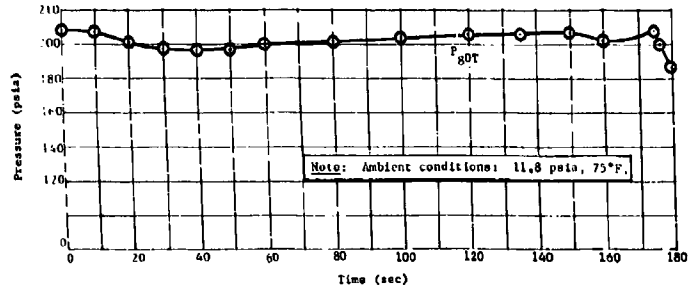
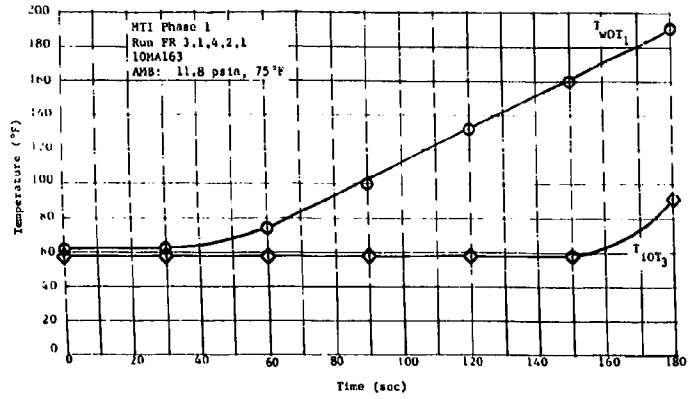
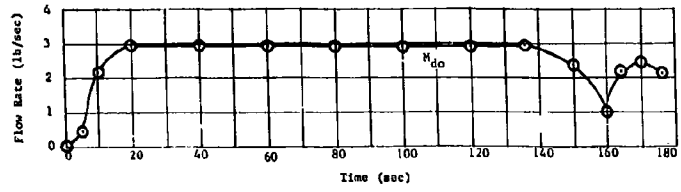


Fig. II-112 Parametric Test Oxidizer Tank System Performance at 200 psia

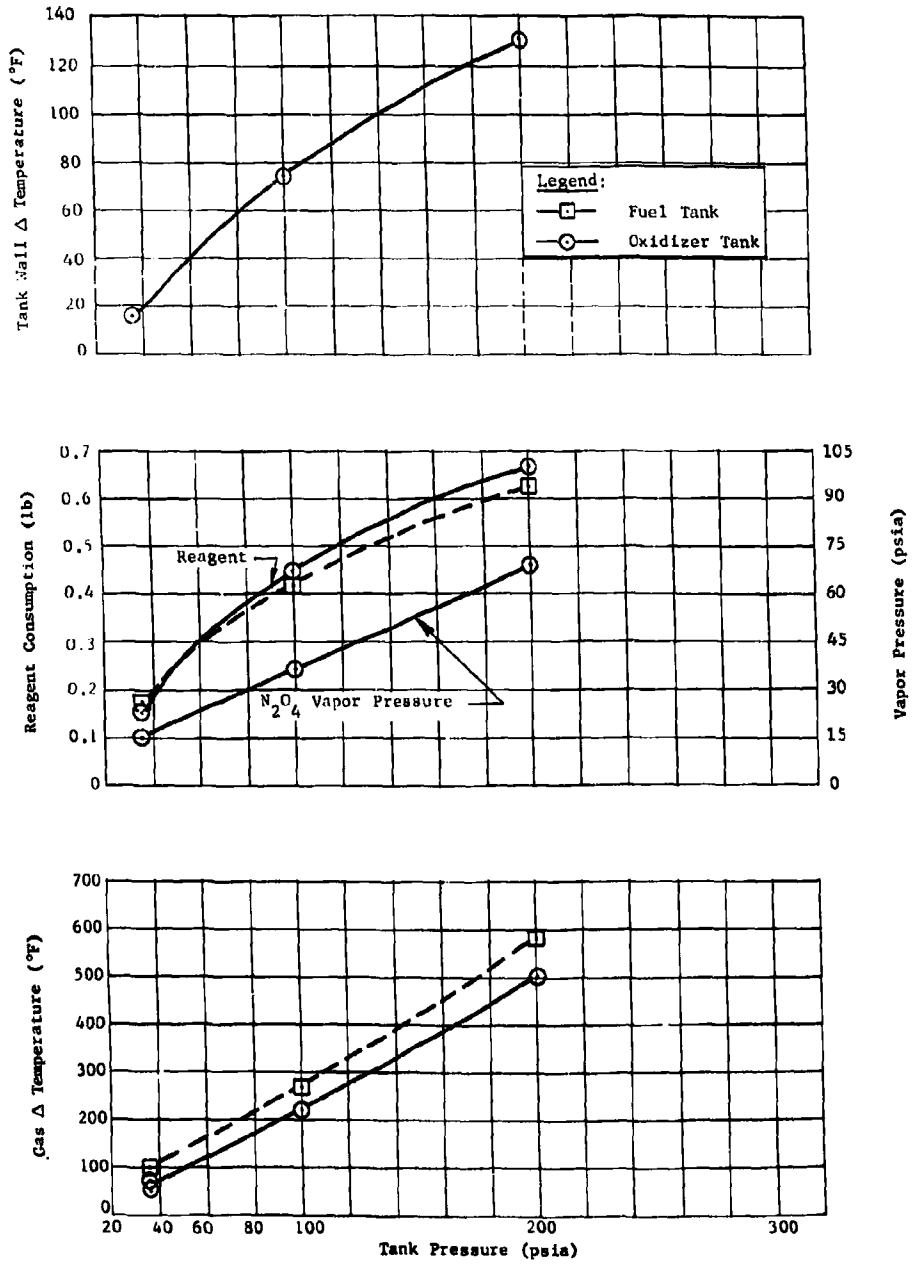


Fig. II-113 Parametric Test Data Summary

G. CHEMICAL ANALYSIS

Chemical analysis of the propellants and combustion gases was required for complete MTI pressurization system evaluation. Propellant specimens that were acquired before and after each test were analyzed by the Martin Quality Control organization to assess the extent of degradation experienced from the various injection techniques. Available apparatus was not accurate enough to perform continuous combustion gas analysis, consequently propellants were periodically sampled. The specimens acquired during each test were subsequently analyzed by mass spectrometer at the National Bureau of Standards in Boulder, Colorado. The gas composition and molecular weight, reaction ratio, and extent of propellant vapor saturation of the ullage were established by interpreting the acquired data. Approximately 75 tests were made on the Phase I system with 120 gas specimens analyzed. A good description of MTI process gas has been established for both the dual injection and common ullage systems with various injection techniques and covering the 36 to 200 psia propellant tank pressure range. Propellants were analyzed on almost every run. Small changes in propellant composition were detected that resulted in a certain amount of inconsistency. Consequently, the data were carefully examined and the more certain effects are reported. Analytical investigations of the condensate formed in the fuel tank system were not entirely successful due to the complex nature of the substance. However, the quantity (less than 10%) is composed primarily of UDMH and may be treated accordingly.

1. Gas Analysis

During the injector development three analytical techniques were used to determine propellant tank ullage gas composition. The most satisfactory method was mass spectrometer analysis. The other methods included a gravimetric technique and an on-site gas chromatograph. Periodic sampling during the tests verified actual composition. The data were theoretically reduced from the actual composition of the ullage gas to obtain the composition and quantity of the combustion products. Since the research fixture propellant tank was initially pressurized with nitrogen containing a small amount of vaporized propellant (less than 1%), the continuous gas bleed in the gas sampling system required development of a small computer program (described in App A) to interpret the test data. In subsequent tests helium was used for prepressurization to permit a more accurate identification of the combustion products. The established average molecular weight of the combustion products was used to evaluate the performance and affects of

a variety of mixing techniques. In addition, the actual composition of the fuel tank pressurant enabled the calculation of thermodynamic properties and reactivity of the gas with nitrogen tetroxide before initiation of the common ullage test series. The analysis of the oxidizer tank pressurizing gas obtained from both common ullage and direct fuel injection allowed a comparison of system weight advantages by relating the pressurant-molecular weights.

Analytical Techniques - The National Bureau of Standards, Boulder, Colorado, performed the mass spectrometer gas analysis for this test program. Although the method of obtaining the specimens did not provide continuous analysis, the four samples taken during each test did permit reaction process characteristics to be determined. In addition to providing the gas composition accurate to ± 200 parts per million the main propellant consumed and molecular weight of the ullage gas was determined. The repetition of this information sufficiently defines performance for the solid stream surface injection pressurization process so that various mixing techniques can be compared.

A schematic of the gas sampling system is shown in Fig. II-47. The system is heated to the expected gas temperature range before test initiation and evacuated to 10 microns. After 10 sec from test start the sample valve is opened allowing gas to flow through the lines, flow control orifice, manifold, and out the 2.5 psig backpressure regulator, and 1/4 psig check valve to the atmosphere. The specimens are obtained at 20, 60, 120, and 160 sec by opening the stop cock on the evacuated sample bottle. It takes approximately 2 to 4 sec to fill each bottle. Sufficient time is available so that conditions can stabilize between each sample. The last sample is taken approximately 10 sec after test termination to ensure actual final gas composition. The 0.025-in. orifice allows sufficient response for minimum sampling duration and keeps pressurizing gas losses during overboard bleed to a minimum. The total amount of gas lost from the system due to the overboard bleed and gas specimen acquisition is approximately 4% of the total mass of gas generated. After a constant combustion product composition was verified, continuous bleed sampling was abandoned and only final samples were taken. This technique involved bleeding the final gas into an evacuated sample bottle. All of the samples were analyzed within 48 hr of test termination. The standardized samples were reheated to the approximate test temperature and the analysis performed.

The on-site gas chromatograph provided a qualitative means for determining ullage gas composition on a test-to-test basis. These data were used to tentatively assess the relative merits of changes in MFI test parameters and the consistency of test results. The gas samples were procured in the same manner as for the mass spectrometer with the 0.051 ml sample gas density adjusted to ambient temperature and pressure before injection into the analyzer by a syringe. The analyzer is standardized with air and a known mixture of hydrogen and nitrogen before and after each series of analyses to establish standard reference points and baseline drift. Standardizing insures an accuracy of less than $\pm 2\%$. The air standardization also provides a check of nitrogen sensitivity and a basis for correcting for any air leaks, as indicated by the presence of O_2 in the sample. Helium is used as a carrier to transport the sample and provide an output baseline. Sample gas composition is determined by comparing the hydrogen and nitrogen readouts to those obtained during standardization with the check gas. The relative concentration of hydrogen detected in the gas mixture provided approximate ullage gas weight information in the development of desirable injection techniques.

A gravimetric analysis was initially performed on all specimens procured for gas analysis by mass spectrometer and gas chromatograph to determine the quantity of condensibles not identified by the vapor phase analytical techniques. The average density of the sample determined by this method was not sufficiently accurate to support any valid conclusions. The 125 cc sample bottles were precisely measured before being used to collect the ullage gas specimens. The change in volume due to temperature changes was considered. An analytical balance established the weight of the empty and filled bottle to within 0.01%. Since the actual quantity of gas collected weighed considerably less than the sample bottle, the overall accuracy in gas density would amount to approximately 10%.

Results - From the actual composition of the gas obtained the molecular weight can be determined. The data were further analyzed to obtain combustion product molecular weight by using theoretical techniques programed on the IBM 1620 computer. The ullage gas dilution program (detailed in App D), computes the theoretical mole fraction of pressurizing gas in the ullage as a function of time based on the actual test temperature history and system operating

characteristics for a particular combustion gas, Figure II-114 shows the change in composition with gas bleed when the fuel tank system is being pressurized with combustion products that have a molecular weight of 13. Several values of combustion gas molecular weight were selected with the corresponding ullage gas molecular weight plotted for a typical test run in Fig. II-115. Comparable performance curves for the two-tank common ullage system are shown in Fig. II-116 thru II-118 for helium prepressurization. The molecular weight of the test specimens were plotted to show the degree of correlation, which indicates the response of the sampling system appears to be approximately 10 sec slow. If the curve is shifted to allow for this condition, the test data almost matches the theoretical curve for a combustion product molecular weight of 13. The slight discrepancy in dilution rate is probably due to a small error in the gas bleed calculation resulting from the assumed orifice discharge coefficients and gas specific heat ratio.

Since nitrogen was used for prepressurization and the combustion products also contain nitrogen, the actual molecular weight of the combustion products cannot be determined directly from the mass spectrometer analysis. For this reason helium prepressurization was used in later tests. The total weight of gaseous combustion products produced, however, was still computed by the theoretical method due to the change in mixture composition with gas bleed. Total weight of gaseous combustion products, in addition to the weight of condensible formed, is important to obtain the amount of main propellant consumed in the reaction. Since the quantity of reagent being reacted in the combustion process is known, the main propellant consumed can be obtained from a mass balance. From the difference in molecular weight of the vapor determined by mass spectrometer and average molecular weight calculated from a gravimetric analysis the resultant quantity of condensibles can be determined from Fig. II-17. For the single tank tests performed the average difference in ullage gas molecular weight has been less than three, corresponding to an equivalent weight of condensibles of less than 0.08 lb or approximately half of that required for the material balance.

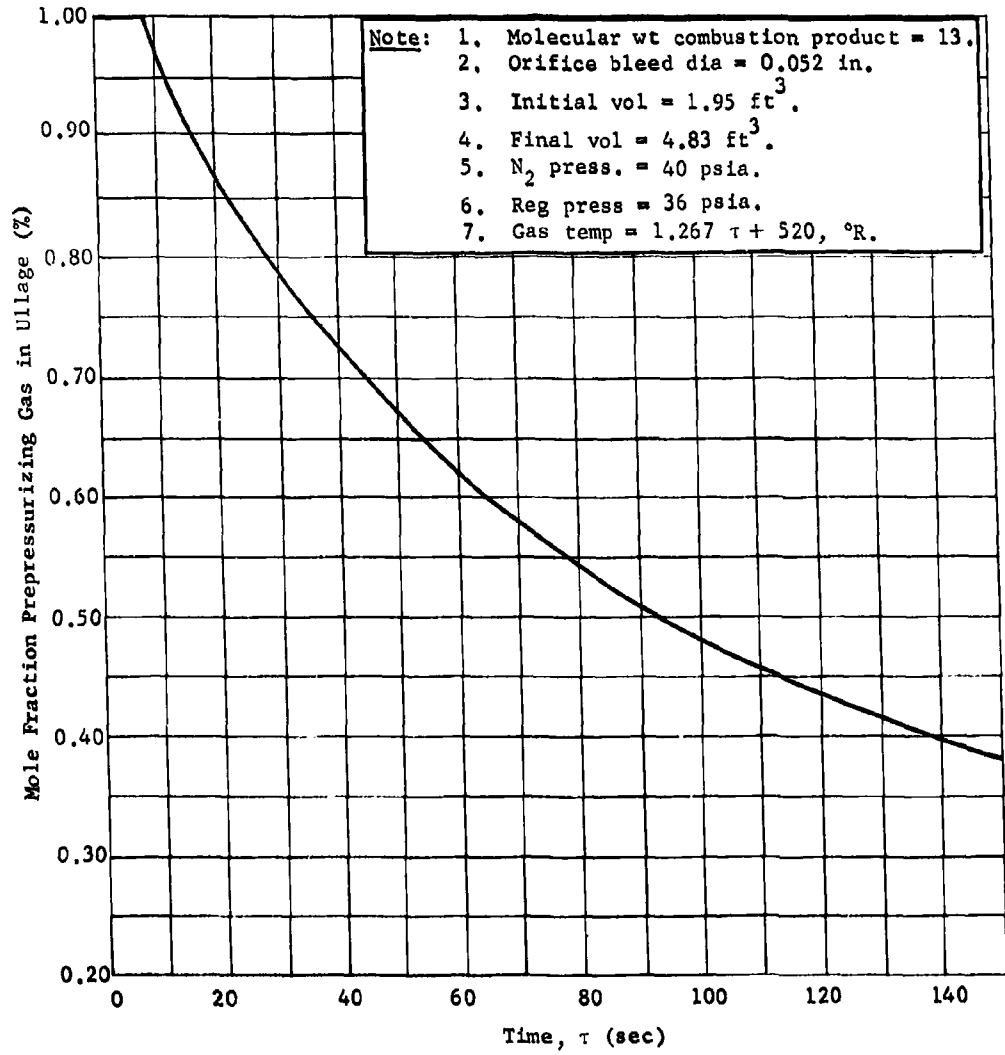


Fig. II-114 Ullage Gas Dilution for the Small Scale Single Tank System

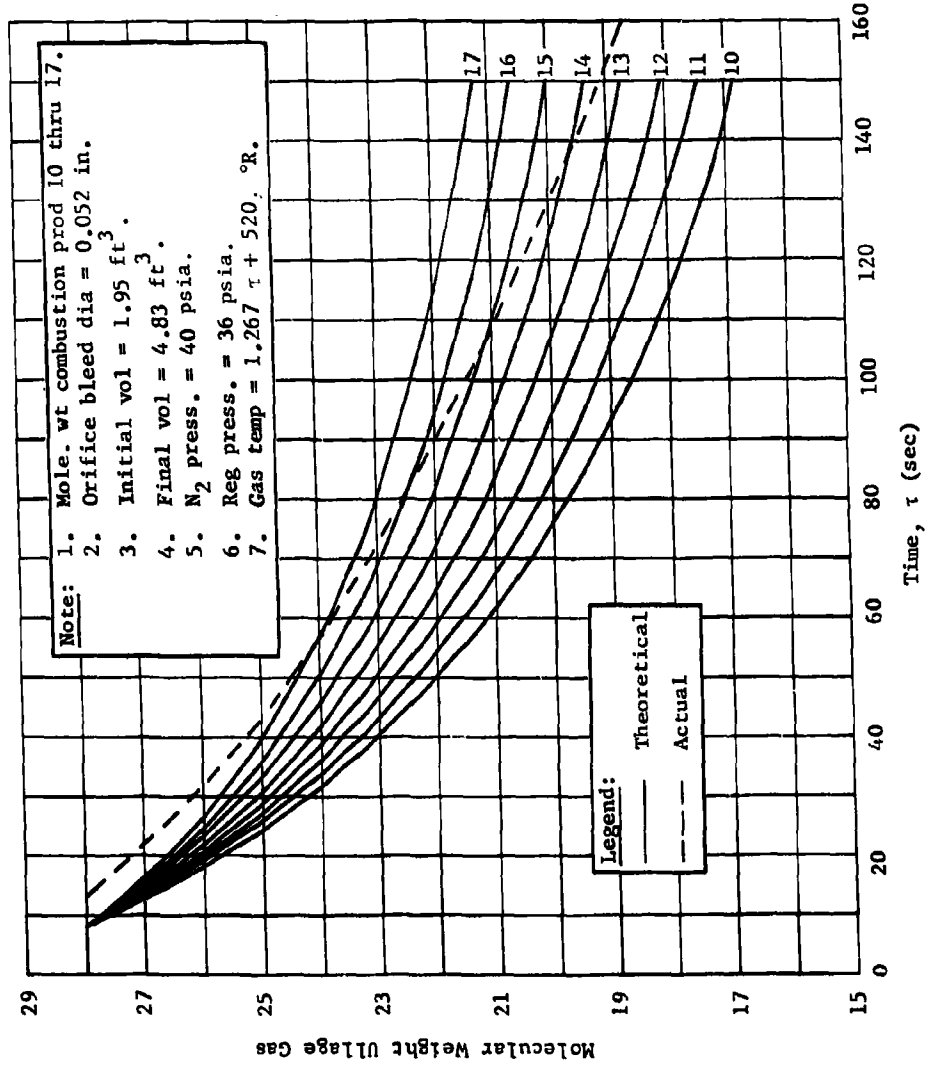


Fig. II-115 Fuel Tank Ullage Gas Molecular Weight vs Time-Single Tank Test N₂ Initial Pressurization

RTD-TDR-63-1123

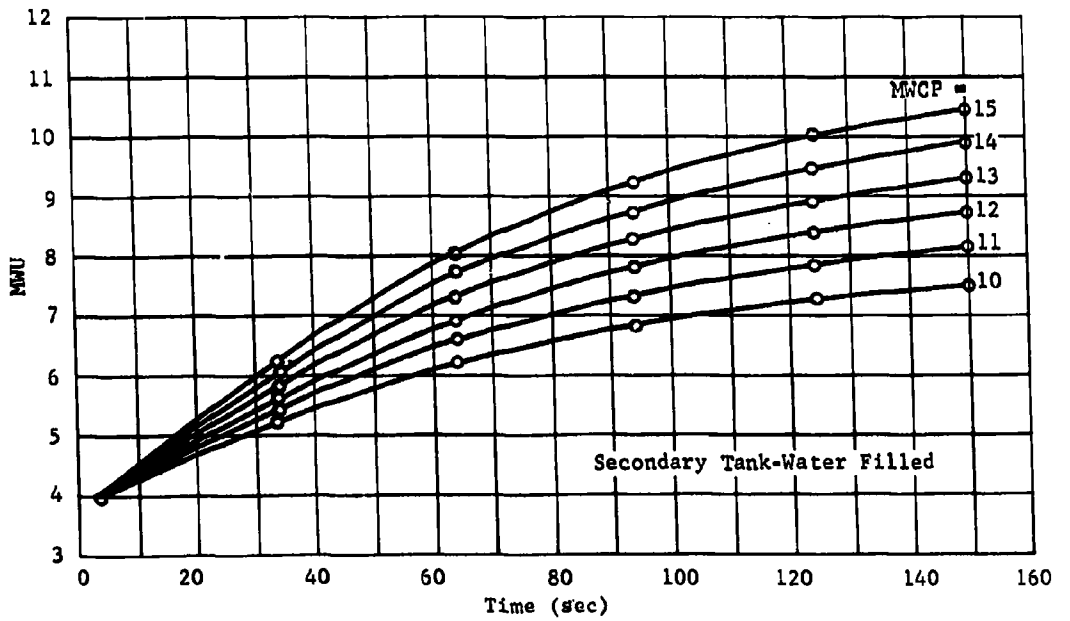
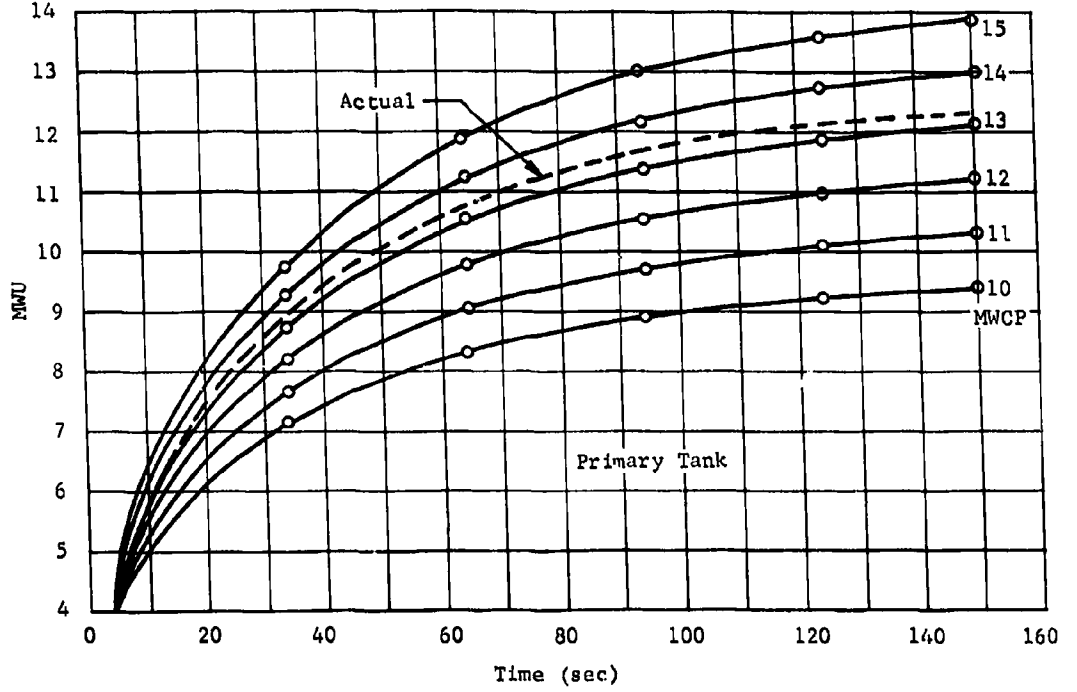


Fig. II-116 Phase I Predicted Pressurizing Gas Dilution

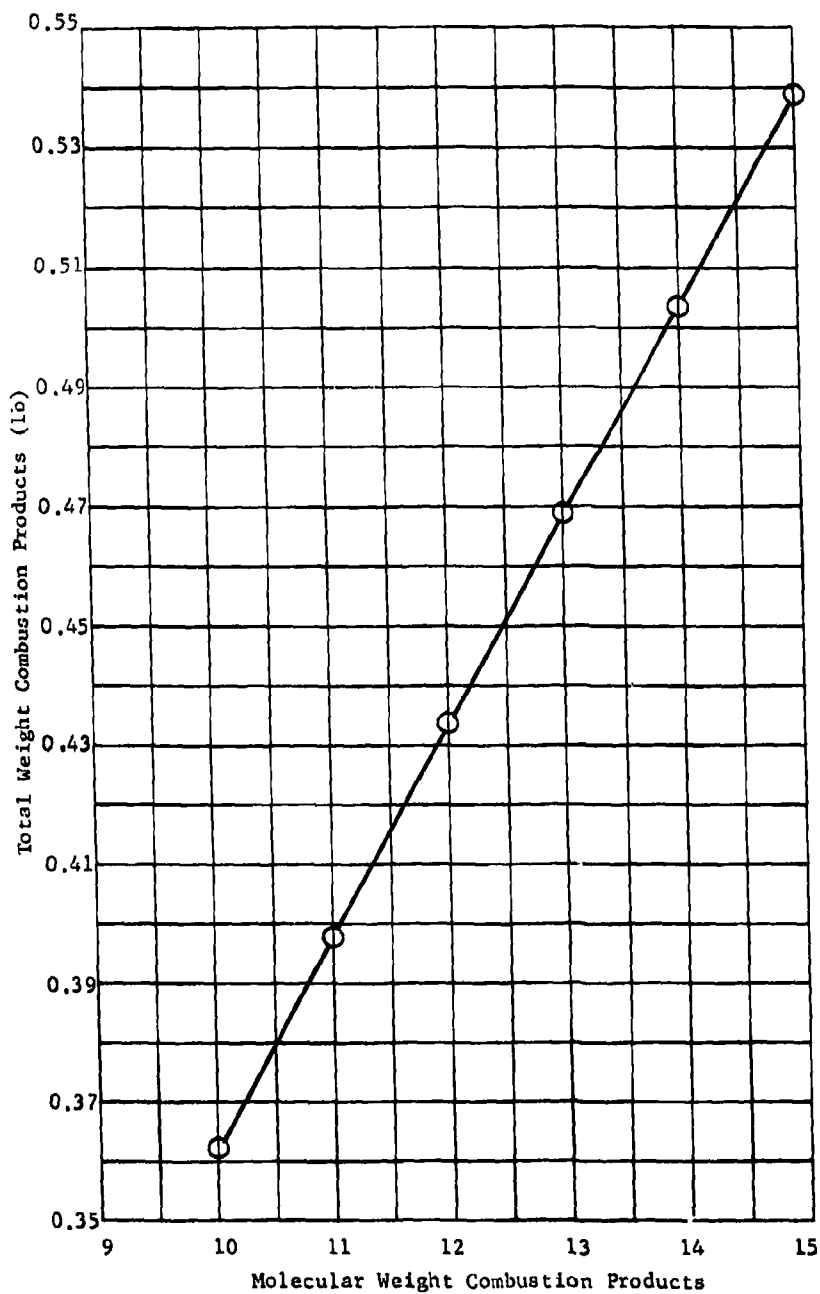
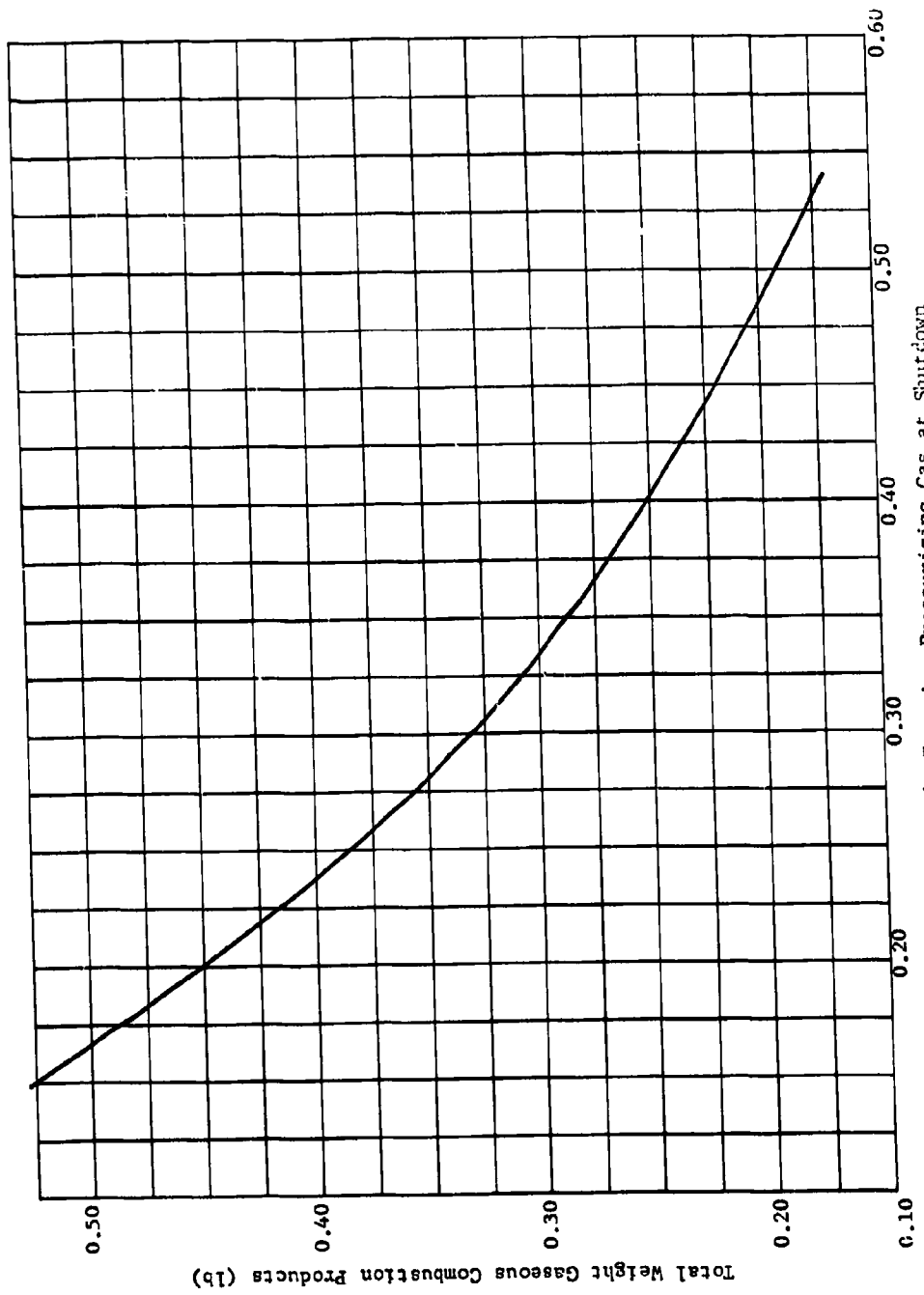


Fig. II-117 Phase I Pressurizing Gas Requirements vs Molecular Weight



Fuel Tank Mole Fraction Pressurizing Gas at Shutdown
Fig. II-118 Combustion Product vs Residual Pressurizing Gas

Fuel Tank System - A tabulation of fuel tank combustion product composition is contained in Table II-17, based on the 36 psia injection system evaluation test series. Testing was performed on the two-tank common ullage configuration with a water-filled oxidizer tank. Gas sampling, was as described previously with gas specimens acquired periodically by the heated constant bleed system. A significant change in fuel tank ullage gas composition was experienced by varying mixing techniques with the lowest gas molecular weight obtained with the solid stream surface injection process. Subsequent gas analysis performed on the fuel tank with the solid stream surface reagent injector indicated an increase in combustion product molecular weight resulting from a change to the evacuated bottle no bleed sampling technique. The comparison between the various injection techniques is believed valid. For design purposes the gas composition and molecular weight indicated in the parametric test portion of this section is recommended. The inert prepressurizing gas and vaporized propellant data were removed from all combustion product data. Since the quantity of vaporized fuel was extremely small (mole fraction less than 1%) the effect on ullage molecular weight was considered insignificant. The change in propellant vapor concentration is shown in Fig. II-119 for several injection processes and theoretical conditions.

Common Ullage System - Ullage gas composition and molecular weight of the oxidizer tank pressurant is shown in Table II-18 for various gas impingement techniques. The system configuration is described in detail in Chap. II.B.2 with a combination of gas sampling techniques used. A detailed analysis of the oxidizer tank gas was achieved by periodic sampling through the constant bleed system while only final gas specimens were obtained from the fuel tank. Both combustion product molecular weight and ullage gas molecular weight on a helium-free basis is reported. A detailed presentation of rate of saturation of the ullage with oxidizer vapors is shown in Fig. II-120 for two impingement techniques and two hypothetical cases.

Although the common ullage system represents the MTI system with the lowest oxidizer tank molecular weight, the system has a tendency to random pressure surges and high temperatures for the surface gas impingement technique. Subsurface gas impingement has been successfully demonstrated in several tests. However, ignition of hydrogen in the oxidizer tank ullage requires careful system design. Gas specimen analysis before and after an extreme pressure surge with an unsuccessful gas diffuser design showed almost complete elimination of the contained hydrogen.

The reaction is set off by the heat released when gunk reacts with oxidizer. Figure II-121 shows a normal hydrogen profile in the oxidizer tank as opposed to a run in which a violent pressure surge was encountered. All other constituents showed a normal increase during the run.

Table II-17 NTI Fuel Tank Combustion Product Composition at 36 psia with Variations in N_2O_4 Injection Technique

Injection Technique		Combustion Products Analysis (Vol %)										Molecular Weight Combustion Product	
Fuel Tank	Oxidizer Tank	N_2	H_2	CH_4	NH_3	NO	CO_2	CO	H_2O	O_2	Fuel Tank	Fuel Tank with Vapor	
Surface Solid	Common Ullage	30.0	47.4	11.1	9.2	1.6	0.4	-	-	-	13.4	13.4	
Surface Spray	Common Ullage	60.0	11.8	18.6	3.4	3.1	3.0	-	-	-	22.9	22.9	
Subsurface Solid	Common Ullage	28.1	41.3	10.1	4.9	1.0	0.4	14.5	-	-	15.6	15.6	
Subsurface Spray	Common Ullage	35.8	37.5	13.0	3.4	1.0	0.2	9.5	-	-	16.4	16.4	

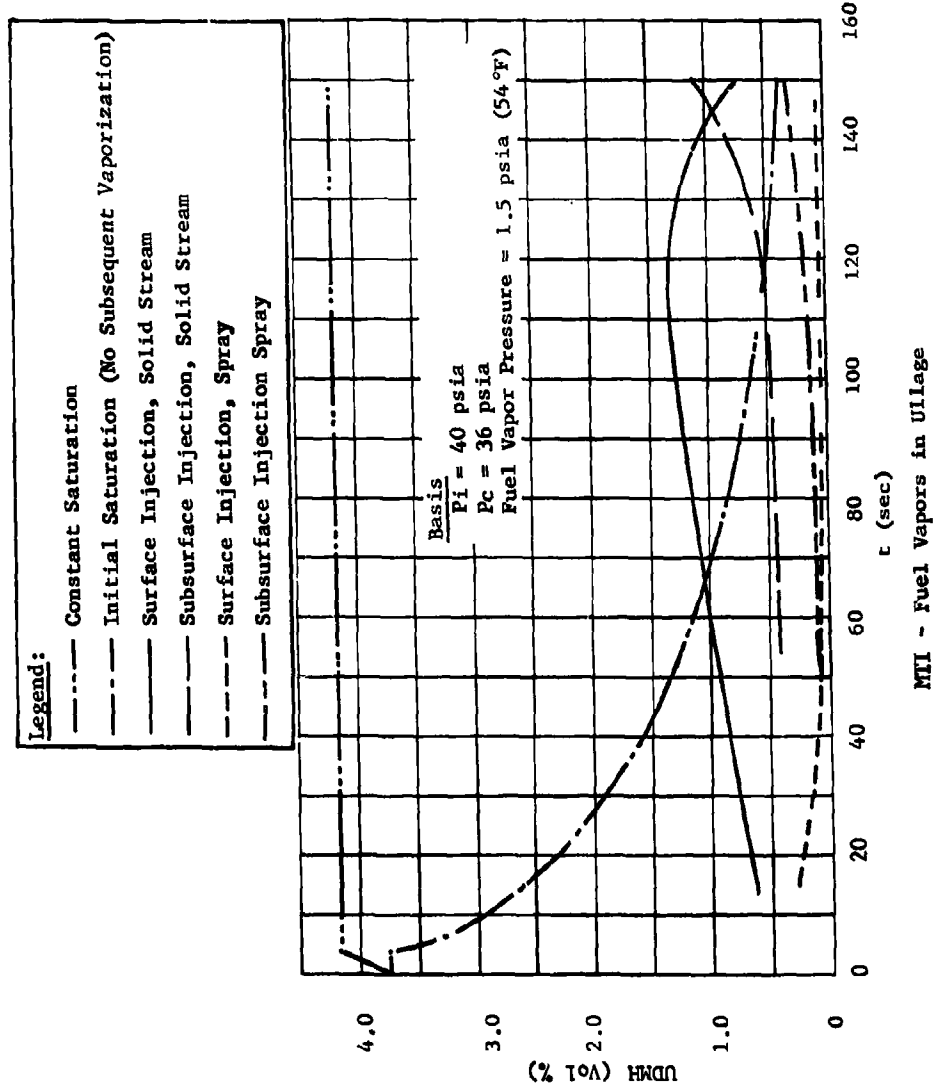
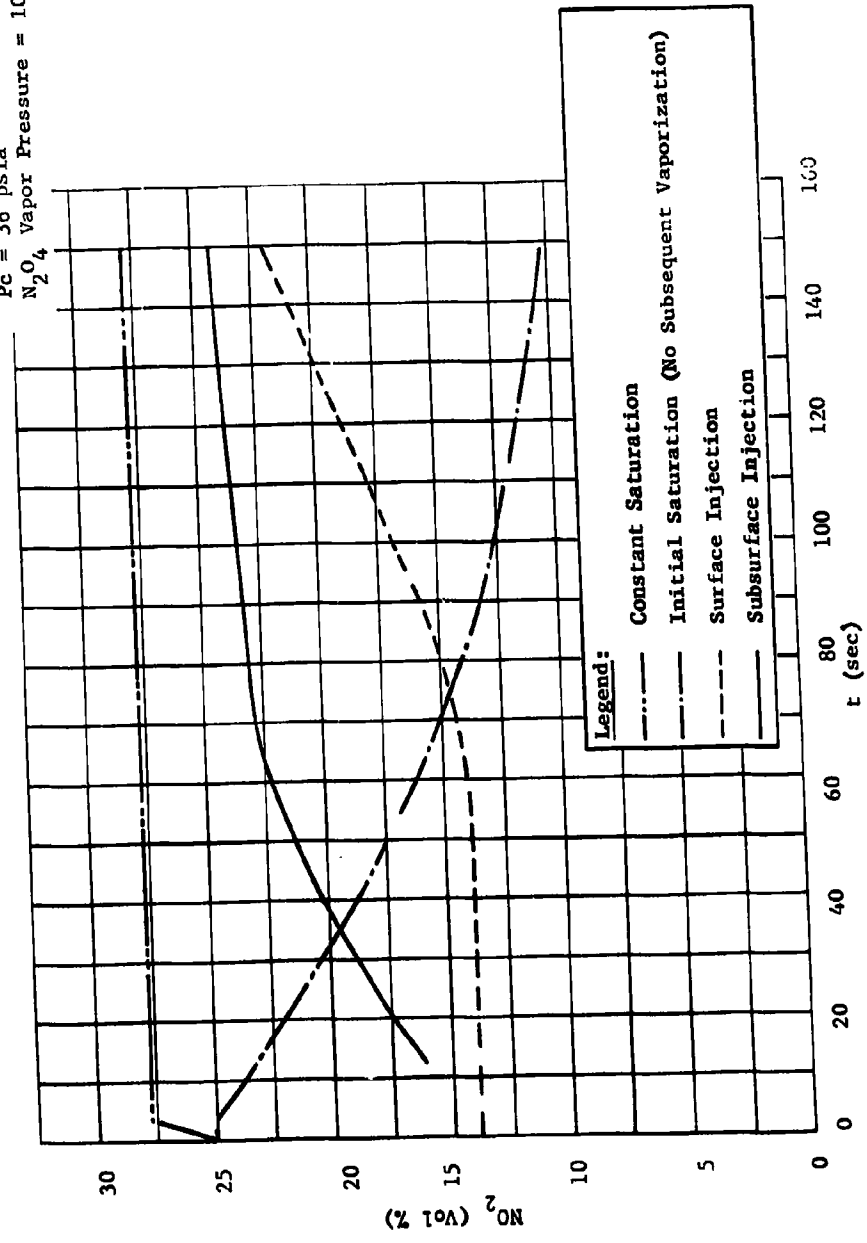


Fig. II-119 Fuel Tank Ullage Saturation with UDMH Vapors

Table II-18 MTL Oxidizer Tank Combustion Product Composition of Various Common Ullage Systems at 36 psia

Injection Technique		Combustion Products Analysis (Vol %)											Molecular Weight Combustion Product	
Fuel Tank	Oxidizer Tank	N ₂	H ₂	CH ₄	NH ₃	NO	CO ₂	CO	H ₂ O	O ₂	Fuel Tank	Oxidizer Tank	Oxidizer Tank with Vapor	
Surface Solid	Surface	60.1	18.2	5.5			5.2	11.0			18.48	23.43	27.83	
Subsurface Spray	Surface	68.4	18.7	9.0			3.9	-			24.8	22.67	25.71	
Surface Solid	Surface with Gunk Condenser	52.1	34.5	10.0			3.3	-			14.07	18.35	21.65	
Surface Solid	Surface with Gunk Filter	46.7	37.1	11.4			2.0	-	3.0		16.0	17.03	23.62	
Surface Solid	Surface with Gunk Reaction	46.4	26.5	12.8			8.8	-	5.4		16.0	20.43	27.0	
Surface Solid	Subsurface	59.9	19.4	5.8			4.4	-	2.5	8.1	16.02	23.04	30.5	

Basis
 $P_i = 40$ psia
 $P_c = 36$ psia
 N_2O_4 Vapor Pressure = 10 psia (54°F)



MTI - Oxidizer Vapors in Ullage

Fig. II-120 Oxidizer Tank Ullage Saturation with NO_2 for Common Ullage System

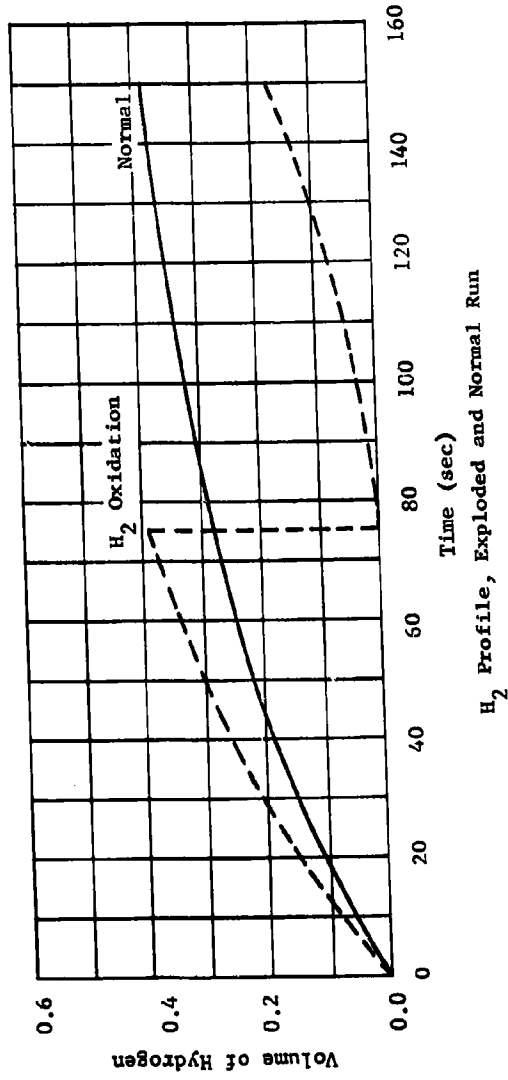


Fig. II-121 Verification of Hydrogen Reaction in Oxidizer Tank

Oxidizer Tank System - A detailed investigation of the influence of injection technique on the products of reaction was not made for the oxidizer tank because of the experience gained from the fuel tank injection system evaluation test program. However, Table II-19 shows available semispray surface injection data to compare solid stream surface fuel injection process and common ullage subsurface gas impingement. High gas temperatures were encountered with the surface spray fuel injection system due to a lack of penetration of the oxidizer. However, the combustion gas composition was not appreciably affected. A lower ullage molecular weight is obtained with the surface spray injection when compared to the solid stream injection because of the decrease in nonreacted vaporized propellant. A comparison with the common ullage data indicates a slightly higher gas molecular weight is obtained by direct fuel injection. The lower combustion product molecular weight realized with the common ullage system resulted from the increased quantity of unburned hydrogen in the oxidizer ullage with somewhat less carbon dioxide present. Propellant vapor ullage saturation profiles are shown in Fig. II-122 with comparisons of two theoretical possibilities.

Table II-19 MTI Oxidizer Tank Combustion Products Composition at 36 psia for Various Pressurization Techniques

Injection Technique		Combustion Products Analysis (Vol %)									Molecular Weight Combustion Product	
Fuel Tank	Oxidizer Tank	N ₂	H ₂	CH ₄	NH ₃	NO	CO ₂	CO	H ₂ O	O ₂	Oxidizer Tank	Oxidizer Tank with Vapor
N/A	Surface Spray	59.8	3.5	0.6	1.4	-	11.4	-	8.4	15.0	28.45	34.77
N/A	Surface Solid	58.6	1.9	1.0	-	-	17.9	-	14.1	6.7	29.11	38.52
N/A	Subsurface Gas	59.9	19.4	5.8	-	-	4.4	-	2.5	8.1	23.04	30.5

Parametric Tests - A summary of MTI pressurization system performance at pressures of 36, 100, and 200 psia is contained in Table II-20 for both the direct injection and the common ullage process. The gas composition data were based on specimens acquired at test termination by the evacuated bottle sampling technique. A solid stream surface reagent injection process was used for the direct injection system with a subsurface gas diffuser used to pressurize the oxidizer tank by the common ullage technique. Fuel tank pressurization resulted in a distinct increase in combustion

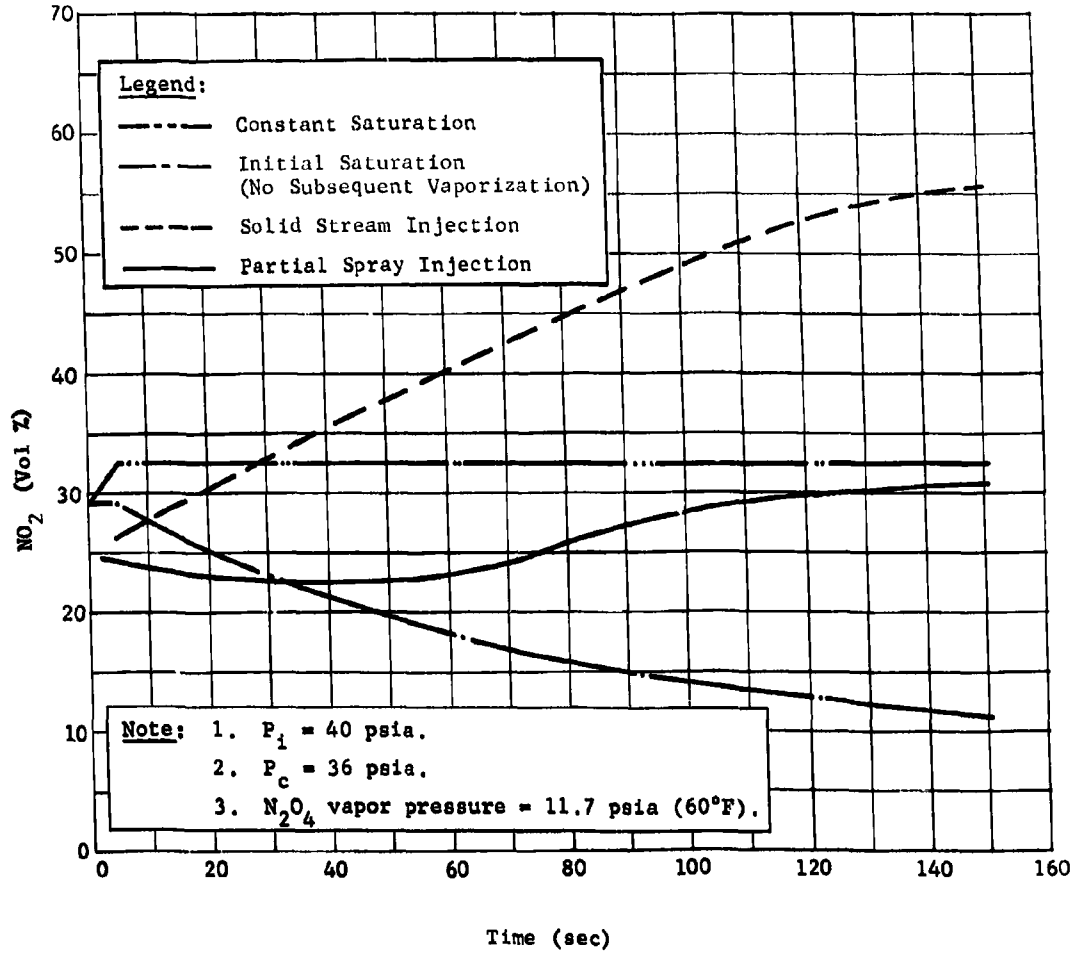


Fig. II-122 Oxidizer Tank Ullage Saturation with NO_2

product molecular weight at the higher pressures due to a 50% reduction in hydrogen concentration. The slight discrepancy between the 100- and 200-psia test data appears to be within the accuracy of the analytical technique and does not necessarily indicate a change in molecular weight between 100 and 200 psia. The absence of ammonia and UDMH in the gas analysis was contrary to initial data and later results of the full-scale demonstration system. However, the increase in combustion product molecular weight is believed valid (shown in Fig. V-1 along with the oxidizer tank gas for the direct injection and common ullage system). Although the combustion product molecular weight in the oxidizer tank is relatively insensitive to increases in ullage pressure for the direct injection system, propellant vaporization increased noticeably due to the greater heat input to the liquid in the area of the combustion zone. The change in mole fraction of oxidizer vapor in the tank ullage is shown in Fig. V-2 as a function of operating pressure for direct fuel injection. Figure II-113 shows the equivalent vapor pressure of the liquid. The bulk temperature of the liquid was considerably less than indicated by the high vapor pressure of the liquid. Local heating from the combustion zone is apparently responsible for this condition and could possibly be reduced by multiple or combination injectors in large capacity systems.

Table II-20 MTI Combustion Product Composition Parametric Data

Injection Technique		Combustion Products Analysis (Vol %)										Molecular Weight Combustion Product		
Fuel Tank	Oxidizer Tank	N ₂	H ₂	CH ₄	NH ₃	NO	CO ₂	CO	H ₂ O	O ₂	Fuel Tank	Oxidizer Tank	Oxidizer Tank with Vapor	
Surface Solid (36 psia)	N/A	44.3	39.3	14.9	-	1.2	0.2	-	-	-	16.02	N/A	N/A	
Surface Solid (100 psia)	N/A	55.0	18.6	18.3	-	2.7	2.3	-	0.2	3.0	21.5	N/A	N/A	
Surface Solid (200 psia)	N/A	51.7	19.7	20.5	1.7	3.6	1.2	-	0.6	0.9	20.46	N/A	N/A	
Oxidizer Tank														
N/A	Surface Solid (36 psia)	58.6	1.9	1.0	-	-	17.9	-	14.1	6.7	N/A	29.11	38.52	
N/A	Surface Solid (100 psia)	63.1	-	-	1.1	-	11.7	-	6.0	17.9	N/A	29.87	35.79	
N/A	Surface Solid (200 psia)	65.8	1.7	0.8	0.8	-	11.3	-	3.2	16.1	N/A	29.54	35.30	
Oxidizer Tank (Common Ullage)														
Surface Solid (36 psia)	Subsurface (Common Ullage)	59.9	19.4	5.8	-	-	4.4	-	2.5	8.1	16.02	23.04	30.5	
Surface Solid (100 psia)	Subsurface (Common Ullage)	66.4	3.1	1.7	1.0	-	3.2	-	2.7	21.9	21.5	28.0	32.79	

2. Propellant Analysis

The propellant analysis can also furnish considerable information to determine MTI pressurization system process characteristics. Particular emphasis has been on securing data for heat transfer analysis and to determine condensed products of reaction to establish a material balance. Determining propellant degradation was considered primarily to evaluate pressurization system performance. The effects on rocket engine specific impulse are also needed. Engine performance was considered to establish the method of securing propellant samples. The extent of propellant contamination for the 2.5 min tests was so small that the effect on rocket engine performance was negligible.

Immediately before each test, a propellant specimen is taken from the main propellant tank discharge port and sealed in a bottle. The final sample is acquired in the same manner from the residual 0.42 cu ft remaining in the bottom of the propellant tank at the end of the run. From a chromatograph analysis of the specimen, the increase in water content of the fuel attributed to the MTI reaction process can be determined from a chromatograph analysis of the specimen. Changes in composition were determined by wet chemistry techniques. Oxidizer specimens are analyzed for water only by either a thermal conductivity or acidity test. The analysis of the contaminated propellants is assumed to be representative of the maximum concentration of contaminants that a rocket engine would be subjected to during actual operation with an MTI pressurization system. When an average percent increase in water content was desired to establish approximate quantities contained, the propellant was mixed before acquiring the final specimen. After nine tests on the fuel with a surface reagent injection process and 3.6 psia tank pressure the following composition was noted:

	<u>Actual</u>	<u>Specification</u>
N_2H_4	54.52%	51.0 \pm 0.8%
UDMH	43.75%	47.0% (min)
H_2O	1.72%	1.8% (max)

Similarly, the oxidizer contamination showed 1.9% water after 14 common ullage tests (0.2% max specification). No measurement of propellant contamination due to higher operating pressures was made; however, the extent of degradation is expected to be proportional to the reagent consumption.

Analytical Technique - Propellant analysis for the MTI program was performed in the Martin Chemical Laboratories by Quality Control personnel. Specimens were acquired before and after each test from the discharge port of each tank. The final specimen represented the condition of the propellant that would enter the engine just before burnout. Specimens were also obtained by recycling the propellant at the end of the test to obtain the average change in propellant composition or contamination. Based on this analysis, the absolute quantity of water generated was identified and included in a material balance of the reaction process. Separate techniques were used on the fuel and oxidizer. They are explained generally in the following paragraphs, with a brief description of the improved technique used in some of the laboratory work.

Fuel composition was determined by two wet chemistry techniques. The first method used was a total alkalinity method combined with an oxidation-reduction method. Alkalinity was determined by a color indicator from a titration of perchloric acid solution in a sample prepared in glacial acetic acid. The oxidation-reduction method involved the potentiometric determination of the electrical conductivity of the specimen reacted with a normal solution of potassium iodate (KIO_3). From the alkalinity and electrical conductivity, the ratio of hydrazine to UDMH could be determined. Fuel composition was also determined by the new specification acetylation method (Martin specification 8021310000), permitting a 60% reduction in laboratory time per specimen with an accuracy of 0.1%. This method used the titration of an acetic anhydride solution in the specimen prepared in glacial acetic acid.

Due to the extent of the acetylene reaction of the hydrazines, color indications, were noted, giving a direct correlation with the actual concentrations of each of the two constituents. Water content was determined directly from the diffusion and thermal conductivity of the material by a Beckman GC-2 chromatograph. From the results of the two investigations, the total assay was assured with an accuracy of more than 98%.

The nitrogen tetroxide was analyzed for water content only by two methods. The predominant method used was a Martin technique involving the determination of electrical conductivity. A specially designed stainless steel resistance cell unit was used

in conjunction with a Wheatstone bridge. This apparatus was calibrated constantly against the specification method to assure system accuracy. The second method was the standard specification method (Martin specification 8021310000) using the Haberman bulb to determine the concentration of nitric acid in the specimen by an evaporation process.

Results - Table II-21 presents data acquired from an analysis of the fuel used in the two-tank tests with a water-filled secondary tank. Although the fuel was not within specification requirements because it had been used several times, no significant effect on pressurization system performance was detected in subsequent tests. Table II-22 presents comparable propellant analysis performed on a series of 150-sec tests with solid-stream surface injection in the primary tank and common ullage pressurization of the oxidizer-filled secondary tank. The corresponding change in water concentration in the oxidizer was included for the subsurface gas impingement process. No significant change occurred in the oxidizer with the surface gas impingement system.

From the tabulated data, it was apparent that some decrease in UDMH, the more volatile constituent of the 50/50 fuel blend, resulted from the pressurization process; the amount being a function of the type of reagent injection. The increase in hydrazine content was only relative, and does not indicate any additional formation. The change in water concentration, however, did show an actual increase that was caused by the injection technique. From the theoretical studies performed on the reaction process, the increase in water formation would indicate a more oxidizer-rich reaction. This theory was substantiated by the significant increase of water in the fuel tank for the surface spray injection test and high-ullage gas molecular weight characteristic of an oxidizer-rich reaction. The unknowns detected in the fuel were believed to be condensibles generated by the reaction process that were also observed in the pressurization system. A positive identification of the material was not established, but the fluid was similar to a reddish light oil with a density of 68.5 lb/cu ft, and was hypergolic with nitrogen tetroxide.

The average 0.3% increase in water content of the fuel and oxidizer during the 150-sec test was not considered excessive, but will require further investigation to determine the effect on rocket engine performance. A significant reduction in water concentration occurred when the propellant was mixed, giving an indication of the actual amount of water formed. The theoretical maximum water content in each propellant is shown in Fig. II-123 as a function of quantity of reagent injected. Since an insignificant quantity of hydrogen compounds were detected in the oxidizer tank ullage gas analysis with an absence of gunk, the theoretical water concentration is believed to be representative of the actual condition although no measurement was made for the direct fuel injection process.

Table II-21 Propellant Analysis for Two-Tank Test with Water-Filled Second Tank

Type Test	Condition	UDMH (%)	N ₂ H ₄ (%)	H ₂ O (%)	Unknown (%)
Surface Solid	Before	46.1	52.0	0.55	1.35
	After	44.8	52.9	0.95	1.55
Surface Spray	Before	44.3	53.5	0.79	0.41
	After	40.6	53.6	2.37	3.43
Subsurface Solid	Before	45.1	52.7	0.90	1.3
	After	43.9	53.4	1.19	1.51
Subsurface Spray	Before	45.5	52.9	0.79	0.81
	After	44.4	53.5	1.04	1.06

Table II-22 Typical Propellant Analysis for Two-Tank Test Series with Oxidizer-Filled Second Tank

Type Test	Condition	Fuel				Oxidizer H ₂ O (%)
		UDMH (%)	N ₂ H ₄ (%)	H ₂ O (%)	Unknown (%)	
(Unmixed Propellant) (P) Solid Stream (S) Subsurface	Before	48.4	50.9	0.31	0.39	0.10
	After	48.1	50.3	0.63	0.97	0.47
(Mixed Propellant) (P) Solid Stream (S) Subsurface	Before	45.3	53.1	0.32	1.01	0.27
	After	44.5	53.4	0.53	1.20	0.37

Note: (P) Primary Tank (fuel); (S) Secondary Tank (oxidizer)

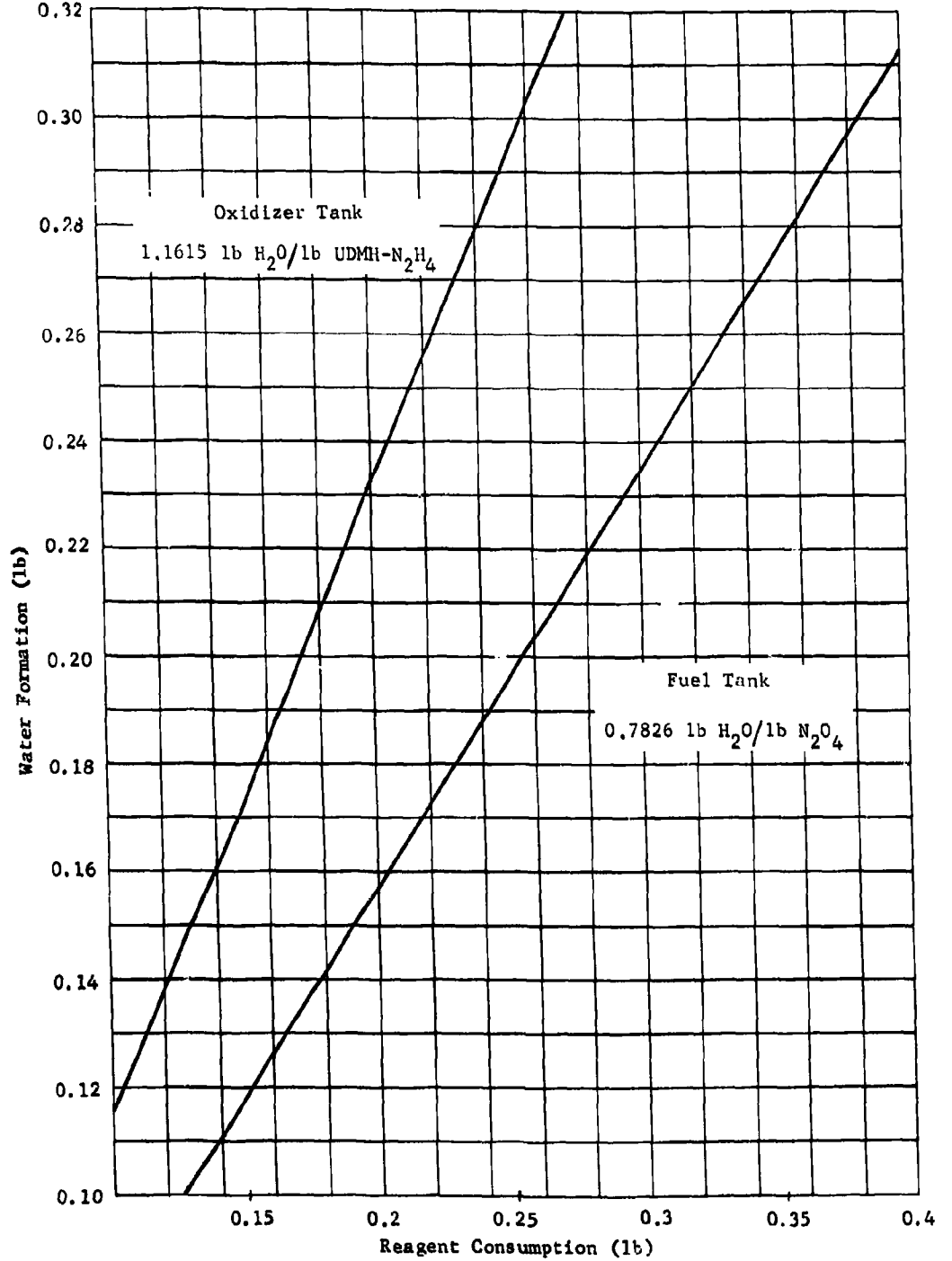


Fig. II-123 Theoretical Maximum Water Concentration in the Fuel vs Reagent Consumption

The average increase in water concentration of approximately 0.45% in the oxidizer was noted in the restart tests, where an explosion had occurred. This fact appears to support the conclusion that a hydrogen-oxygen reaction, triggered by a hypergolic reaction with condensed fluids carried in the cross-flow gas, caused the additional water formation. In addition to the chemical changes to the propellants noted, an analysis of the fuel specimen after one test showed a negligible change in specific gravity and viscosity. For the fuel specimen obtained after one of the tests with an oxidizer-filled second tank, the specific gravity changed from 0.8987 to 0.9064, and viscosity increased from 0.96 to 0.98 centistokes (equivalent to a 4°F temperature change).

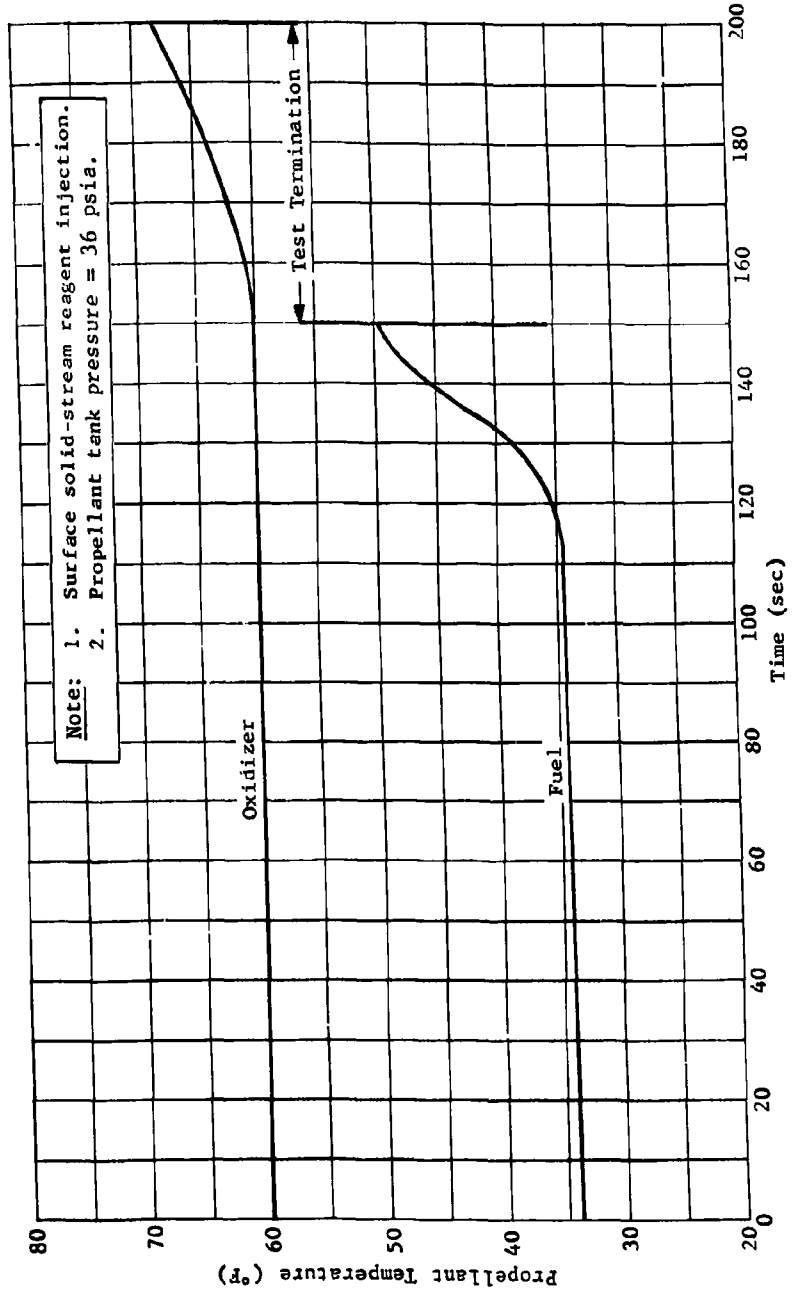


Fig. II-124 Propellant Temperature at Tank Outlet vs Time

Several factors connected with the propellant and combustion process apparently aid the mixing of the contaminated and uncontaminated fuel. Although the fuel is infinitely soluble in water, the increased density of the fuel near the surface with the solid stream surface injection process or from ullage gas condensation will tend to sink to the bottom of the tank. At the same time, heavier products of combustion at a higher temperature will likewise cause a certain amount of turbulence in the propellant due to natural convection. The actual amount of temperature stratification in the propellant occurring during a test can be seen from Fig. II-123, which shows the temperature in the discharge line. The 15°F propellant temperature rise noted for the solid stream surface injection process is also representative of the average bulk temperature of the 0.42 ft³ residual and has been used in heat balance studies. A slight decrease in temperature noticed earlier in the test program has never been satisfactorily explained but appears to have been due to an instrumentation problem in view of the consistent additional data accumulated.

In general the condition of the fuel after each test was good with no evidence of undissolved reaction by-products. A slight discoloration of the fuel was noticeable after each test probably due to the solubility of condensed reaction products. After a maximum of five full duration tests was performed on one load of fuel the only evidence of contamination was the light yellow color of the fuel. After five full-duration tests with direct fuel injection into the oxidizer tank, the propellant was beginning to darken slightly from the amount of entrained water.

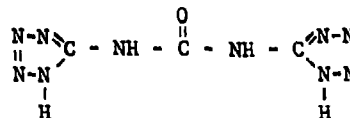
3. Condensate Analysis

A viscous reddish brown liquid (gunk) was observed in the common ullage line during the initial MTI fuel tank pressurization tests. The gunk caused considerable interest due to propellant contamination and later because of the severe reactions encountered in the oxidizer tank. A brief investigation showed the substance to be hypergolic with N₂O₄ and hypergolic to a lesser extent with a variety of other elements. Since the gunk reaction detonated the hydrogen in the common ullage oxidizer tank pressurization tests, the composition of the material and reactive characteristics were investigated. The first investigations by wet chemistry qualitative methods indicated the gunk was similar to hydrogen nitrate. When the liquid specimen evaporated, an X-ray diffraction was performed on the residue at the Denver Research Institute. The substance was found not to be crystalline, consequently, identification was impossible by this technique. Subsequent gunk specimens were procured by a vortex separator in the common ullage line to obtain larger quantities for investigation of reaction characteristics. Since the gunk apparently exists in both the liquid and gaseous phase, an attempt was made to separate the substance by condensation. This method was moderately successful, although the ice-cooled common ullage line configuration was considered impractical for future system application.

Various physical and chemical methods were attempted to remove the gunk from the pressurizing gas generated in the fuel tank. Traps containing oxidizing agents were provided in the common ullage line to break down the gunk into H_2 , N_2 , NO_2 , H_2O , and other substances nonhypergolic with nitrogen tetroxide. A more detailed description of the laboratory experiment with CrO_3 , Drierite, Zeolite, $KMnO_4$, silica gel, activated charcoal, and firebrick is contained in Sec A of this chapter. A glass wool filter was used in all tests that involved combinations of the above materials. The basic idea was to either absorb or react all the potential hypergolic constituents. In general the absorbent ingredients of the filter were fairly successful in eliminating liquids of the two-phase fluid. However, the reactants were only moderately successful in reducing the reactive vapors. Catalytic-type powdered molybdenum and copper oxide wool filters were also unsuccessful in decomposing the vapor phase hypergols.

The liquid condensate was further investigated because of the partial success obtained with the common ullage reactive filter. A fairly comprehensive analysis of the condensate in the vapor phase was obtained by mass spectrometer analysis at the National Bureau of Standards at Boulder, Colorado. Primary constituents were UDMH and a large amount of the NH_3 radical with smaller quantities of CH_3 , NO_2 , and CO_2 .

The gunk was consequently identified as consisting of 50% UDMH and NH_3 remaining in a partial vapor phase at nominal MTI system operating temperatures (150 to 300°F). The equivalent change in ullage gas molecular weight is shown in Fig. II-125 as a function of vaporized gunk. In addition, the gunk density was 68.5 lb/cu ft with a pH of 10.5 in a water solution, measured by the Beckman pH meter. Subsequent infrared analysis of the condensate minus the UDMH portion was also performed. The results of this investigation indicated the presence of a polymer of x many members with a basic monomeric structure similar to the one shown below:



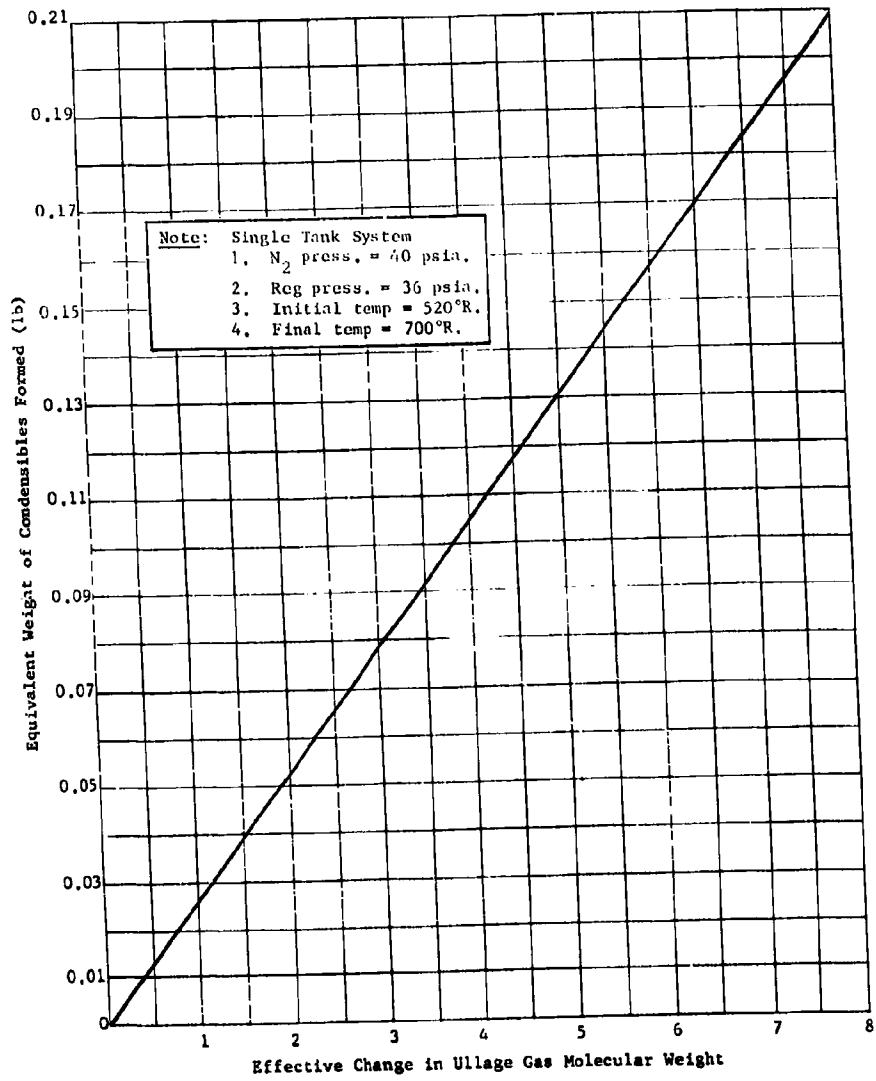


Fig. II-125 Equivalent Ullage Gas Weight as a Function of Changes in Molecular Weight

Along the polymer chain it was indicated that NO_2 groups existed and the polymer probably ended in a carboxyl group (COOH). The presence of the polymer indicates a free radical mechanism taking place in the formation of the gunk. Consequently, the exact nature of the polymer cannot be predicted since it probably differs in structure with each reaction. Further attempts to eliminate the gunk in the common ullage application were abandoned. A successful subsurface gas impingement technique was developed that consumed the reactive material before it reached the hydrogen pressurized oxidizer tank ullage.

D. CONCLUSIONS

As a result of the Phase I research program a definite region of application was established for the MTI pressurization system in future liquid fueled vehicles. Subsequent examination of the reaction process has verified adequate pressure control with satisfactory performance for full-scale system demonstration although additional effort is required to identify reaction kinetics and influence parameters. The results of this program have provided pertinent design information for the full-scale system, based on a dual solid stream surface injection pressurization process. Some of the more significant results of both the analytical and experimental programs are described in detail in this section.

1. Engineering Studies

- 1) The 2,000-gal. Phase III demonstration test article is well within the range of desirable low-pressure MTI system applications.
- 2) A 35 ± 1 psia propellant tank pressure will satisfy the propellant feed requirements of booster vehicles that can be used with small-scale system parametric performance to provide theoretical data for low-pressure space vehicles (100 to 200 psia).
- 3) The development of an on-off constant flow injection system was required, not only for control of the reaction kinetics, but to provide adequate pressure control for variable thrust-restart type missions.

- 4) Maximum system operating temperatures will be determined by tank material considerations, rather than propellant temperature limitations. However, increased oxidizer temperatures will have to be compensated by higher tank pressures for turbopump pressurized propulsion systems.
- 5) For a noncooling process, such as booster or continuous mission, the reaction mixture ratio and consequently combustion product molecular weight will have only a small effect on pressurization system weight because of the low pressurant density resulting from the high operating temperature.
- 6) Initiation of the pressurization process in the fuel tank of a common ullage system is desirable from both a weight and design point of view.
- 7) A fuel-rich reaction is desired not only for temperature control, but also for low system weight of space vehicles in environmentally cooled operations, due to the lower gas molecular weight realized.
- 8) For environment cooling missions, a stored helium system with heat added to cancel the cooling from gas expansion is lighter than an MTI system with a gas molecular weight greater than 15.
- 9) For booster and sustaining vehicle applications, the MTI pressurization system is lighter than the stored gas system.
- 10) The MTI pressurization system is slightly lighter than the gas generator system for all vehicle sizes and applications; however, versatility is its main advantage.
- 11) An MTI pressurization system may be applicable to a variety of propellant combinations in addition to the storeable type specifically investigated.
- 12) The principle advantage of the MTI pressurization technique is the high-density low-pressure storage of the reagents and capability for generation of a low-density pressurant without the aid of a heat exchanger.

2. Experimental Testing

- 1) Smooth combustion and moderate system pressure rise rates are possible with a common ullage or dual reagent injection pressurization system at pressures up to 200 psia.
- 2) The direct reagent injection reaction process can be significantly affected by the mixing technique in the fuel tank, and to a lesser extent in the oxidizer tank.
- 3) By careful system design, secondary reactions occurring when fuel-rich combustion products are introduced into the oxidizer by a subsurface gas diffuser in a common ullage configuration, can be controlled sufficiently for satisfactory pressurization.
- 4) Check valves have been satisfactory in preventing propellant vapor reactions in a common ullage system. However, a more positive isolation valve with differential pressure switch control may be desired in larger systems.
- 5) Propellant heating does not appear to be a significant problem, although, for high-pressure applications a considerable amount of oxidizer is vaporized with direct fuel injection due to local heating in the combustion zone. The slight increase in vapor pressure with a low-pressure system may require higher operating pressures to supply the necessary NPSH of a turbopump pressurized propulsion system.
- 6) Although combustion was not sustained in the dual injection system when injection was terminated, the common ullage system experienced some additional reaction of a small magnitude in the gas cross flow line.
- 7) Propellant tank pressure control can be maintained within close tolerance by a MTI pulse injector system.
- 8) The direct injection process generated combustion gases with a molecular weight of 16 in the fuel tank and 29.5 in the oxidizer tank (23.75 for common ullage pressurization of the oxidizer tank) without a significant change for the 150-sec test duration.

- 9) Precise solid stream surface reagent injection is required to obtain sufficient heat transfer to the propellants for providing an acceptable ullage gas and propellant tank wall temperature.
- 10) The heat of combustion, primarily dissipated in the fuel, did not significantly increase the quantity of propellant vapors in the ullage at low pressures. At high pressure (200 psia) a significant increase in oxidizer vaporization was experienced.
- 11) For a common ullage pressurization system, the reactivity of the MTI combustion gas would be significantly lower than for a gas generator system due to a 60% reduction in ammonia and more complete combustion.
- 12) Propellant contamination resulting from the dual injection process has been less than 0.5% in either the fuel or oxidizer tank.
- 13) Reagent consumption was approximately 50% higher than predicted for the small-scale dual injection system because of the amount of condensibles formed. Approximately 2.5 lb of gas was formed per pound of reagent.
- 14) The reaction mixture ratio, established from a theoretical material balance, was 0.63 in the fuel tank and 2.3 in the oxidizer tank for the small-scale system with direct injection.
- 15) The reaction mixture ratio was independent of operating pressure although an apparent increase in combustion product molecular weight was experienced in the fuel tank at higher operating pressures.
- 16) Reagent consumption did not appear to be affected by orifice size.
- 17) The surface area of the combustion zone appears to be directly proportional to the injector orifice area.
- 18) Condensate generated only in the fuel tank appears to be primarily UDMH and represents less than 10% of the total combustion products.

- 19) Penetration of the liquid propellant by the combustion process with solid stream injection is limited only by injection duration or physical boundaries of the tankage.
- 20) Injection velocity will be limited based on a (200 psi) maximum differential pressure to achieve a good solid stream without any atomization.
- 21) Liquid propellant agitation or distance from the surface solid stream injector did not have any significant effect on pressure control or the reaction process in the 26-in. dia spherical test tank.

III. PHASE II PROGRAM

The second phase of the MTI pressurization system development program was concerned with the design of a 279-cu ft test article for ground demonstration of the 36 psia dual reagent injection pressurization system. This article evolved from small-scale research testing. The experimental test data were analyzed to investigate the effects of heat transfer and establish a mass balance for the MTI process when used in a full-scale flight weight system. From the reaction characteristics observed during the small-scale test program and subsequent analytical investigations of system thermodynamics, two MTI mathematical models were formulated. One model was programed on the IBM 7094, and one model was an abbreviated version on the IBM 1620. Based on the theoretical predictions of full-scale system performance, a design criteria document was generated to aid in the detailed design and fabrication of the prototype MTI demonstration system.

A. THEORETICAL STUDIES

In addition to the ullage gas dilution computer program described for Phase I test data interpretation and the IBM 1620 single tank mathematical model formulated for early studies of expected system performance, several detailed theoretical analyses were also performed. These analyses investigate heat and mass transfer relationships encountered in the MTI pressurization process. Since a purely theoretical prediction of the reaction kinetics was not possible because of the complex nature of the reaction phenomena, empirical relationships based on the experimental data were established. Film coefficients used in the heat transfer analysis of the Phase I system were later employed in the analysis of the Phase II system with appropriate scaling factors considered. The material balance performed on the Phase I system was established from an analysis of the actual products of reaction. Due to the complex nature of the fuel tank MTI process, reaction mixture ratio influence parameters will require additional investigation. However, relationships have been established for the Phase I and Phase II systems. Both the dual injection and common ullage configurations were analyzed and designed. Current test philosophy permitted testing of the small-scale system only.

1. Heat Balance

The heat transfer investigation, based primarily on the small-scale system experimental program, provides a comprehensive description of various MTI process thermodynamic characteristics so that full-scale system design can be verified. A description of the quantitative examination of the time variant ullage gas thermodynamics for the small-scale system was established based on average system properties to allow rapid noncomputer type calculations. From the evaluation of the film coefficients obtained in the small-scale system, estimated values for the full-scale system were computed based on known thermodynamic relationships concerning pressurant gas demand. In view of the lack of correlation with theoretical relationships for the fuel tank pressurization film coefficients, comparable empirical values for the oxidizer tank were obtained by parametric computer runs. Specifically, heat transfer coefficients between the pressurant and tank wall and the liquid surface were established with combustion temperature and apparent reaction mixture ratio determined from a chemical analysis. These results, tabulated in Table III-1 for the injection system development test series show:

- 1) Free convection theory requires adjustment for fuel tank heat transfer because of mass transfer and forced convection effect resulting from the subsurface combustion zone;
- 2) Conventional free convection heat transfer theory can be used for predicting heat transfer within the oxidizer tank for the common ullage system in the absence of secondary chemical reactions;
- 3) Subsurface gas impingement with secondary reactions in the oxidizer tank results in sufficient cooling to minimize the ullage gas temperature increase.

Application of these results to a flight-weight MTI pressurization system (Phase III) was made. The analysis for the prediction of salient system performance parameters is described later in this section. The Phase III system was analyzed for common ullage and with single propellant tank expulsions. Predicted performance results for both conditions are shown in Table III-2.

Wall temperatures of 367°F were estimated for the dual tank expulsion, with a full load of water in the secondary tank. To test tank wall thermal protection could be achieved by 1/8-in. Foam-Sil internal insulation or equivalent. A reduction in pressurization requirements with live oxidizer would eliminate the necessity for insulation, due to the lower primary tank wall temperatures expected. This configuration was not tested, however, to due safety conditions.

Table III-1 Phase I Research Test Tank Correlation of Ullage Gas Thermodynamics, Twin Tank Expulsion (Water in Oxidizer Tank)

	Fuel	Oxidizer
Molecular Weight Combustion Products	13.4	
Inert Gas Weight (lb_m)	0.0486	0.0077
Final Gas Weight (lb_m)	0.31	0.311
Condensed Moisture (lb_m)	0.29	
Reagent Used (lb_m)	0.412 Total	
Wall Film Coefficient ($Btu/hr ft^2 \text{ } ^\circ R$)	18	1.66
(Free Convection Film Coefficient) ($Btu/hr ft^2 \text{ } ^\circ R$)	3.23	1.59
Liquid Surface Film Coefficient ($Btu/hr ft^2 \text{ } ^\circ R$)	104.5	1.41
(Free Convection Film Coefficient) ($Btu/hr ft^2 \text{ } ^\circ R$)	3.73	1.35

Table III-2 Estimated Phase III Pressurization
System Performance

$T_{wb} = 60^{\circ}\text{F}$ $MW_{cp} = 16$	Single-Tank Expulsion	Twin-Tank Expulsion (Full Load of Water in Second Tank)
Maximum Fuel Gas Temperature ($^{\circ}\text{F}$)	290	580
Maximum Fuel Wall Temperature ($^{\circ}\text{F}$)	190	367
Total Helium Weight (lb_m)	1.595	1.96
Total Gas Weight (lb_m)	17.15	31.85
Condensed Moisture (lb_m)	7.	13.5
Reagent Used (lb_m)	10	19.3
Weight Penalty (lb_m)	24.15	45.35

Phase I System Thermodynamic Characteristics - Due to the nature of the combustion reaction, the use of free convection formulas proved unsatisfactory in determining primary tank wall temperatures. The gas generated from combustion appeared to sweep outward against the ullage wall surfaces, introducing some degree of forced convection. This was evidenced in films of the combustion process, where light-colored gases were seen rising above the liquid surface. In addition, the solid stream surface injection technique actually penetrated the liquid surface, resulting in combustion beneath the liquid surface and heat and mass transfer caused by the increased turbulence.

To determine the effective heat transfer coefficients, at the wall and across the bulk liquid surface, several test runs using the research-type spherical tanks were examined. A model diagram of a typical arrangement is shown in Fig. II-47. The general energy equation applied to the ullage gas in either tank is:

change of internal energy = net enthalpy of added pressurant*,
less heat loss†, less flow work,
less enthalpy of any bleed flow.

Fuel Tank - The amount of heat transferred from the pressurant (excluding heat from mass transfer) can be determined from the general equation that reduces to this form when test measurements are used. The combustion temperature, T_c , was carried as a variable, since no adequate measurements were made:

$$Q = C_1 T_c - C_2, \quad \text{[III-1]}$$

where,

C_1 and C_2 were derived from test measurements. The total heat transferred, including the heat from mass transfer, was computed directly by determining the change of thermal capacity of the tank wall and the bulk liquid. That is,

$$Q + Q_M = \sum W C_p \Delta t, \quad \text{[III-2]}$$

*This term excludes the enthalpy of condensed pressurant.

†This term excludes the heat liberated by condensed pressurant.

where,

Q_M is the heat gain from mass transfer,

W is the mass exposed to heat transfer,

Δt is the temperature change.

Furthermore, when mass transfer is identified, the heat from this source is expressed by,

$$Q_M = f(T_s, W_s), \quad \text{[III-3]}$$

where,

W_s is the mass involved in mass transfer,

T_s is the saturation temperature.

Assigning test measured values, Eq [III-1] and [III-2] were plotted as a function of T_c (Fig. III-1) for a typical run.

Chemical analysis of the bulk propellant to determine the amount of steam condensed was found inconclusive. This value was estimated on the basis of the maximum possible amount of steam generated, limited by the number of oxygen atoms available. As shown in Fig. III-1, 93½% of maximum available moisture was considered condensed. This high degree of condensation probably can be expected because of the subsurface combustion. Equations [III-1] and [III-2] intersect, indicating an estimated combustion temperature of 2540°F. More important, the actual heat transfer rate was found to be greater than that expressed by the free convection formula by an overall factor of 6.33 to 1 (28 to 1 for the liquid side and 5.5 to 1 for the wall side).

The greatly accelerated rate for the liquid side was influenced primarily by the mass transfer and the sloshing liquid-level surface. Undoubtedly, the relative absence of mass transfer (condensation) at the tank walls resulted in a lower deviation at the wall surface, although the presence of forced convection affected this value.

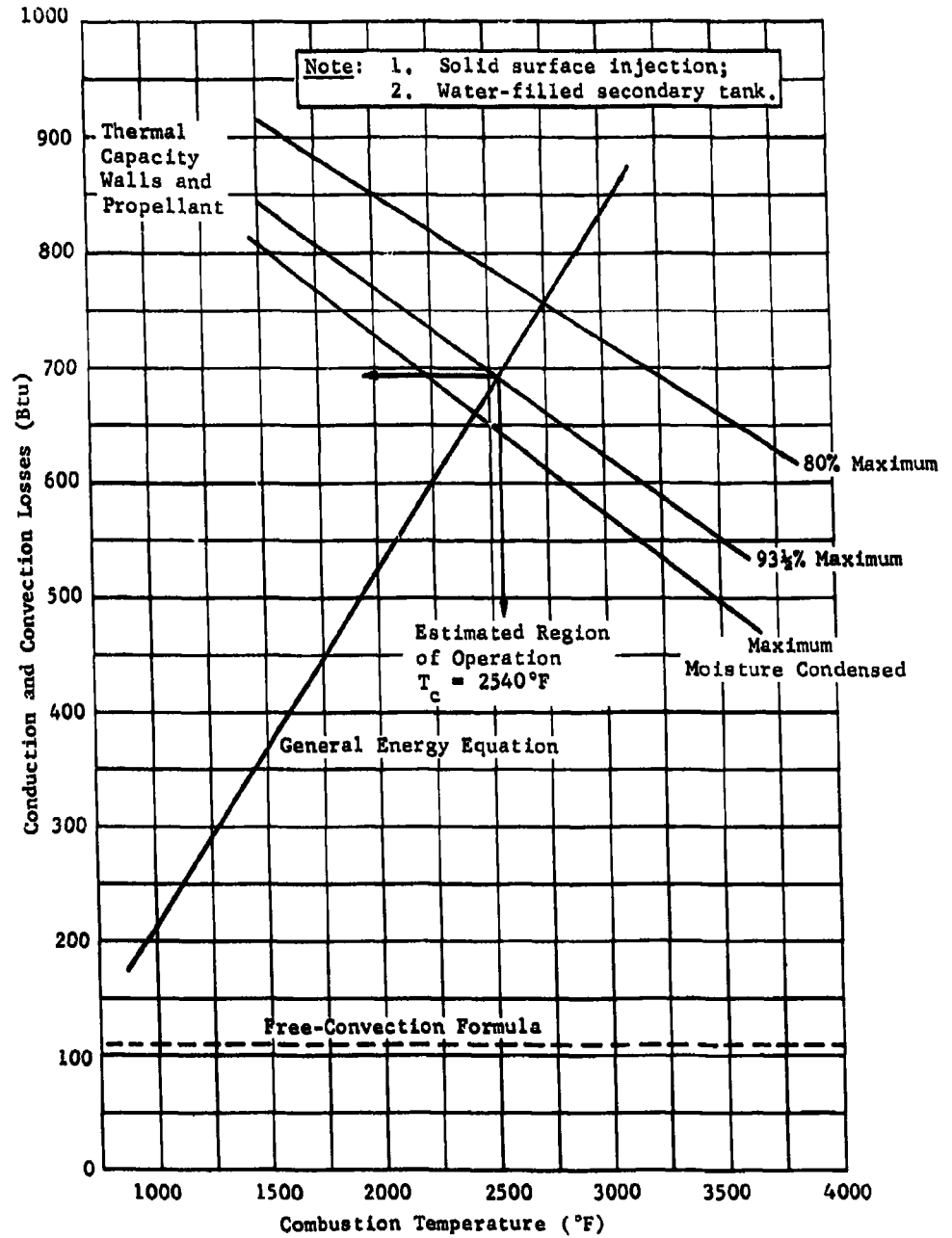


Fig. III-1 Research Test Tank Correlation of Fuel Tank Ullage Gas Thermodynamics

Oxidizer Tank - The treatment of the common ullage oxidizer tank was less complex, since the temperature of the inlet pressurant was known, and an inert-nonvolatile propellant was used. Consequently, the general energy equation, Eq [III-1], reduced to the following form:

$$Q = C_1 - C_2. \quad \text{[III-4]}$$

Unlike the fuel tank, temperatures in the oxidizer tank were relatively cool because of the method of gas pressurant injection. Therefore, the temperature gain of the tank wall and bulk liquid was difficult to accurately identify, and the thermal capacity change of the system could not be measured. Consequently, the heat transferred must be calculated directly by Fourier's law for heat transfer, i.e.,

$$Q = \tau \left[\sum (hA\Delta T)_{\text{wall}} + \sum (hA\Delta T)_{\text{liquid}} \right], \quad \text{[III-5]}$$

where,

h = coefficient of heat transfer,

A = heat transfer surface,

ΔT = temperature gradient,

τ = time of operation.

In the absence of any secondary chemical reaction in the oxidizer tank, the heat transferred expressed by Eq [III-4] and [III-5] must be equal. Substituting free convection film coefficients into Eq [III-5] resulted in an agreement within 10% of the value given by Eq [III-4]. Thus, the validity of the free convection formula is confirmed.

Theoretical Reaction Mixture Ratio - The overall process mixture ratio for the fuel tank was determined from the following equation:

$$\lambda = \frac{W_{\text{oxidizer}}}{W_{\text{fuel}}} = \frac{W_{\text{oxidizer}}}{W_{\text{tot}} - W_{\text{inert}} + W_s - W_{\text{oxidizer}}}$$

where,

W_{oxidizer} is a test measured value,

W_{tot} and W_{inert} are determined from equation of state,

W_s , the amount condensed, is estimated at 70% of the oxidizer used.

The amount of fuel vaporized was found to be insignificant and was not included in this analysis.

Phase III System Thermodynamic Characteristics - The flight-weight full-scale MTI pressurization system was examined with tank configuration assumed spherical, with an equivalent diameter of 8 ft approximately, or 3.69 times larger than the research test tank. Since injection parameters were also correspondingly increased (3 to 5 times larger), dynamic similarity was presumed. For this application, paramount importance was placed on the prediction of the maximum tank wall temperatures and the other system performance parameters to insure that excessive wall temperatures were avoided.

The first step in this computation involved the solution of the heat balance across the tank wall. Since condensation at the wall was assumed negligible, the net heat transferred from the gas to the wall was the sum of:

- 1) Heat retained by the wall;
- 2) Heat flow to the ambient;
- 3) Heat flow via conduction to the wall exposed to liquid propellant.

Simplifying this computation by assuming initial ambient conditions for tank wall and propellant, a linear history of gas and wall temperatures, and a negligible temperature gradient within the nonwetted tank wall (axially and longitudinally), the expression for the wall temperature use became:

$$\text{wall temperature rise} = \frac{(\text{gas temperature rise}) (1 - \alpha_i/U_i)}{2\beta/U_i + 1 + h_o/U_i} \quad [\text{III-6}]$$

where,

U_i and h_o are heat transfer coefficients (internal and external, respectively),

β and α_i are constants being a function of the wall material, surface length, cross section areas and perimeter, and exposure time.

Equation [III-6] was solved for the uninsulated wall, and the results are presented in Fig. III-2. In the event the final gas temperature becomes very high, 1/8 in. of Foam-Sil or equivalent insulation will readily limit the wall temperature. For comparison, the uninsulated research fixture was relatively cool due to the 5/8-in. walls.

The second step required estimating the temperature change in the wall and bulk liquid as a function of heat transferred. This was desired to obtain a reasonable estimate of temperature gradient from which to calculate the actual heat transferred. For this reason, a simplified analytical model in the tank wall and the bulk liquid was used. In either case, the net heat absorbed was calculated from:

$$Q = \int_0^T W c_p dT - \text{heat rejected}, \quad [\text{III-7}]$$

where,

W = exposed mass = $W_{\text{initial}} \pm \dot{W}\tau$ (+ for tank wall)
(- for liquid),

C_p = specific heat of mass,

T = $T_{\text{initial}} + \dot{T}(\tau)$,

$dT = \dot{T} d\tau$,

τ = time of operation.

Note: 1. Phase III flight tank (ft) - 2024Al, 0.075 inch;
143 sec firing time;
2. Phase I research fixture - Al alloy, 0.625 inch;
147 sec firing time.

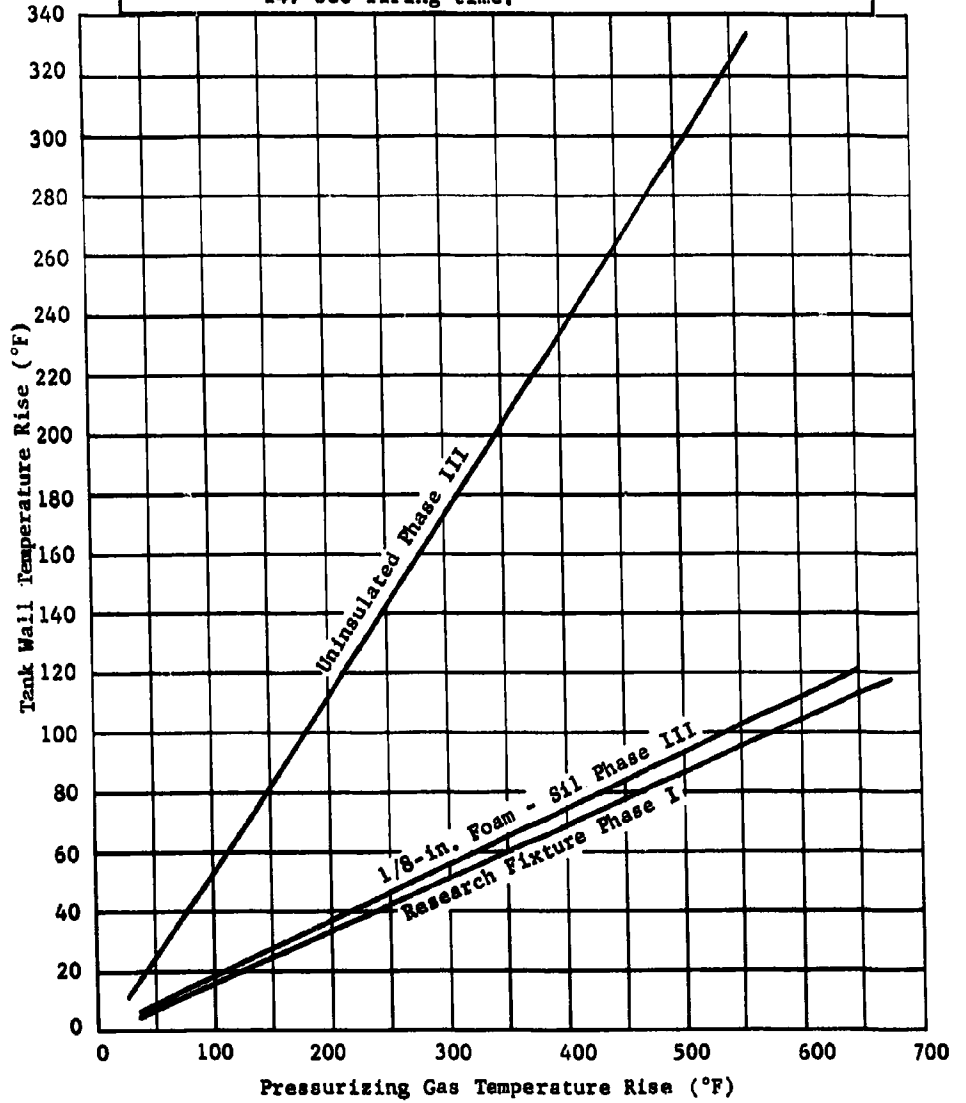


Fig. III-2 Predicted Tank Wall Heating

Since linear change of temperature was assumed,

$$\dot{T} = (T_{\text{final}} - T_{\text{initial}})/\tau.$$

Solution of Eq [III-7] gave the following equation for the temperature change, when the heat rejected was assumed negligible:

$$\Delta T = C_1 \sum Q. \quad \text{[III-8]}$$

Figure III-3 shows the final temperature of the bulk propellant (50/50 blend of UDMH and N_2H_4) and the tank wall (0.075-in. average thickness of aluminum) as a function of heat transferred.

The final step in the calculation of fuel tank ullage thermodynamics relates to the solution of the general energy equation. Since single- and twin-tank expulsions were tested, both conditions were examined.

Estimated values were substituted in the general energy equation, and then simplified, resulting in the following expression for the sensible heat that must be transferred from the fuel tank ullage gas for an energy balance:

$$Q = C_1 + C_2/T_f - C_3 t_f - C_4 t_f/T_f, \quad \text{[III-9]}$$

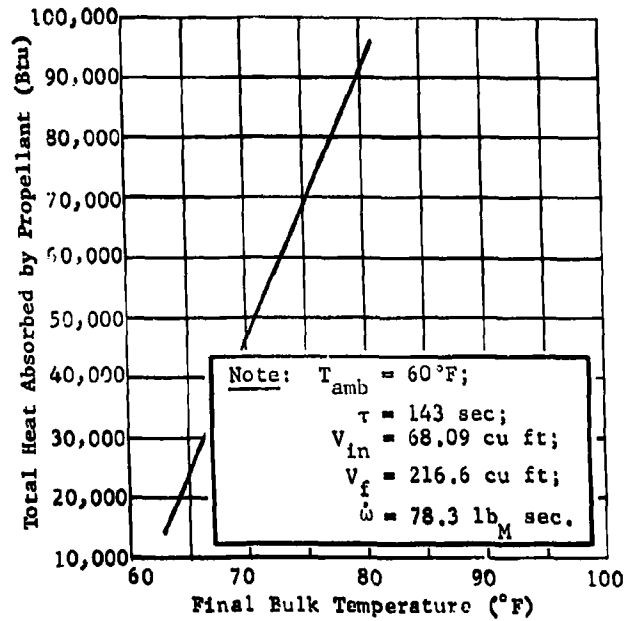
where,

C_1 , C_2 , C_3 , and C_4 are invariant for a given condition ($C_3 = 0$ for single-tank expulsion),

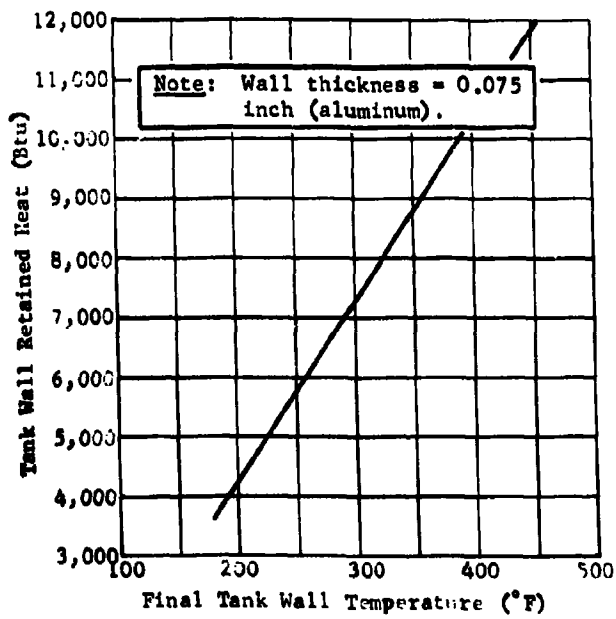
T_f = the final fuel tank gas temperature ($^{\circ}R$),

t_f = the average fuel tank gas temperature ($^{\circ}F$).

Equation [III-9] is plotted in Fig. III-4 for single- and twin-tank expulsion, and shows that the sensible heat loss constraint reduces as ullage temperature increases. Furthermore, sensible heat loss can also be computed directly by means of Eq [III-5].



(a) Propellant Bulk Temperature



(b) Tank Wall Temperature

Fig. III-3 Phase III Fuel Tank Temperature Change vs Heat Transferred

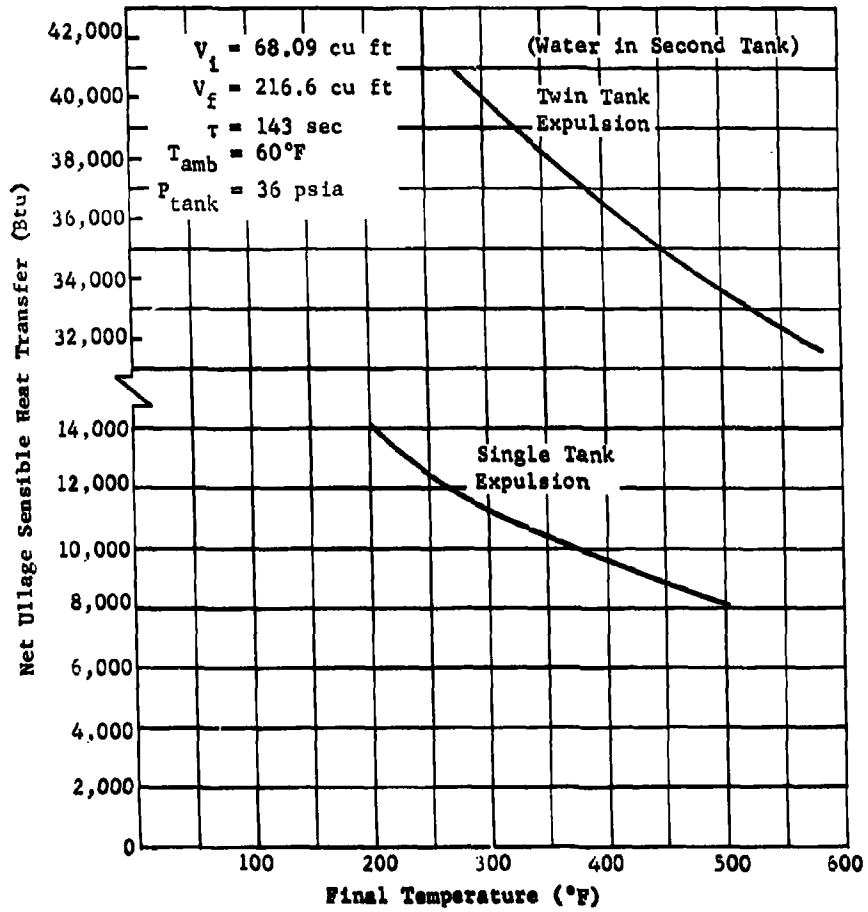
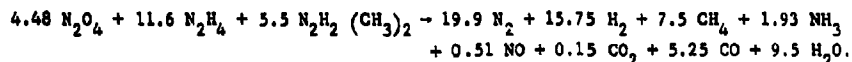


Fig. III-4 Phase III Fuel Tank Ullage Heat Transfer vs Final Pressurant Temperature

The final gas temperatures in the fuel tank were then computed by a trial and error selection of final gas temperature with simultaneous solution of Eq [III-5] and [III-9]. The results are shown in Table III-2, which indicates that wall temperatures will be approximately 367°F for twin-tank operation with a full load of water in the second tank, and 190°F when only the fuel tank is operated.

In an attempt to obtain a better understanding of the heat distribution from the reaction, the established film coefficients and expected temperature relationships were analyzed in conjunction with material balance information reported in Chap. III.A.2. The results of the Phase I heat balance were correlated by chemical heat input calculations before attempting to scale the data to predict Phase III system performance. Since maximum system temperatures and reagent consumption were expected during the water expulsion test series with MTI gas generation process in the primary tank, the results obtained represent the most adverse conditions.

The results of the Phase I heat balance study are summarized in Table III-3, with the corresponding chemical energy released to the system from the reaction process. The heat released from the reaction process was based on the following process, which was established by an analysis of the identified products of reaction:



The heat of reaction for this process occurring at a mixture ratio (W_O/W_F) 0.6 is:

$$H_c = \frac{\sum H_F \text{ products} - \sum H_F \text{ reactants}}{(\text{lb mole N}_2\text{O}_4)(\text{mole weight N}_2\text{O}_4)} = 4800 \text{ Btu lb/N}_2\text{O}_4.$$

Table III-3 Phase I Heat Balance

Heat in Fuel, Expelled	738 Btu
Heat in Fuel, Left in Tank	480 Btu
Heat Flow to Oxidizer Tank	43 Btu
Flow Work (Fuel)	23 Btu
Heat in Fuel Tank Wall	465 Btu
Heat in Ullage Gas	38 Btu
Approximate Heat in System, Assuming No Condensation	2387 Btu
Approximate Heat with 50% H ₂ O Condensation	2087 Btu
Approximate Heat with 80% H ₂ O Condensation	1907 Btu
Chemical Energy Released	2380 Btu (No Condensation)
(Based on Reagent Injected 0.412 lb)	2060 Btu (50% Condensation)
	1900 Btu (80% Condensation)

The basic technique used in the solution to the heat balance, based on chemical energy released to the system, also involved scaling the Phase I heat balance to comparable levels expected in the full-size demonstration system by the techniques contained in Appendix E. Since the heat absorbed by the system was a function of the chemical energy released from the MTI process, the amount of heat absorbed by the system and chemical energy required were computed separately as a function of ullage gas temperature. They were plotted in Fig. III-5 for the secondary tank tests with water and nitrogen tetroxide. The intersection of the two curves represents a heat balance at a primary tank gas temperature of 750°F for the water-filled secondary tank. Figure III-6 is a block diagram showing the energy distribution at this condition, which results in a final tank wall temperature of 474°F. For an oxidizer-filled secondary tank, the maximum expected wall temperature was 338°F. Equivalent primary tank wall temperature for tests with the oxidizer-filled secondary tank were computed from the reduction in reagent consumption, and corresponding chemical energy was dissipated during the Phase I test program.

A summary of the heat absorbed by the Phase III system is presented in Table III-4 for various primary tank gas temperatures based on Phase I system data with a water-filled secondary tank. The corresponding chemical energy released in generating the required quantity of gas at the various temperatures is included, based on the following relationship:

$$Q_{1n2} = (W_{R1}) (4800 \text{ Btu/lb}) \left(\frac{V_2}{V_1} \right) \left(\frac{TGFT_{1f} + 460}{TGFT_{2f} + 460} \right),$$

where,

$$V_2/V_1 = 56.2.$$

Predicted performance for the Phase III common ullage demonstration test configuration is shown in Fig. III-7 and III-8. These curves are based on a nominal 36-psia tank pressure, with an initial 22% primary tank ullage and 5% secondary tank ullage and oxidizer in the secondary tank. Surface solid-stream N_2O_4 injection was used in primary tank pressurization, and the secondary tank was pressurized by subsurface gas impingement. Propellant tank ullage and outlet pressures shown represent the expected variations due to changes in propellant static head. The resulting pressure decay used to expel the residual propellant

by ullage gas expansion was also indicated. Due to a decrease in actual reaction mixture ratio obtained during the Phase III fuel tank tests the reagent consumption predicted is approximately twice that which would be expected from a full-scale system common ullage test. A prediction of dual reagent injection pressurization performance was made with the IBM 7094 computer program and is shown in Chap. V.A.

Table III-4 Phase III Heat Balance

T_{GTF2}	Assumed Final Fuel Tank Ullage Temperature, T_{DFTf2}					
	Item	400°F	500°F	600°F	700°F	800°F
<u>Absorbed (Btu)</u>						
Heat into Fuel	20,300	28,100	35,900	43,400	51,000	
Heat to Oxidizer Tank	4,600	6,200	7,600	8,900	10,300	
Flow Work	1,340	1,340	1,340	1,340	1,340	
Heat to Tank Wall	4,080	5,280	6,470	7,690	8,870	
Heat to Atmosphere	300	410	530	640	760	
Heat in Ullage Gas	4,020	5,200	6,400	7,600	8,700	
Total (Btu)	34,640	46,530	58,240	69,770	80,970	
<u>Generated (Btu)</u>						
Water-Filled Secondary Tank	104,500	93,500	84,800	77,500	71,300	
Oxidizer-Filled Secondary Tank	59,000	53,000	48,000	43,800	40,300	

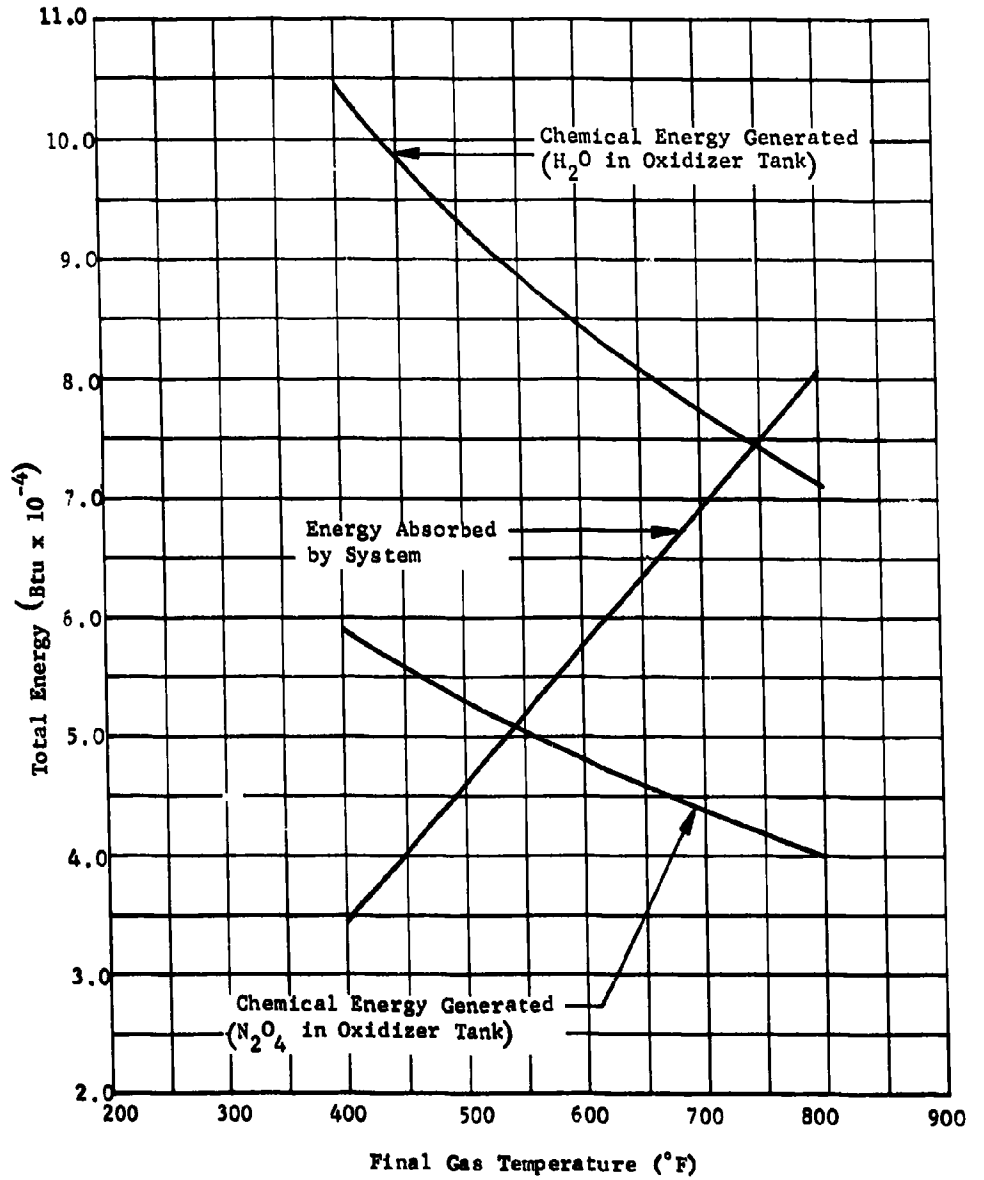


Fig. III-5 Phase III Energy Balance

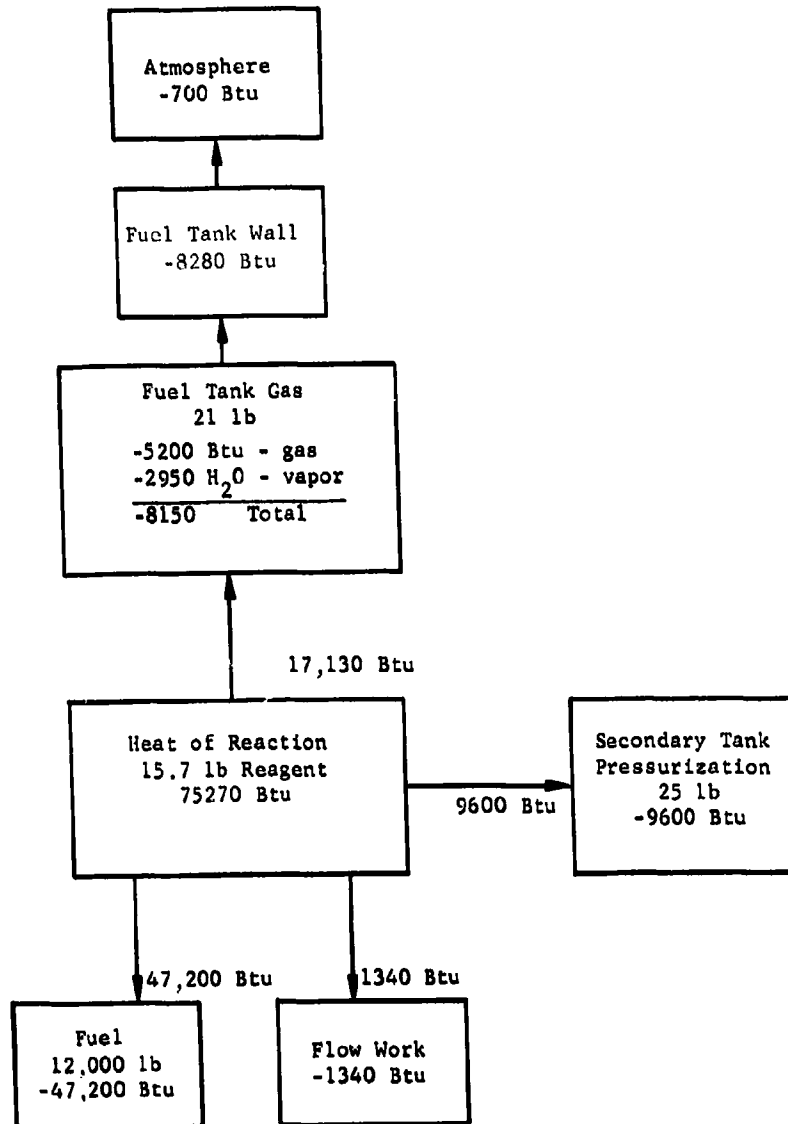
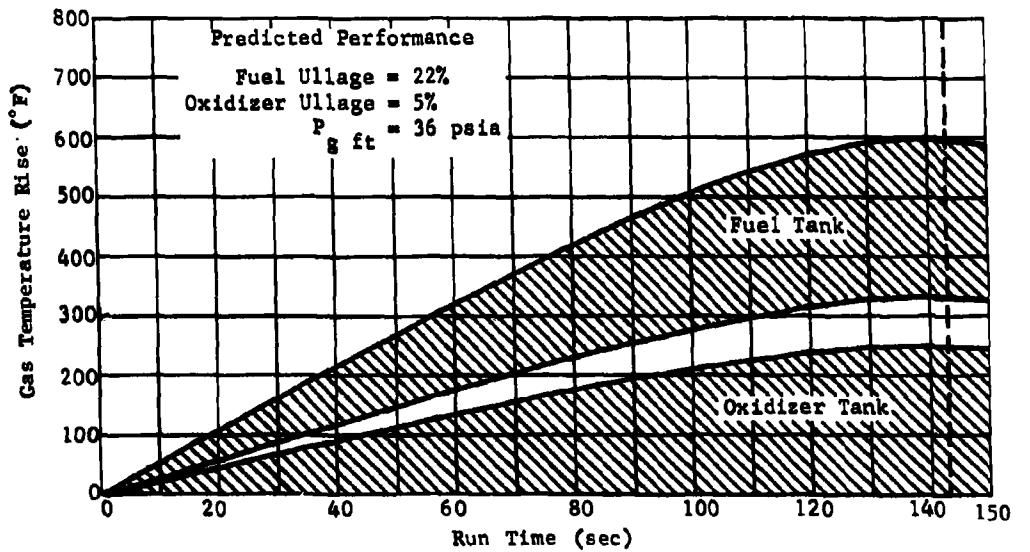
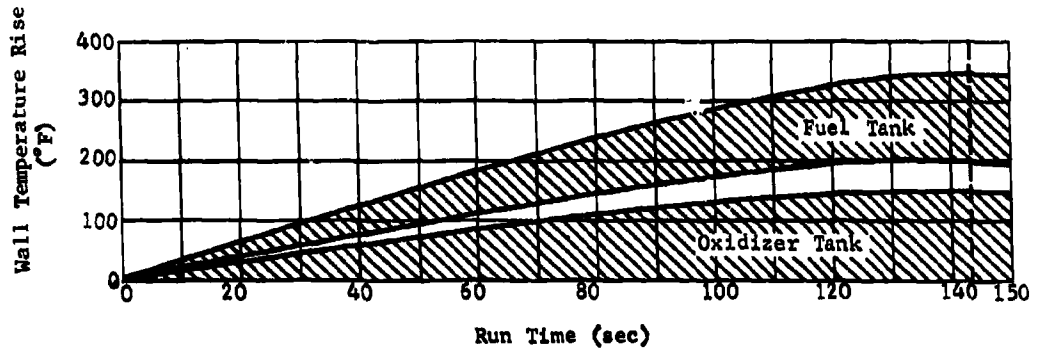
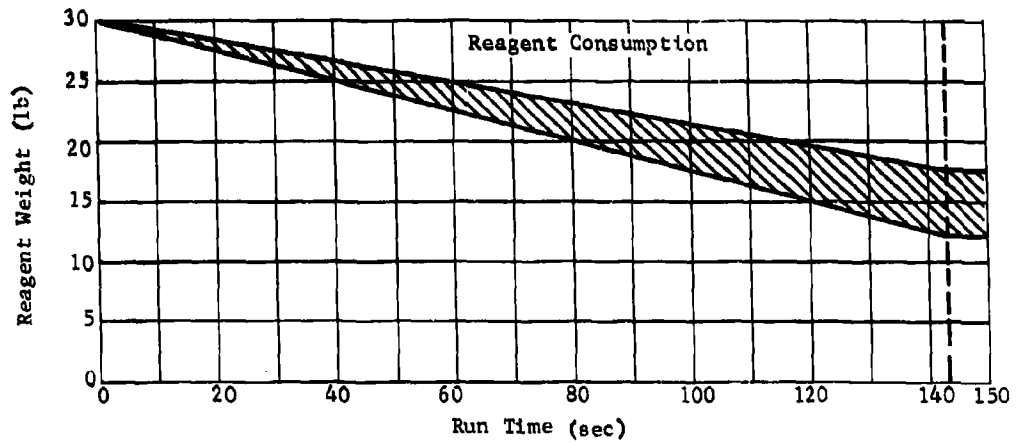


Fig. III-6 Phase III Heat Balance Flow Diagram Inert Oxidizer

RTD-TDR-63-1123



Propellant Tank Temperatures

Fig. III-7 Phase III Predicted Performance Range

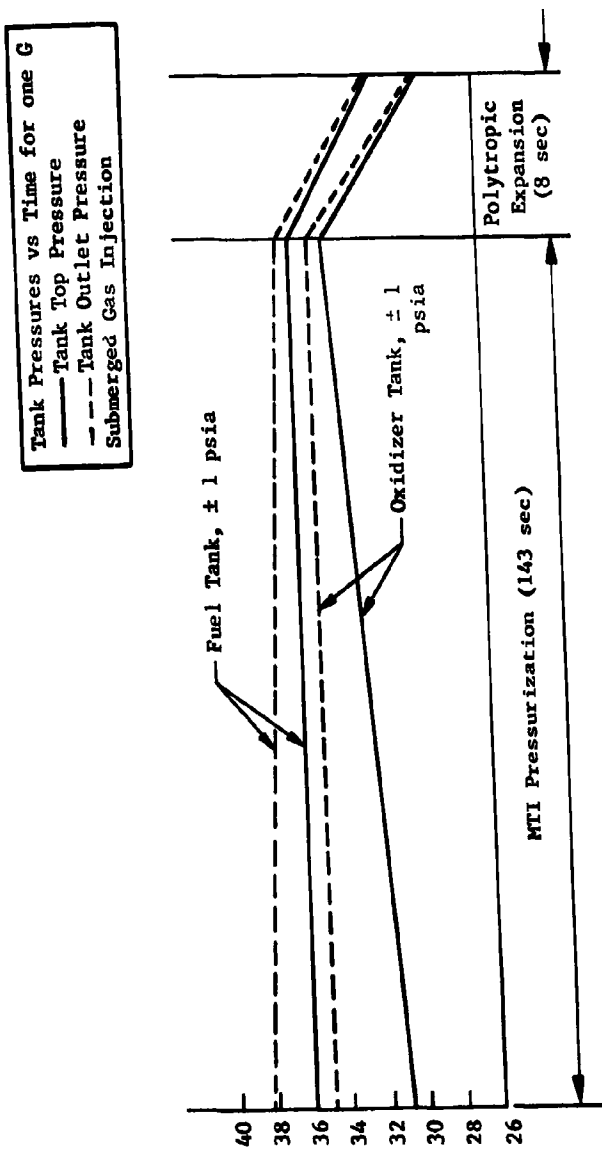


Fig. III-8 Phase III System Propellant Tank Operating Pressure Histories

2. Mass Balance

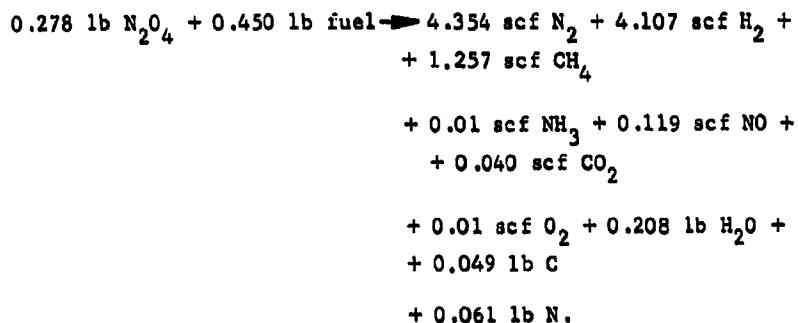
A technique for establishing the actual reaction mixture ratio of the dual injection and common ullage MTI systems was developed based on an analysis of the gaseous products of reaction and the known quantity of injected reagent. Although a hypothetical composition of the condensed products of reaction is obtained, fairly good correlation of actual quantities produced in the experimental program was achieved. A summary of the results of the material balances performed are contained in Table III-5 for both the full-scale and research test system with the analytical technique explained in the following paragraphs. A significant increase in gas generation rate was experienced in the Phase III system (fuel tank from 2.13 to 6.4 lb gas/lb reagent and oxidizer tank from 2.85 to 6.3 lb gas/lb reagent) primarily due to the change in reaction mixture ratio resulting from the increase in injector orifice diameter.

Table III-5 MTI Combustion Product Mass Balance Summary

Configuration	Tank Press. (psia)	Molecular Weight (lb/lb mole)	Comb. Prod (lb) gas	Water Weight (lb)	Total Condensate Weight (lb)	Reagent Weight (lb)	Reaction Mixture Ratio (W_a/W_F)
<u>Phase I</u> Fuel Tank (direct Injection)	36	15.77	0.412	0.208	0.316	0.278	0.62
<u>Phase III</u> Fuel Tank (direct injection)	36	15.98	17.9	1.9	3.6	2.9	0.16
<u>Phase I</u> Oxidizer Tank (direct injection)	36	29.51	0.313	0.165	0.192	0.151	2.34
<u>Phase III</u> Oxidizer Tank (direct injection)	36	30.5	20.8	3.27	16.54	3.3	10.32
<u>Phase I</u> Oxidizer Tank (common ullage)	36	23.04	0.493	0.226	0.258	0.329*	1.28
*Consists of 0.263 lb of fuel(gunk) and the rest primary gaseous combustion products.							

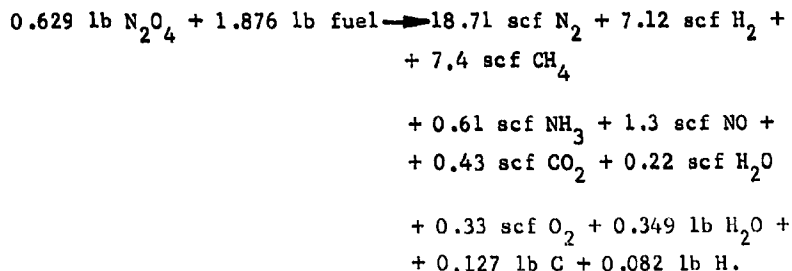
Phase I Small-Scale System - Balanced chemical equations for the dual reagent injection and common ullage systems were first required to determine the actual quantities of reactive constituents and unidentified condensed materials either formed or condensed in the pressurization process. For the common ullage configuration the total weight of gaseous combustion products in the primary tank was computed by the IBM 1620 ullage dilution program. Reagent consumption (an actual test measurement) and gas analysis by mass spectrometer was provided for all tests. The material balance is obtained by attributing all unaccountable oxygen to condensed water and making a hydrogen or nitrogen balance, based on which balance satisfied minimum requirements. The small remaining amount of carbon and nitrogen or hydrogen was attributed to gunk.

Fuel Tank Direct Injection - The chemical reaction investigated for a typical Phase I fuel tank test at 36 psia gave the following balanced equation:



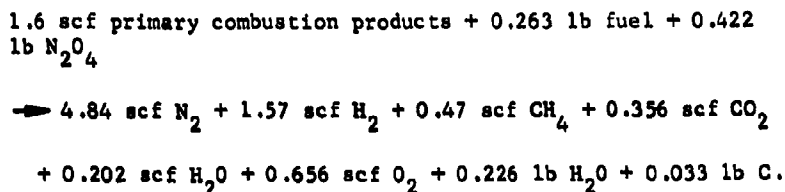
The gaseous combustion products totaled 9.897 scf, equivalent to 0.412 lb, with a molecular weight of 15.77 for the solid stream surface injection process with a 0.014-in. dia injector orifice at a differential pressure of 75 psia. A complete analysis of the gaseous combustion products is presented in Chap. II.C.1.

The increase in combustion product molecular weight at 100 and 200 psia operating pressures precipitated additional study of this reaction. For the 200 psia reaction the following reaction process was established:



A total of 36.12 scf of gaseous combustion products, equivalent to 1.947 lb, was produced at a molecular weight of 20.46 with a reaction mixture ratio of 0.34. Because the amount of test data available on the high pressure process were limited, the results should be considered approximate in view of the large amount of liquid hydrogen compounds required to balance the equation.

Oxidizer Tank Common Ullage System - For the subsurface impingement in the oxidizer tank, the mass of crossflow gas was considered as the difference between the total calculated by the ullage dilution program and the amount remaining in the primary tank at the end of the run. The total secondary reaction gaseous combustion products were also calculated by the ullage dilution program based on the actual concentration of NO₂ vapors in the ullage. Any gunk cross flow was assumed to be essentially fuel and a simultaneous nitrogen and oxygen balance determined the relative amounts of NO₂ (or N₂O₄) and gunk required to complete the equation:



The gaseous combustion products totaled 8.094 scf, equivalent to 0.491 lb, with a molecular weight of 23.04 for the Phase I configuration. Actual composition of the gaseous combustion products is presented in Chap. II.C.1. The total mass balance for both the primary and secondary tanks is represented schematically in Fig. III-9.

Cross Flow
 Primary Combustion
 Products 0.329 lb (0.263 lb gunk)

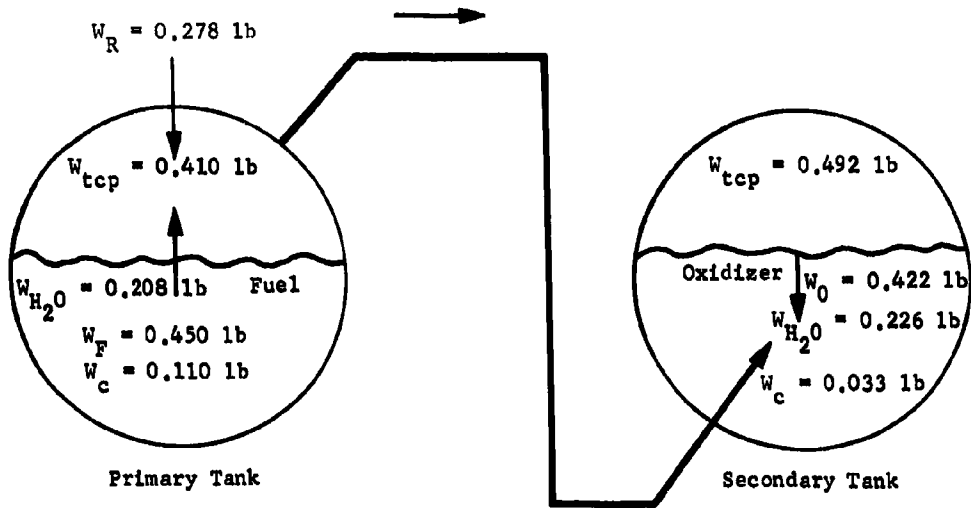
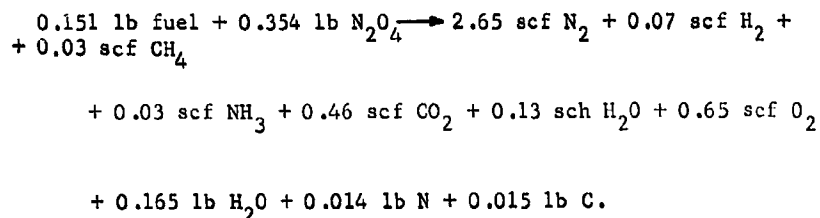


Fig. III-9 Phase I Mass Balance Schematical Representation for the Common Ullage Configuration

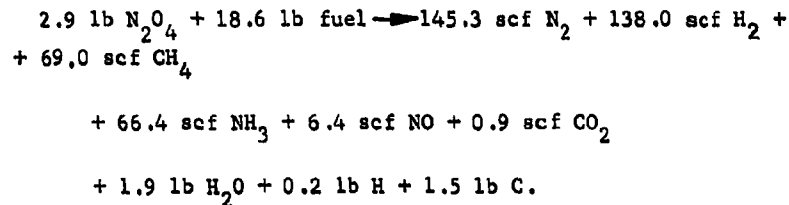
Oxidizer Tank Direct Injection - The pressurization reaction for direct fuel injection in the oxidizer tank is given by the following equation:



The gaseous combustion product totaled 4.02 scf, equivalent to 0.313 lb, with a molecular weight of 29.51. Oxidizer tank injection was at the same condition as in the fuel tank. A description of the actual composition of the combustion products contained in Chap. II.C.1. Since no significant change in gas molecular weight occurred at 100 and 200 psia, additional analysis of the reaction was not necessary.

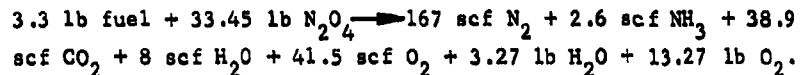
Phase III Full-Scale System - Early predictions of Phase III system performance based on the Phase I data were unsatisfactory due to changes in the reaction process and because the material balance had to be revised based on actual test data. The Phase III system material balance reported was performed similarly to the Phase I reaction. The results are based on a single investigation, and allowance must be made for variation in the calculated values although the combustion product molecular weights correlated with the earlier data obtained. Since the full-scale system was not tested with the common ullage configuration because of safety considerations, only the direct reagent injection method of pressurization was analyzed for each tank. The apparent reaction mixture ratio shift experienced in the Phase I fuel tank at high pressures was again noticed with the full-scale system at low pressures. The shift was probably caused by a change in reaction kinetics brought about by an increase in quantity of reagent injected. Further investigation is warranted to establish empirical relationships defining the influencing parameters.

Fuel Tank Direct Injection - The chemical reaction investigated for the Phase III system operating at 37 psia with solid stream surface nitrogen tetroxide injection gave the following balanced equation:



The gaseous combustion products totaled 425.96 scf, equivalent to 17.9 lb, with a molecular weight of 15.98 for the solid stream surface injection process with a 0.047-in. dia injector orifice at a differential pressure of 75 psi. A complete analysis of the gas is presented in Chap. IV.C.3.

Oxidizer Tank Direct Injection - The Phase III reaction in the oxidizer tank resulting from pressurization to 37 psia by direct fuel injection with the 0.047-in. dia solid stream injector gave the following balanced equation:



For this reaction 258 scf of gaseous combustion products, equivalent to 20.8 lb, were generated at a molecular weight of 30.63. The apparent large quantity of condensed oxygen compounds required for the balance resulted from the amount of gaseous combustion products generated. This quantity of combustion gas was required to perform an energy balance on the Phase III system with the MTI mathematical model. An initial attempt at a pure mass balance indicated that 13.73 lb of gaseous combustion products were formed at a reaction mixture ratio of 5.93. However, 5.84 lb of O₂ would still be required to balance the reaction equation. For additional performance prediction the reaction resulting from the energy balance was used.

3. Predicted Performance

Early attempts to predict MTI pressurization system performance were based on a simplified mathematical model programed on the IBM 1620 computer. Due to the limited capacity of the 1620 computer, a larger model was programed on the IBM 7094 with additional process description and capability for computing common ullage system performance. In predicting MTI pressurization system performance two distinct areas of difficulty were encountered. It was necessary to establish empirical relationships concerning the following items:

- 1) Influence parameters affecting reaction mixture ratio, adiabatic flame temperature, gas molecular weight and condensibles formed.
- 2) Influence parameters affecting the combustion zone area.

These problems were more predominant in the fuel tank as shown by variations in accumulated data. To better understand process characteristics, several theoretical studies (described earlier in this section) were performed to establish heat and mass balances for both the dual injection and common ullage pressurization processes. Most of the early analysis was performed on the common ullage system because of the complexity of the pressurization process. However, techniques of predicting performance without a computer for both the common ullage and dual injection systems were established and are described in Chap. V.B.

As sufficient test data were accumulated from the small-scale test program, the film coefficient and process characteristics identified were used in the IBM 7094 mathematical model to establish correlation with the actual test data. Subsequent prediction of full-scale system performance and the Titan II and Titan III transtage performance was based on the coefficients established. Due to a change in the reaction in the larger system, adjustments were made in the reaction mixture ratio to obtain good correlation. The lack of a suitable method to empirically establish the reaction mixture ratio as a function of the pertinent variables is a problem that warrants further study. Empirical relationships were developed for the combustion zone area, and are incorporated in the computer program as a function of reagent mass flow rate. The effects of changes in orifice area or injector differential pressure are unknown. In arriving at full-scale system performance predictions, the combustion area coefficient was increased in proportion to the orifice area since the injector differential pressure was unchanged. All other coefficients were identical to those established from the Phase I test program and later modified to reflect actual Phase III conditions encountered. The extent of correlation achieved with the 36 psia tests can be seen from Fig. III-10 thru III-12. Due to unresolved problems with the common ullage portion of the MII and mathematical model a comparison was not achieved in Fig. III-12. Insufficient data were available to obtain precise correlation with the higher pressure tests. The best correlation was achieved by assuming the reaction mixture ratio did not change with an increase in operating pressure in the fuel tank. Phase III predicted performance is shown in Fig. III-13 and III-14. A comparison

with actual data obtained is presented in Chap. V.A. In general the predicted gas and tank wall temperatures are lower than the test values since the mathematical model computes the average gas temperature and the test measurement represents the maximum value. A good comparison of predicted and actual propellant temperatures cannot be achieved due to poor resolution of the test measurements for the small temperature changes experienced.

The use of the IBM 7094 mathematical model in predicting MTI pressurization performance requires a knowledge of process characteristics in order to input the proper operating conditions. Pertinent areas involved are system physical characteristics, chemical reaction description, combustion product thermodynamic properties, and heat transfer characteristics of the pressurization process. Physical characteristics of the system are taken from the particular application with the proper option selected (i.e., number tanks, type injection, vapor dissociation, etc).

The injector orifice area and discharge coefficient must be assumed. As the injector orifice area influences the combustion area and the effects of reagent supply pressure are not fully understood, some tolerance on predicted performance should be allowed for applications deviating radically from the conditions of the experimental and development programs.

The description of the reaction process has been obtained from the test programs and primarily represents empirical data. The reaction mixture ratio (RMR), ratio of condensibles to total combustion products generated (RCLP), and molecular weight (XMWCP) of the gaseous combustion products are determined from the experimental test results based primarily on the gas analysis while the heat of vaporization (HLCLP) and specific heat (CPCLP) of the condensed products of reaction are considered to have the same properties as water. The flame temperature (TFP) is determined theoretically by first establishing the heat of reaction:

$$\Delta H_R = \Delta H_C \text{ Reactants} - \Delta H_C \text{ Products}$$

Since the heat of reaction is also equal to the change in enthalpy of the products,

$$\left[\sum_{i=1}^n H_{R_i} = \frac{MF_i}{C_{P_i}} \right] \times C_{P_i} \text{ Btu/lb mole } ^\circ R \times \frac{V_{std}}{379 \text{ scf/lb mole}} \times \Delta T$$

where

MF_i is the mole fraction of each of the combustion product constituents, V_{std} is the standard cubic feet of products, and ΔT is the temperature of reaction minus the initial temperature of the reactants.

The reaction temperature can be solved by a trial and error method based on actual mean heat capacities of the constituents of the products. The theoretical flame temperatures calculated from the actual reaction products are shown in Fig. III-16 as a function of reaction mixture ratio. Combustion product physical properties shown in Fig. III-17, III-18, and III-19 are based on the characteristics of the actual constituents and are calculated before input for the anticipated range in operating temperature. Thermal conductivity (XKCP) based on the following relationship:

$$XKDCP = \sum_{i=1}^n MF_i K_i$$

and heat capacity:

$$GPCP = \sum_{i=1}^n MF_i C_{p_i}$$

The viscosity of the gaseous combustion products (XMVCP) is determined theoretically from:

$$XMVCP = \frac{\sum_{i=1}^n MF_i \mu_i \sqrt{MW_i}}{\sum_{i=1}^n MF_i \sqrt{MW_i}}$$

Heat transfer computation in the mathematical model requires establishing proper coefficients from experimental data for use with standard natural convection relationships. The thermodynamics of the system are based on the transfer of heat from a combustion zone below the liquid surface. Net heat transfer from

the reaction is considered between the combustion gas to the liquid propellant, combustion liquid to the liquid propellant, and combustion gas to the tank ullage. Values for determining the quantity of condensibles formed are shown below with the pertinent heat transfer coefficients based on the Phase I test program results.

Mathematical Model Heat and Mass Transfer Coefficients

	CACP	CHC	XFGWP	CFGWP	XFGLP	CFGLP	XFLWP	CFLWP	RCLP	RM	XMW
Fuel Tank	0.64	0.19	0.25	0.31	0.25	0.31	0.25	0.25	0.44	0.62	16.
Oxygen Tank	0.64	0	0.25	0.05	0.25	0.05	0.25	0.25	0.38	2.34	29.5

The combustion zone area constant (CACP) appears to vary directly as the injector orifice area that was $1.07 \times 10^{-6} \text{ ft}^2$ for the Phase I system while all of the additional heat transfer constants remained unchanged for the larger systems analyzed. This data was generated with a 75 psi injector differential pressure at a 36 psia propellant tank pressure.

The general outline of the computer program is shown in Fig. III-20 and described in detail in Appendix F. This program has been used for the prediction of Phase III full scale system performance as well as the Titan II and Titan III transtage performance with an MTI pressurization system based on the empirically derived heat transfer relationship from the Phase I experimental program. Unique features of this program include the calculation of heat transfer from a combustion zone in the liquid propellant depending on the primary tank theoretical combustion process characteristics in addition to the determination of secondary tank thermodynamics based on a specified amount of reaction occurring in either the tank liquid or ullage in a common ullage arrangement.

Legend:
 - - - - - Predicted
 ——— Actual

Note: N_2O_4 injection into 50-50 UDMH- N_2H_4 ,
 5.33-cu ft Al Tank, 36 ± 0.5 psia.

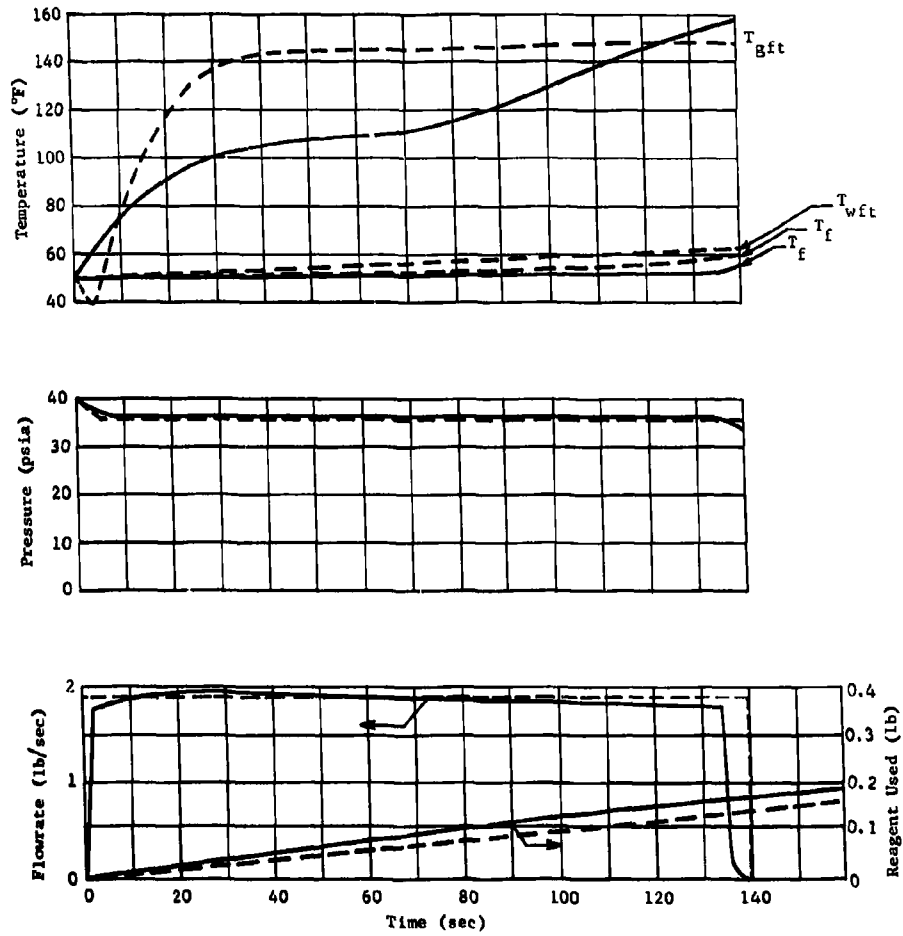
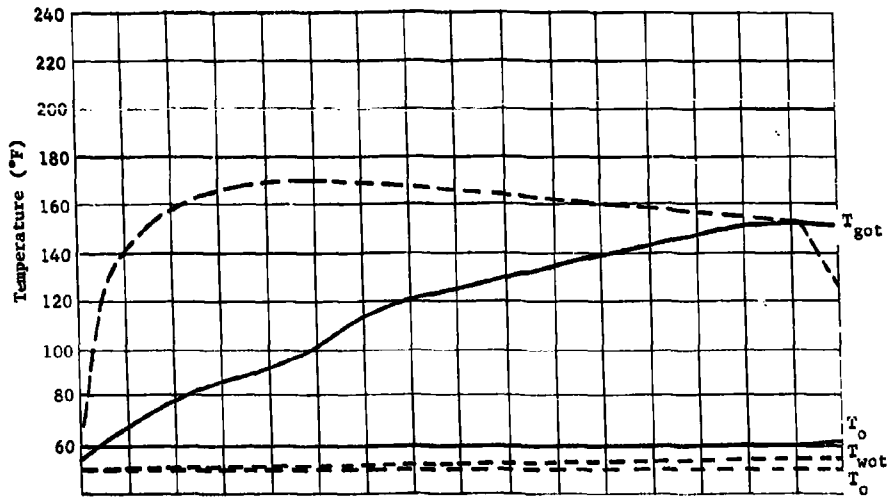
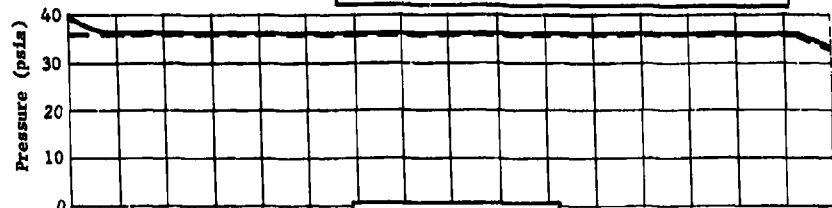


Fig. III-10 MTI Phase I Fuel Tank Performance



Note: 50-50 UDMH-N₂H₄ injection into N₂O₄,
5.33-cu ft Al Tank, 36 ± 0.5 psia.



Legend:
- - - Predicted
— Actual

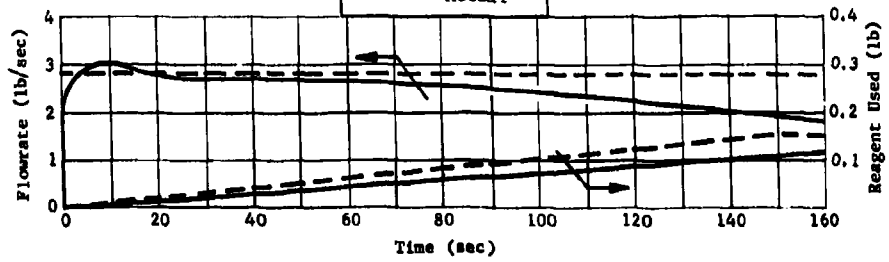


Fig. III-11 MTI Phase I Oxidiser Tank Performance

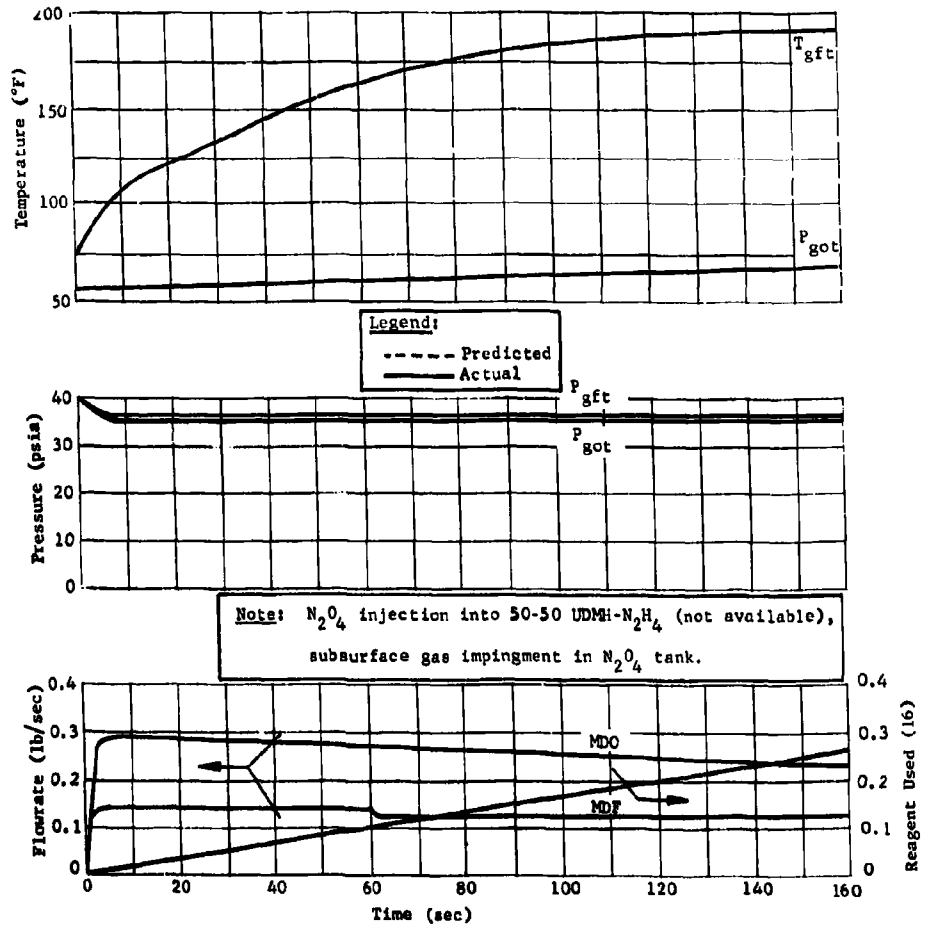


Fig. III-12 MTI Phase I Common Ullage System Performance

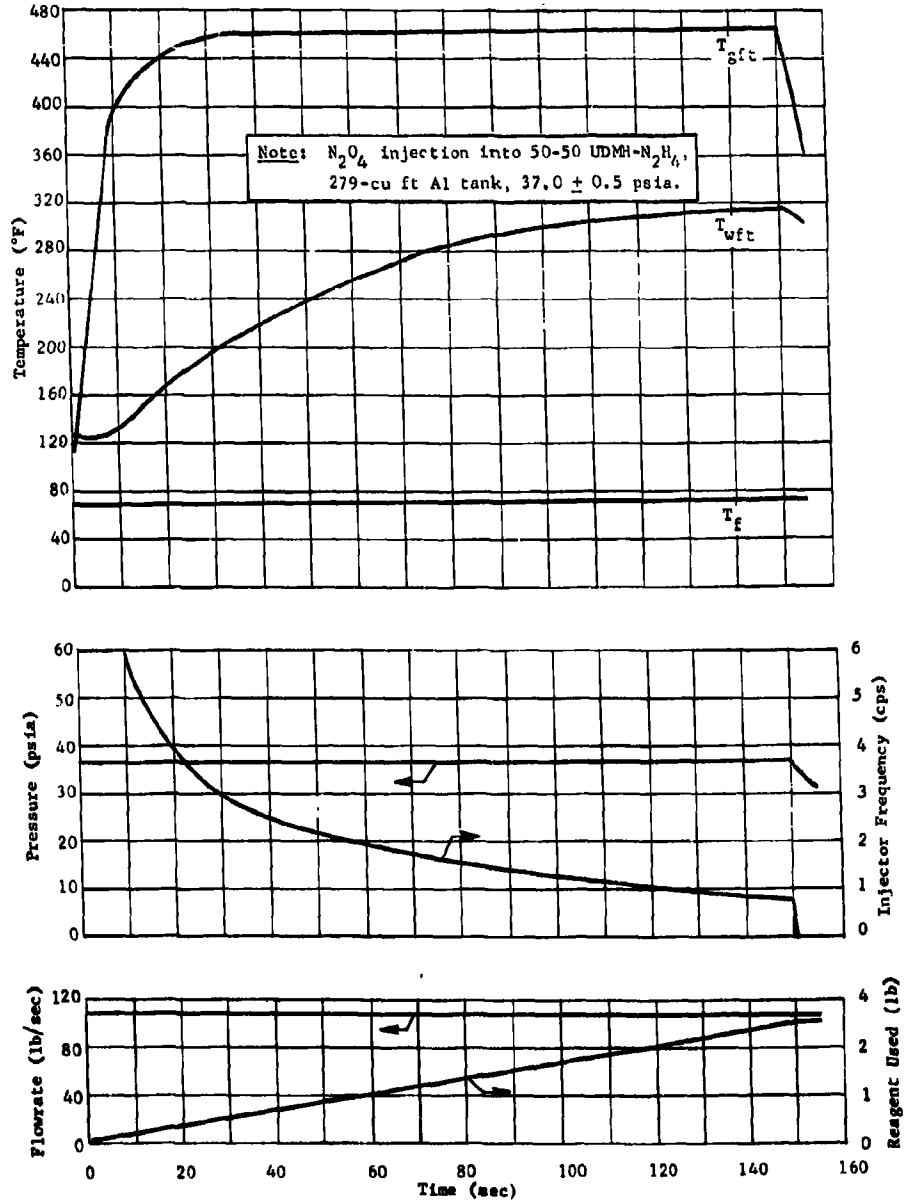


Fig. III-13 Phase III MTI Fuel Tank Performance, Predicted

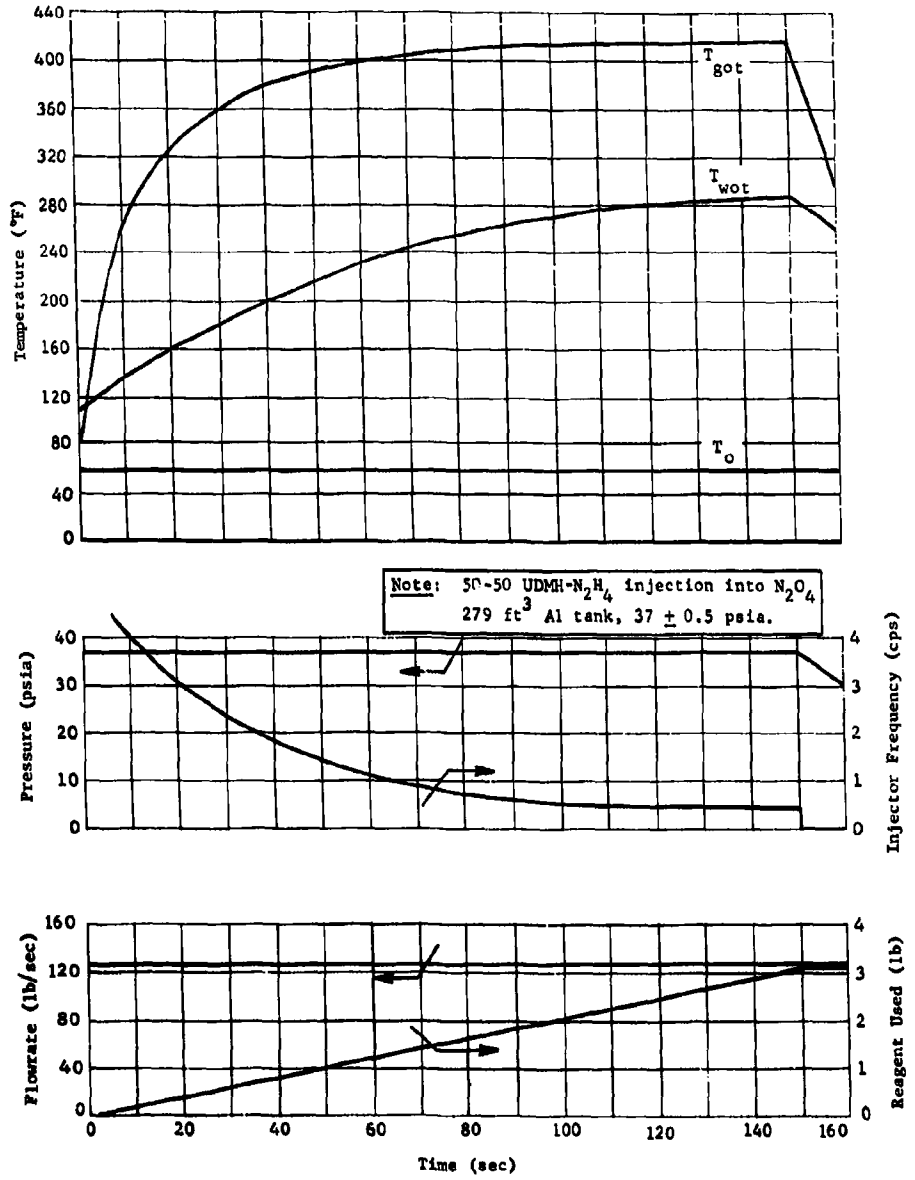


Fig. III-14 Phase III MTI Oxidizer Tank Performance, Predicted

RTD-TDR-63-1123

(Fig. III-15 not used.)

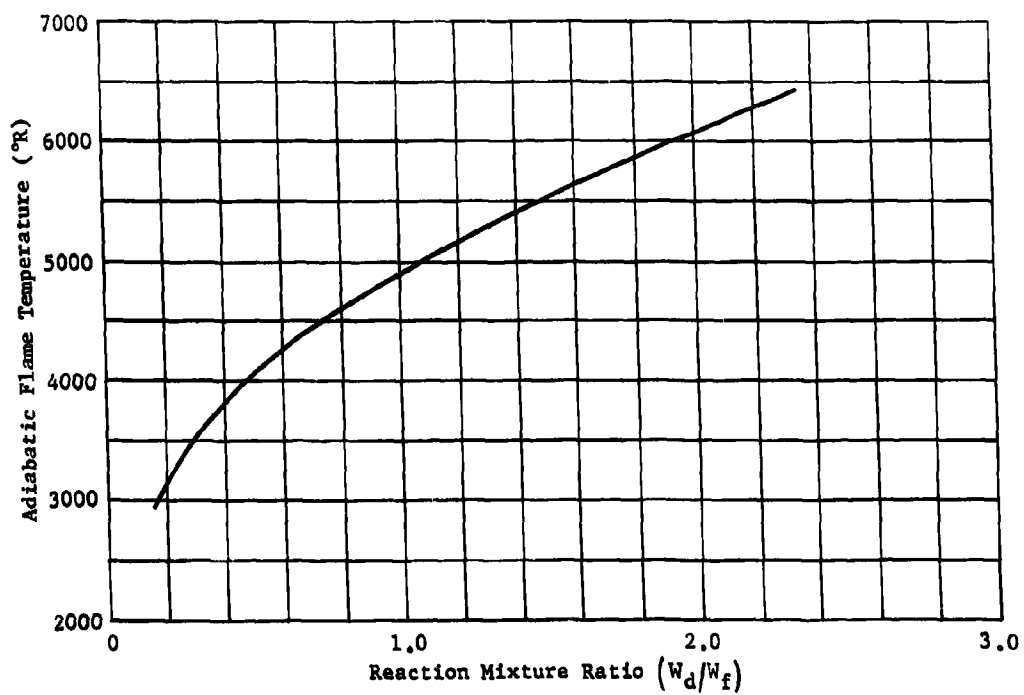


Fig. III-16 Theoretical Reaction Temperature Based on Actual Combustion Products at 36 psia

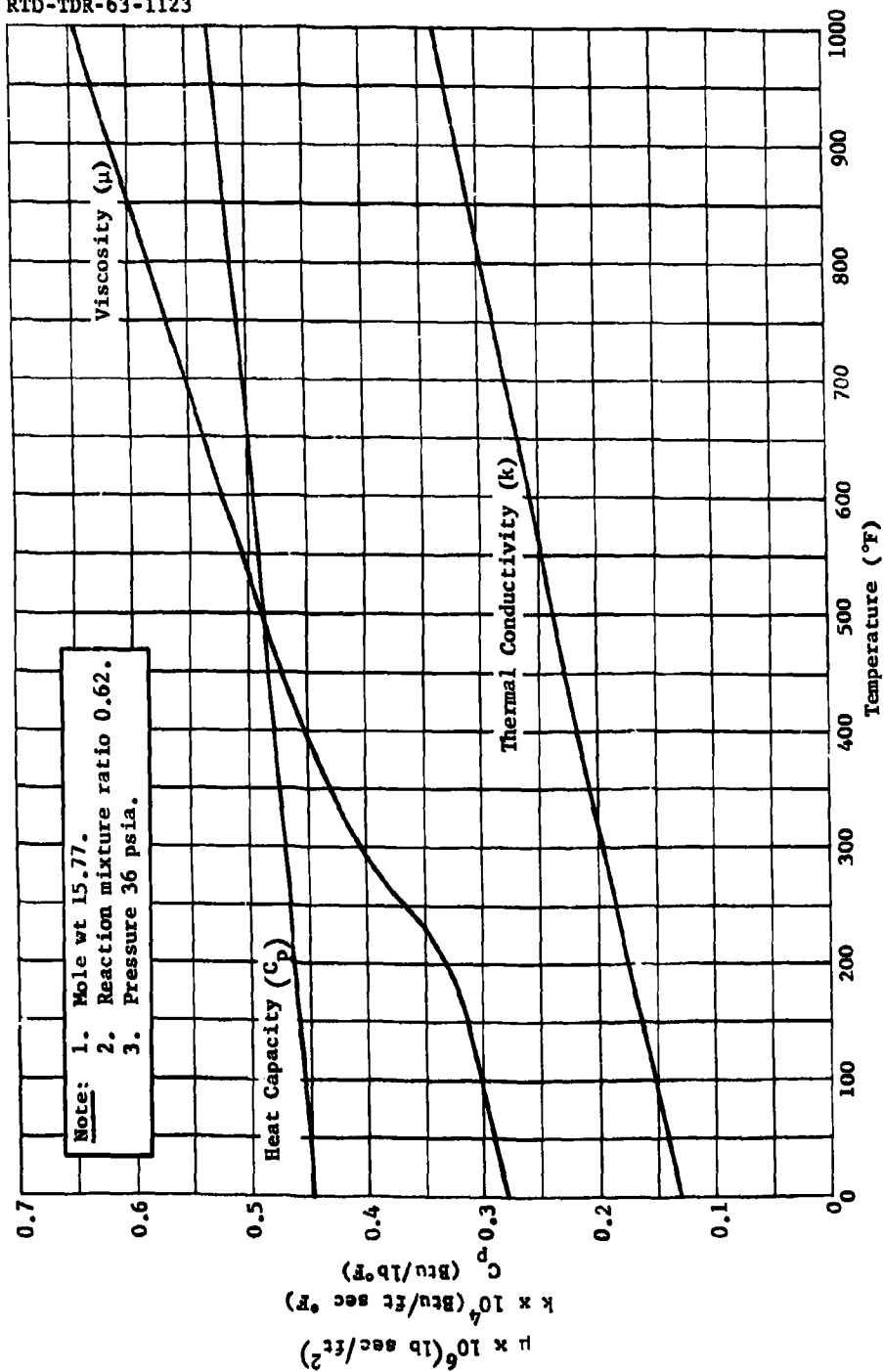
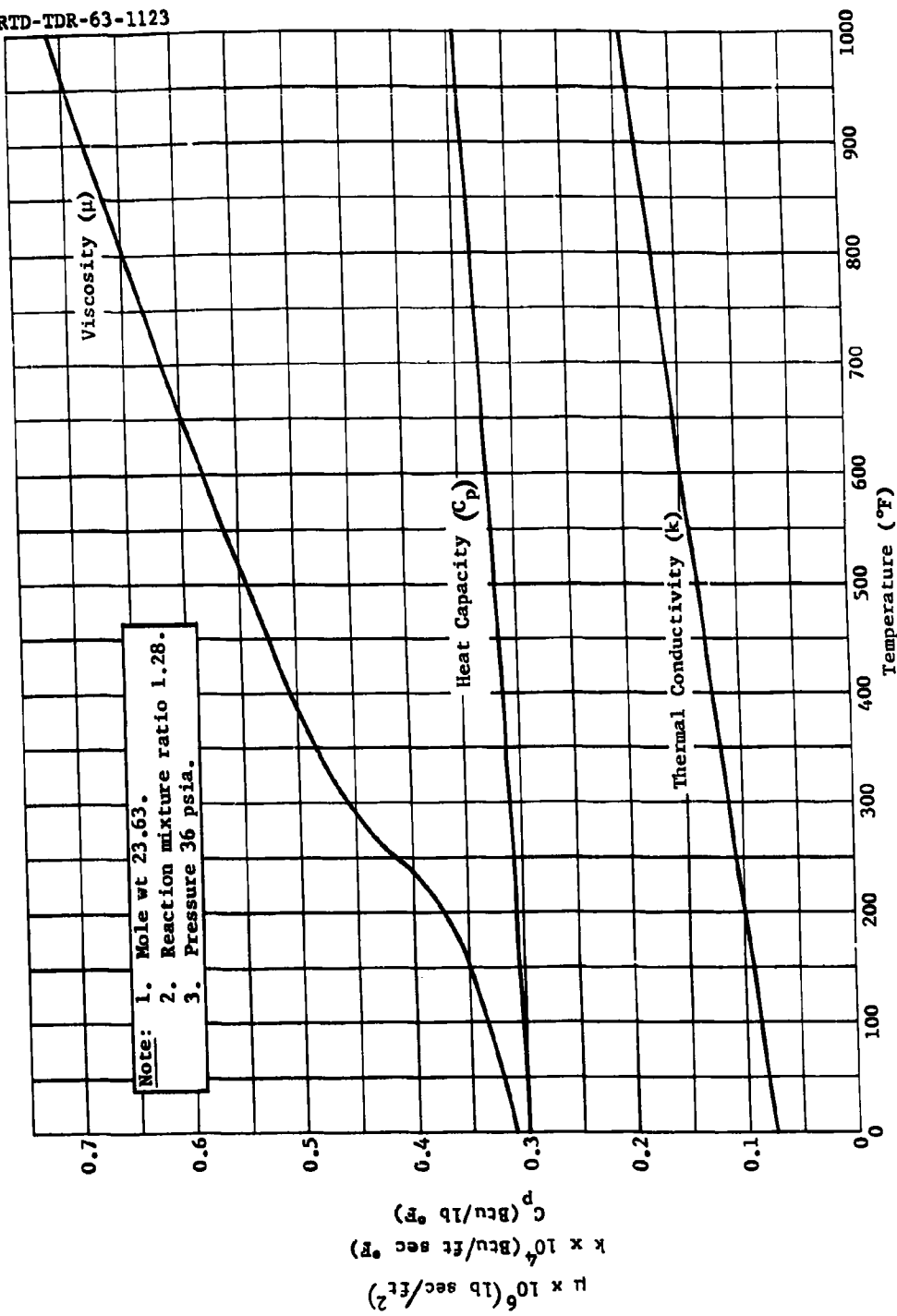


Fig. III-17 Properties of Combustion Gases, Fuel Tank Reaction, N_2O_4 Injection



Note: 1. Mole wt 23.63.
 2. Reaction mixture ratio 1.28.
 3. Pressure 36 psia.

Fig. III-18 Properties of Combustion Gases, Secondary Tank Reaction, Common Ullage

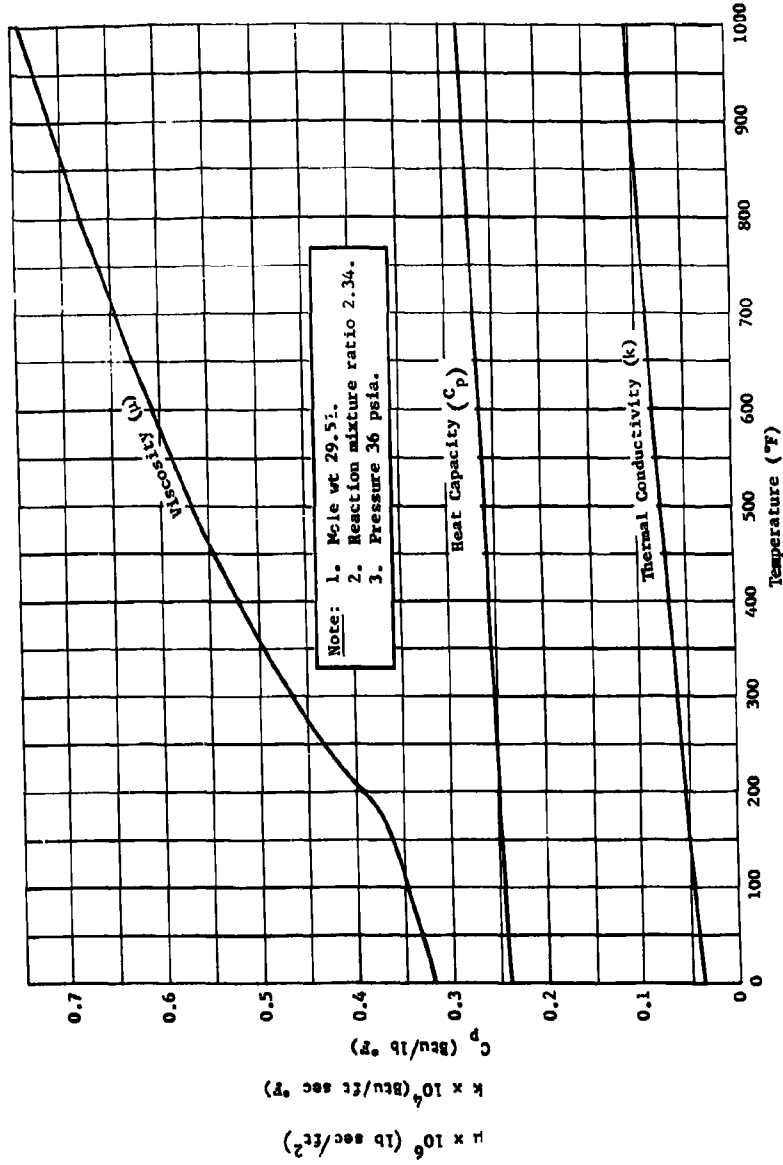


Fig. III-19 Properties of Combustion Gases, Oxidizer Tank Reaction, Fuel Injection

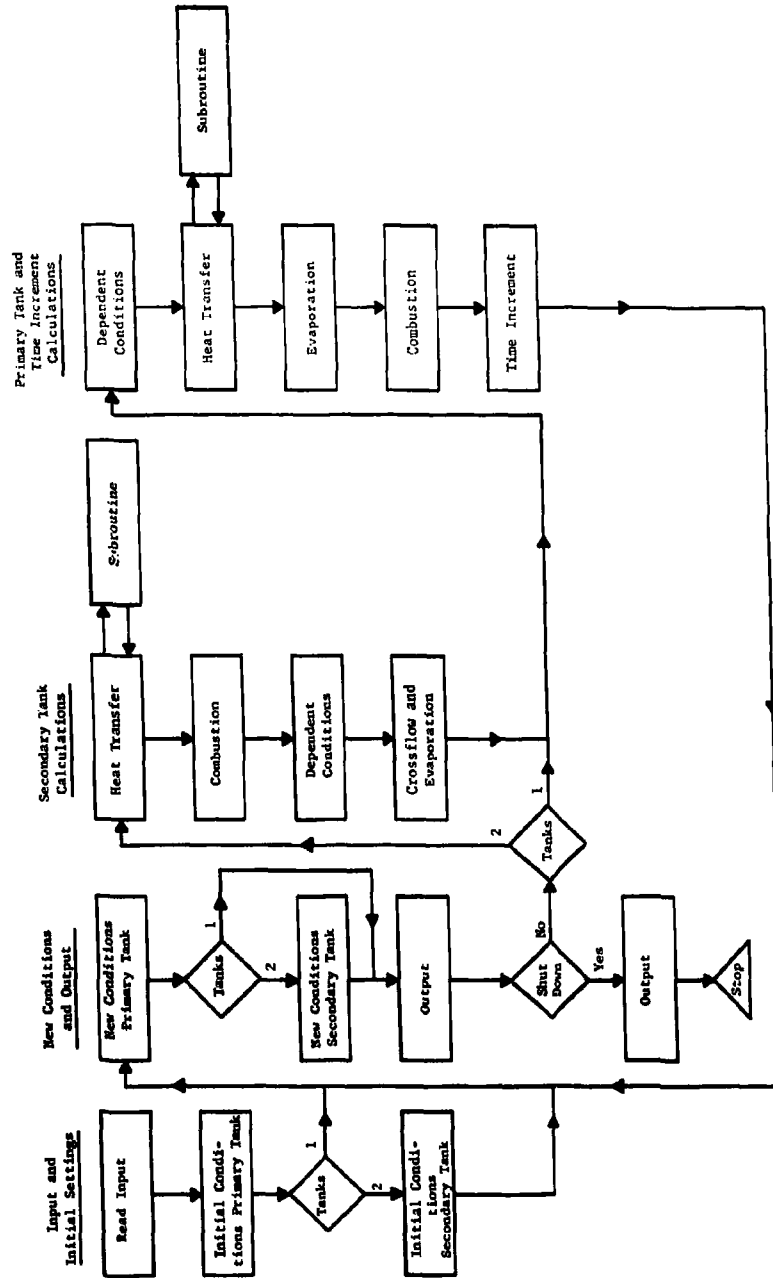


Fig. III-20 Analytical Model of a Main Tank Injection Propellant Pressurization System

The program logic is as follows: after setting the initial conditions, all required tank conditions are calculated. A check for shutdown is made, then secondary tank change rates are computed and the cross flow determined. For a single tank system or dual reagent injection, the cross flow is set to zero and the secondary tank omitted. Next, the primary change rates are calculated and the time increment fixed. The program next calculates the new conditions throughout the system and checks for shutdown. The system conditions are printed out at specified intervals. Shutdown occurs when propellant level in either tank is below an input low limit, or, for the constant-flow orifice injection only, when the primary tank pressure exceeds a specified range. After shutdown, summation of several parameters are printed out and the program stops. Output is time, tank, gas and liquid temperatures, gas and total pressure, gas and total pressure, gas composition and molecular weight, number of calculations made, weight of reactant, and fraction of combustion products in propellant. At shutdown, all of the preceding are output, along with total weight of gaseous liquid combustion products and the total cross flow by component.

Heat transfer computations consider heat exchange between the bulk gas and adjacent tank wall, the bulk gas and liquid surface, the liquid and the adjacent tank wall, and wall to outside atmosphere. Internal heat transfer, excluding that from the combustion zone, is based on the standard convective heat transfer film coefficient;

$$H = C(k/D) \left[D^3 \rho^2 g \beta \Delta T C_p / (\mu k) \right]^X,$$

where C and X have been determined from the Phase I experimental program and a subroutine is used to calculate each gas film heat transfer coefficient. Heat transfer to the liquid from the combustion zone is based on a purely empirical relationship;

$$Q_C = H_C A_C \dot{\omega} R^{0.87} (T_R - T_L)$$

where the combustion film coefficient, H_C (or CHC) and A_C (or CACP) are assumed. Similarly, thermodynamic heating to the tank wall is computed for each time increment by a separate routine from the following relationship;

$$Q_A = H_A A_T (T_A - T_W)$$

where H_A (or HAP) and T_A (or TAWP) have been computed by a separate program for a characteristic missile trajectory and is input as a function of time. H_A is the theoretical heat transfer coefficient and T_A is the adiabatic skin temperature. Since the aerodynamic heating is handled by a separate program, considerable detail has been incorporated to obtain data over typical ranges in Mach number for a given trajectory. Although the aerodynamic heating computation is performed separately, the heating rates are considered valid for the application since the tank wall differential temperature term is not omitted.

In addition to the heat transfer function mentioned, heat transfer to the liquid by condensation of reaction products or the remaining energy from combustion going into the ullage gases is also considered. Similar relationships are also used where a secondary reaction occurs between the cross flow and secondary liquid and/or vapors. In this case, however, the adiabatic flame temperature is corrected to reflect the damping effect of inert pressurizing gas in the cross flow. The calculation of the mass of gas cross flow assumes no heat transfer or time delay in the common ullage line. Pressure drop through the line is input. The program first determines if cross flow is required to maintain a set pressure in the secondary tank, then checks pressures to make sure cross flow is possible. If cross flow is required and permissible, it is calculated for a 1-sec increment, based on existing primary tank gas conditions. Secondary tank pressure may be gas pressure or may include the liquid head. In each computational sequence, the program recalculates the dependent parameters of propellant out flow, work of expelling the propellant, gas heat capacity, and sample bleed for each tank.

If primary injection is by a constant flow orifice, time increments for each calculation are input, and may be time-dependent. If a pulse injection technique is used, an on-off switching sequence computes the time interval for the primary tank pressure to either build up to the high limit or decay to a low limit. These limiting pressures may be ullage gas pressure or may include the liquid head.

Since Phase I tests show that propellant vaporization depends on MTI injection and combustion techniques, the vapor pressure is handled by the relationship, $P = CV$, where V is the vapor pressure based on the liquid temperature and P is the partial pressure of the vapor. C is based on test data and can be time-dependent. Evaporation occurs to satisfy this relationship with accompanying heat transfer.

B. SYSTEM DESIGN

The initial design of the full scale flight weight Main Tank Injection Pressurization System was based on low pressure system criteria established as a result of several preliminary investigations that are reported in Chapter II, A. Consequently an operating pressure of 36 ± 1 psia was selected for the 2,000 gal. tankage with a 150 sec run duration. Although the capacity exceeds the minimum required volume by 100%, the availability of scrap missile aluminum tankage provided a flight type system at a minimum cost. The system has capability for a 3 to 1 variation in propellant outflow rate, coast and restart, and residual propellant expulsion by a polytropic gas expansion process. Flexibility of the design provided early initiation of manufacturing drawings to allow scheduling compatible with current Titan I and Titan II manufacturing effort. The completion of the final design effort was based on recommendations resulting from the small scale experimental test program. A brief description of the Design Criteria, System Design, and Prototype fabrication are contained in the following paragraphs.

Design Criteria - From the results of the preliminary investigations, pertinent MTI system design requirements were incorporated in a Design Criteria Document (LAB 6003251) with additional specific details concerning the full scale demonstration system to be built. The document served to identify specific demonstration system characteristics, as much of the system was defined from earlier investigations, in addition to providing general criteria for chemical pressurization systems. The MTI Systems Design Criteria describes a ground demonstration common ullage system of the type successfully tested on a small scale basis (Fig. III-21). However, subsequent investigation of current Martin safety requirements resulted in the selection of a dual reagent injection system for full scale demonstration. Consequently the description of the demonstrated system would consist of identical systems for fuel and oxidizer tank similar to the existing fuel tank direct reagent injection pressurization system. Functionally, the bi-injection system operated in each tank similar to the fuel tank pressurization system with the common ullage line isolation valve closed thereby providing separate testing of each propellant tank pressurization system.

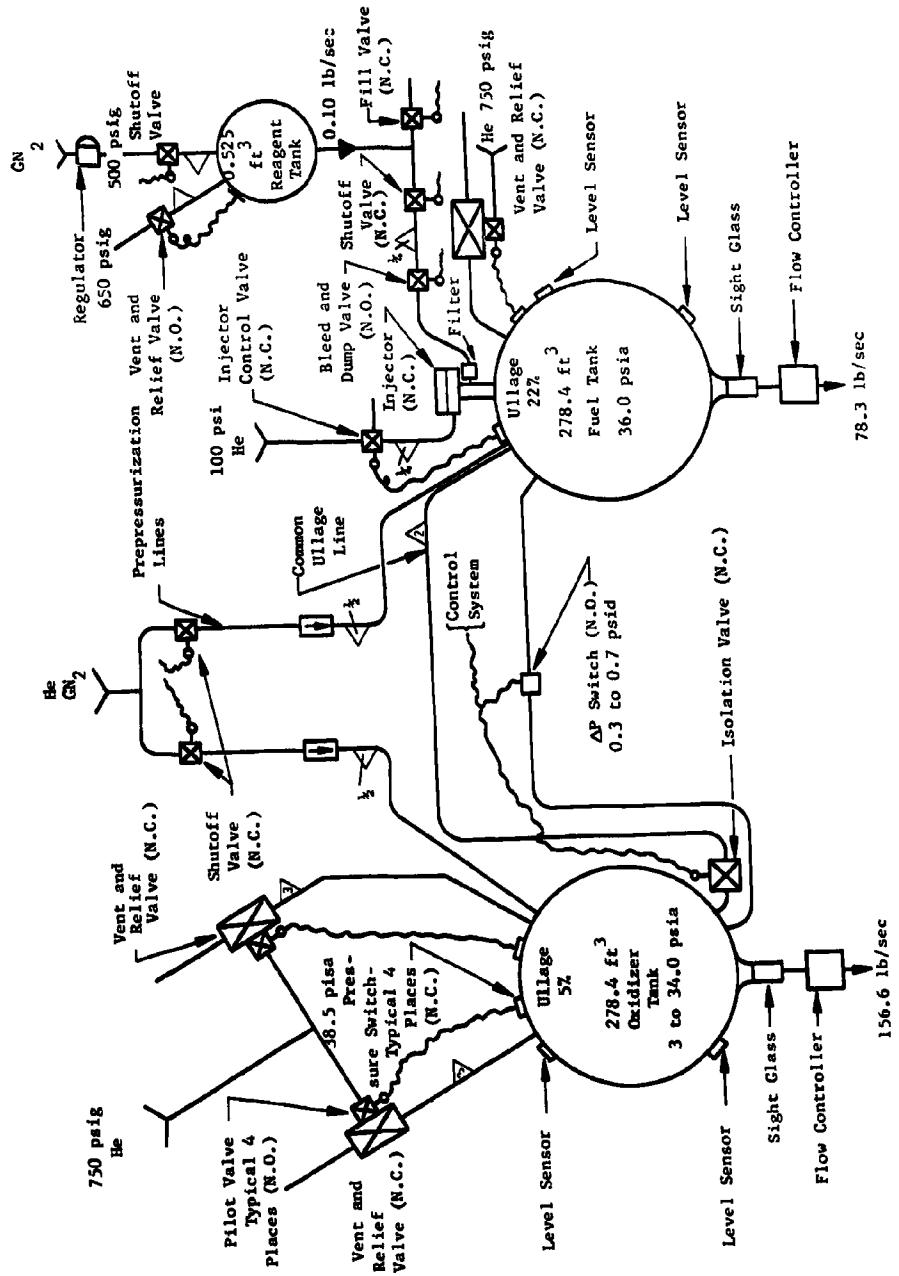


Fig. III-21 Main Tank Injection Phase III Test Schematic (Preliminary)

Pressurization Systems - The basic criteria for pressurization system design was to achieve a light weight low pressure system by generation of a low density pressurant (gas molecular weight less than 15) from relatively high density reactants with an emphasis on increasing system reliability by minimizing the number of components required. Since precise pressure control (within ± 1 psi) was desired a pulse injection system was mandatory to achieve consistent performance and minimize variations in the reaction process due to pressurant demand for a variable propellant outflow rate. For applications where continuous engine operation is anticipated and a greater tolerance in tank pressure is allowed as in a booster application; greater reliability can be achieved by replacing the pressure control mechanism with a calibrated orifice. As a result of initial tests performed on the small scale system, solid stream surface reagent injection was selected for fuel tank pressurization with subsequent pressurization of the oxidizer tank by the combustion products admitted to the tank bottom through a common ullage line and isolation valve. In order to prevent engine mixture ratio shift during operation, it was desired to maintain the discharge pressures equal at each tank outlet, however, the inherent characteristics of the common ullage pressurization process required a small differential pressure between each tank. A nominal 36 psia operating pressure was selected for the fuel tank based on current turbo-pump NPSH requirements. Consequently fuel tank-top pressure was set at 36 ± 1 psia that results in an oxidizer tank-top pressure of 31 ± 1 psia at start and 34 ± 1 psia at termination of injection due to the method of introducing pressurizing gas into the oxidizer tank. This change in ullage pressure is caused by the decreasing oxidizer head since constant pressure control is maintained at the tank outlet.

Pressurizing capability of the system was dictated by the 558 ft^3 total propellant tank volume considering a common ullage configuration with approximately 50% of the oxidizer pressurization requirement supplied by a secondary reaction. Minimum initial ullage volume was established at 5% with the 7% residual propellant, provided for system cooling, expelled by the gas expansion process after injection termination. A pressurized reagent storage system was employed to simulate a possible turbo-pump bleed reagent supply. Provisions for filling, pressurizing, and draining the system were incorporated to facilitate normal missile servicing characteristics and provide fail safe operation of the injection system. Since a demonstration of system flexibility was desired, requirements were established to assure adequate response and control during the planned continuous tests as well as the variable outflow restart tests. The pressurization system criteria was based on pressure

switch controlled pulse injector in the fuel tank due to previous success in the Phase I program while the oxidizer tank common ullage manifold was charged to include an isolation valve and differential pressure switch instead of the check valves employed in the small scale system design to prevent reverse flow. Remote operation of the system was required by a control console to demonstrate sequencing capability. Actual testing, once initiated, was automatic.

The reagent injection system must be capable of maintaining the desired pressure during conditions of maximum propellant outflow and minimum ullage. Specific design recommendations have been made in Chapter V. B, however, a response of approximately 0.050 sec is generally required. Reagent supply pressure will affect the injector control system requirements since final tank pressure during each injection cycle will be a function of reagent injection velocity and the quantity of reagent unreacted at injector shutoff. Based on laboratory experiments the maximum injection velocity is limited to approximately a 200 psi injector differential pressure for obtaining a good solid stream. The influence of unreacted reagent with the 7-ft long tankage was less than 0.2 psi due to the corresponding large ullage volume.

Safety requirements dictated the utilization of a dual pressure relief system will adequate response for prevention of exceeding structural limitations at the expected elevated operating temperatures. In addition all functions were monitored by the control console to permit manual override of any system. The injection system was provided with automatic shutdown and reagent dump capability in the event of an injector failure to reduce the possibility of an over temperature condition. The response of all systems was based on satisfactory performance under the 5% minimum ullage situation.

Propellant System - A propellant tank minimum required volume of 1000 gal. and nominal operating pressure of 36 psia resulted in the acquisition of available scrap Titan I, Stage II fuel tanks for the full scale system demonstration test article. Operating pressures were limited to 40 psia based on the expected operating temperatures and extent of modification of the aluminum tanks. Flowrate requirements were determined by nominal booster system operation during (approximately 150 sec) and a 2:1 (O/F) storable propellant mixture ratio. Since identical tanks were used for the fuel and oxidizer system correct propellant loads were assured by high liquid level sensor indication. Resulting nominal flowrates were 78.3 lb_m/sec fuel and 156.6 lb_m/sec of oxidizer. Injection

termination before fuel exhaustion was made a requirement to prevent tank damage due to the combustion process. The low level sensor used for injection termination also was required for timer actuation during the residual propellant expulsion by ullage gas expansion to accomplish system shutdown. To verify an absence of entrained vapor in the expelled propellant a sight glass was required at the tank outlet.

Propellant tank modifications required to accommodate the MTI pressurization system were provided to permit sufficient flexibility in the design of various pressurization techniques. Fore and aft propellant tank skirts were utilized to permit component mounting and tank support attachments. Complete isolation of each system required a side by side tank arrangement with a separating blast wall.

System Design - The Phase III MTI system was designed using the previously created Design Criteria as a guide. The basic philosophy of the design was to provide a maximum of data at a minimum cost consistent with safety. Due to the potentially hazardous nature of the test, safety was of primary importance. A schematic of the Phase III system is shown in Fig. III-21. As noted previously, the test system was changed from common ullage to bi-injection subsequent to writing of the Design Criteria. This change did not alter the system overall design except for eliminating the common ullage line, isolation valve, ΔP switch and one of the two oxidizer tank relief valves. The oxidizer pressurization system became identical to the fuel tank pressurization system except that fuel rather than oxidizer was used for reagent. System operating parameters remain the same except that oxidizer tank pressures became equal to fuel tank pressure. A schematic of the bi-injection system as tested is shown in Fig. III-22. The primary design effort involved the modification of the main propellant tanks and the definition of facility requirements with the necessary drawings of the common ullage system vent system, and reagent supply system completed. The following paragraphs describe the design of the Phase III MTI system with the exceptions noted.

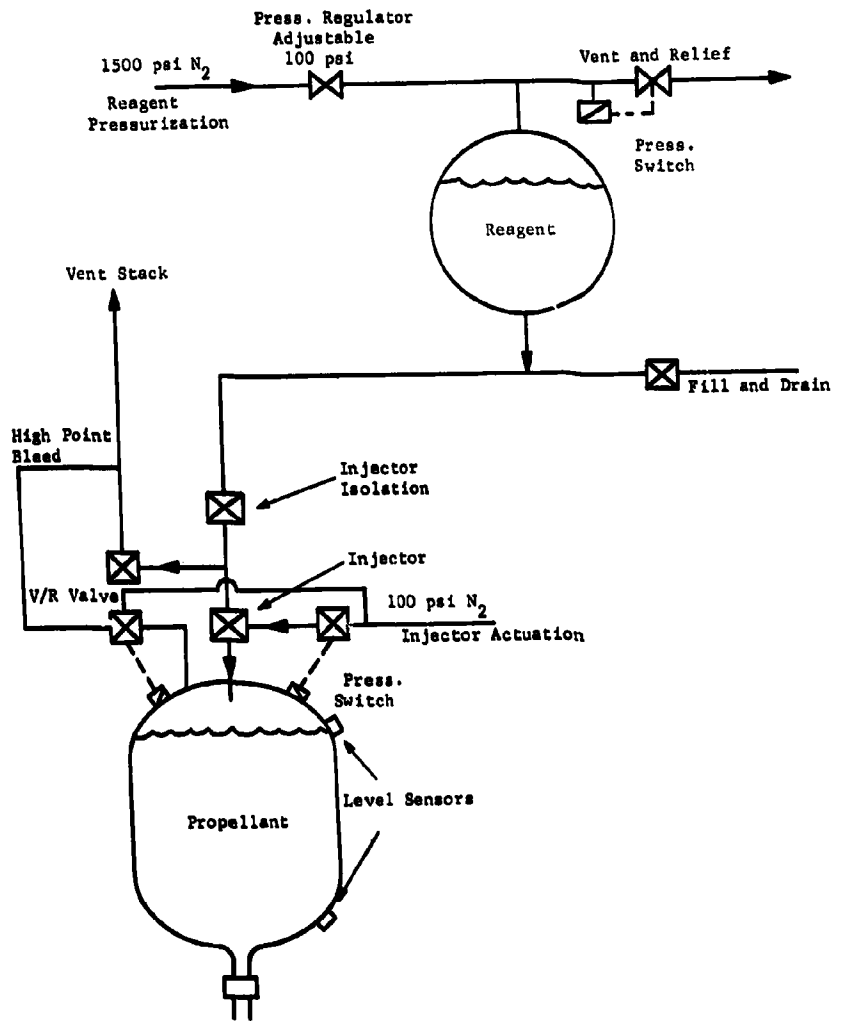


Fig. III-22 Main Tank Injection Phase III Separate Reagent Injection System

Pressurization System - The fuel tank pressurization system includes the reagent storage and injection system and the pressure control system. Reagent flowrate through the injector and storage tank capacity were based on scaling Phase I test data as follows:

Assuming identical reaction mixture ratio of 0.62,

$$W_{r3} = W_{r1} \frac{V_{p3}}{V_{p1}} \frac{T_{gft1}}{T_{gft3}}$$

where

W_{r3} = reagent usage, Phase III,

W_{r1} = reagent usage, Phase I, 0.26 lb_m,

V_{p3} = volume pressurized, Phase III, 445.8 ft³,

V_{p1} = volume pressurized, Phase I, 7.95 ft³,

T_{gft1} = temperature of fuel tank ullage gas, Phase I, approximately 260°F,

T_{gft3} = temperature of fuel tank ullage gas, Phase III, approximately 450°F estimated.

$$W_{r3} = (0.26 \text{ lb}_m) \frac{445.8 \text{ ft}^3}{7.95 \text{ ft}^3} \frac{260 + 460 \text{ }^\circ\text{R}}{450 + 460 \text{ }^\circ\text{R}}$$

$$W_{r3} = 11.6 \text{ lb}_m.$$

For design purposes this was increased to 22 lb_m to allow testing flexibility such as MTI prepressurization, repressurization after a period of coasting, and to allow for reaction uncertainties. The maximum injector reagent flowrate calculated was 0.0738 lb_m/sec for a 0.047-in. dia injector orifice. Although the injector should normally be oversized to assure adequate response during transients and with a 2- to 3-cps frequency during steady-state operation, the injector was originally sized for continuous operation to avoid tank over-pressurization. An injector differential

pressure of 100 psig was used based on Phase I testing and injector orifice development. Phase I tests showed that injection of reagent as a spray resulted in much higher ullage gas temperature than a solid stream injection. Injector orifice development indicated that increasing the pressure drop above 200 psi through the injector resulted in degradation of the injection stream. As a result, 100 psi was chosen as a compromise between penetration and anticipated ullage gas temperature because of degradation of the injector stream. However, the reagent supply system was designed for 650 psig maximum in case testing indicated that reagent injection pressure higher than 125 psig was feasible.

Pressurization line size was 1/4 in. while reagent supply and fill lines were 1/2-in. dia. The reagent tank volume selected was 0.523 ft³ as a tank this size was available that was more than adequate to hold the anticipated maximum reagent consumption of 22 lb. Pressure relief of the reagent tank was provided by a 1/2-in. 3-way solenoid valve controlled by a pressure switch sensing reagent tank pressure. Figure III-23 shows the assembled system.

Early in the MITI program a search was made for a commercially available device that could be used as an injector to preclude design and development of a special component. The injector (Fig. III-24) was made from a commercially available Spraying Systems Company #24AUA-898 spray gun for use in the Phase I test program before use in the Phase III test program. It was capable of withstanding the maximum reagent injection pressure and required a minimum of approximately 45 psig pneumatic pressure to operate. In order to provide maximum response the injector control system was designed to operate at 150 psig. Nitrogen-injector control pressure was supplied to the large dome-shaped operating head shown in Fig. III-25 that causes a teflon piston to retract against a spring, also contained in the operating head. Reaction of the piston pulls a 1/8-in. dia operating rod from a valve seat machined into the orifice mounted on the opposite end of the injector. The orifice is held onto the injector by a retaining nut. The retaining nut is also screwed into a mounting port on the tank dome to provide a mounting point for the injector and assure axial injection. Control of the injector is discussed later in this section. The Phase III Injector Orifice is shown in Fig. III-26 and performance presented in Fig. III-27.

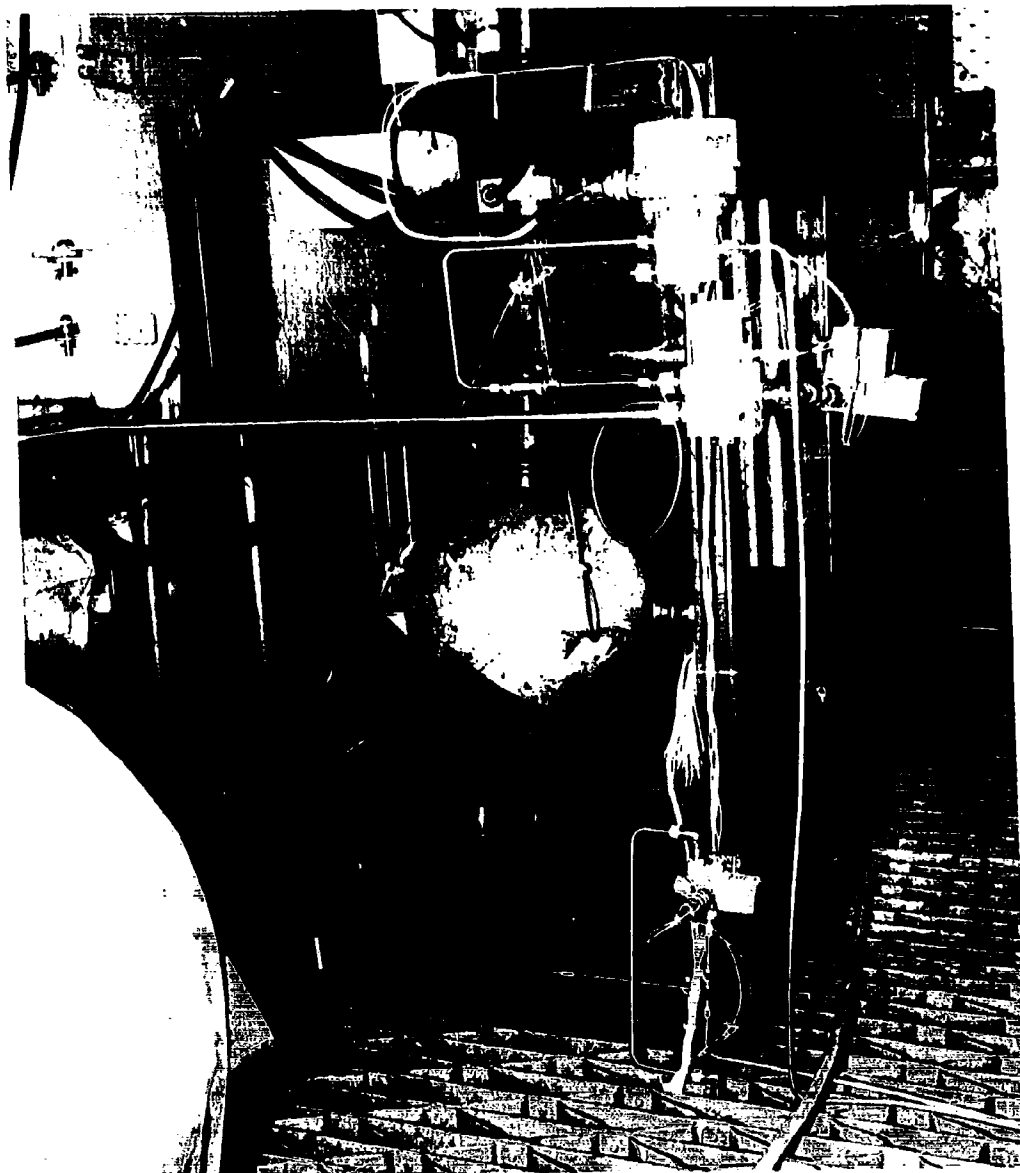


Fig. III-23 Phase III MTI Reagent Supply System

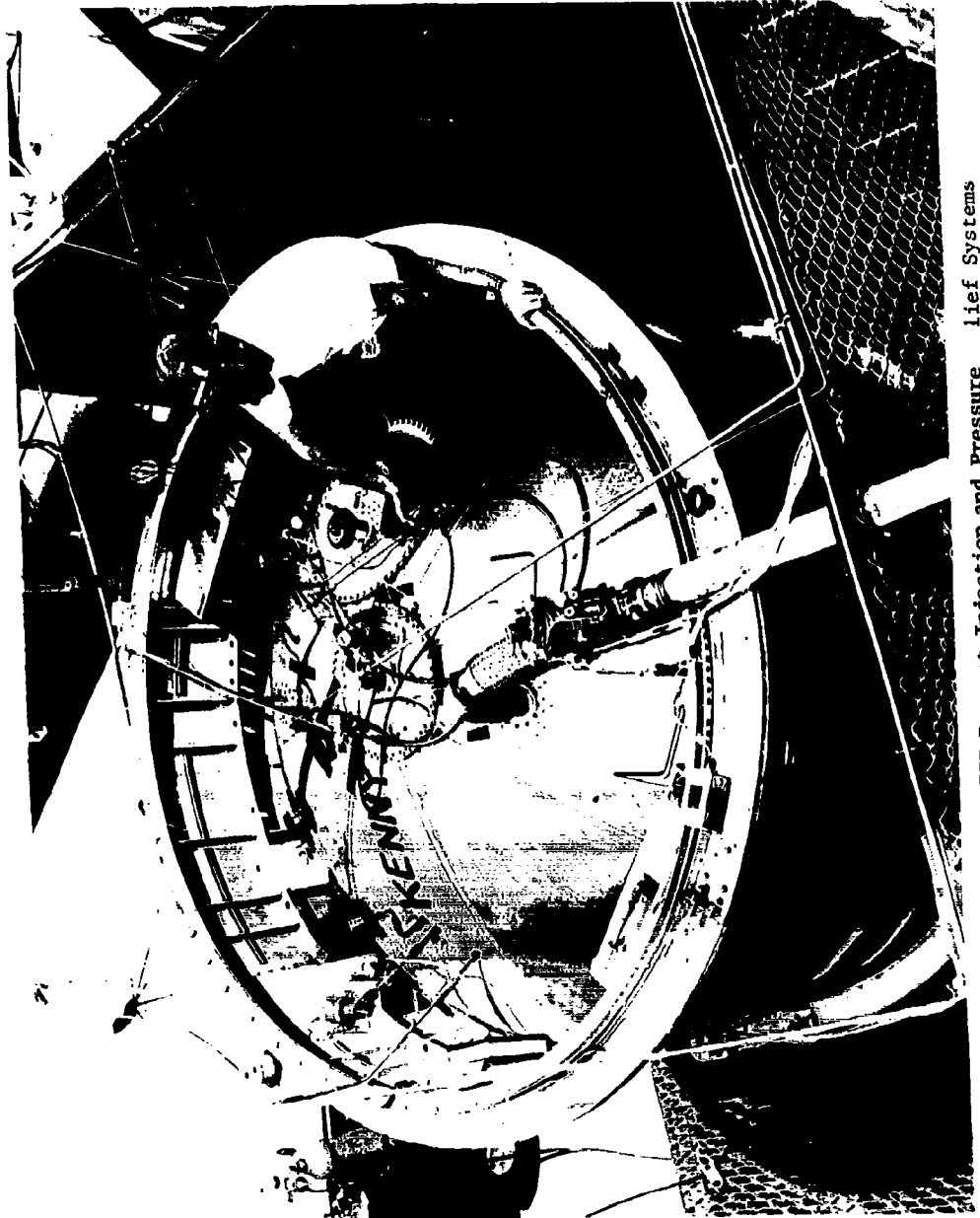


Fig. III-24 Phase III Reagent Injection and Pressure Lief Systems

RTD-TDR-63-1123



Fig. III-25 MTI Injector

RTD-TDR-63-1123

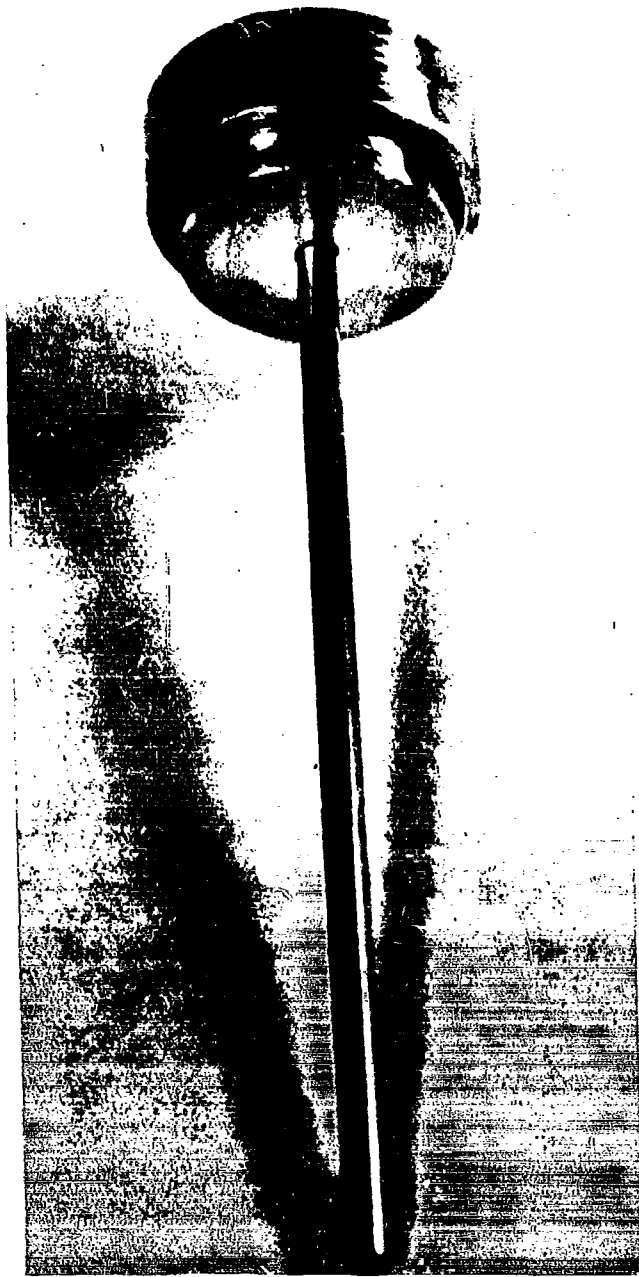


Fig. III-26 MTI Phase III Injector Orifice

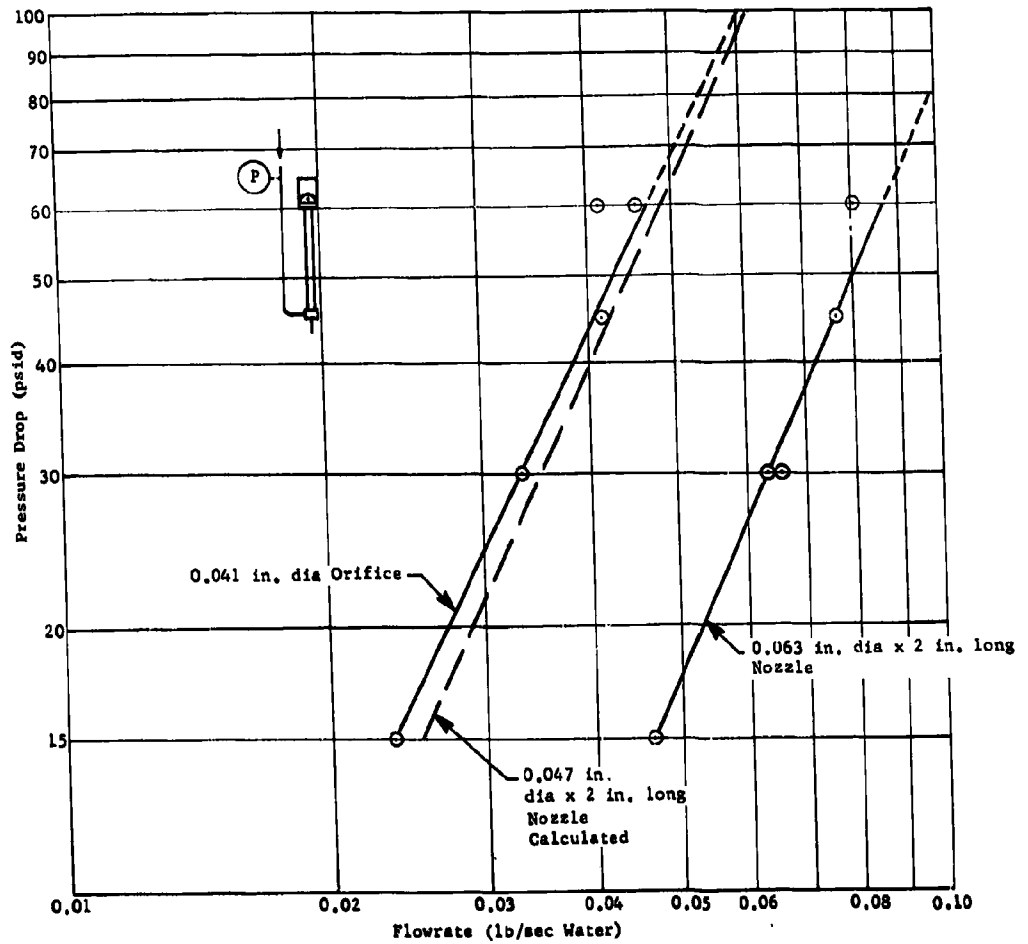


Fig. III-27 Phase III Injector Flow Capacity

Pressurization of the oxidizer tank was to be originally accomplished by introduction of pressurizing gas from the top of the fuel tank into the lower dome of the oxidizer tank, (below the liquid surface) through a common ullage line. A common ullage line was designed using as criteria the pressurization gas velocity used in the most successful Phase I common ullage tests. This velocity was 66 ft/sec and the resulting common ullage line size chosen was 2-in. dia. The 2-in. dia line results in a slightly higher velocity and pressure loss but was chosen because of the availability of hardware and the realization of an optimum pressure drop through the line. The higher pressure drop makes it easier to control the isolation valve as discussed later in this section. To isolate the two propellant tanks and prevent reverse flow through the common ullage line, a 1½-in. dia Annin valve was selected as the isolation valve to be installed at the lowest point in the common ullage line as shown in Fig. III-21. This was considered to be the best location in view of the possibility of condensing gunk out of the pressurizing gas. Control of the isolation valve is discussed later in this section.

Originally oxidizer tank pressurization gas was to be injected into the tank through a 2-in. port on the lower dome with a diffuser inside the tank below the liquid surface (Fig. III-28). A subsurface gas injector was designed from information gained in Phase I testing, which was carried on concurrently with Phase III design. The basic technique for successful operation was to put pressurizing gas into the oxidizer tank below the top of the baffles such that any gunk in the gas reacting with the oxidizer would be completely consumed before reaching the liquid surface. This design routed pressurizing gas in a 2-in. dia tube concentrically up through the inside of the 4-in. dia outflow line terminating in a gas diffuser mounted in the center of the "X" formed by the baffles. The gas diffuser design had a solid top so that pressurizing gas was forced out horizontally along radial lines from the tank center before rising to the surface. The subsurface gas diffuser is shown in Fig. III-29. The subsurface gas diffuser although not used was left as a splash plate for the direct fuel injection tests.

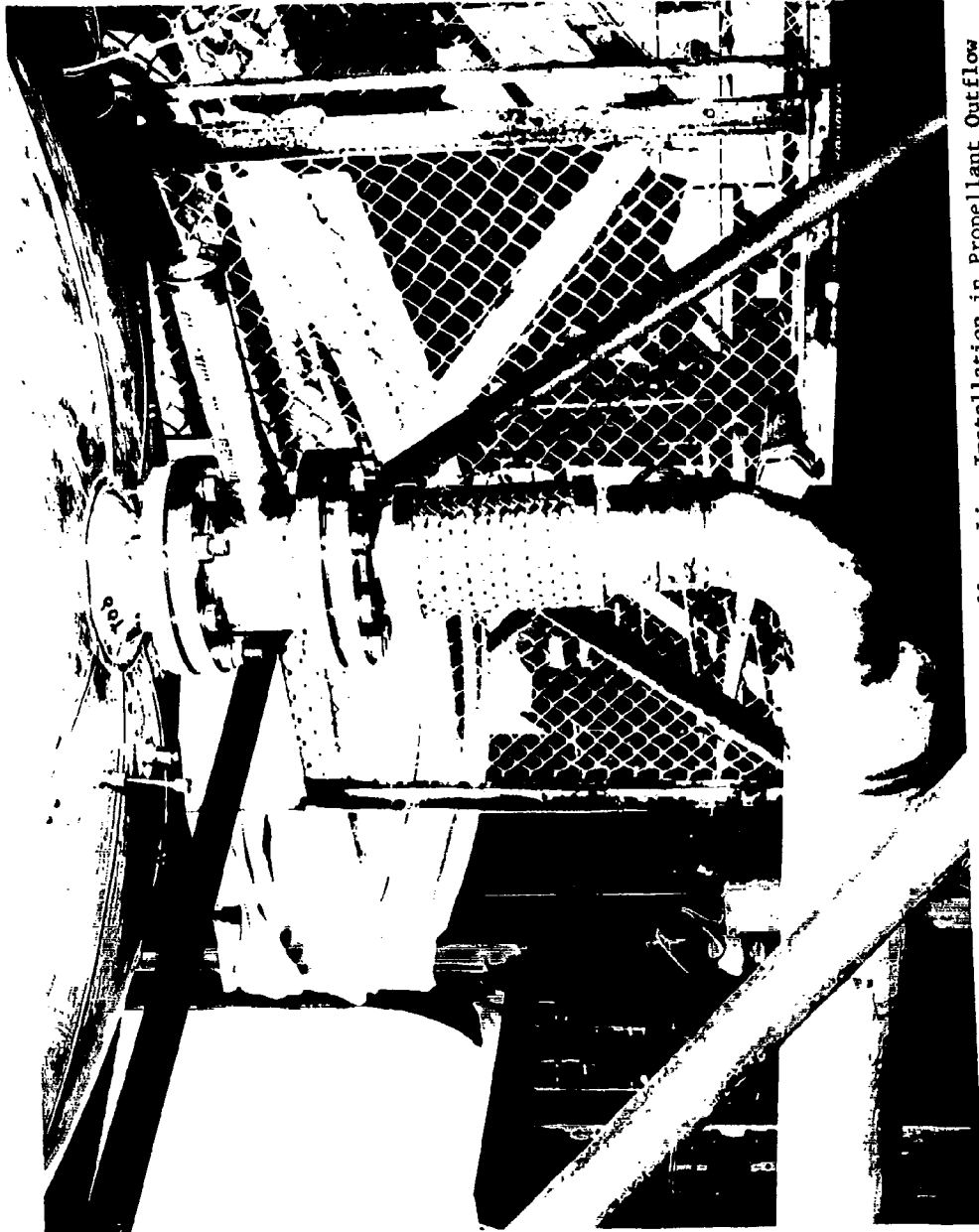


Fig. III-28 Phase III Secondary Tank Common Ullage Line Installation in Propellant Outflow System



Fig. III-29 MTI Phase III Secondary Tank Common Ullage Subsurface Gas Diffuser

Fundamental control of pressure within the system was achieved by pressure switches. The propellant tank pressure control system is shown schematically in Fig. III-22. As stated previously 36 psia was chosen as nominal fuel tank-top pressure, to be controlled ± 1 psi by a pressure switch controlling the injector through a 1/4-in. pneumatic 3-way control valve. The system was designed so that when the fuel tank pressure is below 36 psia the pressure switch is closed, energizing the injector control valve to the open position causing pneumatic pressure to be applied to the injector operating head, opening the injector. When fuel tank pressure is greater than 36 psia, the switch is open and the injector control valve vents the injector operating head causing the injector to be closed. The injector was required to be normally closed and the injector control valve required to be normally closed (vented) for safety in case of either pneumatic or electrical failure. A 1/2-in. shutoff valve, normally closed, located between the reagent tank and injector, was included for isolation of the injector in case of injector malfunction. In order to bleed air out of the injector before testing and dump pressure from the injector should a malfunction occur, a 1/4-in. bleed and dump valve was added to the injector. This valve was required to be normally open so reagent pressure in the injector would be released in case of electrical failure. Both bleed and dump valve and shutoff valve were to be manually controlled, remotely operated from the test console. The reagent supply system is shown in Fig. III-23.

With the injection control system described, initiation of injection was automatic following opening of the reagent shutoff valve, electrically arming the pressure switch and control valve, and starting propellant outflow. Termination of injection was to be accomplished by a fuel tank low level sensor. At fuel low level a signal from the low level sensor interrupted electrical power to the injector control valve causing the injector to close. The low level sensor was also connected to a timer to allow outflow to continue beyond termination of injection. This is described in the propellant feed system section.

The oxidizer tank pressure control system design was based on a differential pressure switch controlling the normally closed isolation valve in the common ullage line. The differential pressure switch high pressure port was connected to sense fuel tank-top pressure while the low pressure port was connected to sense oxidizer tank lower dome pressure. Switching points of the differential pressure switch were chosen as 0.7 psid on decreasing pressure based on calculated common ullage line pressure drop.

The common ullage line was sized for a pressure drop of approximately 0.4 psid during normal propellant outflow rates. Initially, pressure in the oxidizer tank will drop until the ΔP across the common ullage line and ΔP switch is greater than 0.7 psi set point. The normally open ΔP switch then closes, energizing a solenoid valve that opens to supply pneumatic pressure to the isolation valve, which opens to allow pressurizing gas to flow into the oxidizer tank. As a result of the isolation valve opening the differential pressure sensed by the ΔP switch drops to approximately 0.4 psi (the ΔP of the common ullage line) that is between the switching points of the ΔP switch. Thus, at normal flowrates the isolation valve remains open. When oxidizer outflow is at a lower rate, or zero, the isolation valve will be caused to cycle slowly, admitting pressurizing gas to the oxidizer tank whenever pressure drop across the common ullage line (from fuel tank-top dome to oxidizer tank lower dome) is greater than 0.7 psi. Whenever ΔP is less than 0.2 the system was designed to close the isolation valve to prevent reverse flow into the fuel tank. Tank-top and lower dome pressures resulting from this control system are shown in Fig. III-8. Fuel tank-top pressure remains constant 11 psi because of the injector control system. Fuel tank lower dome pressure decreases with outflow because of loss of fuel head at a rate of 0.0328 psi/in. as fuel outflows from the tank until it equals tank-top pressure at fuel exhaustion. Oxidizer lower dome pressure remains constant within 0.7 psi lower than fuel tank-top pressure because of the isolation valve control. Oxidizer tank-top pressure is less than lower dome pressure by the amount of oxidizer head in the tank. As oxidizer outflow commences tank-top pressure increases at a rate of 0.0526 psi/in. until it equals lower dome pressure at oxidizer depletion. The pressure decay during the final eight seconds is due to a polytropic pressure decay following injection termination and residual propellant expulsion.

Over-pressure protection of both fuel and oxidizer tanks was assured by multiple protection methods designed into the system. The primary protection in each tank consisted of shutting off the pressurization source, i.e., the injector in the fuel tank and the isolation valve leading to the oxidizer tank. In case of a serious overpressure, dual relief valves controlled by pressure switches were incorporated on each of the two tanks to increase overall system reliability. Two pressure relief valves were required on the oxidizer tank because of the possibility of secondary reaction occurring following closing of the isolation valve.

Design of the pressure relief system on each tank was based on Phase I maximum pressure rise rate, structural capability of available tankage and allowable maximum tank wall temperatures during testing. Proof pressure of tankage selected for Phase III use was 40 psig at room temperature. Relief valve response requirements were calculated for a combination of worst conditions in order to determine how far below tank proof pressure to set relief pressure. The relief pressure established was 38.5 ±0.5 psia based on response characteristics of available relief valves and pressure switches. Response data indicated a system with an opening response time of 80 msec was required. Based on this relief pressure, a maximum allowable tank wall temperature was determined from the strength vs temperature data specified in MIL HDBK-5 (March 1961) for 1/2-hr temperature exposure of 2014-T6 aluminum.

<u>Temperature (°F)</u>	<u>Yield Strength (%)</u>
0	100
100	99
200	94
300	84
350	77
400	67
450	53

Maximum allowable tank wall temperature was established by applying a safety factor of 1.15 times relief pressure, or (39.0 - 11.8 psig) (1.15) = 31.0 psig;

$$\text{Allowable Strength Reduction} = \frac{31 \text{ psig}}{40 \text{ psig}} = 0.77$$

Therefore, from table, max allowable wall temperature = 305°F. Relief valve and line sizes were specified as 3-in. dia for both tanks based on anticipated gas composition and quantity to be vented. With the maximum gas generation rates (in case of a malfunction) and available pressure drop between tank ullage and atmospheric pressure, the surplus Calmeec vent and relief valves, PD47S0128, were found to fit the design requirements. However, the relief function, altered for pneumatic actuation, was controlled automatically by pressure switches set at 38.5 psia. Venting for fill and drain operations was controlled manually by remote control from the test console. Figure III-24 shows the pressure relief system as installed.

In addition to the controls described for the isolation valve and relief valves, the circuit logic was also designed to close the isolation valve whenever a fuel tank over-pressure occurred. This consisted of connecting the fuel tank overpressure switch lead to the isolation valve circuit so that anytime the fuel tank relief valve was signaled to open, the isolation valve would be closed.

Propellant Feed System - The propellant feed system consists of the main propellant tanks with provisions for filling from a pressurized storage tank, control of the propellant outflow at desired flowrates and termination of outflow. Capability was included for recycling of propellant after each run so that more than one test run could be made on each load of propellants. Loading of each propellant tank was accomplished by including a 2-in. dia return line, flowmeter and shutoff valve running from each catch tank bottom into a "T" in each propellant outflow line just below the bellows, approximately 23-in. below the propellant tank lower dome. Transfer of propellants from catch tank to main propellant tank was done by pressurizing the storage tank to 45 psia. A flowmeter, indicating both rate and total, was called for in the fill line for an accurate determination of propellant loads. A schematic of the propellant feed system is shown in Fig. III-21 and one of the catch tanks shown in Fig. III-30.

Shutdown of the injection system before complete propellant exhaustion was required to prevent damage because of reagent impingement on the tank bottom. Residual propellant expulsion was then accomplished by employing a shutdown timer in the system. A low level sensor, installed in the fuel tank of the common ullage system, when triggered by fuel low level, shutoff injection by interrupting electrical power to the injector control valve. A timer was simultaneously activated by the fuel low level sensor signal to close both fuel and oxidizer outflow control valves after a specified interval. Tank-top pressure is allowed to decay polytropically during the final few seconds of outflow following termination of injection. The length of time allowed for polytropic expansion is dependent on the established fuel tank low level sensor location, anticipated oxidizer outage at shutdown, allowable pressure decay, and anticipated ullage temperature decay rate following termination of injection. Low level sensor location, identified previously, was chosen so that 17.6 ft³ of propellant remain at injection termination in the fuel tank, however, an oxidizer depletion prevents complete expulsion. Based on a maximum tank pressure decay during this time, a time delay of 8 sec was chosen, for the common ullage system to minimize propellant outage. Outflow was started and stopped by a Rockwood ball

valve simulating typical engine start and shutdown transients while flowrate was modulated by a Fisher butterfly valve controlled manually from the test console. The existing baffles used to control vortexing and the nondrop-out tank outlets were designed for flowrates 15% higher than Phase III design flowrates, providing ample margin for the MTI test conditions imposed. Flow capability of the more critical oxidizer system is shown in Fig. III-31.

Structure - Structure for the Phase III test system consisted of the main propellant tanks, propellant tank supports, outflow and service lines, catch tanks, and a blast shield. The aluminum propellant tanks were of semi-monocoque construction not designed specifically for the Phase III test program but were obtained as salvage items from the Titan I program and modified. Total volume of each tank was 278.4 ft^3 , capable of a 1980 gal propellant load. Level sensor locations were calculated for each of the two tanks so that a 150-sec test run could be made with an initial ullage of 5% in the fuel tank and 22% in the oxidizer tank outflowing at 78.3 and $156.6 \text{ lb}_m/\text{sec}$ of fuel and oxidizer, respectively. Level sensor ports at both the 5 and 22% ullage levels were provided in each tank to allow tests to be run to determine control system response with a minimum ullage in both tanks. The tank capacities, when loaded for a bipropellant expulsion at a 2 to 1 oxidizer to fuel mass ratio, result in a 5% oxidizer ullage and 22% fuel ullage, equivalent to 264.6 ft^3 and 216.6 ft^3 , respectively. Propellant tank operating and relief pressures were discussed previously. Access ports large enough for a man to enter were provided in each tank dome.

Propellant tank supports were designed for each of the tanks to be used in conjunction with support skirts and handling rings that were part of the tank structure. The tank supports were designed to support $25,250 \text{ lb}_f$ and to resist wind loads to 90 mph. A blast shield-catch basin structure was designed to physically isolate the tanks and propellants in case of tank rupture. The tank supports, blast shield and catch basin are shown in Fig. III-32 and III-33. The blast shield was designed using steel plate and angle iron to be filled with sand after being erected. The catch basin was designed to be partially filled with water and extends only under the fuel tank. In case of both tanks rupturing, fuel would be retained in the steel catch basin and oxidizer would fall through the grating shown at the left of Fig. III-32 into a concrete pit flushed with water.

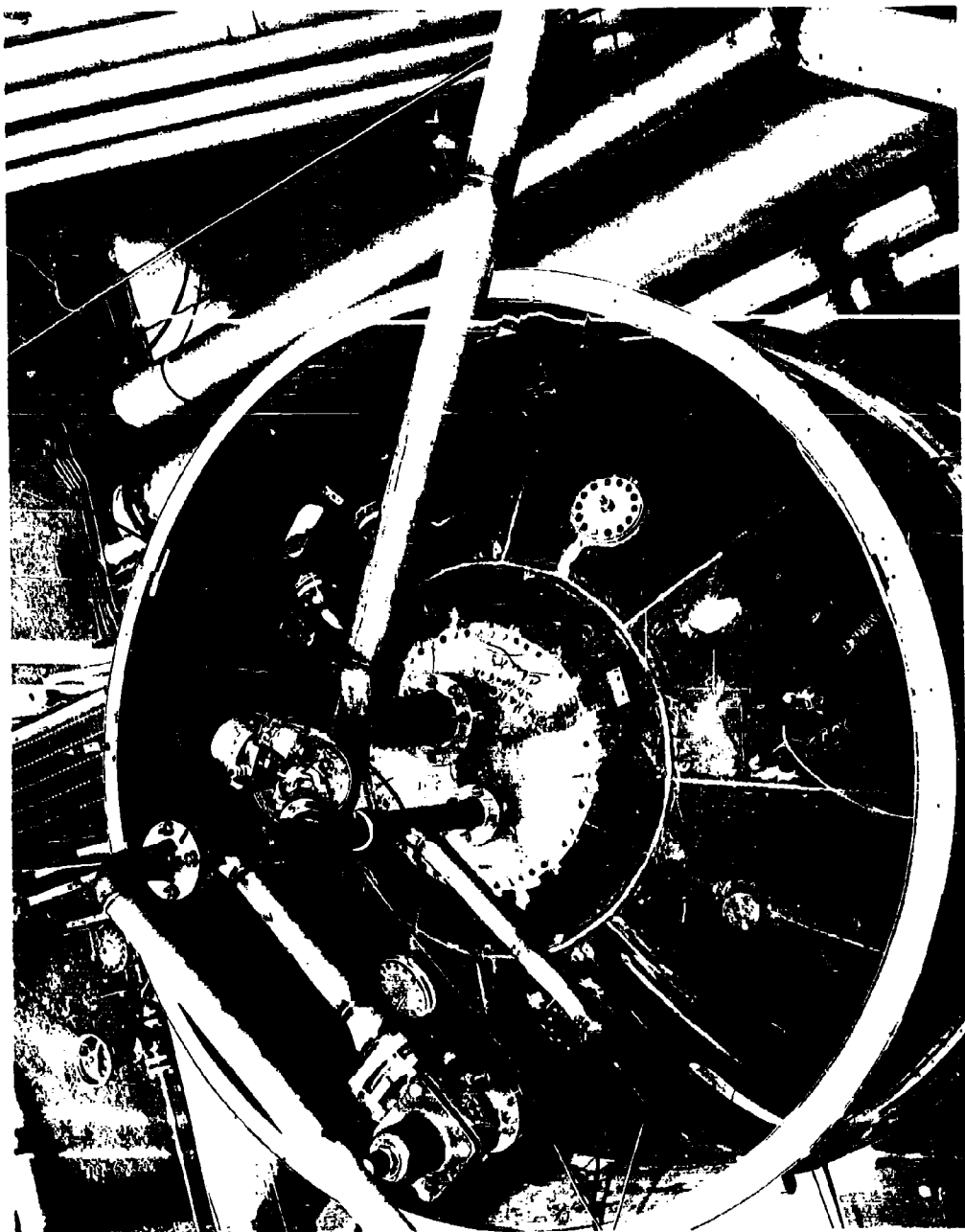


FIG. III-30 Phase III MTI Fuel Catch Tank

Legend:	
1	As Drawn CFL 6100184
2	Concentric C. U. Line Restricted Outlet to 7.4 in. ²
3	Concentric C. U. Line Restriction in 12.5 in. ² Section

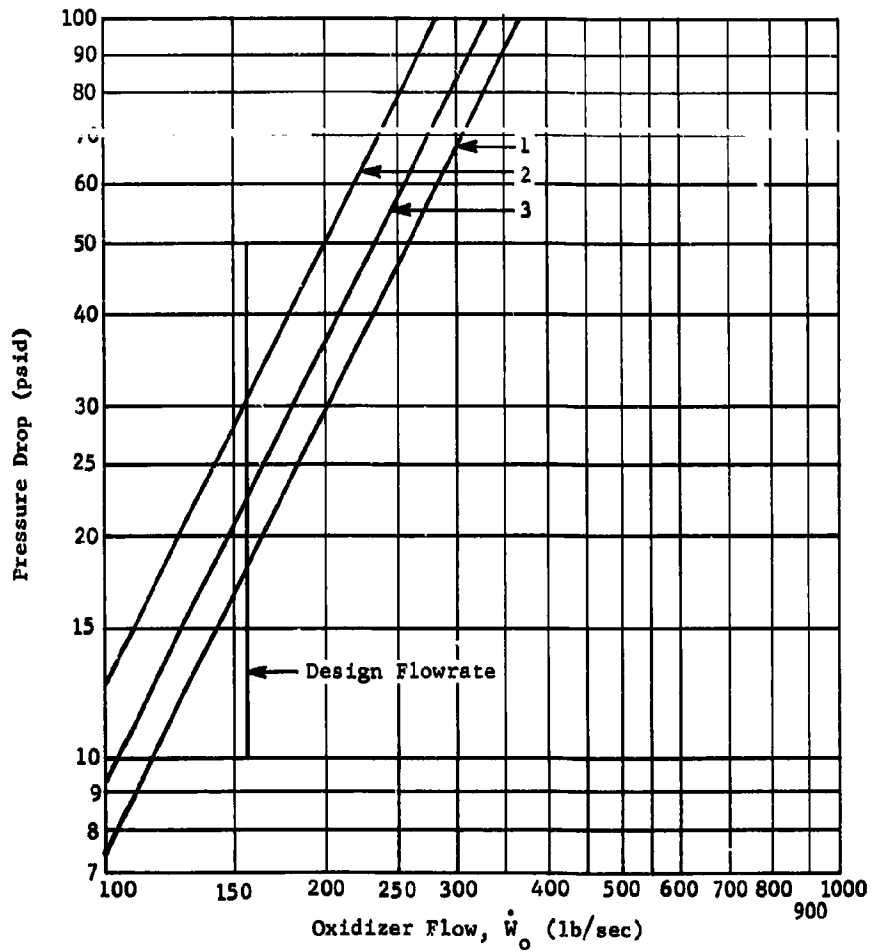


Fig. III-31 Calculated Pressure Drop MTI Phase III Oxidizer System

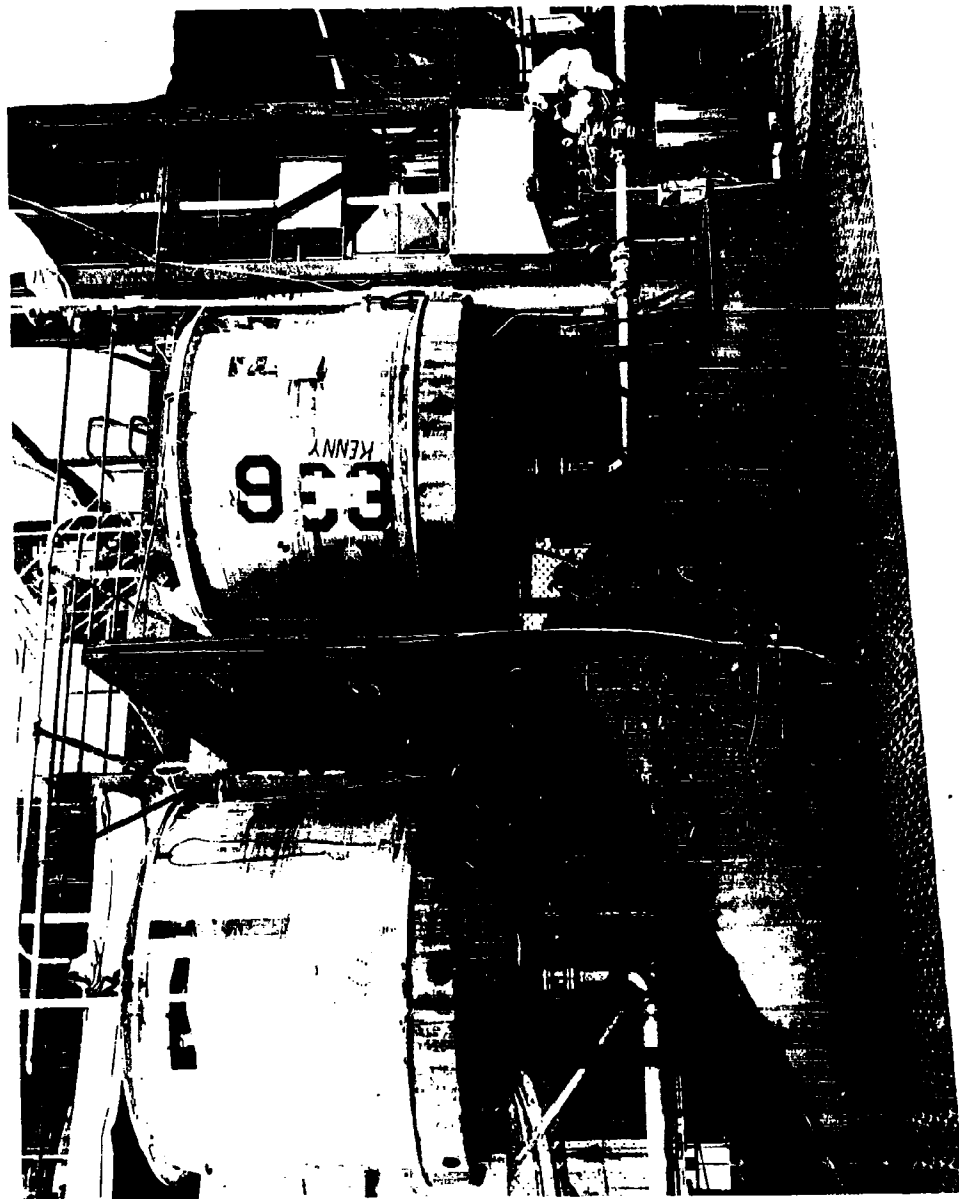


Fig. III-32 Phase III MTI Test Article

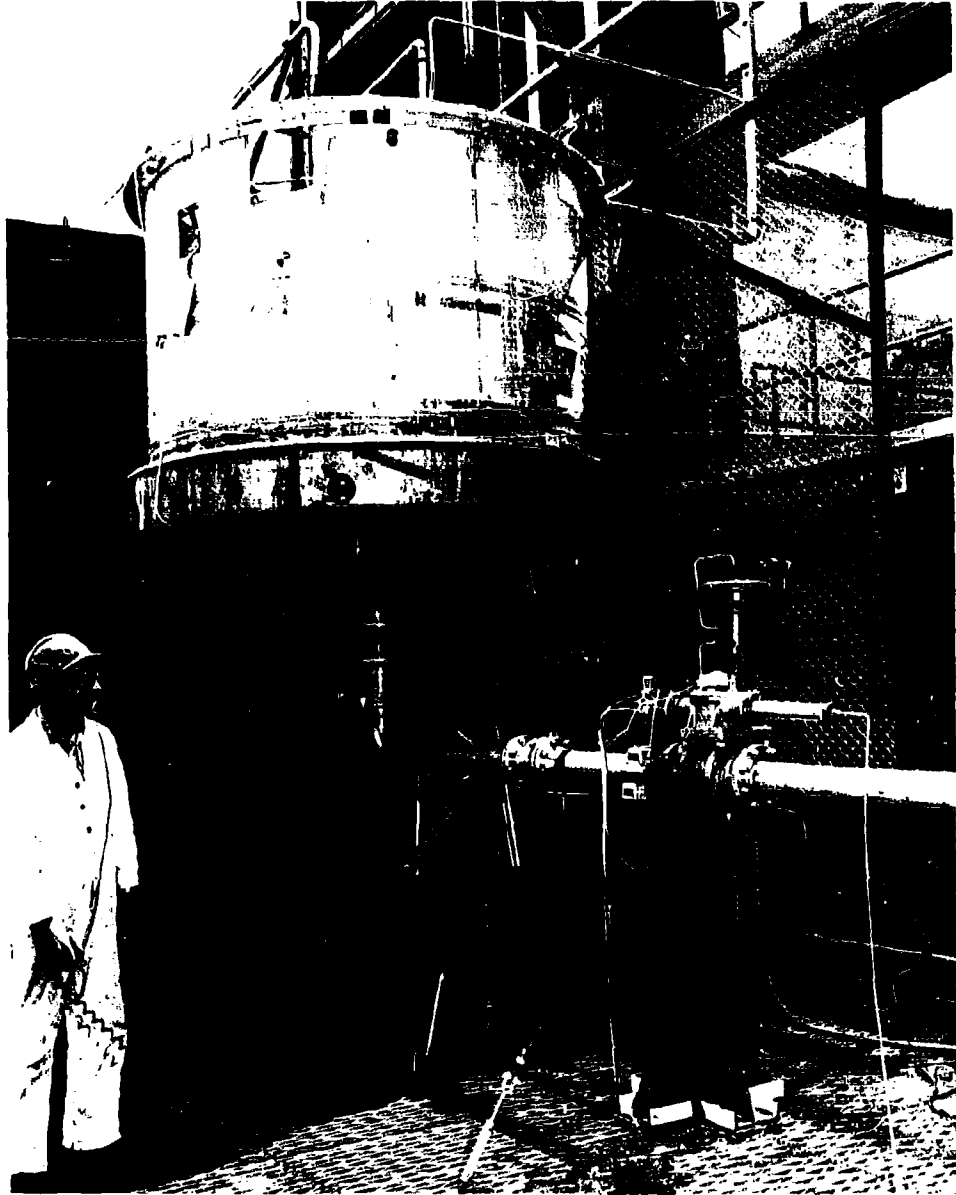


Fig. III-33 Phase III MFI Fuel Tank System and Catch Basin

C. PROTOTYPE FABRICATION

The MTI pressurization system prototype used for Phase III testing consisted of two 278.4 ft³ flight weight aluminum tanks mounted in a side by side arrangement with overpressure protection. Pressurization was accomplished either by direct reagent injection from a pressurized 0.523-ft³ supply or subsurface gas impingement for oxidizer tank pressurization in a common ullage arrangement. The primary fabrication effort was concerned with propellant tank modifications and system assembly and installation at the test site. Approximately 75% of the complete system fabrication was performed in the Martin manufacturing facilities with the remaining portion consisting of procured components and local machining done on the tank supports. The test article was assembled at the Cold Flow Laboratory Titan II System Test Area test stand. Figure III-32 shows the prototype test assembly, the blast shield, and a small portion of the test stand in the background.

Fabrication was started before the completion of Phase I testing in order to cut down time between Phase I and Phase III testing. Basic hardware was fabricated with sufficient capability to incorporate any changes resulting from Phase I program recommendations. In order to facilitate possible late modifications, the availability of existing tooling checkout equipment permitted the manufacturing to be done on the regular production line making this operation less expensive. This enabled easy system modification when the change from a common ullage system to bi-injection was made. The common ullage ports were simply capped and a second injector, fabricated for Phase I oxidizer tank use, was mounted in the oxidizer tank dome in an existing port.

Items having a predominant effect on system thermodynamic characteristics were flight-weight while the remainder of the system was relatively heavy off-the-shelf type. The propellant tanks, baffles, vent and relief valves, and pressure switches were flight-weight. Emphasis was placed on obtaining surplus components and materials in order to keep cost to a minimum. A list of components used in construction of the Phase III MTI prototype is given in Table III-6.

Table III-6 Phase III MEI Pressurization System Components

ITEM	No. Req	Made By	Size Capacity	Remarks
<u>Injection Subsystem</u>				
Injector	1	Spraying Systems Co. #24 AUA-898D	0.047-in. injector orifice diameter	Modified
Injector Control Valve	1	Marotta - SV124	1/4-in. Port	Marotta #202873 113k in. used on Phase I
Regulator	1		1/4-in. Port	150 psig
Bleed and Dump Valve	1	Marotta MV 100 MD	1/4-in. Line	New (2-way)
Shutoff Valve	1	Marotta MV 583K	1/2-in. Line	New (2-way)
Fill Valve	1	Hand Valve	1/2-in. Line	
Reagent Tank	1	Martin #327B-7050015-029	0.523 ft ³ 1-0.079-0.080-in. L.R-5.99 in.	Titan I, Stage II, Accumulator
Vent and Relief Valve	1	Marotta SV 153	1/2-in. Port	(3-way)
Relief Valve Pressure Switch	1	Hydroelectric	38.5 psia	Titan II Modified (Surplus)
<u>Propellant Subsystem</u>				
Fuel Tank	1	Fabricated-Martin LAB 600 3250-059	278.4 ft ³	Scrap Titan I, Stage II Tanks-Repaired
Oxidiser Tank	1	Fabricated-Martin LAB 6003250-069	278.4 ft ³	Scrap Titan I, Stage II Tanks-Repaired
High Level Sensor	2	Powertron #PD 8380115-069		Used on Phase I
Low Level Sensor	2	Powertron #PD 8380115-069		Used on Phase I
Level Sensor Controller	2	Powertron #PD 8380115-059		Used on Phase I
Sight Glass	2	Fabricated	4 in. ID	Glass Tube and Gaskets Corning Glass Works - Flanges Fabricated
<u>Common Ullage Subsystem*</u>				
Common Ullage Line	1	Cold Flow Laboratory	2-in. dia	
Isolation Valve	1	Annin #CV 36	1 1/2-in. dia	CV258
ΔP Switch	1	Spiedel Electric	1/2 psi	New-Spiedel #145-D LAB 6003252
<u>Pressure Control Subsystem</u>				
Injector Pressure Switch	1	Hydro-Electric PD 7180067 3/4 001	36.0 ±0.5 psia	Used on Phase I
Relief Valve Pressure Switch	3	Hydro-Electric	38.5 ±0.5 psia	
Vent and Relief Valve, Fuel	1	Calmec PD4780128	3-in. Port	Titan I Modified
Vent and Relief Valve, Oxidiser	2	Calmec PD4780128	3-in. Port	Titan I Modified
Prepressurisation Shutoff Valves	2	Marotta MV 583K	1/2-in. Port	New (3-way)
Check Valve	2	Republic	1/2-in. Port	

*The common ullage subsystem was designed but not used during Phase III testing.

Propellant Tanks - The Phase III MTI fuel tank came originally from the Titan I, B9 missile. The first stage of this missile had been damaged in a liquid oxygen loading accident and the second stage tanks released for structural testing. The second stage fuel tank upper dome was burst during structural testing and the tank was released as salvage. This tank and another with a dented lower dome were acquired from salvage for MTI use. The B9 missile tank was repaired but found to be structurally inadequate for MTI use requiring the top dome from the other salvage tank removed and welded to the B9 tank. The B9 tank was found to be satisfactory following minor patching, replacement of huck bolts, cleaning, and hydrostatic testing to 40 psig. This tank and the replacement upper dome were not chem-milled. The dome wall thickness was 0.080 in., and the barrel thickness was 0.125 in.

The Phase III MTI oxidizer tank was fabricated originally for a flight-weight ground test Lot G series prototype missile (GX). Following handling, erection, and other tests the second stage fuel tank was released for acoustic tests. These tests were to determine the effect of engine induced acoustic stress because of in-silo starting of first stage missile engines. This tank was subsequently obtained, through salvage, for MTI testing. It required extensive cleaning to remove contamination and a coating of paint inside the tank. Following minor patching, replacement of huck bolts, and hydrostatic testing to 40 psig the tank was found satisfactory for use as the Phase III oxidizer tank. This tank was chem-milled with the following nominal thicknesses:

	<u>Chem-milled Areas</u>	<u>Land Areas</u>
Dome	0.049 in.	0.080 in.
Barrel	0.067 in.	0.125 in.

Each of the two propellant tanks were originally fabricated from two 45-deg elliptical domes, 95-in. dia, welded to a 23-in. long barrel section. Construction was welded skin-stringer type with a floating ring for stabilization. Material was 2014-T6 aluminum. Dimensional characteristics of the identical propellant tanks are shown in Fig. III-34.

Component	Title	Height	Dist (in.)	Vol (ft ³)
A	Oxid High-Level Sensor 5%	H ₃	84.08	264.4
B	Fuel High-Level Sensor 22%	H ₂	68.09	216.6
C	Oxid Low-Level Sensor	H ₁	17.67	17.6
D	Fuel Low-Level Sensor	H ₁	17.67	17.6
E	Propellant Tank	H ₄	94.68	278.4

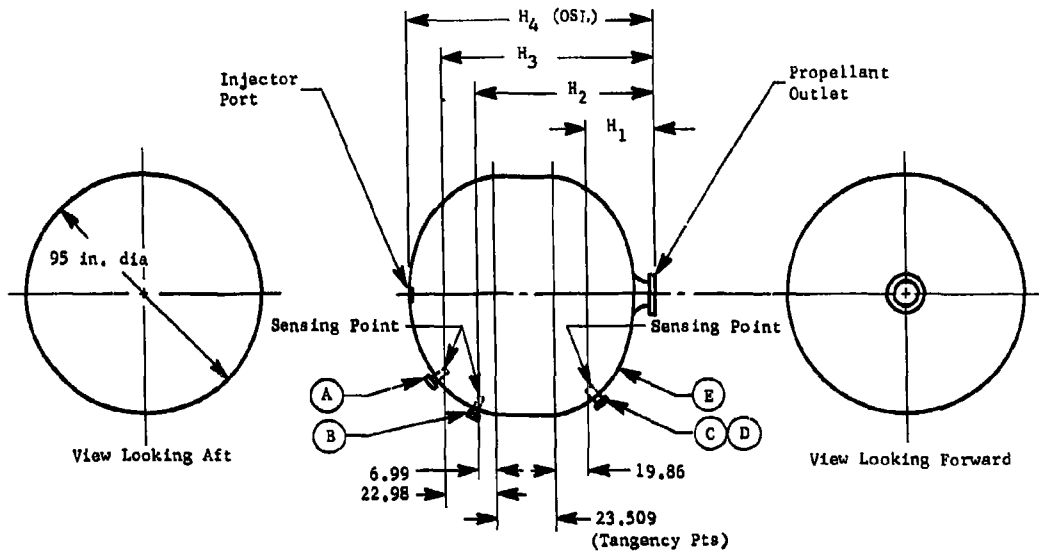


Fig. III-34 Phase III Tankage

Ports in the upper dome of each of the propellant tanks were provided as follows:

Vent and Relief Port - 3-in. dia Marman flange

Common Ullage Line - 3-in. dia Marman flange

Injector Port - 12 tube size AN fitting

Prepressurization Port - 8 tube size AN fitting

Level Sensors

5% Ullage - 1.5-in. conoseal flanges

22% Ullage - 1.5-in. conoseal flanges

Pressure Switches

Injector Switch - 4 tube size AN fitting

Vent and Relief Switch - 4 tube size AN fitting

Instrumentation Ports

Tank Pressure - 4 tube size AN fitting

Tank Temperature - thermocouple fitting

The lower dome of the tanks used standard 4-in. ASA 150 lb raised-face flanges for propellant outlets and 1.5-in. conoseal flanges for mounting of low level sensors. The oxidizer outlet was contoured for drop out and cavitation elimination while the fuel tank outlet was not. In addition, each tank had support skirts fusion welded to the tank structure to provide a mounting surface for handling rings that were used for both handling and mounting of the propellant tanks. Baffles were provided in each of the tanks to prevent vortexing. Figure III-29 shows the baffle used in the oxidizer tank.

Injection System - The injectors were made from commercially available #24 AUA-8980 chemical spray guns manufactured by Spraying Systems Company. A picture of an injector as used in Phase III testing is shown in Fig. III-25. Modification involved putting on extension tubes and operating rods to move the spraying tips further away from the operating heads and provision of a reagent

supply tube welded on near the spray tip. The pneumatic operating heads containing a teflon piston and spring were not modified. The orifice retaining nuts on the spraying tips were modified by welding the retaining nut to a -12 male AN fitting to enable the injector to be mounted in the tank by screwing it into a -12 female AN fitting.

Control of the injectors was provided by a pressure switch mounted on each tank skirt controlling an injector control valve, a $\frac{1}{2}$ -in. solenoid valve. The fuel tank injector pressure switch is shown at the top of Fig. III-33 (small cylindrical object).

Reagent Supply System - The reagent supply system for each of the two injectors was the same except for the reagent used in each. Supply to the injector was through $\frac{1}{2}$ -in. tubing and a $\frac{1}{2}$ -in. reagent shutoff valve. Filling of the reagent tank was accomplished through a $\frac{1}{2}$ -in. tube and hand valve "T'd" into the reagent supply line. The reagent tanks were 0.523-cu ft spheres with 0.080-in. walls. Three tabs welded to the tanks around a diameter were provided so the tanks could be suspended from a load cell by wire rope. A picture of the reagent tank, load cell, support frame, and associated plumbing used in the fuel tank test is shown in Fig. III-23. Vent and relief functions were provided by a pressure switch and solenoid valve. Pressurization of each reagent tank was through a regulator and tubing "T'd" into the vent and relief line.

Common Ullage System - Before completion of Phase I testing, a 3-in. dia aluminum common ullage line joining the forward tank domes was fabricated and planned for usage with a 3-in. dia Calmec isolation valve on the Phase III system. Development of the common ullage concept during Phase I testing revealed that a smaller diameter line was required in order to maintain a higher common ullage gas velocity and also to introduce the gas below the oxidizer tank liquid surface. Consequently, a 2-in. dia stainless steel common ullage line was fabricated to be used with a $1\frac{1}{2}$ -in. dia Annin isolation valve. In order to introduce gas below the oxidizer tank liquid surface a subsurface gas injector was fabricated as shown in Fig. III-29. The subsurface gas injector was an elbow welded into a spool in the propellant outlet line so that the common ullage line ran concentrically up the propellant outflow line and ended in a gas diffuser mounted in the center of the baffle. Figure III-28 shows how the spool piece containing the subsurface gas injector fits between the two flanges provided initially for the sight-glass. The upper diffuser support disc also provides an injector splash plate for use with the direct reagent injection system. When the test system was changed to dual reagent injection the common ullage line was set aside for possible future use and the common ullage ports on each tank were capped.

Pressure Relief System - A separate vent system was used for each tank, fabricated from 3-in. dia aluminum tubing as shown in Fig. III-24. The pressure relief system for each tank was connected to a 3-in. dia Marman flange on the propellant tank, ran vertically about 12-in. to an elbow, and attached to a 3-in. dia Calmec vent and relief valve through 14-in. of bellows. The facility plumbing consisted of a horizontal section of pipe 8 ft long connecting the existing lines on the second floor of Cell 6 and up to the Cell 7 vent and relief package and vent stack on the third floor. When the test system was changed to a bi-injection system, the relief valve requirement was changed to one per tank.

Relief valve pressure switches were obtained from surplus, modified to act as gage pressure switches and adjusted to the actuation pressures required. The pressure switches, mounted on the skirt of each tank as shown on the fuel tank in Fig. III-24 (lower left on skirt), sensing tank pressure through a $\frac{1}{4}$ -in. tube, controlled the pneumatically operated vent and relief valve through a relay and pilot solenoid valve integral with the vent and relief valve. Surplus Calmec liquid oxygen vent and relief valves (PD47S00128) were obtained from surplus and modified for storable propellant usage. Brass main shaft bushings were replaced with aluminum bushings and the automatic vent feature of the valve was blocked off.

IV. PHASE III PROGRAM

The Phase III program encompasses the development testing of a full scale, flight weight, low pressure MTI Pressurization System, the design and fabrication of which was accomplished in Phase II. The overall objectives of the Phase III program are to demonstrate the feasibility of the MTI system in flight-weight tanks; to accumulate data to show reliability, repeatability, and performance; and to provide design data for future system development. The following paragraphs describe the system configuration and the development and demonstration tests conducted.

A. SYSTEM CONFIGURATION

The test system was assembled at the Cold Flow Laboratory Titan II Systems Test area on the east side of the systems test stand. The two propellant tanks were mounted side by side with a sand-filled blast shield between them. The propellant tank support frames were mounted on the blast shield support structure, which also contained a fuel catch basin and oxidizer spill trough. The whole test assembly was mounted on steel gratings over a concrete propellant catch pit. Outflow lines from the propellant tanks ran in opposite directions to stainless steel catch tanks mounted approximately 15 ft below the propellant tanks. Figure III-21 shows the general arrangement of the test system.

1. Test Article

The pressurization system tested was the dual-reagent injection system described in Chapter III.B.2. Because of the hazardous nature of the full-scale system test program, each of the 2000-gal. propellant tanks were tested separately. Capability was provided for helium initial pressurization of the 5% ullage volume. Both fuel and oxidizer systems were essentially identical, each having a similar pressure relief, injection, and control system configuration. Propellant expulsion rates were controlled remotely during the nominal 150-sec test, with pressurization maintained at 36 psia by a solid-stream surface, reagent-injection system. A complete propellant expulsion was accomplished by discharging the residual propellant by a polytropic gas expansion process after injection termination.

The injection system was a pressure switch-controlled, pulse-type system with a pneumatically operated injector. The reagent was supplied from a gas-pressurized tank, which was instrumented for the determination of reagent consumption. Capability was provided for shutoff or dump of the reagent in the event of an injector malfunction. Performance tests were completed with variable propellant outflow, restart, and continuous operation to demonstrate complete system capability.

2. Control Console

The control console used for Phase III testing was located in the Cold Flow Laboratory blockhouse approximately 100 yd from the test area. It provided remote control for all test phases, including propellant loading, pretest pressurization, and automatic test sequencing. Reagent loading, performed on the test article, was not included in the remote-controlled capability of the test console. Important control and operating parameters were monitored by gages and direct-readout recorders while a light indication was provided for important valve positions. Visual coverage was provided by two remote-controlled television cameras. The console provided malfunction detection capability, with automatic shutdown in case of over-pressurization and manual shutdown in the event of control irregularities. The entire system has been designed, as much as possible, to be fail-safe during any part of the test operation. The control console is shown in Fig. IV-1.

3. Instrumentation

Data taken during Phase III testing were recorded by two Sanborn six-channel recorders, five Bristol single-channel recorders, eight Dynac single-channel recorders, and one 78 channel Brush event recorder. Parameters recorded, ranges, symbols, and transducers used are tabulated in Table IV-1. Figures IV-2 and IV-3 give the location of transducers on the Phase III system.

Pressures were measured with Data Sensor and Tabor pressure transducers. Propellant tank pressure and reagent-injection pressure were of primary importance. Propellant tank gas temperature was measured with a chromel-constantan shielded thermocouple mounted so it protruded approximately 1 in. inside the upper dome wall. Three unshielded chromel-constantan thermocouples were spot-welded to the outside of the tank upper dome to measure tank wall temperatures at a location of varying skin thickness. Propellant temperature was recorded 23 in. below the tank outlet in the outflow line to establish the condition of the discharged propellant.

RTD-TDR-63-1123

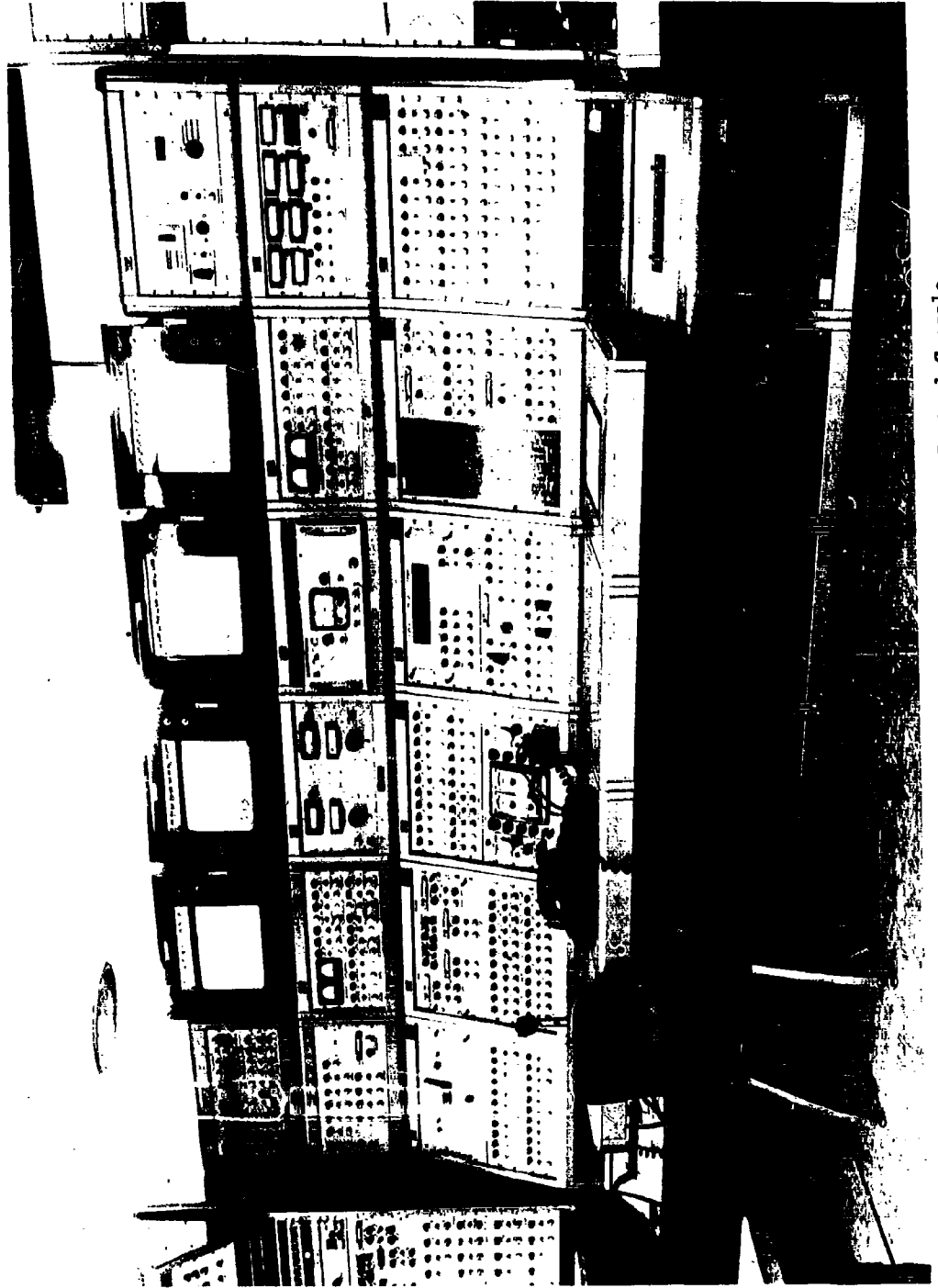


Fig. IV-1 Phase III M1 Pressurization System Control Console

Table IV-1 Phase III Instrumentation List

Symbol:	Measurement Description	Range	Recording Device	Data Accuracy
P _R	Pressure, Reagent	0-500 psig	Bristol	±2%
P _{gFT}	Pressure, Gas, Fuel Tank	0-50 psig	Bristol	±1%
P _{gOT}	Pressure, Gas, Oxidizer Tank	0-50 psig	Bristol	±1%
T _R	Temperature, Reagent	0-100°F	Sanborn	±2%
T _{gFT}	Temperature, Gas, Fuel Tank	0-700°F	Bristol	±2%
T _{gOT}	Temperature, Gas, Oxidizer Tank	0-700°F	Bristol	±2%
T _{wFT₁}	Temperature, Wall, Fuel Tank (3 places)	0-400°F	Sanborn	±2%
T _{wOT₁}	Temperature, Wall, Oxidizer Tank (3 places)	0-400°F	Sanborn	±2%
T _{F0}	Temperature, Fuel, at Outlet	0-150°F	Sanborn	±2%
T _{O0}	Temperature, Oxidizer at Outlet	0-150°F	Sanborn	±2%
W _R	Weight Reagent Tank	0-50 lb	Bristol	±1%
M _{DFO}	Mass Flow Rate, Fuel	0-8000 gpm	Dynac	±1%
M _{D00}	Mass Flow Rate, Oxidizer	0-800 gpm	Dynac	±1%

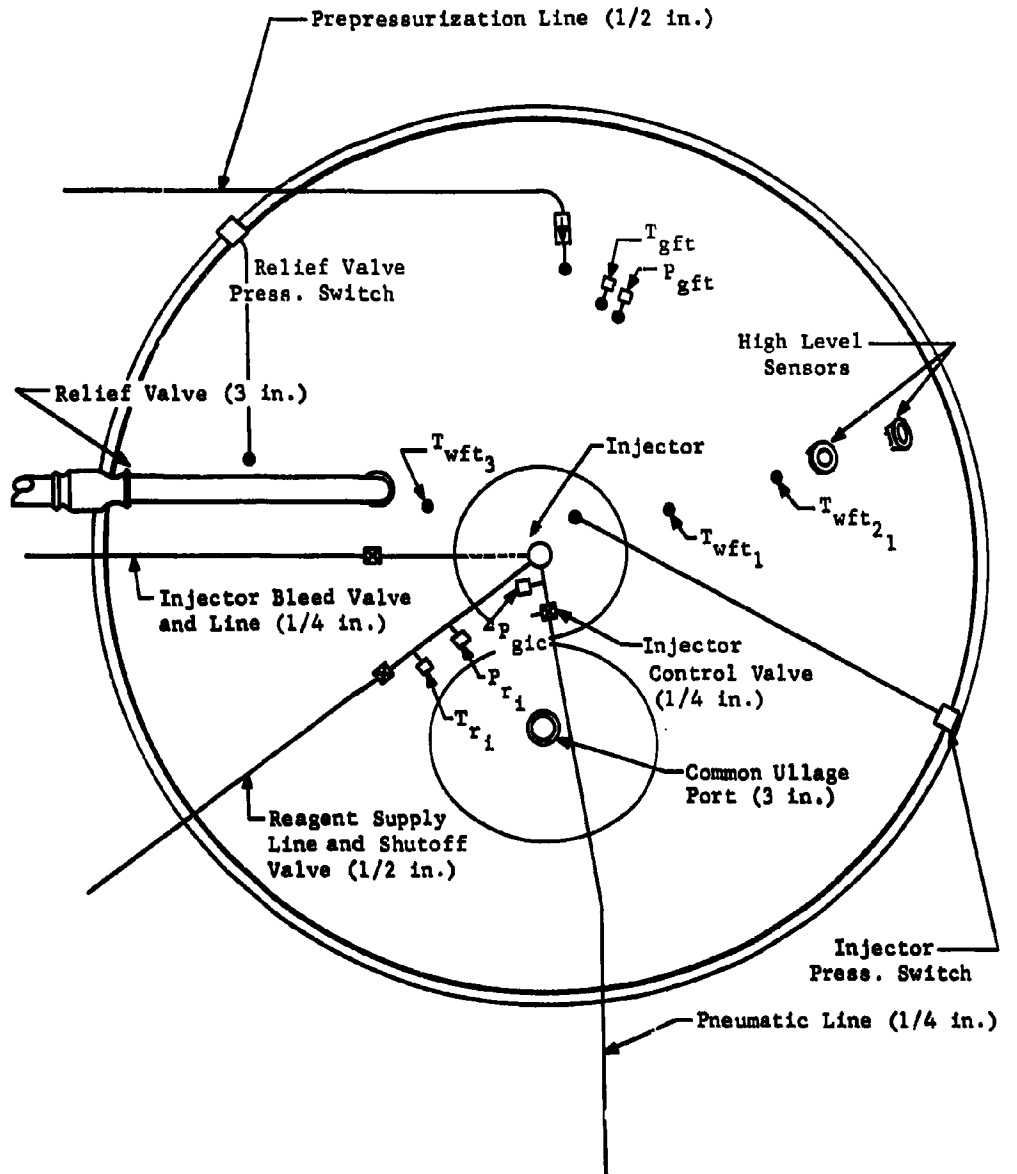


Fig. IV-2 Instrumentation Location Phase III Tank Plan (Top) View

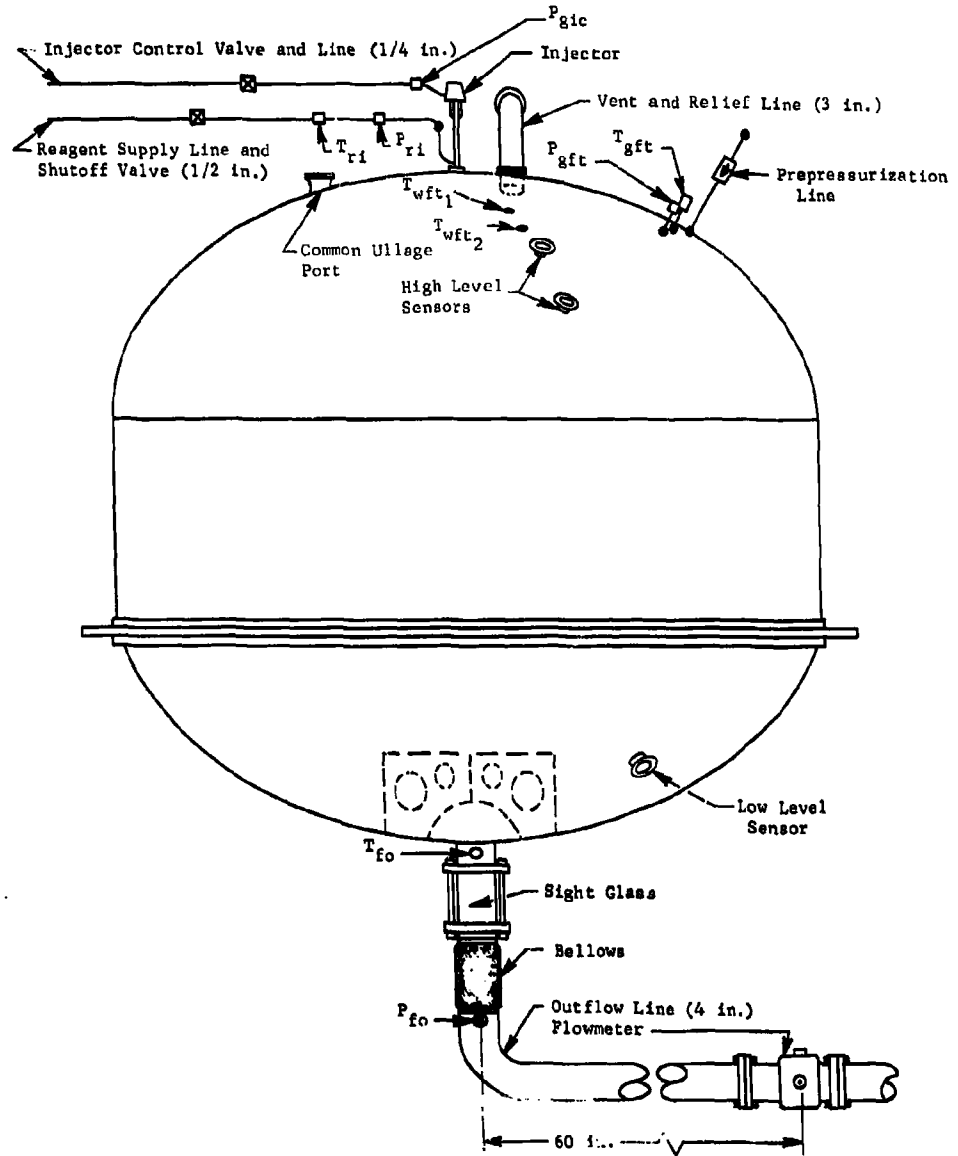


Fig. IV-3 Instrumentation Locations, Phase III Fuel Tank-Side View

Potter turbine -- type flowmeters, used for flow measurements, were connected to digital direct readout Dynac recorders. Reagent usage was measured and recorded by suspending the reagent tank from a Baldwin-Lima-Hamilton 50-lb load cell connected to a Bristol direct-inking recorder. The load cell-tank suspension arrangement is shown in Fig. III-23.

Combustion gas composition data were obtained with a simple gas-sampling apparatus similar to that used on the Phase I test article. Analysis of the gas samples was accomplished at the National Bureau of Standards Laboratories in Boulder, Colorado, using a mass spectrometer.

B. DEMONSTRATION TEST SERIES

A reduction in the planned developmental effort on the Phase III MTI Pressurization System was realized because of the initial success of the system that evolved from an extensive Phase I experimental program. Consequently, a single verification test of the complete system was performed before initiation of the demonstration test program. The development and functional testing of the individual components and subsystems, however, required a significant effort because of the changes in subsystem design and test technique of the larger system. A summary of the developmental work performed is contained in the following paragraphs.

1. Component Tests

These tests were to verify adequate strength, actuating response, and leakage of the individual components before their installation into various subsystems. In some cases, namely the injector and pressure switches, some development effort was required to achieve the desired adjustment or level of performance. A parts list giving component make, model number, and size is given in Table III-6.

Solenoid Valves - Solenoid valves tested were for prepressurization, injector control, and reagent control. They were proof-tested to 750 psig and tested for leakage using soap bubbles with GN_2 at 500 psig applied to the inlet port. Allowable leakage was 10 SCCM from outlet port and no visible leakage externally. Actuation of the valve was to be smooth, with no evidence of hanging up or excessive electrical requirements. Each of the solenoid valves passed the tests successfully.

Check Valves - Check valves to be used in the prepressurization lines were tested for proof pressure at 750 psig. External leakage was checked using GN₂ at 30 psig applied to the inlet port. No visible leakage was allowed using soap bubbles. Reverse flow leakage was checked using GN₂ at 24 psig applied to the inlet port. A maximum of 10 SCCM reverse flow leakage was allowed. Cracking and reseal pressure was to be less than 3 psig. Both check valves successfully passed the test requirements.

Vent and Relief Valves - Vent and relief valves were tested following modification as described in Chap III.C.5. Tests conducted and results are tabulated in Table IV-2.

Table IV-2 Phase III Vent and Relief Valve Test Results

Test Applied	Results		
	Item tested		
	PD47S0128	PD47S0128	PD47S0128
Leakage at outlet port with GN ₂ pressure applied to 3-in. inlet port	S/N DI 100 SCCM at 10 psig	S/N 0000113 7000 SCCM at 25 psig	S/N0000161 10,000 SCCM at 25 psig
Actuation, closed to open and open to closed several times	Smooth	Smooth	Smooth
Position switch actuation when valve actuated	Good	Good	Closed position good; open position bad
Pilot solenoid operation and current draw at 28v dc	Good (0.5 amp)	Good (0.5 amp)	No good

Reagent Storage Tank - The reagent storage tank was proof pressure tested at 750 psig, leak checked at 650 psig, and was found to be satisfactory following repair of a small leak near the top fitting. Leak testing was performed by pressurizing to 650 psig with water and monitoring tank pressure for 2 minutes. No pressure was observed.

Pressure Switches - Pressure switches, except injector control pressure switches, were checked for leakage and actuation pressures using a Wallace and Tiernan 0 to 40 psi, two-turn pressure gage. Because the same injector pressure switches were used for both Phase I and Phase III, no additional checkout was required. No leakage was observed on any of the pressure switches. Actuation pressures are listed in Table IV-3.

Table IV-3 Phase III Pressure Switch Test Results

Switch	Pressure	
	Increasing	Decreasing
Relief Valve Pressure Switches		
PD71S0066-023 S/N 042	27.25 psig	27.74 psig
PD71S0066-023 S/N 065	26.60 psig	26.11 psig
PD71S0066-015 S/N 006*	26.65 psig	26.35 psig
PD71S0066-015 S/N 007*	26.64 psig	26.22 psig
Injector Control Pressure Switches		
PD71S0067-001 S/N	26.0 psig	25.5 psig
PD71S0067-001 S/N		
Differential Pressure Switch		
Spiedel No. 145-D S/N 101	0.65 psid	0.35 psid
*Not Used		

Injector - The injector was rebuilt following completion of the Phase I experimental program. It was used to develop an injector orifice that would provide a good solid stream of liquid when operated at various supply pressures. Phase I testing demonstrated the importance of injecting a solid stream of reagent rather than a spray. Consequently, additional effort was devoted to development of such an orifice. Testing consisted of flowing water at various pressures through the injector and observing the resulting spray pattern.

The initial tests were performed with a scaled up version of the 0.013-in. dia orifice used in Phase I testing as it had provided a good solid stream of liquid. Injector tips were machined with 0.040-in. dia orifices having different L/D ratios as shown in Fig. II-53. The lower L/D ratio appeared to improve the spray pattern but it was not satisfactory. Other configurations, as shown in Fig. II-53, were tried with little success. Finally, a 0.047-in. dia injector tube was made with an extremely large L/D ratio (64) and tested. It showed considerably better results, so another was made and a series of tests performed. They showed a lowering of the L/D ratio each time until the configuration shown in Fig. III-26 was obtained (L/D = 64). The solid stream provided was much better than any other orifice tested, so it was selected for the Phase III system. Following the orifice tests, the injector was cleaned and a new actuating rod lapped to the new orifice. The injector was leak checked with GN_2 and soap bubbles, with no visible leakage. A second injector, identical to the first and used in the Phase I oxidizer tank, was rebuilt, tested, and found to be satisfactory for Phase III oxidizer tank tests.

2. Subsystem Tests

Tests were made on each of the subsystems to verify their proper operation before final connection and integration into a complete test system. A verification of injection system operation was particularly important because of the increase in size and distance of the reagent supply from the test article over the Phase I configuration. The demonstration of proper subsystem operation also provided a calibration of both the reagent injection and propellant control systems before an MTI-pressurized propellant expulsion. The subsystem tests described in the following sections were divided into three main areas: injection system, pressure control system, and propellant system.

Injection Subsystem - The injection subsystem was tested by filling the reagent storage tank, pressurizing it, and flowing reagent through the injector with the injector mounted outside the propellant tank. The tests were made to verify the system flow capacity, reagent control valve operation, and injector operation. The load cell measuring reagent usage was also calibrated to assure a 2% accuracy. Following modifications to the fuel tank injector supply line to eliminate excessive pressure drop, the injection subsystem was considered satisfactory for use.

3. System Tests

The MTI Pressurization System development tests were conducted at the Martin Cold Flow Laboratory Titan II Systems Test Area. Tests were run to demonstrate the feasibility of the MTI technique for flight weight propellant tank pressurization and to accumulate sufficient data to establish performance, repeatability, and feasibility. The tests were also to provide guidelines for future missile applications. Five tests were performed on the fuel tank during June 1963, and two tests were run on the oxidizer tank. Fuel tank tests were in two categories, including one nitrogen and four MTI pressurized propellant expulsions. Because of the independent nature of the fuel and oxidizer tank systems when using the bi-injection technique, it was possible to test each tank separately. The following paragraphs describe the complete system tests conducted and the results obtained. The description of tests conducted is given with no specific reference to either fuel or oxidizer because the same tests were run separately on each tank.

Inert Pressurization - Inert pressurization tests were conducted using GN_2 supplied through the prepressurization lines to check the operation and capability of the complete system before a hot test. The reagent tank was not filled, and the reagent shutoff valve remained closed. Before filling the propellant tank, a functional check of the system was made by actuating all valves and the injector from the test console, and checking their operation on the test article. The propellant tank was then filled with propellant, checked for leaks, and pressurized to operating pressure. The outflow modulating valve (butterfly valve) was set at a position corresponding approximately to design outflow rate. The outflow shutoff valve (ball valve) was opened and outflow rate adjusted to design flow rate by adjusting the modulation valve. Flow commenced until the low level sensor signalled the shutoff timer to start. Then a check was made to determine if the injector control valve was signalled by the low level sensor to close. Following the preset interval, the shutoff time caused the outflow shutoff valve to close. Pressure was vented from the tank; the outflow shutoff valve reopened, and the residual propellant was drained from the tank into the catch tank.

Fuel Tank Results - Fuel tank pressure was set at 32 psia before the test (Test 1). Fuel outflow rate was held at 610 to 620 gpm for 163 sec. The low level sensor then started the timer

Pressure Control Subsystem - The pressure control subsystem was tested by pressurizing each propellant tank with nitrogen to various levels to verify actuation of the vent and relief valves, injector control valve, and proper functioning of the prepressurization system. The helium prepressurization system was used to pressurize the propellant tanks individually. Pressure in the propellant tank was increased until the injector pressure switch opened, causing the injector control valve to close. The pressure was then decreased until the injector pressure switch caused the injector control valve to open. This was done to determine if the injector control valve closing point was within 36 ± 1 psia and if the dead band between open and closing points was 0.5 psi maximum. Pressure was then increased until the relief valve pressure switch opened, causing the relief valve to open. The tank pressure decayed through the open relief valve. When the valve closed the pressure was noted. The pressure at which the relief valve opened was 38.5 ± 0.5 psia with the dead band between open and closing points of 0.5 psi maximum. Actuating pressures for the fuel tank were:

Injector control: open -37.3 psia, closed -37.8 psia;

Relief valve: open -39.3 psia, closed -38.8 psia.

The injector control actuating pressures were 0.8 psia higher than anticipated but were considered satisfactory.

Propellant Subsystem - The propellant tank was partially filled, and the outflow control system was checked for proper operation by flowing propellant out of the tank into the catch tank. Outflow control valve operation and visual observation through the propellant tank outflow line sight-glass were checked. It was found that a television camera viewing the outflow sight-glass gave a clear indication anytime there were bubbles in the fuel tank. The sight-glass was omitted from the oxidizer tank with the installation of the common ullage configuration.

A check for leakage was performed by filling and pressurizing the tank to 26 psig. Several leaking huck bolts were found on the top dome along with leaking sight-glass flanges and a patch leak on the tank barrel section. All except the patch leak and about three huck bolt leaks were completely stopped. Pressure decay data were taken before each MTI test run so test data could be corrected to account for leakage. The level sensors were checked and found to be functioning properly.

and signalled the injector control valve to close. Six sec later the time caused outflow to stop. The tank pressure was vented, and the residual propellants were drained from the tank. No cavitation or vapor entrainment was observed during the test in the outflow sight glass. No discrepancies were observed in the test system during the inert pressurization outflow test, verifying that the fuel tank system was ready for MTI tests.

Oxidizer Tank Results - The inert pressurized propellant expulsion was not required for the oxidizer tank, because system verification was achieved during prepressurization in the initial MTI tests.

MTI Pressurization Tests - MTI pressurization tests were conducted with the complete system assembled as described in Chapter IV-A. The fuel and oxidizer tanks were tested independently, however, identical test procedures were employed. A constant outflow test for approximately 150 sec and a restart test with variable propellant outflow and system shutdown for 10 min after 60 sec of constant pressure propellant expulsion were made. (The latter test was to simulate a vehicle coasting without propulsion.) Following the 10-min coast period the injector was returned to automatic control to repressurize the propellant tank before restarting propellant outflow. Run termination by use of the low level sensor and outflow shutoff timer was the same for both tests.

A functional test of the test system was made before loading propellant and after notifying safety personnel and obtaining test clearance from environmental control concerning weather conditions. The reagent tank was filled after verifying that the injector was closed. During filling, the reagent tank air was bled out of the injector through the reagent isolation and bleed valves. The reagent tank was then pressurized and the pressure was monitored to be sure the injector was not leaking. Following this determination, reagent tank pressure was vented and the test area was cleared of personnel except for two cell technicians. Propellant was loaded through the 2-in. dia propellant return line T'd into the 4-in. dia outflow line just below the propellant tank outlet. Rate and total propellant flow were monitored by the propellant return line flowmeter. Level sensors were used to confirm that propellant tanks were accurately loaded. Following propellant loading, an inspection was made for leakage. The outflow shutoff timer was set for 6-sec delay; the outflow modulating valve was opened to a position corresponding to the required flowrate, and the propellant tank was pressurized with helium to approximately 37.5 psia. Another leakage check was made by monitoring the propellant tank pressure decay. Pressure changes observed were recorded for use in adjusting test data.

The reagent tank was gradually repressurized while watching propellant tank pressure for any indication of reagent leaking through the injector. The reagent isolation valve was opened, and the reagent bleed valve was cycled to assure elimination of entrained vapor in the reagent supply system. The injector control switch was moved from closed to automatic position on the test console after verifying that propellant tank pressure was approximately 37.5 psia. At this point the system was ready for countdown.

During the countdown data recorders and cameras were turned on and the test was initiated by opening the propellant outflow shutoff valve. The injection system operated automatically to maintain propellant tank ullage pressure between 37 and 38 psia until injection was terminated by the low level sensor. Propellant outflow rate was monitored by Dynac digital recorder and adjusted manually by the Swartout Autronic System. Tank wall and gas temperatures were visually displayed by Bristol recorders to verify adequate temperature control. Television and photographic observation were provided for general system inspection and were specifically provided for detecting vapor entrainment in the propellant at the outflow sight-glass. Propellant tank overpressure protection was provided by the test console. In the event of a malfunction automatic corrective actions would have resulted in a shutdown.

Following outflow termination by the outflow shutoff timer, propellant tank pressure was vented and residual propellant drained slowly from the propellant tank. Propellant tank pressure was monitored during outflow to prevent tank implosion resulting from propellant draining and temperature reduction.

The reagent isolation valve was closed and the reagent tank drained and vented. Reagent was bled from the injector and a nitrogen purge initiated to clear the injector of reagent and fumes. The propellant tank was then purged with hot nitrogen by flowing it in through the propellant fill line. A propellant sample was obtained manually from the catch tank after each run. Propellant was stored between test runs in the catch tank by maintaining a 5 psig nitrogen blanket in the tank. After completion of the tests the propellant was stored briefly in the catch tank with dry ice on the dome to prevent boiloff and subsequently returned to the facility for reuse at the direction of Edwards Air Force Base since the propellants were still within specifications.

Fuel Tank Results - Four fuel tank MTI pressurization tests were conducted on 11 and 12 June 1963. Three of the tests were constant outflow runs and the fourth was a restart test in which propellant outflow and injection were shutoff for 10 min after 70 sec of operation. All four tests were completely successful. The first of the three 150-sec constant outflow runs was considered a development test to verify injection system capability and to allow adjustment of the reagent supply pressure and propellant flowrate. As a result of the initial success, the remaining two constant flow tests and the restart test were identified as demonstration tests in which the Martin Quality Control organization was responsible for data verification. The results of the four tests conducted on the fuel tanks are discussed in the following paragraphs.

Test data for the three constant flow runs (Tests 2, 3, and 4) are shown in Fig. IV-4 thru IV-12. No vapor entrainment in the propellant was observed in the outflow line and there was no noticeable vibration; however, a sound recording made of the combustion process indicated moderate detonations. Maximum propellant tank wall temperatures ranged from 228 to 266°F, the difference being caused by the initial ullage and the amount of sunlight incident on the tank dome. Test 2 (the initial MTI pressurization test) was with a 22% initial ullage, 620 gpm propellant outflow rate, and a 175 psig reagent injection pressure maximum wall temperature of 228°F. Tests 3 and 4 had a 5% ullage volume, 680 and 750 gpm propellant outflow rate, respectively, and a 100 psig reagent injection pressure indicating maximum temperatures of 246 and 366°F. The slight variation in wall temperature being due to differences in the amount of solar radiation as evidenced by the higher initial wall temperature for Test 4. As noted in the instrumentation section, wall temperatures were taken at three different locations on the tank dome. In each of the fuel tank tests all three of these dome temperatures were within 7°F. Temperature of the fuel tank gas (T_{gft}) was recorded to be approximately 50°F below tank wall temperature on each of the runs. This apparent divergence in tank temperatures has not been explained. The thermocouple was checked and calibrated before each run and rechecked against a bulb thermometer in air following the tests. Each check showed the thermocouple and readout equipment operated accurately. Temperature increase in the fuel at the tank outlet was a maximum of 7°F. Part of this variation was a decrease of 1 to 2°F during the run because of propellant stratification. The remaining variation reflected an increase due to heating from the MTI reaction.

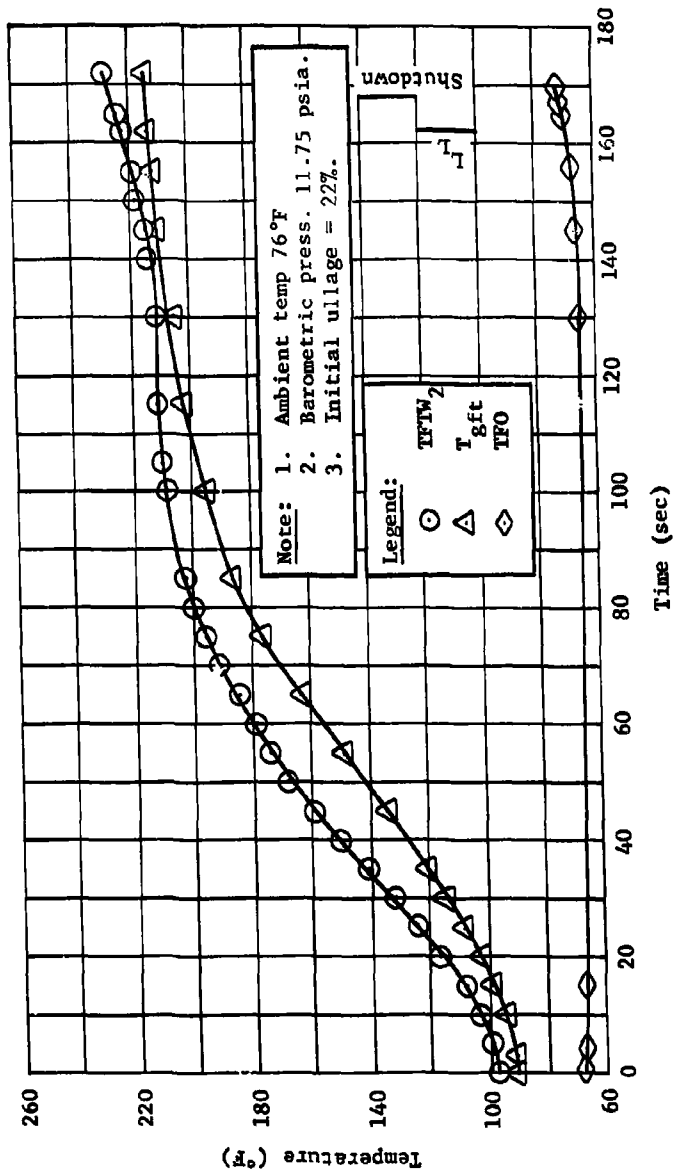


Fig. IV-4 Run 2 Phase III Fuel Tank System Temperatures

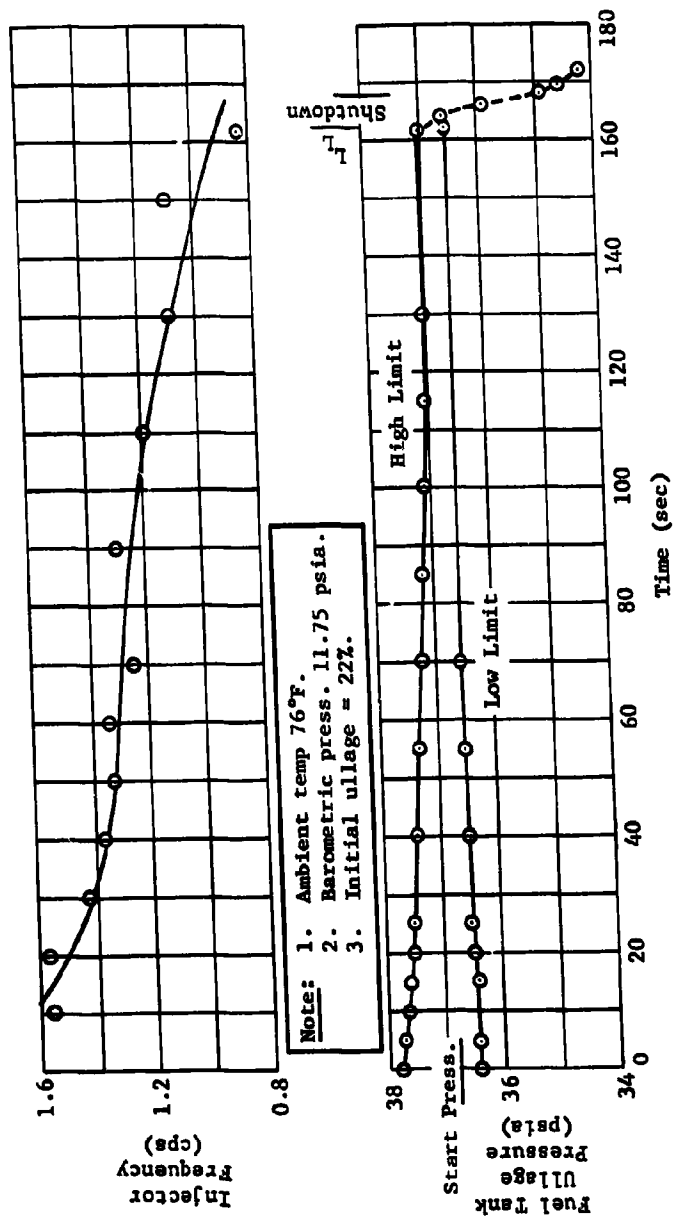


Fig. IV-5 Run 2 Phase III Fuel Tank Injector Performance

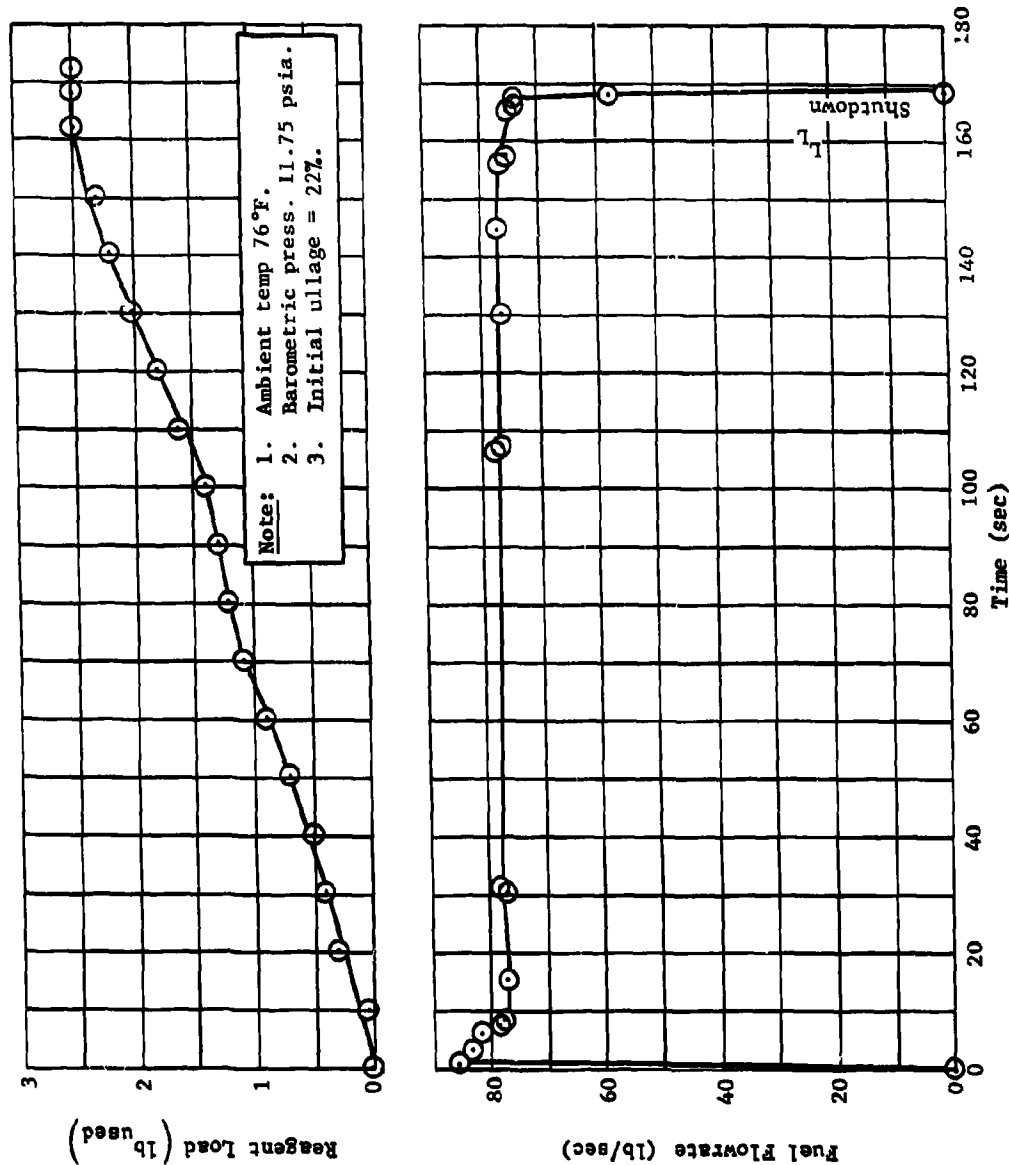


Fig. IV-6 Run 2 Phase III Fuel Tank Pressurization and Propellant Flowrates

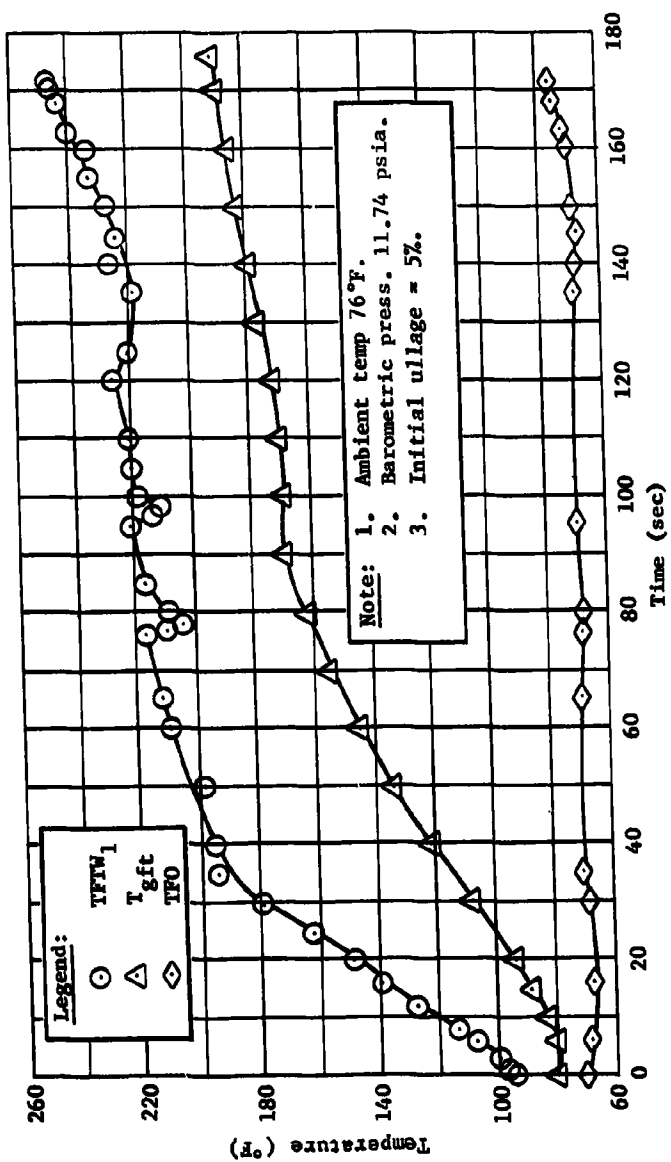


Fig. IV-7 Run 3 Phase III Fuel Tank System Temperatures

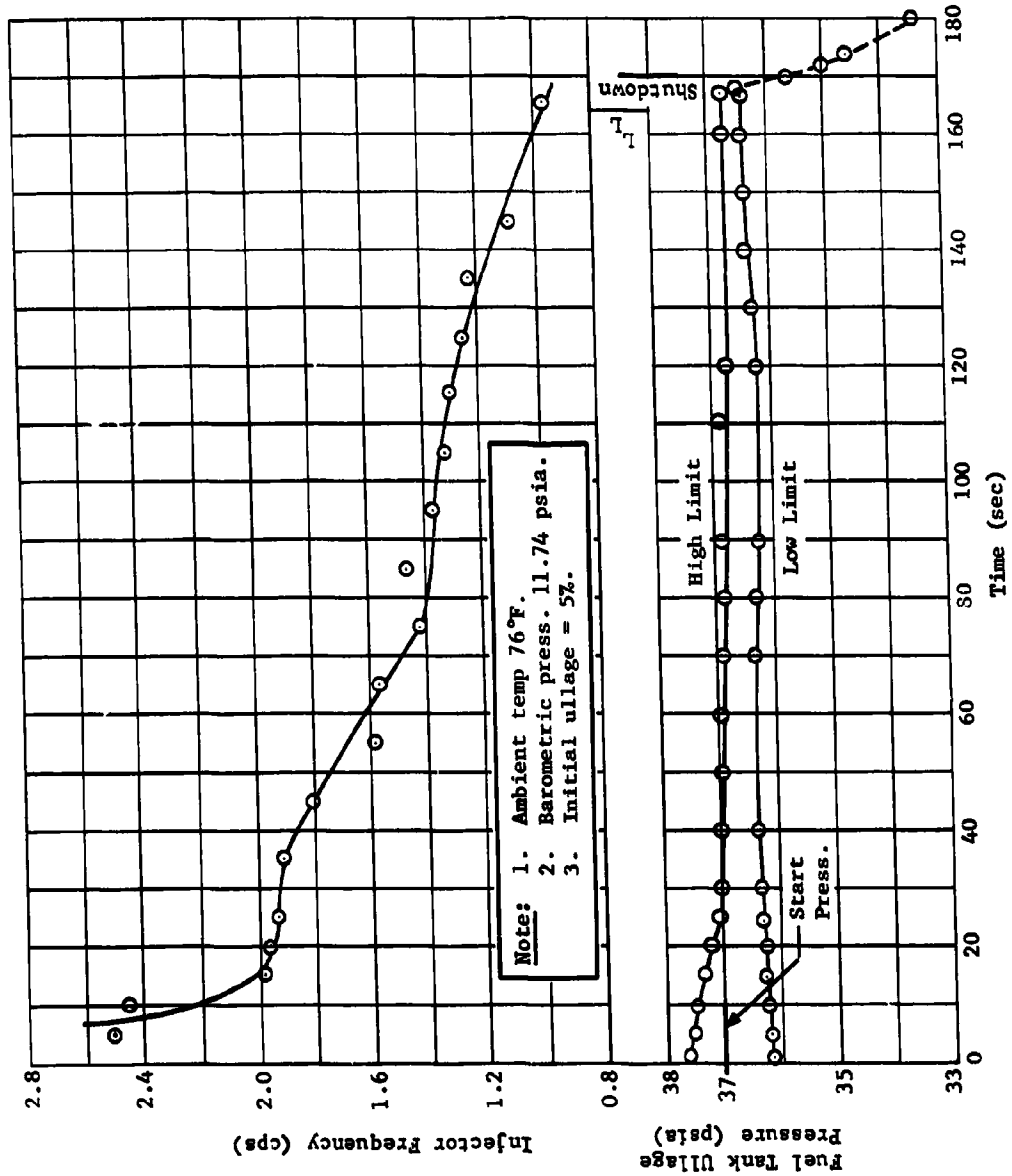


Fig. IV-8 Run 3 Phase III Fuel Tank Injector Performance

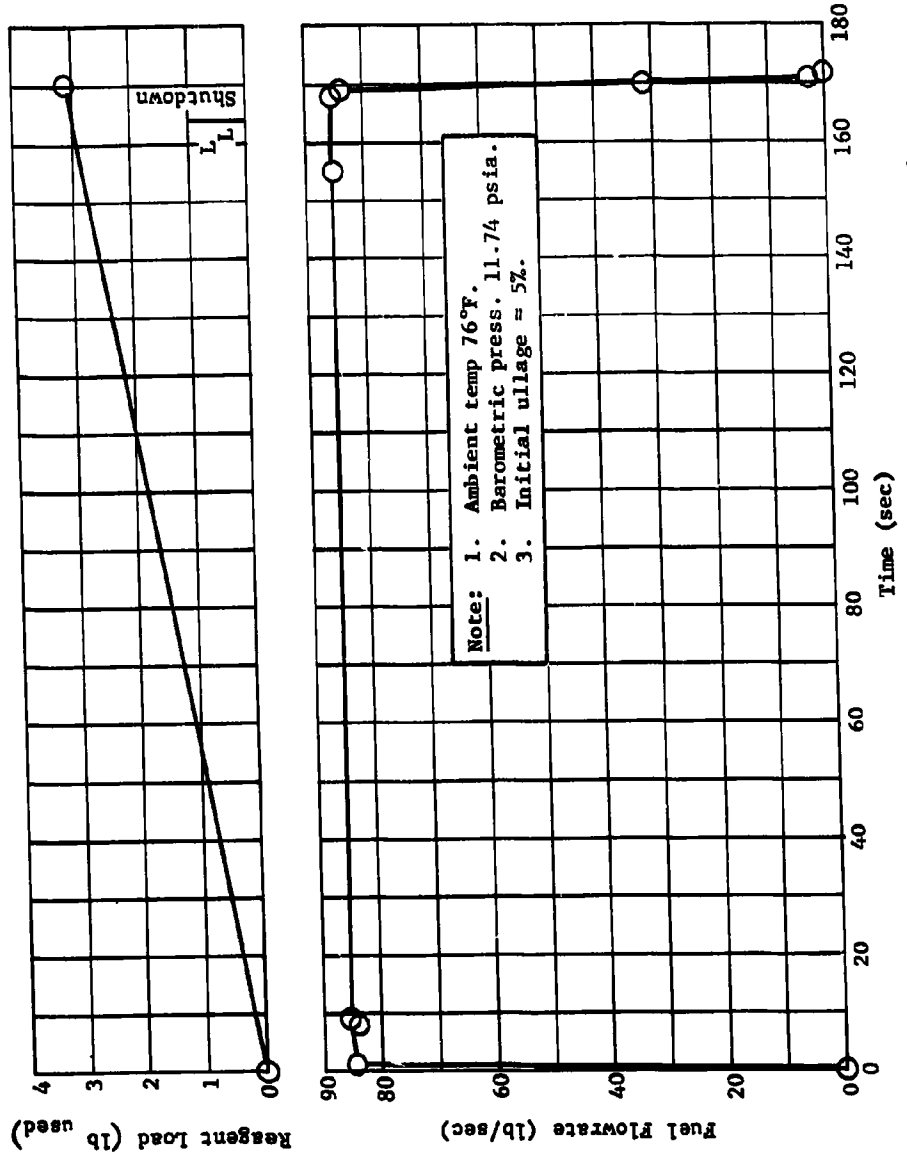


Fig. IV-9 Run 3 Phase III Fuel Tank Pressurization and Propellant Flowrates

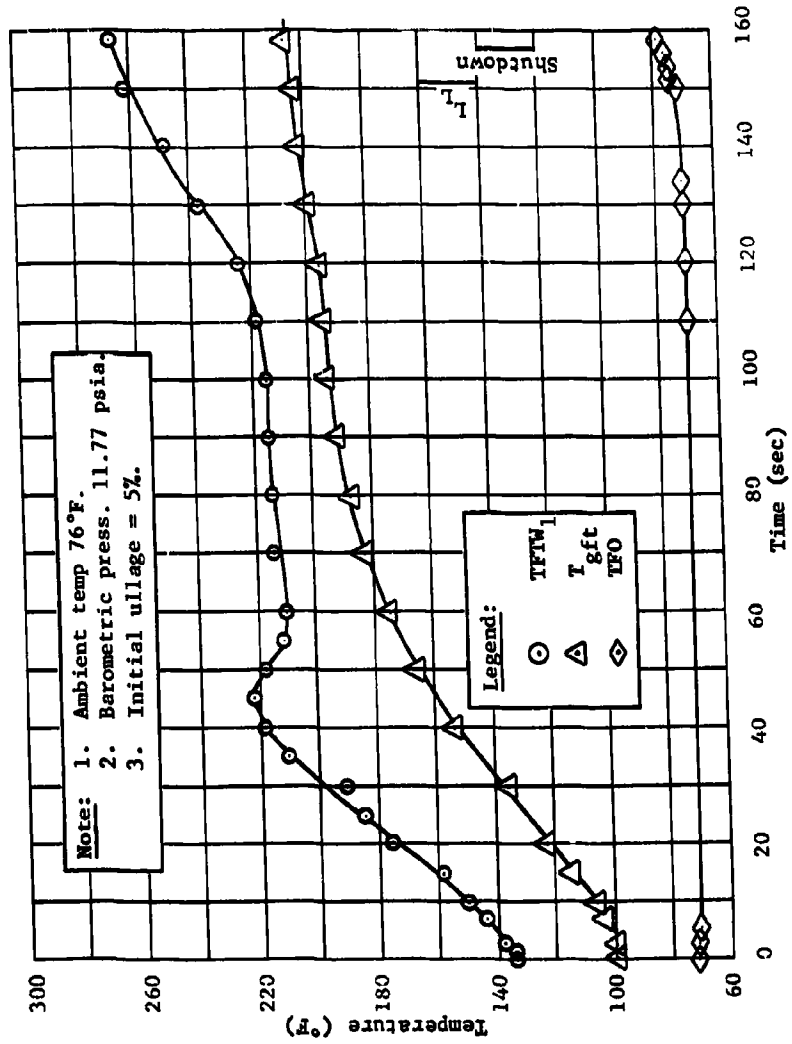


Fig. IV-10 Run 4 Phase III Fuel Tank System Temperatures

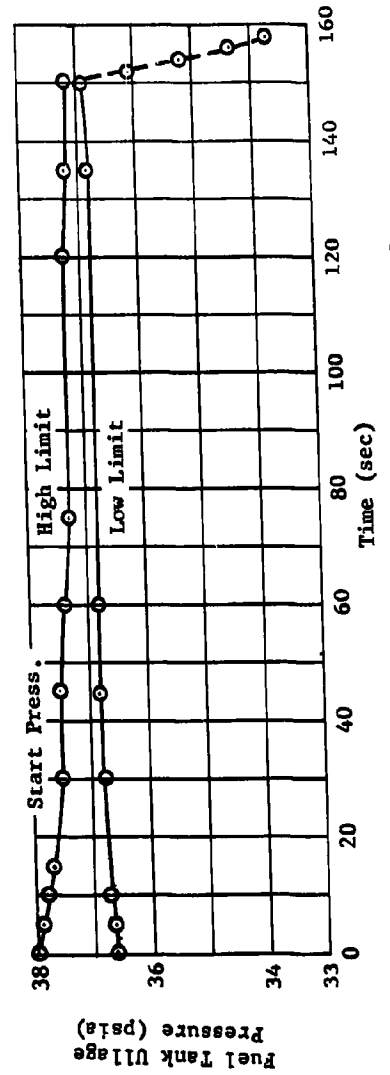
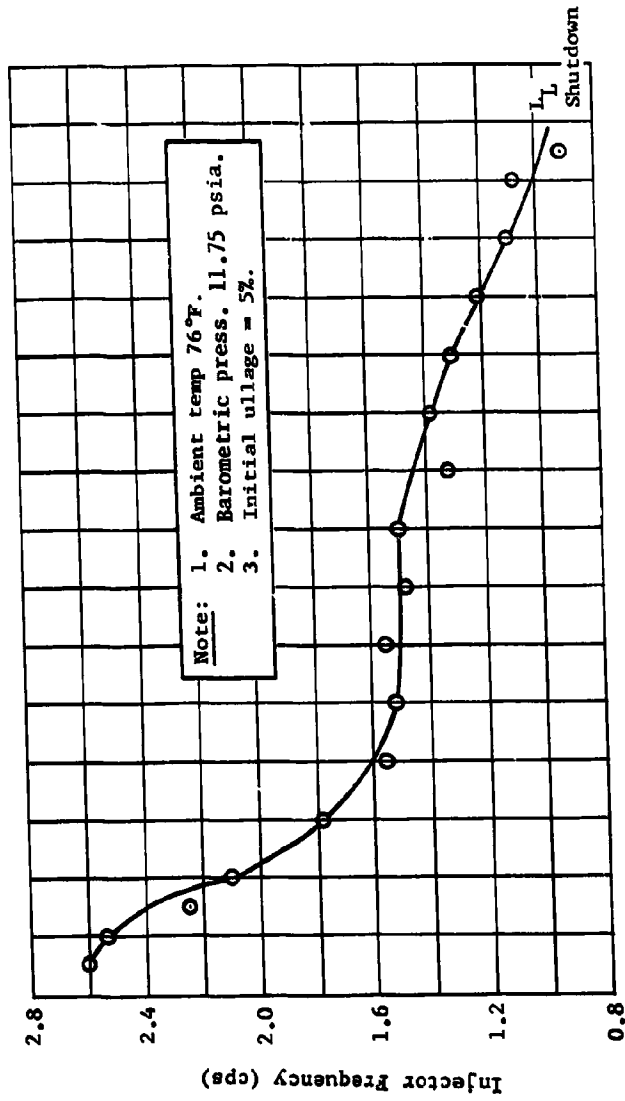


Fig. IV-11 Run 4 Phase III Fuel Tank Injector Performance

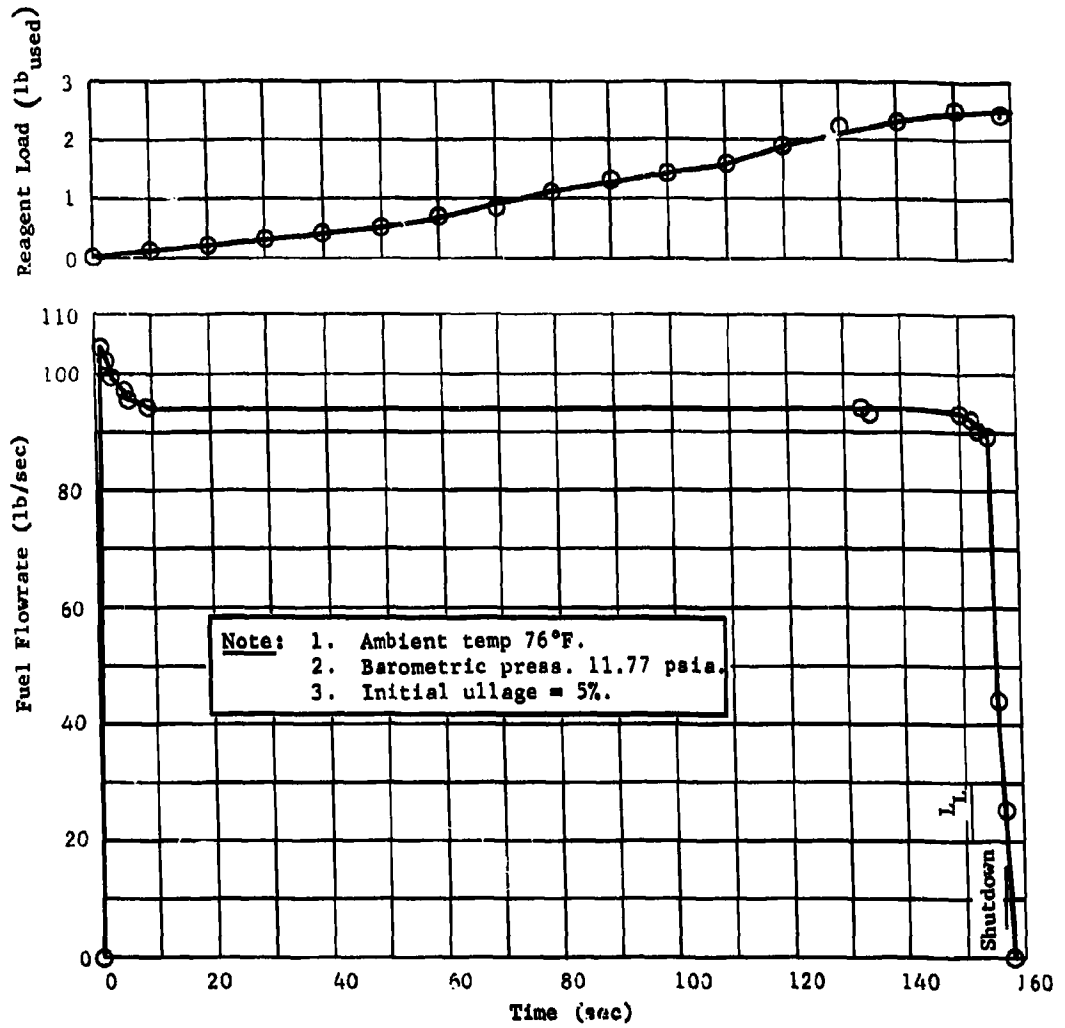


Fig. IV-12 Run 4 Phase III Fuel Tank Pressurization and Propellant Flowrates

Because of the close tolerance between injector operating pressure and relief valve actuation pressure, injector operation would commence when the system was in the automatic mode. This occurred because the amount of prepressurization was generally within the operating pressure control range because of minor system gas leakage. Leakage from the propellant tank was checked before each test run and was found to be between 0.048 psi/sec to 0.12 psi/sec at 38 psia tank pressure when prepressurized with helium. Pressure control at the start of each test was within +1.0 psi and -0.4 psi maximum with variation decreasing during each run as ullage volume increased. Pressure control is indicated in Fig. IV-5, IV-8, and IV-11 by a high and low limit envelope of the pressure trace. At no time during the tests did an uncontrolled pressure surge occur in the fuel tank. A sketch of a typical pressure cycle during the first few seconds of a test is shown in Fig. IV-13. Reagent injection pressure was 175 psig decaying to 146 psig for Run 2, 93 psig for Run 3, and 84 psig for Run 4. Injection pressure was reduced because of the lower than anticipated reagent usage.

Reagent consumption was 2.6 to 3.2 lb as determined by the reagent tank load cell. This measurement was also checked by manually integrating the injector control pressure traces to obtain injector on time and multiplying this time by the injector flowrate obtained from an injector calibration curve for the 0.047-in. dia nozzle. The result verified the load cell readings noted above. Injector cycling rate (Fig. IV-14) varied from a maximum of 2.5 cps to 0.8 cps; the maximum rate occurred at the start of each run, and decreased as the propellant was expelled because of the larger ullage.

The restart Test 5 was conducted in the same manner as the constant flow tests except that both outflow and injection were shut off for a period of 10 min after 65 sec of constant outflow. Propellant shutoff was controlled so that it occurred over a period of 9 sec rather than approximately 3 sec as in the previous tests. This was done to determine the effect on injector operation under throttling conditions. During the 10-min coast period tank temperatures and pressure were allowed to decay. Following the 10-min coast period the injector was returned to automatic control to repressurize the propellant tank after which outflow was re-established.

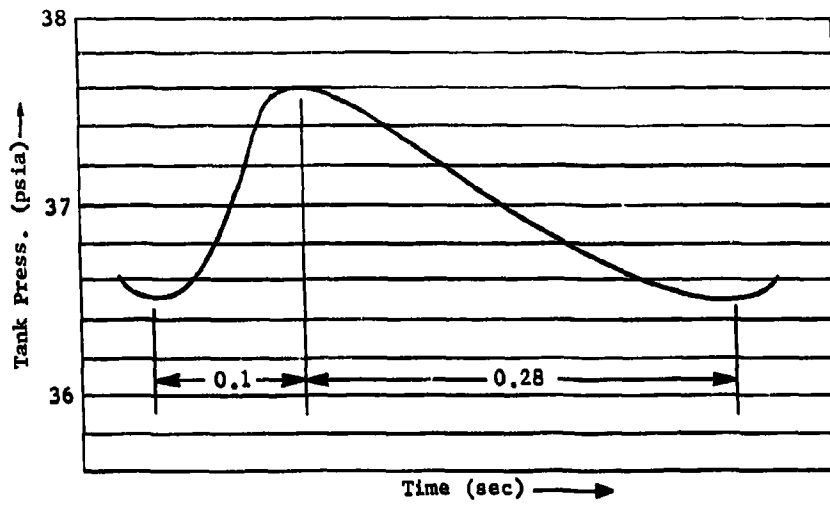
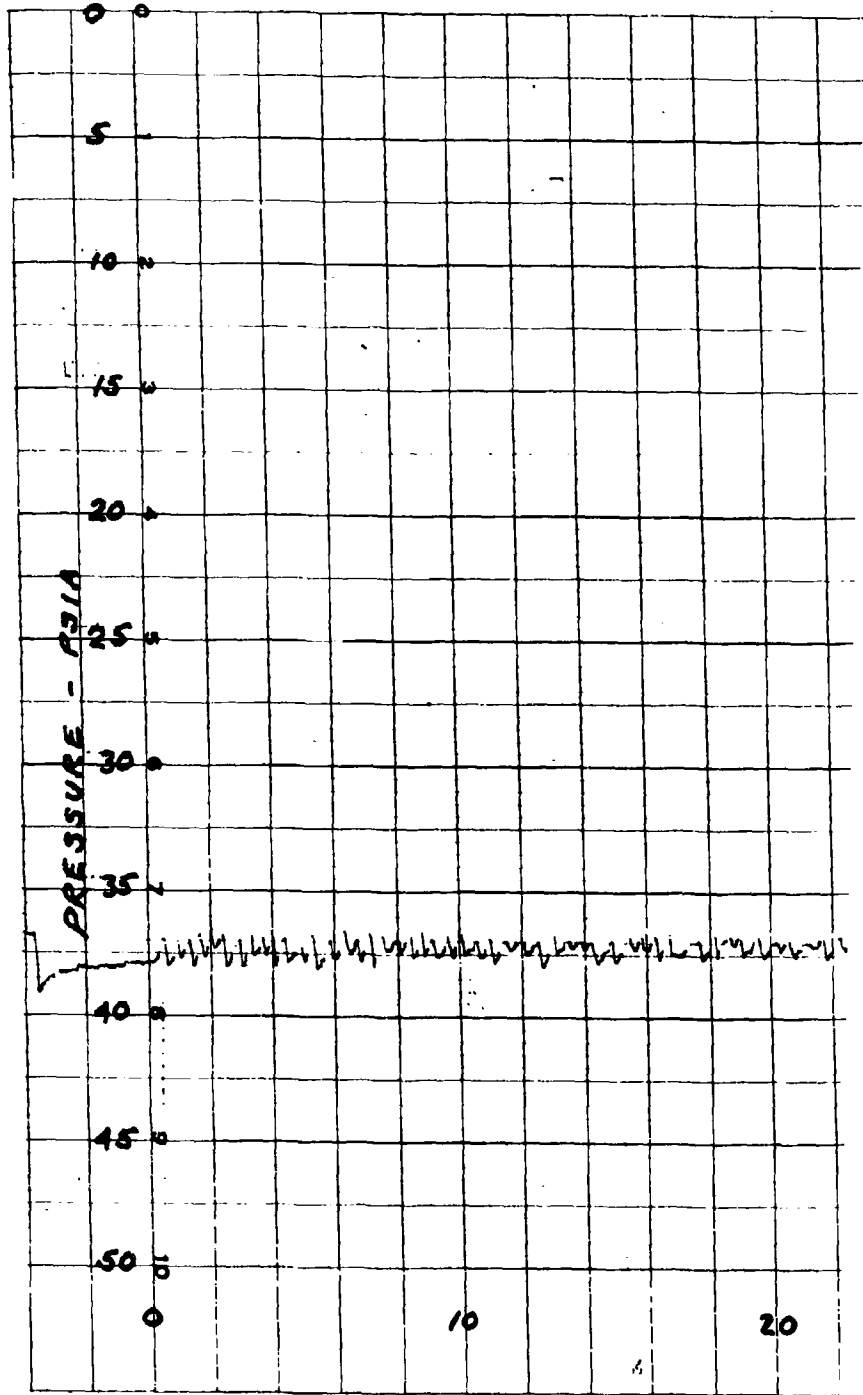
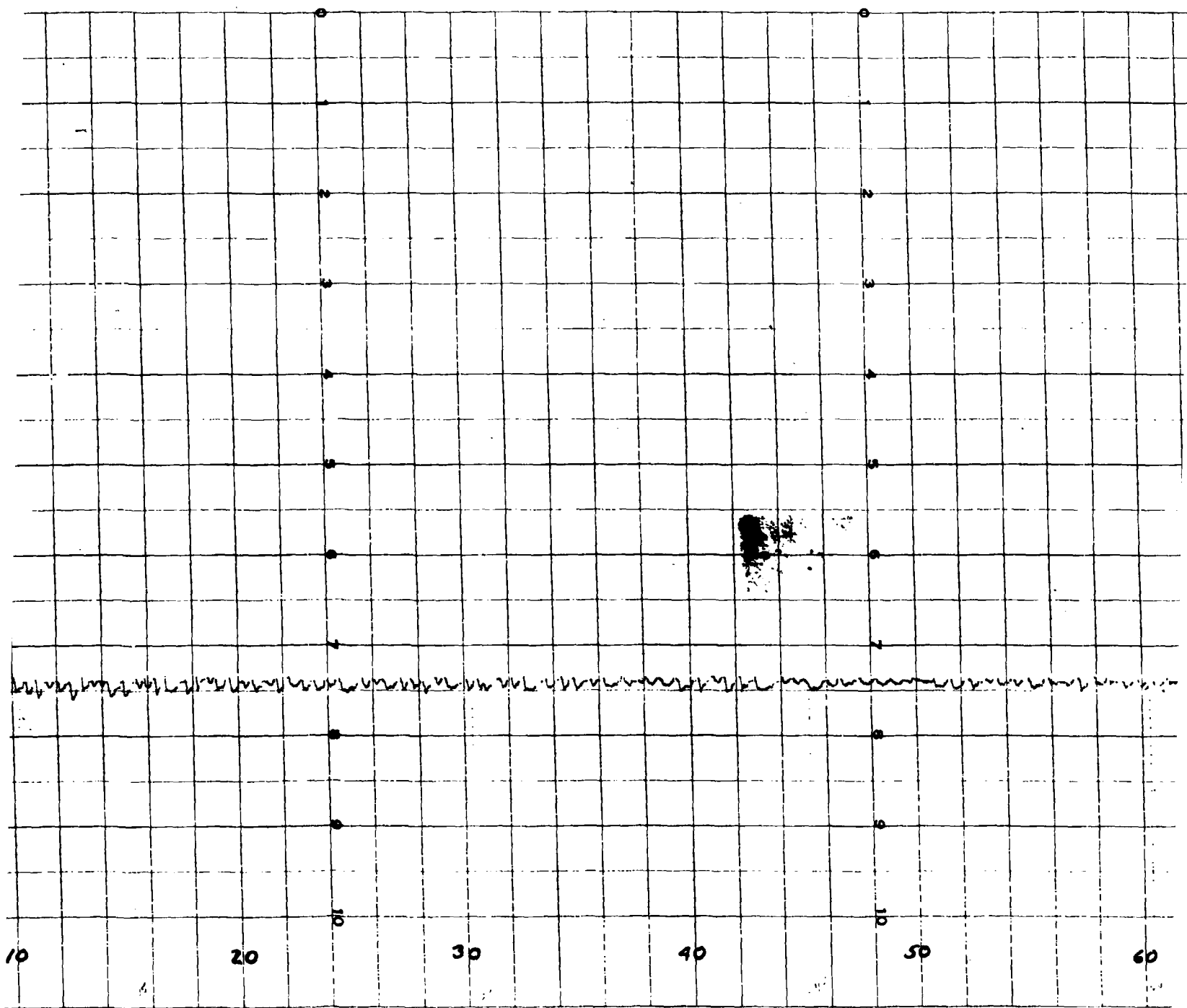


Fig. IV-13 Typical Pressure Cycle at 5% Ullage

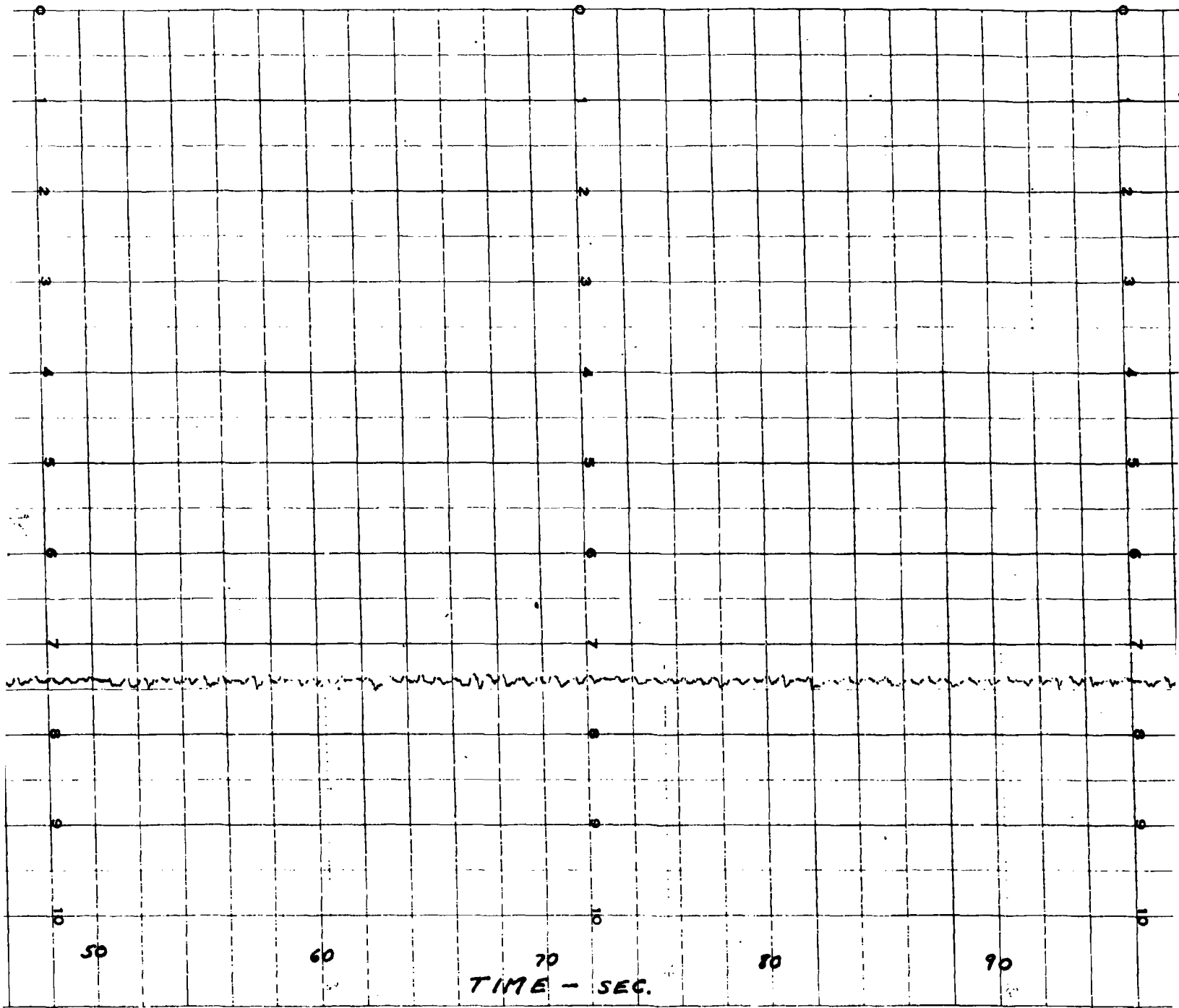
1

SAME SIZE RECORD

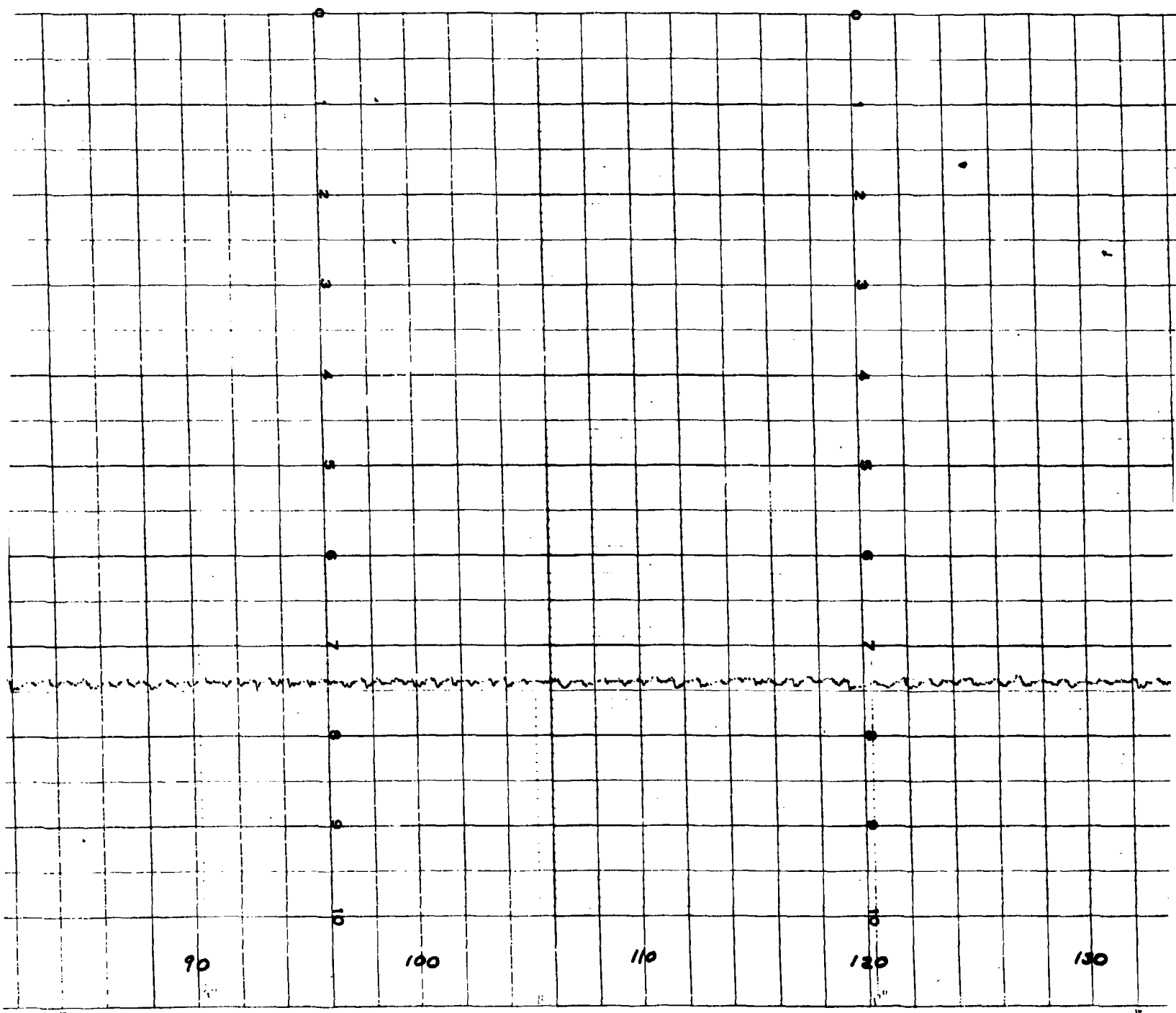




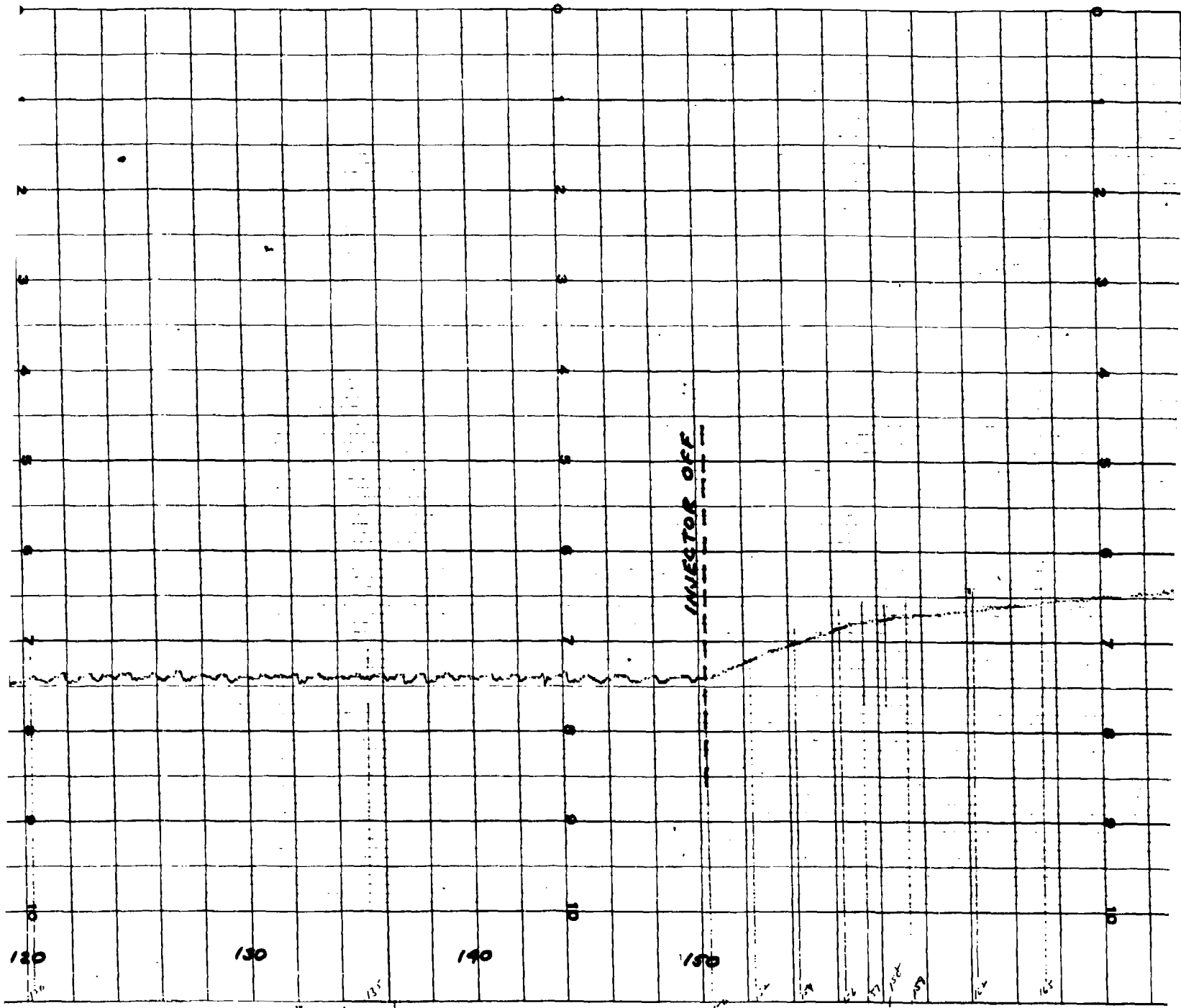
2



3



4



5

Fig. IV-14 Actual Pha

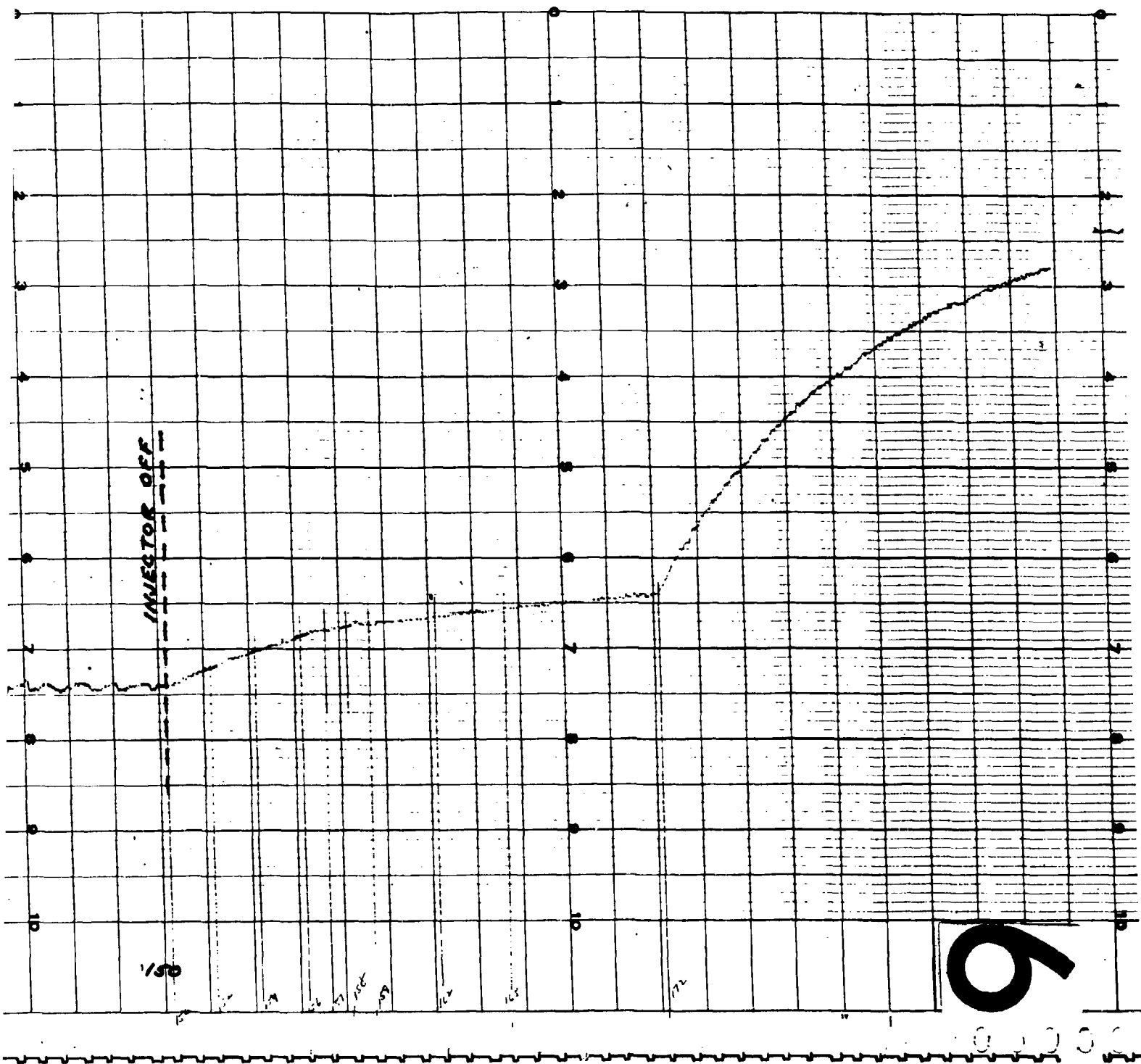


Fig. IV-14 Actual Phase III Pressure Trace with 5% Initial Ullage, Fuel Tank IV-27 and IV-28

Data for the restart test are shown in Fig. IV-15 and IV-16. During the coast period, tank pressure decayed to 25.5 psia because of decreasing temperature and leakage from the tank. Wall temperatures decayed to 128°F. After energizing the pressurization system, following the coast period, the injector stayed on continuously for 3.9 sec to increase tank pressure from 25.5 to 36.8 psia. The ullage volume is approximately 140 ft³ at this time. No pressure overshoot or temperature spikes occurred during the repressurization process. Variation in outflow rate, as in outflow termination, had no effect on injector performance except to change the injector cycling rate. Reagent usage during the repressurization process was 0.4 lb. Reagent consumption for the entire run was 2.9 lb. The actual pressure trace for this run is shown in Fig. IV-17.

Tank wall temperature was 233°F maximum for the restart test. Propellant temperature at the outlet decreased 1.8°F during the first 30 sec of the test run and increased during the final 50 sec by 6.3°F. No system vibration or bubble entrainment in the propellant was observed on the television monitor. A sound recording was made during the test by fastening an intercom headset to the outer tank wall above the high level sensor. The tank reaction makes a considerable amount of noise as it could be heard approximately 100 yd from the test site while testing was in progress.

Gas sampling was accomplished using the same equipment and technique used during Phase I testing. Two samples were taken following the completion of the restart test and analyzed at the National Bureau of Standards in Boulder, Colorado. The results were as follows on a helium free basis:

<u>Combustion Products</u>	<u>Volume (%)</u>
N ₂	32.5
H ₂	30.9
CH ₄	15.5
NH ₃	14.9
NO	1.4
CO ₂	0.2
UDMH	4.6

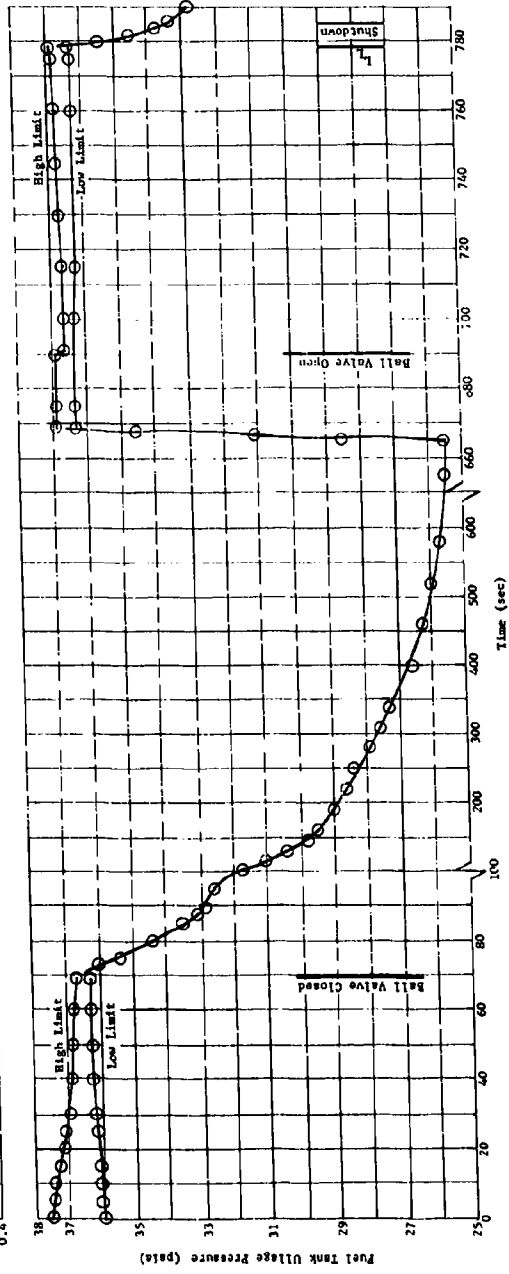
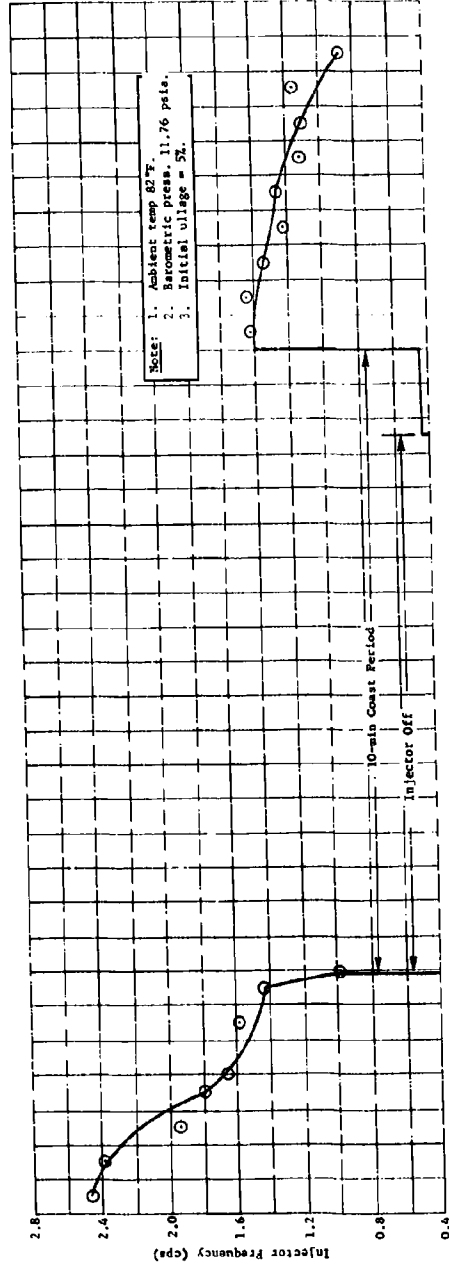


Fig. IV-15 Run 5 Phase III Fuel Tank Injector Performance

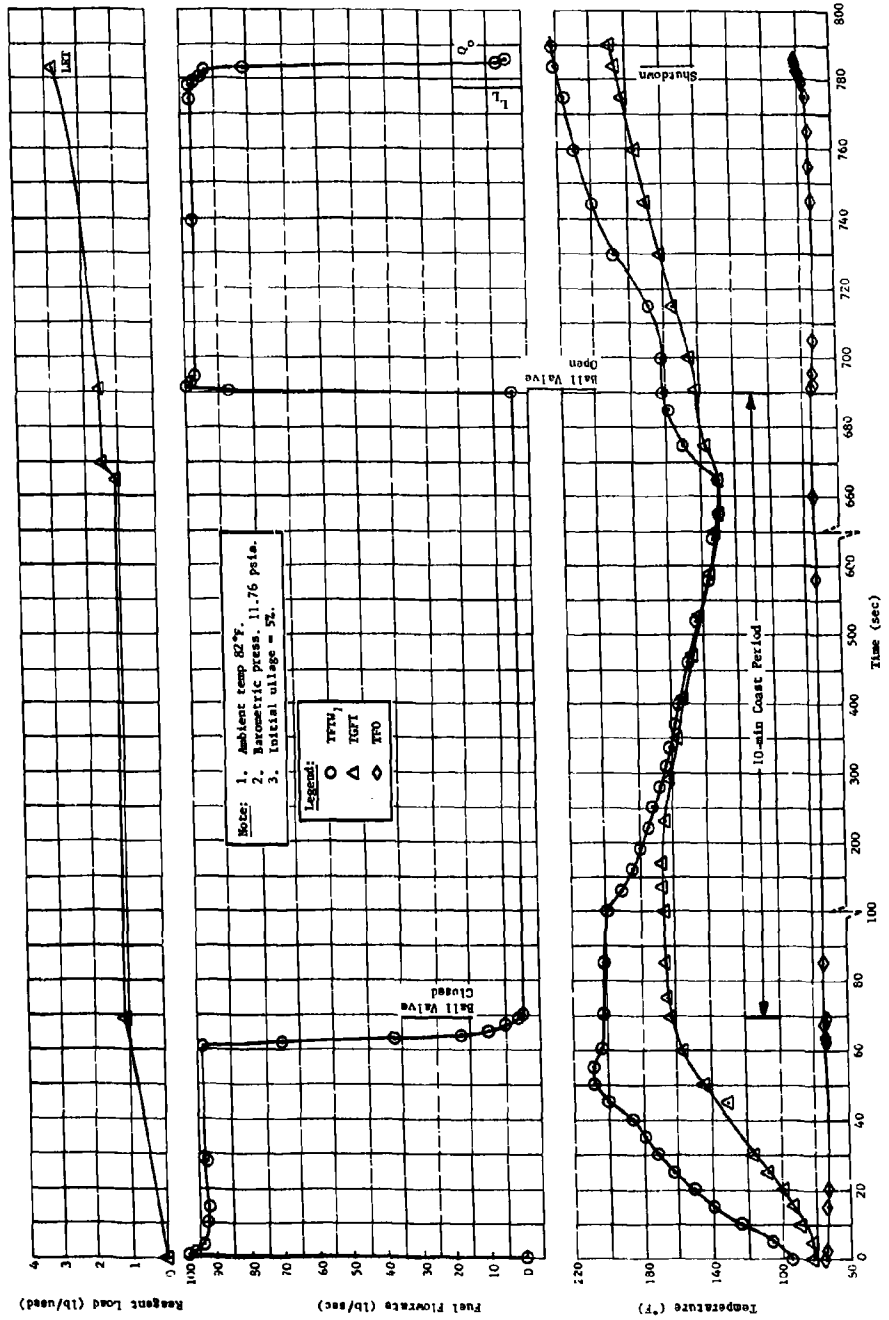


Fig. IV-16 Run 5 Phase III Fuel Tank MFI System Performance

Molecular Weight of Combustion Products = 15.98
Molecular Weight of Ullage Gas = 17.02
Molecular Weight of Ullage Gas (No Helium) = 18.00

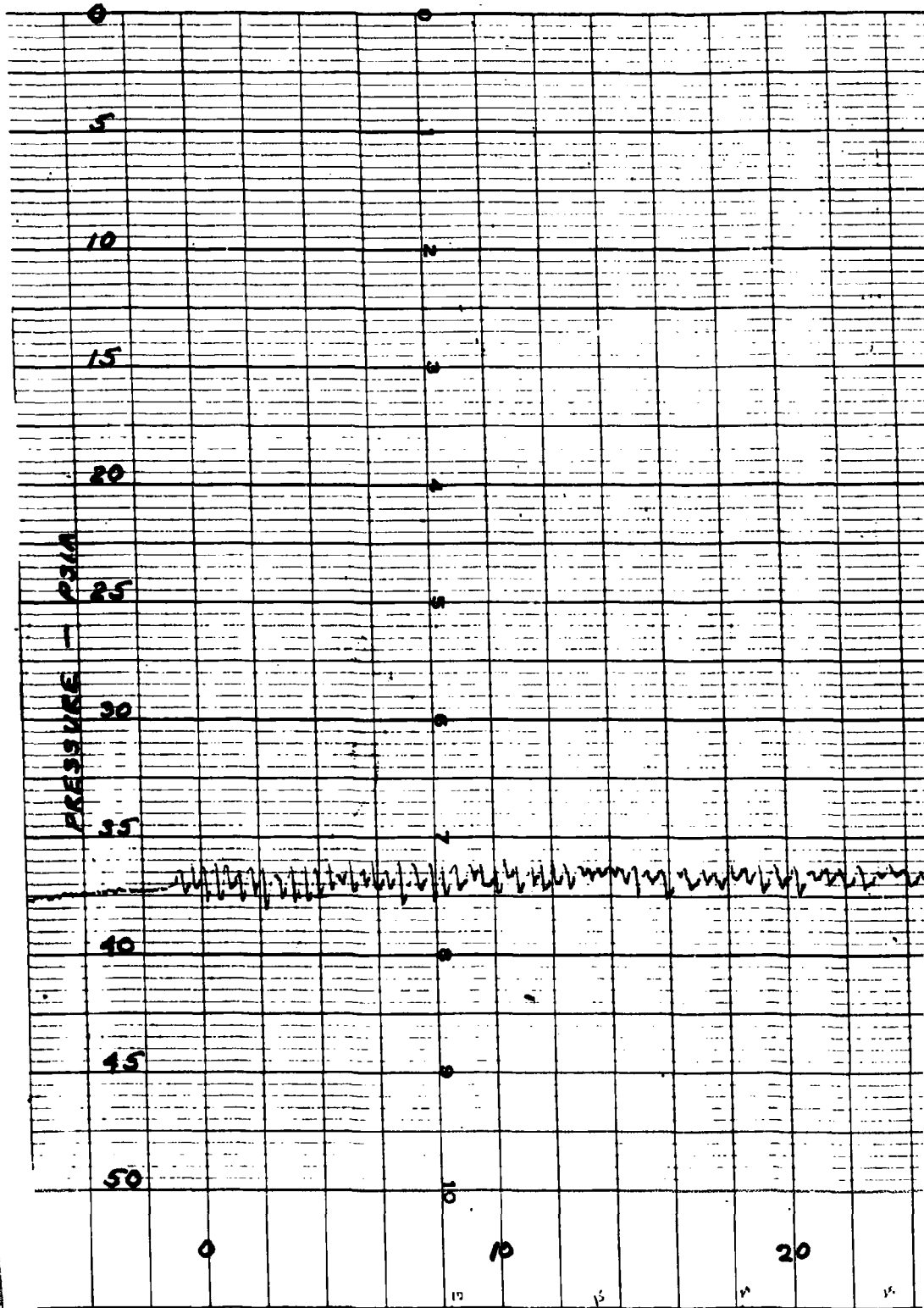
Propellant analysis was performed at the Martin Quality Control Laboratories as described in Chapter IIC2. The fuel was found to be within specification limits after completion of four full duration tests and subsequently returned to storage.

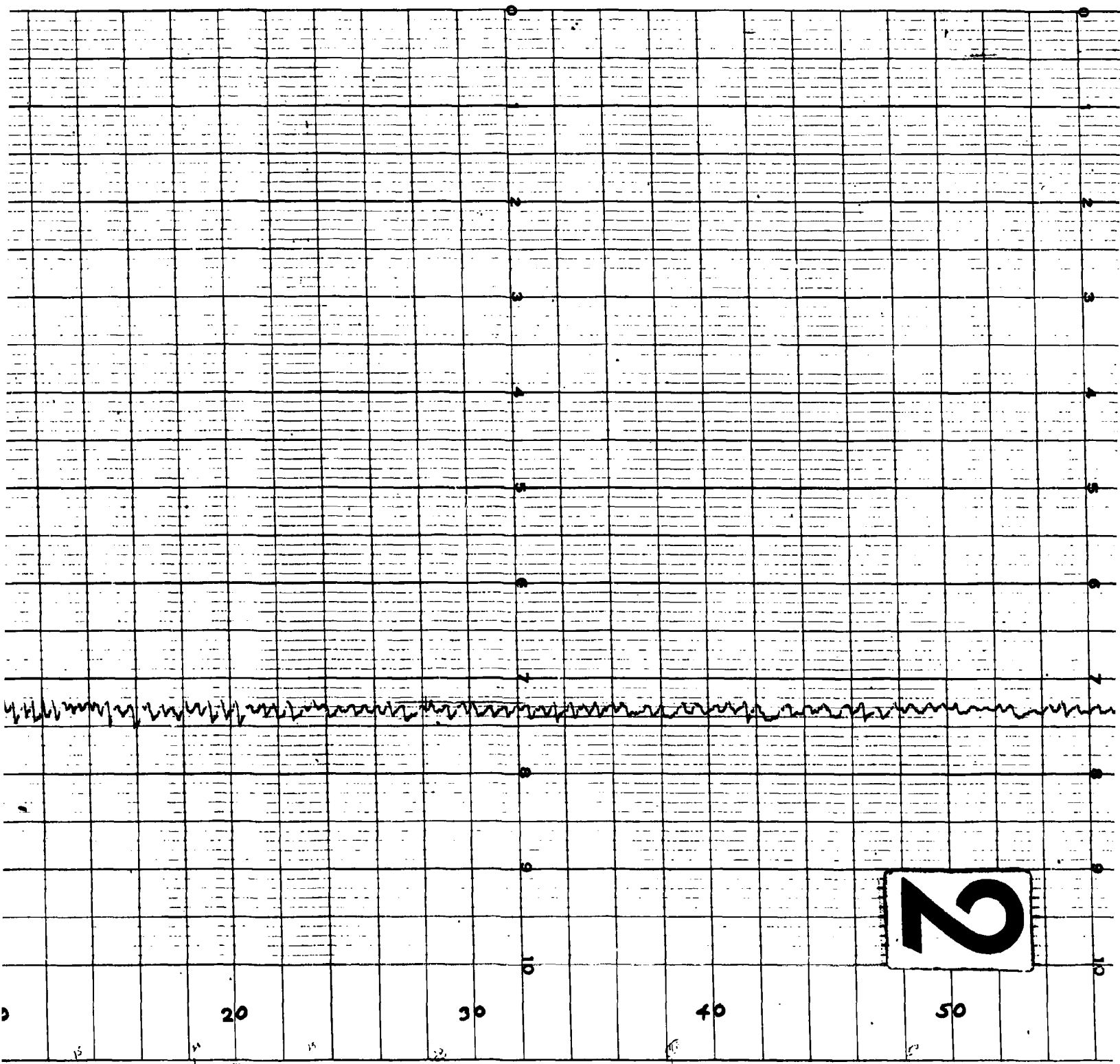
Oxidizer Tank Results - The initial oxidizer tank MTI pressurization test was performed on 13 September 1963. Pressurization during the 150-sec continuous test was achieved by direct fuel injection through the 0.047-in. dia, solid-stream injector nozzle. In general, the performance was good and quite similar to the fuel tank. All critical parameters were recorded except for the ullage gas temperature and propellant flow rate. Approximate values have been determined for these two parameters, however. They are based on tank wall temperature measurements and propellant level sensor indication. Photographic observation of the system during the run was also achieved, as well as a sound recording of the actual pressurization process.

The results of the initial oxidizer tank MTI test (No. 6) are shown in Fig. IV-18 thru IV-21. This test was performed with the initial 5% ullage prepressurized with helium to 38 psia. A leak check before test initiation indicated a pressure decay of approximately 2 psi/min. Instrumentation locations are indicated in Fig IV-2 and IV-3 with a tabulation of the nomenclature contained in Table IV-1. A headset installed on the propellant tank forward skirt indicated moderate detonations from the reaction. No vibration was observed, however. The sound has been described as analogous to rapid helium pressurization of the ullage.

Pressure control was within 37.5 ± 1 psia at the start of the test and narrowed to ± 0.25 psi near the end. Injector frequency (5 cps) was higher in the fuel tank and diminished to 2 cps toward the end of the test. The maximum wall temperature of 267°F was obtained from the No. 3 position on the tank dome, with a range over the surface to 234°F. Because of solar heating, the average initial tank wall temperature was 100°F, with an ambient temperature of 81°F. A 17°F rise in propellant temperature was detected during the run, which reduced the pressurization requirements somewhat. Reagent consumption was lower than anticipated at 3.3 lb, resulting in only fair pressure control due to the oversized injector.

1





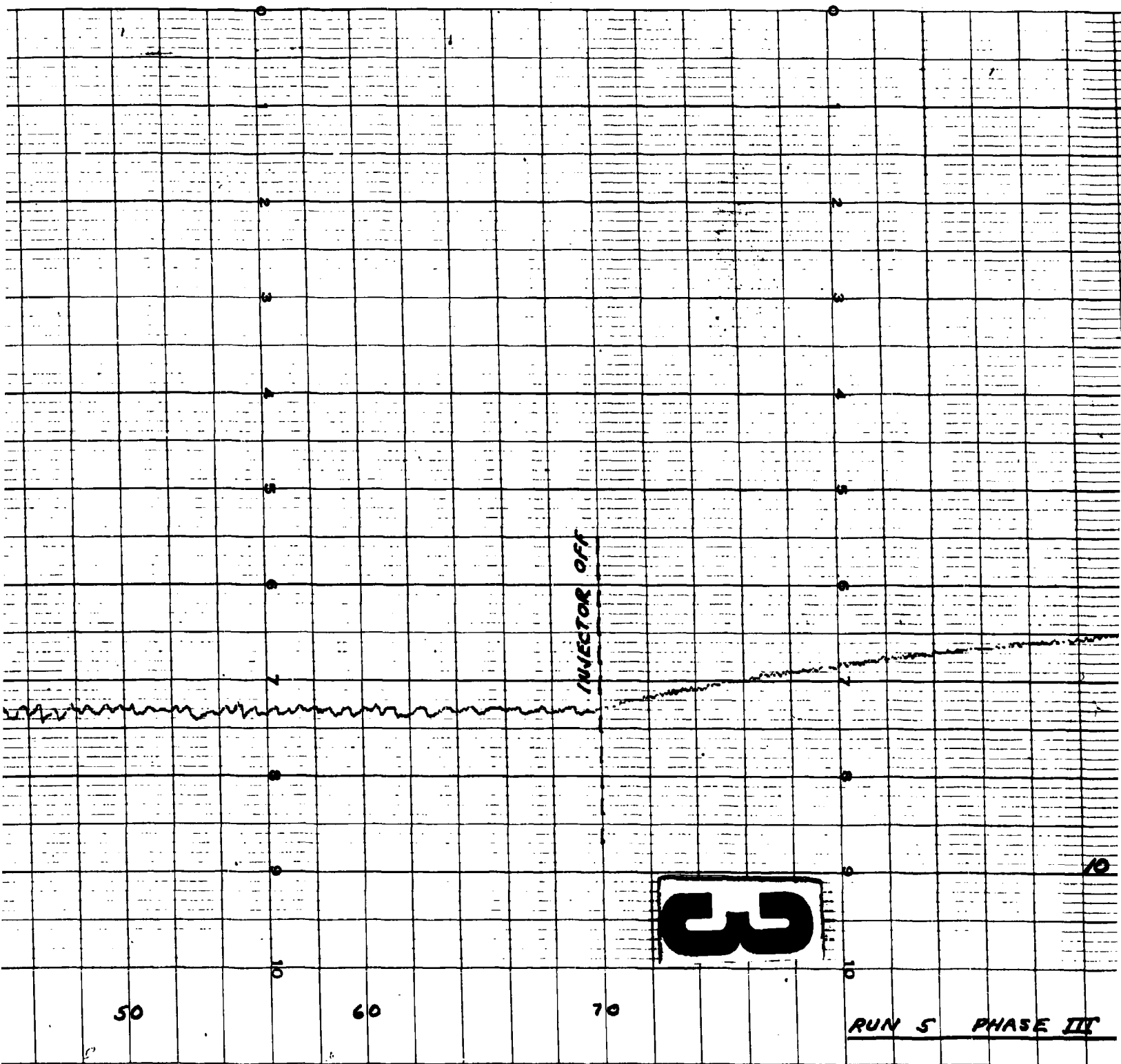
II

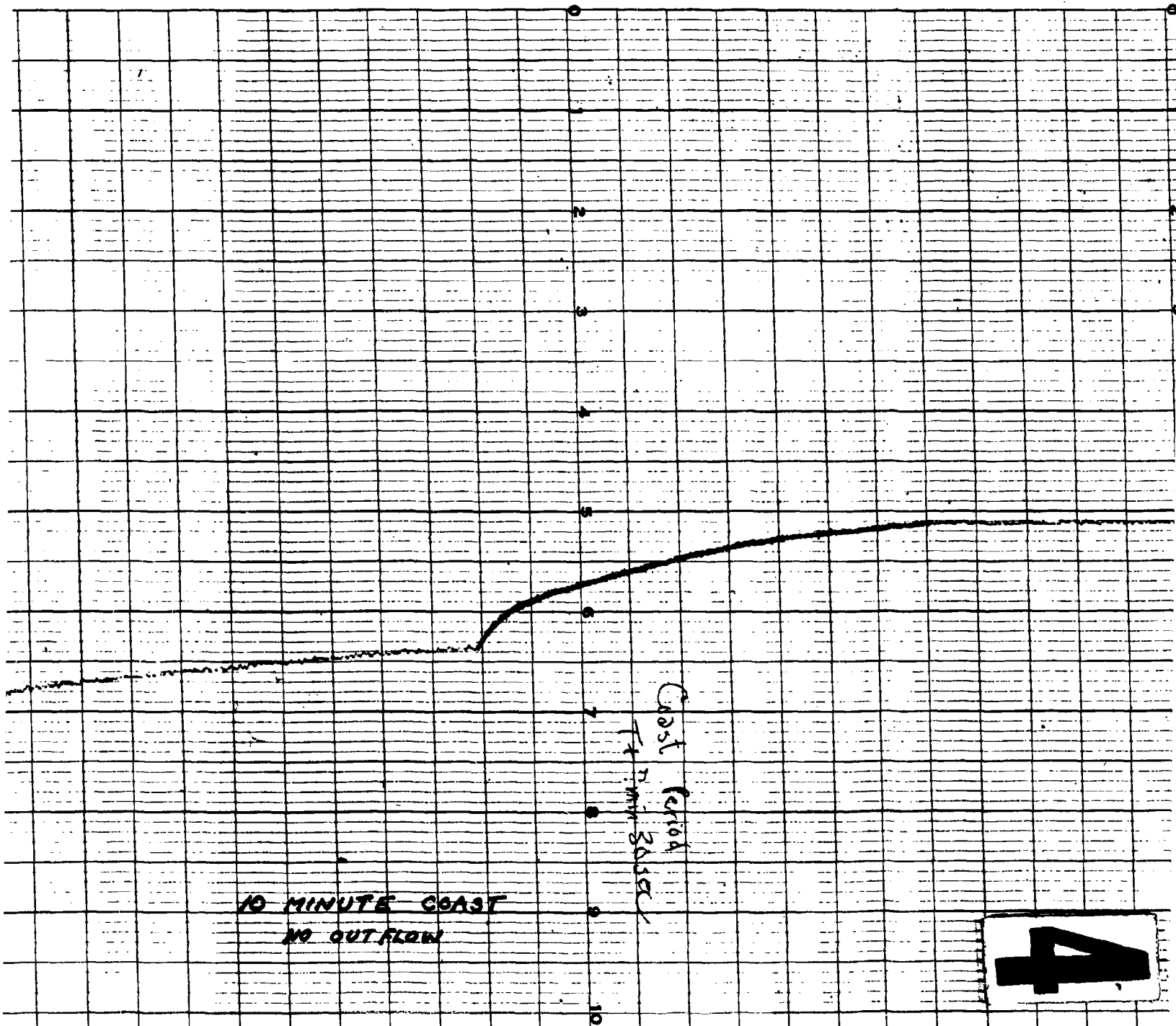
20

30

40

50





10 MINUTE COAST
NO OUTFLOW

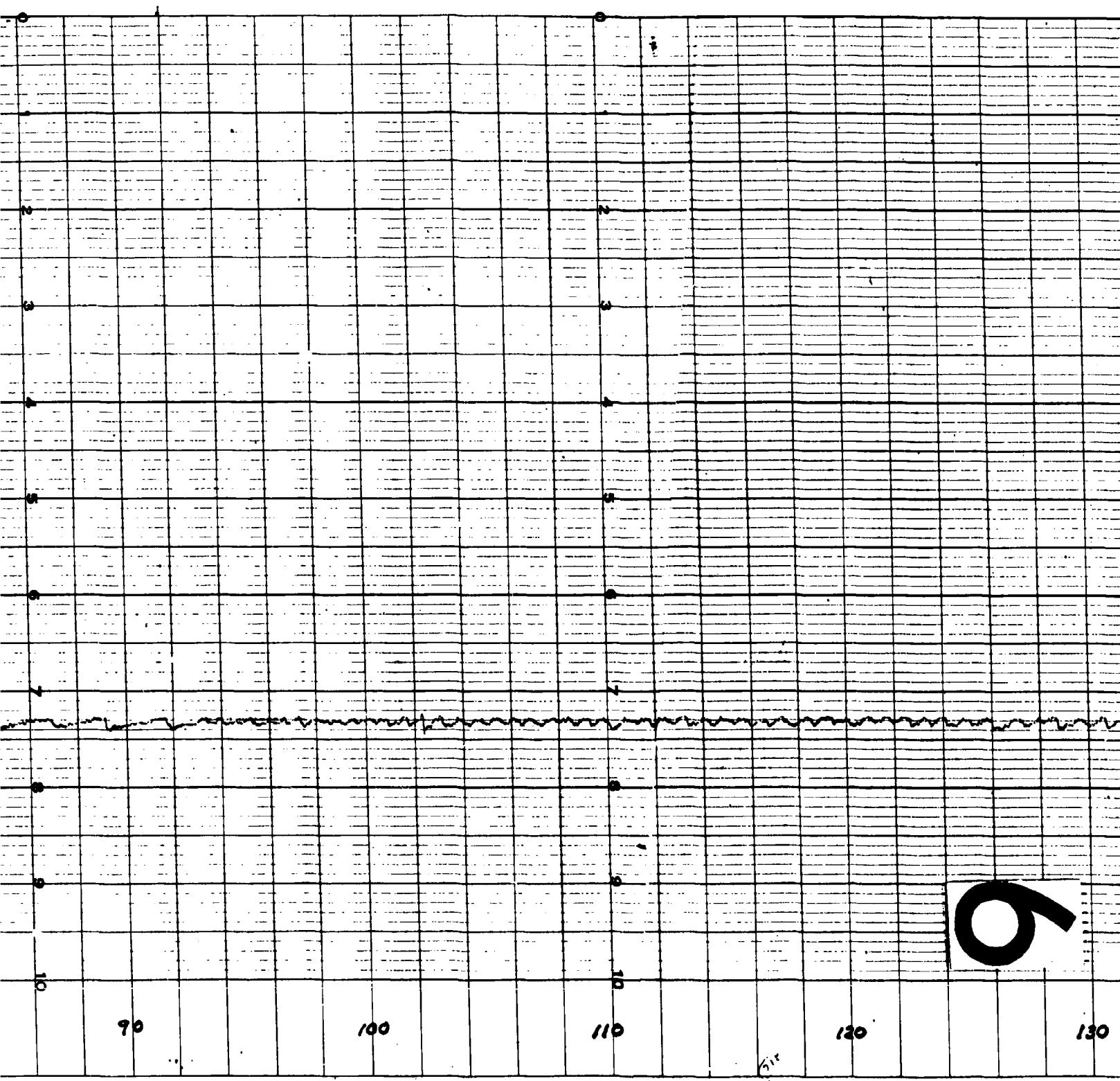
Coast Period
7 min 30 sec

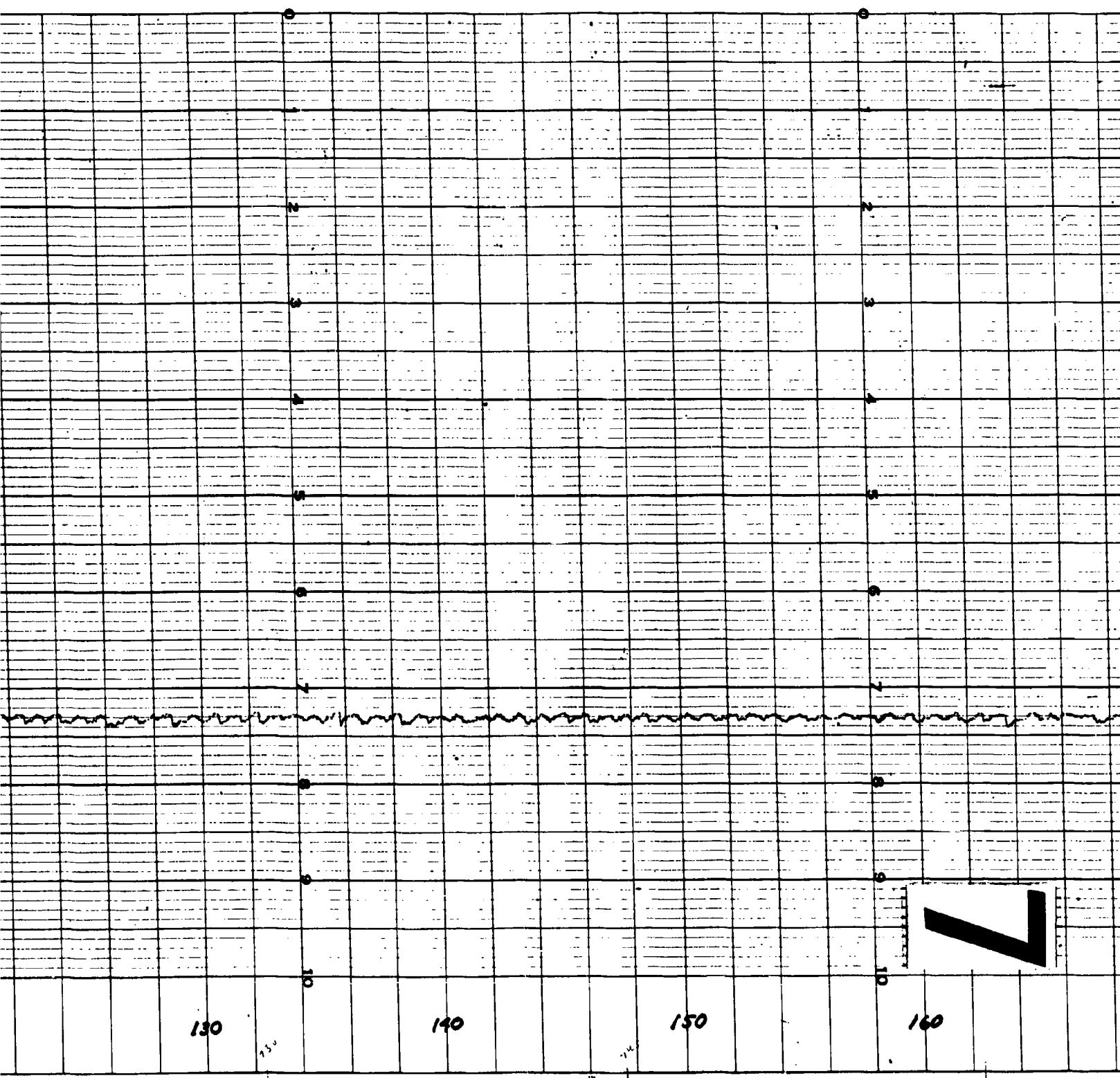
4

RUN 5 PHASE III FUEL TANK - RESTART

653







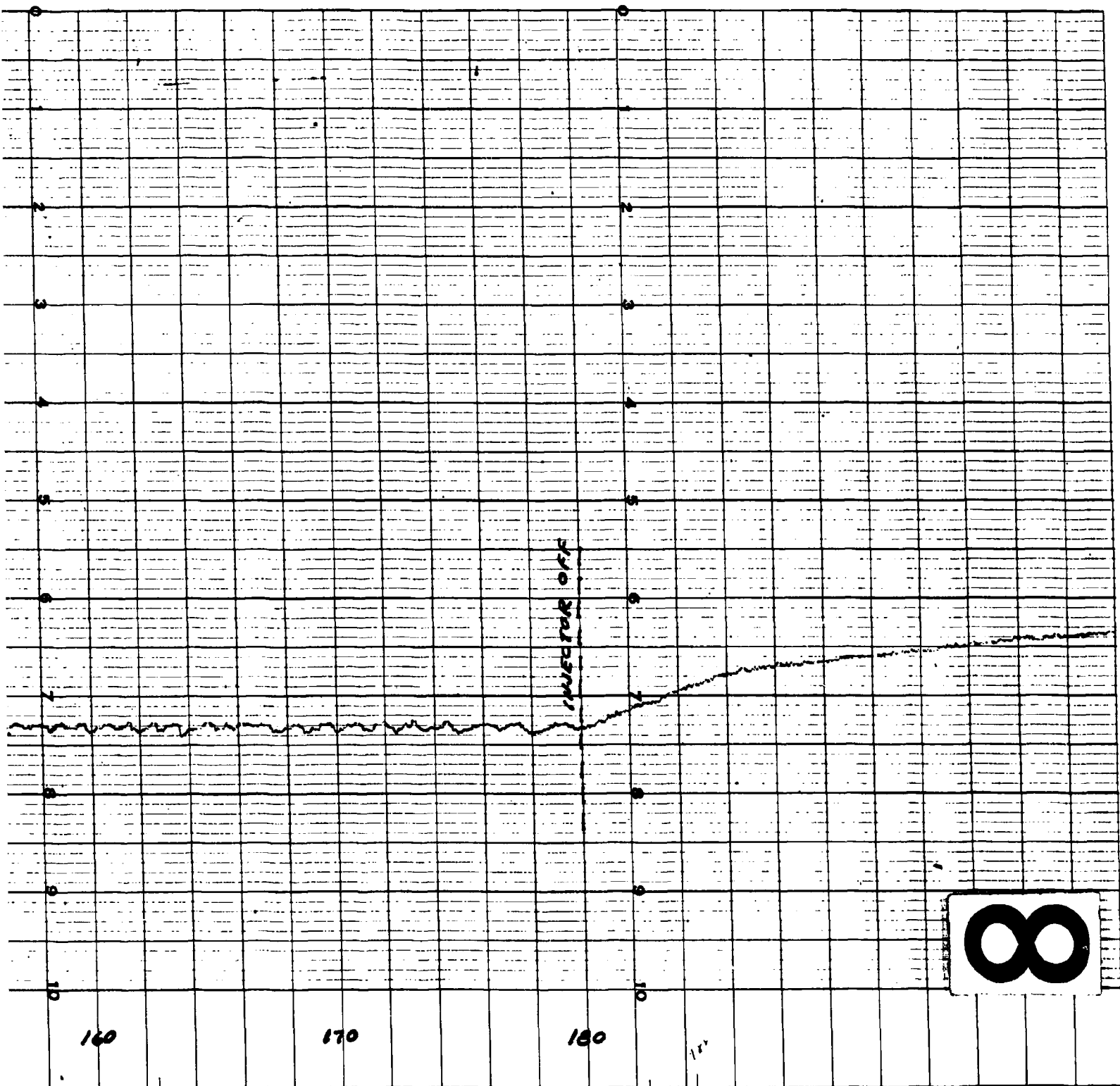


Fig. IV-17 Run 5 Actual Phase III Fuel Tank Pressure Trace, Restart Test IV-33 and IV-34

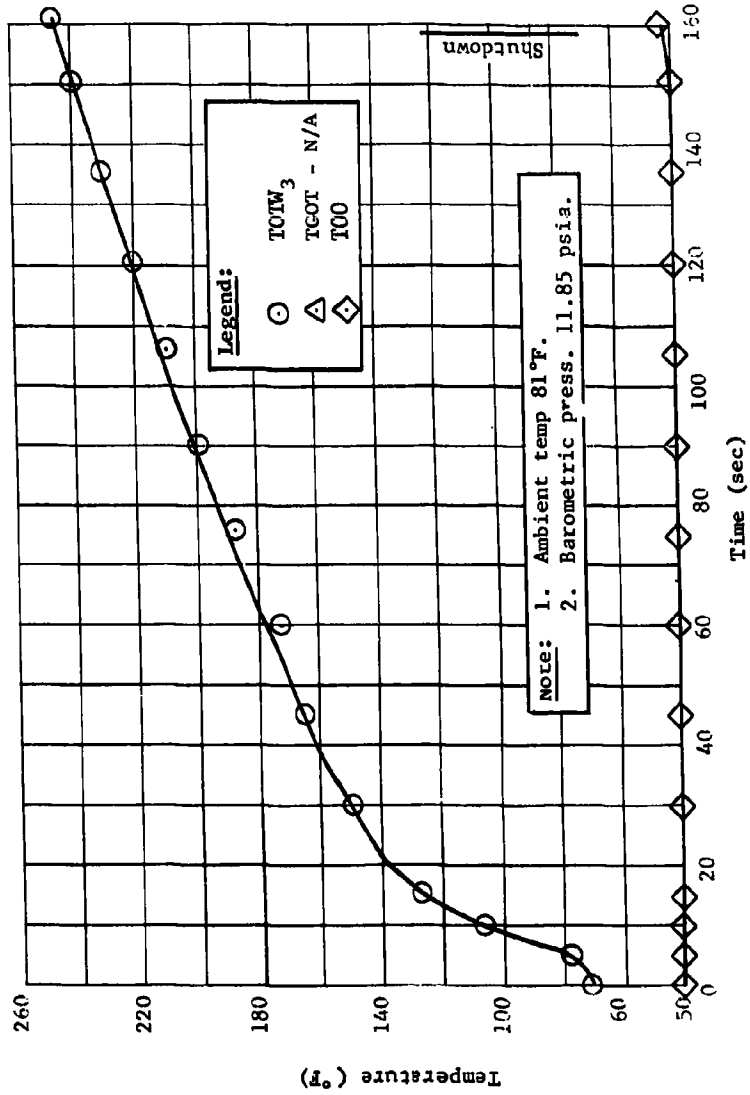


Fig. IV-18 Run 6 Phase III Oxidizer Tank System Temperatures

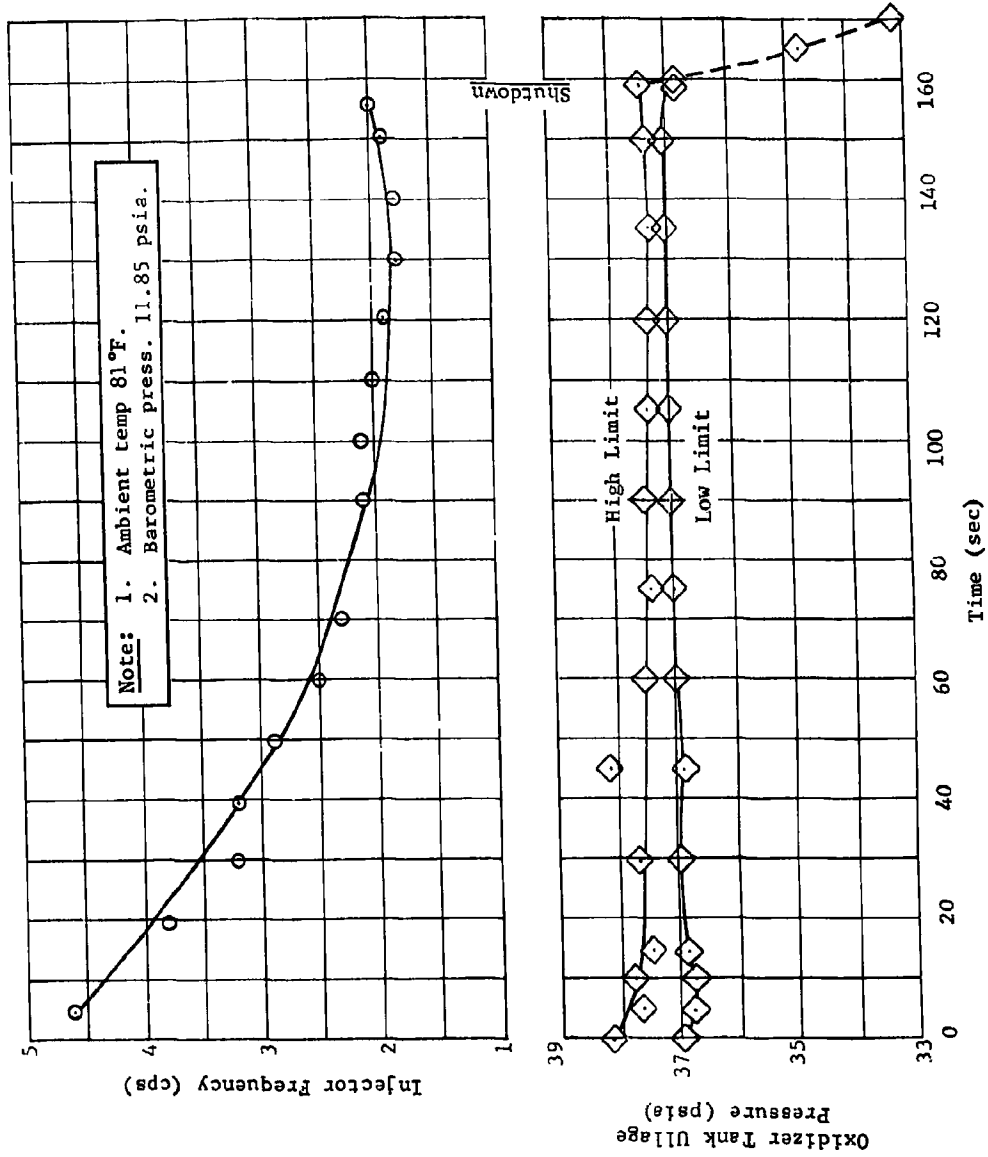


Fig. IV-19 Run 6 Phase III Oxidizer Tank Injector Performance

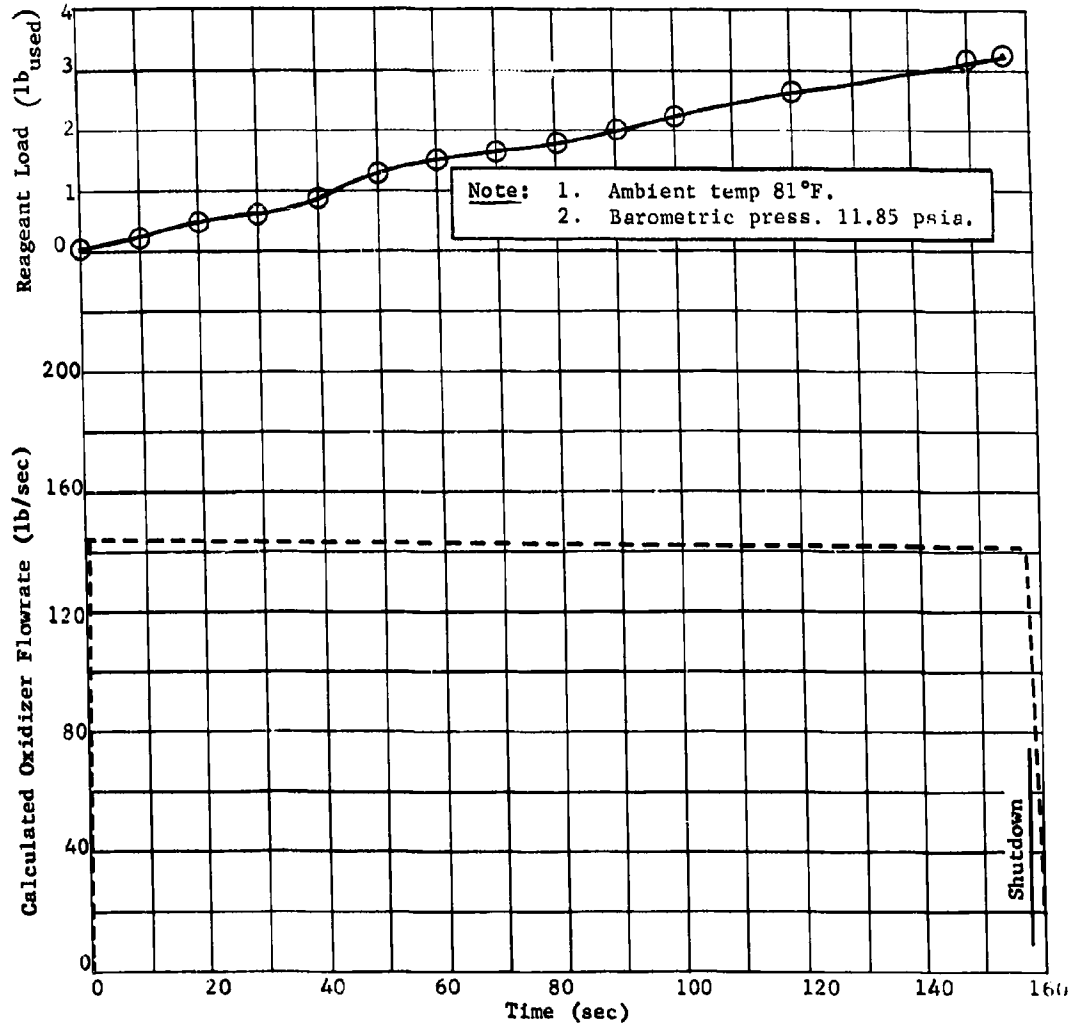


Fig. IV-20 Run 6 Phase III Oxidizer Tank Pressurization and Propellant Flowrates

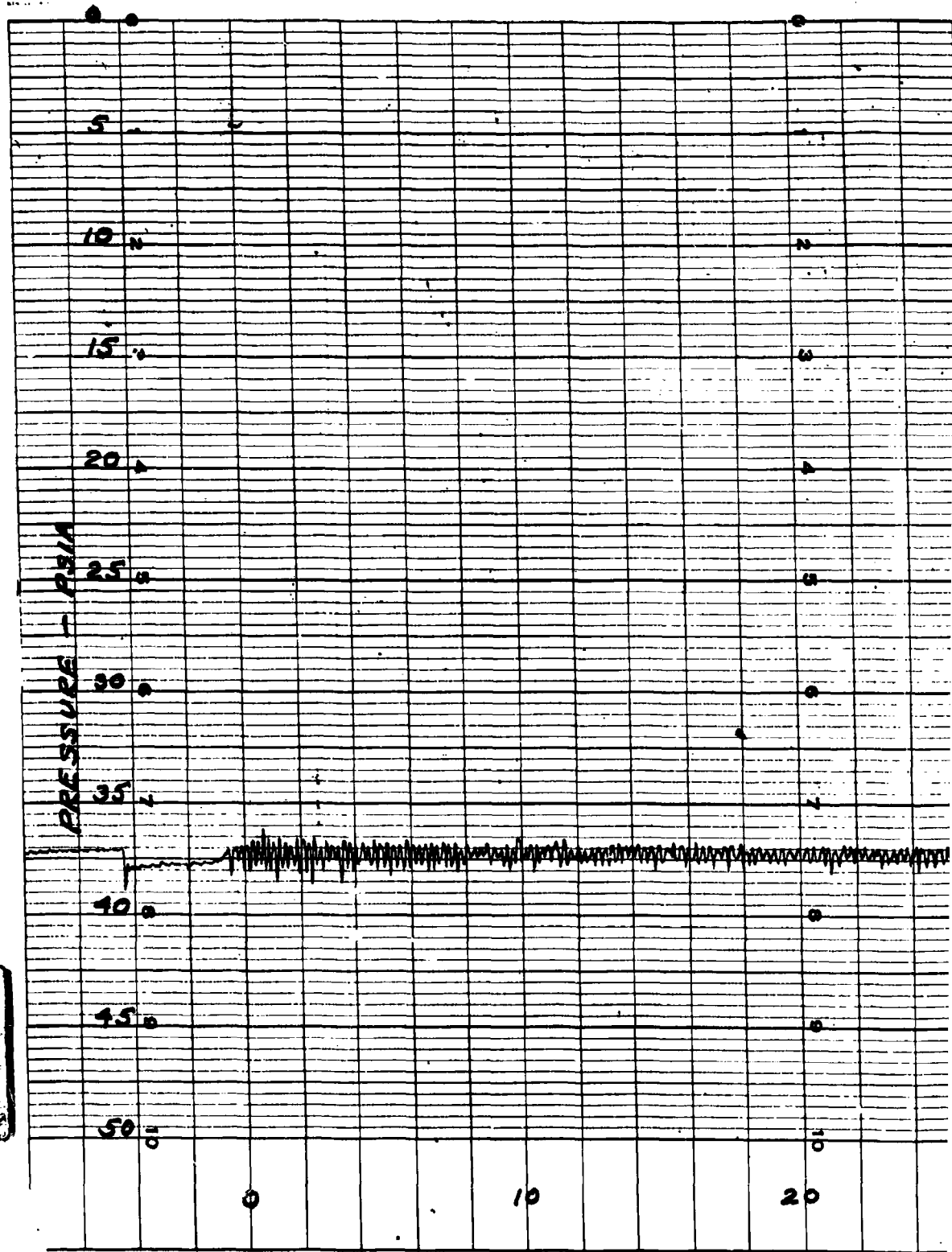
Average propellant flowrate was determined from the 158-sec duration of the test and volume between the liquid level sensors. Propellant analysis performed on oxidizer specimens taken before and after the test indicated a negligible increase in water content. The entire propellant was then returned to storage at direction of the procuring officer. Chemical analysis conducted on a gas sample taken after the test indicated the following composition on a helium-free basis:

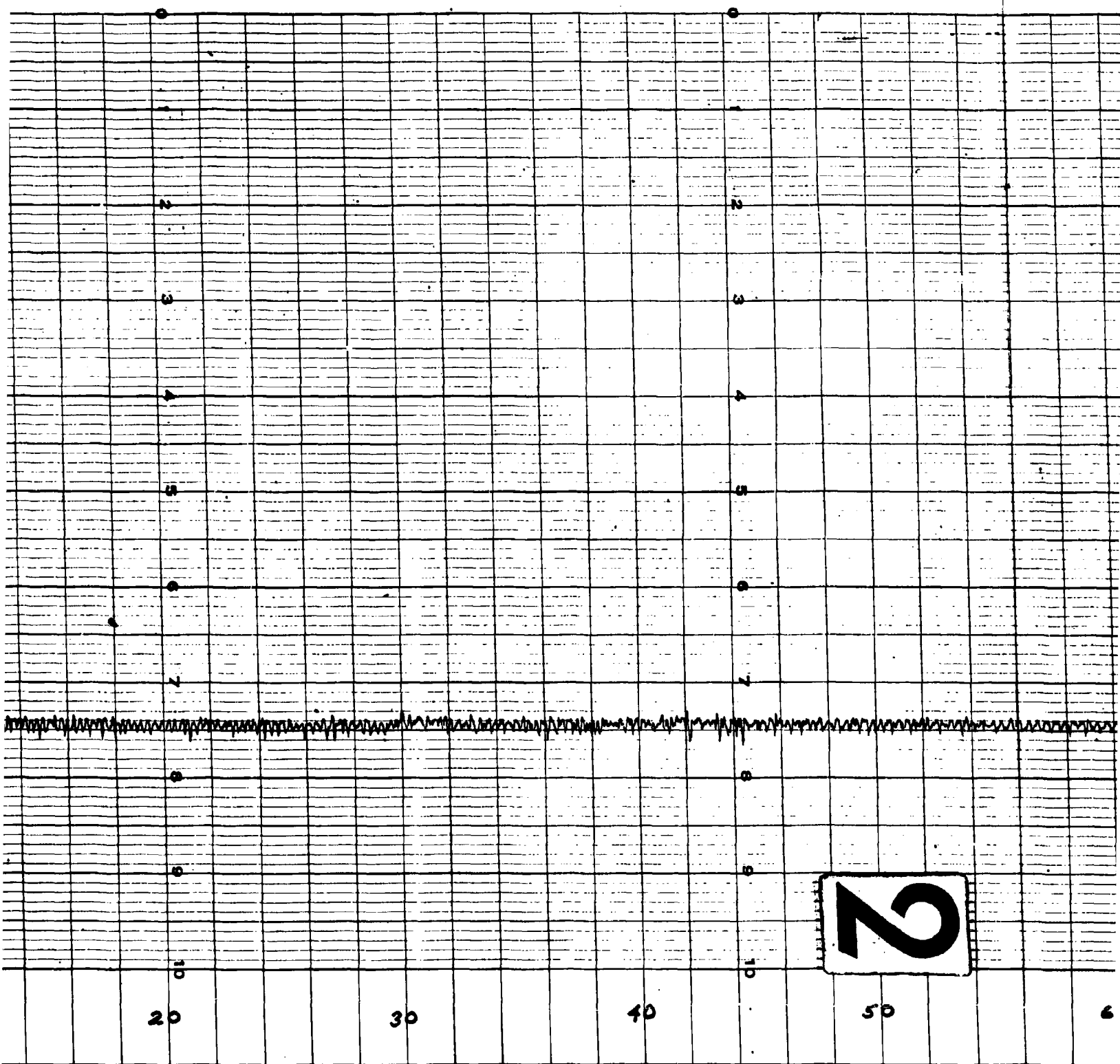
<u>Constituent</u>	<u>Volume (%)</u>
NO ₂	59.75
N ₂	26.05
H ₂	Trace
O ₂	6.47
CO ₂	6.06
H ₂ O	1.25
NH ₃	0.42

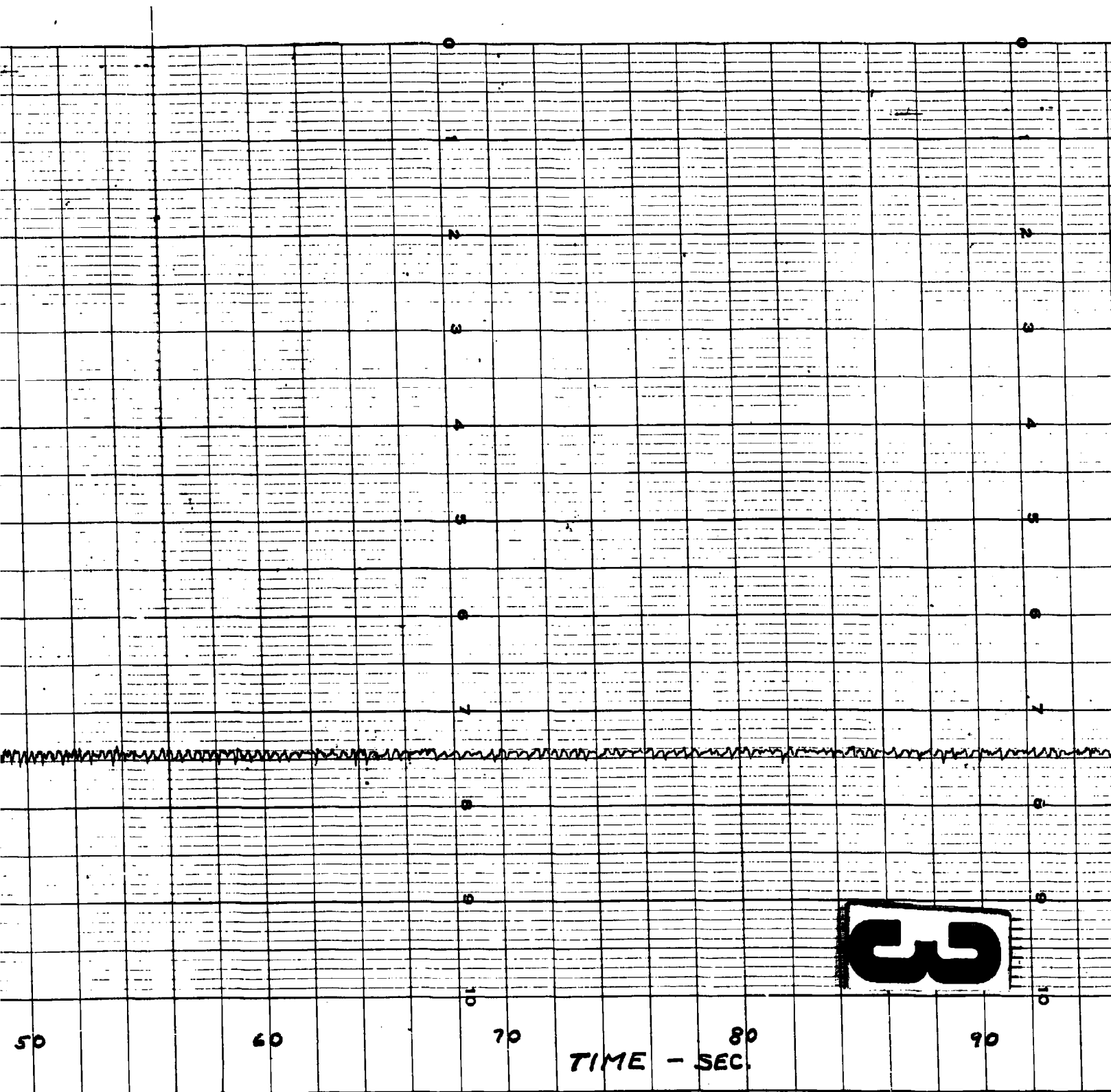
Combustion product molecular weight was 30.63 with a total gas molecular weight of 38.28 or 39.81 with no helium.

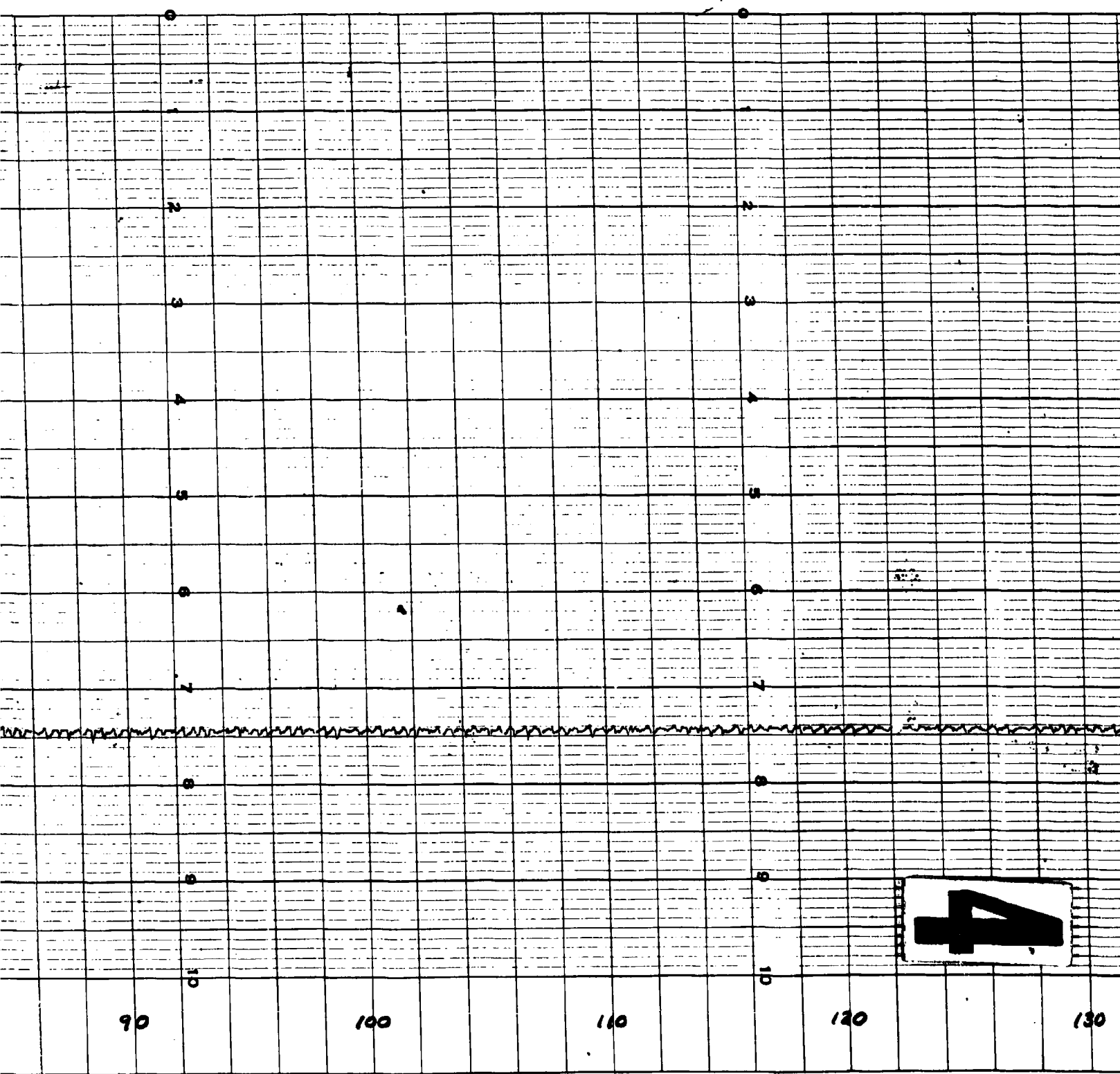
A second test was performed on the oxidizer tank September 17, 1963. System configuration was identical to the previous test except for replacement of an inoperative vent and relief valve, repair of the propellant flowmeter, and replacement of the propellant tank ullage thermocouple. The planned test procedure incorporated a 10-min coast period after the first 60 sec of variable outflow operation. It then resumed outflow at a variable rate until propellant depletion. A loss of propellant flow indication prevented an accurate indication of the flow adjustment achieved, but modulation was believed less than 20%. In general, the performance was good and quite similar to the fuel tank restart test except that several seconds lapsed before resumption of propellant flow following the 10-min coast. All critical parameters were recorded except for the loss of the propellant flow rate and one tank wall thermocouple. A sound recording of the MTI pressurization process was also made in the same manner as was accomplished on the fuel tank.

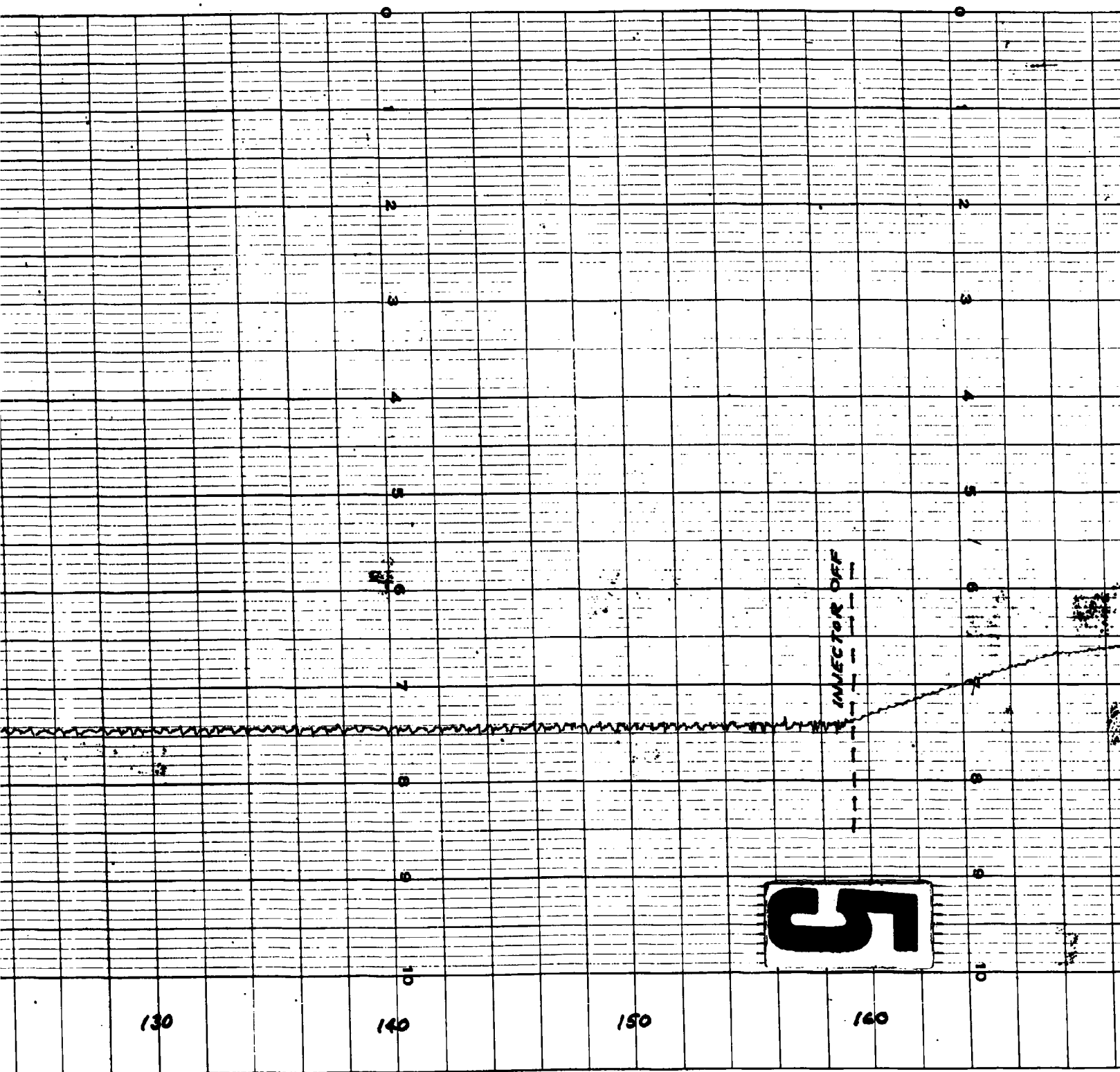
1











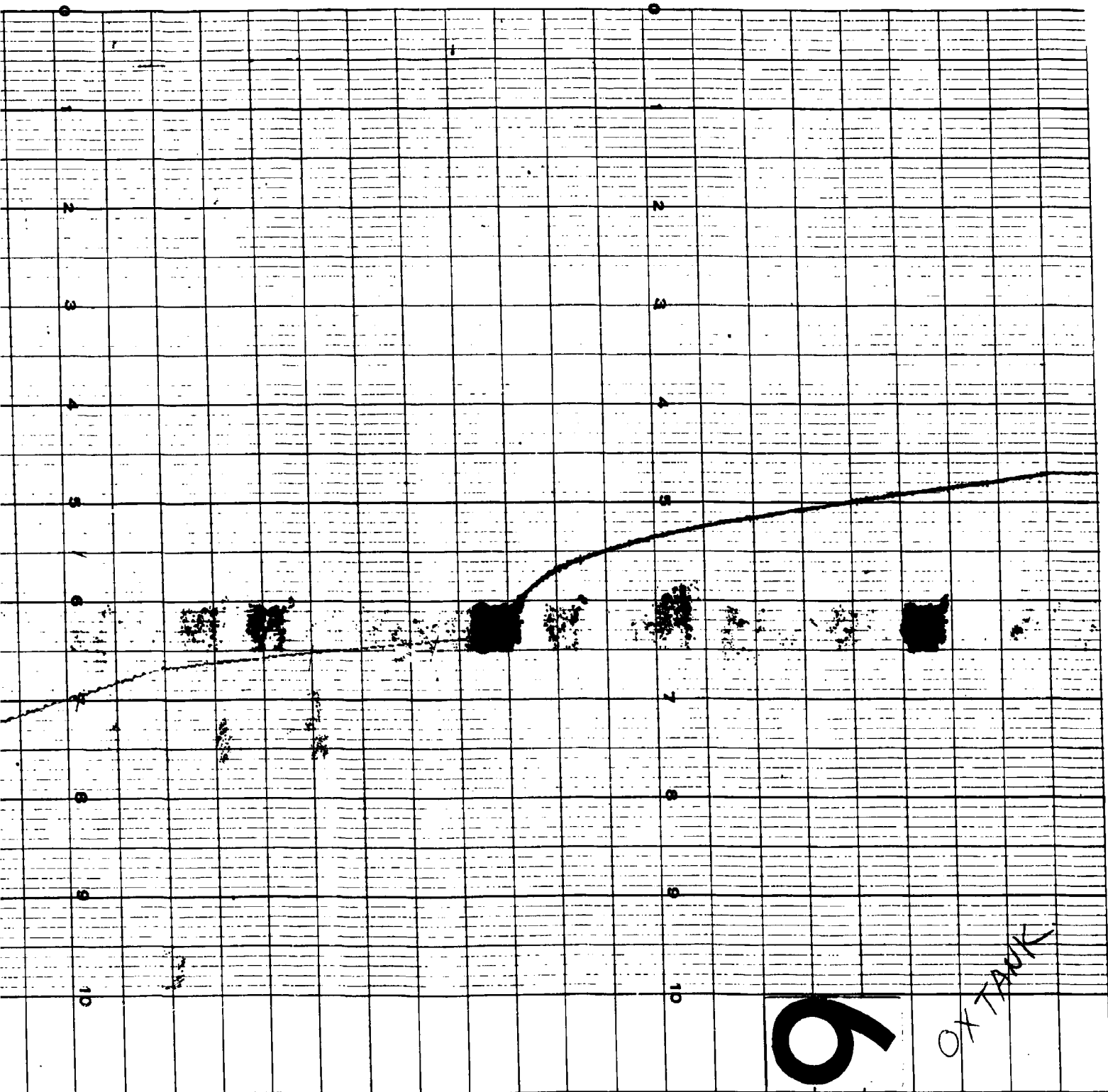


Fig. IV-21 Actual Phase III Pressure Trace with 5% Initial Ullage, Oxidizer Tank IV-39 and IV-40

The results of the oxidizer tank restart test (No. 7) are shown in Fig. IV-22 thru IV-24. The initial 5% propellant tank ullage volume was prepressurized with helium to 38 psia. A leak check before test initiation indicated a pressure decay of approximately 1.5 psi/min. Instrumentation was the same as the previous test except T_{got} was located 6 in. inside the tank forward dome and 2 ft radially from the injector. The headset was installed on the forward dome for this run to obtain better sound definition. Again no vibrations or pressure surges were noted. Pressure control was within 37 ± 1 psia at the start of the test, decreasing to 37 ± 0.25 psi after 20 sec. Injector frequency was 5 cps initially and diminished to 2 cps after restart. The maximum wall temperature of 216°F occurring at shutdown was obtained from the No. 1 and 2 positions on the tank dome. Initial wall temperatures were between 72 and 84°F due to the solar heating effects. Ambient temperature was 79°F, with the initial ullage temperature 74°F and propellant temperature 56°F. A 20°F rise in propellant temperature was detected during the run, which increased the amount of propellant vaporization with resultant decrease in reagent consumption. The relatively high final gas temperature of 326°F results in almost complete dissociation of the vaporized propellant and a low reagent consumption of 3.4 lb. During repressurization, 0.4 lb of reagent was required to bring the ullage pressure up from 27.1 psia to 37 psia in 7 sec.

An average propellant flow rate of 129.36 lb/sec was determined from the 174-sec test duration and 246.8 ft³ volume between level sensors. Results of the propellant analysis performed at the Martin Quality Control Laboratories indicated the oxidizer water content increased from 0.06% before Run 6 to 0.17% after Run 7 (0.20 max Spec AGC-44055A). No analysis of the pressurizing gas was performed on this test.

Phase III Data Summary - Satisfactory pressurization of the 279 ft³ flightweight aluminum propellant tanks has been demonstrated by the direct injection of nitrogen tetroxide into the 50/50 UDMH hydrazine fuel blend and vice versa with the pulse mode, solid stream, surface injection system. Pressure was controlled to within ± 0.7 psi at 37 psia with the 5% initial ullage volume in each propellant tank. The control band decreased to ± 0.25 psi after approximately 20 sec of operation with the increasing ullage. Four MTI pressurization tests were made on the fuel tank and two on the oxidizer tank. Of the tests performed, all were of 150-sec nominal duration, with one test on each tank

designated as a restart test. During the restart test, pressurization system capability was demonstrated by varying the propellant outflow rate, repressurizing after the 10-min coast period, and employing an injector shutoff sequence before propellant-flow termination. In all of the tests, adequate thermal protection was achieved because of the inherent regenerative cooling capability of the main propellant. In addition, no pressure surges or entrained vapor were detected at the expelled propellant. A summary of the data obtained is presented in Table IV-4.

Table IV-4 Phase III Demonstration System Test Results

Fuel Tank								
Type Run	ΔT Gas (°F)	ΔT Liquid (°F)	ΔT Wall (°F)	Comb. Prod. Mole. Wt.	W_P (lb)	Pressure Cont (psi)	H ₂ O (%)	Injector Frequency (cps)
Surface Solid - 37 psia (150-sec continuous)	N/A	6 (72 max)	131 (228 max)	N/A	2.5	± 0.7	1.02	1.6 to 0.8
Surface Solid - 37 psia (150-sec continuous)	N/A	10 (76 max)	152 (246 max)	N/A	3.1	± 0.7	N/A	2.5 to 1.0
Surface Solid - 37 psia (150-sec continuous)	N/A	5 (70 max)	232 (266 max)	N/A	2.5	± 0.7	N/A	2.6 to 0.9
Surface Solid - 37 psia (Restart Test)	N/A	8 (82 max)	128 (222 max)	16.0 18.0 (Total)	2.8	± 0.7	0.72	2.5 to 0.9
Oxidizer Tank								
Surface Solid - 37 psia (150-sec continuous)	N/A	3 (53 max)	174 (246 max)	30.6 39.8 (Total)	3.3	± 0.7	0.06 (Before Test)	4.6 to 1.8
Surface Solid - 37 psia (Restart Test)	250 325 @ FS ₂ to 357 max ($T + 70$)	20 (75 max)	130 (215 max)	N/A	3.4	± 0.7	0.17 (After 2nd Test)	4.7 to 1.7
N/A = Not Available								

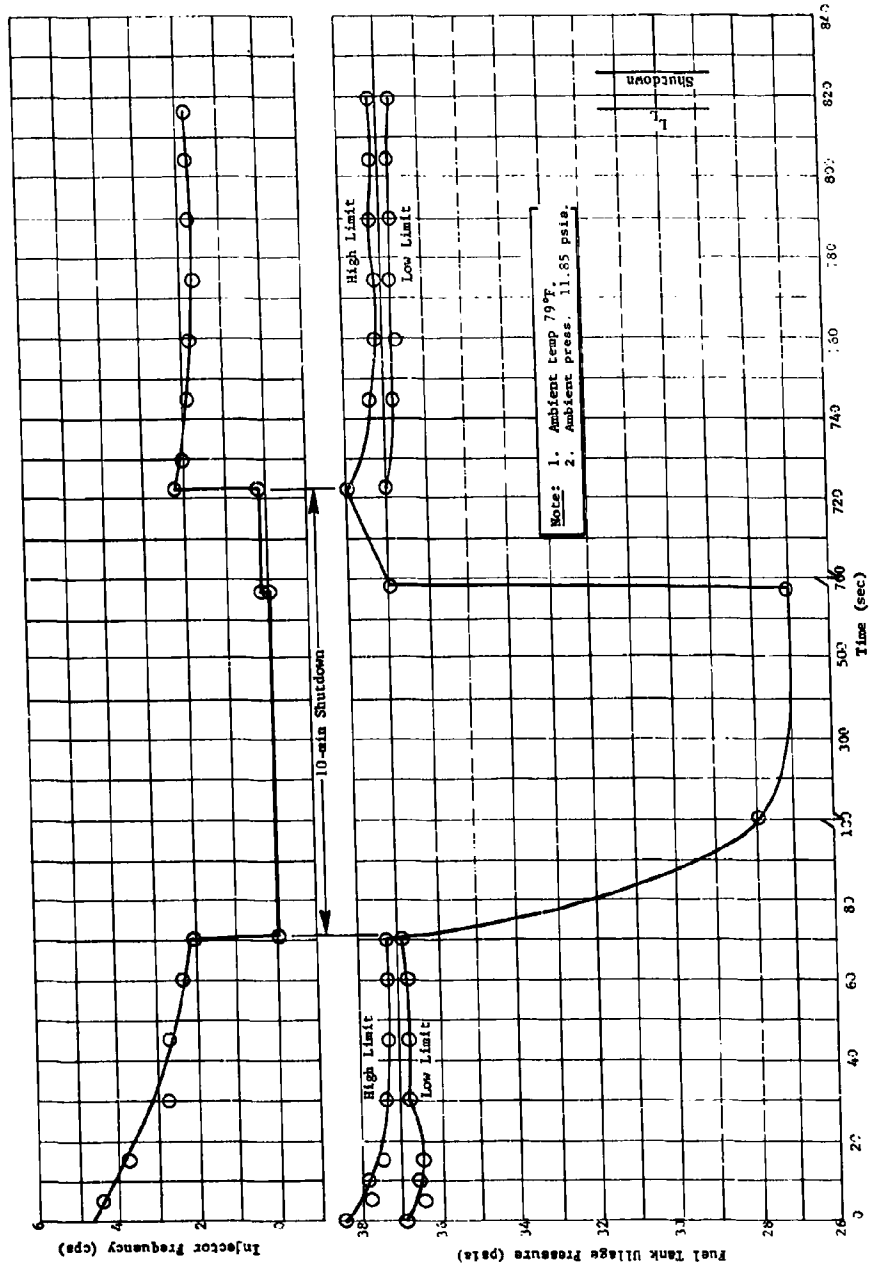


Fig. IV-22 Run 7 Phase III Oxidizer Tank Injector Performance

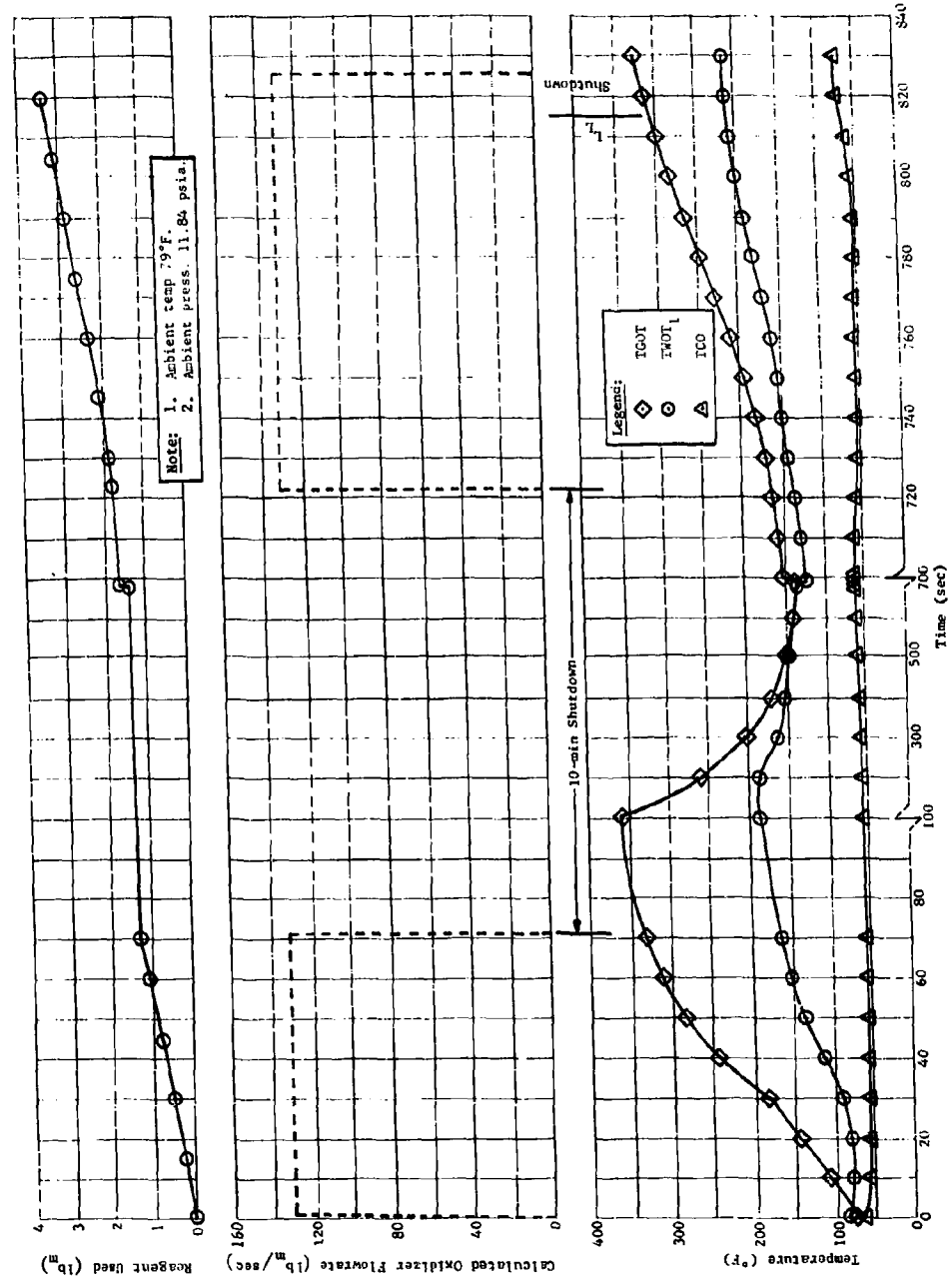
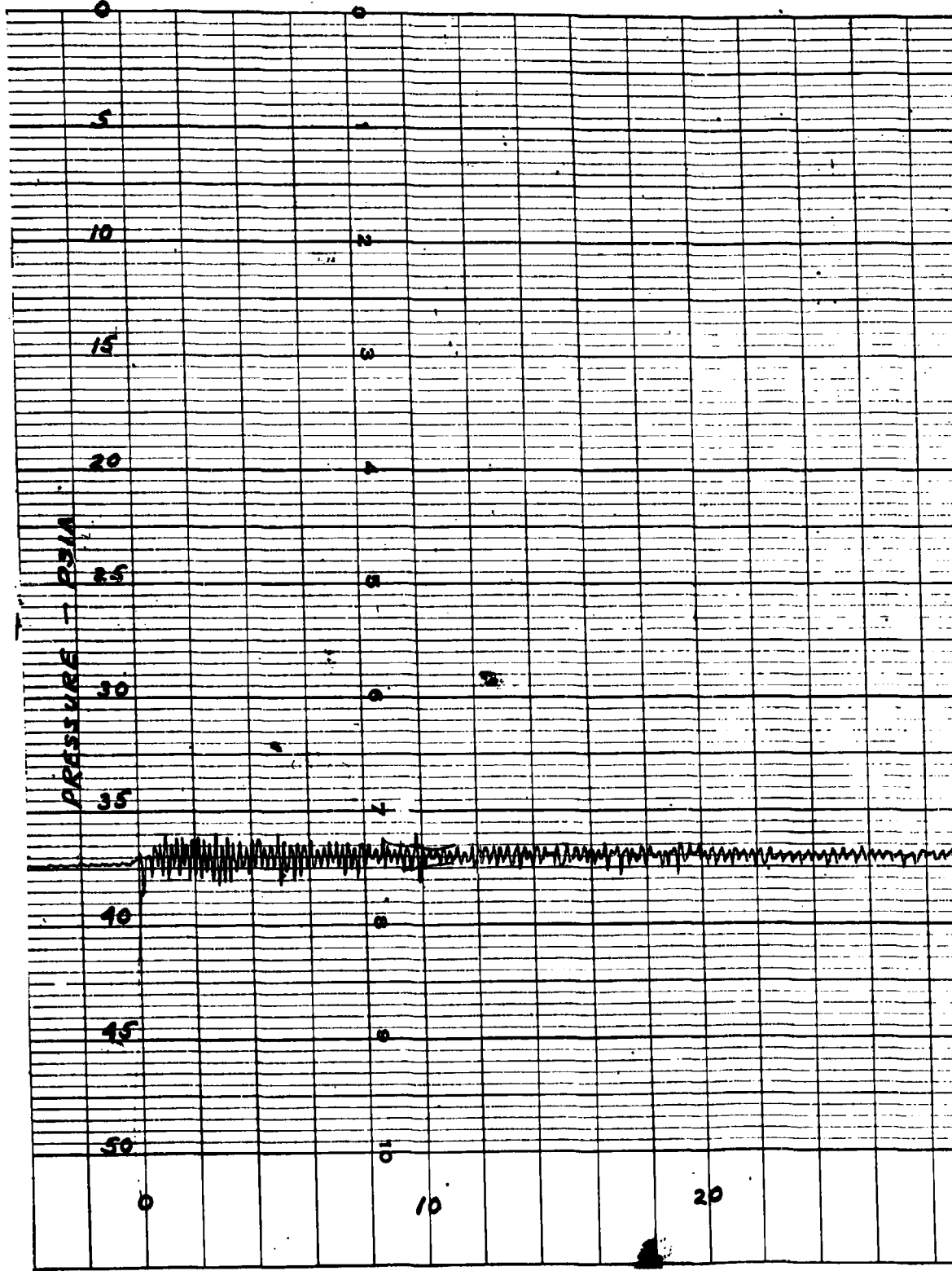
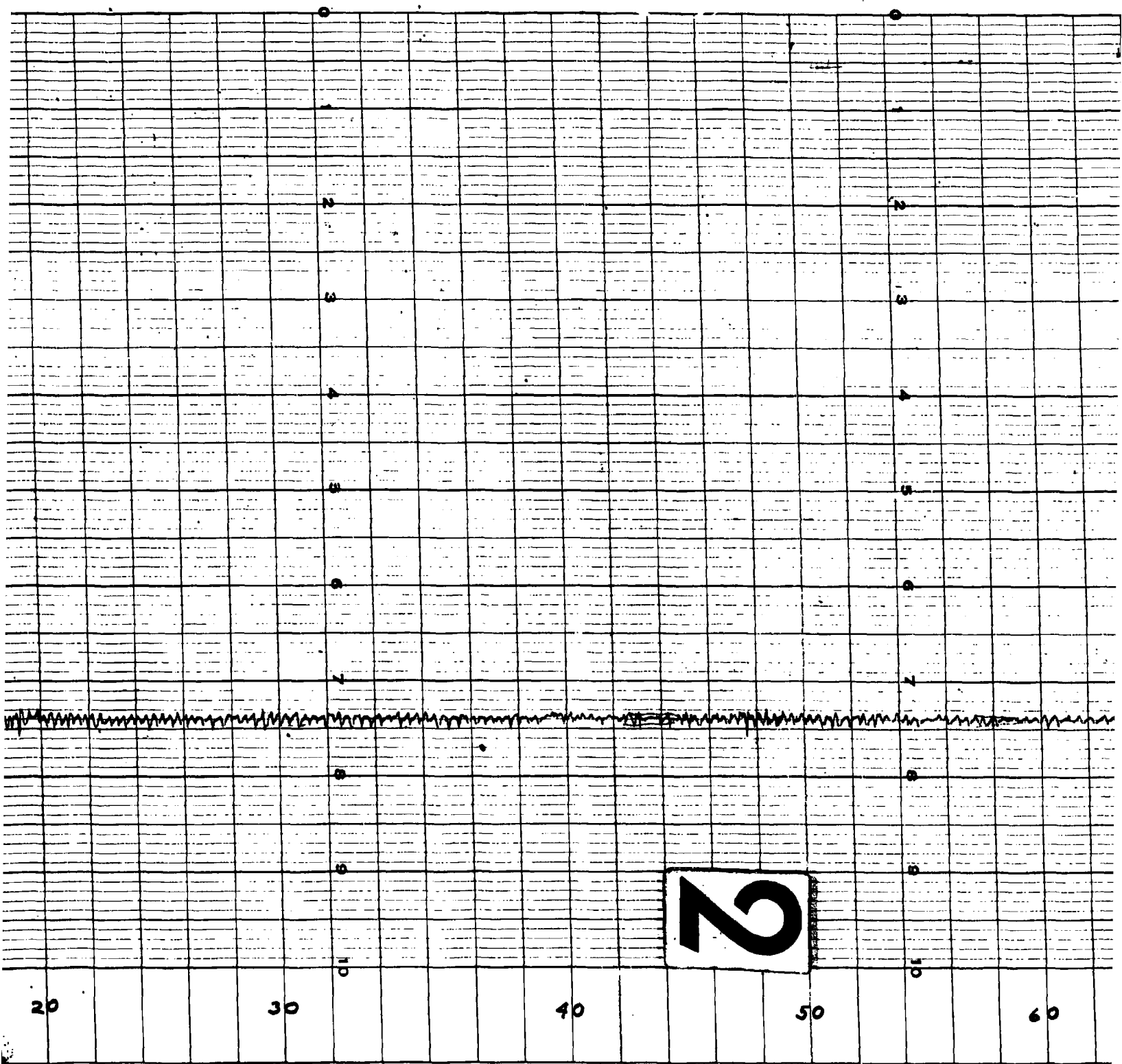
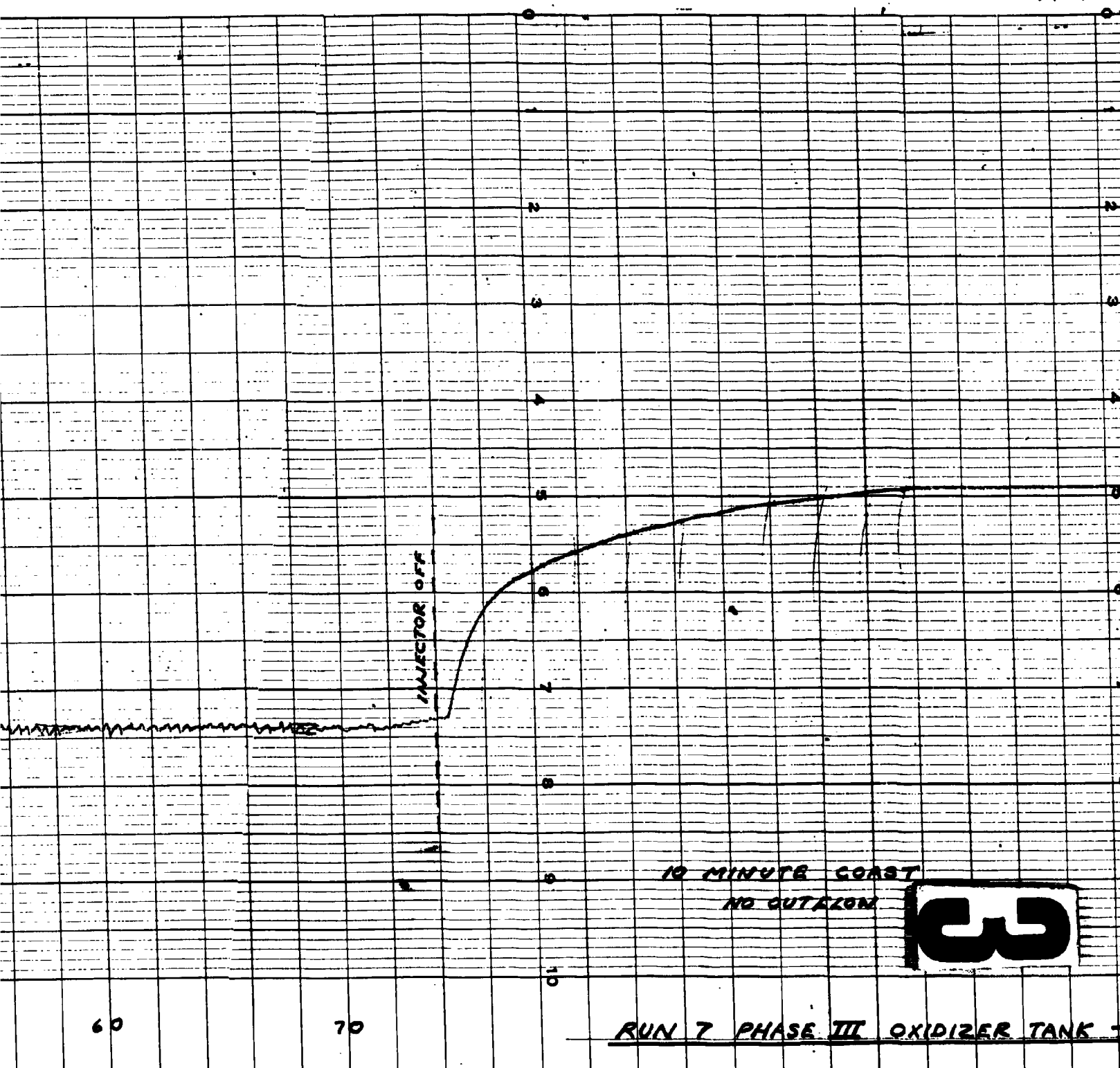


Fig. IV-23 Run 7 Phase III Oxidizer Tank MII System Performance

1



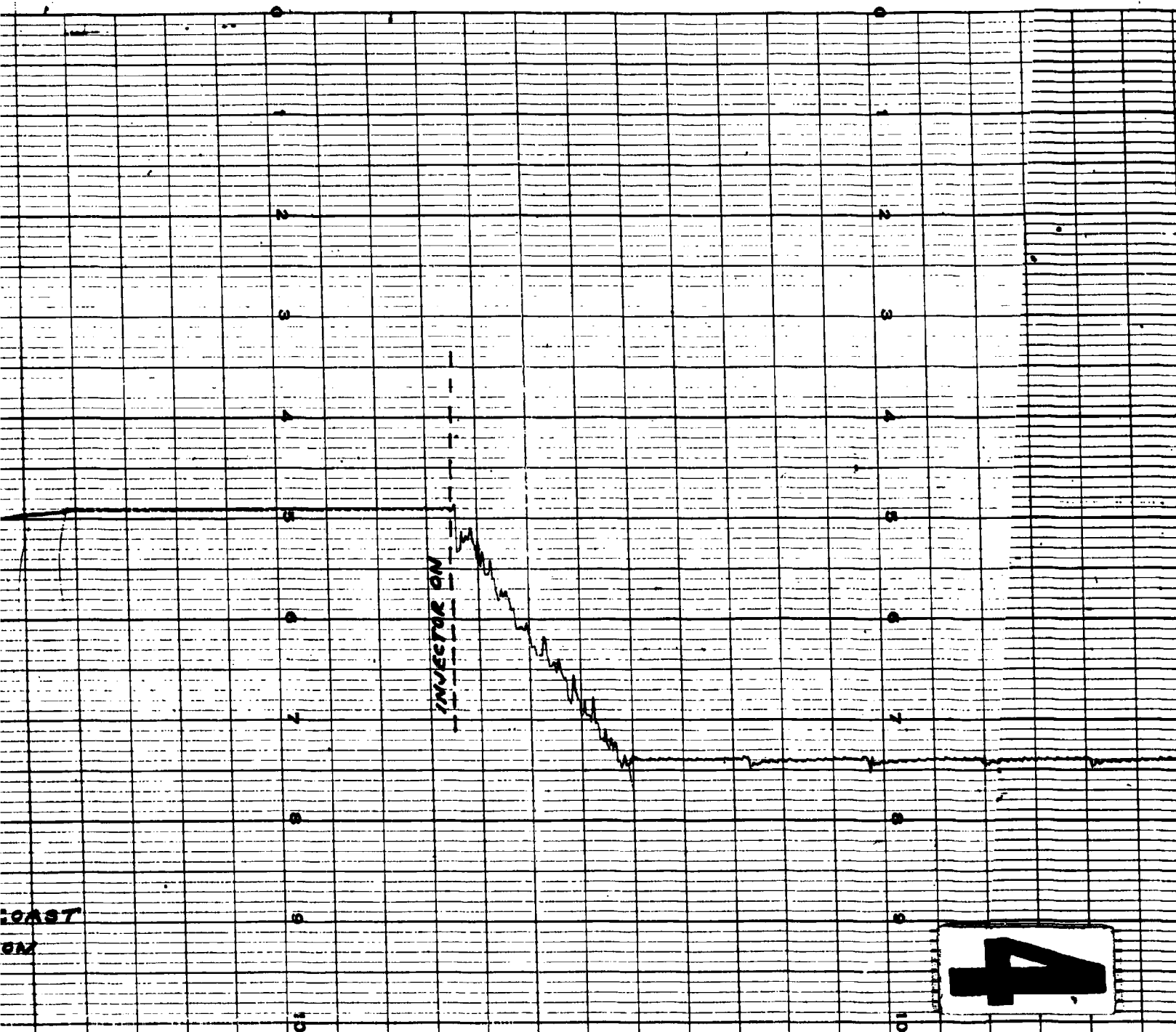




10 MINUTE COAST
NO OUTFLOW

3

RUN 7 PHASE III OXIDIZER TANK



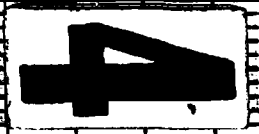
COAST
ON

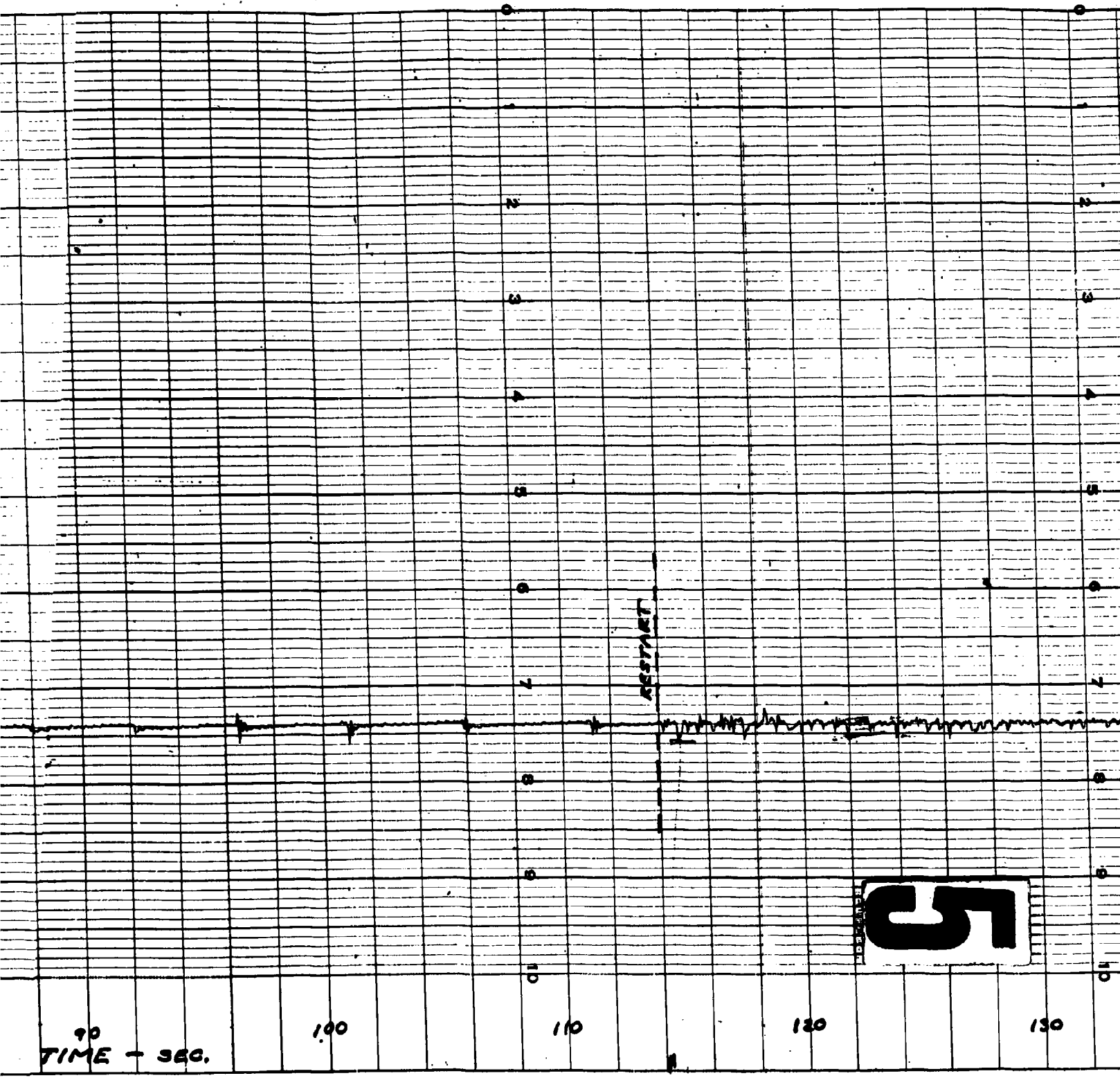
INJECTOR ON

OXIDIZER TANK - RESTART

80

90
TIME - SEC.





90
TIME - SEC.

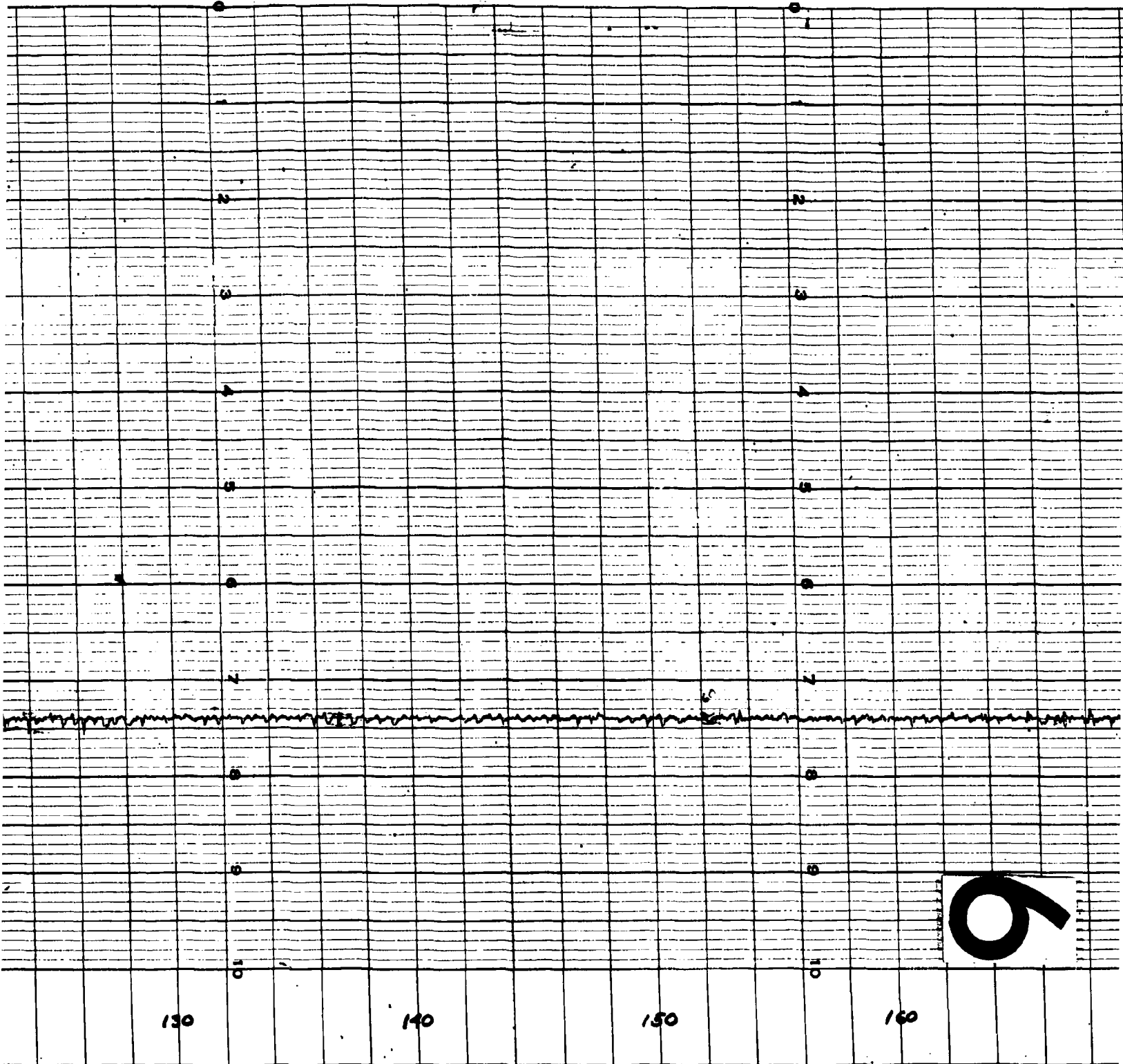
100

110

120

130

5



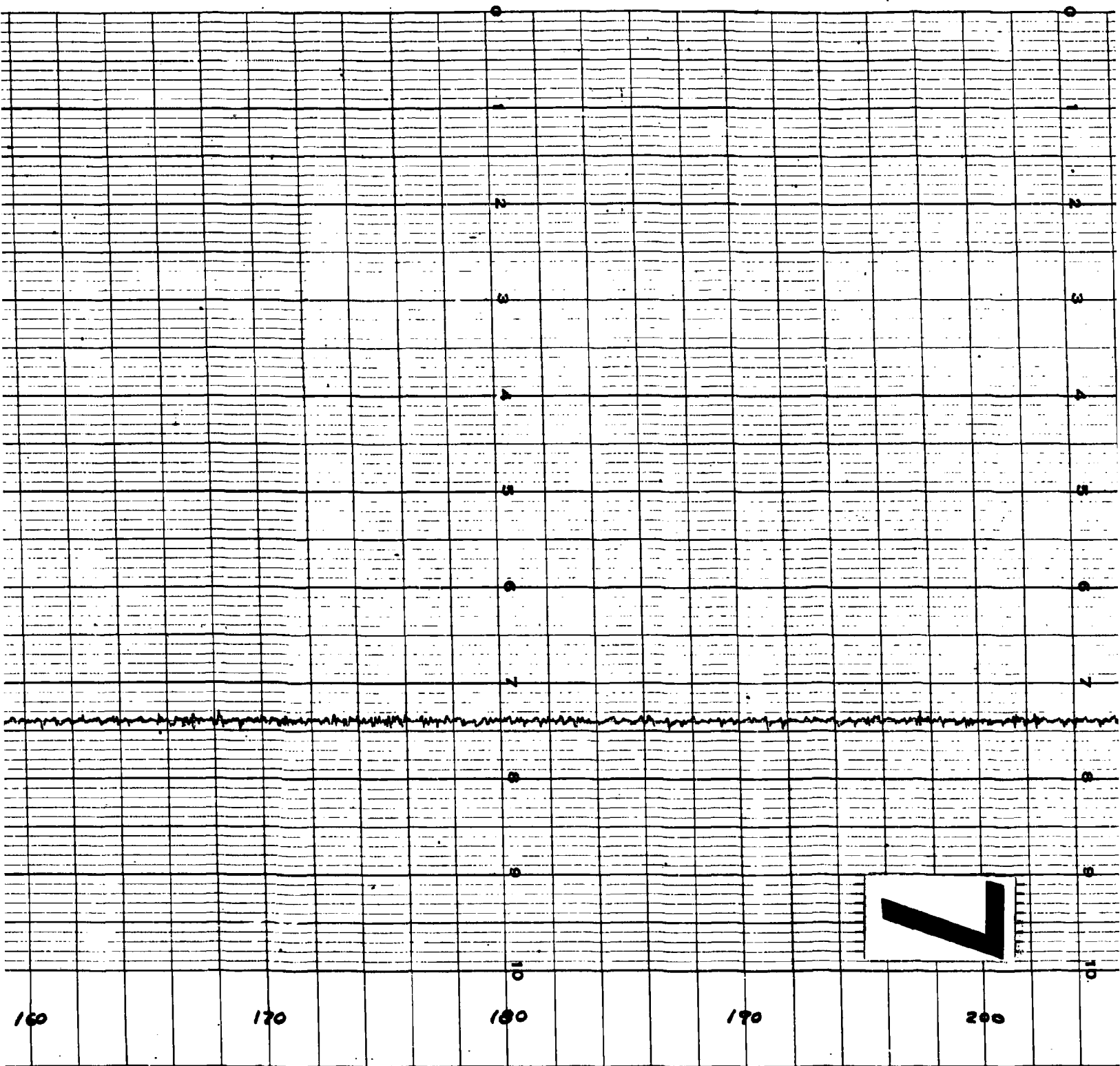
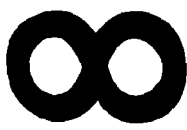
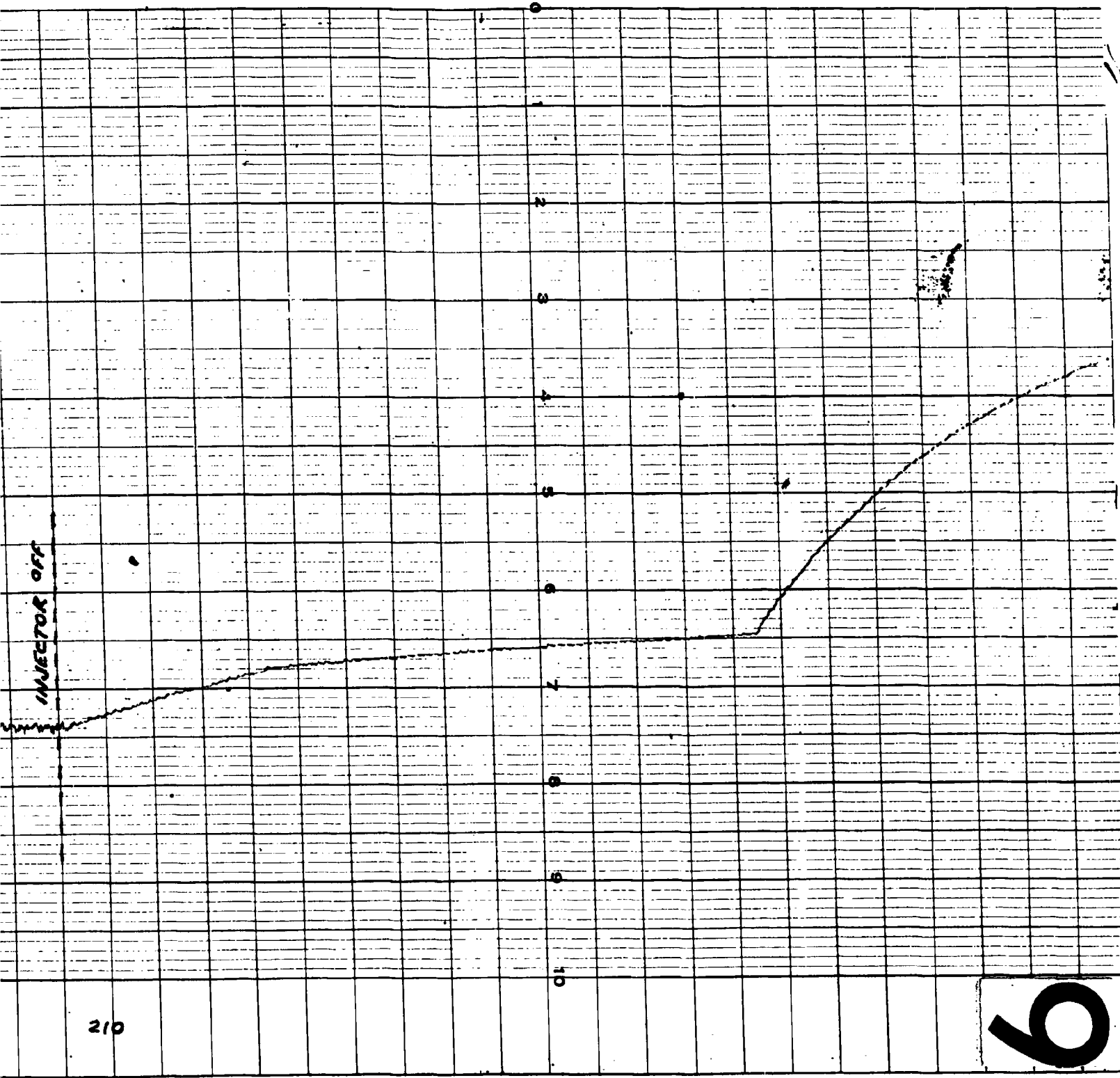




Fig. IV-24 Run 7 Actual Phase III
IV-45 an





210

6

Fig. IV-24 Run 7 Actual Phase III Oxidizer Tank Pressure Trace, Restart Test IV-45 and IV-46

V. PHASE IV PROGRAM

The final portion of the MTI program involved the analysis and interpretation of the Phase I and Phase III test data, with the basic thermo-chemical relationships compiled in the form of a Design Handbook. Results of the Martin test programs have been compared with theoretical predictions and previous data reported under AFO4(611)-6087 to establish the extent of correlation and to verify the accuracy of performance prediction. An MTI mathematical model formulated on the IBM 7094 digital computer was used to predict the Phase III pressurization system performance as well as to determine the feasibility of adopting an MTI pressurization system to the Titan II and Titan III transtage. A cost, weight, and reliability analysis of the possible Titan missile application of an MTI pressurization system with preliminary design schematics has also been completed to aid in the evaluation.

A. CORRELATION OF TEST DATA

The MTI pressurization system test results have been reviewed to determine correlation and accuracy of predicting performance of future flight systems. Test data for the Phase I Martin test program under Contract AFO4(611)-8198 have been compared with Lockheed's previous work resulting in Contract AFO4(611)-6087. Theoretical performance predictions obtained with the IBM-7094 mathematical model are compared with the Phase III data only, since the Phase I test data were used to establish the proper heat and mass transfer coefficients.

The Phase I tests were performed on a 5.33 cu ft spherical aluminum propellant tank with 5/8 in. thick walls and on a 279 cu ft aluminum cylindrical tank with elliptical domes and walls averaging 0.075 in. thick. The Lockheed test article was a 1.0 cu ft, thick walled stainless steel tank. System operating temperatures reported naturally show some divergence due to differences in heat capacity, initial temperature, and duration of exposure for the various systems. Theoretical performance is compared with the Martin data only, since the exact physical characteristics and method of operation of the Lockheed system were not known.

In general, excellent correlation was found between the actual and predicted performance of the input reaction processes of the Phase III system. Divergences in performance reported can be attributed to unidentified process influence parameters requiring further study. Comparisons of AF04(611)-6087 data previously acquired shows a serious conflict with AF04(611)-8198 data, in that a combustion gas molecular weight and apparent reaction mixture ratio are virtually reversed for direct injection process of both the fuel and the oxidizer tank. Although common ullage pressurization of the oxidizer tank was also studied, no test data are available at this time for comparison with theoretical predictions. Process gas characteristics have been compared for the various test systems with data obtained by mass spectrometer gas analysis.

1. Process Gas Characteristics

The molecular weight and composition of the process gas have been compared for the various experimental programs. Since the mixing technique affects the reaction significantly, factors such as injector nozzle contour, differential pressure, and physical characteristics of the system will alter the resultant composition of the combustion products. The results presented in this section are based on a solid stream surface reagent injection process for the single-tank tests and subsurface gas impingement for the oxidizer tank of the common ullage configuration. All tests were performed at 36 psia tank pressure and 75 psi injector differential pressure; however, the operating pressure has not been specified for the Lockheed results, but is believed to be in the 30 to 350 psig range.

A comparison of the MTI pressurizing gas molecular weight obtained from the Lockheed data and from Phase I and Phase III Martin programs are shown in Fig. V-1 and V-2 with the composition described in Table V-1. The oxidizer tank data indicate the gaseous combustion product characteristics and the resultant molecular weight of the pressurant, including the 35% mole fraction of vaporized oxidizer. Fuel vaporization was generally small in the Phase I program due to relatively cool (50°F) ambient temperatures. Consequently an increase in molecular weight of the gas was not encountered. All data are reported on a helium-free basis.

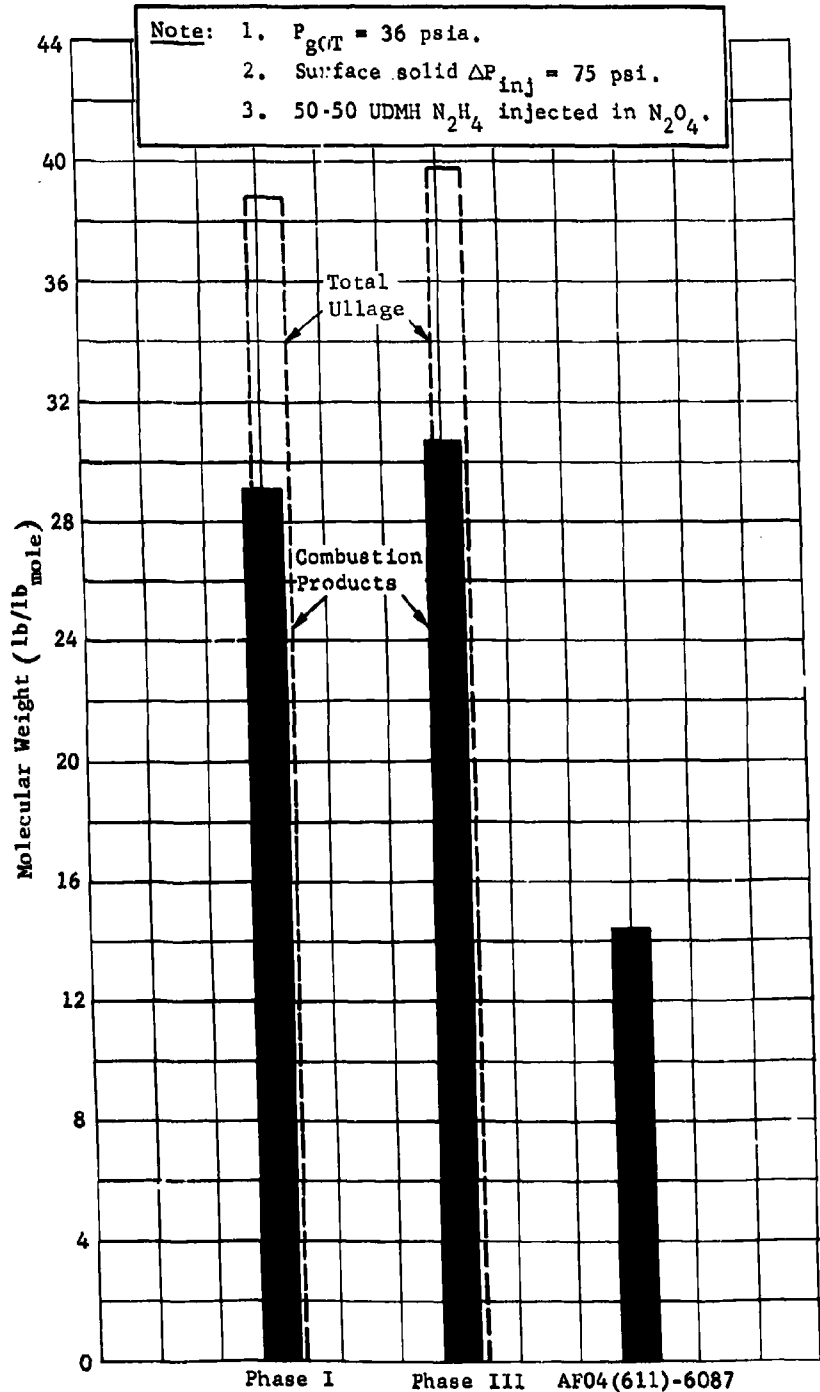


Fig. V-1 Molecular Weight Correlation, MTI in Oxidizer Tank

Note: 1. $P_{gFT} = 36$ psia
2. Surface solid $\Delta P_{inj} = 75$ psi.
3. N_2O_4 injected in 50-50 UDMH/ N_2H_4

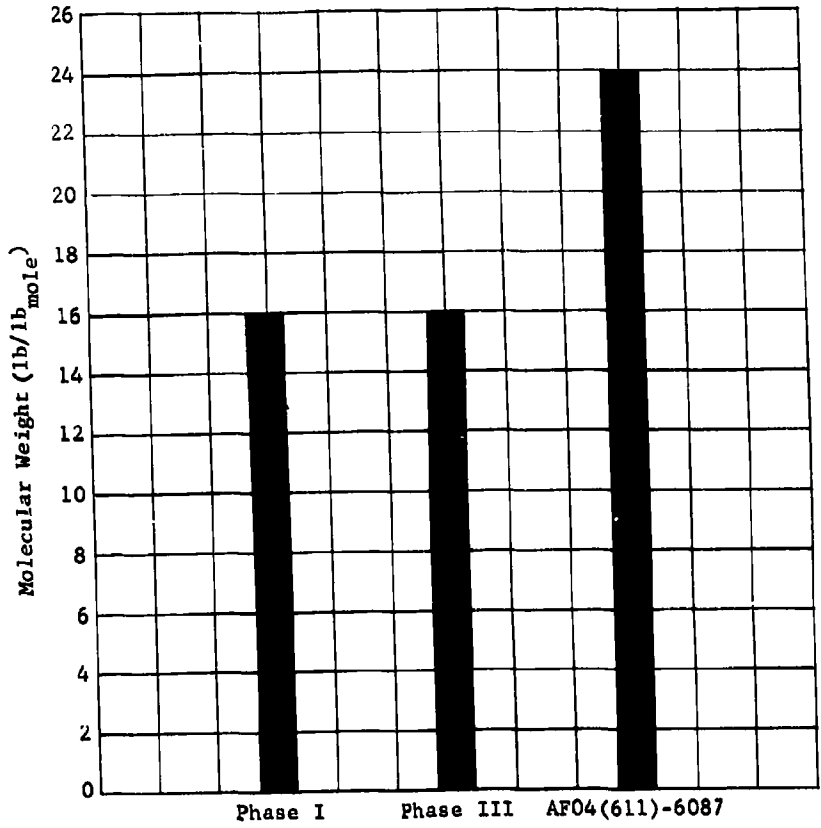


Fig. V-2 Molecular Weight Correlation - MTI in Fuel Tank

Table V-1 MTI Combustion Product Composition (Solid-Stream Surface Reagent Injection;
Correlation in Volume Percent; P = 36 psia; $\Delta P_{inj} = 75 \text{ psi}$)

Oxidizer Tank												
	H ₂	N ₂	NH ₃	CO ₂	H ₂ O	O ₂	CH ₄	CO	C	MW _{cp}	MW _u	
Phase I	1.9	58.6		17.9	14.1	6.7	1.0	-	-	29.13	38.52	
Phase III	Trace	64.7	1.04	15.04	3.12	16.10	-	-	-	30.63	39.81	
AF04(611)-6087	41.1	21.5	Trace	1.1	5.0	-	9.3	14.0	8.0	14.6	N/A	
Fuel Tank												
	H ₂	N ₂	NH ₃	CO ₂	H ₂ O	O ₂	CH ₃	CO	NO	OH	MW _{cp}	MW _u
Phase I	39.3	44.3	-	0.2	-	-	14.9	-	1.2	-	16.02	16.02
Phase III	32.4	34.1	15.6	0.2	-	-	16.2	-	1.5	-	15.98	18.00
AF04(611)-6087	6.4	29.2	-	9.73	35.8	1.5	-	12.2	-	3.2	24.00	N/A

Although excellent correlation of molecular weights was achieved from the Phase I and Phase III programs, the gas characteristics reported under AF04(611)-6087 were not in agreement. Likewise, the apparent reaction mixture ratio obtained with the solid stream surface reagent injection process showed poor correlation for all configurations. Oxidizer tank process characteristics shown in Fig. V-3 indicate the variation between Phase I and Phase III, a slight variation in fuel tank reaction mixture ratio was also obtained (see Fig. V-4). The lower reaction mixture ratio realized in the Phase III fuel tank and higher reaction mixture ratio in the oxidizer tank are probably due to a change in injector design. (The Phase I injector was a flat plate of 0.013 in. dia orifice, and the Phase III injector employed a 2 in. long, 0.047 in. dia injector tube.) The exact flow characteristics of the Lockheed injector are not known but crimped injector tubes 3/32 to 5/32 in. in dia were used to give a fan spray. The injector differential pressure, however, was apparently sufficiently low to prevent atomization of the reagent.

Table V-2 compares data from a gas generator process with data on typical fuel tank ullage gas composition for a 150-sec MTI pressurization test with solid stream surface injection of nitrogen Tetroxide. The average molecular weight of the ullage gas shows the dilution of the initial nitrogen, used for prepressurization, by combustion products with a variation in gas molecular weight from 27.22 near the start of the test to 18.71 at the end. The change in molecular weight of the ullage gas corresponds to that predicted with a constant combustion product molecular weight of approximately 13. The average composition of the MTI combustion products were determined by extracting the fuel vapor and a portion of the nitrogen present from prepressurization, with a resultant molecular weight of 12.39. In later tests, an increase in molecular weight was obtained due to a change in gas analysis technique. A comparison with typical gas generator products of combustion indicates that only a slightly lower molecular weight is achieved with the MTI pressurization process. The reactive constituent ammonia is reduced by approximately 60%. The absence of water in the MTI combustion products is due to condensation occurring in the actual system and is not considered a particular advantage over the small percentage detected with the gas generator system.

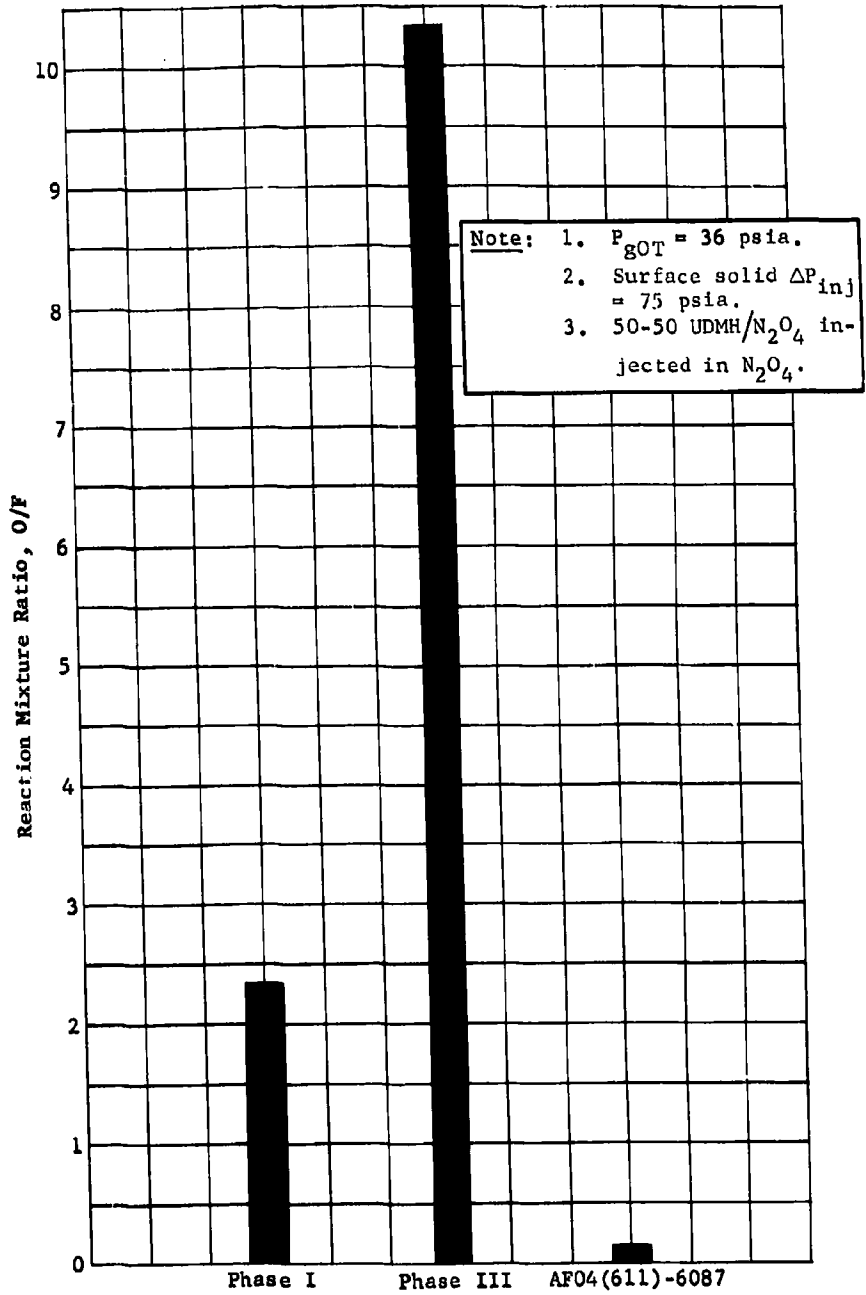


Fig. V-3 Reaction Mixture Ratio - MTI Oxidizer Tank

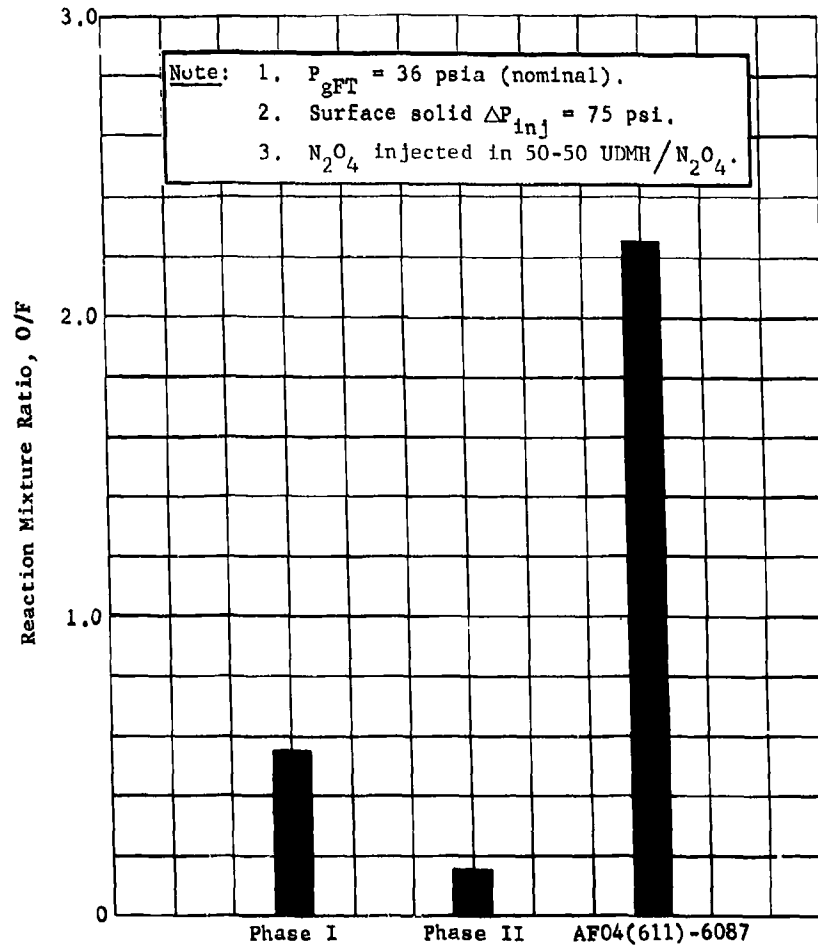


Fig. V-4 Reaction Mixture Ratio - MTI Fuel Tank

Table V-2 Propellant Tank Pressurizing Gas Composition, Volume Percent

Time (sec)	MTI Ullage Gas				MTI Combustion Products	Gas Generator Combustion Products
	20	60	120	160		
N ₂	93.33	77.31	56.52	53.40	23.0	22.53
H ₂	2.23	13.48	24.76	30.36	48.3	26.74
CH ₄	0.42	3.84	6.91	7.32	12.5	11.10
NH ₃	2.97	3.90	8.86	7.02	14.2	35.17
NO	0.52	0.73	1.01	1.15	1.9	-
UDMH	0.52	0.73	1.94	0.74	-	-
CO	-	-	-	-	-	1.96
CO ₂	0.1	0.1	0.1	0.1	0.1	0.1
H ₂ O	-	-	-	-	-	0.34
Miscellaneous (less than 1%)					-	2.14
Actual Molecular Weight	27.22	23.85	20.40	18.71	12.39	15.86

2. Small-Scale System Performance

The performance of the Phase I small-scale MTI pressurization system developed under AFO4(611)-8198 has been compared with the data generated under AFO4(611)-6087 for a direct reagent injection process. Comparisons were based on the amount of reagent required to pressurize a given volume at operating pressures of 36 to 200 psia. The final ullage volume in the case of AFO4(611)-8198 was 4.91 cu ft; and for the AFO4(611)-6087 program, 1 cu ft. The corresponding maximum ullage gas temperatures for the two systems are shown in Fig. V-5 indicating a slight divergence primarily due to a difference in reported apparent process reaction mixture ratios of the two systems (the higher gas temperature corresponding to a higher reaction mixture ratio).

Pressurant demand for the small-scale single tank systems is compared in Fig. V-6 and V-7 with a presentation of comparable performance for the common ullage Phase I system shown in Fig. V-8. The pressurant demand curves indicate the quantity of fuel and oxidizer required to pressurize a given volume with the extent of vaporization, condensate formation, and final system temperatures encountered. Significant variances in the AFO4(611)-6087 data are due to the differences in reaction mixture ratio, lack of condensate formation or propellant vaporization, or both, and a slight change in final gas temperature.

3. Full-Scale System Performance

The performance of the Phase III full-scale MTI pressurization system developed under AFO4(611)-8198 has been compared with the theoretical performance obtained from the IBM-7094 mathematical model for the direct reagent injection process. Predictions are based on the actual reaction mixture ratio with the previously established heat and mass transfer coefficients obtained from the Phase I program. Performance histories for typical continuous 150-sec runs are shown in Fig. V-9 and V-10, with a comparison for the theoretical values. Pressure control at the start of the run was not within the ± 0.5 psia predicted range. Due to a slightly oversized injector, the actual fuel tank bulk gas temperature measurement was not functioning properly, consequently, the quantity of gas generated was approximated with a partial verification of expected reagent consumption obtained for the conditions encountered.

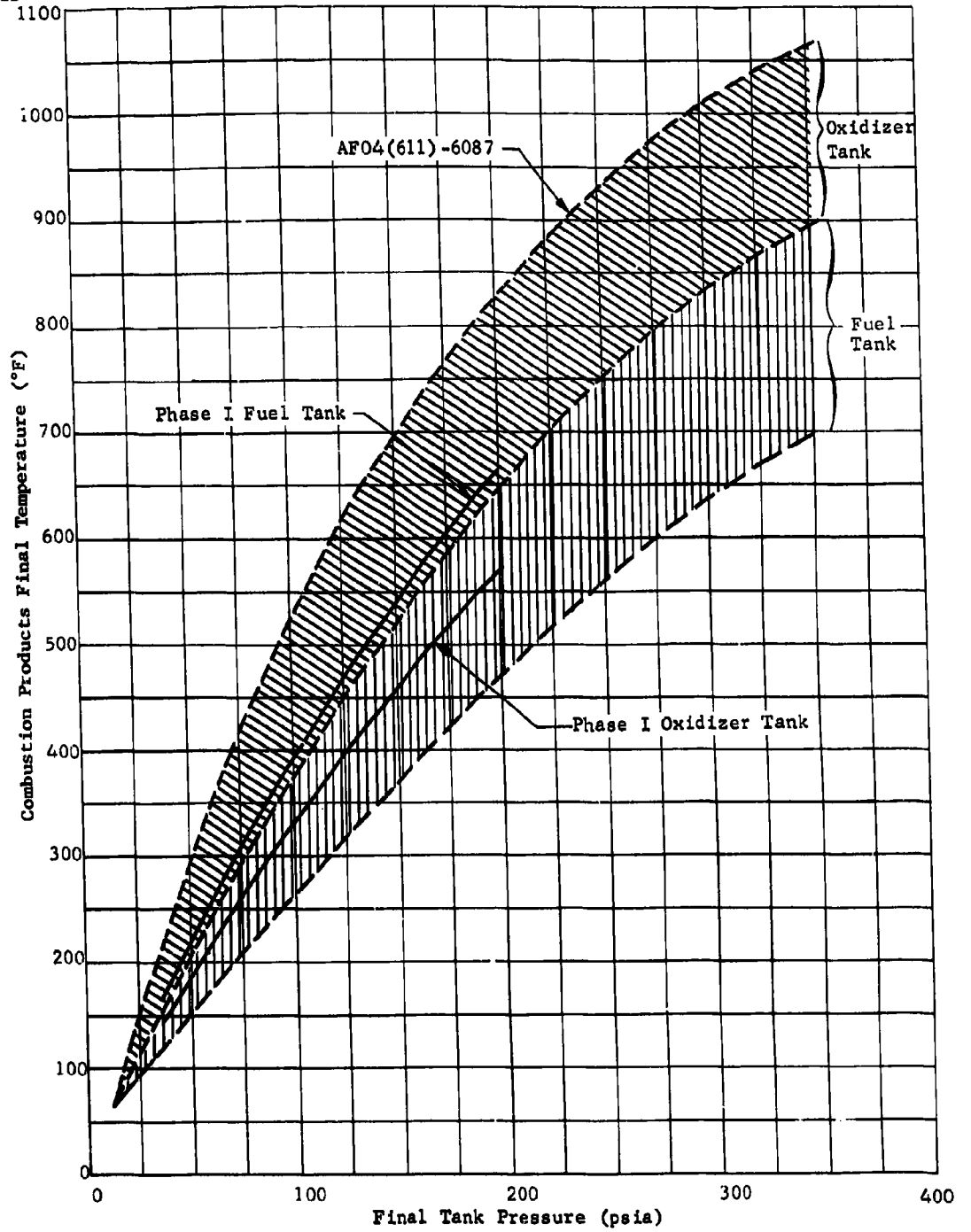


Fig. V-5 MTI Final Gas Temperature Comparisons, Small-Scale Systems

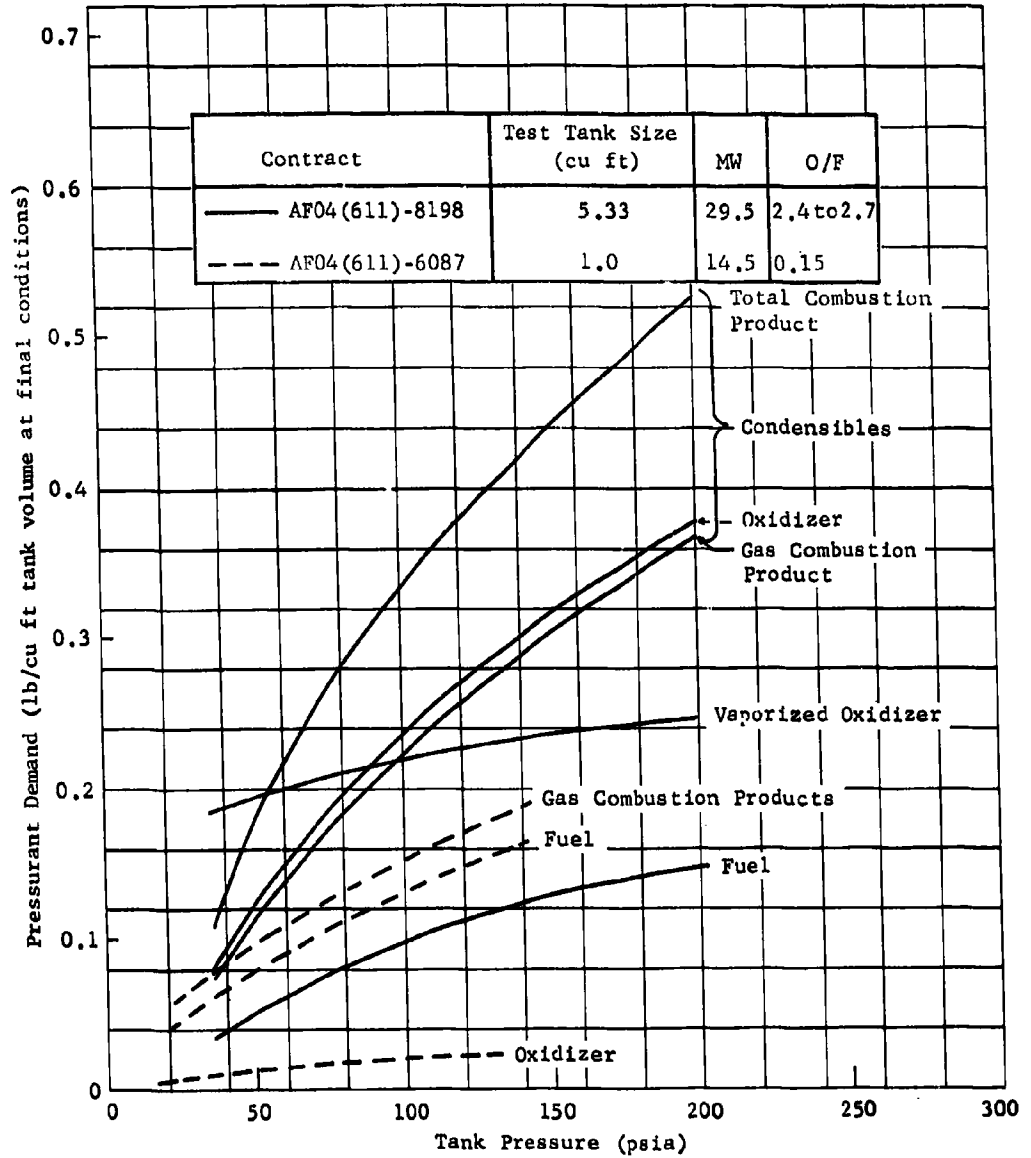


Fig. V-6 MTI Pressurant Weight, Oxidizer Tank, Comparison of Results from AF04(611)-6087 and AF04(611)-8198

Contract	Test Tank Size (cu ft)	MW	O/F
AF04(611)-8198	5.33	16	0.45 to 0.55
AF04(611)-6087	1.0	24	2.25

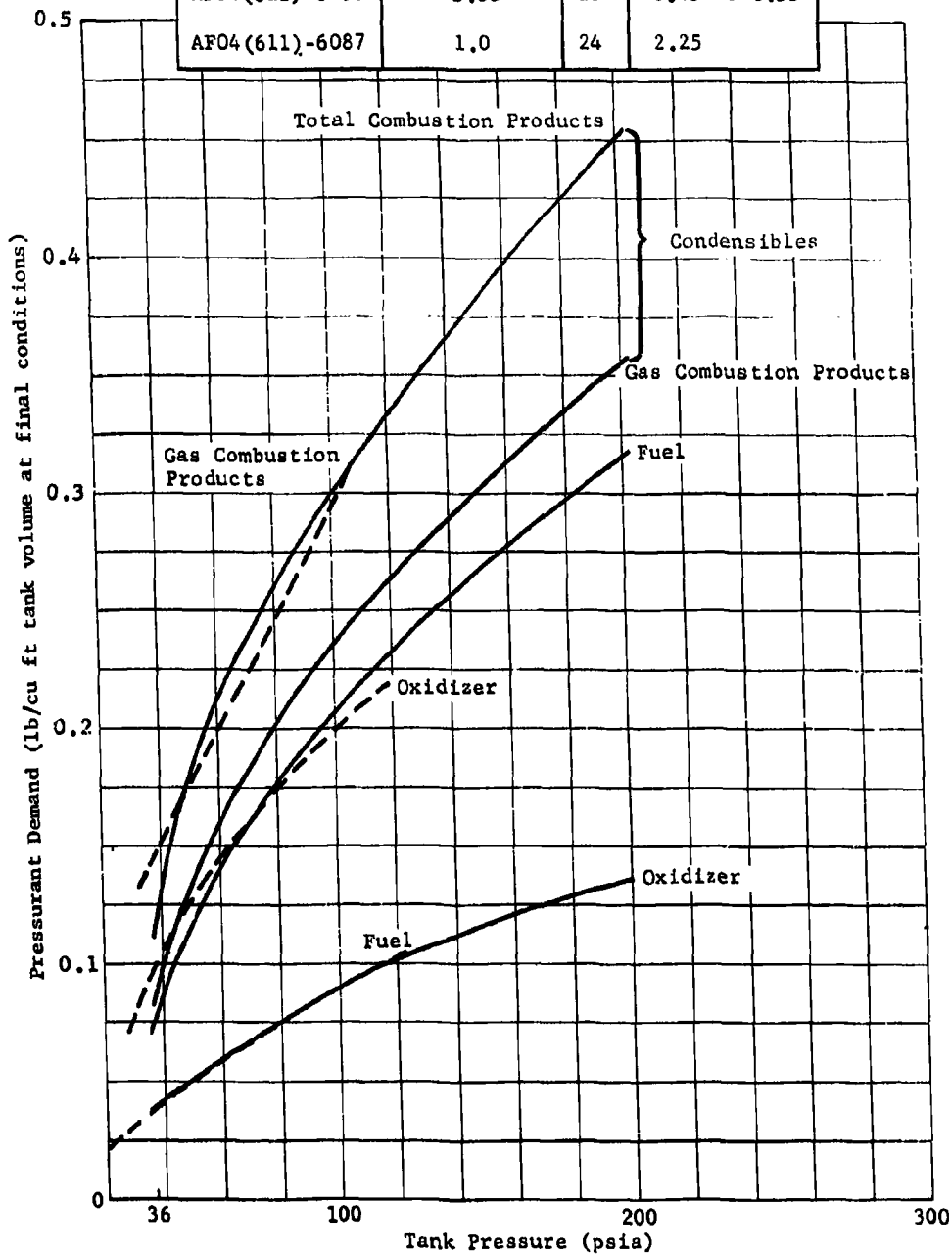


Fig. V-7 MII Pressurant Weight, Fuel Tank, Comparison of Results from AF04(611)-6087 and AF04(611)-8198

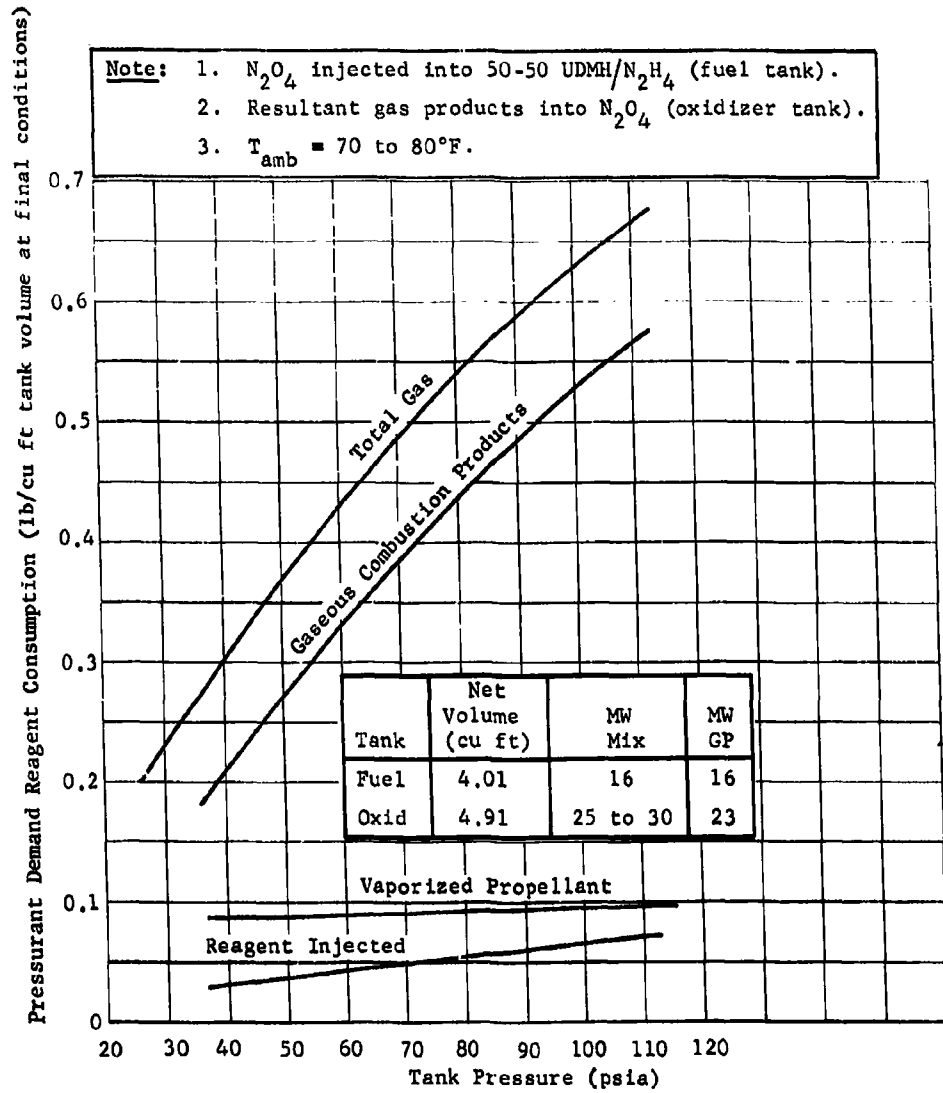


Fig. V-8 MII Common Ullage Pressurant Weight

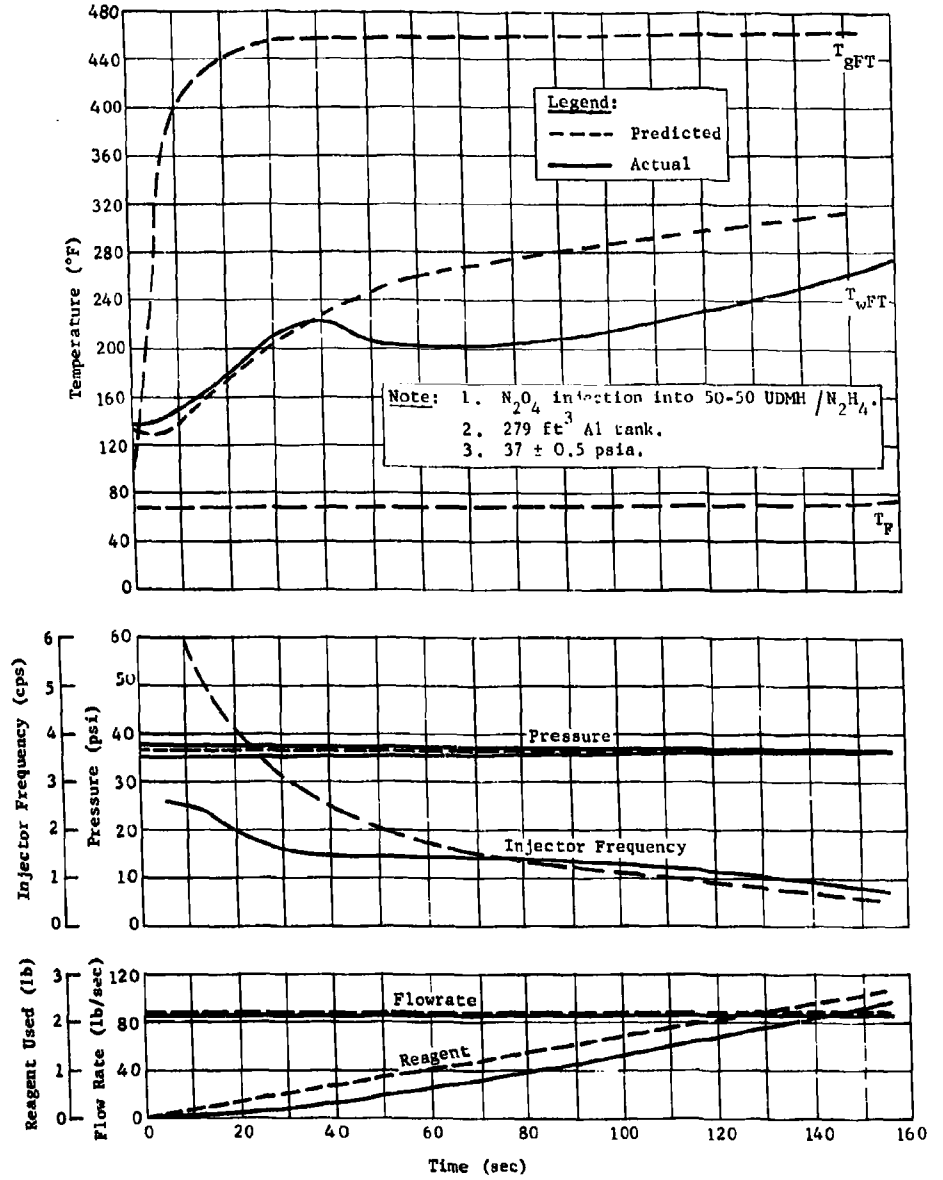


Fig. V-9 Phase III MTI Fuel Tank Performance

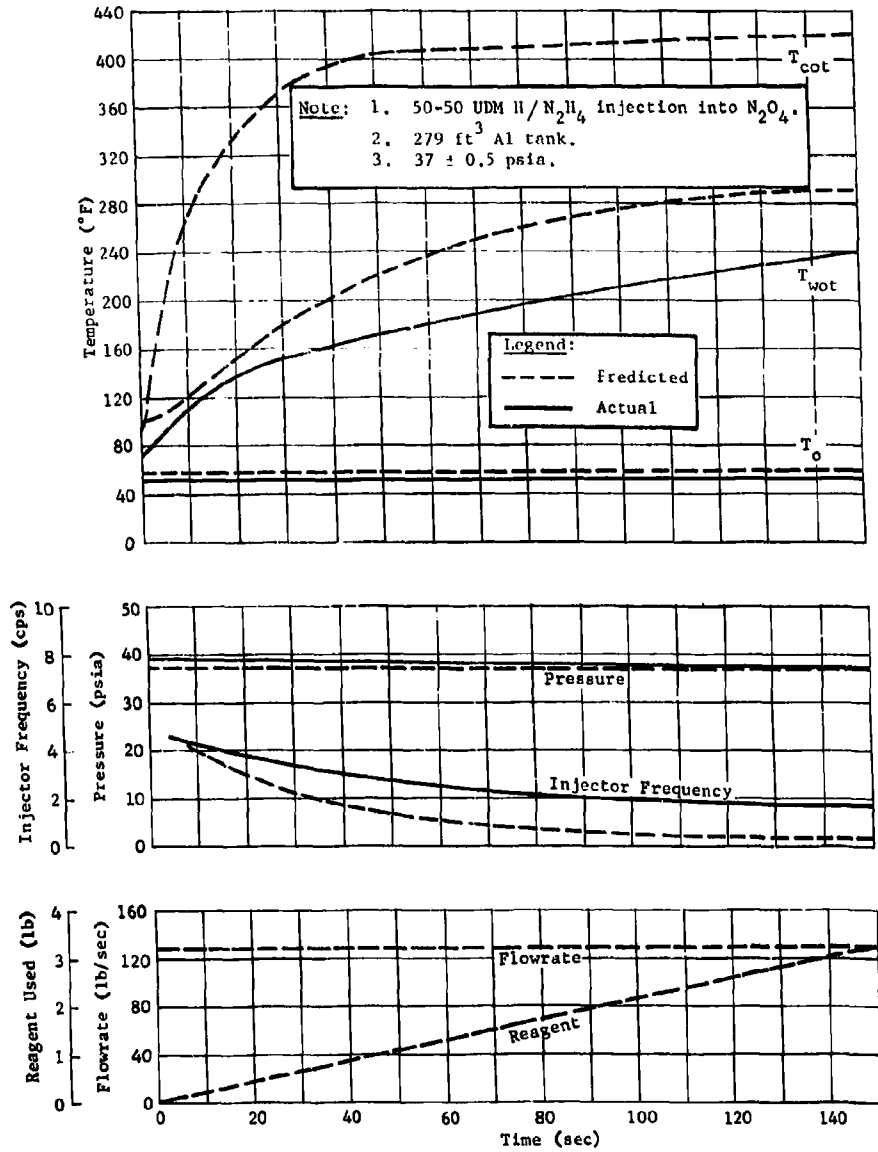


Fig. V-10 Phase III MTI Oxidizer Tank Performance

B. MTI SYSTEM DESIGN HANDBOOK

In this section design information is presented to permit preliminary sizing of main tank injection pressurization systems for N_2O_4 -50/50 mixture of UDMH and N_2H_4 propellant combination. It must be recognized that the thermodynamic actions occurring during the process are not completely understood. Consequently, certain approximations are made that may require revision pending further investigation. Due to the rapid time-varying nature of the process, non-steady-state conditions prevail so that no method, short of an exact solution of the differential equation expressing the energy transfer during the expulsion process, will give accurate results. A satisfactory substitute for this is the digital computer program described in Chap. III, Sec A.3, which solves the energy transfer differential equation on an incremental time basis.

In some applications where rapid preliminary design information is desired, the use of such computer program may be discouraged due to cost, time, or similar considerations. It is expressly for these situations that the MTI design method is directed. Certainly, complete re-examination of these results by the computer program should follow when the MTI process appears to be attractive for the particular application under consideration and when greater accuracy is desired.

1. General Design Considerations

The design of any MTI pressurization system is governed by the following requirements:

- 1) Mission profile;
- 2) Tank pressure;
- 3) Reliability emphasis.

They are discussed in the following paragraphs.

Mission Profile - A feature of the MTI system is the low gas density pressurant generated. This is due primarily to operation at elevated gas temperatures, although a moderate gas molecular weight (16 to 30) is also beneficial. However, when mission profile is such that the influence of heat loss from the pressurant becomes extensive, such as for long-term in-space storage applications, the advantages of low gas density tend to disappear.

Tank Pressure - Equilibrium gas temperatures of MTI systems rise appreciably under increasing tank pressure levels. Figure II-113 shows a typical range valid for 5/8-in. aluminum walls under exposure at atmospheric temperatures (40 to 80°F). It should be evident that for flight-weight tanks, wall temperatures become greater for the thinner walls. Consequently, wall temperature limitations and wall material selections influence the design.

Reliability - Reliability considerations govern the design of all flight systems. For this discussion, it is presumed that the overall reliability of MTI systems are comparable to other types of tank pressurization systems. The principle difference, then, of the MTI System is that pressurant gas properties are not fixed but may show certain variations. These differences can be explained partly by imperfect injection patterns, although more study is needed for quantitative definition. Evidence shows that wide reagent spray patterns elevate gas temperatures excessively. Besides increasing the wall temperatures, increases in molecular weight and reaction mixture ratio influences are sustained.

Thus solid-stream injection is considered the best injection arrangement because of desirable products of reaction and heat dissipation to the liquid propellant. Additionally, the MTI systems should incorporate protective devices to prevent developing partial spray patterns from contaminated propellants.

2. Sizing of Propellant Tanks

For a given vehicle application, the following parameters are generally known or can easily be computed from standard thermodynamic relationships:

Propellant Mixture Ratio	= λ (O/F)
Thrust	= F lb _f
Burning Time	= τ sec
Specific Impulse	= I_{sp} (lb _f -sec)/lb _m
<u>Initial Ullage Volume</u> Total Tank Volume	= $K_u \approx 0.05$
Acceleration	= g/g_c

$$\text{Tank Pressure Requirement, } P_t = \frac{\text{NPSH}_p}{144} + P_v - \frac{h\rho_a}{144g_c} + \Delta P_{\text{line}}, \quad [1]$$

$$P_t = P_c - \frac{h\rho_a}{144g_c} + \Delta P_{\text{line}}. \quad [2]$$

Equation [1] applies to pump-feed propulsion systems and Eq [2] to pressure-fed engines.

Total tank volumes may now be computed:

$$\text{Usable Propellant, } W_o = \frac{(F)(\tau)}{I_{sp}} \left(\frac{\lambda}{1 + \lambda} \right), \text{ lb}_m$$

$$W_f = \frac{(F)(\tau)}{I_{sp}} \left(\frac{1}{1 + \lambda} \right), \text{ lb}_m$$

Vaporized and Trapped Propellant (Unusable) = W_{to} and W_{tf} (given),

$$\text{Total Tank Volume, } V_o = (W_o + W_{to}) / \rho_o (1 - K_{uo}),$$

$$V_f = (W_f + W_{tf}) / \rho_f (1 - K_{uf}).$$

Tank sizes may require minor adjustments to account for pressurant liquid storage and condensables. Following the sizing of propellant tanks, the selection of tank material and wall thickness must be made. Generally, stress considerations based on launch or in-flight loads predominate, although for the MTI systems, the additional wall heating from the hot gas pressurant must be considered for the established operating tank pressure. Tank shape and tank thermal capacity will then be reasonably identified for the determination of pertinent MTI pressurization system performance parameters.

3. System Operating Temperatures

Reagent consumption is primarily a function of the molecular weight and equilibrium temperature of the gas, the wall thermal capacity, and injection dynamics. Other less critical functions are burning time, external environment, and tank pressure volume. It is evident that these factors are interdependent and must be evaluated concurrently; however, an approximation of the ullage gas temperature may be made from an inspection of the heat capacity of the system.

The design method is essentially a solution of the general energy Eq [3] applied to the ullage gas. Because of the time-varying nature of the gas conditions during the expulsion process, weighted average value properties are substituted and the equation solved on a steady-state basis.

The general energy equation applied to the ullage gas for a single tank injection is:

$$U_f - U_i = \Delta H_{\text{gas}} + \Delta H_v - \int_1^2 P dV - \sum Q - \Delta H_b. \quad [3]$$

The term ΔH_b is the enthalpy of gas bled from the main tank (common ullage pressurization). The term ΔH_g is the total enthalpy of the generated gas products excluding the enthalpy of condensables. Consequently, $\sum Q$, the total heat exchange, includes only the convective and radiative heat exchange to the walls and propellant. Such heat exchange is also determined independently from the standard heat transfer relationship, i.e.,

$$\sum Q = hA\Delta T_{\text{liq}}\Delta\tau + hA\Delta T_{\text{wall}}\Delta\tau \quad [4]$$

The value for $\sum Q$ for Eq [4] is then substituted into Eq [3], which may now be solved for the final equilibrium gas temperature. Direct solution of Eq [3] is accomplished by trial and error. A final gas temperature is repeatedly selected, until the identity is obtained. Generally three trials are required to obtain a reasonable agreement.

To aid in the solution, only the convective heat transferred to the wall in Eq [4] need be calculated. This is related to total convective heat by means of the empirical ratio, $(Q_{\text{conv liq}})/Q_{\text{conv}} = C_1$, and $Q_{\text{conv}} = (Q_{\text{conv wall}})/(1 - C_1)$. The term C_1 , an empirical constant, is primarily a function of the injection dynamics, tank configuration, and ullage temperature.

In addition, a predominate influencing factor for C_1 is the combustion reaction process. For example, for the fuel tank reaction, the value is approximately 0.87, but for the oxidizer tank the value decreases to 0.37.

The simultaneous solution of Eq [3] and [4] with the modification noted above results in the Eq [5], for a zero bleed application.

Certain constants for any given application are noted. These are identified in the section that follows:

$$\frac{C_9 \bar{T}_g - \bar{T}_w^{4/3}}{T_g} = \frac{C_3 - C_5 t_{gf}}{T_{gf}} + C_6 - C_4 + C_{10} C_{11}. \quad [5]$$

In addition, equations defining the average gas and wall temperatures are required. To simplify the problem, it is assumed that the wall temperature history is linear and the entire gas-exposed wall surface is at equilibrium temperature. The wall temperature rise becomes

$$\Delta t_w = \frac{\Delta \tau h_g (\bar{T}_g - \bar{T}_w) + \sum (Q/A)_{ext}}{144 C_p \rho t}, \quad [6]$$

and the mean wall temperature is

$$\bar{T}_w = \frac{2 t w_1 + C_2 h_g \bar{T}_g + \frac{\sum (Q/A)_{ext}}{144 C_p \rho t}}{2 + C_2 h_g}. \quad [7]$$

When the influence of wall temperature from aerodynamic or space heating or both is negligible, $(Q/A)_{ext}$ is virtually zero and Eq [6] and [7] reduce to:

$$\Delta t_w = C_2 h_g (\bar{T}_g - \bar{T}_w), \quad [8]$$

$$\bar{T}_w = \frac{2 t w_1 + C_2 h_g \bar{T}_g}{2 + C_2 h_g}. \quad [9]$$

The mean gas temperature is

$$\bar{T}_g = t_{g1} + \eta (t_{gf} - t_{g1}), \quad [10]$$

where η is based on the actual variation of gas temperature with time. Typical test traces show that $\eta \approx 0.667$. The wall heat transfer coefficient, h_g , is expressed by conventional free convection heat transfer moduli, which reduce to:

$$h_g = C_8 \frac{(\bar{T}_g - \bar{T}_w)^{1/3}}{(\bar{T}_g)}, \quad [11]$$

where

$$C_8 = f \left(\frac{2 \text{ MW}^2 C_p a k^2}{\mu} \right)^{1/3}$$

4. Gas Properties

Chemical analysis of the test gas samples indicate the following properties of the MTI combustion gas:

- 1) Molecular Weight. The molecular weight of resultant MTI combustion gas products are shown in Fig. V-11. These were obtained either from surface solid stream injection for single-tank pressurization or subsurface gas impingement in the oxidizer tank for common ullage pressurization.
- 2) Thermodynamic Properties. Gas properties such as specific heat, thermal conductivity, and viscosity are given in the following tabulation. These properties represent combustion gas mixtures diluted with 5% initial ullage prepressurization helium and vaporized oxidizer in the oxidizer tank. Slight modification should be made when prepressurizing with nitrogen.

	C_p (Btu/lb °R)	k (Btu/sec °R ft)	μ (lb/ft sec)	MW (@ 36 psia)
Fuel Tank Injection	0.56	1.7×10^{-5}	1.14×10^{-5}	15.2
Oxidizer Tank Injection	0.85	1.648×10^{-5}	1.11×10^{-5}	41.0

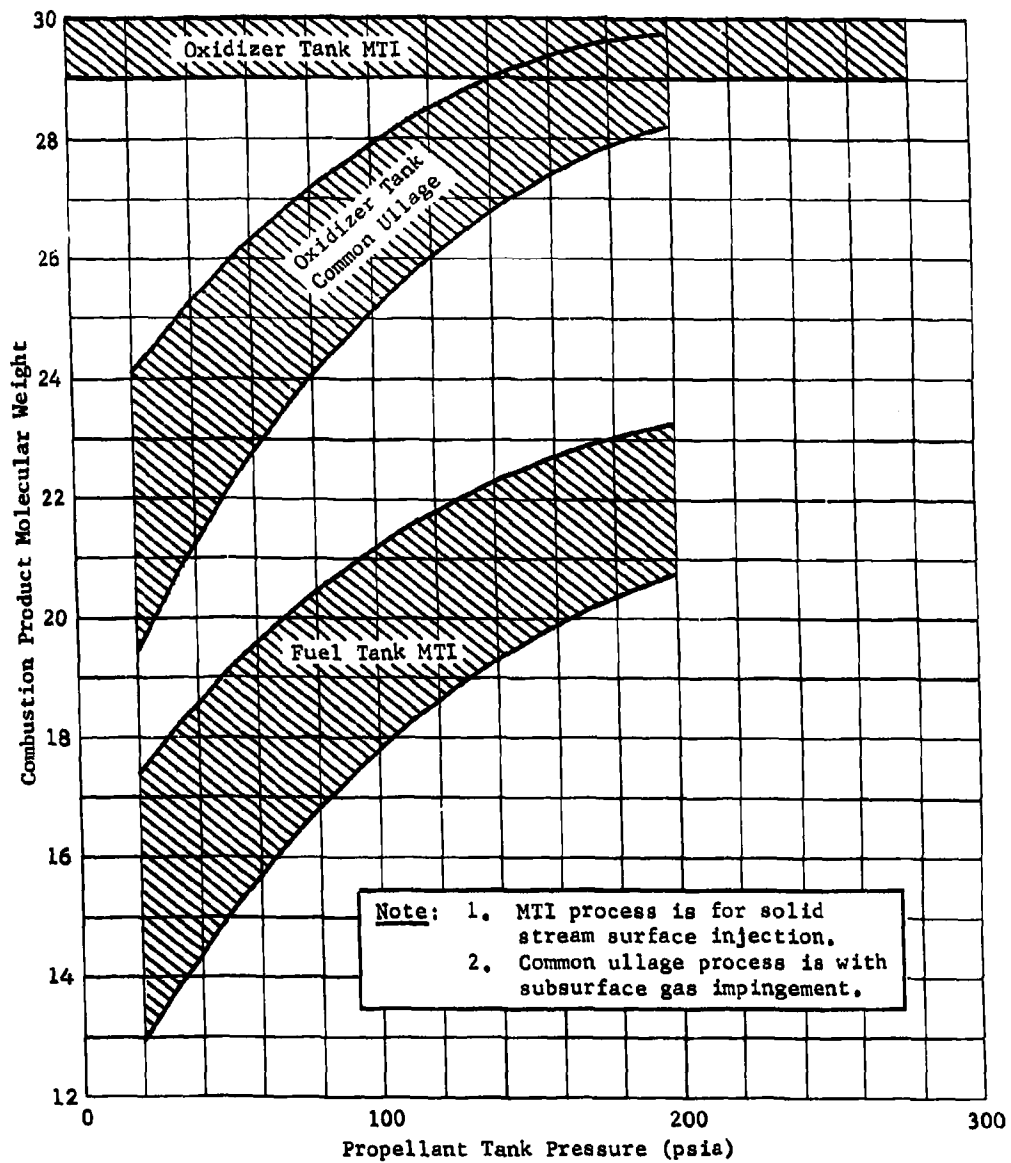


Fig. V-11 Combustion Product Molecular Weight for MTI Pressurization Systems

- 3) Vaporized Propellant. The amount of vaporized propellant in the fuel tank is virtually zero and normally can be neglected. However, the fraction of vaporized oxidizer must always be considered. The mechanism of propellant vaporization in conjunction with the MTI reaction is not fully known. The best quantitative data available are the results from spectrographic examination of gas samples immediately following the tests. These show that tank pressure has a remarkable influence on propellant vapor mole fraction, exceeding, bulk liquid-saturated conditions. Figure V-12 presents these results. The influence of expulsion time between 100 to 200 sec was not pronounced. Expulsion times greater or less than this range were not examined. The thermodynamic properties of the vaporized oxidizer are shown in Fig. V-13.

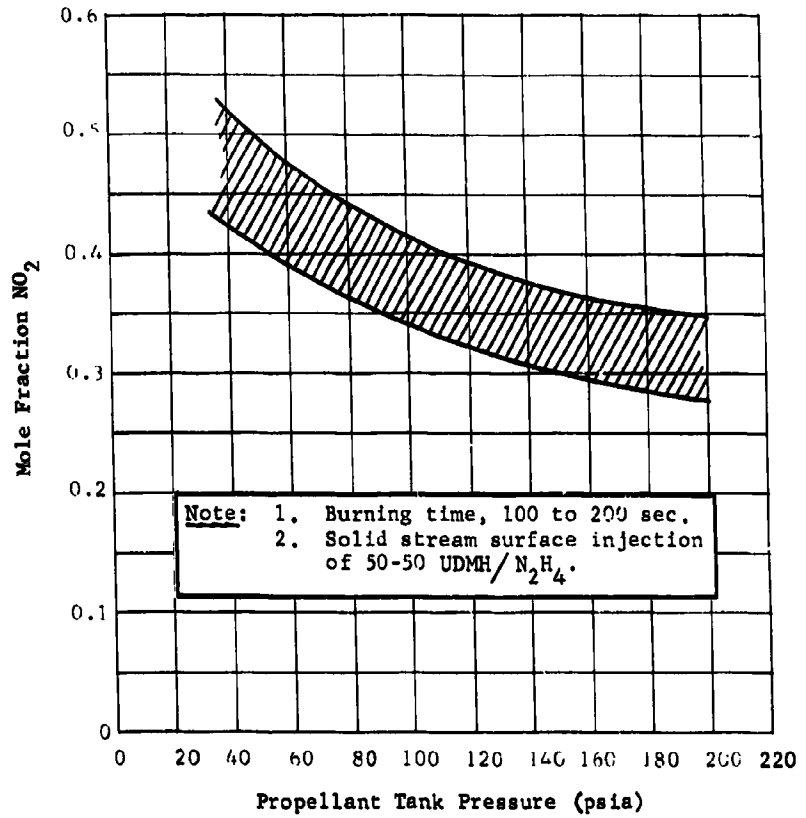


Fig. V-12 Vaporized N_2O_4 Propellant

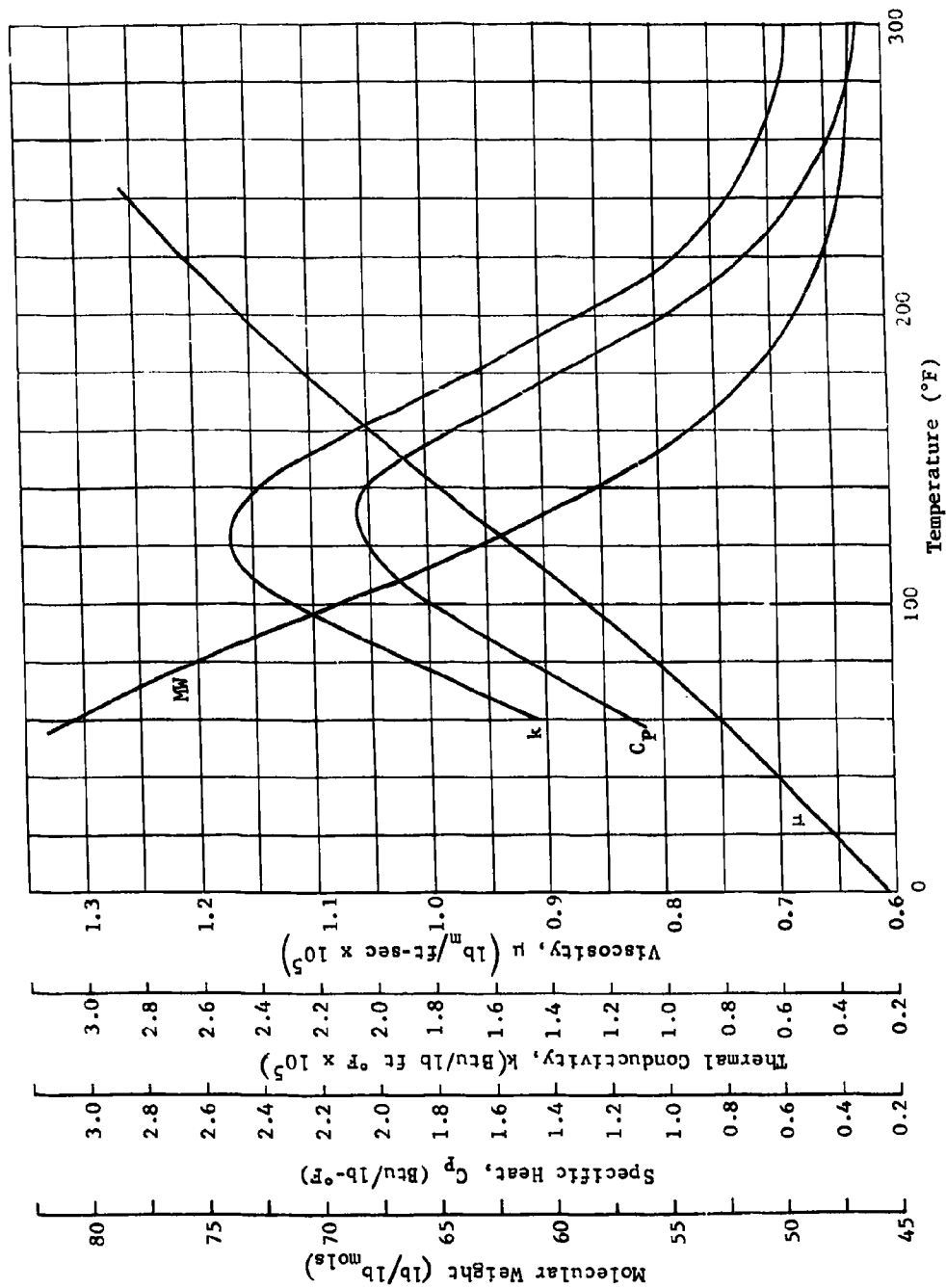


Fig. V-13 Gaseous Nitrogen Tetroxide Thermodynamic Properties at 12 psia

RTD-TDR-63-1123

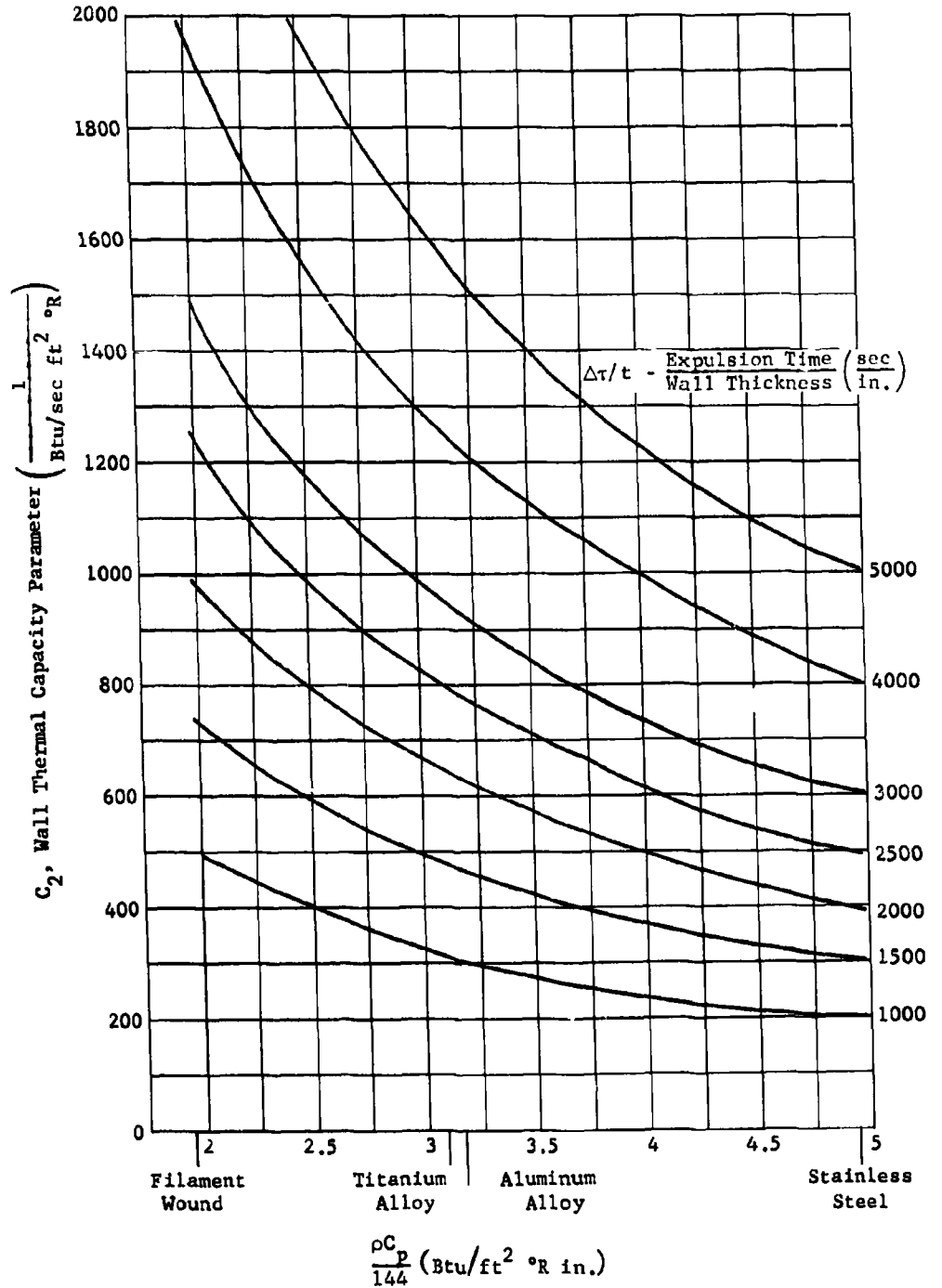


Fig. V-14 Tank Wall Thermal Capacity

5. Reagent Consumption

The determination of the amount of reagent required depends on the precise knowledge of the reaction process mixture ratio experienced and the amount of condensables formed. The equation expressing this is:

$$\text{Total products} = W_g + W_c = \frac{W_o (1 + \lambda)}{\lambda} = W_f (1 + \lambda). \quad [12]$$

Before Eq [12] can be solved, the amount of condensables in the propellant must be evaluated. For direct injection, MTI processes, steam is virtually the major condensable. The maximum quantity of steam formed is limited by the quantity of oxygen present in the fuel tank or hydrogen in the oxidizer tank. Thus the amount of steam generated can be described as some function of the injected reagent. Postfiring examination of the bulk propellant revealed certain changes in moisture concentration resulting in the following estimates of condensables. These are empirical values and probably vary with changes in tank configuration and injection dynamics.

$$W_c = 0.71 \frac{\text{Lb}_m \text{H}_2\text{O}}{\text{Lb}_m \text{N}_2\text{O}_4} \text{ (reagent),}$$

$$W_c = 1.09 \frac{\text{Lb}_m \text{H}_2\text{O}}{\text{Lb}_m 50/50 \text{ UDMH} - \text{N}_2\text{H}_4} \text{ (reagent).}$$

Substituting these values in Eq [12] and solving for the weight of reagent,

$$W_o = \frac{W_g}{\frac{\lambda + 1}{\lambda} - 0.71}; \quad [13]$$

$$W_f = \frac{W_g}{(\lambda + 1) - 1.09} = \frac{W_g}{\lambda - 0.09}. \quad [14]$$

Gas weight (exclusively combustion products) is expressed by the equation of state

$$W_g = \frac{P V_f (\text{MW})_{cp} (\text{MF})_{cp}}{10.72 T_f}. \quad [15]$$

The reaction process mixture ratio is relatively constant for the fixed injection dynamics employed and is given below for the Phase I tests.

Oxidizer tank injection	$\frac{\lambda}{2. - 2.5}$
Fuel tank injection	0.55 - 0.65

6. Injector Dynamics

Surface solid stream injection has been found satisfactory and is, therefore, recommended for the single-tank MTI process. Subsurface gas impingement tests for common ullage tank pressurization of the oxidizer tank is noted although additional development effort is required.

The metering orifices for these injection systems may be either sharp-edged or straight-tube design. Orifice pressure drops for the sharp-edge configuration should be between 75 and 100 psi for the propellants and total pressures examined. At pressure drops above this range, the solid stream tends to break down, resulting ultimately in excessive wall temperatures. Discharge coefficients of 0.6 to 0.7 are recommended. For the straight tube orifice, injection patterns are satisfactory up to 200 psi differential pressure, though a small reduction in discharge coefficient is indicated. The design of the injection system should minimize the propellant volume between the injector seat (where shutoff is accomplished) and the orifice to avoid the possibility of transient tank overpressures. This problem is related to system response. The tank pressure control system may be of the constant flow (full-on), variable flow (modulating), or pulse mode (on-off) type. Constant flow is generally not recommended for systems of variable gas demand, since precise tank pressure control can be accomplished only by tank venting. Variable flow control is possible, but is seldom used because of the development difficulties inherent in the modulating mechanism. Pulse mode systems being relatively easy to develop are therefore selected whenever the resultant tank pressure fluctuations are acceptable. In addition, they are particularly desirable for low pressurant demand rate systems. This is because orifice diameters are correspondingly larger than for the other system control methods, and larger orifices are less sensitive to contamination and partial blockage, thus eliminating undesirable spray patterns. Because of the larger orifice used, the response characteristics of the pulse-mode control systems tend to be more critical than for the other control methods. Consequently, the sizing of the pulse-mode orifice is more dependent on the response of the control system. Orifice design proceeds as follows for a single tank injection system.

The equation of state applied to the ullage gas mixture in the fuel tank is

$$P_{\text{tot}} = \left(\frac{10.72 \text{ TW}}{\text{MW V}} \right)_{\text{inert}} + \left(\frac{10.72 \text{ TW}}{\text{MW V}} \right)_{\text{cp}} \quad [16]$$

Differentiating with respect to time and noting that $(\dot{W})_{\text{inert}} = 0$, the pressure rate change during the "on" position can be expressed as

$$\dot{P} = \frac{(10.72)W}{\text{MW V}} \left(\dot{T} - \frac{T \dot{V}}{V} \right)_{\text{inert}} + \frac{10.72}{\text{MW V}} \left(T\dot{W} + W\dot{T} - \frac{TW}{V} \dot{V} \right)_{\text{cp}} \quad [17]$$

Substituting $(\dot{W})_{\text{cp}} = 0$ in Eq [17], the expression for tank pressure decay rate during the off position is also obtained.

For constant thrust engines,

$$\dot{V} = \frac{V_f - V_i}{\Delta\tau} \quad [18]$$

The term (\dot{P}) varies depending on the instantaneous values of mass, temperature, and ullage volume. The largest single influence is ullage volume. Consequently, (\dot{P}) is most critical initially when ullage volume is smallest. Before solving Eq [17], values of W , T , and \dot{T} must be known. For this calculation, it is sufficiently accurate to estimate these values at minimum ullage. Certainly test data should be relied on if at all possible when establishing these assumptions. On this basis, Eq [17] reduces to an expression for $(\dot{W})_{\text{cp}}$ in terms of (\dot{P}) , the allowable tank pressure variation rate:

$$(\dot{W})_{\text{cp}} = \frac{(\dot{P}) - \frac{10.72 W}{(\text{MW}) V} \left(\dot{T} - \frac{T \dot{V}}{V} \right)_{\text{inert}} - \frac{10.72}{\text{MW V}} \left(W\dot{T} - \frac{TW}{V} \dot{V} \right)_{\text{cp}}}{\frac{10.72 T}{(\text{MW})_{\text{cp}} V}} \quad [19]$$

Let ΔP_{max} be the maximum allowable tank pressure variation above the nominal setting (psi). Then $(\dot{P}) = \Delta P_{\text{max}} / \Delta\tau_r$, where $\Delta\tau_r$ is the total system response time in seconds. This expression is substituted in Eq [19], which can now be solved for $(\dot{W})_{\text{cp}}$.

The reagent flow rate N_2O_4 is then obtained from Eq [13], employing suitable values for λ , the process mixture ratio (0.55 to 0.65).

$$\dot{W}_o = \frac{(\dot{W})_{cp}}{\frac{\lambda + 1}{\lambda} - 0.71} \quad [20]$$

The orifice size is obtained from the incompressible flow equation

$$(A)_o = \frac{144 \dot{W}_o}{v \rho_o} = \frac{144 \dot{W}_o}{C_d \sqrt{2 g_c 144 \Delta P_o} \rho_o} \quad (\text{in.}^2), \quad [21]$$

employing suitable values for orifice pressure drop ΔP_o and discharge coefficient C_d .

A similar procedure is valid for the oxidizer system except that Eq [16] and the subsequent equations are modified to account for propellant vaporization. This must be estimated before the solution and later confirmed. In addition, Eq [20] is replaced by

$$\dot{W}_f = \frac{(\dot{W})_{cp}}{\lambda - 0.09},$$

where

$$\lambda = 2 - 2.5.$$

7. Determination of Constants

The constants discussed in the following paragraphs are useful for solving Eq [5].

C_1 is the ratio of the convective heat transfer to the propellant to the total convective gas heat transfer, i.e.,

$$C_1 = \frac{Q_{11g}}{\Sigma Q}.$$

This constant, being a function of the injection dynamics and tank configuration, must be empirically determined. Estimated values from the Phase I tests are:

Oxidizer tank injection	$\frac{C_1}{0.37}$
Fuel tank injection	0.87

C_2 is the measure of the thermal capacity of the tank walls and the exposure time.

$$C_2 = \frac{\Delta t}{t \rho_m C_{pm}/144} \frac{1}{\text{Btu/sec ft}^2 \text{ } ^\circ\text{R}}$$

Figure V-14 presents this parameter as a function of the density specific heat characteristics of typical wall materials.

C_3 is the measure of the total enthalpy of the generated gas products.

$$C_3 = \frac{P V_f C_p t_c (MW)_{cp} (MF)_{cp}}{10.72}$$

	$\frac{C_p t_c 10.72}{P}$
Oxidizer tank injection	115
Fuel tank injection	143.5

C_4 is the measure of the work being done on the liquid. For constant pressure systems.

$$C_4 = 0.185 P(V_f - V_i) \text{ (Btu)}.$$

C_5 is the measure of the final internal energy of the ullage gas.

$$C_5 = \frac{P V_f (MW)_{mix} C_{vf}}{10.72}$$

Typical values of C_{vf} for gas mixtures prepressurized with helium (5% initial ullage) are:

	C_{vf} Btu/lb °R
Oxidizer tank	1.2
Fuel tank	0.34

C_6 is the measure of the initial internal energy of the prepressurizing gas.

$$C_6 = \frac{P V_i C_{vf} t_{gi} (M_{wi})}{10.72 t_{gi}} = \alpha P V_i.$$

Values of α as a function of the more common prepressurants are shown in Fig. V-15.

C_7 aids in computing wall heat transfer:

$$C_7 = A_g \Delta \tau \text{ (sec-ft}^2\text{)}.$$

C_8 is a measure of the wall heating rate:

$$C_8 = 0.394 \xi_p \times \xi_{mv} \times \xi_{cp} \times \xi_\mu \xi_k.$$

Values of ξ are shown in Fig. V-16 as a function of the applicable gas property.

C_9 is a measure of the total heat exchange from the ullage:

$$C_9 = \frac{C_7 C_8}{1 - C_1}.$$

C_{10} and C_{11} measure the enthalpy of vaporized propellant.

C_{10} is the amount vaporized. C_{11} is the enthalpy release, which for N_2O_4 propellant, is 181.6 B/lb vaporizing at 70°F.

For the fuel tank, this product is essentially zero. For the oxidizer tank vaporized propellant can be computed by means of Fig. V-12.

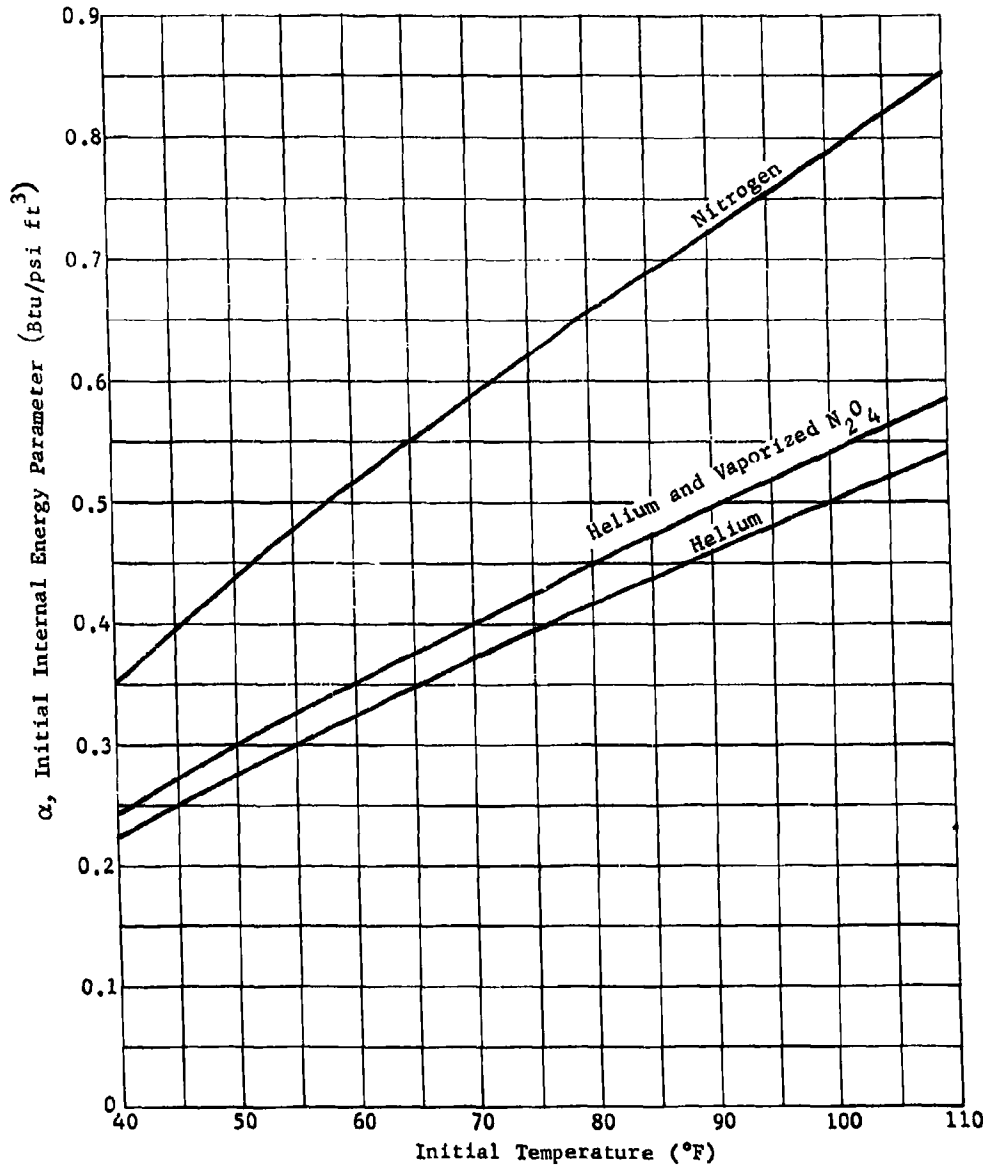


Fig. V-15 Initial Internal Energy of Prepressurants

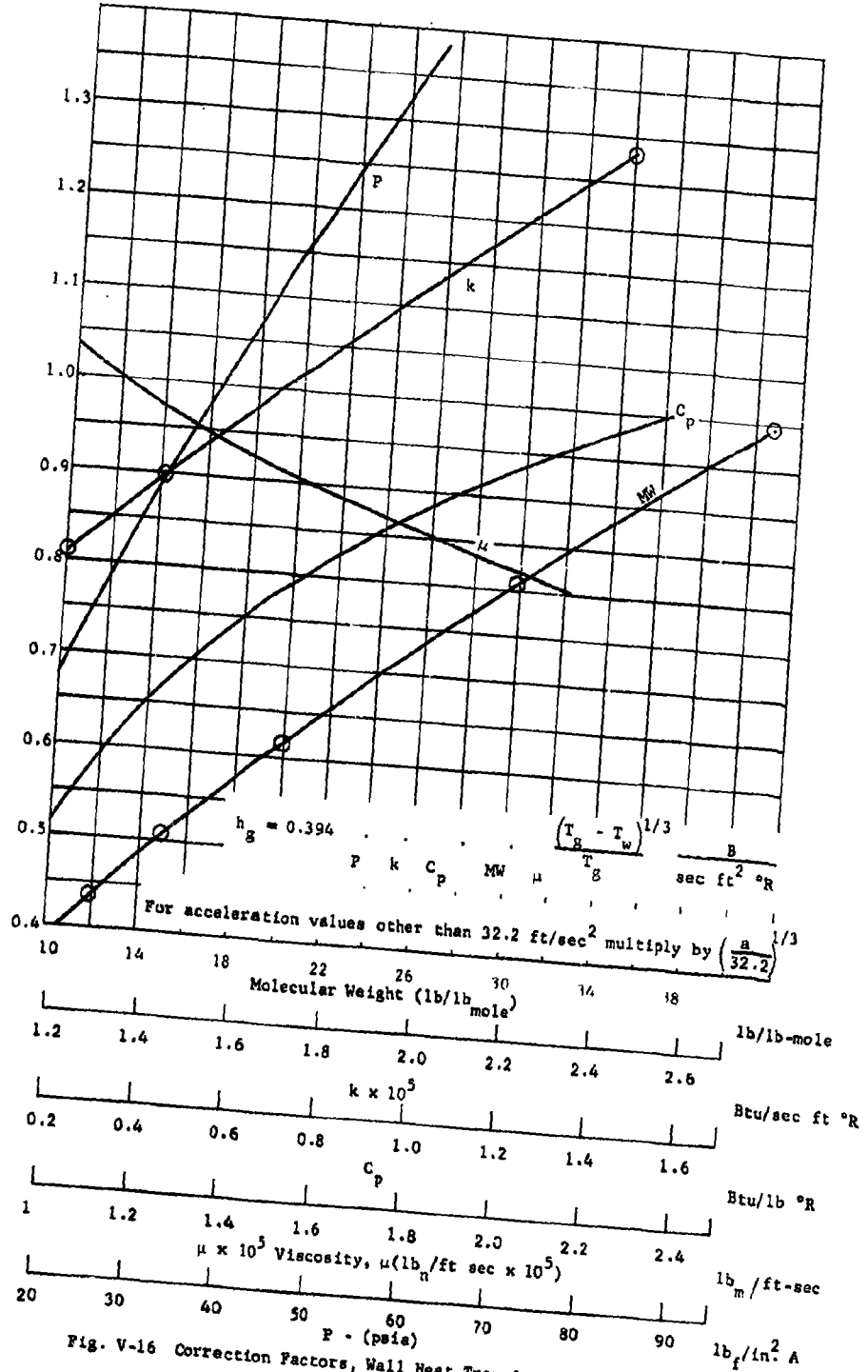


Fig. V-16 Correction Factors, Wall Heat Transfer Coefficient

8. Method of Solution

- 1) Assume the final ullage gas temperature, t_{g_f} ;
- 2) Compute \bar{t}_g (Eq. [10]);
- 3) Compute constants C_1 through C_{11} ;
- 4) Assume h_g (0.001 initially);
- 5) Solve for \bar{t}_w (Eq [7] or [9]);
- 6) Check value of h_g from Eq [11];
- 7) Substitute that value for h_g into Step 5 (convergence is rapid);
- 8) Solve Eq [5];
- 9) When the identity holds, the assumption of t_{g_f} is confirmed; otherwise repeat;
- 10) Compute wall temperature rise (Eq [6] or [8]);
- 11) Compute the gaseous combustion product weight by Eq [15];
- 12) Solve for reagent consumption by means of Eq [13] or [14]. Use proper values for λ ;
- 13) Compute vaporized propellant for the oxidizer tank by Eq [15], modified by the MW and MF of the propellant vapor.

Sample calculations demonstrating the design methods are presented. For illustrative purposes, the Phase I tests are examined. Consequently, test measurements will be used to confirm the validity of the design procedure. It cannot be overemphasized that certain empirically determined factors, such as C_1 and the amount of condensable, and even the gas properties may change for different configurations.

9. Sample Calculations

MFI Pressurization of Fuel Tank: N_2O_4 into 50/50 UDMH- N_2H_4

Given:

Initial volume - 0.267 cu ft

Final volume - 4.91 cu ft

Tank Pressure - 36 psia

Initial gas and wall temperature - 550°R

Expulsion time - 140 sec

Average wall surface exposed to gas - 7.1 sq ft

Prepressurized to 36 psia with helium

Aluminum alloy tank - 5/8-in. wall

Solution:

Determination of constants:

$$C_1 = 0.873. \text{ For aluminum, } \rho C_p / 144 = 3.17 \text{ (Fig. V-14)}$$

$$C_2 = \frac{140}{(0.625)(3.17)} = 70.8$$

$$C_3 = (143.5)(36)(16)(0.93)(4.91) = 377,000$$

$$C_4 = (0.185)(36)(4.91 - 0.267) = 30.9 \text{ Btu}$$

$$MW_{\text{mix}} = (0.93)(16.1) + (0.07)(4) = 15.18$$

$$C_5 = \frac{(36)(4.91)(0.34)(15.18)}{10.72} = 85. \text{ For helium, } \alpha = 0.374 \text{ (Fig. V-15)}$$

$$C_6 = (0.374)(0.267)(36)\left(\frac{55}{70}\right)\left(\frac{530}{515}\right) = 2.9$$

$$C_7 = (7.1)(140) = 993$$

From Fig. V-16 read

$$\xi_{MW} = 0.51, \xi_{cp} = 0.69, \xi_k = 1.02, \xi_\mu = 0.99, \xi_p = 1$$

$$C_8 = (0.394)(0.51)(0.69)(1.02)(0.99)(1) = 0.14$$

$$C_9 = \frac{(993)(0.14)}{1 - 0.873} = 1095$$

$$C_{10} \text{ and } C_{11} = 0$$

As a trial assumption, assume the final gas temperature, $t_{gf} = 163^\circ\text{F}$. From Eq [10], using $\eta = 0.667$,

$$\bar{t}_g = 55 + [0.667 (163 - 55)] = 127$$

$$\text{Assume } h_g = 0.001$$

$$\bar{t}_w = \frac{2(55) + (70.8)(126.8)(0.001)}{2 + (0.001)(70.8)} = 57.5^\circ\text{F}$$

Verifying h_g by Eq [11],

$$h_g = \frac{(0.14)(126.8 - 57.5)^{1/3}}{586.8} = 0.001$$

Substitute into Eq [5],

$$\frac{(1095)(126.8 - 57.5)^{4/3}}{586.8} = \frac{377,000 - 85(163)}{623} + 2.9 - 30.9$$

$$533 \approx 541.8$$

This is a reasonable agreement and no further trials are necessary.

From Eq [8]:

$$\text{Wall temperature rise, } \Delta t_w = (70.8)(0.001)(126.8 - 57.5) = 4.9^\circ\text{F}$$

$$\text{Combustion gas weight} = \frac{(36)(4.91)(16)(0.93)}{(10.72)(623)} = 0.394 \text{ lb}_m$$

(Eq [13])

$$\text{Reagent consumption, } W_o = \frac{0.394}{\frac{1.555}{0.555} - 0.71} = 0.188 \text{ lb}_m \text{ (Eq [11])}$$

Sample Calculations

MTI Pressurization of Oxidizer Tank: 50/50 UDMH-N₂H₄ into
N₂O₄

Given:

Initial volume - 0.267 cu ft

Final volume - 4.91 cu ft

Tank pressure - 35 psia

Initial gas temperature - 51°F

Initial wall temperature - 60°F

Expulsion time - 204 sec

Average wall surface exposed to gas - 7.1 sq ft

Prepressurized to 40 psia with helium

Aluminum alloy tank - 5/8-in. wall

Solution:

Determination of constants

$$C_1 = 0.37$$

$$C_2 = \frac{\Delta\tau}{(t)(P_m)C_{P_m}/144} = \frac{204}{(0.625)(3.17)} = 103$$

$$C_3 = 115 P V_f MW_{cp} MF_{cp}$$

From Fig. V-11 read: $MW_{cp} = 29.1$; due to dissociation
 $(MW)_v = 55$

From Fig. V-12 read: $MF_v = 0.52$

$$MF_{cp} = 1 - 0.52 - MF_{inert} = 0.437$$

$$C_3 = (115)(35)(4.91)(29.1)(0.437) = 251,000$$

$$C_4 = 0.185 P (V_f - V_i) = 0.185(35)(4.91 - 0.267) = 30.2$$

$$C_5 = \frac{P V C_v MW_{mix}}{10.72}$$

$$MW_{mix} = \Sigma(MW)(MF) = (0.52)(55) + (0.437)(29.1) + 4(0.043) \\ = 41.1$$

$$C_5 = \frac{(35)(4.91)(1.2)(41.1)}{10.72} = 792$$

$C_6 = \alpha P_i V_i$ For helium and NO_2 vapor, $\alpha = 305$ (Fig. V-15)

$$C_6 = (0.305)(40)(0.267) = 3.26$$

$$C_7 = \Delta\tau A_g = (204)(7.1) = 1450$$

$$C_8 = 0.394 \xi_p \cdot \xi_{cp} \cdot \xi_\mu \cdot \xi_k \cdot \xi_{MW}$$

$$\text{Since } \xi_p = \xi_{cp} = \xi_\mu = \xi_k = \xi_{MW} = 1$$

$$C_8 = 0.394$$

$$C_9 = \frac{C_7 C_8}{1 - C_1} = \frac{(1450)(0.394)}{(1 - 0.37)} = 907$$

As a trial assumption, assume the final gas temperature is $153^\circ F$ (test measured).

Substituting into Eq [10], we obtain

$$\bar{t}_g = 51 + [0.667(153 - 51)] = 118.3^\circ F$$

Assume $h_g = 0.00254 \text{ Btu/sec ft}^2 \text{ }^\circ\text{R}$

Substitute into Eq [9]

$$\bar{T}_w = \frac{2(60) + (103)(118.3)(0.00254)}{2 + (103)(0.00254)} = 66.8^\circ\text{F}$$

Check h_g from Eq [11]

$$h_g = 0.394 \frac{(118.3 - 66.8)^{1/3}}{(118.3 + 460)} = 0.00254$$

Before solving Eq [5], the parameters C_{10} and C_{11} , the total enthalpy of the vaporized propellant must be determined.

Assuming vaporization at 70°F , $\Delta h_v = 181.6 \text{ Btu/lb}_m$,

$$W_{\text{vap}} = W_{\text{vap}_f} - W_{\text{vap}_i}$$

Based on 60°F bulk temperature, and saturated initial conditions.

$$W_{\text{vap}_i} = \frac{(11.4)(0.267)}{(10.72)(511)} \left(\frac{92}{1 + 0.152} \right) = 0.0442 \text{ lb}_m$$

where

$\alpha = 0.152$ dissociation degree

$$W_{\text{vap}_f} = \frac{(35)(4.91)}{(10.72)(613)} \left(\frac{92}{1 + 0.595} \right) = 0.784 \text{ lb}_m \quad (0.52)$$

$$W_{\text{vap}} = 0.784 - 0.0442 = 0.74 \text{ lb}_m$$

$$C_{10} C_{11} = (181.6)(0.74) = 134.6 \text{ Btu.}$$

The reagent flow rate from Eq [20], using $\lambda = 0.555$, becomes:

$$\dot{W}_o = \frac{0.00648}{\frac{0.555 + 1}{0.555} - 0.71} = 0.00595 \text{ lb}_m/\text{sec.}$$

Employ a sharp-edged orifice, $C_d \approx 0.70$, and a maximum $\Delta P = 75$ psi,

$$v = \sqrt{\frac{2g_c 144 \Delta P}{\rho}} = \sqrt{\frac{(2)(32.2)(144)(75)}{90.5}} = 87.4 \text{ fps.}$$

Orifice diameter is obtained from the continuity equation;

$$D = \sqrt{\frac{4 \dot{W} (144)}{\pi C_d v \rho}} = \sqrt{\frac{4 (0.00595) (144)}{\pi (0.70) (87.4) (90.5)}} = 0.014 \text{ in.}$$

With the injector off during propellant outflow the tank under-pressure condition can also be determined from Eq [19], setting $\dot{W}_{cp} = 0$. During the initial conditions, Eq [19] reduces to

$$\frac{\Delta P}{\Delta t_r} = \frac{10.72 \dot{W}}{MW V} \left(t - \frac{TV}{V} \right)_{\text{inert}} = -4.27 \text{ psi/sec.}$$

Allowing 0.02-sec lag for system filling the total response becomes $0.12 + 0.02 = 0.14$ sec, and the maximum system underpressure becomes

$$\Delta P = - (0.14) [4.27] = 0.6 \text{ psi.}$$

Substituting known values into Eq [5],

$$(907) \frac{(118.3 - 66.3)^{1/3}}{578.6} = \frac{251,000 - (792)(153)}{613} + 3.26 - \\ - 30.2 + 134.6. \\ 301 \approx 319.6.$$

This is a reasonable agreement and no additional refinement is necessary.

Wall temperature rise is calculated from Eq [8]:

$$t_w = (103)(0.00254)(118.3 - 66.8) = 13.47^\circ\text{F.}$$

Combustion gas weight from Eq [13] is

$$W_{cg} = \frac{(35)(4.91)(0.437)(29.1)}{10.72 (613)} = 0.333 \text{ lb}_m.$$

Reagent consumption is determined from Eq [12]. Use $\lambda = 2.34$.

$$W_f = 0.333 / (2.34 - 0.09) = 0.148 \text{ lb}_m$$

Sample Calculations

Pulse Mode Injection System

The design of a pulse mode orifice-type MFI pressurization control system is presented for the 50-50 UDMH/N₂H₄ propellant tank. The task is to size the fixed orifice for a maximum tank pressure variation of ± 1 psi, with an estimated system response time of 120 msec.

Given:

Initial volume - 0.267 cu ft

Final volume - 4.91 cu ft

Expulsion time - 140 sec

Normal tank pressure - 36 psia

Initial gas temperature - 55°F

Final gas temperature - 163°F

Initial pressurization - helium

Mol. weight combustion products - 16

Total response time - 0.12 sec

Maximum tank pressure variation - ± 1 psi

From Eq [19], the flow rate of pressurant can be calculated:

$$(\dot{W})_{cp} = \frac{\frac{\Delta P}{\Delta \tau} - \frac{10.72 W}{MW V} \left(\frac{\dot{T}}{T} - \frac{T \dot{V}}{V} \right)_{inert} - \frac{10.72}{(MW) V} W \dot{t} - \left(\frac{TW}{V} \dot{V} \right)_{cp}}{\frac{10.72 T}{V (MW)_{cp}}} \quad [19]$$

The most critical condition is during the initial outflow when ullage volume is minimum. During this condition, Eq [19] simplifies to:

$$(\dot{W})_{cp} = \frac{\frac{\Delta P}{\Delta \tau} - \frac{10.72 W}{MW V} \left(\dot{T} - \frac{T \dot{V}}{V} \right)_{inert}}{\frac{10.72 T}{V (MW)_{cp}}}$$

$$\dot{V} = \frac{V_i - V_f}{\Delta \tau} = \frac{4.91 - 0.267}{140} = 0.0332 \frac{ft^3}{sec}$$

\dot{T} is estimated at 3°F/sec

$$W_{inert} = \frac{(36)(0.267)(4)}{(10.72)(515)} = 0.00696 \text{ lb}_m$$

Substitution into the above equation,

$$\begin{aligned} (\dot{W})_{cp} &= \frac{\frac{1}{0.12} - \frac{(10.72)(0.00696)}{(4)(0.267)} \left(3 - \frac{515(0.0332)}{0.267} \right)}{\frac{(10.72)(515)}{(0.267)(16)}} \\ &= \frac{8.34 + 4.27}{1293} = 0.00975 \text{ lb}_m / \text{sec}. \end{aligned}$$

Another factor in system response that is difficult to evaluate directly is the effect following injection shutdown of unreacted reagent that continues to flow for a few moments and pressurizes the tanks. This condition, determined from the stream diameter and distance from injector to propellant surface, is usually unimportant. Fair correlation with test results have been obtained by assuming an equivalence of two-thirds of the generated gas flow. On this basis, the maximum allowable generated gas flow reduces to:

$$\dot{W}_{cp} = (0.00975)(2/3) = 0.00648 \text{ lb}_m / \text{sec}.$$

C. APPLICATION STUDY

The high-density pressurant storage of the MTI pressurization system and low-density pressurizing gas obtained without a heat exchanger have required a re-evaluation of present pressurization concepts of specific vehicles to obtain relative cost, weight, reliability, and performance information. Consequently, a study has been performed of the Titan II autogeneous pressurization system (using vaporized and partially dissociated nitrogen tetroxide for oxidizer tank pressurization, molecular weight of approximately 75, and gas generator combustion products, molecular weight of approximately 16, for fuel tank) and the Titan III transtage unheated helium system. Preliminary design concepts have been created to establish possible pressurization system configurations. Although a slight reduction in the Titan II missile weight can be realized by a change in the pressurization system, the slight performance increase does not justify the additional time and money expenditures. However, for a future booster, an additional gain could be realized by more efficient tankage and propulsion system design. Due to possible 250-lb weight saving on the Titan III transtage with the MTI pressurization system, further effort would be warranted for this application.

1. Titan II

Titan II is a two-stage vehicle employing a twin engine 430,000-lb thrust booster and 100,000-lb thrust sustainer. The Stage I engine operates for approximately 149 sec, at which time the engine is shut down by either an oxidizer incipient exhaustion signal or fuel tank low-level sensor, whichever occurs first. The Stage II engine is started at altitude during Stage I engine shutdown, maintaining a positive acceleration during staging. Propulsion of the Stage II vehicle is also continuous, lasting approximately 180 sec; the guidance system initiates shutdown before propellant depletion. Total nominal propellant outage is 0.22% for Stage I and 0.25% for Stage II based on the total usable propellant load. This outage is unburned fuel 70% of the time as determined by a probability analysis.

Propellants are supplied from tanks mounted concentrically, one above the other, with the oxidizer tank in the forward position in each stage. Consequently, an oxidizer feedline runs through each of the fuel tanks to the engines. The storable propellants used are identical to the MTI test fluids; nitrogen tetroxide as the oxidizer and a 50/50 blend of hydrazine and unsymmetrical dimethylhydrazine as the fuel.

All propellant tanks are of aluminum construction, 10 ft in diameter, containing slosh and antivortex baffles. Pertinent design data are tabulated below:

	Stage I		Stage II	
	Fuel	Oxidizer	Fuel	Oxidizer
Tank Volume (cu ft)	1626.5	1920.2	401.7	500.8
Usable Propellant (lb)	246,846		57,902	
Nominal Flow Rate (lb/sec)	567	1094	113.3	204.3
NPSH (ft)	43	44	100	30

The pressurization system is autogenous or self-generating in nature. The Stage I and Stage II fuel tanks are pressurized using gas-generator-produced gas bled from the turbine inlet manifold as the pressurant. The hot (1650°F) gas is cooled to 220°F in a heat exchanger using liquid fuel as the heat sink. The gas then passes through an orifice that is the flow-controlling device of the system, a high-pressure burst disc, the airborne autogenous lines, and a low-pressure burst disc, and then enters the propellant tank through a diffuser. The Stage I oxidizer tank is pressurized with gaseous nitrogen tetroxide. Liquid nitrogen tetroxide is bled from the propellant line below the pump. The liquid passes through a cavitating venturi that is the flow control of the system, a high-pressure burst disc, and a heat exchanger using turbine exhaust gas as the heat source. In the heat exchanger, the liquid is both vaporized and dissociated in being heated to about 350°F. The gas then passes through a back-pressure orifice, the airborne autogenous lines, a low-pressure burst disc, and enters the propellant tank through a diffuser. The Stage II oxidizer tank has no pressurization system. The initial charge of nitrogen plus vehicle acceleration and propellant vaporization satisfy the NPSH and structural requirements without augmentation.

The Stage I and Stage II autogenous pressurization systems are shown schematically in Fig. V-17 and V-18, respectively. The low-pressure burst discs near the top of the Stage I and Stage II fuel tanks and Stage I oxidizer tanks minimize leakage during long-term storage. The high-pressure burst discs eliminate the possibility of solid particles from the start cartridge entering the propellant tanks on the fuel pressurization system and giving a good start transient of the autogenous system on the oxidizer pressurization system. Titan II tank-top pressure requirements for flight are shown in Fig. V-19 thru V-22.

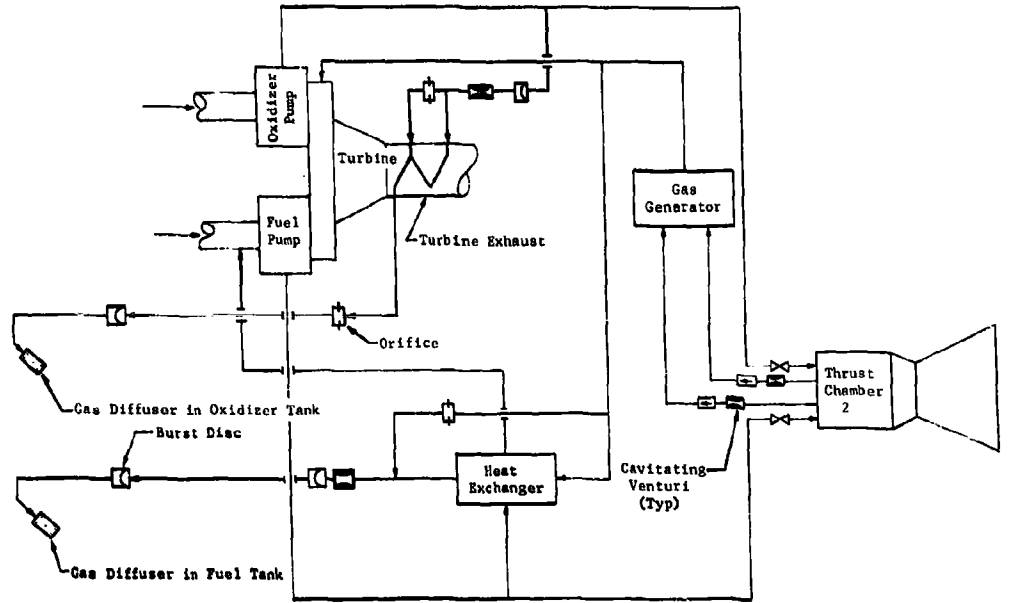


Fig. V-17 Existing Titan II Pressurization System, Stage I

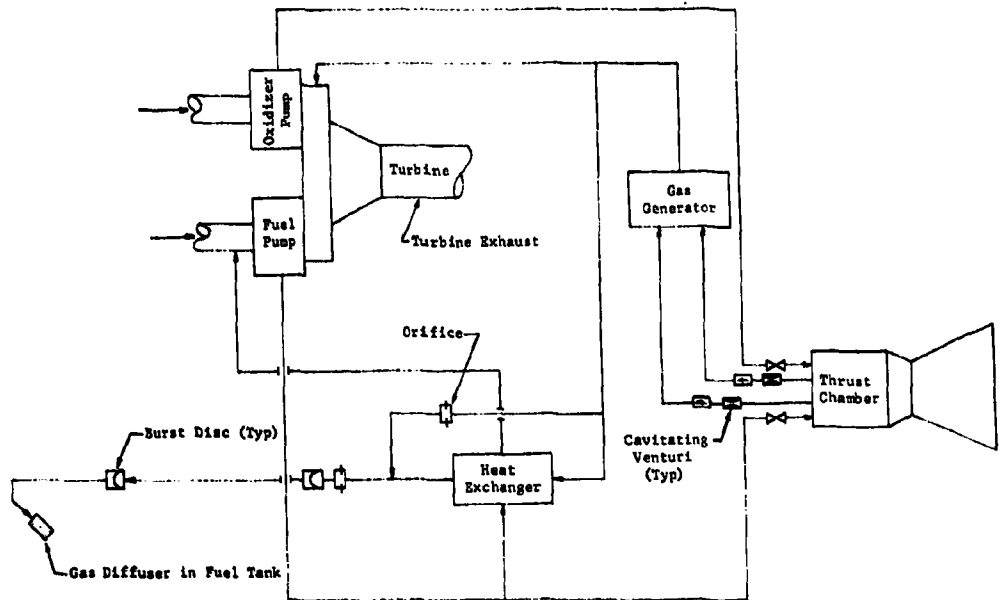


Fig. V-18 Existing Titan II Pressurization System, Stage II

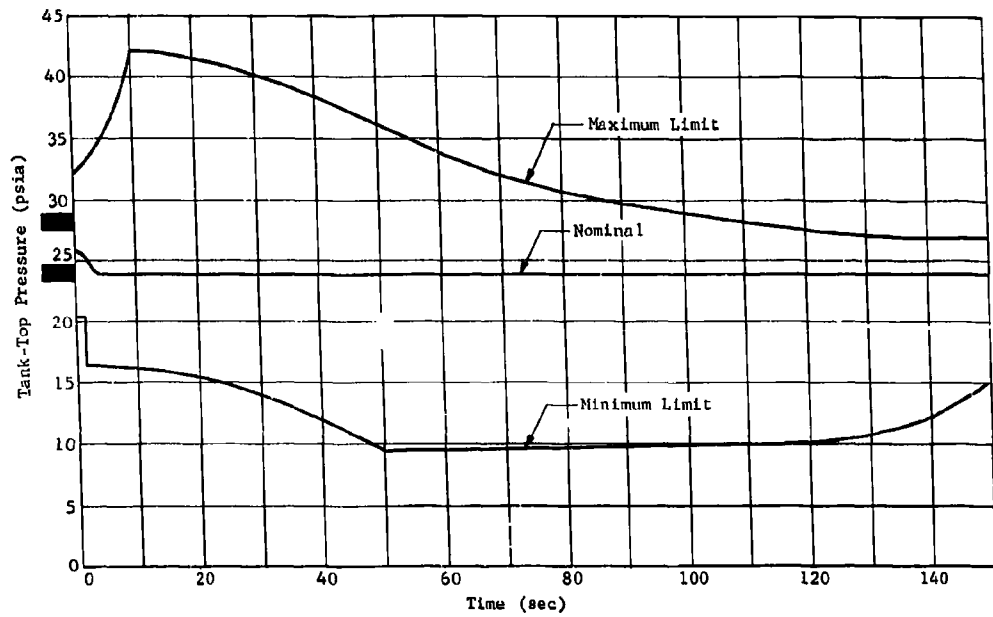


Fig. V-19 Flight Tank Pressure, Stage I Fuel Tank

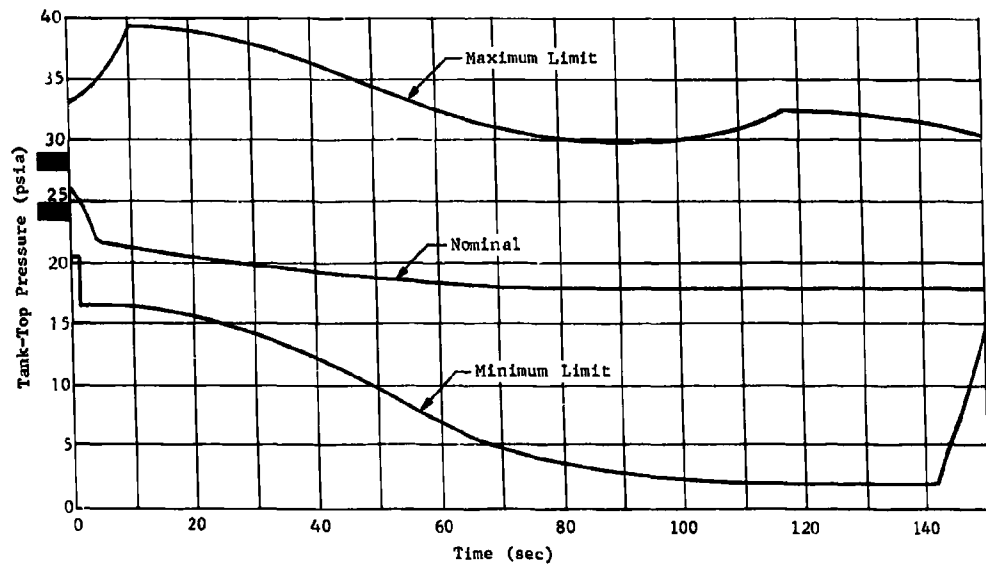


Fig. V-20 Flight Tank Pressure, Stage I Oxidizer Tank

RTD-TDR-63-1123

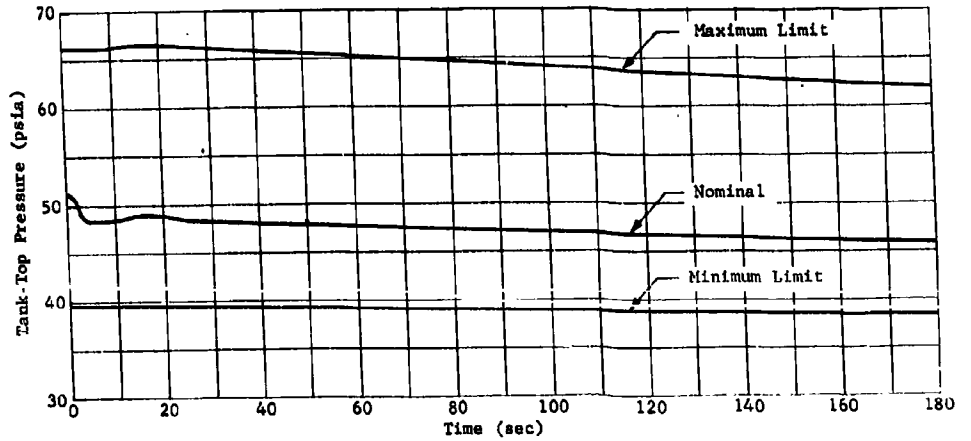


Fig. V-21 Flight Tank Pressure, Stage II Fuel Tank

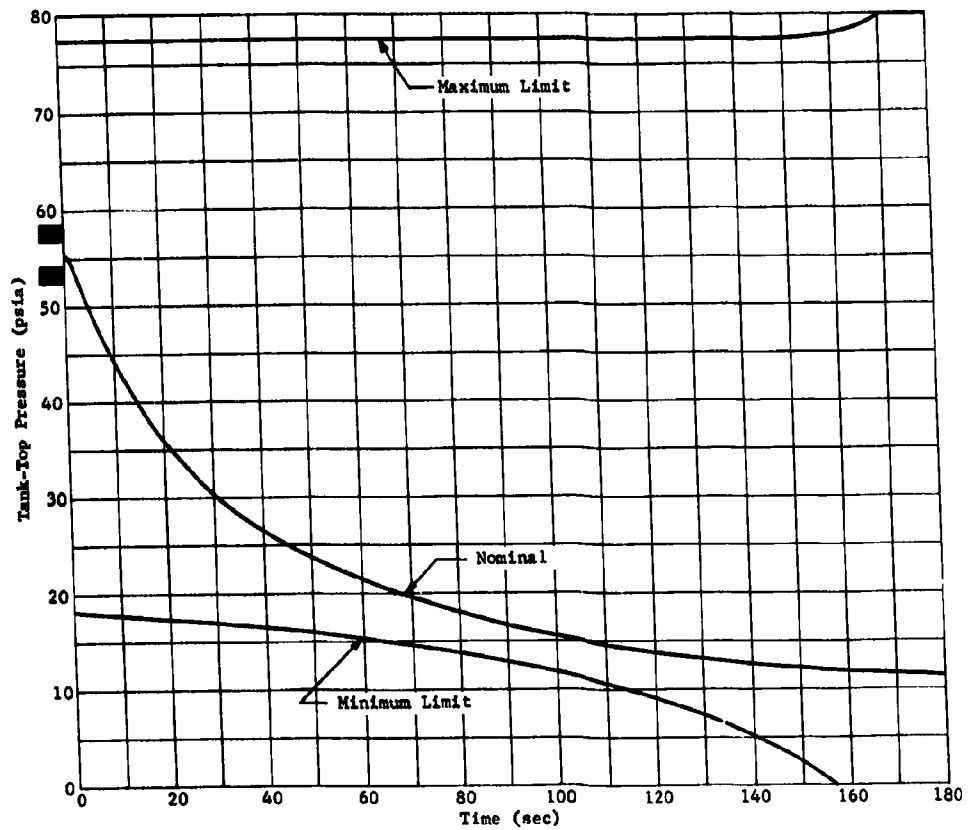


Fig. V-22 Flight Tank Pressure, Stage II Oxidizer Tank

A detailed study of the Titan II pressurization requirements has indicated a slight increase in reliability. A weight saving of approximately 102 lb can be achieved by employing a dual-reagent injection MTI pressurization system in Stage I and 37 lb by a direct injection system in the Stage II fuel tank. Since the Stage II oxidizer tank has no airborne pressurization system, replacement of the polytropic pressurization process with an MTI process was not considered practical. For this particular application, the common ullage pressurization of the oxidizer tank was found to offer no significant advantage over the dual-reagent injection system and, consequently, is not recommended. Performance of the dual-reagent injection system is compatible with the existing structure and is comparable to the Phase III flightweight demonstration system. As a result of this application study, the following conclusions have been established:

- 1) Continuous flow dual-reagent injection is the lightest and potentially the most reliable injection technique due to its simplicity (System D);
- 2) Separate reagent storage is more desirable for use on an existing missile than turbopump-bleed reagent supply, since
 - a) A modular-type arrangement is easily applied to existing missiles with a minimum of rework and eliminates long pressurization lines running the length of the missile,
 - b) The decreasing injector flow rate can be tailored to fit the decreasing pressurizing gas demand by adjusting the reagent tank ullage volume,
 - c) It requires no turbopump modification to incorporate a propellant bleed, either in the housing or at the outlet,
 - d) Separate reagent storage near the forward dome eliminates the effects of missile acceleration on reagent supply pressure;
- 3) Turbopump bleed reagent supply, when used with a continuous flow injector, is the most reliable and appears to be the best system for an operational missile due to its simplicity and minimum of servicing requirements.

Because of the present stage of Titan II development, this study concentrated on system improvement techniques involving a minimum amount of time and cost in the change over. Based on the present amount of development of a flight type system, the following additional effort is recommended for application of an MTI pressurization system to the Titan II missile:

- 1) Development of a modular-type direct reagent injection MTI pressurization system for the Stage I and Stage II fuel tank employing a continuous flow injector with separate reagent storage;
- 2) Installation of the unit developed above in a Titan II missile for static test firings with the existing fuel tank pressurization system capped off and oxidizer tank system left intact;
- 3) Flight demonstration in conjunction with remaining developmental effort or launch crew training of the system tested in Item 2;
- 4) Pending successful development of the modular system, develop a turbopump bleed continuous flow injection system as System C shown in Fig. V-25;
- 5) Simultaneous or subsequent development and flight testing of the oxidizer tank direct-injection pressurization system.

Preliminary Design Schematics - The systems presented are combinations of four methods of pressurizing the fuel tank and five methods of oxidizer tank pressurization by the MTI process. Four of the systems are applicable to both fuel and oxidizer tank pressurization. As noted previously, the Stage II oxidizer has no pressurization system and, therefore, will not be included. The systems are as follows:

- System A - Pulse flow injection, turbopump bleed, used on either fuel or oxidizer tank;
- System B - Pulse flow injection, separate reagent tank used on either fuel or oxidizer tank;
- System C - Continuous flow injection, turbopump bleed used on either fuel or oxidizer tank;

System D - Continuous flow injection, separate reagent tank used on either fuel or oxidizer tank;

System E - Common ullage from fuel tank, applicable only on oxidizer tank with either Systems A thru D used on fuel tank.

System A, shown in Fig. V-23 applied to Stage I propellant tanks, uses propellant bled from the turbopump, injecting it through a pulse-type injector subsystem. Intermittent reagent flow is controlled by a pressure-switch-actuated (normally closed) injector. When tank ullage pressure drops to the pressure-switch set point, the switch signals the injector to open, initiating reaction in the tank to increase pressure. When pressure reaches an upper pressure limit, the injector is closed, stopping the reaction. Propellant is bled from a point on the turbopump where pressure is approximately 265 psia, through a burst disc (required for long-term ground storage) up to the injector on the tank dome. Reagent supply is maintained by the engine turbopump after pressure builds up during start and ruptures the burst disc. Propellant is bled at 265 psig from the pump housing rather than at 1200 to 1400 psig at the pump outlet due to the intermittent-type injection. Each time the injector closed, the injector supply pressure would approach 1200 psi if bled from the pump outlet resulting in atomization of the injection stream. The injector supply line size required is 1/4-in. diameter for fuel and 3/8-in. diameter for oxidizer tank pressurization. The injector used would be similar in size to a 1/4-in., airborne-type solenoid valve and would mount on the tank dome with a 0.070-in. diameter solid-stream nozzle projecting into the tank. Due to the distance from turbopump to tank dome and the acceleration of the missile, supply pressure to the injector will decrease during flight from approximately 210 to 90 psig on the oxidizer tank and from approximately 210 to 105 psig on the fuel tank. As the supply pressure decreases, the injector will stay open a greater percentage of each cycle to compensate for the lower flow rate.

This same configuration can also be used on the Stage II fuel tank. A 1/4-in. supply line bleeding oxidizer from the oxidizer turbopump housing at 145 psig would supply oxidizer to the injector, after passing through a burst disc, at 125 to 90 psig, depending on the Stage II acceleration rate.

System B, shown in Fig. V-24, applied to the oxidizer tank, is the same as System A, except propellant supply to the injector is from a small (12-in. diameter) storage tank mounted near or on the tank dome. The small tank is pressurized to 160 psig before engine start and allowed to decay polytropically to 115 psig during the engine run, resulting in an injector flow rate reduction of 13%. The reagent storage tank is desirable for two reasons: (1) it eliminates the necessity of tapping off propellant at 265 psig from the turbopump housing, and (2) it avoids the injector pressure decrease due to the effects of increasing missile acceleration. Injection is initiated by supplying electrical power to the injector pressure switch at engine start. When tank pressure decays due to outflow, the injector automatically operates. Injection can be terminated by the same propellant low-level signal that shuts off the engine, a separate level sensor, or merely by letting it stop automatically as outflow ceases.

System C, shown in Fig. V-25, applied to the fuel tank, is the most simple of the systems discussed. It consists only of passive elements -- an orifice, burst disc, tubing, and injection nozzle. Propellant supply for the injector is taken from the turbopump outlet and reduced to approximately 265 psig by the orifice. This is possible as constant flow is maintained rather than pulsing flow as in Systems A and B. The primary advantage of constant flow is that it allows injector supply to be tapped off at high pressure (1200 to 1400 psia), which is readily available, and this, in turn, eliminates most of the effect of missile acceleration on injector pressure. For example, if fuel is bled from the turbopump at 1420 psia to supply the injector at 200 psia, a 5-g acceleration results in a reduction of only 10 psia in injector supply pressure.

System D, not shown, is a combination of the separate tank discussed in System B and the continuous flow injector discussed as System C. The reagent storage tank is the same size (12-in. diameter) and is pressurized to the same pressures. Theoretically the reagent demand is reduced approximately 20% during an engine run due to the increasing ullage gas temperature. As stated for System B, the flow rate decrease resulting from the polytropic pressure decay in the storage tank is 13%, but could be adjusted to match the reagent demand by decreasing the storage tank ullage. A shutoff valve between the reagent storage tank and injector is required in this system for prerun isolation, initiation of injection, and termination of injection. A simple solenoid shutoff valve controlled by either low-level sensors or a signal from the engine during the start and shutdown sequences.

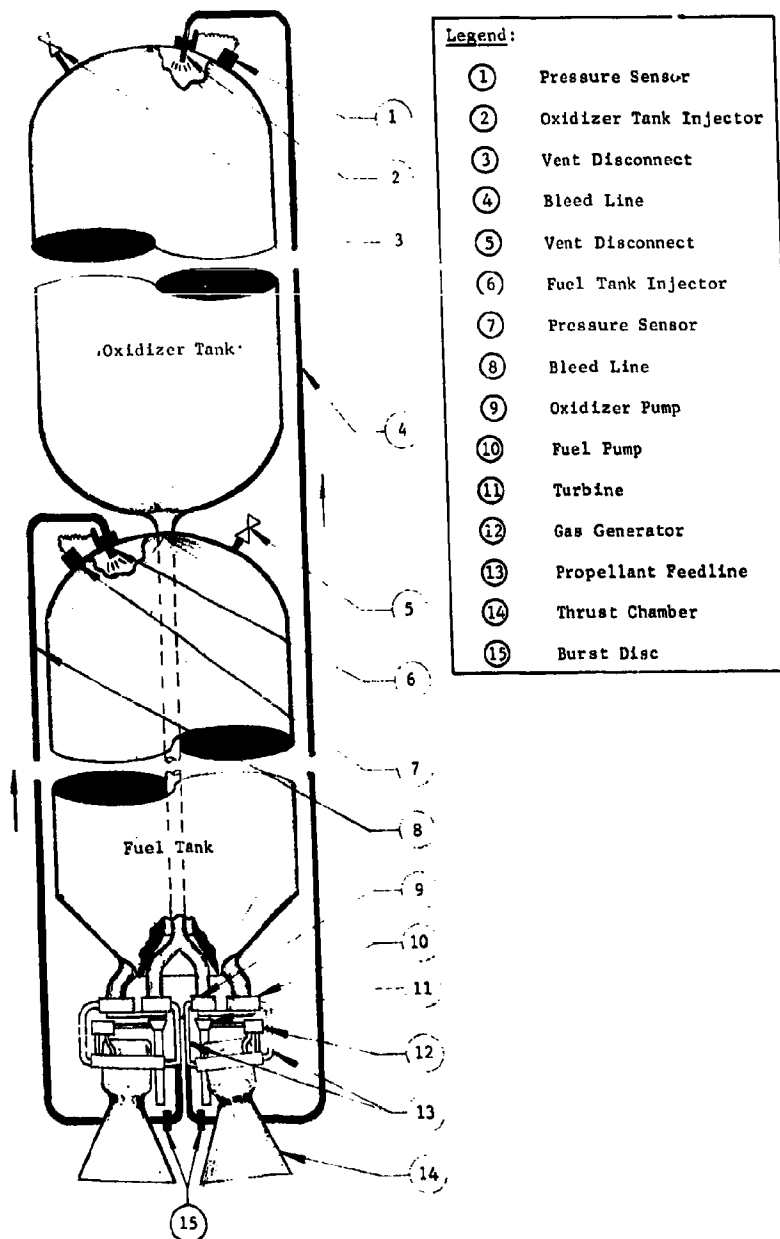


Fig. V-23 Pulse-Type MTI with Turbopump Bleed

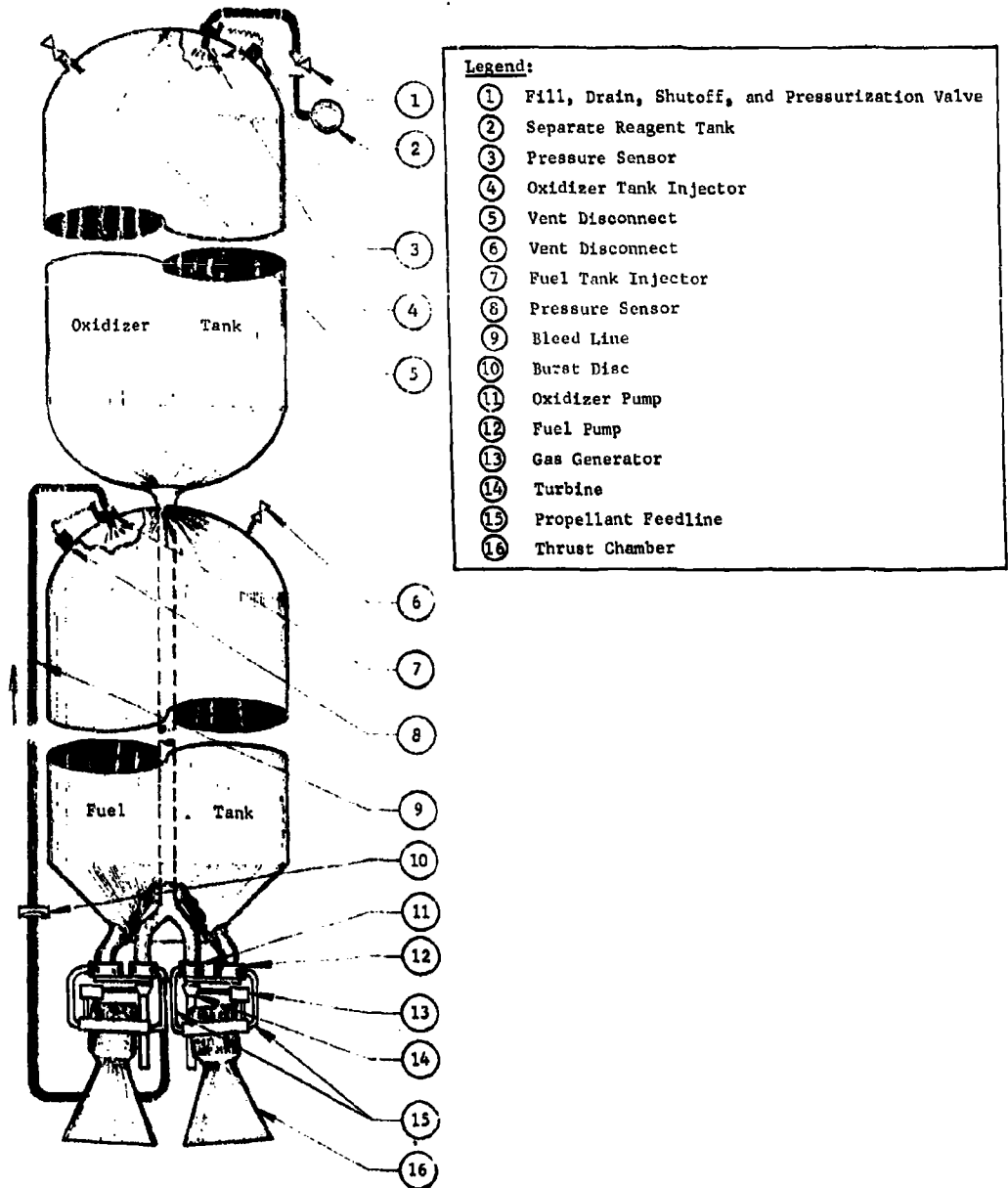


Fig. V-24 Pulse-Type MTL, Turbopump Bleed Fuel Tank and Separate Reagent Supply Oxidizer

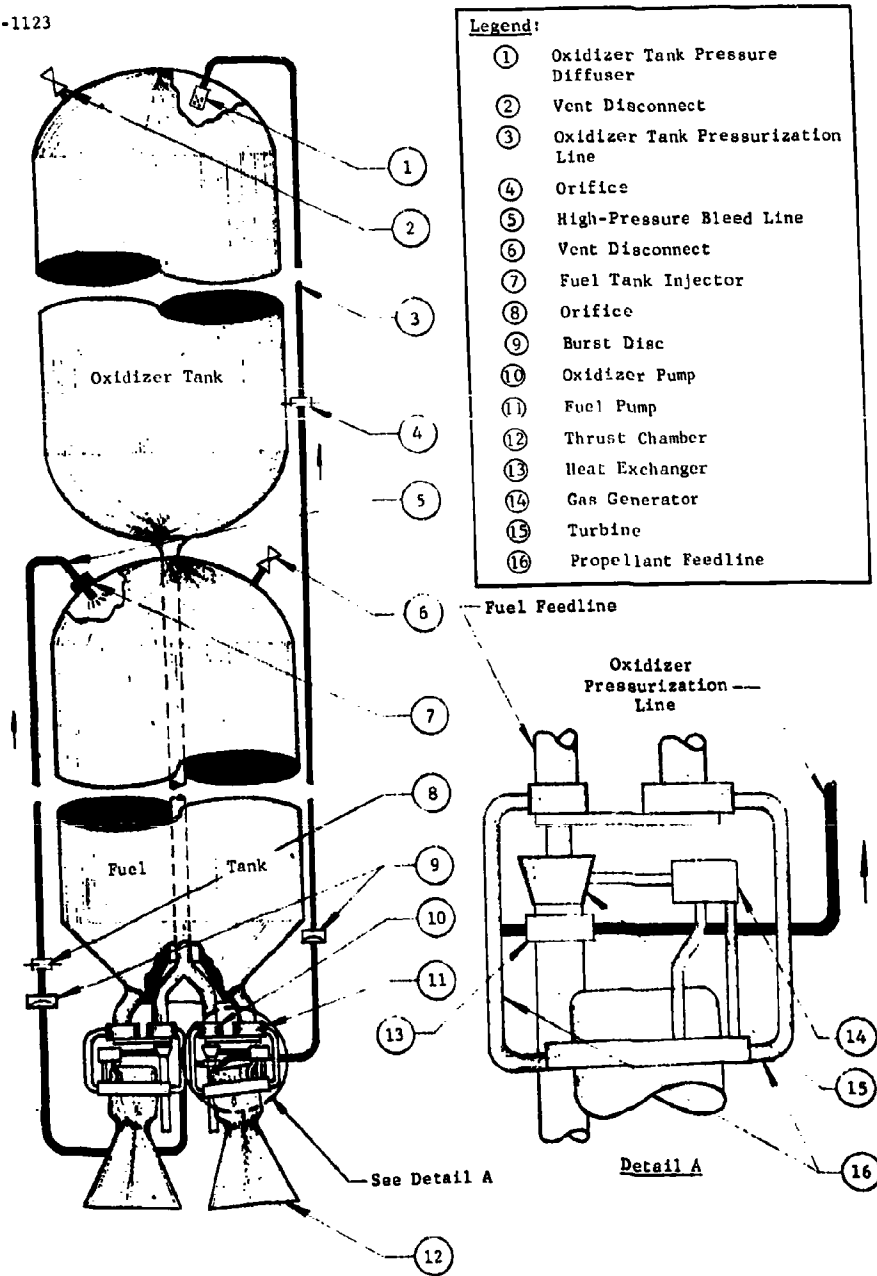


Fig. V-25 Constant Flow-Type MTL, Turbopump, Bleed Fuel Tank Pressurization, Evaporated Propellant Oxidizer Pressurization

Reliability - Predicted reliability factors were calculated for each of the systems considered for use in the boost and sustainer phases. Using the same method, the existing Titan II pressurization system was analyzed; the results are included in Table V-6. The Stage II oxidizer tank was not included as it has no pressurization system.

Calculation of reliability was based on the following definitions and formulas:

Generic failure rate (GF_r) - The inherent number of failures per unit of time, cycles, or trials that will occur under a laboratory-type installation;

Equipment operating mode factor (K_{op}) - A failure rate modifier that adjusts the generic failure rate for various external operating environments;

Equipment application factor (K_a) - A failure rate modifier that adjusts the generic failure rate for various internal operating conditions such as speed, temperature, etc. It is assumed to be unity when no factor has been established;

Adjusted Failure Rate (F_r) = (GF_r) (K_a) (K_{op});

Duration of operating phase being considered (t) (hr)

$$tF_r = GF_r \frac{(\text{failures})}{(10^6 \text{ hr})} (K_{op} - \text{dimensionless})$$

$$(K_a - \text{dimensionless}) (t - \text{hr})$$

$$(\text{Number in system}), (\text{Failures} \times 10^{-6})$$

$$R = e^{-tF_r} (1 \approx tF_r, \text{ where } tF_r < 0.01).$$

Reference: M-63-3.*

It is noted that reliabilities for Stage II are in general slightly higher than Stage I. This is due to the K_{op} being higher for Stage I making the Stage II reliability factors slightly higher.

*Engineering Reliability Policy and Procedures Manual M-63-3.
Martin Company, Denver, Colorado.

System E, shown in Fig. V-26, applied to the oxidizer tank, uses a common ullage line to transfer pressurizing gas from fuel to oxidizer tanks. An isolation valve with differential pressure-switch control in the common ullage line prevents flow from oxidizer to fuel tanks. An injector in the fuel tank supplies enough reagent to pressurize both tanks. Due to secondary reaction of oxidizer with the pressurizing gas from the fuel tank and amount of propellant vapor, the amount of reagent required is increased approximately 40% while the volume to be pressurized is increased 120%. The common ullage line is approximately 4 in. in diameter due to the low density of the pressurizing gas. The isolation valve is a zero leakage valve similar to the existing propellant pre valve in that a diaphragm or some similar device is required to positively seal the valve before engine start. Injection initiation and termination would be the same as described for Systems A, B, C, or D, depending on which is used for the fuel tank. The differential pressure-switch-controlled isolation valve opens to pressurize the oxidizer tank, based on oxidizer tank demand sensed by the pressure switch.

Weight - Weights for the proposed systems were determined by assuming the same pressurization line lengths as the present autogenous pressurization system and component weights of presently available hardware. Present pressurization line lengths are approximately 680 and 370 in. for Stage I oxidizer and fuel, respectively, and 150 in. for Stage II fuel tanks. The pulse-type injector, while not presently available, is similar to existing solenoid valves, from which weights were estimated. The separate reagent tank weight was calculated for aluminum with a safety factor of 1.5 based on a nominal reagent load and 75% ullage. Pressurization gas weights were calculated from MTI development test data, gas laws, Titan II test data, and nitrogen tetroxide dissociation data. Calculated weights based on the preliminary design schematics are shown in Table V-3. Also shown are weights for the existing Titan II missile pressurization system.

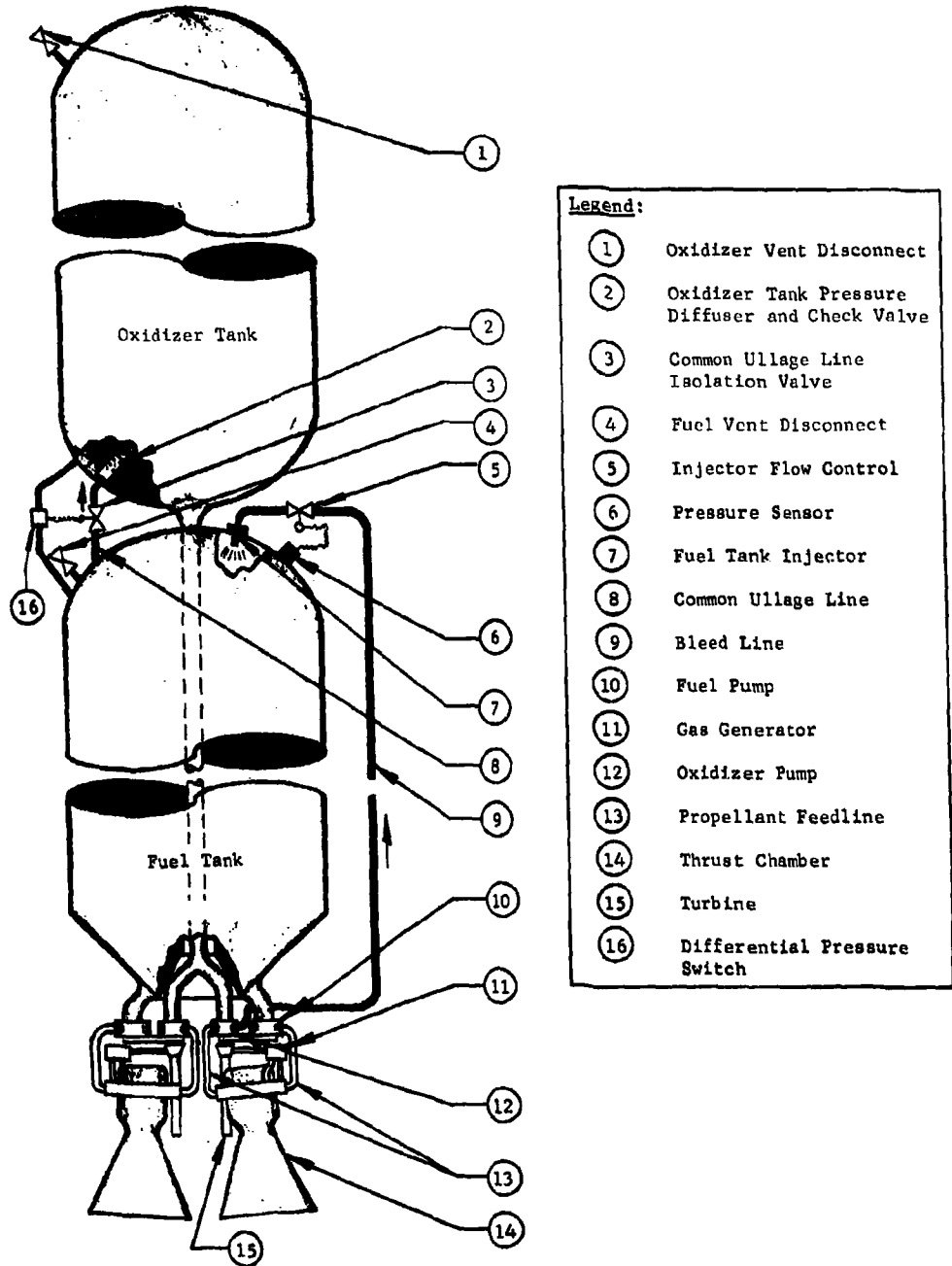


Fig. V-26 Pulse-Type MTI with Turbopump Bleed, Common Ullage System

Table V-3 Titan II Fuel and Oxidizer Tank Pressurization System Weights

	Weight (lb)							
	Stage I Fuel Tank Hardware	Stage I Fuel Tank Pressurization Gas (24 psia)	Stage I Oxidizer Tank Hardware	Stage I Oxidizer Tank Pressurization Gas (20 psia)	Stage I Total System	Stage II Fuel Tank Hardware	Stage II Pressurization Gas (4 psia)	Stage II Total System
<u>Fuel Tank</u>								
Existing Titan II	49	101			150	29	54	83
Pulse Flow - Turbopump Bleed	17	91			108	11	41	52
Pulse Flow - Separate Reagent Tank	8	991			99	6	41	47
Continuous Flow - Turbopump Bleed	12	91			103	9	41	50
Continuous Flow - Separate Reagent Tank	6	91			97	5	41	40
<u>Oxidizer Tank</u>								
Existing Titan II			46	281	327			
Pulse Flow - Turbopump Bleed			22	270	292			
Pulse Flow - Separate Reagent Tank			10	270	280			
Continuous Flow - Turbopump Bleed			17	270	287			
Continuous Flow - Separate Reagent Tank			8	270	278			
Common Ullage from Fuel Tank			13	334	347			

RTD-TDR-63-1123

Using the weight data given in Table V-4, total pressurization system weights for both fuel and oxidizer tanks were calculated and are given in Tables V-5 and V-6 along with the resulting weight savings over the existing systems. The weight decrease shown for the Stage I fuel tank pressurization systems when applied with a common ullage is due to an increase in fuel tank ullage temperature, which reduces gas weight 4 lb, and an increase in the fuel tank injector capacity, which increases hardware weight 2 lb. The high weight of the common ullage system is due to the low ullage temperature and large amount of undissociated oxidizer vapor in the oxidizer tank. Although the molecular weight of the combustion products is substantially lower than dissociated oxidizer, the small amount of pressurization required (equivalent to partial pressure of 5 psia) does not result in a significant weight reduction in the Stage I oxidizer tank.

As shown, weight savings over the existing Titan II pressurization system range from 29 to 102 lb for Stage I (a reduction of 6 to 21%), and from 31 to 37 lb for Stage II (a reduction of 37 to 45%). The system offering the greatest potential from a weight standpoint is continuous flow injection from a separate tank for Stage I fuel and oxidizer tanks and Stage II fuel tank.

Table V-4 Titan II, Stage I, Total Pressurization System Weights

Pressurization System Used		Pressurization System Weight Total (lb)	Weight Savings over Existing Titan II (lb)
Fuel Tank Weight (lb)	Oxidizer Tank Weight (lb)		
Existing Titan II -150	Existing Titan II - 327	477	0
Pulse Flow, Turbopump Bleed - 108	Pulse Flow, Turbopump Bleed - 292	400	77
Pulse Flow, Separate Tank - 99	Pulse Flow, Separate Tank - 280	379	98
Continuous Flow, Turbopump Bleed - 103	Continuous Flow, Turbopump Bleed - 287	390	87
Continuous Flow, Separate Tank - 97	Continuous Flow, Separate Tank - 278	375	102
Pulse Flow, Turbopump Bleed - 108	Pulse Flow, Separate Tank - 280	388	89
Pulse Flow, Turbopump Bleed - 106	Common Ullage - 347	453	24
Pulse Flow, Separate Tank - 99	Existing Titan II - 327	426	51
Continuous Flow, Turbopump Bleed - 101	Common Ullage - 347	448	29
Continuous Flow, Separate Tank - 97	Common Ullage - 347	444	33

Table V-5 Titan II, Stage II, Fuel Tank Pressurization System Weights

System	Weight (lb)	Weight Savings over Existing System (lb)
Existing Titan II	83	0
Pulse Flow, Turbopump Bleed	52	31
Pulse Flow, Separate Reagent Tank	47	36
Continuous Flow, Turbopump Bleed	50	33
Continuous Flow, Separate Reagent Tank	46	37

From Table V-6 it is seen that the system employing constant flow injection with turbopump bleed supply is predicted to be the most reliable for both fuel and oxidizer tanks in Stage I and the fuel tank in Stage II.

Table V-6 Titan II Candidate MTI Pressurization Systems Reliabilities

Type Subsystem	Stage I		Stage II	
	Reliability	Rank	Reliability	Rank
Fuel Tank				
Existing Titan II	0.9992	2	0.9994	2
Pulse Flow, Turbopump Bleed	0.9988	3	0.9990	3
Pulse Flow, Separate Reagent Tank	0.9983	5	0.9986	5
Continuous Flow, Turbopump Bleed	0.9996	1	0.9997	1
Continuous Flow, Separate Reagent Tank	0.9985	4	0.9988	4
Oxidizer Tank				
Existing Titan II	0.9991	2	N/A	
Pulse Flow, Turbopump Bleed	0.9988	3	N/A	
Pulse Flow, Separate Reagent Tank	0.9983	6	N/A	
Continuous Flow, Turbopump Bleed	0.9996	1	N/A	
Continuous Flow, Separate Reagent Tank	0.9985	5	N/A	
Common Ullage from Fuel Tank	0.9988	4	N/A	

Performance - The theoretical pressurization system performance of the Titan II booster has been computed by the IBM-7094 MTI mathematical model. Pertinent pressurization data are shown in Fig. V-27 and V-28 for the Stage I and Stage II systems employing the solid-stream surface reagent injection process in each tank. The Stage II oxidizer tank has not been analyzed because of the satisfactory method now used (nitrogen initial pressurization and ullage gas expansion). However, for certain missions with a heavier payload, the MTI system could be employed to satisfy the increased pressurization requirements. Nominal mission durations have been analyzed for a typical trajectory with the expected aerodynamic heating. Pressure control was limited to +0.5 psia for the run based on minimum pressure requirements considering a 6- to 8-sec ullage gas expansion process for expelling the residual propellants. Maximum predicted wall temperatures are within the allowable limits for the aluminum structure and are considered realistic in view of the results obtained from the similar tankage tested during Phase III. Reagent consumption was moderate for each system, permitting either turbopump bleed or separate storage without difficulty.

In comparing the performance of the existing Titan II pressurization system with the MTI system, an increase in reliability can be realized by a change; however, the weight saving with the MTI system is a relatively small percentage of the total propulsion system weight. The elimination of the heat exchanger and control of hot gases are the primary factors affecting the reliability of the present systems. Only a small decrease in the Stage I oxidizer tank pressurization system weight is realized due to the relatively low operating pressure and large amount of vaporized N_2O_4 . An ullage gas temperature of 150°F was assumed for the MTI pressurization process and 200°F for the present system. By operating the MTI system at higher temperatures (300°F) an additional 20% weight saving can be obtained due to further dissociation of the propellant vapor. The decrease in fuel tank pressurization system weight is primarily due to a reduction in components as the gas pressurizing gas molecular weight is essentially the same for both systems.

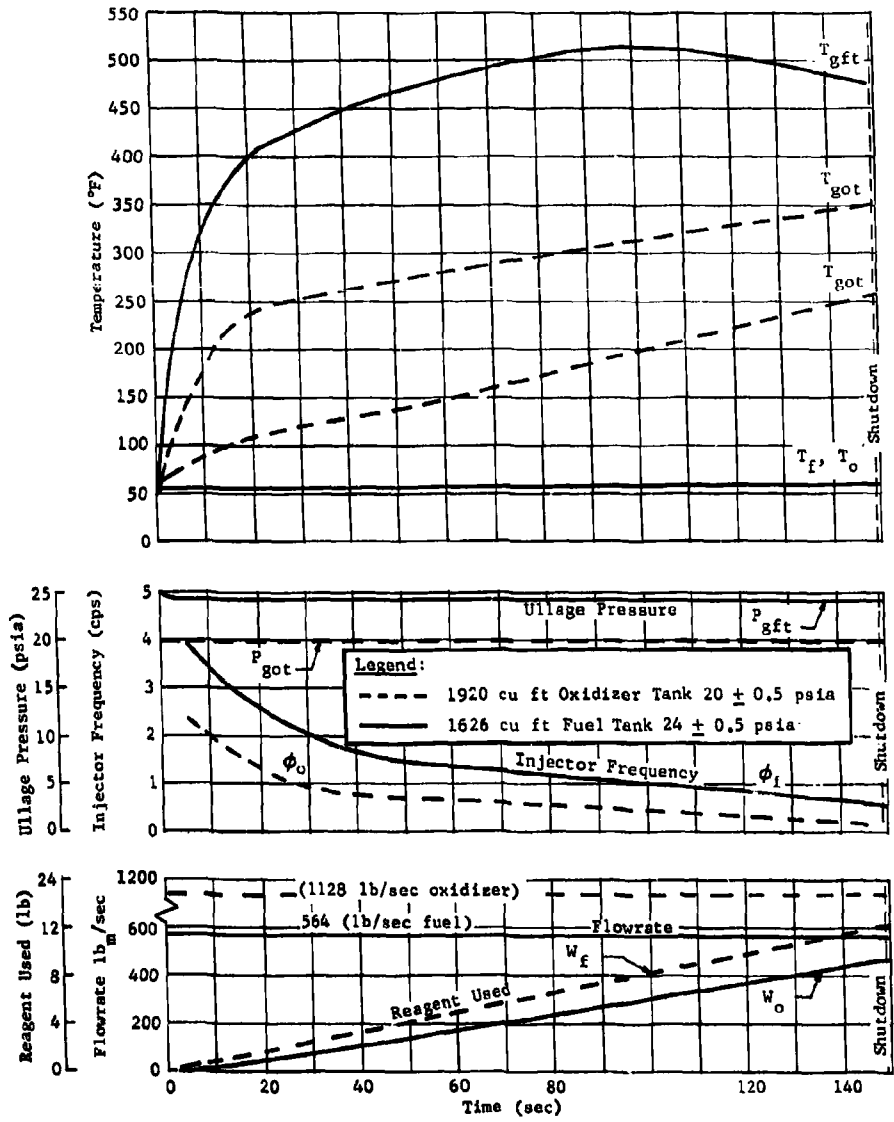
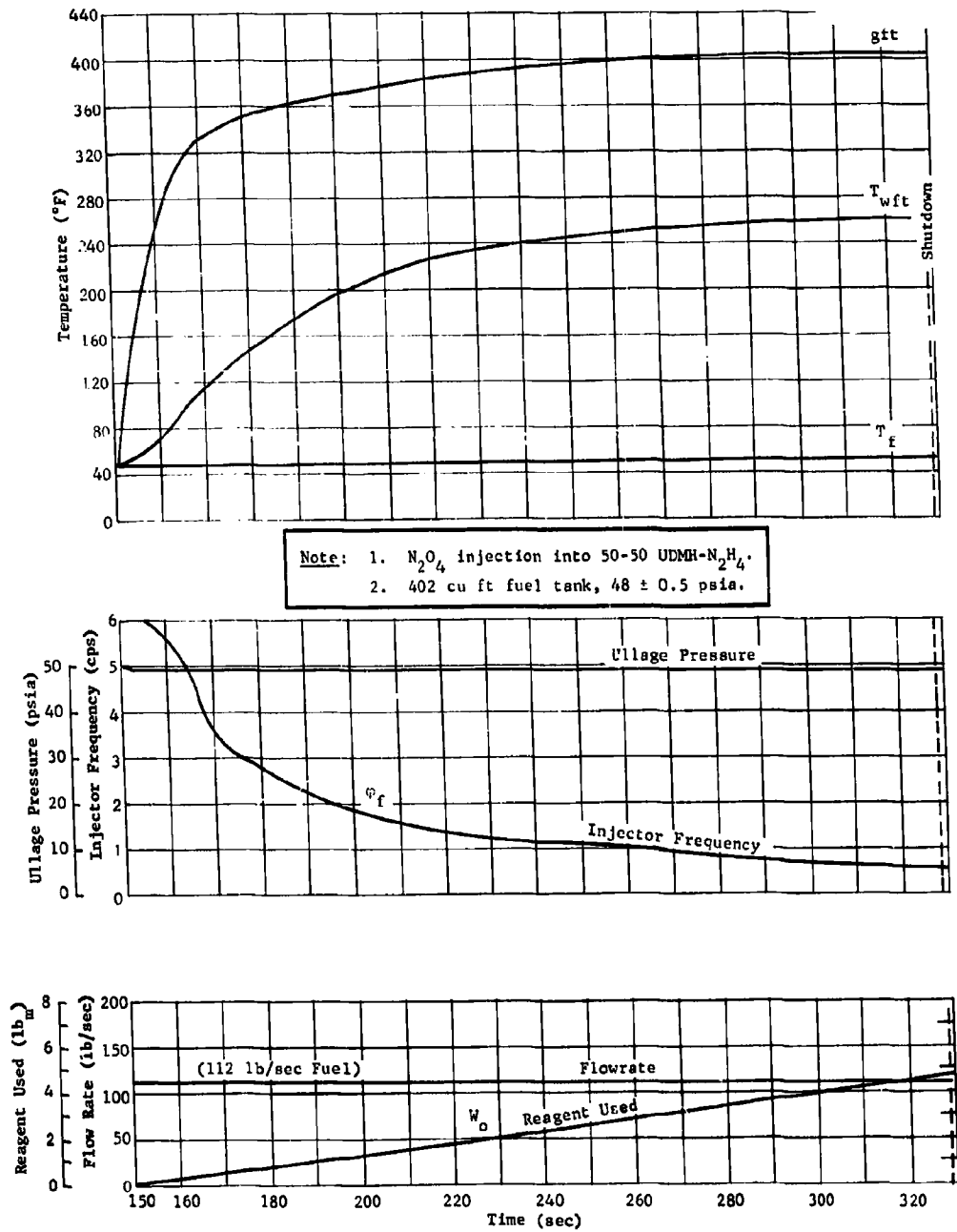


Fig. V-27 MTL Titan II Stage I Predicted Performance



Note: 1. N_2O_4 injection into 50-50 UDMH- N_2H_4 .
 2. 402 cu ft fuel tank, 48 ± 0.5 psia.

Fig. V-28 MTI Titan II Stage II Predicted Performance

Cost - A preliminary study of the effort required for the development and testing of a Titan II MTI pressurization system has been made to determine the program duration and cost. Based on a modular concept, an estimated 4 months would be required from program initiation to flight demonstration at a cost of approximately \$26,400 per system (plus G and A, overhead, and fee) excluding the flight test cost and assuming a government-furnished missile or installation on one of the remaining R&D vehicles. This is a preliminary engineering estimate performed on a typical system indicated in Fig. V-29 for the pressurization of the Titan II Stage I fuel tank. A continuous solid stream surface reagent injection system was selected for each tank due to its high reliability and easy installation. This concept could be used for pressurization of the other tanks with modification to the injector for achieving the proper gas generation rate. All components are standard shelf items with only a small percentage of manufactured parts required. Ample room for installation has been assumed. However, the Stage II installation would be hampered by space limitations.

The total manpower estimate for the 4-month program outlined is 2200 man-hours (equivalent to approximately \$22,000). The detailed cost breakdown contained in Table V-7 based on the development of a single system; for a larger order, the cost per system would be reduced due to a 50% decrease in labor per system (i.e., 2 units \$25,900 each, 5 units \$17,600 each).

Table V-7 Basis for Cost Estimate, Titan II, MTI (Based on One System)

	Cost (\$)
Material	
1 Reagent Storage Sphere (0.295 cu ft)	1,500
1 Injector Isolation Valve (1/4 in.)	750
1 Injector	100
1 Reagent Fill and Drain Valve (1/4 in.)	750
1 Reagent Pressurization Disconnect (1/4 in)	1,000
Plumbing, Wiring, Supports, etc.	<u>300</u>
Total	4,400
Manpower	
2200 man-hours (\$10/man-hour)	<u>22,000</u>
System Cost	
Total	26,400

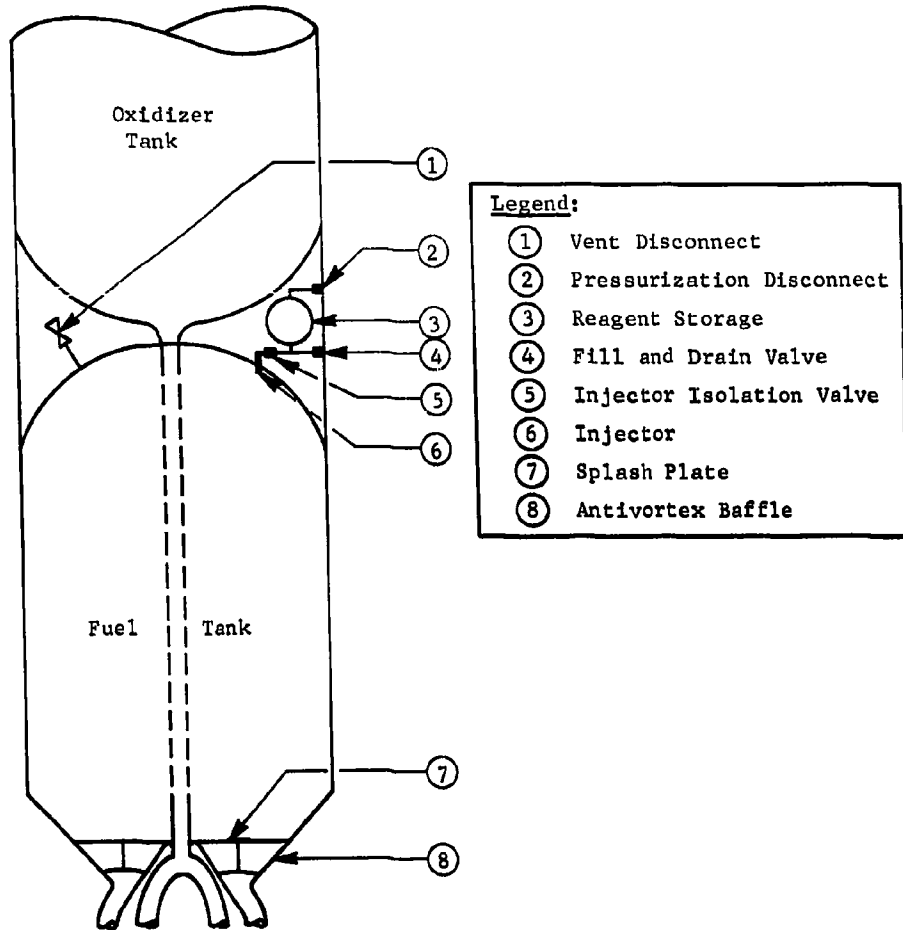


Fig. V-29 Titan II, Stage I Fuel Tank, MTI Pressurization System

RTD-TDR-63-1123

The development schedule is shown in Fig. V-30. Initial effort would be concerned with the generation of a design criteria document indicating pertinent system requirements from which detailed design drawings can be completed. The detailed design would be based on a thorough analytical examination of pressurization and operational characteristics to establish optimum flow capacity and response. Anticipated problems would center on the space limitations of the system and structural support requirements of the individual components. The fire-in-the-hole staging technique would present some difficulty in assuring Stage I oxidizer tank MTI system structure integrity during the Stage II engine operation environment. In addition, heat transfer through the oxidizer conduit will warrant careful study. Thermodynamic analysis of the pressurization system would be provided by the existing mathematical model developed during the present MTI program. Resultant injector and reagent designs would be adjusted, if required, during verification testing.

Since all the basic components would be off-the-shelf procured items, the minimum procurement effort would be handled by design and engineering personnel. Manufacturing effort would involve the fabrication of necessary component supports, plumbing, and performing existing system modifications. Existing quality assurance programs on similar components would be imposed to obtain satisfactory component performance. System development would be accomplished during the system verification tests. During this phase of the program, a full-scale mockup of the MTI pressurization system would be constructed and flow-tested to the design performance levels before installation on the flight article. Due to the extensive testing performed on similar tankage with a pulse-type system, no full-scale battleship tests would be required. Adequate overpressure protection during the 20-sec captive firing would be achieved by the present vent and pressurization system. In the event of inadequate pressurization due to a low gas generation rate, shutdown would be initiated and an additional test required for the increased capacity injector.

Work Item	Months				Men	Man-Hours
	1	2	3	4		
1. System and Criteria Definition	█				2	240
2. System Design		█			2	320
3. Procurement			█		*	—
4. Manufacturing			█		3	480
5. System Verification Tests			█	█	5	600
6. System Installation and Checkout				█	3	240
7. Captive Test				█	8	320
8. Flight Demonstration				█		
Total						2200

*Included in design and engineering effort.

Fig. V-30 Titan II MTI Pressurization System Development Schedule

2. Titan III Transtage

The transtage is the third stage of the Titan III core and has a basic configuration as shown in Fig. V-31. The titanium main propellant tanks are in a side-by-side position within the 10-ft-diameter module formed by the aluminum missile skin. Fuel tank capacity is approximately 137 cu ft of a 50/50 blend of hydrazine and UDMH, while the oxidizer tank contains approximately 169 cu ft of N_2O_4 . The total tank length of 14 ft was not considered a significant problem for the MII pressurization system application. Two pressure-fed 8000-lb-thrust engines are located toward the aft end of the propellant tanks, oriented along an axis perpendicular to a line joining the tank centerlines. The complete transtage consists of two sections, the propulsion module and the control module. Propellant tanks, engines, and the pressurization system are contained in the propulsion module, while the control module houses the transtage instrumentation and the attitude-control system. The attitude-control rocket motors are on the missile skin immediately above the separation line of the two modules.

Transtage applications will include use as an extra booster stage for high orbits or heavier payloads. Since it will also be used to transfer the payload from one orbit to another, it requires a capability of three restarts in zero-g environment. For a zero-g engine startup, the attitude-control rocket motors are fired for a period of about 10 sec, providing acceleration to begin bottoming the propellants. After the 10-sec period but before the propellants have completely bottomed, the transtage engines are started, using the propellant trapped beneath a false bottom in each tank. The propellant is completely bottomed by the acceleration from the transtage engines. The transtage is capable of 500 seconds of continuous operation after 6.5 hr in orbit (in the zero-g environment). The entire transtage weighs about 28,000 lb loaded with propellants, with weight kept at an absolute minimum.

The configuration of the propulsion system now adopted for the Titan III transtage is shown in Fig. V-31. Helium gas is compressed to 3600 psi in two 10.25-cu-ft storage spheres. These spheres are made of titanium and weigh 235 lb each. Each contains 23 lb of helium gas, which passes through regulator valves to maintain propellant tank pressures at approximately 163 psi.

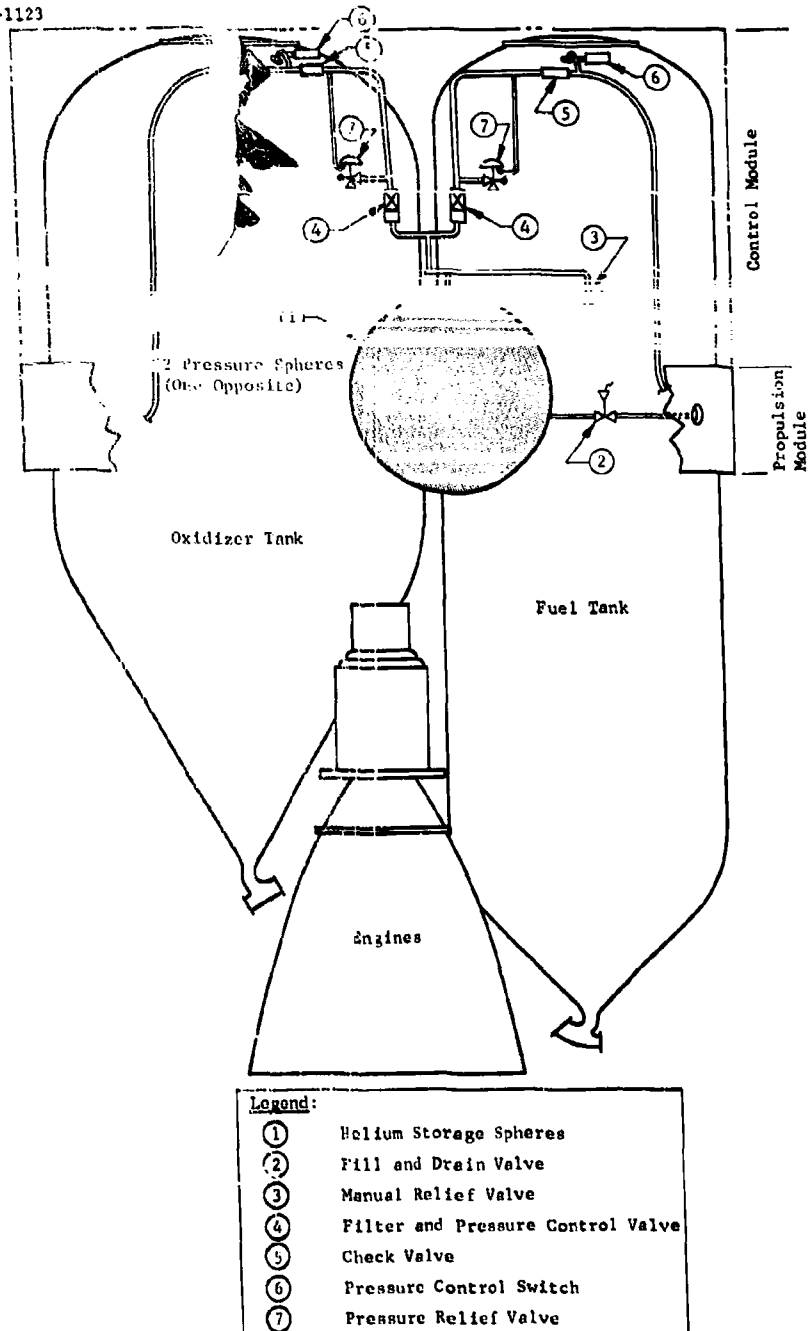


Fig. V-31 Titan III Transtage Helium Pressurization System (Configuration 1)

The results of this study indicated that approximately 250 lb can be saved by using a dual-injection MTI pressurization system instead of the present helium configuration, with only a slight reduction in reliability. A modular-type system has been proposed. It could be developed during the Titan II test program and later incorporated in the Titan III design. Because of elimination of the helium spheres, a re-evaluation of vehicle dynamics would be required to verify stability and control requirements. In view of the zero-mission requirements and uncertainty of the reaction process, continuous pressurization or adoption of the common ullage MTI pressurization concept is not recommended. The titanium tankage is particularly desirable for the MTI pressurization system since high operating temperatures could be efficiently used for continuous missions. For discontinuous missions, the high operating temperatures would be less desirable since pressurization could not be provided by the MTI system during a zero-g cooldown. An investigation of repressurization requirements indicated that approximately 25 sec may be required unless a special high-capacity injector is used during this period.

Preliminary Design Schematics - Figures V-32 thru V-36 show design schematics of the MTI pressurization systems considered most promising for Titan III transtage application. In all the MTI systems, the injector is a self-contained (modular-type) unit attached to the inside of the tank manhole cover. The injection duration is controlled by an electrically operated solenoid, with its movement perpendicular to the reagent flow direction, reducing the power requirement. The solenoid is activated by a pressure switch monitoring propellant tank pressure. The tank is pressurized by controlled combustion of the hypergolic propellant and reagent within the tanks. (The term "reagent" refers to fuel when injected into the oxidizer tank and to oxidizer when injected into the fuel tank.) Overpressure protection is provided by the existing pressure vent and relief system, with an additional capability of closing the reagent supply valve in the event of a failed open injector.

When an MTI system is used in a restart mission, it is not intended that tank pressures be maintained throughout the coast period. Instead, the injection process would be activated up to 5 sec before engine start, allowing the tank pressure to rise sufficiently for propellant feed. An auxiliary injector could be added to cut down on the time needed for prepressurization. This would be especially advantageous in conserving the attitude-control system propellant supply when firing in a zero-g environment, where the attitude-control system is used to provide

acceleration to bottom the propellants in the main tanks. The propellants must be bottomed before the injection begins, since the injected reagent must come into contact with the propellant for the process to be controllable. Detailed descriptions of the operation of the proposed systems are contained in the following paragraphs.

MTI Dual Injection, Titan III Transtage, Gas Pressurized Reagent Supply (Fig. V-32) - Helium or nitrogen gas at 1700 psi is released from a 1/3-cu-ft titanium sphere through a pressure-control valve into the two reagent storage tanks, which are titanium spheres with volumes of 1 cu ft and 1/3 cu ft. The pressurized reagent passes through the reagent supply through the reagent supply valves to the injectors.

MTI Dual Injection, Titan III Transtage, N₂ Pressurized Reagent Supply (Fig. V-33) - This configuration is similar to the previous configuration, except that an existing pressurized gas source is used. Nitrogen gas at 3000 psi is used to supply pressure to the transtage attitude-control system propellant tanks and, in this configuration, also supplies pressure to the MTI reagent storage tanks. A break-away-type coupling in the nitrogen line provides for separation of the two systems when the control module separates from the propulsion module. Reagent is supplied from two titanium spheres, having volumes of 1 cu ft and 1/3 cu ft. The reagent passes through the reagent supply valves into the injectors.

MTI Dual Injection, Titan III Transtage, Pump Fed, Main Tank Reagent Supply (Fig. V-34) - Pumps are used to supply reagent under pressure to the injectors. The reagent is tapped from locations beneath the false bottom of the main propellant tanks, insuring a constant reagent supply during accelerations from zero-g. Based on estimates of component weights, this configuration was found to be the lightest system.

MTI Dual Injection, Titan III Transtage, Mechanically Pressurized Reagent Supply (Fig. V-35) - Reagent is stored in collapsible bellows encased in gastight chambers. Inside each chamber and behind the bellows is a spring with a minimum spring force per square inch of 100 lb, equal to the desired pressure differential across the injector. An open line from the spring chamber is tapped into the main tank ullage; consequently, the pressure behind the reagent filled bellows is the sum of the pressures exerted by the gas and by the spring.

Since the gas pressure is equal to the ullage pressure, the required ΔP across the injector is always maintained by the spring.

MTI Single Tank Injection, Common Ullage (Fig. V-36) - Although a spring-loaded reagent storage chamber is shown in Fig. V-36, any of the preceding reagent storage and pressurization techniques can be used for this system. Reagent is supplied to only one tank, and part of the pressurizing gas is passed from the ullage of the primary tank into the secondary tank through a thin-walled stainless steel common ullage line $1\frac{1}{2}$ in. in diameter. The proposed method of gas entrance into the secondary tank is called subsurface gas injection, found to be the most successful technique in the Phase I experimental program.

Weight - To compare weights of the various pressurization systems presented for Titan III transtage use, conservative estimates were made based on the preliminary design configurations. The final pressurization system weights are compared at engine shut-off, so the pressurant weight includes the combustion products with condensibles, the initial pressurizing gas, and the vaporized propellant. It was assumed that, for the MTI systems, an ambient cooldown of the saturated ullage gases to 100°F was the condition determining the amount of pressurant required. This assumption is conservative since it represents an extreme case for a transtage mission using the MTI system. In all cases, weight estimates were based on gas storage tanks made of titanium and initially pressurized with helium to 3600 psi. Approximations of component weights were obtained from similar existing units.

Weight comparisons of the six pressurization systems evaluated are given in Table V-8 and Fig. V-37. Total hardware weight comprises pressurization and service lines, switches, valves, supports, reagent storage containers, gas pressurant tanks, pumps, and injector. It was found that using any of the MTI systems rather than the present helium system would result in a saving of 238 to 271 lb.

Best Available Copy

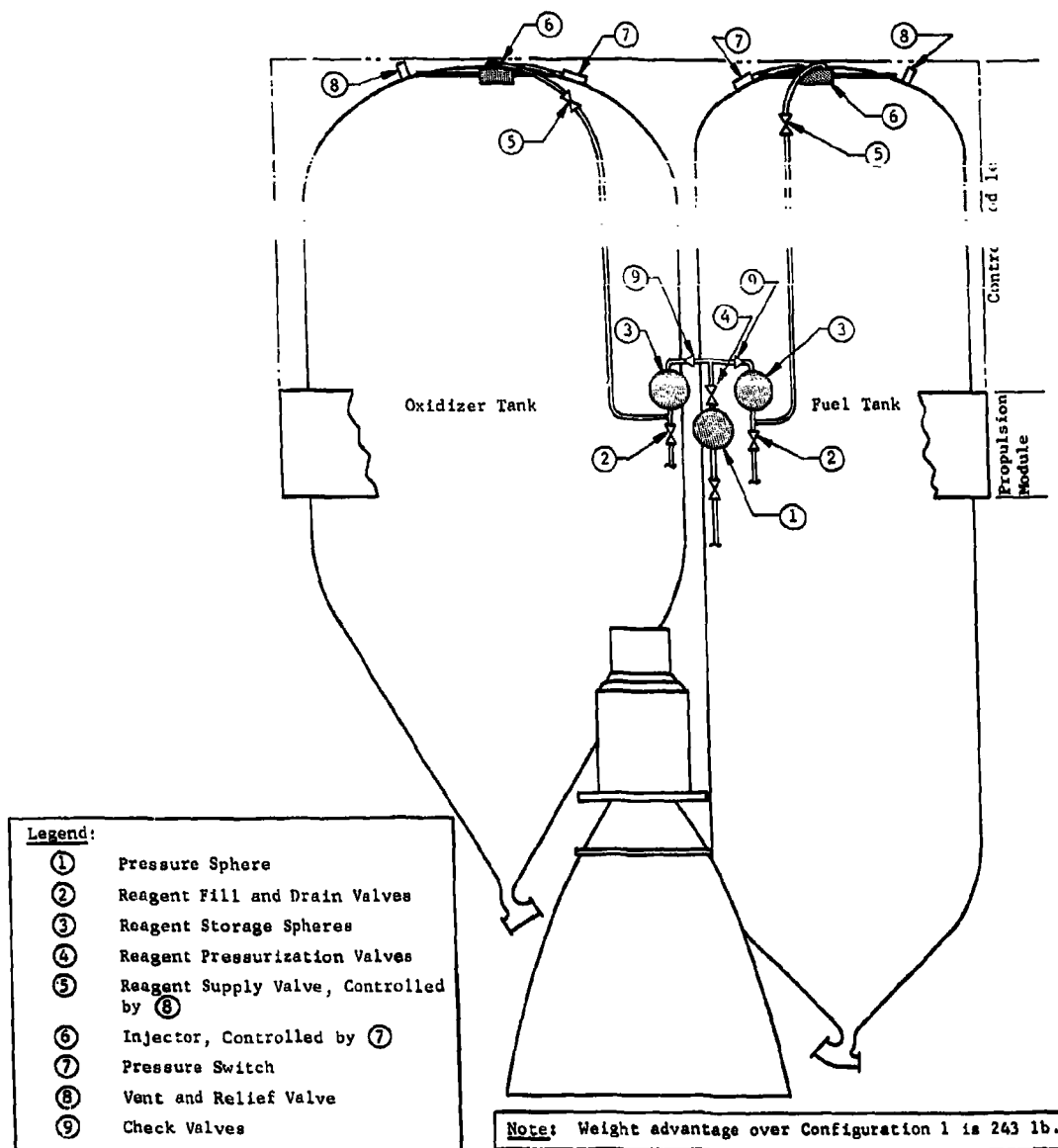


Fig. V-32 MTI Dual-Injection, Titan III Transtage, Gas-Pressurized Reagent Supply (Configuration 2)

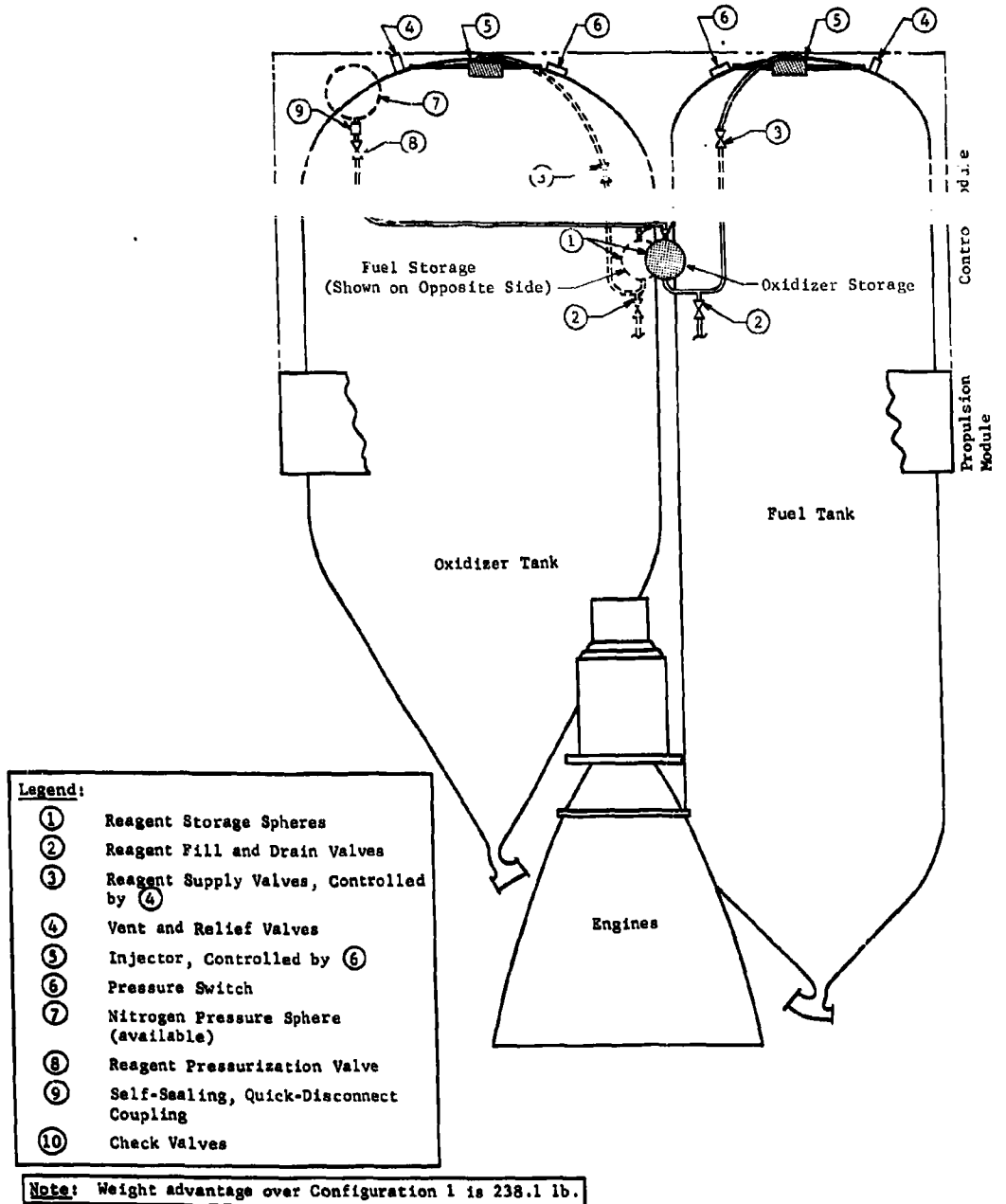


Fig. V-33 MTI Dual-Injection, Titan III Transtage, Nitrogen-Pressurized Reagent Supply (Configuration 3)

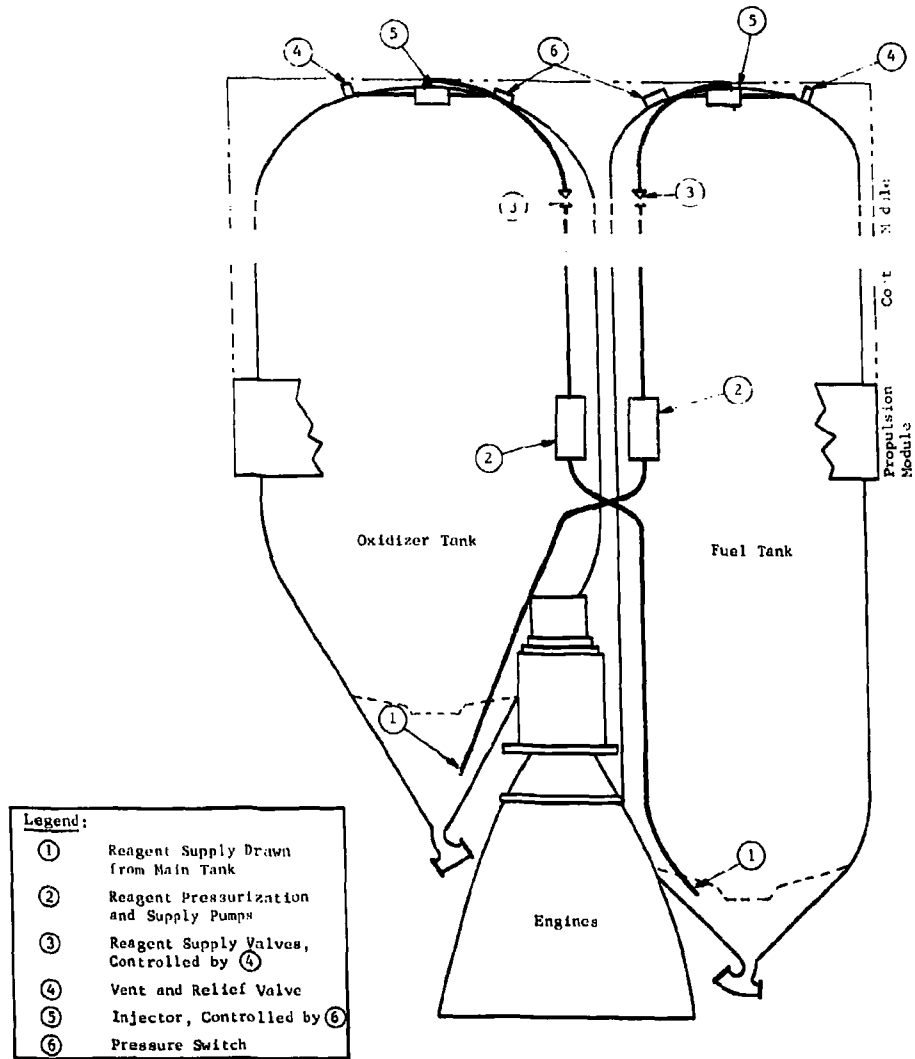
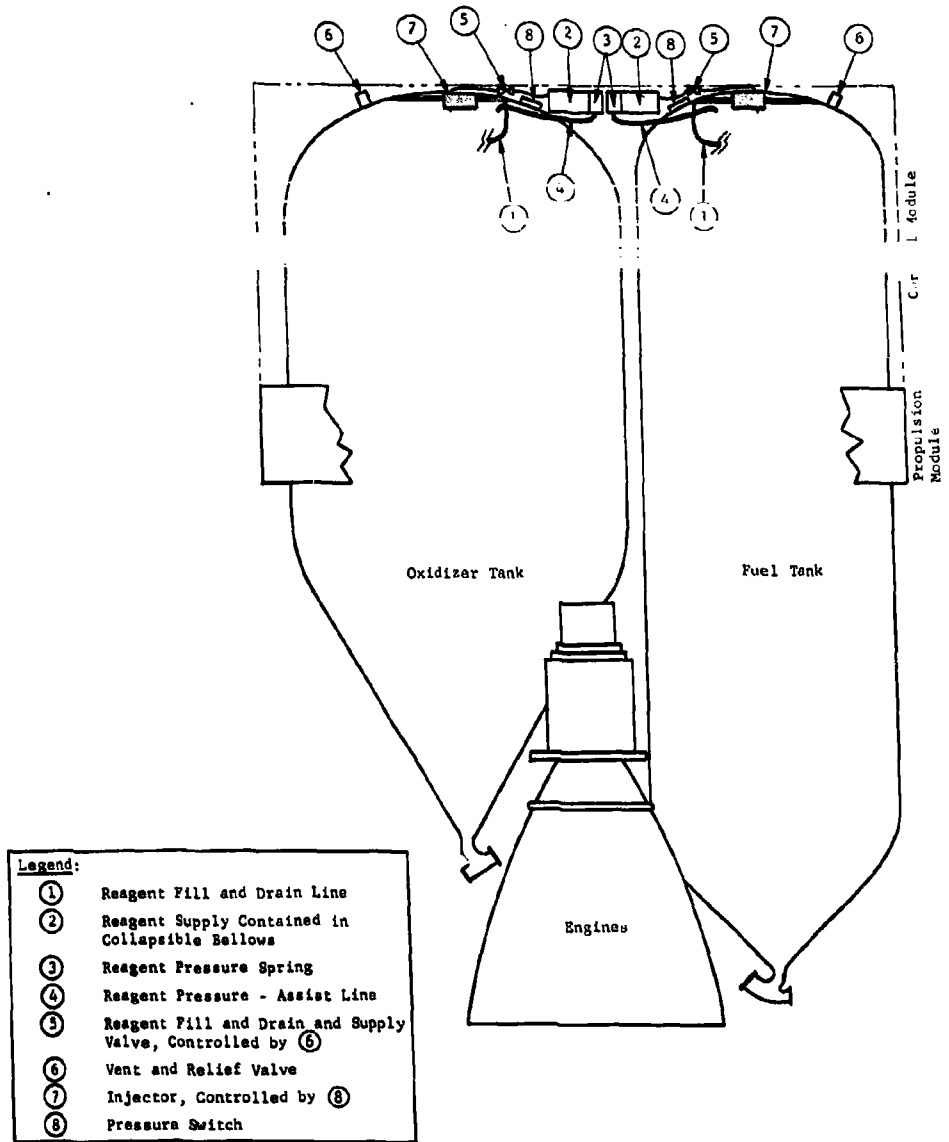


Fig. V-34 MTL Dual-Injection, Titan III Transtage, Pump-Fed, Main Tank Reagent Supply (Configuration 4)



Note: Weight advantage over Configuration 1 is 238.1 lb.

Fig. V-35 MTI Dual-Injection, Titan III Transtage, Mechanically Pressurized Reagent Supply (Configuration 5)

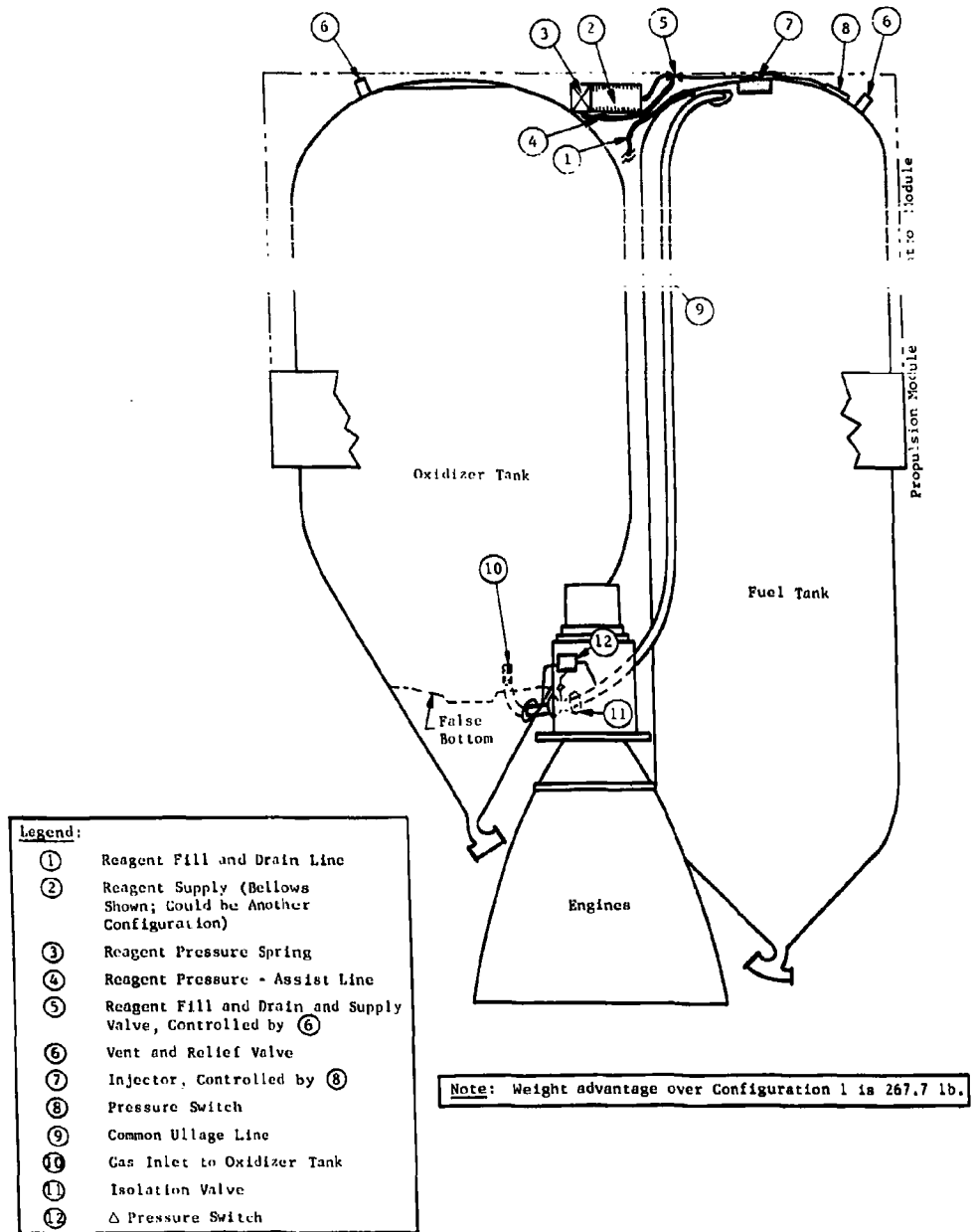


Fig. V-36 MTI Single-Tank Injection, Common Ullage (Configuration 6)

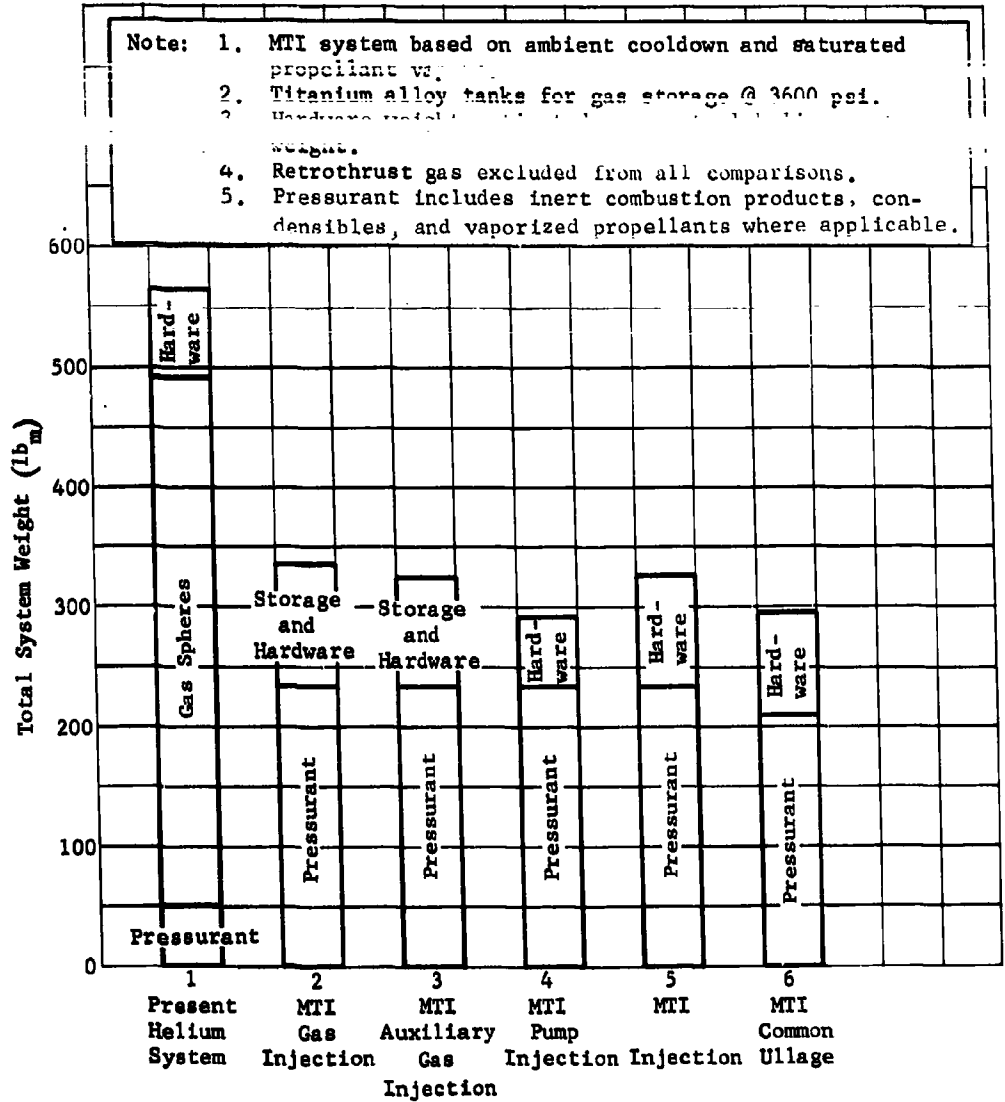


Fig. V-37 Comparative Pressurization System Weight, Titan III Transtage

Table V-8 Summary of Titan III Transtage Pressurization System Weights (Lb)

System	Present Helium System	MTI Gas Injection	MTI Auxiliary Gas Injection	MTI Pump Injection	Structural	MTI Common Ullage
Accessories (lines, switches, valves, supports)	81	61	61	48		66
Subequipment (reagent storage, pressurant spheres, pumps, bellows)	438	25	20	10		20
Total Hardware	519	86	81	58		86
Pressurant (inerts, combustion products, vapor)	43.8	233.7	233.7	233.7	7	209.1
Total	562.8	319.7	314.7	291.7	7	295.1
Weight Savings Relative to Helium Pressurization	0	243	248.1	271.1	33.1	267.7

V. RELIABILITY

The reliabilities of the various pressurizing systems for the Titan III Transtage are presented in Table V-9. A summary is contained in Table V-10. The results indicate the present helium-pressurized system to be the most reliable, the dual-injection (nitrogen, independent gas source, and mechanical pressurization) and the single-tank injection (common ullage) system to be the next most reliable. The pump-driven dual-injection system is indicated to be the least reliable.

Calculation of the reliabilities was based on the latest revision of Martin's Engineering Reliability Policy and Procedures Manual, as indicated in the preceding section. A simplifying assumption was made in the calculation of the reliabilities, namely that the mission consisted of a 500-sec (0.139-hr) firing. No attempt was made to calculate reliabilities during the coast period or for restarts. In addition, the determination of the generic failure rate, GF_r , for the MTI injectors was established by assuming that this failure rate was equal to that of the most unreliable component, the reagent supply valve. It is probable that if the GF_r were more accurately determined, the reliabilities of the various MTI systems would have compared more favorably with the present helium pressurization system.

Table V-9 Pressurization System Reliability Comparison

a. Titan III Transtage					
Component	No. Required	$GF_r \times 10^6$	K_a	K_{op}	$tF_r \times 10^6$
Reagent Supply Valve	2	11.0	1	145	443.4
Airborne Pressure Control Switch	2	0.1	1	145	29.0
Vent and Relief Valve	2	2.85	1	145	114.9
Helium Storage Tank	2	0.07	1	145	2.8
Helium Check Valve	2	5.0	1	145	201.6
Helium Filter	2	0.3	1	145	12.1
Diffuser	2	0	1	145	0
Flexible Line and Fittings	10	0.448	1	145	90.3
Hard Line and Fittings	18	0.224	1	145	81.3
Total =					975.4
Reliability = 0.9990					

Table V-9 (cont)

Component	No. Required	$GF_r \times 10^6$	K_a	K_{op}	$tF_r \times 10^6$
Reagent Supply Valve	2	11.0	1	145	443.4
Airborne Pressure Control Switch	2	0.1	1	145	29.0
Pressurant Load Hand Valve	1	0.112	1	145	2.3
Pressurant Storage Container	1	0.07	1	145	1.4
Pressure Check Valve	2	5.0	1	145	201.6
Injector	2	11.0	1	145	3100.0
Flexible Line and Fittings	2	0.448	1	145	13.0
Hard Line and Fittings	6	0.224	1	145	19.6
Vent and Relief Valve	2	2.85	1	145	114.9
Total = 3925.2					
Reliability = 0.9961					
c. MTI Dual-Injection, Pump-Fed, Main Tank Reagent Supply					
Component	No. Required	$GF_r \times 10^6$	K_a	K_{op}	$tF_r \times 10^6$
Reagent Supply Valve	2	11.0	1	145	443.4
Airborne Pressure Control Switch	2	0.1	1	145	29.0
Vent and Relief Valve	2	2.85	1	145	114.9
Injector	2	11.00	1	145	3100.0
Pumps	2	13.5	1	145	3920.0
Flexible Line and Fittings	6	0.448	1	145	390.0
Hard Line and Fittings	2	0.224	1	145	6.3
Total = 8003.6					
Reliability = 0.9920					

Table V-9 (Contd)

Pressurized Reagent Supply					
Component	No. Required	GF $\times 10^6$	K_a	K_{op}	tF $\times 10^6$
Reagent Supply Valve	2	11.0	1	145	443.4
Airborne Pressure Control Switch	2	0.1	1	145	29.0
Vent and Relief Valve	2	2.85	1	145	114.9
Injector	2	11.00	1	145	3100.0
Bellows	2	2.2	1	145	640.0
Springs	2	0.1	1	145	29.0
Flexible Line and Fittings	2	0.448	1	145	13.0
Hard Line and Fittings	6	0.224	1	145	19.6
Total =					4388.9
Reliability = 0.9956					
e. MTI Single-Tank-Injection, Common Ullage					
Component	No. Required	GF _r $\times 10^6$	K_a	K_{op}	tF _r $\times 10^6$
Reagent Supply Valve	1	11.0	1	145	221.9
Airborne Pressure Control Switch	1	0.1	1	145	14.5
Vent and Relief Valve	1	2.85	1	145	107.5
Injector	1	11.00	1	145	1550.0
Bellows	1	2.2	1	145	320.0
Spring	1	0.1	1	145	14.5
Isolation Valve	1	5.0	1	145	725.0
Gas Diffuser	1	11.0	1	145	1550.0
Δ Pressure Switch	1	0.1	1	145	14.5
Flexible Line and Fittings	2	0.448	1	145	13.0
Hard Line and Fittings	3	0.224	1	145	10.0
Total =					4540.9
Reliability = 0.9955					

Table V-10 Summary of Pressurization System Reliability, Titan III Transtage

Type System	Reliability
Present Helium Pressurization System	0.9990
MTI Dual-Injection, Gas Pressurized Reagent Supply (both nitrogen and independent gas)	0.9961
MTI Dual-Injection, Mechanically Pressurized Reagent Supply	0.9956
MTI Single-Tank-Injection, Common Ullage	0.9955
MTI Dual-Injection, Pump-Fed Main Tank Reagent Supply	0.9920

Performance - The theoretical pressurization system performance of the Titan III transtage has been computed with the IBM-7094 MTI mathematical model. Individual tanks are pressurized by the direct reagent injection process for a continuous 450-sec mission. System thermodynamic characteristics are shown in Fig. V-38 and V-39, with a polytropic gas expansion process used for the final 15 sec of mission duration. Pressure control is maintained within the 1% tolerance range by the existing pressure switches. Maximum expected tank wall temperatures are well within the allowable for the titanium structure, and the low reagent consumption minimizes pressurant storage requirements.

In comparing the performance of the Titan III transtage equipped with an MTI pressurization system with that of the present helium system, two significant factors must be considered. For a continuous mission, the helium system absorbs a large weight penalty because of the cooling caused by gas expansion, whereas the heat generated in the MTI system is used effectively to reduce the pressurant density. Conversely, for an environment cooled mission, as could be encountered in a 6.5-hr period, the higher gas molecular weight inherent in the MTI process would invoke a weight penalty on the MTI pressurization system. For comparison, however, the vehicle was assumed to be capable of either type of mission, and a weight saving of 250 lb was still realized with the MTI pressurization process.

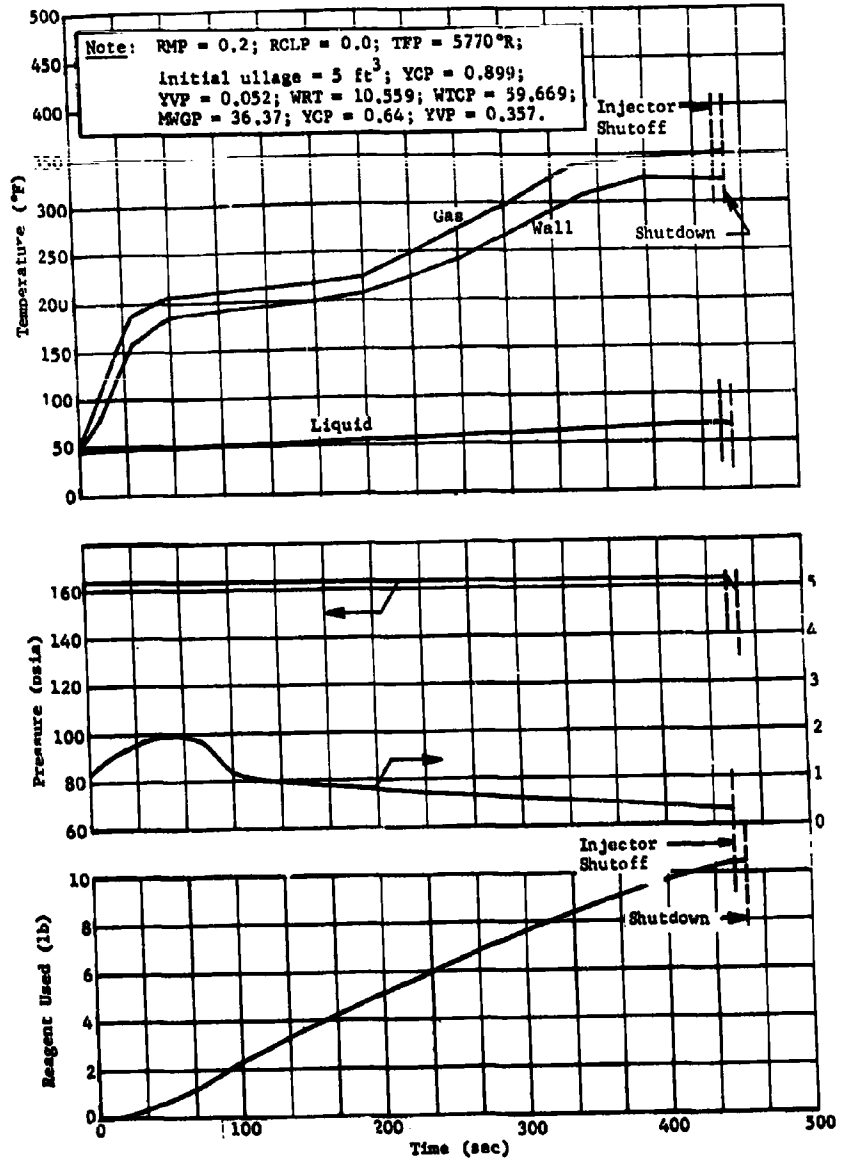


Fig. V-38 Titan III Transtage MTI Predicted Performance, Oxidiser Tank

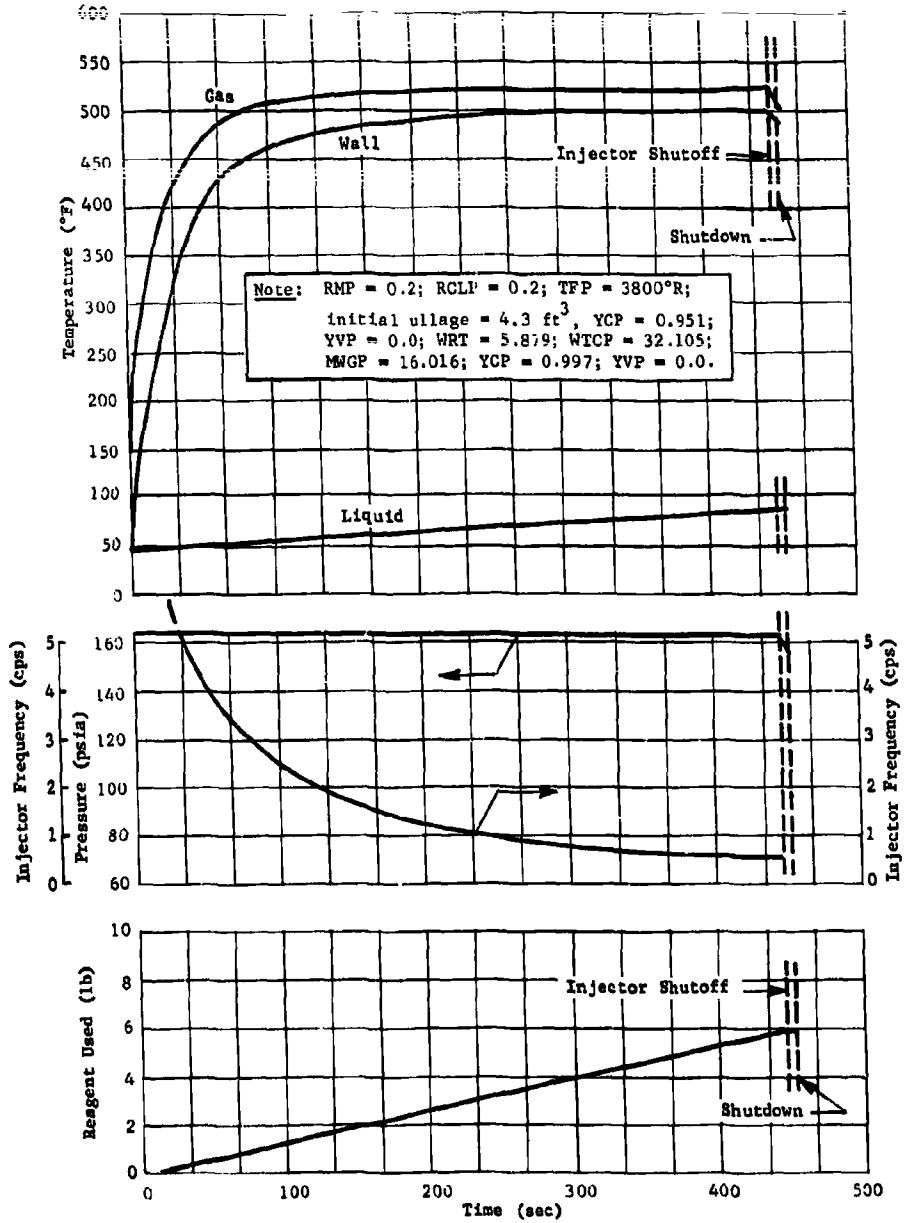


Fig. V-39 Titan III Transtage MTI Predicted Performance, Fuel Tank

From the foregoing reliability study, it is indicated that an MTI system using a gas pressurized reagent supply (such as presented in Fig. V-32 and V-33) would give the best overall performance for continuous operation of the transtage. The reliability valve for the pump-fed reagent configuration (Fig. V-34), which represents the greatest weight saving, is significantly low. A fair evaluation of the single-injection, common ullage system (Fig. V-36), which also represents a substantial saving in weight, cannot be made at this time due to a lack of test data. Moreover, current pressurization system design philosophy prevents pressurization of an oxidizer tank with a fuel-rich gas.

When evaluating the performance requirements of the coast-inject mission, several problems prohibit the use of an MTI system in its present stage of development. In addition to the problem of the pressurizing gases cooling down during a coast period, there is also an undemonstrated ability of the MTI system to operate effectively in the zero-g environment. Although propellant orientation is accomplished by the attitude-control system used to provide initial acceleration for restarts from zero-g, bottoming the propellants is doubly important in an MTI system, since the injected reagent must come into contact with the propellant for the process to be controllable. This situation would increase the demand on the attitude-control system if it were used, and its capacity would possibly have to be increased, thus reducing the weight advantage. The configurations shown in Fig. V-32 and V-33 depend on acceleration to orient the reagent supply, unless a bladder or other reagent container is used. In the single-tank-injection, common ullage configuration of Fig. V-36, additional valving would be needed in the common ullage line to keep the propellants from undesirable mixing.

The present sequence of operations requires that the propellant tank pressures be increased from the 8-psig nitrogen blanket pressure to 92 psia before launch to verify airborne pressurization system operations. With the adoption of the MTI pressurization process, it is recommended that the pressure be raised to 60 psia with nitrogen just before MTI pressurization to 92 psia, to avoid an underpressure kill from cooling of the pressurants. A second benefit is derived from this procedure since the injector differential pressure will not exceed the 200-psi maximum for a significant period of time. For the purpose of the preliminary study effort performed, however, the MTI pressurization process has been used from 8 to 92 psi to obtain maximum system heating and reagent consumption.

During the 110 sec of solid rocket motor operation and 140 sec of the liquid core boost, the MTI system is inoperative. It is anticipated that a slight reduction in transtage propellant tank pressure because of cooling before launch would be offset by aerodynamic heating in flight, but for the purpose of this study it was assumed that tank pressures were at 90 psia initially during the 165 sec of the second stage of the liquid core. At this time, the transtage propellant tanks are brought up to the 163-psia operating pressure by the MTI process. System response and maximum temperatures have been predicted to enable a structural analysis of the tankage during this critical period.

Steady-state operation of the transtage propulsion system has been based on the 163-psia initial pressure and 45°F minimum system operating temperature with the minimum ullages and nominal propellant flow rates. Before the first burn, a hand computation was performed to determine the reagent consumption for this condition.

A specific restart mission was selected to establish maximum reagent consumption. For this case, ullage temperatures were assumed to reach bulk propellant temperature during coast. Before the second and third burns, MTI system response is predicted with the aid of the IBM-7094 computer program. Since the repressurization occurs just before restart for this mission, the initial temperatures are the same at the start of propellant expulsion. A detailed representation of the complete mission and characteristics of the pressurization process are shown in Fig. V-40 and V-41. To provide residual propellants for cooling, the injector has been shut off when the propellant level reaches the false bottom. Based on the possible elimination of liquid level sensors for injection termination, a study of the amount of pressure decay experienced with various volumetric changes indicated that the rate is equivalent to 1 psia/sec.

Cost - A preliminary cost analysis has indicated that an MTI pressurization system could be installed in a Titan III transtage in 4 months for a cost of approximately \$40,000 (plus G+A, overhead, and fee), assuming no additional problems requiring a redesign of the system or its components are encountered. Additional transtage units could be converted to MTI for \$17,400 each. The MTI configuration shown in Fig. V-32 was used as the basis for the engineering cost study. Except for the injector, which would be a newly developed part, all the components needed to construct the MTI system are either shelf items or are in use on the helium pressurization system. Consequently, the injector accounts for most of the labor allocated to component design, manufacturing, and component testing (Fig. V-42).

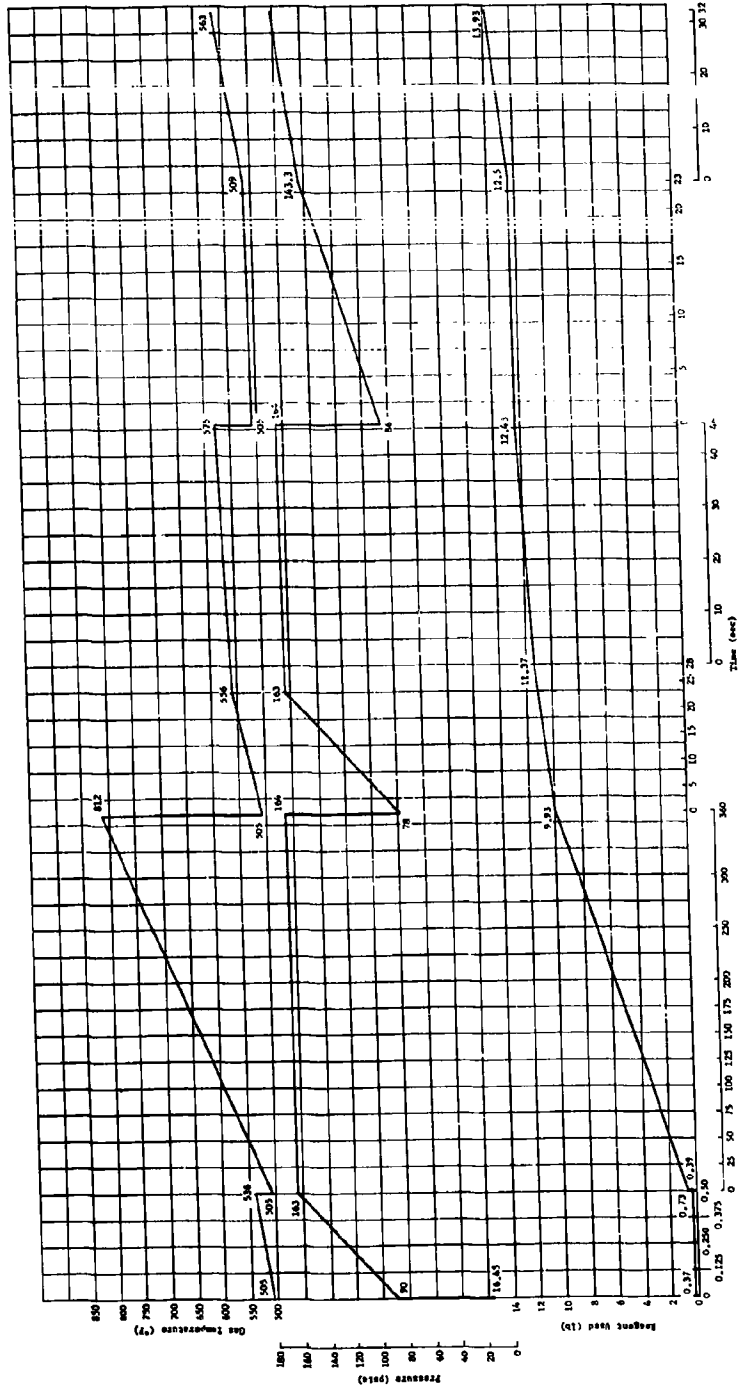


Fig. 7-40 Titan III Thrustage RTI Performance, Boost Mission, Oxidant Tank

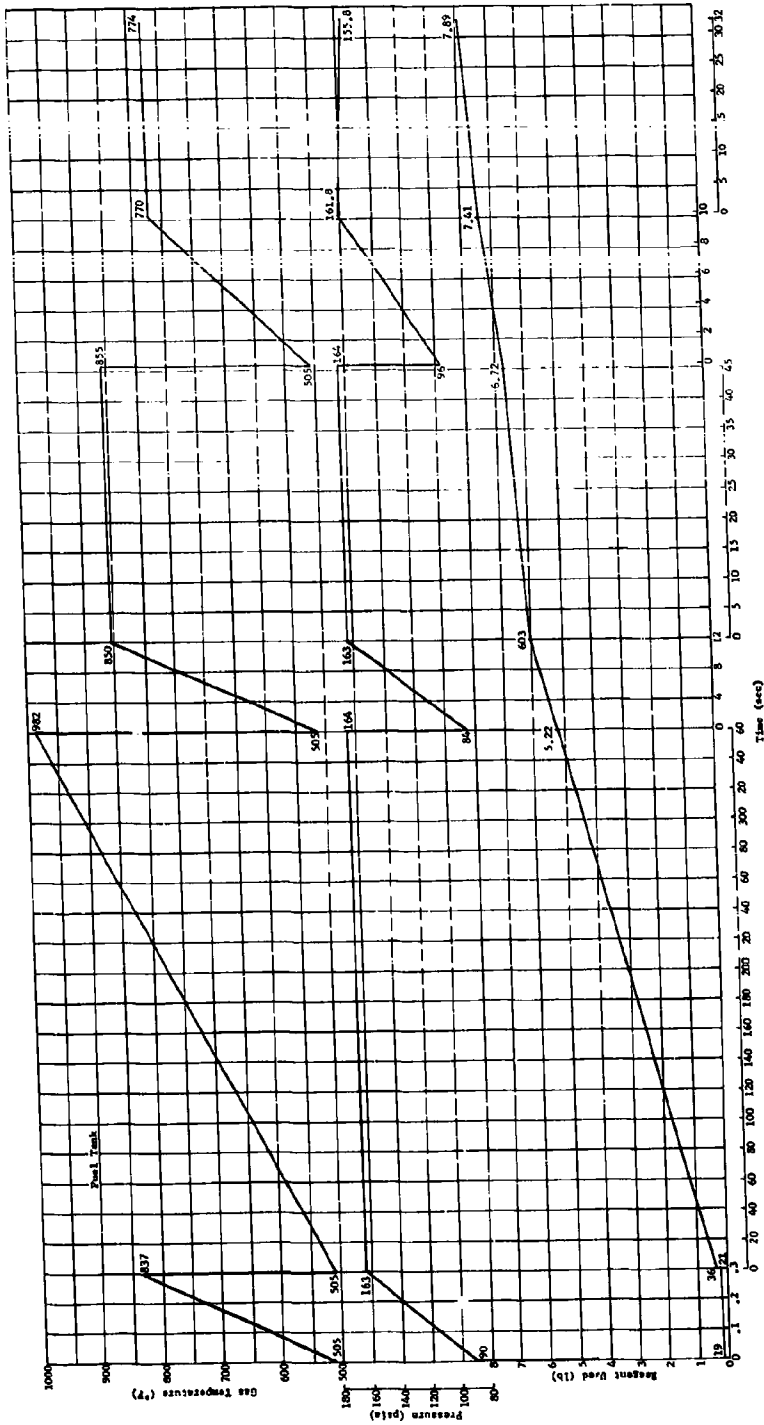
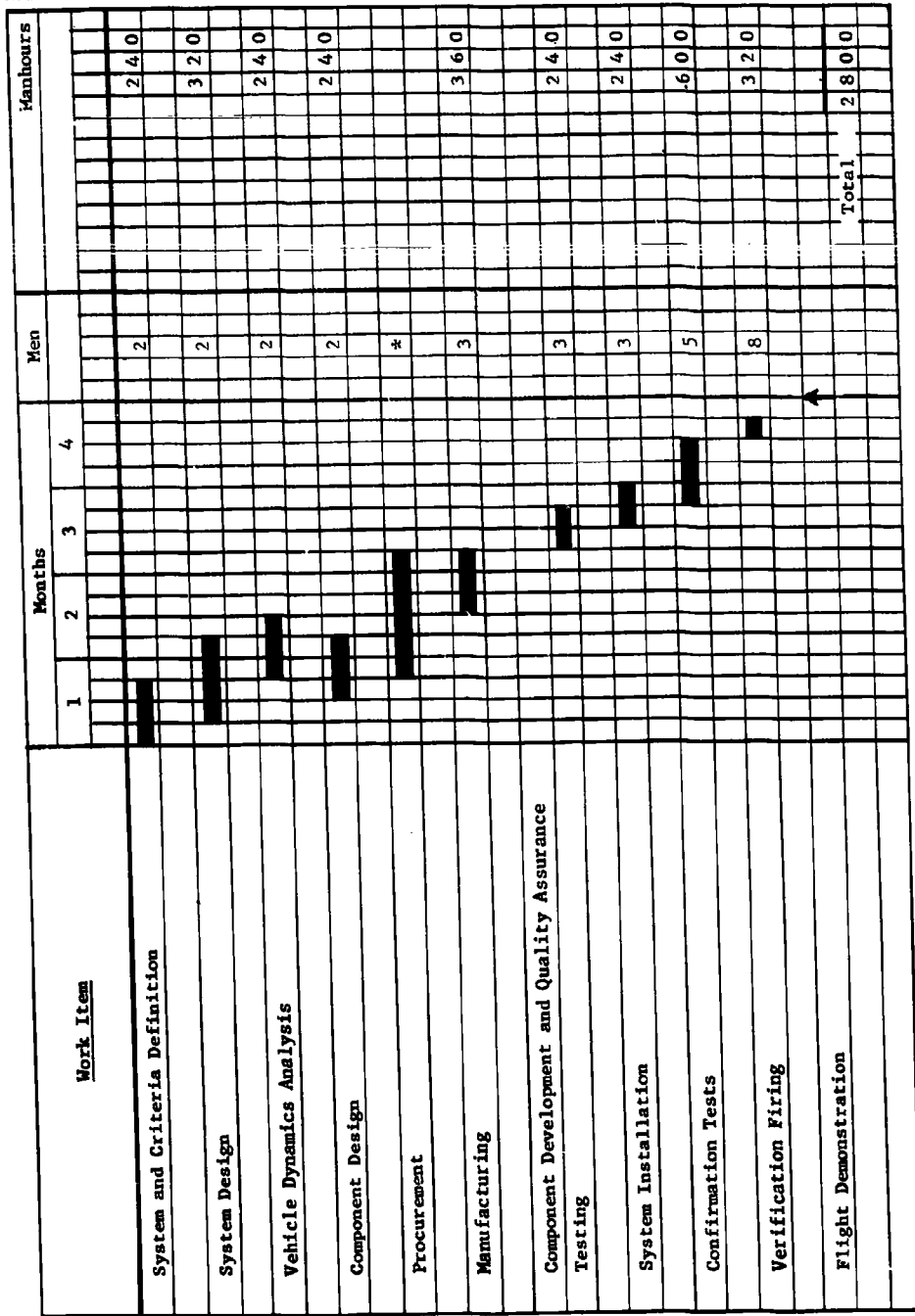


Fig. V-21 Titan III Intermediate III Performance, Restart Mission, Fuel Tank



*Included in design and engineering effort

Fig. V-42 Titan III Transtage MTI Pressurization System Development Schedule

The total work load allowed for the 4-month program outlined is 2600 manhours, estimated to cost \$26,000. The component cost, including testing, for the first transtage unit is \$12,000, making the total cost \$38,000. Additional units, when development and testing have been completed, could be attached to the transtage for \$17,400 each. A detailed cost breakdown for a typical MTI installation has been provided in Table V-11.

The initial step in developing the Titan III transtage MTI pressurization system is to outline the performance requirements of the MTI system and prepare a criteria document. The performance criteria would probably parallel the requirements for the helium system, but since it is not being proposed that the MTI system be capable of a restart from zero-g, the performance criteria for an MTI system may not be so demanding. Once the requirements were stated, the entire MTI system would be accurately designed to achieve the proper size, weight, and performance requirements for each line and component. Also included in this effort is the determination of what alterations the transtage tanks must have to accept the MTI unit. Since the MTI is attached to the tanks as a modular unit, such alterations, except for the manhole cover, would be minor. However, some components not in the MTI system itself would have to be rearranged so the transtage center of gravity is not shifted from its present axis. This relocation of components would be studied in the work effort entitled "Vehicle Dynamics Analysis." The group performing this analysis would also be responsible for the design of adequate supports for the relocated components, since the supports enter into the weight balance.

To establish the man-loading, it has been assumed that the job of procurement can be absorbed into the other manhour allocations. The procurement phase of the program consists of preparing the paperwork involved in buying shelf items and arranging for in-house manufacture of components.

To meet the missile performance criteria, all new components or parts would have to comply with the quality assurance test requirements specified in the applicable documents. Such testing would be conducted at Martin test facilities or be subcontracted to a testing agency. During the test phase of the new components, installation of the MTI system in the transtage could be started, using the parts already available. System installation would be completed when the tested components were ready for use.

RTD-TDR-63-1123

Confirmation tests would consist of tank pressurization and propellant outflow tests and would be performed on the first transtage unit only. Any minor design alterations resulting from the test results would be used in all subsequent units. The transtage would also be verification fired, thus proving the capability of the MTI system. The system would finally be tested in a demonstration flight and its performance in flight monitored by existing telemetry.

Table V-11 Basis for Cost Estimate - Titan III Transtage

Parts Usable from Helium System:		
Two Pressure Switches		
Two Vent and Relief Valves		
Two Gas Fill and Drain Valves		
Two Check Valves (gas)		
One Gas Line Disconnect		
Extra Components Needed in the MTI System (based on one transtage Unit):		
	<u>Cost Each</u>	<u>Total</u>
Two Injectors	\$ 1,200	\$ 2,400*
Two Reagent Supply Valves	1,500	3,000
Two Reagent Fill and Drain Valves	750	1,500
Two Reagent Fill and Drain Disconnects	1,000	2,000
Plumbing	--	300*
Two Manhole Covers (altered)	350	700*
Supports	--	200*
One 1-cu-ft Reagent Sphere	2,500	2,500
One 1/3-cu-ft Reagent Sphere	1,500	1,500
One 1/3-cu-ft Gas Sphere	1,500	1,500
		<u>\$15,600</u>
		*Included in Manhour Cost \$3600
		Total Material Cost = \$12,000
<u>No. 1 -- One Missile</u>		
Total Manhours = 2800 at \$10/Manhour		
Manpower Cost	= \$ 28,000	
Material Cost	= 12,000	
		<u>Total \$ 40,000</u>
<u>No. 2 -- Five Missiles</u>		
Manpower Cost	= \$ 5,400	
Material Cost	= 12,000	
		<u>Total \$ 17,400 Each</u>

VI. CONCLUSIONS AND RECOMMENDATIONS

As a result of the Phase III test program, the feasibility and reliability of the main tank injection gas generation process for missile propellant tank pressurization has been established. However, additional test effort is recommended to establish process influence parameters before a flight demonstration can be attempted. The efficiency of the pressurization process has established a definite weight advantage over the unheated stored gas system in high-pressure systems with only a slight advantage when compared to present autogenous or stored gas pressurization systems of low-pressure booster stages. Based on current pressurization system usage, the common ullage pressurization of the oxidizer tank is not recommended (though successfully demonstrated during the small-scale experimental program) because of the presence of a hydrogen atmosphere in the oxidizer tank. Consequently, the pulse mode, solid stream surface, dual reagent, injection process demonstrated on the flight-weight tanks is advocated for future applications. For missions involving a zero-gravity coast period, present pressurization techniques will require propellant orientation before repressurization at this time.

During the course of the program, it became evident that variations in process reaction mixture ratio particularly in the fuel tank caused a variation in gas molecular weight and in the amount of condensibles formed although pressure control within ± 0.5 psi was obtained. The extent of propellant degradation resulting from the quantity of condensibles formed was found to be relatively low with a negligible effect on theoretical rocket engine specific impulse for 2- to 3-min propellant expulsions. Consistency of the reaction mixture ratio is an area for future study; however, good repeatability was obtained with the Phase III injection system.

1. Detailed Conclusions

The following study conclusions are offered.

- 1) Precise pressure control can be accomplished by the pulse-mode, direct-injection method in a full-scale propellant system;
- 2) Moderate temperatures can be achieved by adequate propellant penetration with the solid-stream surface, reagent-injection process to permit the use of thin-wall aluminum tankage in a low-pressure, flight-type system;

- 3) Propellant degradation resulting from the reaction process is not an important consideration since the amount of contamination encountered in a nominal 3-min mission would be less than 0.5%;
- 4) Theoretical performance predictions computed with the IBM 7094 MTI Mathematical Model show good correlation with actual Phase III test results;
- 5) A significant weight saving with a high degree of reliability can be realized by employing an MTI propellant tank pressurization system in current booster, and space vehicles.

2. Specific Recommendations

Martin makes the following specific recommendations.

- 1) Allow further investigation of reaction-influence parameters concerning reaction mixture ratio, combustion zone, injector design, and quantity of condensed products of reaction;
- 2) Develop a multipurpose, flight weight, modular pulse mode, solid stream surface, reagent injection system;
- 3) Initiate a flight demonstration program employing remaining Titan II R&D missiles;
- 4) Study adaption of an MTI pressurization system to the Titan III transtage;
- 5) Study adaption of an MTI pressurization system to the Titan III solid rocket motor, fluid injection, thrust vector control system.

VII. FUTURE STUDIES

The successful application of a chemical pressurization system to a flight-weight, full-scale system has established the feasibility of the MTI pressurization technique for the nitrogen tetroxide and 50/50 fuel blend of hydrazine and unsymmetrical dimethylhydrazine storable liquid propellants. Although some additional knowledge concerning the nature of the combustion process and influence parameters is still needed, this technique shows considerable promise for propellant tank pressurization of both booster and space vehicles. The availability of energy sources such as turbopumps, gas generators, radiant engine heat, etc will obviously influence the selection of a pressurization system for a particular application. However, the inherent high-density, low-pressure storage of the pressurant and relatively low molecular weight of the gaseous combustion product produced allows the design of a highly efficient modular-type unit that can be adapted to a variety of configurations. Based on the extent of investigation completed, several areas of additional study appear warranted.

A. HYDROGEN PRESSURIZATION OF AN OXIDIZER TANK

Before complete development of a common-ullage MTI pressurization system can be attempted, a detailed examination of the feasibility of hydrogen pressurization of an oxidizer tank is required. The use of hydrogen as a pressurant in the presence of an oxygen atmosphere is particularly important in cryogenic or MTI systems due to the capability for high-density storage. Since this is the lightest gas available, the extent of weight reduction may be desirable if methods of eliminating the potential hazard can be identified. On completion of this feasibility-type study, an extensive investigation of techniques to eliminate a flammable reaction inside the oxidizer tank with the common-ullage configuration would be required. In addition to the present method developed of subsurface cross-flow gas impingement with storable propellants, further study of ways to eliminate the hypergolic reactants by suitable gas conditioning methods should be considered. The feasibility of common ullage or hydrogen pressurization of cryogenic systems should be determined in view of currently planned propulsion systems. Final verification of systems developed would then be subjected to a full-scale, battleship-tank test program in an isolated area.

B. INVESTIGATION OF OTHER REAGENTS

If generation of a noncombustible gas or elimination of hazardous reactive constituents is desired in a flammable pressurant, a variety of different gaseous byproducts can be achieved by using reactants other than the main hypergolic propellants. Several possible reactants for the storable propellants investigated are presented in Table II-4. In general, heavier gases would be evolved by reactants other than the storable propellants; however, eliminating undesirable byproducts may offset this disadvantage, particularly in a common-ullage system. System thermodynamics and propellant contamination would be analyzed in addition to gas composition, preferably on a small-scale.

C. MTI WITH OTHER PROPELLANT COMBINATIONS

The continual search for high-energy, high-density liquid propellants necessitates advancing pressurization system technology. Unique problems associated with the MTI process concerning reaction mixture ratios, process gas composition, and condensed products of reaction require initiation of a research program when promising propellant combinations are identified. Since the MTI pressurization process is applicable to both ambient-stored and cryogenic propellants, studies should be extended beyond the effort completed under AF04(611)-6087. Besides the small-scale primary research contemplated, effort would be expended on a performance demonstration with hydrogen peroxide, chlorine trifluoride, hybaline, and cryogenic propellants with a simulated full-scale test article.

D. MTI THERMAL GRADIENT STUDY

Successful development of an MTI pressurization system requires a thorough knowledge of gas, liquid, and wall temperature profiles. The anticipated thermal gradient study would be essentially a follow-on to a test program similar to that conducted under AF04(611)-8198 Phase III. Particular emphasis would be placed on obtaining oxidizer tank combustion temperatures and liquid temperature stratification by infrared photography techniques to supplement ullage temperature data previously accumulated. Wall heat distribution data would be obtained during the full-scale system test by temperature indication from heat-sensitive paint and color photography. Information acquired would be used to establish precise internal heat transfer film coefficients to aid in thermodynamic analysis of space vehicle applications.

E. MTI WITH THIXOTROPIC PROPELLANTS

In addition to the new high-energy liquid propellants proposed for MTI pressurization investigation, the semiliquid gelled propellants under present development should be examined for possible application of an MTI pressurization system. Since many of the high-energy thixotropes employ either powdered beryllium or aluminum as a thickening agent, the possibility of coring or developing large sintered particles must be determined. The anticipated high reaction temperatures associated with the type of propellant and reduced natural convective cooling inherent in the high viscosity fluid will require considerable study to assure elimination of fuel autoignition. The development of an MTI pressurization system for gelled propellants would be particularly advantageous for long-term, zero-gravity space vehicle applications. Initial experimental work would require considerable small-scale system testing to establish the process feasibility and the desirable techniques followed by a full-scale system development program based on probable future applications.

F. MTI ZERO GRAVITY PRESSURIZATION ANALYSIS

Before an MTI pressurization system can be successfully applied to a space vehicle, a detailed investigation of pressurization system requirements must be completed including analytical studies with a relatively short full-scale ground test program. The analytical work would concentrate on heat transfer encountered in space with the resultant pressurant demand. If continuous pressurization is required during a zero-gravity coast period, considerable analysis of propellant orientation and reaction characteristics would be required to study the feasibility of precise pressure control. Studies would also be made concerning response characteristics of a system, initiating repressurization just before engine ignition using a propellant orientation device. Included in this program, logically, would be an investigation of possible unique configurations to eliminate associated zero-gravity and space environment cooling problems.

VIII. BIBLIOGRAPHY

- Adams, G. K. and Stock, G. W.: "Development of Reaction Velocity Constants and Some Insight Into Mechanisms Occuring for Hydrazine Combustion." The Combustion of Hydrazine. 4th Symposium on Combustion, Cambridge, Massachusetts 1952 239-248 (Pub. 1953).
- Agnew, J. T.: "Combustion Studies Using the Goly Photothermal Detection With an Infrared Monochromator." Trans. A.S.M.E., 1949.
- Altman, David and Thomas, Delbert D.: "Evaluation of Hydrazine as a Monopropellant and a Gas Generant." Jet Propulsion Laboratories, April 1949.
- "A Technique for the Computer Solution of Complex Equilibrium Problems." A.I.Ch.E (Abstract 64) Denver Meeting, August 1962.
- Audrieth, L. F.: "New Development In the Field of Hydrazine Chemistry." Österr Chemiker Ztg 58, 2-8 (1957).
- Autogenous Pressurization System Expulsion Testing. LRP 240. Aerojet-General Corp., October 1961.
- Bailey, N. P.: "Abrupt Energy Transformation in Flowing Gases." Trans. A.S.M.E., 1947.
- Beardsley, E. G.: "Study of Oil Sprays for Fuel Injection Engines by Means of High Speed Motion Pictures." Trans. A.S.M.E., 1927-1928, O.G.P. 50-3.
- Binkhoff, G. and Zarentovelle, E.: Jets, Wakes and Cavities. Academic Press, New York, N.Y. 1957.
- Davis, C. W., et al.: "Fuel Injection and Positive Ignition-Basis for Improved Efficiency and Economy." S.A.E. Trans. (Paper 190A) June 5-10, 1960.
- De Corse, S. M.: "Effect of Ambient and Fuel Pressure on Spray Drop Size." Engineering for Power, January 1960.
- Development of Inert Gas Pressurization System. 8160-01Q-6F Aerojet-General Corp. (Confidential).
- Development of Self Generating Propellant Pressurization System. AFFTC TR6-68, Parts I and II, Aerojet-General Corp. (Confidential).

Donovan, T. M., et al.: "The Heat of Combustion of Tetramethylhydrazine and 1, 1-dimethylhydrazine." J. Phys. Chem. 64 281 (1960).

Edelman, G. M. and Shapiro, Ascher H.: "Tables for Numerical Solution of Problems in the Mechanics and Thermodynamics of Steady One-Dimensional Gas Flow Without Discontinuity." Trans. A.S.M.E. 1947.

Edmister, W. C. and Yarborough, Lyman: "Enthalpies of Vapor Phase Mixture." A.I.Ch.E. (Abstract 87) Denver Meeting, August 1962.

Errede, L.A.: "Simple Equations for Calculating Bond Dissociation Energies." J. Phys. Chem. 64 1031-4 (1960).

F-1 Pressurization System Analysis: ASTIA AD 320212, Rocketdyne Confidential).

Fenn, John B. and Calcote, H. W.: "Activation Energies in High Temperature Combustion." 4th Symposium on Combustion, Cambridge, Massachusetts (1952) 231-9 (Pub. 1953).

Fergenbutz, L. V., et al.: "Combustion Charts for High Energy Fuels." (Pt I, Thermodynamics Properties of Combustion Products) Convair, General Dynamics.

Flocke, E. F., et al.: "Definitions of Heats of Combustion of a Fuel and Current Methods for Their Determination." Trans. A.S.M.E., 1948.

"Fuel Injector Comparator." : Diesel Progress, January 1959.

Giesbrecht, Ernesto: "The Chemistry of Hydrazine and Its Practical Importance." "Selecta Chim" No. 14, 89-114 (1955).

Gigurre, Paul A. and Liu, I. D.: "The Infra-Red Spectrum of N_2H_4 ." J. chim phys. 20 136-40 (1952).

Glendenning, E. B. and Black, A. R., et al.: "Atomization of Oil By Small Pressure-Atomizing Nozzles." Trans. A.S.M.E., 1939.

Goldthwaite, J. L.: "High Speed Oil Engine Pumps and Injection Valves." Trans. A.S.M.E., 1929.

Goodger, E. M.: "Manifold Tuning." Automotive Engineer, December 1958.

- Grant, Arthur F.: "Development of Hydrazine as a Monopropellant and Gas Generant." Jet Propulsion Laboratories, March 1, 1950.
- Gray, P. and Lee, J. C.: "Total Pressures Required for Explosion of Mixtures of N_2H_4 and O_2 Were Determined from 370 to 540°C." Trans. Faraday Soc. 50, 719-28 (1954).
- Green, W. A. and G. R.: "Notes on Jerk Systems of Fuel Injection." Diesel Engineers and Users Association, March 1959.
- Gregory, C. A., Jr. and Calcote, H. F.: "Combustion Studies of Droplet-Vapor Systems." 4th Symposium on Combustion. Cambridge, Mass. 1952 830-7 (Pub. 1953).
- Kobe, K. A. and Harrison, R. H.: "Heat Capacities, Free Energies of Formation, Heats of Formation and Comb., Enthalpies, and Entropies of NH_3 , N_2H_4 , $MeNH_2$, Me_2NH and Me_3N are given." (Univ. of Texas) Pat. Ref 33, No. 11 161-4 (1954).
- Hogeman, H.: "Fuel Injection Equipment for Multi-Fuel Engines." S.A.E. Trans. (Paper S221), November 12, 1959.
- Holtz, John C. and Elliot, M. A.: "The Significance of Diesel-Exhaust-Gas Analysis." Trans. A.S.M.E., 1941.
- Hornetz, D., et al.: Hydrazine Derivatives. Metaelectro Corp., March 1956 (Confidential)
- Joachim, W. F.: "Oil Spray Investigations of N.A.C.A." Trans. A.S.M.E., 1927-1928.
- Johnson, Donald F.: Literature Survey on the Use of Hydrazine as a Rocket Fuel. Aerojet-General Corp., Azusa, California, April 1950 (Confidential).
- Lee, D. W.: The Effect of Nozzle Design and Operating Conditions on the Atomization and Distribution of Fuel Sprays. NACA Report 425g, 1952.
- Liberto, Ralph R.: Research and Development on the Basic Design of Storeable High-Energy Propellant Systems and Components. Bell Aircraft, Buffalo, New York, January 1960 (Confidential).

- Livingston, S.: Determination of the Characteristics of Liquid Propellants. Picatinning Arsenal, May 1946 (Confidential).
- Lloyd, Peter: "Determination of Gas Turbine Combustion-Chamber Efficiency By Chemical Means." Trans. A.S.M.E., 1948.
- Lorell, Jack and Wise, Henry: "The Flame Equation Corresponding to the Steady State Combustion of a Liquid Droplet as Adapted to a Monopropellant with Chemical Reaction Diffused through the Gas Phase." J. Phys. Chem. 23, 1928-32 (1955).
- Lutz, O., et al.: "Reaction Enthalpy-Entropy Table for a Stoichiometric Mixture of Hydrazine-Nitric Acid." Deut. Forschungsanstalt Luftfahrt e. V., Forschber FBS 10/54 (1954).
- Main Propellant Tank Pressurization System Study and Test Program. SSD-TR-61-21 (Vol III) Design Handbook, Lockheed Aircraft Corp. Marietta, Georgia, December 1961.
- Meckle, Olson, and Quillian: "An Apparatus for Determining Fuel Spray Characteristics." S.A.E. Trans. Paper 436-A, November 1961.
- Morey, T. F.: N₂O₄ Thermodynamic Properties. TM 0431-302, The Martin Company, October 1960.
- Morino, Yonezo, et al.: "An Electron Diffraction Investigation of the Molecular Structure of Hydrazine," Bull. Chem. Soc., Japan, 33 46-8 (1960).
- Obert, Edward F: Internal Combustion Engine Analysis and Practice. (2nd Edition), International Textbook Company, Scranton, Pennsylvania, 1952.
- Perlee, Henry E.: "Flammability Characteristics of Hydrazine Fuels in Nitrogen Tetroxide Atmospheres." J. Chemical and Engineering Data, July 1962.
- Preliminary Analysis of Gas Generator Combustion Products from A-50 and N₂O₄. TM 0431-334, The Martin Company, November 30, 1961.
- "Research on the Fire and Explosive Hazards Associated with New Liquid Propellants." NAonr 11-60, Bureau of Mines, Pittsburgh, Pennsylvania.
- Revers, N. M., Schmidt, R. C., and Perr, J. P.: "Cummins Next PT Fuel Pump." S.A.E. Trans. (Paper 258B) October 31 - November 2, 1960.

- Rieke, K. L.: "Temperature and Gas Analysis Surveys in the Combustion Zone of a Gas-Fired Turbine Combuster." Trans. A.S.M.E., 1953.
- Scott, D. W.: "Heat Capacity, Heats of Fusion and Vaporization, Vapor Pressure, Entropy and Thermodynamic Functions." J. Am. Chem. Soc. 71 2293-7 (1949).
- Scott, F. E., et al.: Explosive Properties of Hydrazine. Bureau of Mines Report R.I. 4460, Pittsburgh, Pennsylvania, 1949.
- Shapiro, Ascher H. and Hawthorne, W. R.: "The Mechanics and Thermodynamics of Steady One-Dimensional Gas Flow." Trans. A.S.M.E., 1947, 1948.
- Somogyi, Dezso and Feiler, C. E.: "Liquid Phase Heat Release Rates of the Systems Hydrazine Nitric Acid and 1, 1 Dimethylhydrazine-Nitric Acid." NACA Tech Note D469 (1960).
- Sutton, J. F., et al.: Main Propellant Tank Pressurization System Study and Test Program. FTRL-TOR-61-22, February, 1961 Lockheed Aircraft Corp., Marietta, Georgia.
- Taylor, G. F. and E. S.: The Internal Combustion Engine. (2nd Edition) International Textbook Company, Scranton, Pennsylvania, 1961.
- Thisza, Laszlo: "The Thermodynamics of Phase Equilibrium." Ann. phys. 13, 1, 1-92 (1961).
- Titan II Storeable Propellant Handbook. AFBSD-TR-62-2, Bell Aerodynamics, March 1962.
- Wakuri, Y. et al.: "Studies on Penetration of Fuel Spray on Diesel Engines." Soc. Mech. Eng., February 1960.
- Walther, Kleinpaul: "Calculation of Activation Energies" (I Introduction). Z. physik, Chem. (Frankfurt) 26 313-24 (1960).
- Walther, Kleinpaul: "Calculation of Activation Energies" (II Present Results. Z. physik, Chem. (Frankfurt) 27 343-56 (1961).
- Weissberger, A.: Investigation of Ratio and Mechanisms of Reactors (Vol VIII, Pt I), Interscience Publishers, Inc., New York, 1961.
- Weitzsch, Fritz: "A New Approach for Treating Gas-Dynamic Problems at Large Deviations From Thermodynamic Equilibrium." Ann. Physik, 7 403-17 (1961).

RTD-TDR-63-1123

Yamaguchi, Akiko: "Normal Vibrations of Hydrazine." Nippon Kagaku Zasshi 80 1109-12 (1959).

Zimmer, Hans: "New Developments in the Field of Hydrazine Chemistry." Chemiker Ztg. 79 599-605 (1955).

APPENDIX A

PROPULSION SYSTEM OPTIMIZATION PROGRAM

The Propulsion System Optimization Program is an analytical technique for determining propulsion system weight with the IBM 1620 digital computer. The program computes the size and weight of the pressurization system, propellant system, and engine system for a storable bipropellant configuration. Propulsion system mass fraction, impulse, density, and ideal velocity increment are also computed. Capability is provided for variation in thrust, total impulse, and engine design. Since spherical propellant tanks are assumed, the total impulse is limited to 1×10^7 lb-sec. Ambient stored gas pressurization is used with single-stage regulation.

1. Engine System

The engine system computations are performed in two separate areas. The first area involves the calculation of the engine size from both theoretical and empirical formulas. In the second area engine system weight is determined based on empirical data and equations derived from weight data on existing systems and influence parameters. These relationships establish the total engine system weight for a regeneratively cooled engine with either gimballed or fixed vector control. Capability is also provided for selecting a gas- or pump-pressurized propellant feed system.

The assumptions used for engine system computations are:

- 1) One regeneratively cooled engine;
- 2) Combustion chamber efficiency, $\eta_c = 0.96$;
- 3) Chamber convergence angle = 30 deg;
- 4) Chamber area = five times the throat area;
- 5) Injection pressure drop = $0.2 P_c + 15$.

2. Propellant System

The propellant system includes the propellant, tankage, and storage valves required for a liquid bipropellant system. Storage valve size, propellant quantity, and tank volume, are theoretical. Valve weights are empirical and a function of size. Tank thickness is based on allowable hemispherical stress with a minimum thickness established by manufacturing limitations.

The assumptions concerning the propellant system are:

- 1) Two spherical tanks;
- 2) 5% ullage volume;
- 3) Overall stress factor = 1.65;
- 4) Two storage valves ($\Delta P = 0.1$ psi).

3. Pressurization System

Calculation of storage container, regulator, and vent valve size is theoretical; valve weights are empirically determined from size. Pressurizing gas requirements are determined by an adiabatic energy balance with provision for simulated heat transfer. A 5% margin is allowed for residual unusable pressurizing gas. Mass transfer at the gas-liquid interface is neglected. Tank pressures are a function of engine chamber pressure for a gas-pressurized propellant feed system, or NPSH of a turbopump system.

The assumptions with respect to the pressurization system are:

- 1) Residual gas is based on a final storage container pressure 100 psi above regulated pressure;
- 2) One spherical storage container;
- 3) Overall safety factor = 1.5;
- 4) Gas required includes 5% margin;
- 5) Equal propellant tank pressures;
- 6) Propellant vapor pressure = 0.

APPENDIX B

COMPUTER PROGRAM DESCRIPTION FOR MTI APPLICATION STUDY

1. Heated and Unheated Stored Gas Systems

The general energy equation is applied to the heated and unheated systems, with internal tank heat transfer and Joule-Thompson effects neglected. These assumptions are generally conservative, since heat absorption by the ullage gas occurs and thus reduces pressurizing gas requirements.

The heated stored gas system differs in that auxiliary heating (engine-originated) of the pressurant gas is applied before propellant tank inflow. Conservatively, the amount of heating is assumed sufficient only to maintain the ullage gas temperature at bulk propellant conditions. The effect of extended space storage time on both types of stored gas systems is considered by accounting for gas leakage from the high-pressure gas valves. A leaktight system is assumed except for the high-pressure valves (four per system), with leakage parameters comparable to those experienced by superior valve designs. Average storage pressures (measured from initial to final) are used in the leakage computations over the total space storage life. Vaporized propellant (N_2O_4) is determined in a similar manner to the MTI system.

The weights of valves, accessories, hardware, and related fittings are obtained by empirical factors, and are proportional to the storage container size with a prescribed minimum value. Storage container weights are computed directly using a high-strength titanium alloy Ti-13CR-11V-3al.

a. Unheated Stored Gas System

The total system weight penalty consists of the following:

- 1) Stored inert pressurant;
- 2) Stored inert gas to cover leakage;
- 3) Vaporized oxidizer;
- 4) Storage container;
- 5) Hardware, valves, etc.

Neglecting heat transfer and the Joule-Thompson effect, the weight of initially stored inert pressurant is expressed by the following equation:

$$W_{sci} = \frac{P_T V_T \gamma}{R T_{sci}} \left(1 - \frac{P_{scf} Z_{sci}}{P_{sci} A_{scf}} \right). \quad [B-1]$$

Initial storage pressure of 3000 psia and a final storage pressure of 200 psia or two times the tank pressure (whichever is larger) is assumed.

The amount of vaporized oxidizer (N_2O_4) is computed from empirical equations of the following form:

$$\frac{\partial P_v}{P_T} = C_1 \left(P_T \right)^{-C_2}. \quad [B-2]$$

Values for C_1 and C_2 were determined empirically from analytical programs considering identical mass transfer processes. These were found to vary, principally as a function of burning time, and to a lesser extent, as a function of type of inert gas and gas temperature. Exceptions were allowed to account for special conditions. Namely, the amount of vapor must always be equal to or greater than the amount required to saturate the initial ullage. Furthermore, for extended space storage times, the vapor is determined directly from a saturated total oxidizer propellant tank.

Dalton's Law is used to relate the partial pressures thus determined for a gas or propellant vapor weight penalty. Gas leakage across the four high-pressure valves is determined from basic leakage parameters:

- 1) $\frac{1}{4}$ -in. valve, 10 cc/hr - helium gas @ 3000 psi, related to 14.7 psia and 60°F;
- 2) $\frac{1}{2}$ -in. valve, 80 cc/hr - helium gas @ 3000 psi, related to 14.7 psia and 60°F.

The size of the valve is a function of the thrust rating; however, since leakage considerations concerned space vehicles and the lower thrust levels, the $\frac{1}{4}$ -in. valve size leakage was used.

$$C_t = 0.011 \text{ lb}_m/\text{mo for helium}$$

$$C_t = 0.0275 \text{ lb}_m/\text{mo for nitrogen}$$

$$\text{Total Leakage} = \frac{C_t \times \text{Storage Time}}{3000} \times \left(\frac{P_{\text{initial}} + P_{\text{final}}}{2} \right) \quad [\text{B-3}]$$

Leakage computed from Eq [B-3] is related to a stored weight penalty by the product factor $\left(\frac{1}{1 - \frac{P_{\text{scf}} Z_{\text{sci}}}{P_{\text{sci}} Z_{\text{scf}}}} \right)$.

Storage container weight is calculated from thin-wall hoop stress formulas for internally pressurized spheres.

$$V_{\text{sc}} = \frac{\text{Total Mass Inert Gas}}{\text{Initial Gas Density}} \quad [\text{B-4}]$$

$$W_{\text{sc}} = \frac{(1728) (1.5) P_{\text{initial}} \times V_{\text{sc}} \times \text{Safety Factor}}{(\text{Stress/Density Ratio})} \quad [\text{B-5}]$$

The program has provisions for a minimum wall thickness; therefore, the wall thickness dictated by stress considerations is initially computed, and the container weight increased accordingly if the resultant thickness is below the minimum value established, which for this application is 0.02 in.

The weight of hardware, valves, lines, and accessories is computed as 20% of the storage container weight, with a minimum value of 12 lb. The size of propellant tanks is based on a mixture ratio, engine expansion ratio, and combustion pressure consistent with the vehicle mission-trajectory and feed system, as indicated in Table B-1.

Table B-1 Propellant Tank Sizing Factors

Case	Feed System	Engine Mixture Ratio	Engine Expansion Ratio	Combustion Pressure (psia)	Specific Impulse $\left(\frac{\text{lb}_f}{\text{lb}_m \text{ sec}}\right)$
I	Pump	1.9	8	750	277
II	Pump	2.0	12	750	277 to 288.8
III	Pressure	2.0	12	$P_T - 50$	253 to 282
IV	Pump	2.0	12	750	277 to 288.8
V	Pressure	2.0	12	$P_T - 50$	253 to 282
VI	Pressure	2.0	40	$P_T - 50$	309 to 312.5
VII	Pressure	2.0	40	$P_T - 50$	309 to 312.5

The size of the propellant tanks is computed by:

$$v_{to} = \left(\frac{\lambda}{1 + \lambda}\right) \frac{I_t}{I_s} \frac{(1 + K_u)}{\rho_o} \quad [\text{B-6}]$$

$$v_{tf} = \left(\frac{1}{1 + \lambda}\right) \frac{I_t}{I_s} \frac{(1 + K_u)}{\rho_f} \quad [\text{B-7}]$$

b. Heated Stored Gas System

The heated stored gas system program is essentially the same as the unheated system except the assumption is made that the heat added is sufficient to remove the expansion and work cooling effects in the propellant tank. This is the same as if Eq [B-1] were multiplied by $\left(\frac{1}{\gamma}\right)$. A nominal amount is added to the accessories to account for the heat exchanger weight. No penalty is introduced for bleeding heat from the rocket engine.

2. MTI Pressurization System

The general energy equation is applied with heat transfer to lines and walls. A combustion mixture ratio, and thus gas product molecular weight, is estimated for both pressurizing methods. Experience gained from test data from concurrent pressurization programs forms the basis of those estimations. Molecular weight and gas temperature variations between propellant tanks are used to account for line heat transfer and secondary chemical reactions occurring in the nitrogen tetroxide propellant tank. The effects of extended space storage time on system performance are accountable by assuming gas temperatures cool to bulk liquid temperatures coincident with a net increase in molecular weight.

The total system weight penalty consists of the following, where applicable:

- 1) Pressurant gas reaction products;
- 2) Vaporized oxidizer;
- 3) Additional main propellant tankage to store pressurant reactants;
- 4) Hardware, lines, control valves, etc;
- 5) Injection system.

The weight of the pressurant gas reaction products in either propellant tank is computed by the equation of state:

$$W_g = \frac{T_t}{P_t} \frac{1545}{V_t \text{ MW}} \quad [B-8]$$

Ullage gas temperature and molecular weight of gas products are fixed inputs for this program. At the present time, these are considered to be a function of reaction mixture ratio (λR), secondary reactions with N_2O_4 vapor, and tank-top temperature. The respective values for this program are tabulated in Table B-2. It is recognized that adjustment may be warranted as additional test data become available.

Table B-2 Inputs for MTI Pressurization

Case	Tank Pressure (psia)	λR	Fuel		Oxidizer		Remarks
			MW	T_t ($^{\circ}R$)	MW	T_t ($^{\circ}R$)	
I	20 to 50	0.4	15	850	24	760	} Space Storage
II	20 to 50	0.4	15	850	24	760	
III	100	0.4	15	900	24	800	
	200	0.4	15	950	24	850	
	300	0.4	15	1000	24	900	
IV	20 to 50	0.4	20	530	24	530	
V	100 to 300	0.4	20	530	24	530	
VI	100 to 300	0.4	20	530	24	530	
VII	100 to 300	0.4	20	530	24	530	

The amount of vaporized oxidizer is computed in a similar manner to the stored gas system. Constants in Eq [B-2] vary from the stored gas values to account for minor differences in mass transfer rates. The resultant partial pressure of the reaction products in the oxidizer tank is used in Eq [B-8] to determine the respective weight penalty.

The rocket engine data used to size the propellant tanks are identical to the data used for stored gas pressurization, Table B-3. However, since pressurant propellant storage in the main propellant tanks is assumed, the capacity of the main propellant tanks must be enlarged. This in turn increases the amount of reaction products required, as well as the vaporized propellant penalty. The tank weight penalty is obtained by assuming spherical storage of the total propellants (both engine and pressurant) when ID < 120 in. For larger tank volumes, cylindrical storage with hemispherical ends is assumed with the ID = 120 in. minimum and an L/D = 2.5.

$$\text{Volume of metal, } V_m = \pi D^2 (t) \quad (\text{sphere})$$

$$V_m = \pi D^2 (1 + L/D) (t) \quad (\text{cylindrical with hemispherical ends})$$

Wall thickness is determined from hoop stress considerations with a minimum thickness of 0.05 in. assumed for the high-strength aluminum alloy used (maximum stress = 25,000 psi). The actual weight penalty then becomes:

$$\text{Tank Weight Penalty} = \left[\frac{\text{Incremental Volume}}{V_t \text{ ideal} + \text{Incremental Volume}} \right] V_m \times \rho_m$$

computed individually for each propellant tank.

Associated hardware, lines, and control valves, such as orifices, are estimated at 10% of the total reaction gas products with a minimum value of 12 lb.

The weight of the injection system is assumed negligible for pump-feed systems, and 2% of the total reaction gas products for pressure-feed systems.

3. Gas Generator Pressurization Systems

The program for the gas generator system is virtually the same as the MTI program except that gas products are precooled to 760°F by an auxiliary heat exchanger before they enter the propellant tank inlet. No penalty is introduced for cooling the pressurant except that the accessory weight is adjusted to account for the heat exchanger. Table B-3 lists the respective input values for this program.

Table B-3 Inputs for Gas Generator Pressurization

Case	Tank Pressure (psia)	R	Fuel		Oxidizer		Remarks
			MW	T _t (°R)	MW	T _t (°R)	
I	20 to 50	0.09	16	760	28	760	Space Storage
II	20 to 50	0.09	16	760	28	760	
III	100	0.09	16	760	28	760	
	200	0.09	16	760	28	760	
	300	0.09	16	760	28	760	
IV	20 to 50	0.09	20	530	28	530	
V	100 to 300	0.09	20	530	28	530	
VI	100 to 300	0.09	20	530	28	530	
VII	100 to 300	0.09	20	530	28	530	

RTD-TDR-63-1123

Associated hardware, lines, gas generator, and heat exchanger are estimated at 15% of the total reaction gas products with a minimum value of 12 lb. The weight of the feed system for the gas generator is assumed negligible for pump-feed engines and 2% of the total reaction gas products for pressure-feed engines.

APPENDIX C

MTI PRESSURIZATION SYSTEM PROGRAM

A schematic of the MTI pressurization system as considered by this analytical model is given in Fig. III-9. The system consists of a single propellant tank pressurized with combustion gases generated by the injection of a hypergolic reactant during propellant outflow. The flow of reactant is controlled by an orifice, an on-off valve, and a supply pressure. The tank gas is a mixture of three components, inert gas used for prepressurization, propellant vapors that may be dissociating, and combustion gas produced by the reaction. This mixed gas may be allowed to overflow into a secondary tank at a rate proportional to the combustion gas production.

A pressure switch in the propellant tank controls the on-off solenoid valve to maintain the tank pressure between the set limits. Computations are made over small time increments that start and end at times of valve actuation, as well as at specified intervals. Valve actuation times occur at a specified interval after the tank pressure reaches the high or low switch setting. The reactant flow may also be terminated at any specific time and the tank pressure allowed to decay.

The combustion gas is produced and propellant is consumed in proportion to the reactant flow rate. The proportions depend on the assumed effective burned mixture ratio based on test data. The combustion temperature, the molecular weight, and specific heat of the combustion gas also depend on this ratio. The combustion between propellant and injected reactant is assumed to occur primarily in a relatively well-defined zone at the liquid surface. The size of this zone is proportional to the volume of combustion gases produced. Mass transfer from the liquid in the combustion zone is assumed to be just sufficient to furnish propellant for the reaction. Heat transfer from the hot gas to the liquid reduces the combustion gas temperature before it mixes with the bulk gas. This heat transfer is obtained by a simplified forced convection relationship.

Heat transfer occurs between the bulk gas and the adjacent tank wall. Both heat and mass transfer take place between the bulk gas and the liquid at the noncombustion surface. These rates depend on simplified gas phase free convection and diffusion relationships. Liquid side heat transfer is obtained by a heat balance at the surface. External tank wall heat transfer is not considered.

An explanation of the basic equations employed in the mathematical model are contained below.

1. Reagent Consumption and Gas Generation

During the time interval when the propellant tank pressure is less than the input minimum the injector is on and the reagent flow rate is:

$$\dot{W}_R = A_v C_{dv} \left[288 g_c R (P_{RS} - P_{GPT}) \right]^{\frac{1}{2}} \quad [C-1]$$

where

- A_v = injector orifice area (sq ft),
- C_{dv} = discharge coefficient,
- P_{RS} = reagent supply pressure (psia),
- P_{GPT} = propellant tank gas pressure (psia).

The total weight of reagent consumed during the propellant expulsion is:

$$W_T = \sum \dot{W}_R t \quad [C-2]$$

where

t = time that the injector is on (sec).

The amount of propellant used is:

$$\dot{W}_{LR} = \dot{W}_{CR} - \dot{W}_R \text{ or } W_{IRT} = \sum (\dot{W}_{CR} - \dot{W}_R) t \quad [C-3]$$

where

\dot{W}_{CR} = gas generation rate, defined as

$$W_{CR} = W_R (\lambda + 1) / \lambda.$$

The reaction mixture ratio, λ , is the oxidizer-to-fuel ratio of the reaction process. If the fuel is the reagent, the reciprocal of λ must be used: $\lambda = \dot{W}_R / \dot{W}_{LR}$.

2. Gas Properties

The significant gas properties required to compute ullage gas characteristics have been reduced to the following equations:

- 1) Propellant Vapor Pressure

$$P_{VPT} = e^{(C_{PVP1} - C_{PVP2} / T_{LPT})} \quad [C-4]$$

where

$C_{PVP1,2}$ are specific heat constants for the propellant,

and

T_{LPT} is temperature of the liquid ($^{\circ}R$);

- 2) Vapor Dissociation

$$K_{PV} = e^{(C_{KPV1} / T_{GPT} - C_{KPV2})} \quad [C-5]$$

where

$C_{KPV1,2}$ are vapor dissociation constants for the propellant,

and

T_{GPT} is the temperature of the gas ($^{\circ}R$);

- 3) Propellant Vapor, Constant Volume Specific Heat

$$C_{VV} = C_{CPV1} + C_{CPV2} T_{GPT} - (1.987 / M_{VP}) + D_{ADTV} D_{MD} \quad [C-6]$$

where

$$D_{ADTV} = \left(C_{KPV_1} - T_{GPT} \right) \left(A_{VPT} - A_{VPT}^2 \right) / \left(2 - A_{VPT} \right) T_{GPT}^2$$

and

$$A_{VPT} = \left(1 + 4K_{PV} P_{VPT} \right);$$

4) Combustion Products, Specific Heat

$$C_{PC} = C_{CPC_1} + C_{CPC_2} T_{GPT} \quad [C-7]$$

and

$$C_{VC} = C_{PC} - 1.987/MW_{CP}.$$

3. Mass Transfer

The mass transfer at the propellant surface is computed from the simplified relationship:

$$\dot{W}_{VSP} = C_{VSP} (P_{VLP} - P_{VPT}) / (P_{GPT} - P_{VLP}) \left[(T_{GPT} - T_{LPT}) / T_{GPT} \right]^k \quad [C-8]$$

where

C_{VSP} combines the gas diffusivity and other influencing factors.

4. Heat Transfer

Heat transfer characteristics at the tank wall and liquid surface have been reduced to the following relationships:

$$\text{for the tank wall, } \dot{Q}_{PTG} = C_{HW} A_W (T_{PTG} - T_{GPT})^{1.333},$$

$$\text{and for the liquid surface, } \dot{Q}_{PSG} = C_{HL} A_L (T_{LPT} - T_{GPT})^{1.25} \quad [C-9]$$

where the C_H terms combine the free-convection coefficient with the gas properties in the Prandtl, Grashoff, and Nusselt numbers as they occur in the free-convection correlation.

Heat transfer from the combustion zone to the liquid propellant is similarly calculated as follows:

$$\dot{Q}_{RL} = C_{HC} AC (T_C - T_{LPT}) \quad [C-10]$$

where C_{HC} combines the forced-convection coefficient with gas velocity and physical properties. All areas are in sq ft.

5. Heat Balance

Gas temperature change rates are computed from an energy balance on the system which reduces to the following equation:

$$\begin{aligned} \dot{T}_{GPT} = & \left[\dot{Q}_{PTG} + \dot{Q}_{PSG} + R_u T_{GPT} (\dot{W}_{VPT}/MW_{VP} + \dot{W}_{IPT}/MW_I) + \dot{W}_{CR} H_{CR} - \right. \\ & \left. - \dot{W}_{CT} H_{CPT} - \dot{W}_{CPT} (H_{CPT} - R_u T_{GPT}/MW_{CP}) + 144 P_{GPT} \dot{V}_{LPT}/J \right] / \\ & \dot{W}_{GPT} C_{VGPT} \end{aligned} \quad [C-11]$$

6. Gas Molecular Weight

The change in gas molecular weight due to the dilution of the initial pressurizing gas with propellant vapors and combustion products is computed as follows:

$$\begin{aligned} \dot{MW}_{GPT} = & \dot{W}_{GPT} / \sum MW_{GPT} - W_{GPT} (\dot{W}_{CPT}/MW_{CP} + \dot{W}_{VPT}/MW_{VP} + \dot{W}_{PT}/MW_I) / \sum \\ & MW_{GPT}^2 \end{aligned} \quad [C-12]$$

7. Propellant Tank Pressure

The rate of change in gas pressure is:

$$\dot{P}_{GPT} = P_{GPT} (\dot{W}_{GPT}/W_{GPT} + \dot{T}_{GPT}/T_{GPT} + \dot{V}_{LPT}/V_{GPT} - \dot{MW}_{GPT}/MW_{GPT}) \quad [C-13]$$

8. Final Conditions

The final liquid conditions are computed from the following relationships:

$$\left. \begin{aligned} T_{LP} &= (Q_{RL} - Q_{PSG} - W_{VSP} D_{HVP})(W_{LP} C_{PLP}), \\ W_{LP} &= W_{LP} (N - 1) - \dot{W}_{LP} \Delta t, \\ V_{LP} &= W_{LP} / \rho_{LP}. \end{aligned} \right\} \quad [C-14]$$

The final gas conditions are determined as follows:

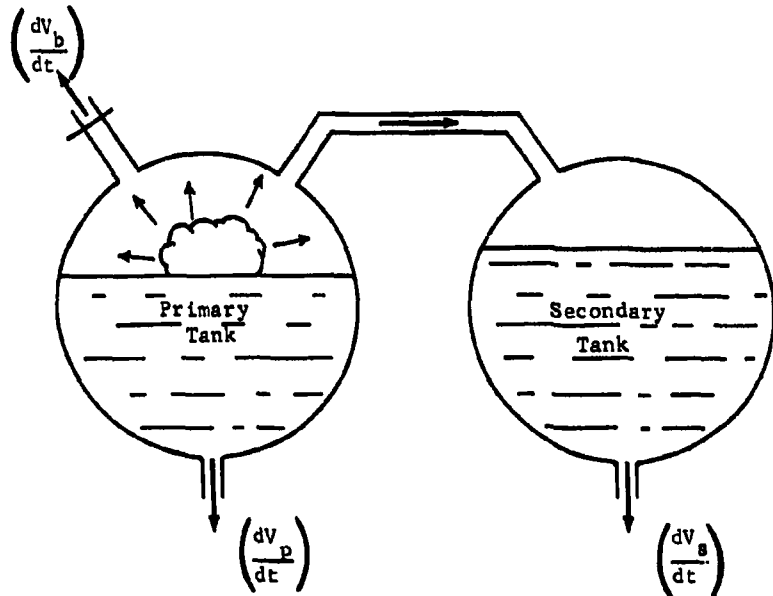
$$\left. \begin{aligned} T_{GPT} &= T_{GPT} (N - 1) - \dot{T}_{GPT} \Delta t \\ W_{GPT} &= W_{VPT} + W_{IPT} + W_{CPT} \\ V_{GPT} &= V_{PT} - V_{LP} \\ MW_{GPT} &= W_{GPT} / (W_{IPT} / MW_I + W_{CPT} / MW_{CP} + W_{VPT} / MW_{VP}) \\ P_{GPT} &= R_u T_{GPT} / 144 MW_{GPT} V_{GPT}. \end{aligned} \right\} \quad [C-15]$$

APPENDIX D

PROPELLANT TANK ULLAGE GAS DILUTION COMPUTER PROGRAM

The computer program described here has been formulated on the IBM 1620 for the interpretation of single or dual propellant tank ullage gas test data for an inert oxidizer and a nonvolatile fuel. Analysis of the properties of the MTI combustion gas and interpretation of test results is complicated by the fact that the ullage gas mixture concentration is time variant. During the Phase I tests, an unusually large amount of prepressurizing inert gas in the fuel tank is prescribed for safety considerations. Consequently the diluting effect of the inert gas is significant and must be considered in all computations. Furthermore, the pressurant gas in the fuel tank is continuously bled for pressurizing the oxidizer tank and for gas sampling, resulting in a continual change in the dilution rate of the inert gas in each tank. Valid test data interpretation demands a precise analytical representation of the gas-mixture concentration history in both tanks and determination of total quantity of combustion gas generated.

The solution of this problem is achieved by performing a mass balance on the MTI common ullage pressurization system to effect a constant pressure process. Computations are made on an incremental time basis to determine the quantity of combustion gas required to maintain the pressure of each tank, considering gas cross flow, with gas sample bleed and propellant outflow.



To complete this solution, certain simplifying assumptions must be made:

- 1) Tank pressures are constant;
- 2) The change in volume due to reaction or condensation is insignificant;
- 3) No propellant vaporization occurs during the run;
- 4) The molecular weight of the added combustion products is constant with time;
- 5) The gas mixture is homogeneous.

Since the ullage gas temperature histories must be known, these are approximated (based on average test results) by a simple function of time:

$$T_p = T_{i,p} + \left(\frac{dT_p}{dt}\right)t \quad [D-1]$$

$$T_s = T_{i,s} + \left(\frac{dT_s}{dt}\right)t \quad [D-2]$$

The total volume change from either tank due to propellant outflow, for this constant engine thrust application, is known and is expressed by:

$$\left(\frac{dV_p}{dt}\right) = \frac{\dot{W}_p}{\rho_p} \quad [D-3]$$

$$\left(\frac{dV_s}{dt}\right) = \frac{\dot{W}_s}{\rho_s} \quad [D-4]$$

For variable thrust applications, $\dot{W} = \theta(t)$ can be substituted.

In addition to propellant outflow, bleed from the fuel tank for gas sampling must be considered. Sampling flow passes through a sharp edge orifice that is expressed by the following equation:

$$\left(\frac{dv_b}{dt}\right) = 1.548 C_d A \sqrt{\frac{T_p}{MW_p}} \phi(\gamma) \quad [D-5]$$

where

$$\phi(\gamma) = \sqrt{\gamma \frac{2}{\gamma+1}}^{\gamma+1/\gamma-1}$$

$$C_d \approx 0.60$$

The function, $\phi(\gamma)$ does not vary significantly for reasonable ranges of (γ) . [From $1.25 \leq \gamma \leq 1.4$, $\phi(\gamma)$ varies less than 5%]. Consequently $\phi(\gamma) = 0.628$ (based on $\gamma = 1.35$) can be used with negligible error. For a throat size of 0.025 inch, the flow equation reduces to:

$$\left(\frac{dv_b}{dt}\right) = 0.000308 \sqrt{\frac{T_p}{MW_{up}}} \quad [D-6]$$

As indicated previously, the calculation will be accomplished on a step-by-step basis beginning at time = 0 to time of shutoff. A time increment of 1 sec is used. Gas conditions of the preceding time interval become the initial conditions for the next increment under evaluation. At a given time (n) the computation procedure is as follows:

1. Secondary Tank

The net volume cross-flow to the secondary tank is:

$$Q_{s,n} = V_{i,s} + n \frac{dv_s}{dt} - \left(\frac{T_{s,n}}{T_{s,n-1}}\right) \left(V_{i,s} + (n-1) \frac{dv_s}{dt}\right) \quad [D-7]$$

where $T_{s,n}$ and $T_{s,n-1}$ are computed from Eq [D-2].

The corrected total volume of the initial pressurizing gas in the secondary tank becomes:

$$V_{pg,s,n} = V_{pg,s,n-1} \frac{T_{s,n}}{T_{s,n-1}} + Q_{s,n} MF_{pg,p,n-1} \quad [D-8]$$

The mole fraction of the initial pressurizing gas in the secondary tank can now be determined.

$$MF_{pg,p,n} = \frac{V_{pg,s,n}}{V_{i,s} + n \frac{dV_s}{dt}} \quad [D-9]$$

The molecular weight of the ullage gas mixture in the secondary tank is expressed:

$$MW_u = MF_{pg,s,n} MW_{pg} + (1 - MF_{pg,s,n}) MW_{cp} \quad [D-10]$$

2. Primary Tank

The net gas flow volume leaving the primary tank is the sum of the sampling gas bleed volume and the secondary tank cross-flow volume corrected to the conditions in the primary tank.

Equation [D-1] expresses the gas temperature $T_{p,n}$

$$T_{p,n} = T_{i,p} + \left(\frac{dT_p}{dt} \right) t$$

Equation [D-6] gives the bleed flow, $Q_{b,p}$ for a time increment of 1 sec:

$$Q_{b,p} = \left(\frac{dV_p}{dt} \right) (\Delta t) = 0.000308 \sqrt{\frac{T_p}{MW_{up}}}$$

The net volume outflow (to the secondary tank) corrected to primary tank conditions is,

$$Q_{s,p,n} = Q_{s,n} \left(\frac{P_{c,s} T_{p,n}}{P_{c,p} T_{s,n}} \right)$$

The total net volume outflow from the primary tank is,

$$Q_{t,p,n} = Q_{b,p,n} + Q_{s,p,n}$$

The new volume of pressurizing gas in the primary tank is,

$$V_{pg,p,n} = \frac{T_{p,n}}{T_{p,n-1}} \left(V_{pg,p,n-1} - MF_{pg,p,n-1} Q_{t,p,n} \right)$$

The mole fraction of the pressurizing gas in the primary tank at time increment (n) becomes:

$$MF_{pg,n} = \frac{V_{pg,p,n}}{V_{i,p} + n \left(\frac{dV_p}{dt} \right)}$$

The instantaneous molecular weight of the ullage gas mixture in the primary tank can now be found by substituting appropriate tank values into Eq [D-10].

$$MW_{up} = MF_{pg,p,n} MW_{pg} + (1 - MF_{pg,p,n}) MW_{cp}$$

The total weight of combustion products in the summation of the weight of combustion products to time (n-1), and the additional weight of combustion products required to balance the net volume change in the primary tank.

$$W_{cp,n} = W_{cp,n-1} + Q_{t,p,n} (1 - MF_{pg,p,n}) \frac{P_{cp} MW_{cp}}{10.73 T_{pn}}$$

Calculations are repeated for all time intervals until the shut-off time is reached.

APPENDIX E

MTI PRESSURIZATION SYSTEM THERMODYNAMIC ANALYSIS

Full-scale system operating temperature predictions have been based on an analysis of the small-scale system thermodynamic process. This technique involves the solution to the general energy equation without secondary reactions. By assuming various final gas ullage temperatures, an iterative process is used to achieve a satisfactory heat balance. Since small-scale system heat transfer coefficients have been established by analyzing acquired test data, the interrelationship of the thermodynamic processes can be determined and computation time reduced. Complications resulting from secondary reactions have not been considered here since an MTI pressurization system mathematical model now being assembled will provide a more satisfactory solution. The configuration studied in this analysis is described below.

- | | |
|---|-----------------------------|
| 1) V_{i_f} = 61.8 cu ft; | 6) T = 143 sec; |
| 2) V_{FF} = 260.3 cu ft; | 7) P_{T_f} = 36 psia; |
| 3) W_f = 78.3 lb _m /sec; | 8) V_{i_o} = 14 cu ft; |
| 4) D_f = 8 ft; | 9) V_{f_o} = 260.3 cu ft. |
| 5) t_f = 0.075 in.
(average
aluminum
wall
thickness); | |

Tables E-1 and E-2 describe the gas mixture properties believed to represent the MTI process.

Table E-1 Phase I Research Tests ($MW_{cp} = 14$)

	Average		Final	
	Fuel Tank	Oxidizer Tank	Fuel Tank	Oxidizer Tank
MW ($lb_m/lb\text{-mole}$)	10.5	7.0	12.4	9.9
C_p Btu/ lb_m °R	0.627	0.87	0.569	0.72
$\mu \times 10^5$ lb_m/ft sec	1.14	1.097	1.13	1.087
$k \times 10^5$ Btu/sec ft °R	2.442	2.337	2.432	2.300
N_{pr}	0.293	0.446	0.265	0.34
C_v - Btu/ lb_m °R	0.439	0.586	0.41	0.52
γ	1.43	1.485	1.388	1.385

Table E-2 Phase III System ($MW_{cp} = 16$)

	Average		Final	
	Fuel Tank	Oxidizer Tank	Fuel Tank	Oxidizer Tank
MW	12.04	--	14.7	11.1
C_p	0.622	--	0.566	--
$\mu \times 10^5$	1.14	--	1.13	--
$k \times 10^5$	2.45	--	2.436	--
N_{pr}	0.289	--	0.263	--
C_v	0.457	--	0.431	--
γ	1.36	--	1.313	--

Note: Two-tank system = -24.4% fuel ullage initial, 5% oxidizer ullage.

1. General Energy Equation

For the full-scale system with a water-filled secondary tank, the general energy equation for the fuel tank may be described as follows:

$$U_f - U_i = H_c - H_o - \frac{PdV}{J} - \Sigma Q, \quad [E-1]$$

where,

Initial internal energy

$$U_i = W_i C_{vi} t_i = 72 \text{ Btu}; \quad [E-2]$$

Final internal energy

$$U_f = \frac{P_f (\text{MW})_f V_f C_{vf} t_f}{10.72 T_f} = \frac{5540 t_f}{T_f} \text{ Btu}; \quad [E-3]$$

Oxidizer tank demand

$$H_o = \Sigma W_o \bar{C}_p \bar{t}_f = 9.6 \bar{t}_f \text{ Btu}. \quad [E-4]$$

In the absence of secondary thermochemical reaction, an average MW of 11.1 at a 60°F temperature is estimated,

$$\text{where} \quad \Sigma W_o = \bar{W} \left(\frac{P_o V_o \text{MW}_{of}}{10.72 T_{of}} \right) \quad [E-5]$$

RTD-TDR-63-1123

and $\bar{W} = 0.8523$ (final weight fraction of combustion products in oxidizer tank)

Fuel tank energy demand

$$H_c = \Sigma W_{cp} \bar{C}_p \bar{t}_f, \quad [E-6]$$

but
$$\Sigma W_{cp} = \Sigma W_o + \Sigma W_f = 17.84 + \frac{12480}{T_{ff}};$$

therefore
$$H_c = 1380 \left(\frac{12,480}{T_{ff}} + 15.46 \right) \text{ Btu}$$

Expulsion work

$$\frac{PdV}{J} = 1330 \text{ Btu.} \quad [E-7]$$

Substituting in the general energy equation,

$$Q = 21,350 + \frac{17.2 \times 10^6}{T_{ff}} - 9.6 \bar{t}_f - \frac{5540}{T_{tf}} t_f \quad [E-8]$$

Equation [E-8] is plotted in Fig. II-4 as noted for the two-tank system.

For single fuel-tank tests, Eq [E-8] simplifies to

$$Q = \frac{11 \times 10^6}{T_{ff}} - 1258 - \frac{3980}{T_{ff}} t_f \quad [E-9]$$

This is also shown in Fig. II-4.

2. Heat Transfer to Walls

From free-convection formulas, in turbulent region $(N_{Gr} N_{Pr}) > 10^9$

$$N_{Nu} = 0.14 (N_{Gr} N_{Pr})^{1/3},$$

$$h_g = \frac{0.14 k}{D} \left(\frac{\rho^2 g_c \beta (T-T_w)}{\mu^2} D^3 \frac{C_p \mu}{k} \right)^{1/3};$$

But
$$\rho = \frac{P \text{ (MW)}}{10.72 T_{fw}}, \quad [E-10]$$

$$\beta = \frac{1}{T}.$$

Based on average gas conditions during the run, and to account for the influences of some degree of forced convection, increase coefficient by 5.55; i.e.

$$h_{gw} = \frac{3350 (\bar{T} - T_w)^{1/3}}{T_{fw}} \text{ Btu/hr-sq ft } ^\circ\text{R.} \quad [\text{E-11}]$$

The wall surface area exposed to ullage gas was integrated over the total firing cycle and the average area exposed calculated: $\bar{A}_w = 118$ sq ft. Therefore,

$$Q_w = \frac{h_{gw} A_w (\bar{T} - T_w)}{3600} \tau = \frac{15700 (\bar{T} - T_w)^{4/3}}{T_{fw}} \quad [\text{E-12}]$$

3. Heat Transfer Across Liquid Interface

The heat transfer rate across the gas/liquid interface was controlled by both the gas-side and liquid-side film coefficients.

In actuality, the heat transfer across the gas/liquid interface is considerably lower than calculated; however, with the limited information available on the combustion process, this technique was considered the best representation to allow prediction of full-scale system performance.

For both films, the free convection coefficient was determined by

$$N_{Nu} = 0.14 (N_{Gr} N_{Pr})^{1/3} \quad [\text{E-13}]$$

For the gas:

$$h_{gL} = \frac{(603) (\Delta T_{gas})^{1/3}}{T_{fL}} \text{ Btu/hr ft}^2 \text{ } ^\circ\text{R} \quad [\text{E-14}]$$

For the liquid:

$$\begin{aligned}
 h_{LL} &= (0.14)k \left[\frac{g_c \beta \rho^2}{\mu^2} N_{Pr} \Delta T_{liq} \right]^{1/3} \\
 &= 25.2 (\Delta T_{liq})^{1/3} \text{ Btu/hr ft}^2 \text{ } ^\circ\text{R}
 \end{aligned}
 \tag{E-15}$$

To account primarily for the influences of mass transfer, the film coefficients are increased by 28.

$$\text{Therefore, } h_{gL} = 16,750 \frac{(\Delta T_{gas})^{1/3}}{T_{fL}}
 \tag{E-16}$$

$$h_{LL} = 700 (T_{liq})^{1/3}
 \tag{E-17}$$

$$\text{But } \Delta T_{gas} + \Delta T_{liq} = \Delta T_{total} = \bar{T} - \bar{T}_{liq}$$

$$\text{and } (h_{gL}) \Delta T_{gas} = h_{LL} \Delta T_{liq}$$

Solving these equations simultaneously yields:

$$\Delta T_{gas} = \frac{\bar{T} - \bar{T}_{liq}}{1 + \frac{10.8}{(T_{fL})^{3/4}}}
 \tag{E-18}$$

$$\Delta T_{liq} = \frac{\bar{T} - \bar{T}_{liq}}{1 + \frac{(T_{fL})^{3/4}}{10.8}}
 \tag{E-19}$$

The overall film coefficient across the liquid interface becomes

$$U = \frac{1}{\frac{1}{h_{gL}} + \frac{1}{h_{LL}}}$$

and the total heat transferred (convection only) based in a time-integrated average exposed area of 44.1 sq ft becomes:

$$Q_{liq} = 1.75 U (\bar{T} - \bar{T}_{liq}) \text{ Btu.} \quad [E-20]$$

Research tests on the MTI system indicate nonhomogenous gas temperatures, and gas temperatures near the liquid surface are approximately 50% of the upper gas temperature. Consequently, \bar{T} should be adjusted accordingly.

4. Total Heat Transferred from Pressurant

Excluding the heat from mass transfer, this value becomes

$$\Sigma Q = Q_w + Q_{liq}. \quad [E-21]$$

5. Determination of Wall Temperature Rise

For negligible temperature gradients in the wall, a heat balance at the wall results in

$$h_{gw} \bar{A}_w [\bar{T} - \bar{T}_w] = \frac{\rho C_p V_w}{\tau} - h_o \bar{A}_w' [\bar{T}_w - T_a] - \sqrt{h_{gw} b k S} (\bar{T} - \bar{T}_{liq}), \quad [E-22]$$

where the last term of the equation identifies the heat flow rate conducted through the wall to the propellant.

Noting that $V_w \approx \bar{A}_w(t)$ cu in. of wall material,

$$S_b \approx \pi^2 D_m^2 (t), \text{ the product of surface and perimeter of wall cross section, and}$$

$$\bar{A}_w \approx \bar{A}_w'.$$

Initial conditions were ambient.

Since linear temperature histories are assumed, the resultant equation becomes:

$$\Delta T_{wall} = \frac{(1 - \alpha/h_{gw}) (\bar{T}_{sfinal} - T_a)}{1 + \frac{h_o}{h_{gw}} + \frac{2\beta}{h_{gw}}} \cdot R, \quad [E-23]$$

where,

$$\alpha = \sqrt{h_{gw} k t \left(\frac{\pi D}{A_w} \right)}, \text{ and}$$

$$\beta = \frac{\rho c t}{\tau}.$$

Figure II-2 shows the predicted tank wall heating as a function of the gas temperature rise.

6. Determination of Liquid Temperature Rise

This calculation is to permit rapid determination of bulk temperature rise to evaluate film coefficients and average temperature gradient. In this manner the heat transferred across the liquid interface can be easily checked in a rapidly converging trial and error solution.

$$\Sigma Q = \int W C_p dT, \quad [E-24]$$

since, $\dot{w}_f = \text{constant}$, and

$$W = w_{\text{initial}} - \dot{w}_f (T).$$

A linear temperature history is assumed. This will introduce some error that will be adjusted if necessary.

$$T = T_{\text{initial}} + \dot{T} (\tau)$$

$$dT = \dot{T} d\tau$$

Substituting in Eq [E-12] gives:

$$\Sigma Q = C_p \int_0^f \left(W_{\text{initial}} - \dot{w}_f \tau \right) \dot{T} d\tau \quad [E-25]$$

Integrating with \dot{T} assumed constant,

$$\Sigma Q = C_p \tau \dot{T} \left(W_{\text{initial}} - \frac{\dot{w}_f \tau}{2} \right).$$

$$\text{But } \dot{T} = \frac{T_{\text{final}} - T_{\text{initial}}}{\tau}.$$

Therefore,

$$\Sigma Q = C_p \left[W_{\text{initial}} - \frac{\dot{w}_T \tau}{2} \right] (T_{\text{final}} - T_{\text{initial}}). \quad [\text{E-26}]$$

Since this value includes the heat from mass transfer and wall conduction, these must be estimated before Eq [E-26] can be used to obtain the bulk liquid temperature rise.

Figure II-3 presents the temperature rise of the bulk liquid as a function of the total heat absorbed. Also shown is the temperature rise of the wall as a function of retained heat.

APPENDIX F

IBM 7094 MTI MATHEMATICAL MODEL

This program calculates the transient conditions during operation of an MTI (main tank injection) propellant pressurization system (Fig. F-1). The system provides tank ullage pressure by injecting a hypergolic reactant into a propellant tank to generate gaseous combustion products. Tanks may be pressurized independently, or two tanks may be pressurized in series with ullage gas from the primary tank used to pressurize the secondary tank. In this case, the program considers any additional reaction that may occur in the secondary tank. Although the program is intended to analyze the MTI pressurization system, proper selection of input data will provide simulation of a stored gas pressurization system.

Both the size of the combustion zone and the reaction are affected by reactant flow rate and the injection technique. Although the primary tank reaction occurs in the liquid, any secondary tank reaction may take place either in the ullage or the liquid. Mass transfer in the combustion zone is just sufficient to provide propellant in the desired reaction mixture ratio. The composition and temperatures of the combustion products are based either on empirical data or theoretical equilibrium calculations.

Injection of reactant into the primary tank may be controlled by a pressure-actuated on-off valve or by a constant-flow orifice. For constant-flow operation, a time increment is an input, and transient conditions are calculated at the end of each interval until shutdown occurs. For cyclic on-off operation, a high and low pressure value for the primary tank is an input, and the dependent time interval is calculated for either pressure decay to the low level or pressure generation by reaction to the high level. The time and transient conditions are calculated at the end of each interval until shutdown occurs.

If two tanks are pressurized in series, gas crossflow may occur only from the primary to the secondary tank, and then only if the primary tank ullage pressure is sufficiently above the ullage pressure in the secondary tank. The crossflow is just sufficient to maintain a specific pressure in the secondary tank, and no heat loss or pressure drop effects of the transfer line are considered. Pressure-sensing points may be either at tank top or bottom. If at bottom, the pressure is the sum of ullage gas pressure plus propellant head.

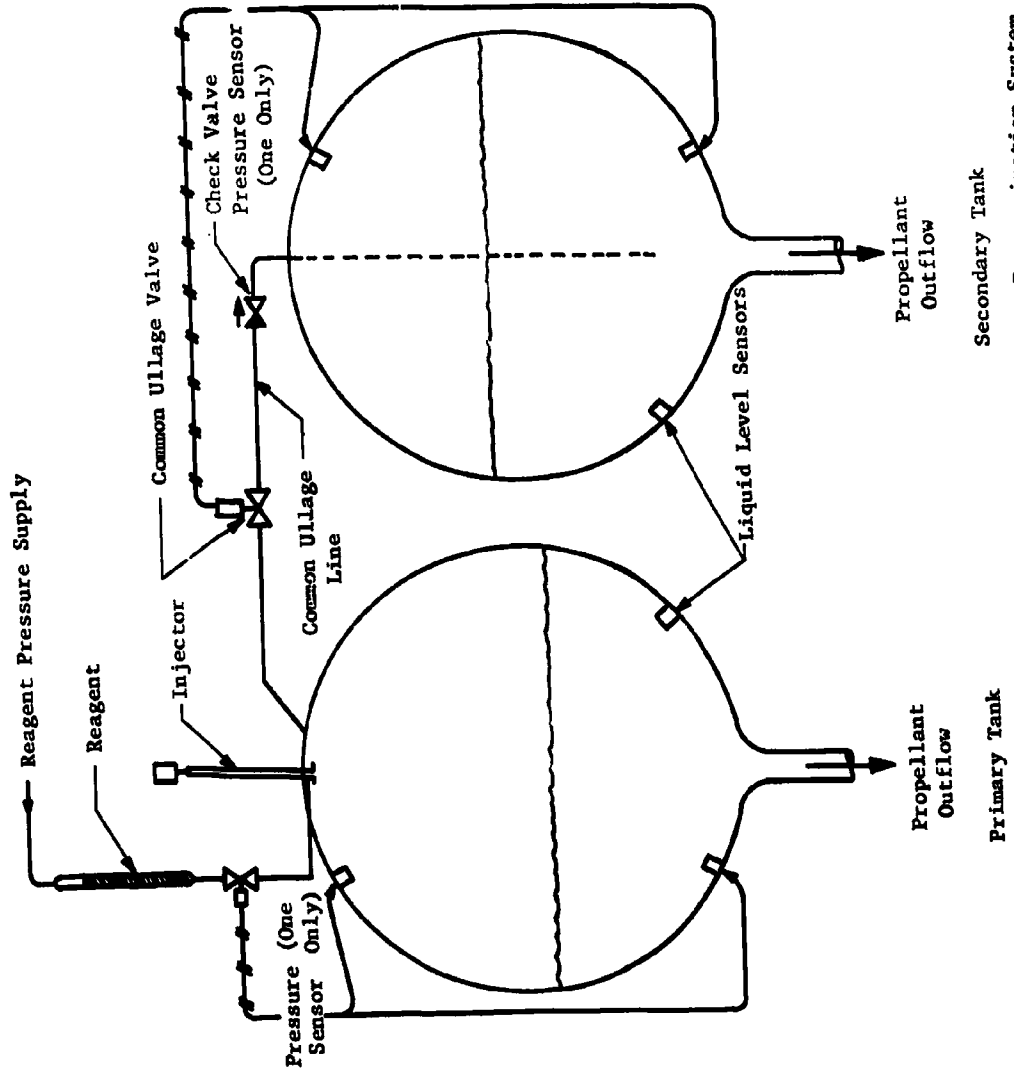


Fig. F-1 Analytical Model of a Main Tank Injection Propellant Pressurization System

Heat is transferred by convection between the gas the adjacent tank wall, the liquid and the adjacent tank wall, the outside wall and the adjacent atmosphere, and across the tranquil portion of the gas-liquid interface. For subsurface reaction, heat transfer is also considered between the combustion zone and the liquid. Evaporation and subsequent vapor dissociation can be treated in either tank, with heat and mass transfer across the ullage gas-liquid interface. Provisions for a sample bleed have been included on both tanks to duplicate conditions encountered in ground test experiments.

A general outline of the analytical model sequence of computations is shown in Fig. F-2. More specific details of the circuit logic are schematically represented in Fig. F-3. Additional program details are contained in the following paragraphs.

A. PROGRAM QUALIFICATIONS

1. Assumptions

The following assumptions were made to simplify the mathematical relationships used in the Analytical Model of a Main Tank Injection Propellant Pressurization System:

- 1) The ideal gas law applies to constituents of the ullage at all times;
- 2) The ullage is considered homogeneous at all times with regard to mixing and temperature;
- 3) The tank wall adjacent to the ullage is considered to be at an average bulk temperature at any time;
- 4) The propellant is considered homogeneous at all times with regard to mixing and temperature;
- 5) The tank wall adjacent to the propellant is considered to be at an average bulk temperature at any time;
- 6) Propellant vapor partial pressure is considered to be some temperature-dependent fraction of the saturated vapor pressure;

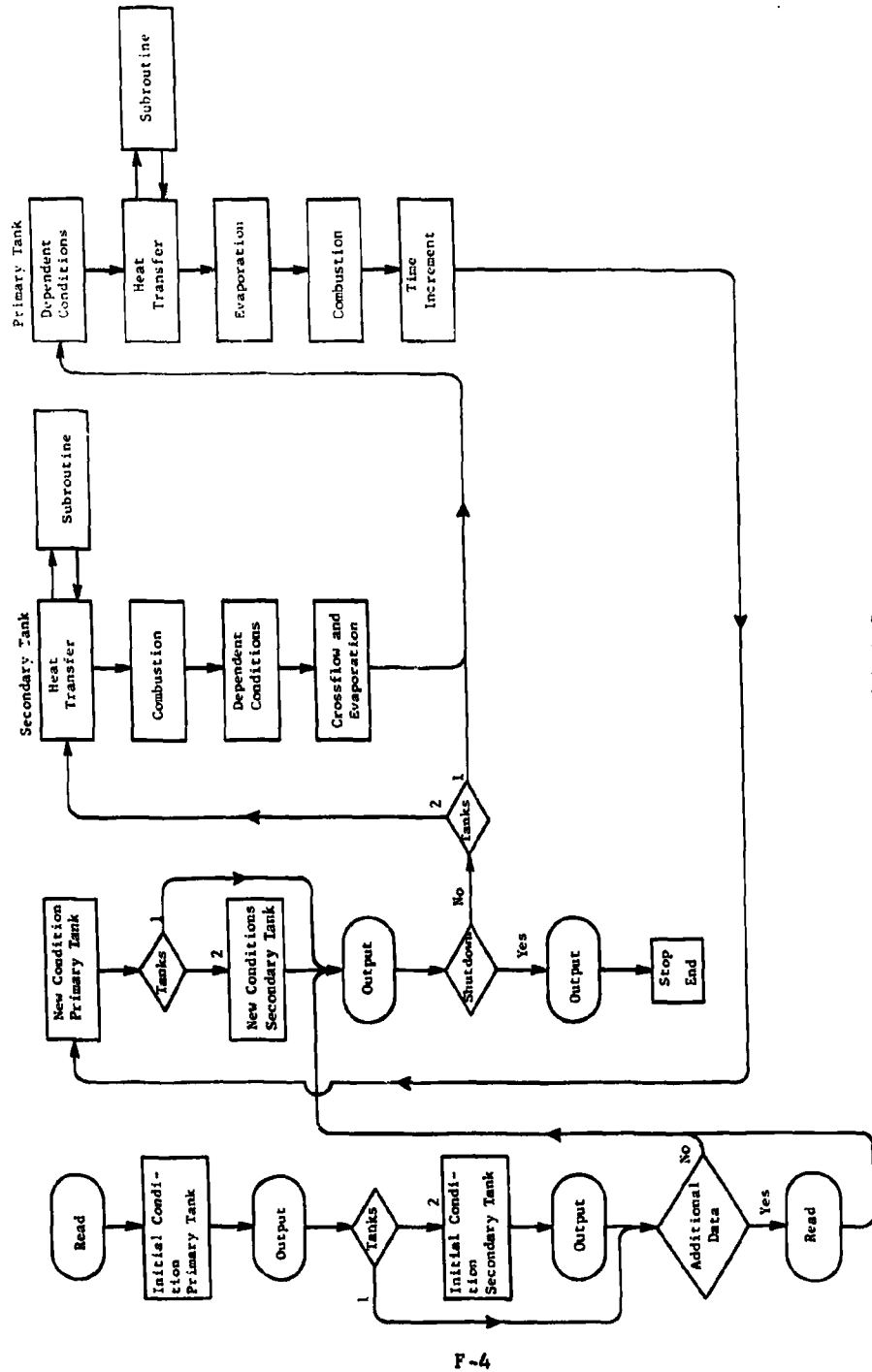


Fig. F-2 General Logic Sequence

- 7) Propellant properties of heat capacity and density are considered to be linear functions of temperature;
- 8) Linear interpolation is used on all tabular input.

2. Options (binary code meaning assignments)

OPAD	Additional Data 0 = No 1 = Yes
OPBP	Bleed, Primary Tank 0 = No 1 = Yes
OPBS	Bleed, Secondary Tank 0 = No 1 = Yes
OPCS	Combustion, Secondary Tank 0 = No 1 = Yes
OP1P	Reagent Injection, Primary Tank 0 = Constant Flow 1 = Pulse Flow
OPIS	Crossflow Injection, Secondary Tank 0 = Into Ullage 1 = Into Liquid
OPPCP	Pressure Control, Primary Tank 0 = Ullage Pressure 1 = Ullage Pressure Plus Propellant Head
OPPCS	Pressure Control, Secondary Tank 0 = Ullage Pressure 1 = Ullage Pressure Plus Propellant Head
OPTNK	Tanks 0 = Primary 1 = Primary Plus Secondary
OPVDP	Vapor Dissociation, Primary Tank 0 = No 1 = Yes
OPVDS	Vapor Dissociation, Secondary Tank 0 = No 1 = Yes

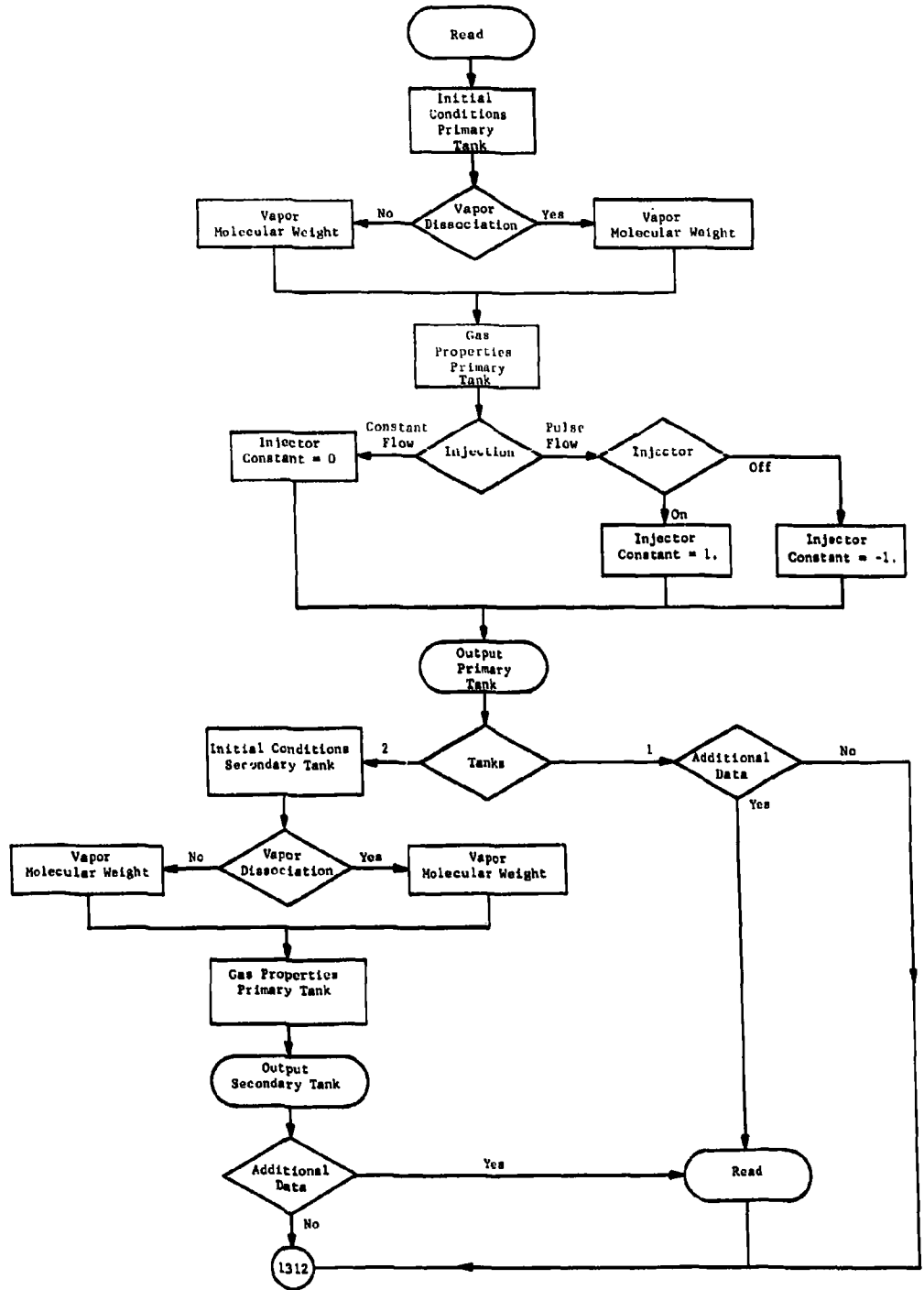


Fig. F-3 Detailed Logic Sequence

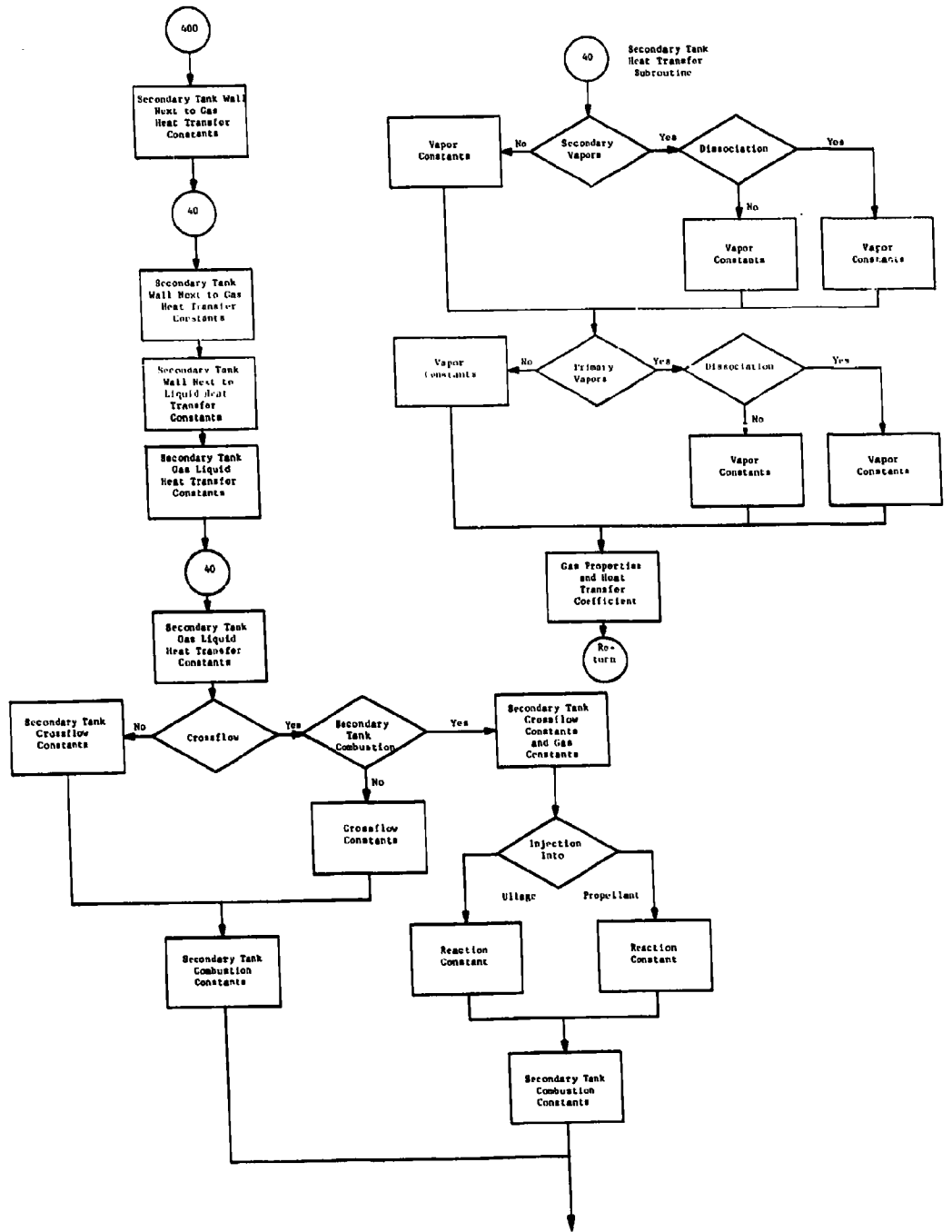


Fig. F-3 (cont)

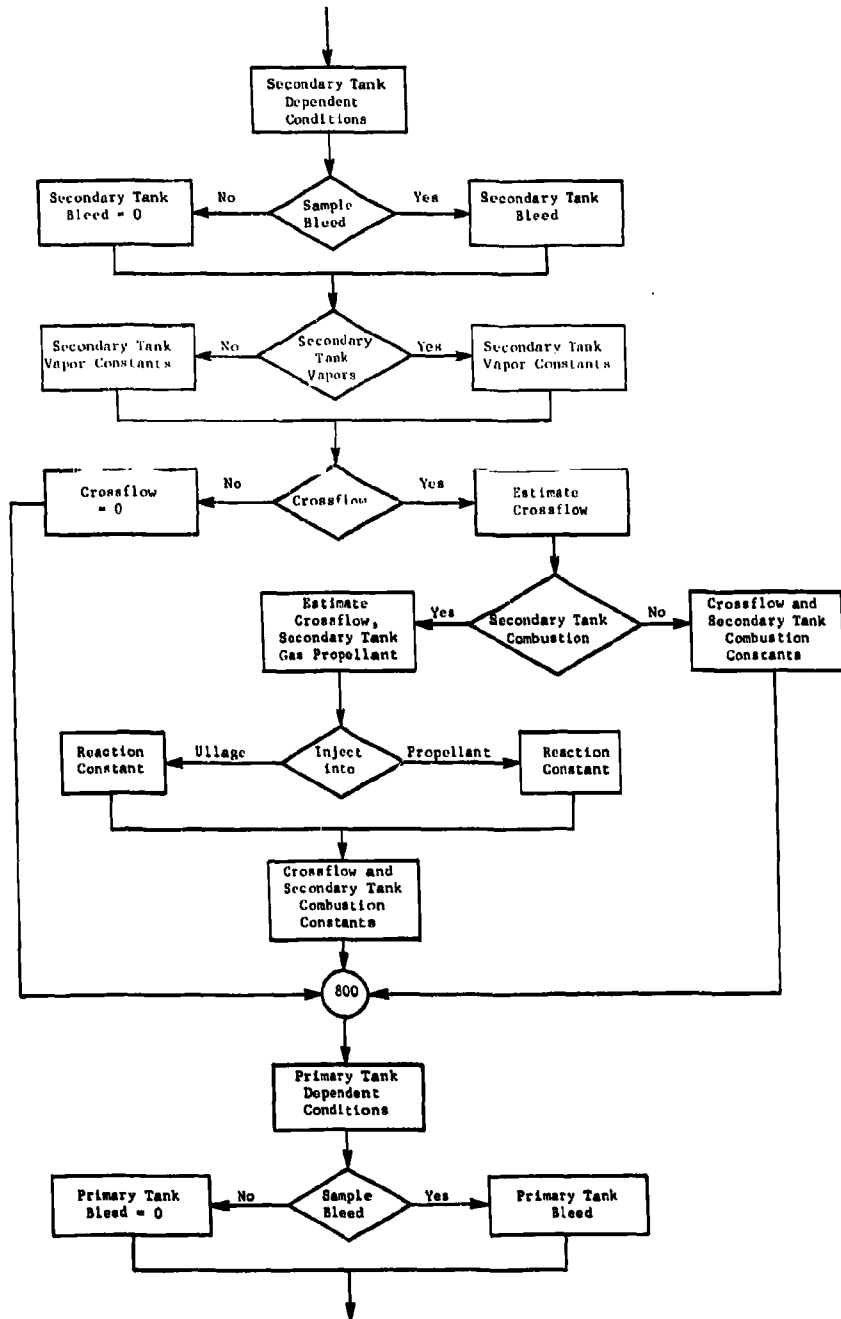


Fig. F-3 (cont)

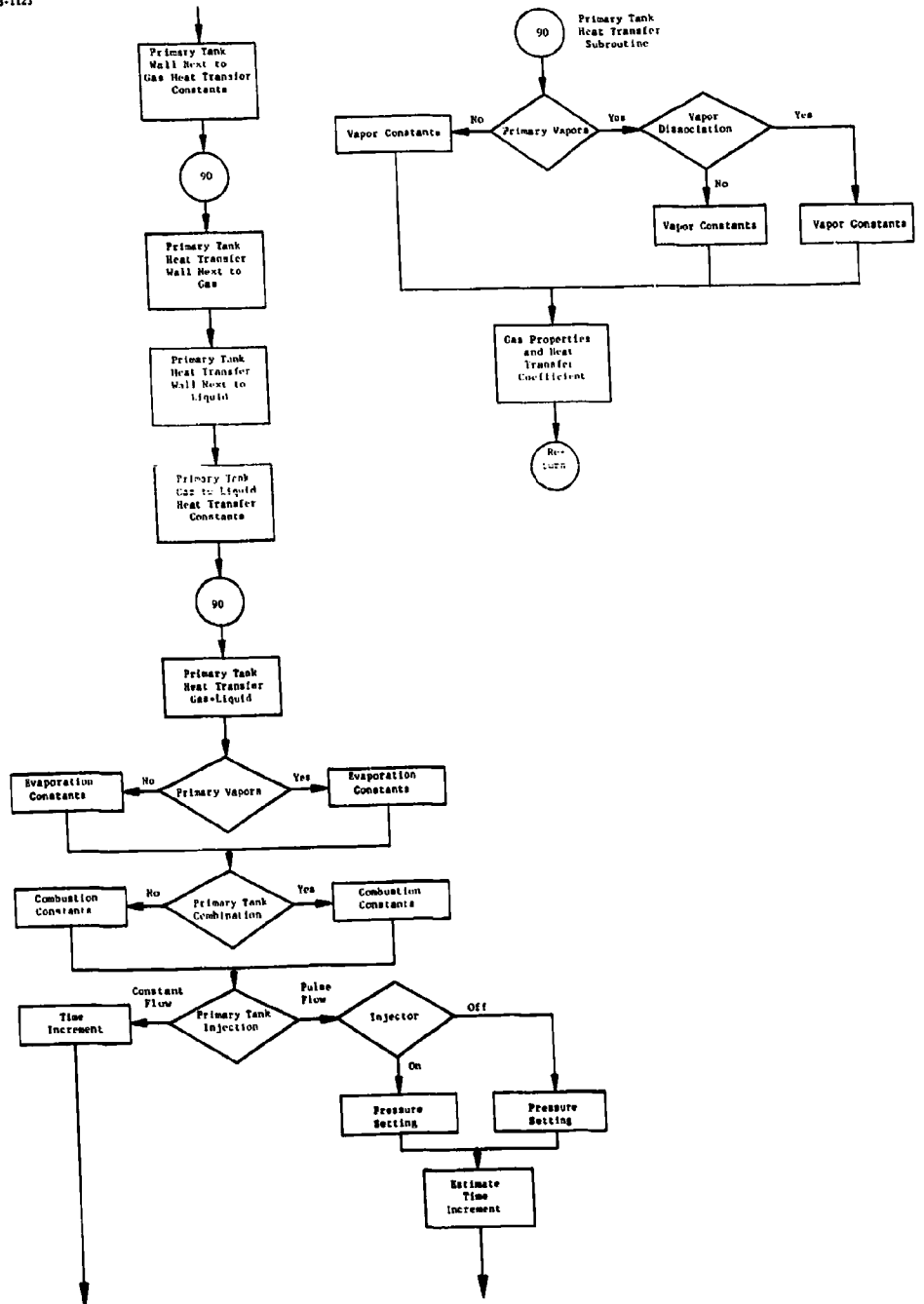


Fig. 7-3 (cont)

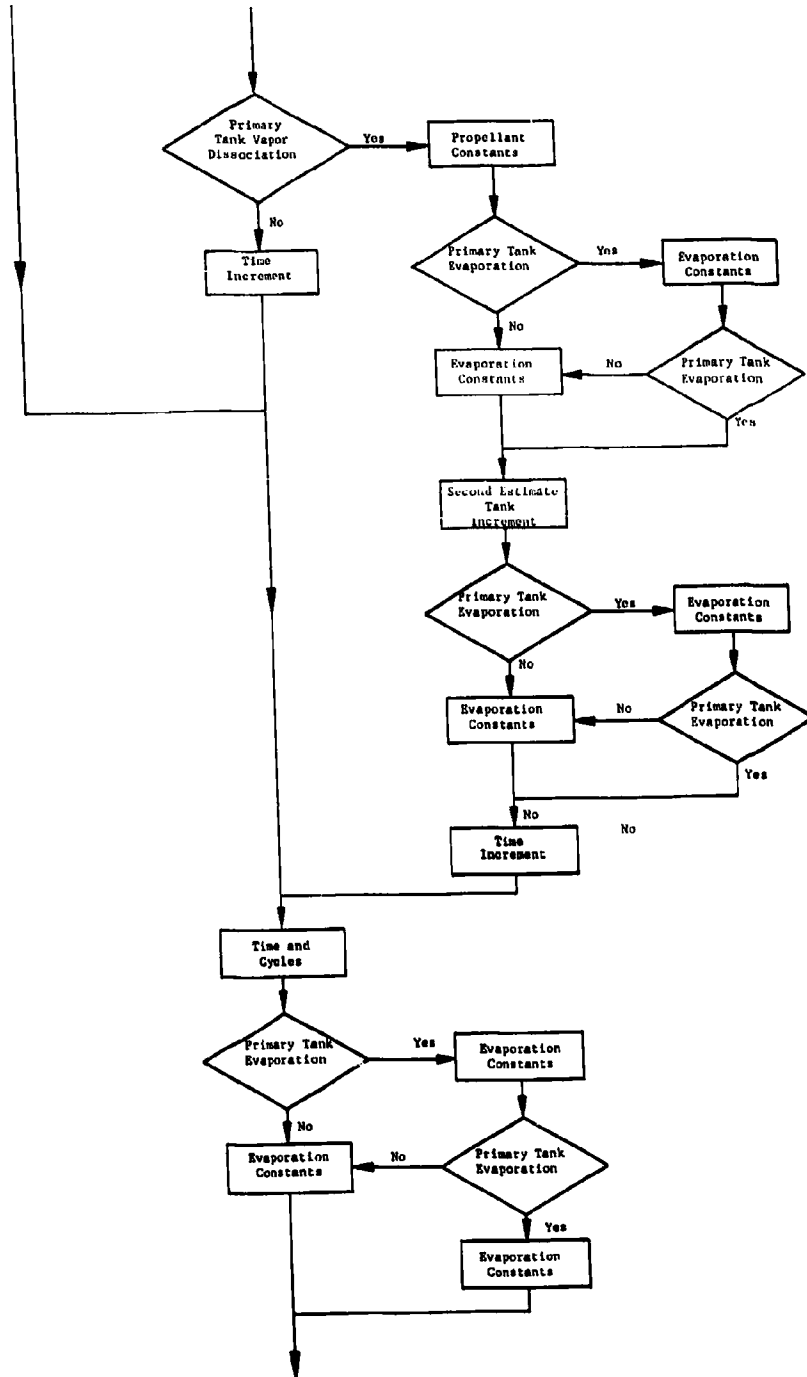


Fig. P-3 (cont)

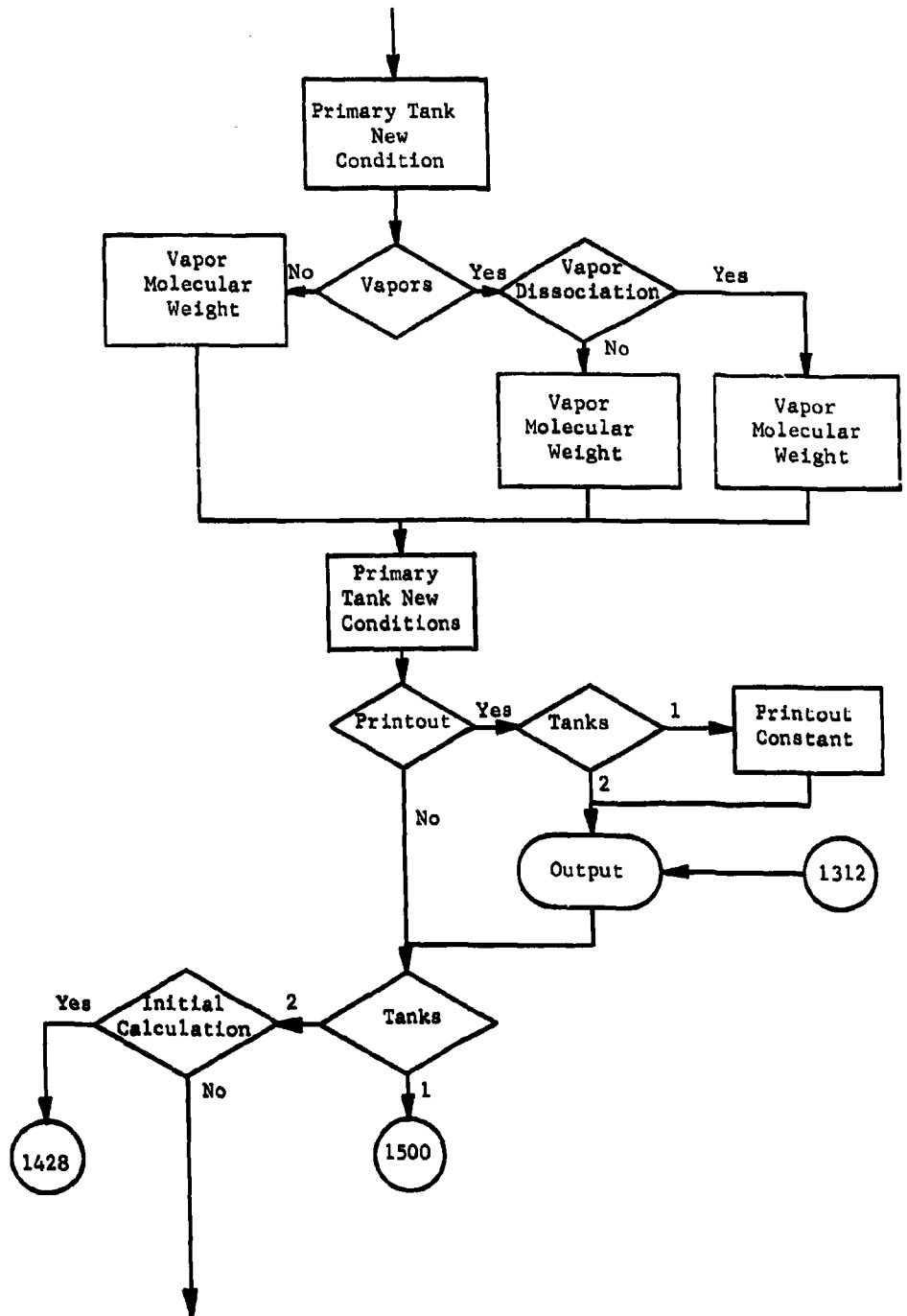


Fig. F-3 (cont)

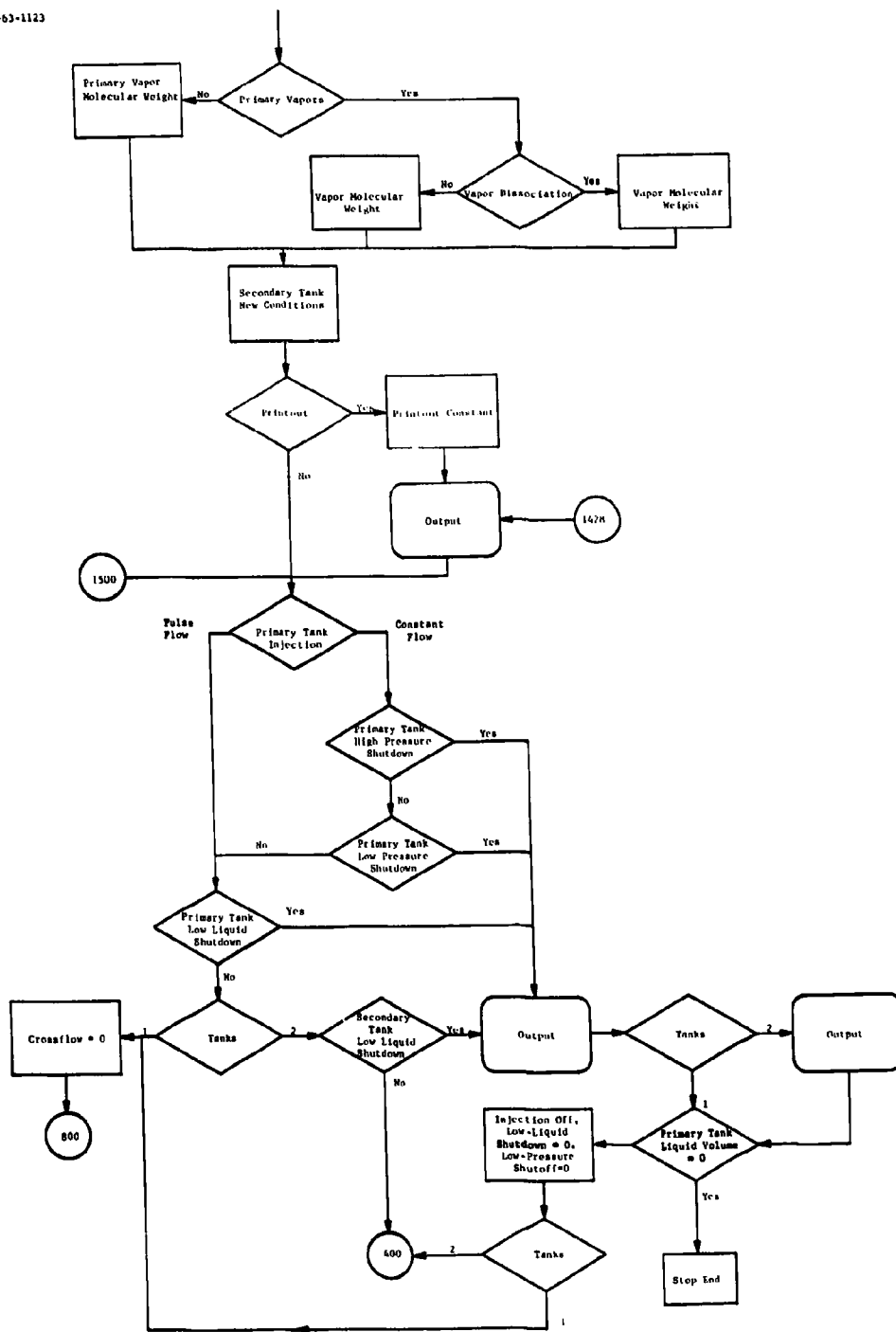


Fig. F-3 (concl)

B. PROGRAM INTERNAL OPERATION SEQUENCE

1. Initial Conditions (Fig. F-2 and F-3)

After reading the input data, initial conditions of the system, such as gaseous composition of the ullage, are calculated. Initial settings are made for a system at time zero (no previous MTI reaction), and specific constants to control the injector and printout are determined.

If required, use of the option for additional data, OPAD, permits additional input at this time to override specific initial conditions as determined in the program. As an example, the program sets the temperature of the tank adjacent to the ullage equal to the input ullage temperature. If such is not the case, the desired wall temperature is inserted after all the initial input has been read and the initial conditions section completed. At this point, the program prints out the system initial conditions.

2. Heat Transfer

Heat transfer is considered between the gas and adjacent tank wall, this wall and the outside environment, the gas and liquid, the liquid and the adjacent tank wall, and this wall and the outside environment.

For determination of internal-film heat transfer coefficients, the fluid properties are calculated at the average film temperature, and the heat transfer coefficient derived from the natural convection relationship:

$$h_f \frac{D}{k_f} = \left(\frac{1}{\alpha} \frac{D^3 \rho_f^2 g_L \beta \Delta t}{\mu_f^2} \right)^n \left(\frac{C_p \mu_f}{k_f} \right)^m \quad [F-1]$$

By assuming $n = m$ and simplifying, we have

$$h_f = \left(C_f \frac{k_f}{D} \left(\frac{D^3 \rho_f^2 g_L \beta \Delta t C_p}{\mu_f k_f} \right)^{X_f} \right) \quad [F-2]$$

where C_f and X_f need to be determined empirically from test data. The symbol, T , is taken as the difference between the bulk temperatures of the source and sink, and the average film temperature as the average of these two bulk temperatures. Subroutines are provided to calculate gas film properties at the average film temperature in the primary and secondary tanks.

To account for aerodynamic heating of the tank walls, available data are inserted as tables of heat transfer coefficient, h_a , and adiabatic wall temperature, T_{aw} , versus time, and calculated as $Q = h_a A_{wall} (T_{aw} - T_{wall})$. Heat transfer is calculated separately for the tank wall adjacent to the ullage and propellant. For application where aerodynamic heating does not occur, suitable input may be used to account for heat transfer based on ambient conditions.

3. Combustion

Reaction mixture ratio, R_m , adiabatic flame temperatures, T_f , and the ratio of condensible products to total products, R_{CL} , are required input to calculate effects of the combustion reaction. In the primary tank, R_{mp} is the ratio of the weight of reagent injected, W_R , to the propellant consumed by the reaction. In the secondary tank, R_{ms} is the ratio of weight of propellant consumed to weight of reactants in the crossflow, considered to be primary vapors plus gaseous combustion products.

The heat of reaction is calculated by integrating the combustion products' heat capacity between the reaction temperature and the adiabatic flame temperature to get the enthalpy change, H_{cp} , per pound of products. Then the heat of reaction is this enthalpy change multiplied by the mass of products

$$Q_{RP} = (W_{CP} + W_{CLR}) \int_{T_R}^{T_{FP}} C_{PCP} dT_t \quad [F-3]$$

The heat of reaction is corrected to account for contributions of the reactants, and then a corrected flame temperature is calculated:

$$T_{FCP} = T_R + \frac{Q_{FR}(T_{FP} - T_R)}{H_{CP}(W_{CP} + W_{CLR})} \quad [F-4]$$

In the secondary tank, this also includes the temperature-reducing effect of inert gas in the crossflow. A new enthalpy change is calculated, based on the corrected adiabatic flame temperature, and is then used to provide a more accurate calculation of T_{FCP} .

For convective heat transfer between the hot gases in the combustion zone and the surrounding liquid, an empirically derived relationship was used to determine the area of combustion, A_C , and the film-heat transfer coefficient, h_c , as a function of the reagent flow rate:

$$A_C = C_{AC}(\dot{w}_R)^{.67}$$

and

$$h_c = C_{HC}(\dot{w}_R)^{.2} \quad [F-5]$$

where C_{AC} and C_{HC} are constants.

Simplifying the heat transfer between the hot gases and the surrounding liquid,

$$Q_{LPC} = C_{AC}C_{HC}(\dot{w}_R)^{.87} (T_{FLP} - T_L) \quad [F-6]$$

The heat loss from cooling and condensation of the condensible combustion products, Q_{CLP} , occurs in the combustion zone, and is calculated from the latent and sensible heat change of the condensibles:

$$Q_{CLP} = W_{CLP} (H_{LCLP} + H_{SCLP}) \quad [F-7]$$

The total energy available to the system (above the ullage temperature) from primary and secondary results of the combustion reaction, Q_{SPC} , is the sum of the corrected heat of reaction and the latent heat of the condensibles, less the energy required to raise the gaseous combustion products to the bulk gas temperatures:

$$Q_{SPC} = Q_{FR} - W_{CP} C_{PCP} (T_{GP} - T_R) + W_{CLP} H_{LCLP} \quad [F-8]$$

4. Time Increment

For the case with constant flow orifice, the time increment is constant and is used as an input to the program.

For pulse-flow injection, the ideal gas law is differentiated with regard to time as follows:

$$P = \frac{WRT}{MV}$$

$$\frac{dP}{dt} = \frac{WR}{MV} \frac{\partial T}{\partial t} + \frac{RT}{MV} \frac{\partial W}{\partial t} - \frac{WRT}{MV^2} \frac{\partial V}{\partial t} - \frac{WRT}{M^2V} \frac{\partial M}{\partial t} \quad [F-9]$$

The partials are evaluated from the previous calculations in each time increment, and the expression is solved for $\frac{dP}{dt}$. By determining the required pressure change, ΔP , and using the approximate relationship (for small Δt 's)

$$\frac{\Delta P}{\Delta t} = \frac{dP}{dt},$$

then

$$\Delta t = \Delta P \times \frac{1}{\frac{dP}{dt}}.$$

The required pressure change is equal to the difference between the pressure and either the high or low pressure limit, depending, respectively, on whether the system is on a combustion or pressure-decay part of the cycle. An iterative calculation of ΔT is used to increase accuracy when vapor dissociation occurs in the primary tank.

5. New Conditions

System conditions at the end of the time increment are now calculated and checked to see if output is to be made at this time. The program then checks to see if any shutdown criteria have been met.

6. Shutdown

For a constant-flow injection system, the program first checks to see if system pressure is within permissible limits. If it is not, the shutdown sequence is initiated; otherwise, the program checks tank propellant volume(s) to see if the liquid level is at or below an input minimum. If not, the program continues with a new cycle; otherwise, shutdown is initiated.

When shutdown occurs, the system conditions are printed, and the program then checks the liquid-level setting. If they are zero, the program is ended (the program actually seeks input for a new case).

If not zero, they are reset to zero, and several other constants are also reset so the program continues, but no injection takes place. Rather, the ullage undergoes a polytropic expansion while the rest of the liquid is expelled until final shutdown is encountered.

7. Output

Data printout of the identified parameters will occur under any of the following situations:

1) Initial Condition

Primary Tank: RUNNO, PLIG, RMP, RCLP, TFP, OPIP, OPVDP, OPEP, OPPCP.

Secondary Tank: SLIQ, RMS, RCLS, TFS, OPIS, OPVDS, OPBS, OPCS, OPPCS.

2) Periodic Output

Primary Tank: T, CYC, TGP, TPTG, TLP, TPTL, PGP, PTP, MWGP, VGP, YCP, YVP, WFCLP, WTR.

Secondary Tank: TGS, TSTG, TLS, TSTL, PGS, PTS, MWGS, VGS, YCS, YVS, YPUS, WFCLS.

3) Shutdown

Primary Tank: T, CYC, TGP, TPTG, TLP, TPTL, PGP, PTP, MWGP, VGP, YCP, YVP, WFCLP, WTR, WTCP, WTCLP.

Secondary Tank: TGS, TSTG, TLS, TSTL, PGS, PTS, MWGS, VGS, YCS, YVS, YPUS, WFCLS, WTCLS, WTVPF, WTCCF, WTILF.

C. PROGRAM INPUT

1. Data Sheets (Table F-1)

- 1) Column 1 must contain a 2, 3, 8, 9 or 0; where 2 represents a floating point number, and 3 represents a symbolic name which may contain up to 6 characters (numeric or alphabetic). An 8 in column 1 is necessary for the second card in each input case. The last card in each input case must contain a 9 in column 1. The first card in a case is an identification card and has a 0 in column 1;
- 2) Column 2 contains a 1 only when a 3 is used in column 1 and in all other cases is left blank;
- 3) Columns 3 thru 7 contain the location at the first piece of input data on a card (Table F-1);
- 4) Columns 8, 21, 34, 47, and 60 are always blank;
- 5) When 3 is used in column 1, the 6-character name must be right-adjusted to column 14 (See Table F-1);
- 6) A zero in column 1 enables the customer to identify his input by some comment;
- 7) Columns 9 thru 20, 22 thru 33, 35 thru 46, 48 thru 59, and 61 thru 72 with a 2 in column 1 contain floating point numbers in any position in the 12-character field. Zeros may be read in as follows: 0. or 0.0. If one or more of the 12-character fields are left blank, no more data will be read from that card;
- 8) Columns 73 thru 76 should be left blank for machine operations personnel to punch the last four digits of the run request number;
- 9) Data punch in columns 73 thru 80 are for identification only;
- 10) Columns 77 thru 80 should be punched for card sequencing.

Table F-1 Sample Data Sheet

MARTIN CODING FORM NO. 1

SHEET 1 OF 1

PROG. NO.	ENGINEER	EXT.	CHARACT. NO.	STATION	LABEL
1					
2					
3					
4					
5					
6					
7					
8					
9					
10					
11					
12					
13					
14					
15					
16					
17					
18					
19					
20					
21					
22					
23					
24					
25					
26					
27					
28					
29					
30					
31					
32					
33					
34					
35					
36					
37					
38					
39					
40					
41					
42					
43					
44					
45					
46					
47					
48					
49					
50					
51					
52					
53					
54					
55					
56					
57					
58					
59					
60					
61					
62					
63					
64					
65					
66					
67					
68					
69					
70					
71					
72					
73					
74					
75					
76					
77					
78					
79					
80					
81					
82					
83					
84					
85					
86					
87					
88					
89					
90					
91					
92					
93					
94					
95					
96					
97					
98					
99					
100					

2. Data Types

- 1) Floating point numbers: every floating point number must contain a decimal point and may be modified by powers of 10 where the power of 10 follows the number. Exponents may be introduced by E±XX, EXX, or ±XX and must be right-adjusted in the data field. The following are equivalent representations of the same floating point number.

7532, +.7532E+4 75.32E+2 7.532E+3 75.32+2

- 2) Comments: columns 2 thru 8 are left blank, and the comment can be written in any column through 72 except 21, 34, 47, and 60.

3. Input Cases

There are four cases of input data.

- 1) The original primary tank data include tabular values for functions that are looked up in the program. The data in tabular or functional form are indicated in Tables F-2 and F-3 by identifying the dependent parameter as a function of the independent variable [e.g. XKCS (TT)]. This is followed by the address of the first value of the independent variable, maximum number of points in the table, and the address of the first value of the dependent variable in sequence. It is not necessary to use the maximum number of points, but the number of points must be specified in the previously mentioned location.

Example:

	<u>LOC</u>
XKCP (TT)	46
161.	47
20.	48
181.	49

If the dependent variable is constant in a table look-up, then 1. goes into the position for the number of points in the table followed by the constant.

Example:

	<u>LOC</u>
CPI (TT)	108
761.	109
1.	110
1.244	111;

- 2) The original secondary tank data include the same type of data as the original primary tank data;
- 3) Precalculated data (for either the primary tank or for the secondary tank calculations);
- 4) Additional data to change the conditions for the primary and/or secondary calculations;
- 5) The locations for the input parameters are found in Tables F-2, F-3, and F-4.

4. Program Run Duration

This program was written for the IBM 7094 computer (FORTRAN), and the running time can be estimated by

$$T = NC (OPTNK + 1) .6 \quad [F-10]$$

where

T = approximate run time in minutes,

NC = number of cases,

OPTNK = 0 for single tank system

1 for dual tank system.

Table F-2 Locations of Input Parameters for Primary Tank

<u>Data Symbol</u>	<u>Location</u>	<u>Data Symbol</u>	<u>Location</u>
RUNNO	1	CHC	33
PLIQ	2	CDT	34
TI	3	XFGWP	35
VPT	4	CFGWP	36
VGP	5	XFGLP	37
PGP	6	CFGLP	38
TGP	7	XFLWP	39
TLP	8	CFLWP	40
CPO	9	RMP	41
PPL	10	RCLP	42
PPH	11	TFP	43
VLPL	12	TR	44
OPVDP	13	XMWCP	45
OPIP	14	XKCP (TT)	46*
OPBP	15	161.	47
OPTNK	16	20.	48
OPPCP	17	181.	49
DOP	18	XMUCP (TT)	50*
GDOP	19	201.	51
FR	20	20.	52
TRP	21	221.	53
RHOR	22	CPCP (TT)	54*
AV	23	241.	55
CDV	24	20.	56
CPR1	25	261.	57
CPR2	26	HLCLP (TT)	58*
DPT	27	281.	59
SPT	28	20.	60
CWSP	29	301.	61
CPTO	30	CPCLP (TT)	62*
CPPT	31	321.	63
CACP	32	20.	64

Table F-2 (cont)

<u>Data Symbol</u>	<u>Location</u>	<u>Data Symbol</u>	<u>Location</u>
341.	65	XKI (TT)	100*
XMWPV	66*	681.	101
PPV (TT)	67	20.	102
361.	68	701.	103
20.	69	XMWI (TT)	104*
281.	70	721.	105
CVAPP (TT)	71*	20.	106
401.	72	741.	107
20.	73	CPI (TT)	108*
421.	74	761.	109
CKPV (TT)	75*	20.	110
441.	76	781.	111
20.	77	XKLP (TT)	112*
461.	78	801.	113
BETVP (TT)	79*	20.	114
481.	80	821.	115
20.	81	XMULP (TT)	116*
501.	82	841.	117
XKVP (TT)	83	20.	118
521.	84	861.	119
20.	85	BETLP (TT)	120*
541.	86	881.	121
XMUVP (TT)	87*	20.	122
561.	88	901.	123
20.	89	CPLP1	124
581.	90	CPLP2	125
CPVP (TT)	91*	CRLP1	125
601.	92	CRLP2	127
20.	93	ACC (T)	128*
621.	94	921.	129
HVAPP (TT)	95*	20.	130
641.	96	941.	131
20.	97	VDLOP (T)	132*
661.	98	961.	133
XMWI	99	20.	134

Table F-2 (concl)

<u>Data Symbol</u>	<u>Location</u>
981.	135
SPTG (VGP)	136*
1001.	137
20.	138
1021.	139
ALGP (VGP)	140*
1041.	141
20.	142
1061.	143
ZP (VGP)	144*
1081.	145
20.	146
1101.	147
DZPBVD (VGP)	148*
1121.	149
20.	150
1141.	151
HAP (T)	152
1161.	153
40.	154
1201.	155
TAWP (T)	156*
1241.	157
40.	158
1281.	159
OPAD	160

Note: The numbers in the column Data Symbol are those to be entered in the corresponding location (e.g. 161 goes into location 47, 20 into location 48, etc).

*No data are to be read into this location.

Table F-3 Locations of Input Parameters for Secondary Tank

<u>Data Symbol</u>	<u>Location</u>	<u>Data Symbol</u>	<u>Location</u>
SLIQ	1501	XMWCS	1532
VST	1502	XKCS (TT)	1533*
VGS	1503	1631.	1534
PGS	1504	20.	1535
TGS	1505	1651.	1536
TLS	1506	XMUCS (TT)	1537*
DELPPS	1507	1671.	1538
PS	1508	20.	1539
VLSL	1509	1691.	1540
OPVDS	1510	CPCS (TT)	1541*
OPIS	1511	1711.	1542
OPBS	1512	20.	1543
OPCS	1513	1731.	1544
OPPCS	1514	HLCLS (TT)	1545*
DOS	1515	1751.	1546
CDOS	1516	20.	1547
DST	1517	1771.	1548
SST	1518	CPCLS (TT)	1549*
CWSS	1519	1791.	1550
CSTO	1520	20.	1551
CPST	1521	1811.	1552
CACS	1522	XMWSV	1553
XFGWS	1523	PSV (TT)	1554*
CFGWS	1524	1831.	1555
XFGLS	1525	20.	1556
CFGLS	1526	1851.	1557
XFLWS	1527	CVAPS (TT)	1558*
CFLWS	1528	1871.	1559
RMS	1529	20.	1560
RCLS	1530	1891.	1561
TFS	1531	CKSV (TT)	1562*

Table F-3 (concl)

<u>Data Symbol</u>	<u>Location</u>	<u>Data Symbol</u>	<u>Location</u>
1911.	1563	CPLS1	1598
20	1564	CPLS2	1599
1931.	1565	CRSL1	1600
BETVS (TT)	1566*	CRSL2	1601
1951.	1567	VDLOS (T)	1602*
20.	1568	2271.	1603
1971.	1569	20.	1604
XKVS (TT)	1570*	2291.	1605
1991.	1571	SSTG (VGS)	1606*
20.	1572	2311.	1607
2011.	1573	20.	1608
XMUVS (TT)	1574*	2331.	1609
2031.	1575	ALGS (VGS)	1610*
20.	1576	2351.	1611
2051.	1577	20.	1612
CPVS (TT)	1578*	2371.	1613
2071.	1579	ZS (VGS)	1614*
20.	1580	2391.	1615
2091.	1581	20.	1616
HVAPS (TT)	1582*	2411.	1617
2101.	1583	DZSBDV (VGS)	1618*
20.	1584	2431.	1619
2131.	1585	20.	1620
XKLS (TT)	1586*	2451.	1621
2151.	1587	HAS (T)	1622*
20.	1588	2471.	1623
2171.	1589	40.	1624
XMULS (TT)	1590*	2511.	1625
2191.	1591	TAWS (T)	1626*
20.	1592	2551.	1627
2211.	1593	40.	1628
BETLS (TT)	1594*	2591.	1629
2231.	1595		
20.	1596		
2251.	1597		

*No input is to be read into this location.

Table F-4 Locations for Additional Input

<u>Data Symbols</u>	<u>Location</u>	<u>Data Symbols</u>	<u>Location</u>
ACC	128	WCP	1477
CCP	1321	WCS	1478
CKPV	75	WFCLP	1439
CKSV	1562	WFCLS	1440
CPO2	1481	WGP	1480
CVAPP	71	WGS	1425
CVAPS	1558	WIP	1426
CYC	1328	WIS	1428
FCP	1338	WPTG	1485
FCS	1339	WSTG	1486
FIP	1335	WICCFX	1484
FIS	1336	WTCLP	1442
FPVS	1341	WTCLS	1443
FVP	1343	WTCS	1445
FVS	1344	WTICFX	1446
PIP	1371	WTR	1447
PIS	1372	WTVCFX	1448
PPV	67	WVP	1433
PSV	1554	WVS	1436
RHOLP	1476	XMWGP	1361
RHOLS	1373	XMWGS	1363
SPTG	136	XMWVP	1366
SPTL	1402	XMWVS	1368
SSTG	1606	YCP	1450
T	1404	YCS	1451
TPTG	1479	YIP	1452
TPTL	1408	YIS	1453
TT	1411	YPVS	1454
TSTG	1409	YVP	1455
TSTL	1410	YVS	1456
VLP	1412	ZP	144
VLS	1413	ZS	1614

Table F-5 Input Parameters Primary Tank

<u>Symbol</u>	<u>Definition</u>	<u>Units</u>
ACC	Acceleration	ft/sec ²
ALGP	Area, Liquid Surface Next to Gas, Primary Tank	ft ²
AV	Area, Injector Valve	ft ²
BETLP	Volumetric Coefficient of Thermal Expansion, Liquid Primary Tank	1/°R
BETVP	Volume Coefficient of Thermal Expansion, Primary Vapor	1/°R
CACP	Constant, Area of Combustion Equation, Primary Tank	--
CPPT	Heat Capacity, Primary Tank	Btu/lb _M °R
CDOF	Coefficient of Discharge, Orifice, Primary Tank	--
CDT	Constant, Time Increment Equation	--
CDV	Coefficient of Discharge, Injector Valve	--
CFGWP	Constant, Film Heat Transfer Coefficient Equation, Gas to Wall, Primary Tank	--
CFGLP	Constant, Film Heat Transfer Coefficient Equation, Gas Liquid, Primary Tank	--
CFLWP	Constant, Film Heat Transfer Coefficient Equation, Liquid to Wall, Primary Tank	--
CKQV	Constant, Dissociation Equation, Primary Tank	--
CMC	Constant, Combustion Zone to Liquid Heat Transfer Coefficient Equation	--
CPCLP	Heat Capacity Liquid from Combustion, Primary Tank	Btu/lb _M °R
CPCP	Specific Heat at Constant Pressure, Combustion Product in Gas, Primary Tank	Btu/lb _M °R
CPI	Specific Heat at Constant Pressure, Inert Gas	Btu/lb _M °R

Table F-5 (cont)

<u>Symbol</u>	<u>Definition</u>	<u>Units</u>
CPLP1	Constants, Specific Heat Equation, Liquid, Primary Tank	--
CPLP2	Constants, Specific Heat Equation, Liquid, Primary Tank	--
CPO	Constant, Printout Equation	--
CPR1	Constant in Heat Capacity Equation, Primary Reagent	--
CPR2	Constant in Heat Capacity Equation, Primary Reagent	--
CPTO	Constant, Surface, Outside/Inside, Primary Tank	--
CPVP	Specific Heat at Constant Pressure, Primary Vapor	Btu/lb _M °R
CRLP1	Constants, Density Equation, Liquid in Primary Tank	lb _M /ft ³
CRLP2	Constants, Density Equation, Liquid in Primary Tank	lb _M /ft ³ °R
CVAPP	Constant, Vaporization Equation, Primary Vapor	--
CWSP	Constant, Weight, Surface, Primary Tank	lb _M /ft ²
DOP	Diameter, Orifice, Primary Tank	ft
DPT	Diameter of Primary Tank	ft
DZPBDV	Change in Liquid Height with Respect to Volume, Primary Tank	--
HAP	Film Coefficient, Aerodynamic Heating, Primary Tank	Btu/ft ² sec °R
HLCLP	Heat of Vaporization, Liquid from Combustion, Primary Tank	Btu/lb _M
HVAPP	Heat of Vaporization, Primary Liquid	Btu/lb _M
OPBP	Option, Bleed Primary Tank	--
OPIP	Option, Injection Primary Tank	--

Table F-5 (cont)

<u>Symbol</u>	<u>Definition</u>	<u>Units</u>
OPPCP	Option, Pressure Sensor	--
OPTNK	Option, Tanks	--
OPVDP	Option, Vapor Dissociation, Primary Tank	--
PGP	Pressure, Gas, Primary Tank	$1b_F/in.^2$
PLIQ	Primary Liquid	--
PPH	Pressure Setting, Primary Tank, High	$1b_F/in.^2$
PPL	Pressure Setting, Primary Tank, Low	$1b_F/in.^2$
PPV	Pressure, Primary Vapor	$1b_F/in.^2$
PR	Pressure, Reagent	$1b_F/in.^2$
RCLP	Weight Ratio, Liquid to Total Products, Primary Reaction	--
RHOR	Density, Reactant	$1b_M/ft^3$
RMP	Reaction Mixture Weight Ratio, Primary Tank	--
RUNNO	Run Number	--
SPTG	Inside Surface, Primary Tank Next to Gas	ft^2
SPT	Inside Surface, Primary Tank	ft^2
T	Time	sec
TAWP	Temperature Adiabatic, Wall, Primary Tank	$^{\circ}R$
TFP	Adiabatic Flame Temperature, Reaction in Primary Tank	$^{\circ}R$
TGP	Temperature, Gas, Primary Tank	$^{\circ}R$
TI	Time, Initial	sec
TLP	Temperature, Liquid, Primary Tank	$^{\circ}R$
TR	Temperature, Reaction (Reference)	$^{\circ}R$
TRP	Temperature, Reactant, Primary Tank	$^{\circ}R$

Table F-5 (concl)

<u>Symbol</u>	<u>Definition</u>	<u>Units</u>
TT	Temperature	$^{\circ}\text{R}$
VDLOP	Volume Flow Rate, Liquid from Primary Tank	ft^3/sec
VGP	Volume Gas, Primary Tank	ft^3
VLPL	Volume Setting, Liquid, Primary Tank, Low	ft^3
VPT	Volume, Primary Tank	ft^3
XFGWP	Exponent, Film Heat Transfer Coefficient Equation, Gas to Wall, Primary Tank	--
XFGLP	Exponent, Film Heat Transfer Coefficient Equation, Gas to Liquid, Primary Tank	--
XFLWP	Exponent, Film Heat Transfer Coefficient Equation, Liquid to Wall, Primary Tank	--
XXCP	Thermal Conductivity, Combustion Products in Gas, Primary Tank	$\text{Btu}/\text{ft}^2\text{sec}^{\circ}\text{R}/\text{ft}$
XXI	Thermal Conductivity, Inert Gas	$\text{Btu}/\text{sec ft}^2 \text{ }^{\circ}\text{R}/\text{ft}$
XXLP	Thermal Conductivity, Liquid Primary Tank	$\text{Btu}/\text{sec ft}^2 \text{ }^{\circ}\text{R}/\text{ft}$
XXVP	Thermal Conductivity, Primary Vapor	$\text{Btu}/\text{sec ft}^2 \text{ }^{\circ}\text{R}/\text{ft}$
XMUCP	Viscosity, Combustion Products in Gas, Primary Tank	$\text{lb}_F\text{-sec}/\text{ft}^2$
XMUI	Viscosity, Inert Gas	$\text{lb}_F\text{-sec}/\text{ft}^2$
XMULP	Viscosity, Liquid, Primary Tank	$\text{lb}_F\text{-sec}/\text{ft}^2$
XMUVP	Viscosity, Primary Vapor	$\text{lb}_F\text{-sec}/\text{ft}^2$
XMWCP	Molecular Weight Combustion Products in Gas, Primary Tank	$\text{lb}_M/\text{lb-mole}$
XMWI	Molecular Weight, Inert Gas	$\text{lb}_M/\text{lb-mole}$
XMWVP	Molecular Weight, Primary Vapor	$\text{lb}_M/\text{lb-mole}$
ZP	Height of Liquid Above Pressure Sensor, Primary Tank	ft

Table F-6 Input Parameters Secondary Tank

<u>Symbol</u>	<u>Definition</u>	<u>Units</u>
ALGS	Area, Liquid Surface Next to Gas, Secondary Tank	ft ²
BETLS	Volumetric Coefficient of Thermal Expansion, Liquid, Secondary Tank	1/°R
BETVS	Volume Coefficient of Thermal Expansion, Secondary Vapor	1/°R
CACS	Constant, Area of Combustion Equation, Secondary Tank	--
GDOS	Coefficient of Discharge, Orifice, Secondary Tank	--
CFGLS	Constant, Film Heat Transfer Coefficient Equation, Gas to Liquid, Secondary Tank	--
CFGWS	Constant, Film Heat Transfer Coefficient Equation, Gas to Wall, Secondary Tank	--
CFLWS	Constant, Film Heat Transfer Coefficient Equation, Liquid to Wall, Secondary Tank	--
CKSV	Constant, Dissociation Equation, Secondary Vapor	--
CPCLS	Heat Capacity Liquid from Combustion, Secondary Tank	Btu/lb _M °R
CPCS	Specific Heat at Constant Pressure, Combustion Product in Gas, Secondary Tank	Btu/lb _M °R
CPLS1	Constants Specific Heat Equation, Liquid, Secondary Tank	--
CPLS2	Constants Specific Heat Equation, Liquid, Secondary Tank	--
CPST	Heat Capacity, Secondary Tank	Btu/lb _M °R
CPVS	Specific Heat at Constant Pressure, Secondary Vapor	Btu/lb _M °R
CRLS1	Constants, Density Equation, Liquid in Secondary Tank	--
CRLS2	Constants, Density Equation, Liquid in Secondary Tank	--

Table F-6 (cont)

<u>Symbol</u>	<u>Definition</u>	<u>Units</u>
CSTO	Constant, Surface, Outside/Inside, Secondary Tank	--
CVAPS	Constant, Vaporization Equation, Secondary Vapor	--
CWSS	Constant, Weight/Surface, Secondary Tank	lb_M/ft^2
DELPPS	Pressure Difference, Gas in Primary Less Gas in Secondary Tank, Minimum	$\text{lb}_F/\text{in.}^2$
DOS	Diameter, Orifice, Secondary Tank	ft
DST	Diameter, Secondary Tank	ft
DZSEBV	Change in Liquid Height with Respect to Volume, Secondary Tank	
HAS	Film Coefficient, Aerodynamic Heating, Secondary Tank	$\text{Btu}/\text{ft}^2\text{-sec}^\circ\text{R}$
HLCLS	Heat of Vaporization, Liquid Combustion Products, Secondary Tank	Btu/lb_M
HVAPS	Heat of Vaporization, Secondary Liquid	Btu/lb_M
OPBS	Option, Bleed, Secondary Tank	--
OPCS	Option, Combustion, Secondary Tank	--
OPIS	Option, Injection, Secondary Tank	--
OPPCS	Option, Pressure Sensor, Secondary Tank	--
OPVDS	Option, Vapor Dissociation, Secondary Tank	--
PGS	Pressure, Gas, Secondary Tank	$\text{lb}_F/\text{in.}^2$
PS	Pressure, Setting, Secondary Tank	$\text{lb}_F/\text{in.}^2$
PSV	Pressure, Secondary Vapor	$\text{lb}_F/\text{in.}^2$
RCLS	Weight Ratio, Liquid to Total Products, Secondary Reaction	--
RMS	Reaction Mixture Weight Ratio, Secondary Tank	--

Table F-6 (cont)

<u>Symbol</u>	<u>Definition</u>	<u>Units</u>
SLIQ	Secondary Liquid	--
SST	Inside Surface, Secondary Tank	ft ²
SSTG	Inside Surface, Secondary Tank Next to Gas	ft ²
TAWS	Temperature Adiabatic, Wall Secondary Tank	°R
TFS	Adiabatic Flame Temperature, Reaction in Secondary Tank	°R
TGS	Temperature of Gas, Secondary Tank	°R
TLS	Temperature of Liquid, Secondary Tank	°R
VGS	Volume of Gas, Secondary Tank	ft ³
VLSL	Volume Setting, Liquid, Secondary Tank, Low	ft ³
VDLOS	Volume Flow Rate, Liquid from Secondary Tank	ft ³
VST	Volume, Secondary Tank	ft ³
XFGLS	Exponent, Film Heat Transfer Coefficient Equation, Gas to Liquid, Secondary Tank	--
XFGWS	Exponent, Film Heat Transfer Coefficient Equation, Gas to Wall, Secondary Tank	--
XFLWS	Exponent, Film Heat Transfer Coefficient Equation, Liquid to Wall, Secondary Tank	--
XKCS	Thermal Conductivity, Combustion Products in Gas, Secondary Tank	Btu/sec ft ² -°R/ft
XKLS	Thermal Conductivity, Liquid, Secondary Tank	Btu/sec ft ² -°R/ft
XKVS	Thermal Conductivity, Secondary Vapor	Btu/sec ft ² -°R/ft

Table F-6 (concl)

<u>Symbol</u>	<u>Definition</u>	<u>Units</u>
XMUCS	Viscosity, Combustion Products in Gas, Secondary Tank	$1b_F\text{-sec/ft}^2$
XMULS	Viscosity of Liquid, Secondary Tank	$1b_F\text{-sec/ft}^2$
XMUVS	Viscosity of Secondary Vapor	$1b_F\text{-sec/ft}^2$
XMWCS	Molecular Weight, Combustion Products in Gas, Secondary Tank	$1b_M / \text{lb-mole}$
XMWSV	Molecular Weight of Secondary Vapor	$1b_M / \text{lb-mole}$
ZS	Height of Liquid Above Pressure Sensor, Secondary Tank	ft

D. PROGRAM OUTPUT

The first two to four pages of output will be a listing of the input data. The following page will be entitled either "Initial Conditions Primary Tank" or "Initial Conditions Secondary Tank" depending on whether the run is for a single or two-tank system. When the volume of the liquid in the tank(s) reaches a preset value, shutdown occurs. The printout continues until the liquid is removed from the tank(s). All of these pages are entitled MAIN TANK INJECTION PROPELLANT PRESSURIZATION SYSTEM PAGE _____. The last page for each run is a TABLE OF OUTPUT SYMBOLS which is so titled. If the run contains consecutive problems, then the above format is repeated for each case.

MAIN TANK INJECTION PROPELLANT PRESSURIZATION SYSTEM

C MAIN PROGRAM

```

COMMON A,C,R
DIMENSION A(1320),B(1130),C(180)
EQUIVALENCE (A(1),RUNNO),(A(2),PLIQ),(A(3),TI),(A(4),VPT),(A(5),VG
1P),(A(6),PGP),(A(7),TGP),(A(8),TLP),(A(9),CPU),(A(10),PPL),(A(11),
2PPH),(A(12),VLP1),(A(13),OPVDP),(A(14),OPIP),(A(15),OPBP),(A(16),O
3PTNK),(A(17),OPPCP),(A(18),DOP),(A(19),CDOP),(A(20),PR),
4(A(21),TRP),(A(22),RHCR),(A(23),AV),(A(24),CDV),(A(25),CPR1),
5(A(26),CPR2),(A(27),DPT),(A(28),SPT),(A(29),CWSP),(A(30),CPTU),
6(A(31),CPPT),(A(32),CACPI),(A(33),CHC),(A(34),CDT),(A(35),XFGWP),
7(A(36),CFGWP),(A(37),XFGLP),(A(38),CFGLP),(A(39),XFLWP),
8(A(40),CELWP),(A(41),RMP),(A(42),RCPI),(A(43),TEP),(A(44),TR),
9(A(45),XMWCP),(A(46),XKCP),(A(50),XMUCP),(A(54),CPCP)
EQUIVALENCE (A(58),HLCLP),(A(62),CPCLP),(A(66),XMWVP),(A(67),PPV),
1(A(71),CVAPP),(A(75),CKPV),(A(79),BETVP),(A(83),XKVP),
2(A(87),XMUVP),(A(91),CPVP),(A(95),HVAPP),(A(99),XMW1),
3(A(103),XKI),(A(104),XMUI),(A(108),CPI),(A(112),XKLP),
4(A(116),XMULP),(A(120),BETLP),(A(124),CPLP),(A(125),CP1),
5(A(126),CRLP1),(A(127),CRLP2),(A(128),ACC),(A(132),VDLUP),
6(A(136),SPTG),(A(140),ALGP),(A(144),ZP),(A(148),DZPBDV),
7(A(152),HAR),(A(156),TAWP),(A(160),OPAD)
EQUIVALENCE (C(1),CCP),(C(2),CF),(C(3),CGFX),(C(4),CPGP),(C(5),CPG
1S),(C(6),CPLP),(C(7),CPLS),(C(8),CYC),(C(9),DMBDT),(C(10),DPBDT),
2(C(11),DTTBDT),(C(12),DVAR1),(C(13),DVRT),(C(14),DWRDT),(C(15),E
3P),(C(16),FIS),(C(17),FISFX),(C(18),FCP),(C(19),FCS),(C(20),FCSFX)
4(C(21),FPVS),(C(22),FPVSFX),(C(23),FVP),(C(24),FVS),(C(25),FVSFX)
5(C(26),FCPEX),(C(27),FPEX),(C(28),FVPEX),(C(29),HCP),(C(30),HCS)
6(C(31),HF),(C(32),HGS),(C(33),HGP),(C(34),HI),(C(35),HSCLP),(C(36
7),HSCLS),(C(37),HVPG),(C(38),HVSG),(C(39),XKGF), (C(41
8),XMWGP),(C(42),XMWGF),(C(43),XMWGS),(C(44),XMWGS2),(C(45),XMWVP)
9),(C(46),XMWVP),(C(47),XMWVP1),(C(48),XMWVS),(C(49),XMWVS1)
EQUIVALENCE (C(51),PIP),(C(52),PIS),(C(53),RHOLS),(C(
154),PTP),(C(155),PTS),(C(156),QDCLP),(C(157),QDCLS),(C(158),QDGLP),(C(
259),QDGLS),(C(160),QDGGP),(C(161),QDQOS),(C(162),QDGS),(C(163),QDQWP),
3(C(164),QDQWS),(C(165),QDLQP),(C(166),QDLOS),(C(167),QDLPC),(C(168),QDL
4BR),(C(169),QDLSC),(C(170),QDLWP),(C(171),QDLWS),(C(172),QDQGR),(C(173)
5,QDQPR),(C(174),QDQPR),(C(175),QDQSPC),(C(176),QDQSR),(C(177),QDQSSC),(C(17
68),QDWP),(C(179),QDWS),(C(182),SPTL),(C(183
7),SSTL),(C(184),T),(C(185),TECP),(C(186),TECS),(C(187),TGS2),(C(188),TP
8TL),(C(189),TSTG),(C(190),TSTL),(C(191),TT),(C(192),VLP),(C(193),VLS),
9(C(194),VLP2),(C(195),VLS2)
DEQUIVALENCE (C(196),WDBP),(C(197),WDWS),(C(198),WDCFX),(C(199),WDGLP),
1(C(100),WDCLS),(C(101),WDCP),(C(102),WCP2),(C(103),WDCS),(C(104),
2WCS2),(C(105),WGS),(C(106),WIP),(C(107),WIP2),(C(108),WIS),(C(1
39),WIS2),(C(110),WRVS2),(C(111),WDR),(C(112),WSTG2),(C(113),WVP),
4(C(114),WDVP),(C(115),WVP2),(C(116),WVS),(C(117),WDVS),(C(118),WVS
52),(C(119),WFCLP),(C(120),WFCLS),(C(121),WTCCF),(C(122),WTCLP),(C(
123),WTCLS),(C(124),WTCP),(C(125),WTCS),(C(126),WTICFX),(C(127),WT
7R),(C(128),WTVCFX),(C(129),XF),(C(130),YCP),(C(131),YCS),(C(132),
8YIP),(C(133),YIS),(C(134),YPVS),(C(135),YVP),(C(136),YVS),(C(137),
9WETGX),(C(138),GANGP),(C(139),GANGS)
DEQUIVALENCE (C(141),DELOGP),(C(142),DELOGS),(C(143),DELQLP),(C(144
1),DELQLS),(C(145),DELOWP),(C(146),DELOWS),(C(147),DELT),(C(148),DE
2LTFX),(C(149),DEWCLS),(C(150),DELWVP),(C(151),DELWVS),(C(152),XNUG
3FX),(C(153),XMUGS),(C(154),RHOGFX),(C(155),PG52),(C(156),RHOLP)
EQUIVALENCE (C(157),WCP),(C(158),WCS)
EQUIVALENCE (C(159),TRTG),(C(160),WGP),(C(161),CPD2)
EQUIVALENCE (C(162),WPVS),(C(163),XMWVPVS),(C(164),WTCCFX)
EQUIVALENCE (C(165),WPTG),(C(166),WSTG)
EQUIVALENCE (B(1),SLD),(B(2),VST),(B(3),VGS),(B(4),PGS)

```

```

1(B(5),TGS),(B(6),TLS),(B(7),DELPPS),(B(8),PS),(B(9),VLSL),
2(B(10),OPVDS),(B(11),CPIS),(B(12),OPBS),(B(13),OPCS),
3(B(14),OPPCS),(B(15),DOS),(B(16),CDO),(B(17),DST),(B(18),SST),
4(B(19),CWSS),(B(20),CSTO),(B(21),CPST),(B(22),CACS),(B(23),XFGWS),
5(B(24),CFGWS),(B(25),XFGLS),(B(26),CFGLS),(B(27),XFLWS),
6(B(28),CFLWS),(B(29),RMS),(B(30),RCLS),(B(31),TES),(B(32),XWWS),
7(B(33),XKCS),(B(37),XMUCS),(B(41),CPCS),(B(45),HLCLS),
8(B(49),CPCLS),(B(53),XMWSV),(B(54),PSV),(B(58),CVAPS),
9(B(62),CKSV),(B(66),BETVS),(B(70),XKVS),(B(74),XWWS),
EQUIVALENCE(B(78),CPVS),(B(82),HVAPS),(B(86),XKLS),(B(90),XMULS),
1(B(94),BETLS),(B(98),CPLS1),(B(99),CPLS2),(B(100),CRLS1),
2(B(101),CRLS2),(B(102),VDLOS),(B(106),SSTG),(B(110),ALGS),
3(B(114),ZS),(B(118),DZSRDV),(B(122),HAS),(B(126),TAWS)
1 CALL FORTN2(M)
IF(OPTNK) 3,3,2
2 CALL FORTN2(M)
CALL ICST
3 CALL ICPT
L = 0
NP = 2
IF(OPAD) 12,12,4
4 CALL FORTN2(M)
12 I1 = T +.9
I2 = TGP +.9
I3 = TPTG+.9
I4 = TLP +.9
I5 = TPTL +.9
IF(L = 54) 51,50,50
50 WRITE OUTPUT TAPE 10, 110, NP
L = 0
NP = NP + 1
51 WRITE OUTPUT TAPE 10,1312,11,CYC,12,13,14,15,PGP,PTP,XMWGP,VGP,YCP
1,YVP,WFCPL,WTR
L = L + 6
13 IF(OPTNK) 18,18,14
14 IF(IT) 17,17,15
15 CALL NCST
IF(IT-CPO2) 18,16,16
16 CPO2 = CPO2 + CPO
17 I1 = TGS +.9
I2 = TSTG +.9
I3 = TLS +.9
I4 = TSTL +.9
IF(L = 54) 53,52,52
52 WRITE OUTPUT TAPE 10, 110, NP
L = 0
NP = NP + 1
53 WRITE OUTPUT TAPE 10,1428, I1,12,13,14,PGS,PTS,XMWGS,VGS,YCS,YVS,
1YPVS,WFCLS
L = L + 6
C SHUTDOWN
18 IF(OPIP) 19,19,21
19 IF(PGP +2P*ACC*RHOLD/4633. -PPH) 20,25,25
20 IF(PGP +2P*ACC*RHOLD/4633. -DPL) 25,25,21
21 IF(VLP-VLPL) 25,23,22
22 IF(OPTNK) 23,23,24
23 WDCFX = 0.
GO TO 31
24 IF(VLS-VLSL) 25,25,?
25 I1 = T +.9
I2 = TGP +.9
I3 = TPTG +.9
I4 = TLP +.9
I5 = TPTL +.9
IF(L = 54) 55,54 ,54

```

```

54  WRITE OUTPUT TAPE 10, 110, NP
    NP = NP + 1
    L = 0
55  WRITE OUTPUT TAPE 10, 1507, 11, CYC, 12, 13, 14, 15, PGP, PTP, XMWGP, YGP
    1, YCP, YVP, WFCLP, WTR, WTCLP
    L = L + 6
26  IF(OPTNK) 27, 27, 26
    I1 = TGS + .9
    I2 = TSTG + .9
    I3 = TLS + .9
    I4 = TSTL + .9
    IF(L = 54) 57, 56, 56
56  WRITE OUTPUT TAPE 10, 1, 0, NP
    NP = NP + 1
    L = 0
57  WRITE OUTPUT TAPE 10, 1508, 11, 12, 13, 14, PGS, PTS, XMWGS, VGS, YCS, YVS,
    1, YPV, WFCLS, WICS, WTCLS, WTVCFX, WTCCFX, WTICFX
    L = L + 6
C   FINAL POLYTROPIC EXPULSION
27  IF(VLPL) 29, 29, 28
28  AV = 0.
    OPIP = 0.
    CCP = 0.
    VLPL = 0.
    VLSL = 0.
    PPL = 0.
    IF(OPTNK) 23, 23, 30
29  WRITE OUTPUT TAPE 10, 40
    WRITE OUTPUT TAPE 10, 41
    WRITE OUTPUT TAPE 10, 42
    WRITE OUTPUT TAPE 10, 43
    GO TO 1
C   SECONDARY TANK CALCULATIONS
30  CALL HTST
    CALL CRST
    CALL BDCST
    CALL GCST
C   PRIMARY TANK CALCULATIONS
31  CALL DCPT
    CALL HIPT
    CALL EVPT
    CALL CRPT
C   TIME INCREMENT
    CALL TINC
    IF(SENSE LIGHT 1) 44, 47
44  I1 = T + .9
    I2 = TGP + .9
    I3 = TPTG + .9
    I4 = TLP + .9
    I5 = TPTL + .9
    WRITE OUTPUT TAPE 10, 1312, 11, CYC, 12, 13, 14, 15, PGP, PTP, XMWGP, YGP, YCP
    1, YVP, WFCLP, WTR
    IF(OPTNK) 45, 46, 45
45  I1 = TGS + .9
    I2 = TSTG + .9
    I3 = TLS + .9
    I4 = TSTL + .9
    WRITE OUTPUT TAPE 10, 1428, 11, 12, 13, 14, PGS, PTS, XMWGS, VGS, YCS, YVS,
    1, YPV, WFCLS
46  WRITE OUTPUT TAPE 10, 100
100  FORMAT(25X, 39H) CASE TERMINATED 5 CONSECUTIVE DELT = 0. / 1H)
    GO TO 1
47  CALL NCPT
    IF(T = CPO2) 13, 32, 32

```

32 IF(OPTNK) 33,33,12

33 CPO2 = CPO2 + CPO

GO TO 12

110 FORMAT(1H110X,52HMAIN TANK INJECTION PROPELLANT PRESSURIZATION SYS
ITEM30X,4HPAGE14////)

1312 FORMAT(6X,10ZHT CYC TGP IPTG TLP TPTL PGP

1 PTP MWGP VGP YCP YVP WFCLP WTR//5X,14,3X,
2F7,1,4(3X,14),2(3X,F5,1),3X,F7,3,3X,F5,1,3(3X,F5,3),3X,F7,3////)

1428 FORMAT(9X,10ZHTGS TSTG TLS TSTL PGS PTS M

1WGS VGS YCS YVS YPVS WFCL3//5X,4(4X,14),2(1
24X,F5,1),4X,F7,3,4X,F5,1,4(4X,F5,3)////)

1507 FORMAT(55X,8HSHUTDOWN////)

1 11X, 98HT CYC TGP TPTG TLP TPTL PGP PTP MWGP

1 VGP YCP YVP WFCLP WTR WTCP WTCLP//

2(14,4X,F7,1,4(4X,14),2(4X,F5,1),X,F7,3,X,F5,0,3(4X,F5,3),3(4X,F7,3)////)

1508 FORMAT(113H TGS TSTG TLS TSTL PGS PTS MWGS VGS YCS

1 YVS YPVS WFCLS WTCS WTCLS WTVCF WTCLF WTICF//5X,4(4X
2,14),2(4X,F5,1),X,F7,3,X,F5,0,4(4X,F5,3),5(4X,F7,3)////)

40 FORMAT(1H1746X,28HDICTIONARY OF OUTPUT SYMBOLS//12X,3HCYC12X,36HC

1UMULATIVE NUMBER OF TIME INCREMENTS/12X,4HWP11X,30HMOLECULAR WLI

2GHT, GAS, P, TANK/12X,4HMWGS11X,30HMOLECULAR WEIGHT, GAS, S, TANK/

312X,4HOPBP11X,22HOPTION, BLEED, P, TANK/12X,4HOPBS11X,22HOPTION, B

4LEED, S, TANK/12X,4HOPCS11X,27HOPTION, COMBUSTION, S, TANK/12X,4HO

5PIP11X,26HOPTION, INJECTION, P, TANK/12X,4HOPIS11X,26HOPTION, INJE

6CTION, S, TANK/12X,5HOPPCS10X,32HOPTION, PRESSURE SENSOR, S, TANK/

712X,5HOPPCP10X,32HOPTION, PRESSURE SENSOR, P, TANK/12X,5HOPVDP10X,

836HOPTION, VAPOR DISSOCIATION, P, VAPOR/12X,5HOPVUS10X,35HOPTION,V

9APOR DISSOCIATION, S, VAPOR)

41 FORMAT(12X,3HPGP12X,22HMPRESSURE, GAS, P, TANK/12X,3HPGS12X,22HPRES

1SURE, GAS, S, TANK/12X,5HP LIQ10X,14HPRIMARY LIQUID/12X,3HPTP12X,2

23HTOTAL PRESSURE, P, TANK/12X,3HPPTS12X,23HTOTAL PRESSURE, S, TANK/

312X,4HRCLP11X,51HWEIGHT RATIO, LIQUID TO TOTAL PRODUCTS, P, REACTIO

4N/12X,4HRCLS11X,51HWEIGHT RATIO, LIQUID TO TOTAL PRODUCTS, S, REAC

5TION/12X,3HRMP12X,38HREACTION MIXTURE WEIGHT RATIO, P, TANK/12X,3H

6RMS12X,38HREACTION MIXTURE WEIGHT RATIO, S, TANK/12X,5HRUNNO10X,1

7HRUN NUMBER/12X,1HT14X,4HTIME/12X,3HTF12X,48HADADIABATIC FLAME TEM

8ERATURE, REACTION IN P, TANK/12X,3HTFS12X,48HADADIABATIC FLAME TEMPE

9RATURE, REACTION IN S, TANK/12X,5HS.LIQ10X,16HSECONDARY LIQUID)

42 FORMAT(12X,3HTGP12X,25HTEMPERATURE, GAS, P, TANK/12X,3HTGS12X,25HT

1TEMPERATURE, GAS, S, TANK/12X,3HTLP12X,28HTEMPERATURE, LIQUID, P, T

2ANK/12X,3HTLS12X,28HTEMPERATURE, LIQUID, S, TANK/12X,4HTPTG11X,32H

3TEMPERATURE, P, TANK NEXT TO GAS/12X,4HTPTL11X,35HTEMPERATURE, P,

4TANK NEXT TO LIQUID/12X,4HTSTG11X,32HTEMPERATURE, S, TANK NEXT TO

5GAS/12X,4HTSTL11X,35HTEMPERATURE, S, TANK NEXT TO LIQUID/12X,3HYGP

612X,20HVOLUME, GAS, P, TANK/12X,3HVG12X,20HVOLUME, GAS, S, TANK/

712X,5HWFCLP10X,48HWEIGHT FRACTION, LIQUID FROM COMB/LIQUID P, TANK

8/12X,5HWFCLS10X,48HWEIGHT FRACTION, LIQUID FROM COMB/LIQUID P, TAN

9K/12X,5HWTCCF10X,41HTOTAL WEIGHT, COMB PRODUCTS IN CROSS FLOW)

43 FORMAT(12X,5HWTCLP10X,39HTOTAL WEIGHT, LIQUID FROM COMB, P, TANK/1

12X,5HWTCLS10X,39HTOTAL WEIGHT, LIQUID FROM COMB, S, TANK/12X,4HWTCL

2P11X,35HTOTAL WEIGHT GAS FROM COMB, P, TANK/12X,4HWTCS11X,42HTOTAL

3 WEIGHT COMB PRODUCTS IN GAS, S, TANK/12X,5HWTICF10X,22HINERT GAS

4 IN CROSSFLOW/12X,3HWTR12X,22HTOTAL WEIGHT, REACTANT/12X,5HWTVCF10X

5,32HTOTAL WEIGHT, VAPOR IN CROSSFLOW/12X,3HYCP12X,44HMOLE FRACTION

6, COMB PRODUCTS IN GAS, P, TANK/12X,3HYCS12X,44HMOLE FRACTION, COM

7B PRODUCTS IN GAS, S, TANK/12X,4HYVPS11X,39HMOLE FRACTION, P, VAPO

8R IN GAS, S, TANK/12X,3HYVP12X,36HMOLE FRACTION, VAPOR IN GAS, P,

9TANK/12X,3HYVS12X,36HMOLE FRACTION, VAPOR IN GAS, S, TANK/1H1)

END

~~C~~ INITIAL CONDITIONS SECONDARY TANK
 SUBROUTINE ICST
 COMMON A,C,B
 DIMENSION A(1320),B(1130),C(180)
 EQUIVALENCE (A(1),RUNNU),(A(2),PLIQ),(A(3),TI),(A(4),VPT),(A(5),VGV
 1P),(A(6),PGP),(A(7),TGP),(A(8),TLP),(A(9),CPU),(A(10),PPL),(A(11),
 2PPH),(A(12),VLR),(A(13),OPVDR),(A(14),OPIR),(A(15),ORHR),(A(16),O
 3PTNK),(A(17),OPPCP),(A(18),DOP),(A(19),CDOP),(A(20),PR),
 4(A(21),TRP),(A(22),RHCR),(A(23),AV),(A(24),CDV),(A(25),CPR1),
 5(A(26),CPR2),(A(27),DPTL),(A(28),SPT),(A(29),CWSB),(A(30),CPTO),
 6(A(31),CPPT),(A(32),CACP),(A(33),CHC),(A(34),CDT),(A(35),XFGWP),
 7(A(36),CFGWF),(A(37),XFGLP),(A(38),CFGLP),(A(39),XFLWP),
 8(A(40),CFLWP),(A(41),RMP),(A(42),RCLP),(A(43),TEP),(A(44),TR),
 9(A(45),XMWCP),(A(46),XKCP),(A(50),XMUCP),(A(54),CPCP)
 EQUIVALENCE(A(58),HLCLP),(A(62),CPCLP),(A(66),XMKPV),(A(67),PPV),
 1(A(71),CVAPP),(A(75),CKPV),(A(79),BETVP),(A(83),XKVP),
 2(A(87),XMUVP),(A(91),CPVP),(A(95),HVAPP),(A(99),Xmw1),
 3(A(104),XKI),(A(104),XMUI),(A(108),CPI),(A(112),XKLP),
 4(A(116),XMULP),(A(120),BETLP),(A(124),CPLP1),(A(125),CPLP2),
 5(A(126),CRLP1),(A(127),CRLP2),(A(128),ACCI),(A(132),VDLOP),
 6(A(136),SPTG),(A(140),ALGP),(A(144),ZP),(A(148),DZPHDV),
 7(A(152),HAP),(A(156),TAWP)
 EQUIVALENCE(C(1),CCP),(C(2),CF),(C(3),CPGFX),(C(4),CPGP),(C(5),CPG
 1S),(C(6),CPLP),(C(7),CPLS),(C(8),CYC),(C(9),DMHDT),(C(10),DPBDT),
 2(C(11),DTTBDT),(C(12),DVAR1),(C(13),DVRT1),(C(14),DWRDT),(C(15),E1
 3P),(C(16),FIS),(C(17),FISFX),(C(18),FCP),(C(19),FCS),(C(20),FC5FX)
 4,(C(21),FPVS),(C(22),FPVSFX),(C(23),FVP),(C(24),FVS),(C(25),FV5FX)
 5,(C(26),FCPEX),(C(27),FIPFX),(C(28),FVPEX),(C(29),HCP),(C(30),HCS)
 6,(C(31),HF),(C(32),HGS),(C(33),HGP),(C(34),HI),(C(35),HSCLP),(C(36
 7),HSCLS),(C(37),HVP),(C(38),HVS),(C(39),XKGF),(C(41
 8),XMWGP),(C(42),XMWGF),(C(43),XMWGS),(C(44),XMWGS2),(C(45),XMWV1
 9),(C(46),XMWVP),(C(47),XMWVP1),(C(48),XMWVS),(C(49),XMWVS1)
 EQUIVALENCE (C(51),PIP),(C(52),PIS),(C(53),RHOLS),(C(1
 154),PIP),(C(155),PTS),(C(156),QDCLP),(C(157),QDCLS),(C(158),QDGLP),(C(1
 259),QDGLS),(C(160),QDGP),(C(161),QDGOS),(C(162),QDGS),(C(163),QDGP,
 3(C(164),QDGLS),(C(165),QDLOP),(C(166),QDLOS),(C(167),QDLPC),(C(168),QDL
 4PR),(C(169),QDLSCR),(C(170),QDLWPI),(C(171),QDLW),(C(172),QDGPGR),(C(173)
 5,QDPR),(C(174),QDRFR),(C(175),QDSPC),(C(176),QDSR),(C(177),QDSSCI),(C(17
 68),QDWP),(C(179),QDWS), (C(182),SPTL),(C(183
 7),SSTL),(C(184),T),(C(185),TECP),(C(186),TFCS),(C(187),TGS2),(C(188),TP
 8TL),(C(189),TSTG),(C(190),TSTL),(C(191),TT),(C(192),VLP),(C(193),VLS),
 9(C(194),VLP2),(C(195),VLS2)
 0EQUIVALENCE (C(196),WDBP),(C(197),WDBS),(C(198),WDCFX),(C(199),WDCLP),
 1(C(100),WDCLS),(C(101),WDCP),(C(102),WCP2),(C(103),WDCS),(C(104),
 2WCS2),(C(105),WGS),(C(106),WIP),(C(107),WIP2),(C(108),WIS),(C(1
 39),WIS2),(C(110),WVVS2),(C(111),WDB),(C(112),WSTG2),(C(113),WVP),
 4(C(114),WDVP),(C(115),WVP2),(C(116),WVS),(C(117),WDVS),(C(118),WVS
 52),(C(119),WFCLP),(C(120),WFCLS),(C(121),WTCCF),(C(122),WTCLP),(C(1
 6123),WTCLS),(C(124),WTCLP),(C(125),WTCS),(C(126),WTCEX),(C(127),WT
 7R),(C(128),WTVCFX),(C(129),XF),(C(130),YCP),(C(131),YCS),(C(132),
 8YIP),(C(133),YIS),(C(134),YPVS),(C(135),YVP),(C(136),YVS),(C(137),
 9BETGEX),(C(138),GANGP),(C(139),GANGS)
 0EQUIVALENCE (C(141),DELOGP),(C(142),DELOGS),(C(143),DELQLP),(C(144
 1),DELQLS),(C(145),DELOWP),(C(146),DELOWS),(C(147),DELT),(C(148),DE
 2LTFX),(C(149),DEWCLS),(C(150),DEWVWP),(C(151),DEWVVS),(C(152),XMUG
 3FX),(C(153),XMUGS),(C(154),RHOGFX),(C(155),PGS2),(C(156),RHOLP)
 EQUIVALENCE (C(157),WCP),(C(158),WCS)
 EQUIVALENCE (C(159),TPTG),(C(160),WGP),(C(161),CPO2)
 EQUIVALENCE (C(162),WPVS),(C(163),XMWVVS),(C(164),WTCCFX)
 EQUIVALENCE (C(165),WPTG),(C(166),WSTG)
 EQUIVALENCE (B(1),SLIQ),(B(2),VST),(B(3),VGS),(B(4),PGS),
 1(B(5),TGS),(B(6),TLS),(B(7),DELPPS),(B(8),PS),(B(9),VLSL),
 2(B(10),OPVDS),(B(11),OPIS),(B(12),OPBS),(B(13),OPCS),
 3(B(14),OPPCS),(B(15),DUS),(B(16),CDUS),(B(17),DST),(B(18),SST),

```

4(B(19),CWSS),(B(20),CSTO),(B(21),CPST),(B(22),CACS),(B(23),XFGWS),
5(B(24),CFGWS),(B(25),XFGLS),(B(26),CFGLS),(B(27),XFLWS),
6(B(28),CFLWS),(B(29),RMS),(B(30),RCLS),(B(31),TFS),(B(32),XMWCS),
7(B(33),XKCS),(B(37),XMUCS),(B(41),CPCS),(B(45),HLCLS),
8(B(49),CPCLS),(B(53),XMWSV),(B(54),PSV),(B(58),CVAPS),
9(B(62),CKSV),(B(66),RFTVS),(B(70),XKVS),(B(74),XNIUS),
EQUIVALENCE(B(78),CPVS),(B(82),HVAPS),(B(86),XKLS),(B(90),XMULS),
1(B(94),BETLS),(B(98),CPLS1),(B(99),CPLS2),(B(100),CRLS1),
2(B(101),CRLS2),(B(102),VDLOS),(B(106),SSTG),(B(110),ALGS),
3(B(114),ZS),(B(118),DZSRDV),(B(122),HAS),(B(126),TAWS)
TSTG = TGS
TSTL = TLS
RHOLS = CRLS1+ CRLS2*TLS
VLS = VST - VGS
CALL TABS(VGS,ZS,1615)
CALL TABS(VGS,SSTG,1607)
WSTG = SSTG*CWSS
SSTL = SST - S5TG
WTCLS = 0.
WFCLS = 0.
WTVCFX = 0.
WTCCFX = 0.
WTICFX = 0.
WTCS = 0.
TT = TLS
CALL TABS(TT,PSV,1555)
CALL TABS(TT,CVAPS,15*9)
PIS = PGS - CVAPS*PSV
WIS = PIS*VGS*XMWI/(10.73*TGS)
WCS = 0.
IF(OPVDS) 301,301,302
301 XMWVS = XMWSV
GO TO 303
302 TT = TGS
CALL TABS(TT,CKSV,1562)
XMWVS = XMWSV/(1. +1./SQRT(1.+4.*CKSV*CVAPS*PSV))
303 WVS = CVAPS*PSV*VGS*XMWVS/(10.73*TGS)
WGS = WVS + WIS
FVS = WVS/WGS
FIS = 1. - FVS
FCS = 0.
FRVS = 0.
WPVS = 0.
XMWPVS = XMWVP
XMWGS = WGS/(WVS/XMWVS + WIS/XMWI)
YVS = FVS*XMWGS/XMWVS
YIS = 1. - YVS
YRVS = 0.
YCS = 0.
I1 = TFS +.9
I2 = OPIS +.9
I3 = OPVDS +.9
I4 = OPBS +.9
I5 = OPCS
I6 = OPPCS
CALL TABS (I,ACC,129)
RTS = PGS + ZS*RHOLS*ACC/4633.
WRITE OUTPUT TAPE 10,304,SLIQ,RMS,RCLS,I1,I2,I3,I4,I5,I6
304 FORMAT(///43X,34HINITIAL CONDITIONS SECONDARY TANK//17X,85HS,L1Q
1 RMS RCLS TFS OPIS OPVDS OPBS 0
2PCS OPPCS//17X,A6,2(5X,F5.1),5X,I4,5(5X,I5)////)
RETURN
END

```

```

C INITIAL CONDITIONS PRIMARY TANK
SUBROUTINE ICPT
COMMON A,C,B
DIMENSION A(1320),R(1130),C(180)
EQUIVALENCE (A(1),RUNNO),(A(2),PLIQ),(A(3),TI),(A(4),VPT),(A(5),VG
1P),(A(6),PGP),(A(7),TGP),(A(8),TLP),(A(9),CPO),(A(10),PPL),(A(11),
2PRH),(A(12),VLR),(A(13),OPVDP),(A(14),OPIP),(A(15),OPBP),(A(16),O
3PTNK),(A(17),OPPCP),(A(18),DOP),(A(19),CDOP),(A(20),PR),
4(A(21),TRP),(A(22),RHCR),(A(23),AV),(A(24),CDV),(A(25),CPR1),
5(A(26),CPR2),(A(27),DPT),(A(28),SPT),(A(29),CWSP),(A(30),CPTO),
6(A(31),CPPT),(A(32),CACP),(A(33),CHC),(A(34),CDT),(A(35),XFGWP),
7(A(36),CFGWP),(A(37),XFLGP),(A(38),CFGLP),(A(39),XFLWP),
8(A(40),CFLWP),(A(41),RMP),(A(42),RCLP),(A(43),TEP),(A(44),TR),
9(A(45),XWVCP),(A(46),XKCP),(A(50),XMUCP),(A(54),CPCP)
EQUIVALENCE (A(58),HLCLP),(A(62),CPLCP),(A(66),XWVPV),(A(67),PPV),
1(A(71),CVAPP),(A(75),CKPV),(A(79),BETVP),(A(83),XKVP),
2(A(87),XMUVV),(A(91),CPVP),(A(95),HVAPP),(A(99),XMWI),
3(A(103),XKI),(A(104),XMUI),(A(108),CPI),(A(112),XKLP),
4(A(116),XMULP),(A(120),BETLP),(A(124),CPLP1),(A(125),CPLP2),
5(A(126),CRLP1),(A(127),CRLP2),(A(128),ACC),(A(132),VDLUP),
6(A(136),SPTG),(A(140),ALGP),(A(144),ZP),(A(148),DZPRDV),
7(A(152),HAP),(A(156),TAWP)
EQUIVALENCE (C(1),CCP),(C(2),CF),(C(3),CPGFX),(C(4),CPGP),(C(5),CPG
1S),(C(6),CPLP),(C(7),CPLS),(C(8),CYC),(C(9),DMBDT),(C(10),DPBDT),
2(C(11),DTBBDT),(C(12),DVARI),(C(13),DVBDT),(C(14),DWBDDT),(C(15),F
3P),(C(16),FIS),(C(17),FISFX),(C(18),FCP),(C(19),FCS),(C(20),FCSFX)
4,(C(21),FPVS),(C(22),FPVSFX),(C(23),FVP),(C(24),FVS),(C(25),FVSFX)
5,(C(26),FCPEFX),(C(27),EIPFX),(C(28),FVPEFX),(C(29),HCP),(C(30),HCS)
6,(C(31),HF),(C(32),HGS),(C(33),HGP),(C(34),HI),(C(35),HSCLP),(C(36
7),HSCLS),(C(37),HVP),(C(38),HMSG),(C(39),XKGF), (C(41
8),XMWGP),(C(42),XMWGF),(C(43),XNWGS),(C(44),XMWGS2),(C(45),XMWVPV)
9),(C(46),XWVVP),(C(47),XWVVP1),(C(48),XWVVS),(C(49),XWVVS1)
EQUIVALENCE (C(51),PIP),(C(52),PIS),(C(53),RHOLS),(C(
134),PTP),(C(55),PTS),(C(56),QDCLP),(C(57),QDCLS),(C(58),QDGLP),(C(
759),QDGLS),(C(60),QDQOP),(C(61),QDQOS),(C(62),QDQGS),(C(63),QDQWP),
3(C(64),QDQWS),(C(65),UDLOP),(C(66),QDLOS),(C(67),QDLPC),(C(68),QDL
4PR),(C(69),QDLSC),(C(70),QDLWP),(C(71),QDLWS),(C(72),QDPGR),(C(73)
5,QDPR),(C(74),QDRPR),(C(75),QDSPC),(C(76),QDSR),(C(77),QDSSC),(C(7
68),QDWP),(C(79),QDWS), (C(82),SPTL),(C(83
7),SSTL),(C(84),T),(C(85),TECP),(C(86),TECS),(C(87),TGS2),(C(88),TP
8TL),(C(89),TSTG),(C(90),TSTL),(C(91),TT),(C(92),VLP),(C(93),VLS),
9(C(94),VLP2),(C(95),VLS2)
EQUIVALENCE (C(96),WDBP),(C(97),WDBS),(C(98),WDCFX),(C(99),WDCLP),
1(C(100),WDCLS),(C(101),WDQP),(C(102),WCP2),(C(103),WDQS),(C(104),
2WCS2),(C(105),WGS),(C(106),WIP),(C(107),WIP2),(C(108),WIS),(C(1
39),WIS2),(C(110),WVVS2),(C(111),WDR),(C(112),WSTG2),(C(113),WVP)
4(C(114),WDVP),(C(115),WVP2),(C(116),WVS),(C(117),WDVS),(C(118),WVS
52),(C(119),WFCLP),(C(120),WFCLS),(C(121),WTCCF),(C(122),WTCLP),(C(
6123),WTCLS),(C(124),WTCP),(C(125),WTCS),(C(126),WTICFX),(C(127),WT
7R),(C(128),WTVCFX),(C(129),XF),(C(130),YCP),(C(131),YCS),(C(132),
8YIP),(C(133),YIS),(C(134),YVS),(C(135),YVP),(C(136),YVS),(C(137),
9BETGFX),(C(138),GAMGP),(C(139),GAMGS)
EQUIVALENCE (C(141),DELQGP),(C(142),DELOGS),(C(143),DELQLP),(C(144
1),DELQLS),(C(145),DELQWP),(C(146),DELQWS),(C(147),DELT),(C(148),DE
2LTFX),(C(149),DENCLS),(C(150),DELWVP),(C(151),DELWVS),(C(152),XMUG
3FX),(C(153),XMUGS),(C(154),RHOGFX),(C(155),PGS2),(C(156),RHOLP)
EQUIVALENCE (C(157),WCP),(C(158),WCS)
EQUIVALENCE (C(159),TPTG),(C(160),WGP),(C(161),CPO2)
EQUIVALENCE (C(165),WPTG),(C(166),WSTG)
EQUIVALENCE (B(1),SLIQ),(B(2),VST),(B(3),VGS),(B(4),PGS),
1(B(5),TGS),(B(6),TLS),(B(7),DELPPS),(B(8),PS),(B(9),VLSL),
2(B(10),OPVDS),(B(11),CPIS),(B(12),OPBS),(B(13),OPCS),
3(B(14),OPPCS),(B(15),DOS),(B(16),CDOS),(B(17),DST),(B(18),SST),
4(B(19),CWSS),(B(20),CSTO),(B(21),CPST),(B(22),CACS),(B(23),XFGWS),
5(B(24),CFGWS),(B(25),XFGLS),(B(26),CFGLS),(B(27),XFLWS),
6(B(28),CFLWS),(B(29),RMS),(B(30),RCLS),(B(31),TFS),(B(32),XMWCS),
7(B(33),XKCS),(B(37),XMUCS),(B(41),CPCS),(B(45),HLCLS)

```

```

8(B(49),CPCLS),(B(53),XMWSV),(B(54),PSV),(B(58),CVAPS),
9(B(62),CKSV),(B(66),BETVS),(B(70),XKVS),(B(74),XMUVS)
EQUIVALENCE(B(78),CPVS),(B(82),HVAPS),(B(86),XKLS),(B(90),XMULS),
1(B(94),BETLS),(B(98),CPLS1),(B(99),CPLS2),(B(100),CRLS1),
2(B(101),CRLS2),(B(102),VDLOS),(B(106),SSTG),(B(110),ALGS),
3(B(114),ZS),(B(118),DZSDV),(B(122),HAS),(B(126),TAW)
T = TI
TPTG = TGP
TPTL = TLP
RHOLP = CRLP1,CRLP2*TLP
VLP = VPT - VGP
CALL TABS(VGP,ZP,145)
CALL TABS(T,ACC,129)
CALL TABS(VGP,SPTG,137)
WPTG = SPTG*CWSP
SPTL = SPT - SPTG
WTCLP = 0.
WTCR = 0.
WFCLP = 0.
WTR = 0.
TT = TLP
CALL TABS(TT,PPV,68)
CALL TABS(TT,CVAPP,72)
PIP = PGP - CVAPP*PPV
WIP = PIP*VGP*XMWI/(10.73*TGP)
WCP = 0.
IF(OPVDP) 201,201,202
201 XMWVP = XMWPV
GO TO 203
202 TT = TGP
CALL TABS(TT,CKPV,76)
XMWVP = XMWPV/(1.+1./SQRT(1.+4.*CKPV*CVAPP*PPV))
203 WVP = CVAPP*PPV*VGP*XMWVP/(10.73*TGP)
WGP = WVP + WIP
FVP = WVP/WC
FIP = 1. - FVP
FCP = 0.
XMWGP = WGP/(WVP/XMWVP + WIP/XMWI)
YVP = FVP*XMWGP/XMWVP
YIP = 1. - YVP
YCP = 0.
CYC = 0.
CPO2 = CPO
IF(OPIP) 204,204,205
204 CCP = 0.
GO TO 210
205 IF(PGP+ZP*RHOLP*ACC/4633.-PPL) 206,206,207
206 CCP = 1.
GO TO 210
207 CCP = -1.
210 I1 = RUNNO + .9
I2 = TFP + .9
I3 = OPIP + .9
I4 = OPVDP + .9
I5 = OPRP + .9
I6 = OPPCP + .9
PTP = PGP + ZP*RHOLP*ACC/4633.
208 WRITE OUTPUT TAPE 10,209,I1 ,PLIQ,RMP,RCLP,I2,I3,I4,I5,I6
209 FORMAT(1H1//44X,32HINITIAL CONDITIONS PRIMARY TANK//17X,85HRUNNO
1 P L I O R M P R C L P T F P O P I P O P V D P O P
28P OPPCP//17X,I5,5X,A6,2(5X,F5.1),5X,I4,4(5X,I5)////)
RETURN
END

```

```

C HEAT TRANSFER SECONDARY TANK
SUBROUTINE HTST
COMMON A,C,B
DIMENSION A(1320),B(1130),C(180)
EQUIVALENCE (A(1),RUNRG),(A(2),PLIQ),(A(3),TI),(A(4),VPT),(A(5),VG
1P),(A(6),PGP),(A(7),TGP),(A(8),TLP),(A(9),CPO),(A(10),PPL),(A(11),
2PRH),(A(12),VPL),(A(13),OPVDP),(A(14),OPIP),(A(15),OPHR),(A(16),O
3PTNK),(A(17),OPPCP),(A(18),DOP),(A(19),CDOP),(A(20),PR),
4(A(21),TRP),(A(22),RHUR),(A(23),AV),(A(24),CDV),(A(25),CPR1),
5(A(26),CPR2),(A(27),DPT),(A(28),SPT),(A(29),CWSP),(A(30),CPTO),
6(A(31),CPPT),(A(32),CACP),(A(33),CHC),(A(34),CDT),(A(35),XFGWP),
7(A(36),CFGWP),(A(37),XFGLP),(A(38),CFGLP),(A(39),XFLWP),
8(A(40),CELWP),(A(41),RMP),(A(42),RCLP),(A(43),TEP),(A(44),TR),
9(A(45),XWUCP),(A(46),XKCP),(A(50),XWUCP),(A(54),CPCP)
EQUIVALENCE (A(58),HLCLP),(A(62),CPCLP),(A(66),XWHPV),(A(67),PPV),
1(A(71),CVAPP),(A(75),CKPV),(A(79),BETVP),(A(83),XWVP),
2(A(87),XWHPV),(A(91),CPVP),(A(95),HVAPP),(A(99),XWVI),
3(A(103),XK1),(A(104),XWUI),(A(108),CPI),(A(112),XKLP),
4(A(116),XWULP),(A(120),BETLP),(A(124),CPLP),(A(128),CPLP2),
5(A(126),CRLP1),(A(127),CRLP2),(A(128),ACC),(A(132),VDLDP),
6(A(136),SPTG),(A(140),ALGP),(A(144),ZP),(A(148),DZPPDV),
7(A(152),HAP),(A(156),TAMP)
EQUIVALENCE (C(1),CCP),(C(2),CF),(C(3),CPGFX),(C(4),CPGP),(C(5),CPG
15),(C(6),CPLP),(C(7),CPLS),(C(8),CYC),(C(9),DMHDT),(C(10),DPHDT),
2(C(11),DTHDT),(C(12),DVAR),(C(13),DVRDT),(C(14),DWBDT),(C(15),D
3P),(C(16),FIS),(C(17),FISFX),(C(18),FCP),(C(19),FCS),(C(20),FCSFX),
4(C(21),FVVS),(C(22),FVVSFX),(C(23),FVP),(C(24),FVS),(C(25),FVSFX),
5(C(26),FCPFX),(C(27),FIPFX),(C(28),FVFPFX),(C(29),HCP),(C(30),HCS),
6(C(31),HF),(C(32),HGS),(C(33),HGP),(C(34),HI),(C(35),HSCLP),(C(36
7),HSCLS),(C(37),HVP),(C(38),HVS),(C(39),XKGF1),(C(41
8),XWGG1),(C(42),XWGG2),(C(43),XWGG3),(C(44),XWGG4),(C(45),XWGG5),
9),(C(46),XWVVP),(C(47),XWVVP1),(C(48),XWVVS),(C(49),XWVVS1)
EQUIVALENCE (C(51),PIP),(C(52),PIS),(C(53),RHOLS),(C(
154),PTP),(C(55),PTS),(C(56),QDCLP),(C(57),QDCLS),(C(58),QDGLP),(C(
259),QDGLS),(C(60),QDQCP),(C(61),QDQOS),(C(62),QDGS),(C(63),QDQWP),
3(C(64),QDQWS),(C(65),QDLOP),(C(66),QDLOS),(C(67),QDLP),(C(68),QDL
4PR),(C(69),QDLSC),(C(70),QDLWP),(C(71),QDLWS),(C(72),QDPGR),(C(73)
5,QDPR),(C(74),QDRPR),(C(75),QDSP),(C(76),QDSR),(C(77),QDSSC),(C(7
68),QDWP),(C(79),QDWS),(C(82),SPTL),(C(83
7),SSTL),(C(84),T),(C(85),TFCP),(C(86),TFCS),(C(87),TGS2),(C(88),TP
8TL),(C(89),TSTG),(C(90),TSTL),(C(91),TT),(C(92),VLP),(C(93),VLS),
9(C(94),VLP2),(C(95),VLS2)
EQUIVALENCE (C(96),WDRP),(C(97),WDWS),(C(98),WDGFX),(C(99),WDCLP),
1(C(100),WDCLS),(C(101),WDCP),(C(102),WCP2),(C(103),WDCS),(C(104),
2WCS2),(C(105),WGS),(C(106),WIP),(C(107),WIP2),(C(108),WIS),(C(1
39),WIS2),(C(110),WVVS2),(C(111),WDR),(C(112),WST2),(C(113),WVP),
4(C(114),WDVP),(C(115),WVP2),(C(116),WV5),(C(117),WDVS),(C(118),WVS
52),(C(119),WFCLP),(C(120),WFCLS),(C(121),WTCCF),(C(122),WTCLP),(C(
6123),WTCLS),(C(124),WTCP),(C(125),WTCS),(C(126),WTCEX),(C(127),WT
7R),(C(128),WTVCFX),(C(129),XF),(C(130),YCP),(C(131),YCS),(C(132),
8YIP),(C(133),YIS),(C(134),YPVS),(C(135),YVP),(C(136),YVS),(C(137),
9BETGEX),(C(138),GANGP),(C(139),GANGS)
EQUIVALENCE (C(141),DELOGP),(C(142),DELOGS),(C(143),DELOLP),(C(144
1),DELOLS),(C(145),DELQWP),(C(146),DELQWS),(C(147),DELT),(C(148),DE
2TEX),(C(149),DEWCLS),(C(150),DELWVP),(C(151),DELWVS),(C(152),XWUG
3FX),(C(153),XWUGS),(C(154),RHOGFX),(C(155),PGS2),(C(156),RHOLP)
EQUIVALENCE (C(157),WCP),(C(158),WCS)
EQUIVALENCE (C(159),TRTG),(C(160),WGP),(C(161),CP02)
EQUIVALENCE (B(1),SLIO),(B(2),VST),(B(3),VGS),(B(4),PGS),
1(B(5),TGS),(B(6),TLS),(B(7),DELPPS),(B(8),PS),(B(9),VLS),
2(B(10),OPVDS),(B(11),CPTS),(B(12),OPBS),(B(13),OPCS),
3(B(14),OPPCS),(B(15),DOS),(B(16),DOS),(B(17),DST),(B(18),SST),
4(B(19),CWSS),(B(20),CS10),(B(21),CPST),(B(22),CACS),(B(23),XFGWS),
5(B(24),CFGWS),(B(25),XFGLS),(B(26),CFGLS),(B(27),XFLWS),
6(B(28),CFLWS),(B(29),RMS),(B(30),RCLS),(B(31),TFS),(B(32),XWMCs),
7(B(33),XKCS),(B(37),XWUCS),(B(41),CPCS),(B(45),HLCLS),
8(B(49),CPCLS),(B(53),XWWSV),(B(54),PSV),(B(58),CVAPS),

```

RTD-TDR-63-1123

```
9(R(62),CKSV),(R(66),BFTVS),(R(70),XKVS),(B(74),XKUVS)
EQUIVALENC(B(78),CPVS),(B(82),HVAPS),(B(86),XKLS),(B(90),X\MULS),
1(R(94),BETLS),(R(98),CPLS1),(B(99),CPLS2),(B(100),CRLS1),
2(R(101),CRLS2),(B(102),VDLUS),(P(106),SSTG),(R(110),ALGS),
3(R(114),ZS),(R(118),DZSPDV),(R(122),HAS),(R(126),TAW5)
C WALL NEXT IC GAS
TT = (TGS + TSTG)/2.
DELTFX = ABS(TGS - TSTG)
XF = XFGWS
CF = CFGWS
CALL HTSST
QDQWS = HF*SSTG*(TGS-TSTG)
CALL TARS(T,HAS,1623)
CALL TARS(T,TAW5,1627)
QDQOS = CSTO*SSTG*HAS*(TSTG-TAW5)
C WALL NEXT TO LIQUID
TT = (TLS + TSTL)/2.
DELTFX = ABS(TLS - TSTL)
CALL TARS(TT,XKLS,1587)
CPLS = CPLS1 + CPLS2*TT
CALL TARS(TT,XMULS,1591)
RHOLS = CRLS1 + CRLS2*TLS
CALL TARS(TT,BETLS,1595)
HF=XKLS*CFLWS/DGT*(DST**3/RHOLS**2*ACC*HLTLS*DELTFX*CRLS*.03108/(
IXMULS*XKLS))**XFLS
QDLWS = HF*SSTL*(TLS - TSTL)
QDLQS = CSTO*SSTL*HAS*(TSTL-TAW5)
C GAS TO LIQUID SURFACE
TT = (TGS + TLS)/2.
DELTFX = ABS(TGS - TLS)
XF = XFGLS
CF = CFGLS
CALL HTSST
CALL TARS(VGS,ALGS,1611)
QDGLS = HF*ALGS*(TGS-TLS)
RETURN
END
```

```

C. HEAT TRANSFER SUBROUTINE SECONDARY TANK
SUBROUTINE HTSST
COMMON A,C,B
DIMENSION A(1320),R(1130),C(180)
EQUIVALENCE (A(1),RUNNO),(A(2),PLIQ),(A(3),TI),(A(4),VPT),(A(5),VG
1P),(A(6),PGP),(A(7),TGP),(A(8),TLP),(A(9),CPL),(A(10),PL),(A(11),
2PPH),(A(12),VPL),(A(13),OPVDP),(A(14),OPIP),(A(15),OPHP),(A(16),O
3PTNK),(A(17),OPPCP),(A(18),DOP),(A(19),CDOP),(A(20),PR),
4(A(21),TRP),(A(22),RHCR),(A(23),AV),(A(24),CDV),(A(25),CPR1),
5(A(26),CPR2),(A(27),DPT),(A(28),SPT),(A(29),CWS),(A(30),CRTG),
6(A(31),CPPT),(A(32),CACP),(A(33),CHC),(A(34),CDT),(A(35),XFGWP),
7(A(36),CFGWF),(A(37),XFGLP),(A(38),CFGLP),(A(39),XFLWP),
8(A(40),CFLWP),(A(41),RMP),(A(42),RCLP),(A(43),TEP),(A(44),TR),
9(A(45),XMWCP),(A(46),XKCP),(A(50),XMUCP),(A(54),CPCP)
EQUIVALENCE (A(58),HLCLP),(A(62),CPLP),(A(66),XMWVP),(A(67),PPV),
1(A(71),CVAPP),(A(75),CKPV),(A(79),BCTVP),(A(83),XKVP),
2(A(87),XMUVV),(A(91),CPVP),(A(95),HVAPP),(A(99),XMWI),
3(A(103),XKI),(A(104),XMI),(A(108),CPI),(A(112),XKLP),
4(A(116),XMULP),(A(120),DCLP),(A(124),CPLP),(A(125),CPLP2),
5(A(126),CRLP1),(A(127),CRLP2),(A(128),ACC),(A(132),VDLDP),
6(A(136),SPTC),(A(140),ALGP),(A(144),ZP),(A(148),DZPRDV),
7(A(152),HAP),(A(156),TAE)
EQUIVALENCE (C(1),CPI),(C(2),CF),(C(3),CPGFX),(C(4),CPGP),(C(5),CPG
1S),(C(6),CPLP),(C(7),CPLS),(C(8),CYC),(C(9),DMHDT),(C(10),DPBBDT),
2(C(11),DTTBDT),(C(12),DVAR),(C(13),DVRT),(C(14),DWBBDT),(C(15),F
3P),(C(16),FIS),(C(17),FISFX),(C(18),FCP),(C(19),FCS),(C(20),FCSFX)
4,(C(21),FPVS),(C(22),FPVSFX),(C(23),FVP),(C(24),FVS),(C(25),FVSFX)
5,(C(26),FVFX),(C(27),FVFX),C(28),FVFX),(C(29),HCP),(C(30),HCS)
6,(C(31),HF),(C(32),HGS),(C(33),HGP),(C(34),HI),(C(35),HSCLP),(C(36
7),HSCLS),(C(37),HVP),(C(38),HVS),(C(39),XKGF),C(41
8),XMG),C(42),XMG),C(43),XMG),C(44),XMG),C(45),XMG)
9,(C(46),XMWVP),(C(47),XMWVP),(C(48),XMWVP),(C(49),XMWVP)
EQUIVALENCE (C(51),PIP),(C(52),PIS),(C(53),RHOLS),(C(
154),PIP),(C(55),PTS),(C(56),QDCLP),(C(57),QDCLS),(C(58),QDGLP),(C(
259),QDGLS),(C(60),QDGGP),(C(61),QDQOS),(C(62),QDGS),(C(63),QDGGP),
3(C(64),QDGS),(C(65),QDLOP),(C(66),QDLOS),(C(67),QDLP),(C(68),QD
4PR),(C(69),QDLS),(C(70),QDLP),(C(71),QDLS),(C(72),QDGR),(C(73)
5,QDPR),(C(74),QDRPR),(C(75),QDSPC),(C(76),QDSR),(C(77),QDSSC),(C(7
68),QDWP),(C(79),QDWS),C(82),SPTL),(C(83
7),S5TL),(C(84),T),(C(85),TFCP),(C(86),TFCS),(C(87),TGS2),(C(88),TP
8TL),(C(89),TSTG),(C(90),TSTL),(C(91),TT),(C(92),VLP),(C(93),VLS),
4(C(94),VIP),(C(95),VIP)
EQUIVALENCE (C(96),WDWP),(C(97),WDHS),(C(98),WDCFX),(C(99),WDCLP),
1(C(100),WDCLS),(C(101),WDCP),(C(102),WCP2),(C(103),WDCS),(C(104),
2WCS2),(C(105),WGS),(C(106),WIP),(C(107),WIP2),(C(108),WIS),(C(1
39),WIS2),(C(110),WVVS2),(C(111),WDR),(C(112),WSTG2),(C(113),WVP),
4(C(114),WDVP),(C(115),WVP2),(C(116),WVS),(C(117),WDVS),(C(118),WVS
52),(C(119),WFCLP),(C(120),WFCLS),(C(121),WTCCF),(C(122),WTCLP),(C(
6123),WTCLS),(C(124),WTCR),(C(125),WTCS),(C(126),WTCF),(C(127),WT
7R),(C(128),WTVCF),(C(129),XF),(C(130),YCP),(C(131),YCS),(C(132),
8YIP),(C(133),YIS),(C(134),YPVS),(C(135),YVP),(C(136),YVS),(C(137),
9BETGFX),(C(138),GAMGP),(C(139),GAMGS)
EQUIVALENCE (C(141),DELOGP),(C(142),DELOGS),(C(143),DELQLP),(C(144
1),DELQLS),(C(145),DELQWP),(C(146),DELOWS),(C(147),DELT),(C(148),DE
2LTFX),(C(149),DEWCS),(C(150),DELWVP),(C(151),DELWVS),(C(152),XMUG
3FX),(C(153),XMUGS),(C(154),RHOGFX),(C(155),PGS2),(C(156),RHOLP)
EQUIVALENCE (C(157),WCP),(C(158),WCS)
EQUIVALENCE (C(159),TPTG),(C(160),WGP),(C(161),CPO2)
EQUIVALENCE (B(1),SLIQ),(B(2),VST),(B(3),VGS),(B(4),PGS),
1(B(5),TGS),(B(6),TLS),(B(7),DELFP),(B(8),PS),(B(9),VLSL),
2(B(10),OPVDS),(B(11),OPIS),(B(12),OPRS),(B(13),OPCS),
3(B(14),OPPCS),(B(15),DOS),(B(16),CDOS),(B(17),DST),(B(18),SST),
4(B(19),CWS),(B(20),CSTO),(B(21),CPST),(B(22),CACS),(B(23),XFGWS),
5(B(24),CEGWS),(B(25),XFGLS),(B(26),CEGLS),(B(27),XFLWS),
6(B(28),CFLWS),(B(29),RMS),(B(30),RCLS),(B(31),TFS),(B(32),XMWCS),
7(B(33),XKCS),(B(37),XMUCS),(B(41),CPCS),(B(45),HLCLS),
8(B(49),CPLS),(B(53),XMWSV),(B(54),PSV),(B(58),CVAPS),J(E(1),CVAPS),

```

```

9(R(62),CKSV), (R(66),BETVS), (R(70),XKVS), (R(74),XKVS)
EQUIVALENCI(B(78),CPVS), (B(82),HVAPS), (B(86),XKLS), (B(90),XKLS),
1(B(94),BETLS), (B(98),CPLS1), (B(99),CPLS2), (B(100),CPLS1),
2(B(111),CRLS2), (B(102),VDLCS), (B(106),SGTG), (B(110),ALSS),
3(B(114),ZS), (B(118),PZSDV), (B(122),HAS), (B(126),TAS)
IF(YVS) 41,41,42
41 XWVSI = 0.
BETVS = 0.
GO TO 45
42 IF(OPVDS) 43,43,44
43 XWVSI = XWVSI
BETVS = 1./TT
GO TO 45
44 CALL TABS(TT,CKSV,1563)
XWVSI = XWVSI/(1.+1./SQRT(1.+4.*CKSV*YVS*PGS))
CALL TABS(TT,BETVS,1567)
45 IF(YPVS) 46,46,47
46 XWVPV = 0.
BETVP = 0.
GO TO 50
47 IF(OPVDP) 48,48,49
48 XWVPV = XWVPV
BETVP = 1./TT
GO TO 50
49 CALL TABS(TT,CKPV,76)
XWVPV = XWVPV/(1.+1./SQRT(1.+4.*CKPV*YPVS*PGS))
CALL TABS(TT,BETVP,80)
50 XWVSI = YVS*XWVSI+YPVS*XWVPV+YIS*XWVI+YCS*XWVSI
FV5FX = YVS*XWVSI/XWVSI
FPV5FX = YPVS*XWVPV/XWVSI
FISFX = 1.-FV5FX-FPV5FX-FCSFX
FCSFX = YCS*XWVSI/XWVSI
RHOGFX = PGS*XWVSI/110.73*TT
CALL TABS(TT,CPVS,1579)
CALL TABS(TT,CPVP,92)
CALL TABS(TT,CPI,109)
CALL TABS(TT,CPCS,1542)
CPGFX = FV5FX*CPVS+FPV5FX*CPVP+FCSFX*CPCS+FISFX*CPI
CALL TABS(TT,XKVS,1571)
CALL TABS(TT,XKVP,84)
CALL TABS(TT,XKI,101)
CALL TABS(TT,XKCS,1534)
XKGF = YVS*XKVS+YPVS*XKVP+YIS*XKI+YCS*XKCS
CALL TABS(TT,XMVS,1575)
CALL TABS(TT,XMVP,88)
CALL TABS(TT,XMVI,105)
CALL TABS(TT,XMUC,1528)
XMUGEX = (YVS*XMVS*SQRT(XWVSI) + YPVS*XMVP*SQRT(XWVPV) +
YIS*XMVI*SQRT(XMVI) + YCS*XMUC*SQRT(XMUC))/(YVS*SQRT(XWVSI)
+ YPVS*SQRT(XWVPV) + YIS*SQRT(XMVI) + YCS*SQRT(XMUC))
BETGX = YVS*BETVS+YPVS*BETVP + (YIS+YCS)/TT
HF=XKGF*CF/DST*(DST**3*RHOGFX**2*ACC*BETGX*DELTFX*CPGFX*.03108/
1(XMUGEX*XKGF))**XF
RETURN
END

```

```

C COMBUSTION SECONDARY TANK
SURROUTINE CBST
COMMON A,C,R
DIMENSION A(1320),B(1130),C(180)
EQUIVALENCE (A(1),RUNNU),(A(2),PLIQ),(A(3),TI),(A(4),VPT),(A(5),VG
1P),(A(6),PGP),(A(7),TGP),(A(8),TLP),(A(9),CPO),(A(10),PPL),(A(11),
2PPH),(A(12),VPL),(A(13),OPVDP),(A(14),OPIP),(A(15),OPHP),(A(16),O
3PTNK),(A(17),OPPCP),(A(18),DOP),(A(19),CDOP),(A(20),PR),
4(A(21),TRP),(A(22),RHCR),(A(23),AV),(A(24),CDV),(A(25),CPR1),
5(A(26),CPR2),(A(27),DPT),(A(28),SPT),(A(29),CASP),(A(30),CPTO),
6(A(31),CPPT),(A(32),CACP),(A(33),CHC),(A(34),CDT),(A(35),XFGWP),
7(A(36),CFGWP),(A(37),XFGLP),(A(38),CFGLP),(A(39),XFLWP),
8(A(40),CFLWP),(A(41),RMP),(A(42),RCLP),(A(43),TEP),(A(44),TRI),
9(A(45),XMWCP),(A(46),XKCP),(A(50),XMUCP),(A(54),CPCP)
FOURIVALFNCE (A(58),HLCPL),(A(62),CPLP),(A(66),XHWVP),(A(67),PPV),
1(A(71),CVAPP),(A(75),CKPV),(A(79),BETVP),(A(83),XKVP),
2(A(87),XMUVP),(A(91),CPVP),(A(95),HVAPP),(A(99),XHWI),
3(A(103),XK1),(A(104),XMU1),(A(108),CPI),(A(112),XKLP),
4(A(116),XMWLP),(A(120),BETLP),(A(124),CPLP1),(A(125),CPLP2),
5(A(126),CRLP1),(A(127),CRLP2),(A(128),ACC),(A(132),VDLUP),
6(A(136),SPTG),(A(140),ALGP),(A(144),ZP),(A(148),DZPBDV),
7(A(152),HAPL),(A(156),TAWP)
EQUIVALENCE (C(1),CCP),(C(2),CF),(C(3),CPGFX),(C(4),CPGP),(C(5),CPG
1S),(C(6),CPLP),(C(7),CPLS),(C(8),CYC),(C(9),DMBDT),(C(10),DPBDT),
2(C(11),DTTBDT),(C(12),DVAR1),(C(13),DVAR2),(C(14),DWBDT),(C(15),FI
3P),(C(16),FIS),(C(17),FISFX),(C(18),FCP),(C(19),FCS),(C(20),FCSFX)
4,(C(21),FPVS),(C(22),FPVSFX),(C(23),FVP),(C(24),FVS),(C(25),FVSFX)
5,(C(26),FCPEX),(C(27),FIPEX),(C(28),FVPEX),(C(29),HCP),(C(30),HCS)
6,(C(31),HF),(C(32),HGS),(C(33),HGP),(C(34),HI),(C(35),HSCLP),(C(36
7),HSCLSI),(C(37),HVPG),(C(38),HVSG),(C(39),XKGF),(C(41
8),XMWGP),(C(42),XMWGF),(C(43),XHWGS),(C(44),XMWGS2),(C(45),XMWVP)
9,(C(46),XMWVP),(C(47),XHWVP1),(C(48),XMWVS),(C(49),XHMVS1)
EQUIVALENCE (C(51),PIP),(C(52),PIS),(C(53),RHOLS),(C(
154),PTP),(C(55),PTS),(C(56),QDCLP),(C(57),QDCLS),(C(58),QDGLP),(C(
259),QDGLS),(C(60),QDQCP),(C(61),QDQOS),(C(62),QDGS),(C(63),QDQWP),
3(C(64),QDQWS),(C(65),QDLOP),(C(66),QDLOS),(C(67),QDLPC),(C(68),QDL
4PR),(C(69),QDLSC),(C(70),QDLWP),(C(71),QDLWS),(C(72),QDPGR),(C(73)
5,QDPR),(C(74),QDRPR),(C(75),QDSPC),(C(76),QDSK),(C(77),QDSSC),(C(7
68),QDWP),(C(79),QDNS), (C(82),SPTL),(C(83
7),SSTL),(C(84),T),(C(85),TFCP),(C(86),TFCS),(C(87),TGS2),(C(88),TP
8TL),(C(89),TSTG),(C(90),TSTL),(C(91),TT),(C(92),VLP),(C(93),VLS)
9(C(94),VLP2),(C(95),VLS2)
OEQUIVALENCE (C(96),WDRP),(C(97),WDBS),(C(98),WDCFX),(C(99),WDCLP),
1(C(100),WDCLS),(C(101),WDCP),(C(102),WCP2),(C(103),WDCS),(C(104),
2WCS2),(C(105),WGS),(C(106),WIP),(C(107),WIP2),(C(108),WIS),(C(1
39),WIS2),(C(110),WRVS2),(C(111),WDR),(C(112),WSTG2),(C(113),WVP),
4(C(114),WDVP),(C(115),WVP2),(C(116),WVS),(C(117),WDVS),(C(118),WVS
52),(C(119),WVCLP),(C(120),WFCLS),(C(121),WTCCF),(C(122),WTCLP),(C(
6123),WTCLS),(C(124),WTCR),(C(128),WTCF),(C(126),WTICFX),(C(127),WT
7R),(C(128),WTVCFX),(C(129),XF),(C(130),YCP),(C(131),YCS),(C(132),
8YIP),(C(133),YIS),(C(134),YPVS),(C(135),YVP),(C(136),YVS),(C(137),
9BETGF),(C(138),GAMGP),(C(139),GAMGS)
OEQUIVALENCE (C(141),DELOGP),(C(142),DELOGS),(C(143),DELOLP),(C(144
1),DELOLS),(C(145),DELOWP),(C(146),DELOWS),(C(147),DELT),(C(148),DE
2LTF),(C(149),DEWCLS),(C(150),DELWVP),(C(151),DELVVS),(C(152),XMWG
3FX),(C(153),XMUGS),(C(154),RHOGFX),(C(155),PGS2),(C(156),RHOLP)
EQUIVALENCE (C(157),WCP),(C(158),WCS)
EQUIVALENCE (C(159),TPTG),(C(160),WGR),(C(161),CPD2)
EQUIVALENCE (B(1),SLIQ),(B(2),VST),(B(3),VGS),(B(4),PGS),
1(B(5),TGS),(B(6),TLS),(B(7),DELPPS),(B(8),PS),(B(9),VLSL),
2(B(10),OPVDS),(B(11),OPIS),(B(12),OPBS),(B(13),OPCS),
3(B(14),OPPCS),(B(15),CDOS),(B(16),CDOS),(B(17),DST),(B(18),SST),
4(B(19),CWSS),(B(20),CSTO),(B(21),CPST),(B(22),CACS),(B(23),XFGWS),
5(B(24),CFGWS),(B(25),XFGLS),(B(26),CEGLS),(B(27),XFLWS),

```

```

6(B(28),CFLWS),(B(29),RMS),(B(30),RCLS),(B(31),TFS),(B(32),XMWCS),
7(B(33),XKCS),(B(37),XMUCS),(B(41),CPCS),(B(45),HLCLS),
8(B(49),CPCLS),(B(53),XMWSV),(B(54),PSV),(B(58),CVAPS),
9(B(62),CKSV),(B(66),RFTVS),(B(70),XKVS),(B(74),XMUVS)
EQUIVALENCE(B(78),CPVS),(B(82),HVAPS),(B(86),XKLS),(B(90),XMULS),
1(B(94),BETLS),(B(98),CPLS1),(B(99),CPLS2),(B(100),CRLS1),
2(B(101),CRLS2),(B(102),VDLOS),(B(106),SSTG),(B(110),ALGS),
3(B(114),ZS),(B(118),DZSRDV),(B(122),HAS),(B(126),TAW)
IF(PGP-PGS-DELPSS) 500,500,502
500 WDCFX = 0.
WDCS = 0.
QDSSC = 0.
501 WDCLS = 0.
QDLSC = 0.
QDCLS = 0.
GO TO 600
502 IF(OPCS) 503,503,504
503 WDCS = FCP
TT = (TGP + TGS)/2.
CALL TABS(TT,CPI,109)
CALL TABS(TT,CPCP,55)
CALL TABS(TT,CPVP,92)
QDSSC = (FIP*CPI+FCP*CPCP+FVP*CPVP)*(TGP - TGS)
GO TO 501
504 WDCS = (FVP+FCP)*(RMS+1.)*(1.-RCLS)
WDCLS = (FVP+FCP)*(RMS+1.)*RCLS
TT = (TGP + TR)/2.
CALL TABS(TT,CPI,109)
CALL TABS(TT,CPCP,55)
CALL INTG (TR,TGP,TT,CPVP,92,HVPG,A)
QPGR=FVP*HVPG*(FIP*CPI + FCP*CPCP)*(TGP-TR)
IF(OPIS) 505,505,506
505 TT = (TGS + TR)/2.
CALL TABS(TT,CPVS,1579)
DVARI = RMS*(FVP + FCP)*CPVS*(TGS - TR)
GO TO 507
506 TT = (TLS + TR)/2.
DVARI = RMS*(FVP + FCP)*(TLS - TR)*(CPLS1 + CPLS2*TT)
507 CALL INTG (TR,TFS,TT,CPCS,1542,HCS,A)
QSR = (WDCS + WDCLS)*HCS + QPGR + DVARI
CALL INTG (TR,TFS,TT,CPI,109,HI,A)
TFCS=TR+QSR*(TFS - TR)/(HI*FIP+HCS*(WDCS+WDCLS))
CALL INTG (TR,TFCS,TT,CPCS,1542,HCS,A)
CALL INTG (TR,TFCS,TT,CPI,109,HI,A)
TFCS = TR + QSR*(TFCS - TR)/(HI*FIP + HCS*(WDCS + WDCLS))
QDLSC = CACS*CHC*(TFCS - TLS)
TT = TLS
CALL TABS(TT,HLCLS,1546)
CALL INTG (TLS,TFCS,TT,CPCLS,1550,HSCLS,A)
QDCLS = (HLCLS + HSCLS)*WDCLS
CALL INTG (TR,TGS,TT,CPCS,1342,HCS,A)
CALL INTG (TR,TGS,TT,CPI,109,HI,A)
CALL INTG (TR,TLS,TT,CPCLS,1550,HSCLS,A)
QDSSC=QSR-WDCS*HCS-FIP*HI+WDCLS*(HLCLS-HSCLS)
600 RETURN
END

```

```

C BLEED AND DEPENDENT CONDITIONS SECONDARY TANK
SUBROUTINE BDCST
COMMON A,C,B
DIMENSION A(1320),B(1130),C(180)
EQUIVALENCE (A(1),RUNNU),(A(2),PLIQ),(A(3),TI),(A(4),VPT),(A(5),VG
1P),(A(6),PGP),(A(7),TGP),(A(8),TLP),(A(9),CPO),(A(10),PPL),(A(11),
2PPH),(A(12),VPL),(A(13),OPVDP),(A(14),OPIP),(A(15),OPBP),(A(16),O
3PTNK),(A(17),OPPCP),(A(18),DOP),(A(19),CDOP),(A(20),PR),
4(A(21),TRP),(A(22),RHCR),(A(23),AV),(A(24),CDV),(A(25),CPR1),
5(A(26),CPR2),(A(27),DPT),(A(28),SPT),(A(29),CWSP),(A(30),CPTO),
6(A(31),CPPT),(A(32),CACP),(A(33),CHC),(A(34),CDT),(A(35),XFGWP),
7(A(36),CFGWP),(A(37),XFGLP),(A(38),CFGLP),(A(39),XFLWP),
8(A(40),CFLWP),(A(41),RMP),(A(42),RCLP),(A(43),TEP),(A(44),TR),
9(A(45),XMWCP),(A(46),XKCP),(A(50),XMUCP),(A(54),CPCP)
EQUIVALENCE (A(58),HLCPL),(A(62),CPCPL),(A(66),XMWVP),(A(67),PPV),
1(A(71),CVAPP),(A(75),CKPV),(A(79),RETVP),(A(83),XKVE),
2(A(87),XMUV), (A(91),CPVP),(A(95),HVAPP),(A(99),XMW1),
3(A(100),XKT),(A(104),XMUI),(A(108),CPI),(A(112),XKLP),
4(A(116),XMIULP),(A(120),RETL), (A(124),CRLP1),(A(128),CRLP2),
5(A(126),CRLP1),(A(127),CRLP2),(A(128),ACC),(A(132),VDLUP),
6(A(136),SPTG),(A(140),ALGP),(A(144),ZP),(A(148),DZPHDV),
7(A(152),HAP),(A(156),TAWP)
EQUIVALENCE (C(1),CCP),(C(2),CF),(C(3),CPGFX),(C(4),CPGP),(C(5),CPG
1S),(C(6),CPLP),(C(7),CPLS),(C(8),CYC),(C(9),DMBDT),(C(10),DPBDT),
2(C(11),DPTBDT),(C(12),DVAR1),(C(13),DVBBDT),(C(14),DWBBDT),(C(15),F
3P),(C(16),FIS),(C(17),FISFX),(C(18),FCP),(C(19),FCS),(C(20),FCSFX)
4,(C(21),FPVS),(C(22),FPVSFX),(C(23),FVP),(C(24),FVS),(C(25),FVSFX)
5,(C(26),FCPEX),(C(27),FPEX),(C(28),FVPEX),(C(29),HCP),(C(30),HCS)
6,(C(31),HF),(C(32),HGS),(C(33),HGP),(C(34),HI),(C(35),HSCLP),(C(36
7),HSCLS),(C(37),HVPG),(C(38),HVSG),(C(39),XKGF), (C(41
8),XMWGP),(C(42),XMWGEX),(C(43),XMWGS),(C(44),XMWGS2),(C(45),XMWVP1
9),(C(46),XMWVP),(C(47),XMWVP1),(C(48),XMWVS),(C(49),XMWVS1)
EQUIVALENCE (C(51),PIP),(C(52),PIS),(C(53),RHOLS),(C(
154),PTP),(C(55),PTS),(C(56),QDCLP),(C(57),QDCLS),(C(58),QDGLP),(C(
259),QDGLS),(C(60),QDGP),(C(61),QDGS),(C(62),QDGS),(C(63),QDGP),
3(C(64),QDGS),(C(65),QDLP),(C(66),QDLOS),(C(67),QDLP),(C(68),QD
4PR),(C(69),QDLS),(C(70),QDWP),(C(71),QDWS),(C(72),QDRPR),(C(73)
5,QDPR),(C(74),QDRPR),(C(75),QDSCP),(C(76),QDSR),(C(77),QDSSC),(C(7
68),QDWP),(C(79),QDWS), (C(82),SPTL),(C(83
7),SSTL),(C(84),T),(C(85),TECP),(C(86),TECS),(C(87),TGS2),(C(88),TP
8TL),(C(89),TSTG),(C(90),TSTL),(C(91),TT),(C(92),VLP),(C(93),VLS),
9(C(94),VLP2),(C(95),VLS2)
DEQUIVALENCE (C(96),WDHP),(C(97),WDUS),(C(98),WDCFX),(C(99),WDCLP),
1(C(100),WDCLS),(C(101),WDCP),(C(102),WCP2),(C(103),WDGS),(C(104),
2WCS2),(C(105),WGS),(C(106),WIP),(C(107),WIP2),(C(108),WIS),(C(1
30),WIS2),(C(110),WVVS2),(C(111),WDR),(C(112),WSTG2),(C(113),WVP),
4(C(114),WDVP),(C(115),WVP2),(C(116),WVS),(C(117),WDVS),(C(118),WVS
52),(C(119),WFCLP),(C(120),WFCLS),(C(121),WTCCF),(C(122),WTCLP),(C(
6123),WTCLS),(C(124),WTCR),(C(125),WTCS),(C(126),WTICEX),(C(127),WT
7R),(C(128),WVCFX),(C(129),XF),(C(130),YCP),(C(131),YCS),(C(132),
8YIP),(C(133),YIS),(C(134),YPVS),(C(135),YVP),(C(136),YVS),(C(137),
9BETGFX),(C(138),GANGP),(C(139),GANGS)
DEQUIVALENCE (C(141),DELQGP),(C(142),DELQGS),(C(143),DELQLP),(C(144
1),DELQLS),(C(145),DELQWP),(C(146),DELQWS),(C(147),DELT),(C(148),DE
2LTEX),(C(149),DENCLS),(C(150),DELWVP),(C(151),DELWVS),(C(152),XWUG
3FX),(C(153),XWUGS),(C(154),RHOGFX),(C(155),PGS2),(C(156),RHULP)
EQUIVALENCE (C(157),WCP),(C(158),WCS)
EQUIVALENCE (C(159),TPTG),(C(160),WGP),(C(161),CPO2)
EQUIVALENCE (B(1),SLIQ),(B(2),VST),(B(3),VGS),(B(4),PGS),
1(B(5),TGS),(B(6),TLS),(B(7),DELPPS),(B(8),PS),(B(9),VLSL),
2(B(10),ORVDS),(B(11),OPIS),(B(12),OPBS),(B(13),OPCS),
3(B(14),OPPCS),(B(15),DOS),(B(16),CDOS),(B(17),DST),(B(18),SST),
4(B(19),CWSS),(B(20),CSTO),(B(21),CPST),(B(22),CACS),(B(23),XFGWS),
5(B(24),CFGWS),(B(25),XFGLS),(B(26),CFGLS),(B(27),XFLWS)

```

RTD-TDR-63-1123

```
6(B(28),CFLWS),(B(29),RMS),(B(30),RCLS),(B(31),TFS),(B(32),XMWCS),
7(B(33),XKCS),(B(37),XMUCS),(B(41),CPCS),(B(45),HLCLS),
8(B(49),CPLS1),(B(53),XMWSV),(B(54),PSV),(B(58),CVAPS),
9(B(62),CKSV),(B(66),BETVS),(B(70),XKVS),(B(74),XMUVS)
EQUIVALENCE(B(78),CPVS),(B(82),HVAPS),(B(86),XKLS),(B(90),XMULS),
1(B(94),BETLS),(B(98),CPLS1),(B(99),CPLS2),(B(100),CRLS1),
2(B(101),CRLS2),(B(102),VDLOS),(B(106),SSTG),(B(110),ALGS),
3(B(114),ZS),(B(118),DZSBDV),(B(122),HAS),(B(126),TAWS)
CALL TABS(T,VDLOS,1602)
ODWS = PGS*VDLOS*.185
TT = TGS
CALL TABS(TT,CPVS,1579)
CALL TABS(TT,CPI,109)
CALL TABS(TT,CPCS,1542)
CALL TABS(TT,CPVP,92)
CPGS = FVS*CPVS + FIS*CPI + FCS*CPCS + FPVS*CPVP
IF(OPBS) 601,601,602
601 WDBS = 0
GO TO 699
602 GAMGS = CPGS/(CPGS - 1.987/XMWGS)
WDBS = .1133*CDOS*DOS**2*PGS*SQRT((XMWGS*GAMGS/TGS)**2./IGAMGS +
11.))**((GAMGS,1.)/(GAMGS-1.))
699 RETURN
END
```

```

C GAS CROSSFLOW AND EVAPORATION SECONDARY TANK
SUBROUTINE GCEST
COMMON A,C,B
DIMENSION A(1320),B(1130),C(180)
EQUIVALENCE (A(1),RUNNO),(A(2),PLIQ),(A(3),TI),(A(4),VPT),(A(5),VG
1P),(A(6),PGP),(A(7),TGP),(A(8),TLP),(A(9),CPO),(A(10),PPL),(A(11),
2PRH),(A(12),VPL),(A(13),OPVDP),(A(14),OPR),(A(15),OPBR),(A(16),O
3PTNK),(A(17),OPPCP),(A(18),DOP),(A(19),CDOP),(A(20),PR),
4(A(21),TRP),(A(22),RHCR),(A(23),AV),(A(24),CDV),(A(25),CPR1),
5(A(26),CPR2),(A(27),DPT),(A(28),SPT),(A(29),CWSP),(A(30),CPTO),
6(A(31),CPPT),(A(32),CACP),(A(33),CHC),(A(34),CDT),(A(35),XFGWP),
7(A(36),CFGWP),(A(37),XFGLP),(A(38),CFGLP),(A(39),XFLWP),
8(A(40),CFLWP),(A(41),RMP),(A(42),RCLP),(A(43),TEP),(A(44),TR),
9(A(45),XMWCP),(A(46),XKCP),(A(50),XMUCP),(A(54),CCPC)
EQUIVALENCE(A(58),HLCLP),(A(62),CPCLP),(A(66),XMPVP),(A(67),PPV),
1(A(71),CVAPP),(A(75),CKPV),(A(79),BETVP),(A(83),XKVP),
2(A(87),XNUVP),(A(91),CPVP),(A(95),HVAPP),(A(99),XMWL),
3(A(100),XKI),(A(104),XMU1),(A(108),CPI),(A(112),XKLP),
4(A(116),XMULP),(A(120),BETLP),(A(124),CPLP),(A(125),CPLP2),
5(A(126),CRLP1),(A(127),CRLP2),(A(128),ACC),(A(132),VMIOP),
6(A(136),SPTG),(A(140),ALGP),(A(144),ZP),(A(148),DZPBVD),
7(A(152),HAR),(A(156),TAWP)
EQUIVALENCE(C(1),CCP),(C(2),CF),(C(3),CPGFX),(C(4),CPGP),(C(5),CPG
1S),(C(6),CPLP),(C(7),CPLS),(C(8),CYC),(C(9),UMBDT),(C(10),DPBDT),
2(C(11),DTTBDT),(C(12),DVARI),(C(13),DVBOT),(C(14),DWRDT),(C(15),F
3P),(C(16),FIS),(C(17),F15FX),(C(18),FCP),(C(19),FCS),(C(20),FCSFX)
4(C(21),FPVS),(C(22),FVVSFX),(C(23),FVP),(C(24),FVS),(C(25),FVSFX)
5(C(26),FCPFX),(C(27),F1PFX),(C(28),FVPEX),(C(29),HCP),(C(30),HCS)
6(C(31),HF),(C(32),HGS),(C(33),HGP),(C(34),HI),(C(35),HSCLP),(C(36
7),HSCLS),(C(37),HVP),(C(38),HVS),(C(39),XKGF), (C(41
8),XMWGP),(C(42),XMGFX),(C(43),XMGWS),(C(44),XMGWS2),(C(45),XMPVP)
9),(C(46),XMPVP),(C(47),XMPVP1),(C(48),XMPVP),(C(49),XMPVP1)
EQUIVALENCE (C(51),PIP),(C(52),PIS),(C(53),RHOLS),(C(
154),PTP),(C(55),PTS),(C(56),QDCLP),(C(57),QDCLS),(C(58),QDGLP),(C(
259),QDGLS),(C(60),QDGP),(C(61),QDGS),(C(62),QDGS1),(C(63),QDGP),
3(C(64),QDGS),(C(65),QDLP),(C(66),QDLOS),(C(67),QDLP),(C(68),QDL
4PR),(C(69),QDLS),(C(70),QDLWP),(C(71),QDLS),(C(72),QDPR),(C(73)
5,QDPR),(C(74),QDRPR),(C(75),QDSP),(C(76),QDSR),(C(77),QDSSC),(C(7
68),QDWP),(C(79),QDWS), (C(82),SPTL),(C(83)
7),SSTL),(C(84),T),(C(85),TECP),(C(86),TECS),(C(87),TGS2),(C(88),TP
8TL),(C(89),TSTG),(C(90),TSTL),(C(91),TT),(C(92),VLP),(C(93),VLS),
9(C(94),VLP2),(C(95),VLS2)
EQUIVALENCE (C(96),WDP),(C(97),WDBS),(C(98),WDBFX),(C(99),WDBLP),
1(C(100),WDCLS),(C(101),WDCP),(C(102),WCP2),(C(103),WDCS),(C(104),
2WCS2),(C(105),WGS),(C(106),WIP),(C(107),WIP2),(C(108),WIS),(C(1
39),WIS2),(C(110),WV62),(C(111),WDR),(C(112),WSTG2),(C(113),WVP),
4(C(114),WDVP),(C(115),WVP2),(C(116),WVS),(C(117),WDVS),(C(118),WVS
52),(C(119),WFCLP),(C(120),WFCLS),(C(121),WTCCF),(C(122),WTCLP),(C(
6123),WTCLS),(C(124),WTCP),(C(125),WTCS),(C(126),WTCEFX),(C(127),WT
7R),(C(128),WTVCFX),(C(129),XF),(C(130),YCP),(C(131),YCS),(C(132),
8YIP),(C(133),YIS),(C(134),YPVS),(C(135),YVP),(C(136),YVS),(C(137),
9BETGEX),(C(138),GANGR),(C(139),GANGS)
EQUIVALENCE (C(141),DELQGP),(C(142),DELOGS),(C(143),DELOLP),(C(144
1),DELOLS),(C(145),DELOWP),(C(146),DELOWS),(C(147),DEL),C(148),DE
21TEX),(C(149),DEWCLS),(C(150),DELVVP),(C(151),DELVWS),(C(152),XMUIG
3FX),(C(153),XMGWS),(C(154),RHOGFX),(C(155),PGS2),(C(156),RHOLP)
EQUIVALENCE (C(157),WCP),(C(158),WCS)
EQUIVALENCE (C(159),TPTG),(C(160),WGP),(C(161),CPO2)
EQUIVALENCE (C(162),WPVS),(C(163),XMPVVS),(C(164),WTCCFX)
EQUIVALENCE(B(1),SLIQ),(B(2),VST),(B(3),VGS),(B(4),PGS),
1(B(5),TGS),(B(6),TIS),(B(7),DFLPPS),(B(8),PS),(B(9),VLS1),
2(B(10),OPVDS),(B(11),OPIS),(B(12),OPBS),(B(13),OPCS),
3(B(14),OPPCS),(B(15),DUS),(B(16),CDOS),(B(17),DST),(B(18),SST),
4(B(19),CWSS),(B(20),CSTO),(B(21),CPST),(B(22),CACS),(B(23),XFGWS),
5(B(24),CFGWS),(B(25),XFGLS),(B(26),CFGLS),(B(27),XFLWS),
6(B(28),CFLWS),(B(29),RMS),(B(30),RCLS),(B(31),TFS),(B(32),XMWCS),
7(B(33),XKCS),(B(37),XMGCS),(B(41),CRCS),(B(45),HLCLS)

```

```

8(R(49),CPCLS),(R(53),XMWSV),(B(54),PSV),(R(58),CVAPS),
9(R(62),CKSV),(B(66),HETVS),(B(70),XKVS),(R(74),XMLVS)
EQUIVALENCE(B(78),CPVS),(B(82),HVAPS),(B(86),XKLS),(B(90),XMLLS),
1(R(94),RFTLS),(R(98),CPLS1),(B(99),CPLS2),(B(100),CRLS1),
2(R(101),CRLS2),(R(102),VDLOS),(R(106),SSTG),(R(110),ALGS),
3(B(114),ZS),(B(118),DZSBDV),(B(122),HAS),(B(126),TAVS)
-----
IF(CVAPS) 701,701,702
701  WDV5 = 0.
     HVSG = 0.
     HVAPS = 0.
     GO TO 703
702  WDV5 = FVS*WDHS + XMWVS*VDLOS*YVS*PGS/(10.73*TGS)
     TT = (TGS + TLS)/2.
     CALL TABS(TT,CPVS,1579)
     HVSG = CPVS*(TGS - TLS)
     TT = TLS
     CALL TABS(TT,HVAPS,1583)
     TT = TGS
     CALL TABS(TT,CPVS,1579)
703  IF(IPGP - PGS - DELPPS) 711,711,704
704  CALL TABS(VGS,DZSBDV,1619)
     PGS2 = PS - (ZS + DZSBDV*VDLOS)*RHOLS*ACC/4633.
     WDCFX = (VGS + VDLOS + WDV5/RHOLS)*PGS2*XMWGS/(10.73*TGS) + WDBS*
111. = FVS) = WGS
-----
WVS2 = WVS - FVS*WDHS + WDV5
IF(OPCS) 705,705,706
705  WPV52 = FVVS*(WGS - WDBS) + FVP*WDCFX
     WCS2 = WCS - FCS*WDHS + FCP*WDCFX
     WIS2*WIS = FIS*WDHS + FIP*WDCFX
     XMWGS2 = (WPV52 + WCS2 + WIS2 + WVS2)/(WPV52/XMWVVS + WCS2/XMWCS +
1WIS2/XMWI + WVS2/XMWVS)
     HGS = WPV52*CPVP + WCS2*CPCS + WIS2*CPI + WVS2*CPVS
     QDGS = WDCFX*QDSSC - QDGS - QDGLS - QDWS - WDV5*HVSG
     TGS2 = TGS + QDGS/HGS
     WDCFX = (VGS + VDLOS + WDV5/RHOLS)*PGS2*XMWGS2/(10.73*TGS2) + WDBS*
111. = FVS) = WGS
-----
GO TO 710
706  WDCFX = WDCFX/(WDCS + FIP)
     WCS2 = WCS - FCS*WDHS + WDCS*WDCFX
     WIS2 = WIS - FIS*WDHS + FIP*WDCFX
     XMWGS2 = (WCS2 + WIS2 + WVS2)/(WVS2/XMWVVS + WCS2/XMWCS + WIS2/XMWI)
     HGS = WPV52*CPVP + WCS2*CPCS + WIS2*CPI
     WDV52 = WDV5 + WDCFX*RMS*(FVP + FCP)
     IF(OPIS) 707,707,708
707  QDGS = WDCFX*(QDSSC - QDCLS) - QDGLS - QDWS - WDV52*HVSG
     GO TO 709
708  QDGS = WDCFX*(QDSSC - QDCLS) - WDCFX**0.87*QDLS - QDGLS - QDWS -
1WDV5*HVSG
-----
709  TGS2 = TGS + QDGS/HGS
     WDCFX = ((VGS + VDLOS + WDV52/RHOLS)*PGS2*XMWGS2/(10.73*TGS2) + WDBS*
111. = FVS) = WGS)/(WDCS + FIP)
-----
710  IF(WDCFX) 711, 799, 799
711  WDCFX = 0.
799  RETURN
     END

```

```

C. -- DEPENDENT CONDITIONS PRIMARY TANK
SUBROUTINE DCPT
COMMON A,C,B
DIMENSION A(1320),H(1130),C(180)
EQUIVALENCE (A(1),RUNNO),(A(2),PLIQ),(A(3),TI),(A(4),VPT),(A(5),VG
1P),(A(6),PGP),(A(7),TGP),(A(8),TLP),(A(9),CPU),(A(10),PPL),(A(11),
2PPH),(A(12),VLP1),(A(13),CPVDP),(A(14),QPIP),(A(15),UPPI),(A(16),U
3PTNK),(A(17),OPPCP),(A(18),DDP),(A(19),CDDP),(A(20),PR),
4(A(21),TRP),(A(22),RHOR),(A(23),AV),(A(24),CDV),(A(25),CPR1),
5(A(26),CPR2),(A(27),DPT),(A(28),SPT),(A(29),CWSP),(A(30),CPTO),
6(A(31),CPPT),(A(32),CACP),(A(33),CHC),(A(34),CDT),(A(35),XFGWP),
7(A(36),CFGWP),(A(37),XFGLP),(A(38),CFGLP),(A(39),XFLWP),
8(A(40),CFLWP),(A(41),RMP),(A(42),KCLP),(A(43),TFP),(A(44),TR),
9(A(45),XWVCP),(A(46),XKCP),(A(50),XMUCP),(A(54),CPCP)
EQUIVALENCE (A(58),HLCLP),(A(62),CPCLP),(A(66),XWVVP),(A(67),PPV),
1(A(71),CVAPP),(A(75),CKPV),(A(79),PETVP),(A(83),XKVP),
2(A(87),XWVVP),(A(91),CPVP),(A(95),HVAPP),(A(99),XHW1),
3(A(103),XK1),(A(104),XWUI),(A(108),CPI),(A(112),XNLP),
4(A(116),XMULP),(A(120),RITLP),(A(124),CPLP1),(A(125),CPLP2),
5(A(126),CRLP1),(A(127),CRLP2),(A(128),ACC),(A(132),VDLDP),
6(A(136),SPTG),(A(140),ALGP),(A(144),ZP),(A(148),DZPRDV),
7(A(152),HAP),(A(156),TAWP)
EQUIVALENCE (C(1),CCP),(C(2),CF),(C(3),CPGFX),(C(4),CPGP),(C(5),CPG
1S),(C(6),CPLP),(C(7),CPLS),(C(8),CYC),(C(9),DMHDT),(C(10),DPBDT),
2(C(11),DTTBDT),(C(12),DVRT1),(C(13),DVRT2),(C(14),DVRT3),(C(15),FI
3P),(C(16),FIS),(C(17),FISFX),(C(18),FCP),(C(19),FCS),(C(20),FCSFX)
4(C(21),FPVS),(C(22),FPVSFX),(C(23),FVP),(C(24),FVS),(C(25),FVSFX)
5(C(26),FCPFX),(C(27),FIPFX),(C(28),FVPEFX),(C(29),HCP),(C(30),HCS)
6(C(31),HF),(C(32),HGS),(C(33),HGP),(C(34),HI),(C(35),HSLP),(C(36
7),HSLCS),(C(37),HVPG),(C(38),HMSG),(C(39),XKGF), (C(41
8),XWVGP),(C(42),XWVFX),(C(43),XWVGS),(C(44),XWVGS2),(C(45),XWVVP)
9),(C(46),XWVVP),(C(47),XWVVP1),(C(48),XWVVS),(C(49),XWVVS1)
EQUIVALENCE (C(51),PIP),(C(52),PIS),(C(53),RHOLS),(C(
134),PTP),(C(55),PTS),(C(56),QDCLP),(C(57),QDCLS),(C(58),QDGLP),(C(
259),QDGLS),(C(60),QDGOP),(C(61),QDGOS),(C(62),QDGS),(C(63),QDQWP),
3(C(64),QDQWS),(C(65),QDLOP),(C(66),QDLOS),(C(67),QDLPC),(C(68),QDL
4PR),(C(69),QDLSC),(C(70),QDLWP),(C(71),QDLWS),(C(72),QDLGK),(C(73)
5,QDPR),(C(74),QDRPR),(C(75),QDQSPC),(C(76),QDSK),(C(77),QDSSC),(C(7
68),QDWP),(C(79),QDWS), (C(82),SPTL),(C(83
7),SSTL),(C(84),T),(C(85),TECP),(C(86),TECS),(C(87),TGS2),(C(88),TP
8TL),(C(89),TSTG),(C(90),TSTL),(C(91),TT),(C(92),VLP),(C(93),VLS),
9(C(94),VLP2),(C(95),VLS2)
0EQUIVALENCE (C(96),WDBP),(C(97),WDHS),(C(98),WDCFX),(C(99),WDCLP),
1(C(100),WDCLS),(C(101),WDCP),(C(102),WCP2),(C(103),WDCS),(C(104),
2WCS2),(C(105),WGS),(C(106),WIP),(C(107),WIP2),(C(108),WIS),(C(1
39),WIS2),(C(110),WVVS2),(C(111),WDR),(C(112),WSTG2),(C(113),WVP),
4(C(114),WDVP),(C(115),WVP2),(C(116),WVS),(C(117),WDVS),(C(118),WVS
2),(C(119),WFCLP),(C(120),WFCLS),(C(121),WTCCF),(C(122),WTCLP),(C(
6123),WTCLS),(C(124),WTCR),(C(125),WTCF),(C(126),WTICFX),(C(127),WT
7R),(C(128),WTVCFX),(C(129),XF),(C(130),YCP),(C(131),YCS),(C(132),
8YIP),(C(133),YIS),(C(134),YPVS),(C(135),YVP),(C(136),YVS),(C(137),
9BETGEX),(C(138),GAMGP),(C(139),GAMGS)
0EQUIVALENCE (C(141),DELQGP),(C(142),DELOGS),(C(143),DELOLP),(C(144
1),DELOLS),(C(145),DELOWP),(C(146),DELQWS),(C(147),DELT),(C(148),DE
2LTFX),(C(149),DEWCLS),(C(150),DELWVP),(C(151),DELWVS),(C(152),XWV
3FX),(C(153),XWVGS),(C(154),RHOGFX),(C(155),PGS2),(C(156),RHOLP)
EQUIVALENCE (C(157),WCP),(C(158),WCS)
EQUIVALENCE (C(159),TRTG),(C(160),WGP),(C(161),CPO2)
EQUIVALENCE (B(1),SLIQ),(B(2),VST),(B(3),VGS),(B(4),PGS),
1(B(5),TGS),(B(6),TLS),(B(7),DELPPS),(B(8),PS),(B(9),VLSL),
2(B(10),ORVDS),(B(11),ORIS),(B(12),ORBS),(B(13),ORCS),
3(B(14),OPPCS),(B(15),DOS),(B(16),CDOS),(B(17),DST),(B(18),SST),
4(B(19),CWSS),(B(20),CSTO),(B(21),CPST),(B(22),CACS),(B(23),XFGWS),
5(B(24),CEGWS),(B(25),XEGLS),(B(26),CEGLS),(B(27),XELWS),
6(B(28),CFLWS),(B(29),RMS),(B(30),RCLS),(B(31),TFS),(B(32),XWVCS),
7(B(33),XKCS),(B(37),XWVCS),(B(41),CPCS),(B(45),HLCLS)

```

```

8(B(69),CPCLS),(B(53),XNWSV),(B(54),RVS),(B(58),CVAPS)
9(B(67),CKSV),(B(66),BFTVS),(B(70),XKVS),(B(74),XMOV5)
EQUIVALENC(B(78),CPVS),(B(82),HVAPS),(B(86),XALS),(B(90),XmUL5),
1(B(94),RETLS),(B(98),CPLS1),(B(99),CPLS2),(B(100),CRLS1),
2(B(101),CRLS2),(B(102),VDLOS),(B(105),SSTG),(B(110),ALGS),
3(B(114),ZS),(B(118),DZSRV),(B(122),HAS),(B(126),TAMS)
CALL TABS(T,VDLQP,133)
WDR = AV*CDV*SGRT*(9266.*RHOR*(PR-PGP))
CDWP = PGP*VDLQP*.185
TT = TGP
CALL TABS(TT,CPVP,92)
CALL TABS(TT,CPI,109)
CALL TABS(TT,CPCP,55)
CPGP = FVP*CPVP + FIP*CPI + FCP*CPCP
IF(OPBP) 801,801,802
801 WDBP = 0.
GO TO 803
802 GAMGP = (CPGP / (CPGP - 1.987/XMWGP)

WDRP = .1133*CDWP*CDWP*2*PGP*SGRTE(L * XMWGP * GAMGP / TGP * 12. / (GAMGP + 1.1)
1*((GAMGP+1.)/(GAMGP - 1.))
803 RETURN
END

```

HEAT TRANSFER PRIMARY TASK

REPORT LINE HTPT

COMMON 5,C:

DIMENSION A(1320),B(1130),C(180)

10 EQUIVALENCE (A(1),R1NGP),(A(2),PLIN),(A(3),TI),(A(4),VPT),(A(5),VG
 11),(A(6),PGP),(A(7),TCP),(A(8),TLPI),(A(9),CPC),(A(10),PPL),(A(11),
 2PP),(A(12),VLPL),(A(13),CPVDP),(A(14),CPIP),(A(15),OPBP),(A(16),O
 3PTK),(A(17),OPPCP),(A(18),DOP),(A(19),CJOP),(A(20),PR),
 4(A(21),TRP),(A(22),RHR),(A(23),AV),(A(24),CLVI),(A(25),CPR1),
 5(A(26),CPR2),(A(27),PPT),(A(28),SPT),(A(29),CWSP),(A(30),CPTU),
 6(A(31),CPPT),(A(32),TACP),(A(33),CPC),(A(34),COT),(A(35),XFGWP),
 7(A(36),CFHP),(A(37),XGLP),(A(38),CFGLP),(A(39),XFLWP),
 8(A(40),CFLBP),(A(41),RBP),(A(42),RCLP),(A(43),TFP),(A(44),TR),
 9(A(45),XMPCP),(A(46),MKCP),(A(47),XMKCP),(A(48),CPCP),
 EQUIVALENCE(A(49),HCLCP),(A(50),CPGLP),(A(51),XNBPV),(A(52),PPV),
 1(A(53),CVAPP),(A(54),CKPV),(A(55),ELTVP),(A(56),XKVP),
 2(A(57),XVVP),(A(58),PVP),(A(59),HVAPP),(A(60),XWV),
 3(A(61),XK1),(A(62),XK4),(A(63),CPI),(A(64),XKLP),
 4(A(65),XKLP),(A(66),RFLR),(A(67),CRLP1),(A(68),CRLP2),
 5(A(69),CRLP),(A(70),CRLP2),(A(71),ACC),(A(72),VLOP),
 6(A(73),SPTC),(A(74),ALGP),(A(75),ZP),(A(76),DZPHDV),
 7(A(77),HAP),(A(78),TAWP),
 EQUIVALENCE(C(1),CCP),(C(2),CF),(C(3),CPGFX),(C(4),CPGP),(C(5),CPG
 15),(C(6),CPLP),(C(7),CPLS),(C(8),CYC),(C(9),DmBDT),(C(10),DPBDT),
 2(C(11),DTBDT),(C(12),JVAB),(C(13),DVBBDT),(C(14),DWBBDT),(C(15),F1
 3P),(C(16),FIS),(C(17),FISFX),(C(18),FCP),(C(19),FCS),(C(20),FCSFX),
 4,(C(21),FVVS),(C(22),FVVSFX),(C(23),FVP),(C(24),FVS),(C(25),FVSFX),
 5,(C(26),FCPFX),(C(27),EIPFX),(C(28),FVPEX),(C(29),HCR),(C(30),HCS),
 6,(C(31),HF),(C(32),HGS),(C(33),HGP),(C(34),HI),(C(35),HSCLP),(C(36
 7),HSL),C(37),HVRG),(C(38),HVS),C(39),XKGF),
 8,XMWGP),(C(42),XMWGX),(C(43),XMWGS),(C(44),XMWGS2),(C(45),XMWV1
 9),(C(46),XMWV2),(C(47),XMWV3),(C(48),XMWVS),(C(49),XMWVS1),
 EQUIVALENCE
 (C(51),PIP),(C(52),PIS),(C(53),RHOLS),(C(54),RTP),(C(55),PTS),(C(56),QDCLP),(C(57),QDCLS),(C(58),QDGLP),(C(59),QDGLS),(C(60),QDGGP),(C(61),QDGGOS),(C(62),QDGS),(C(63),QDGGWP),(C(64),QDGS),C(65),QDLOP),(C(66),QDLOS),(C(67),QDLPC),(C(68),QDL
 4PR),(C(69),QDLSC),(C(70),QDLWP),(C(71),QDLWS),(C(72),QDPGR),(C(73),
 5,QDPR),(C(74),QDRPR),(C(75),QDSPC),(C(76),QDSR),(C(77),QDSSC),(C(78),QDWP),(C(79),QDWS),
 (C(82),SPTL),(C(83
 7),SSTL),(C(84),T),(C(85),TFCP),(C(86),TFCS),(C(87),TGS2),(C(88),TP
 8TL),(C(89),TSTG),(C(90),TSTL),(C(91),TT),(C(92),VLP),(C(93),VLS),
 9(C(94),VLP2),(C(95),VLS2)

```

0EQUIVALENCE (C(96),WDWP),(C(97),WDWS),(C(98),WDCFX),(C(99),WDCLP),
1(C(100),WDCLS),(C(101),WDGP),(C(102),W CP2),(C(103),WDCS),(C(104),
2W CS2),(C(105),W GS),(C(106),WIP),(C(107),WIP2),(C(108),WIS),(C(1
39),WIS2),(C(110),WPVS2),(C(111),WDR),(C(112),WSTG2),(C(113),WVP),
4(C(114),WDVP),(C(115),WVP2),(C(116),WVS),(C(117),WDVS),(C(118),WVS
52),(C(119),WFCLP),(C(120),WFCLS),(C(121),WTCCF),(C(122),WTCLP),(C(
6123),WTCLS),(C(124),WTCP),(C(125),WTCS),(C(126),WTICFX),(C(127),WT
7R),(C(128),WTICFX),(C(129),XF),(C(130),YCP),(C(131),YCS),(C(132),
8YIP),(C(133),YIS),(C(134),YPVS),(C(135),YVP),(C(136),YVS),(C(137),
9BETGFX),(C(138),GAMGP),(C(139),GAMGS)
-----
0EQUIVALENCE (C(141),DFLOGP),(C(142),DFLOGS),(C(143),DELOLP),(C(144
1),DELOLS),(C(145),DELOWP),(C(146),DELOWS),(C(147),DELT),(C(148),DE
2LTFX),(C(149),DEFWCLS),(C(150),DFLWVP),(C(151),DELWVS),(C(152),XNUG
3FX),(C(153),XMUGS),(C(154),RHOGFX),(C(155),PG52),(C(156),RHOLP)
EQUIVALENCE (C(157),WCP),(C(158),WCS)
EQUIVALENCE (C(159),TPTG),(C(160),WGP),(C(161),CRU2)
EQUIVALENCE (B(1),SLIQ),(B(2),VST),(B(3),VGS),(B(4),PGS),
1(B(5),TGS),(B(6),TIS),(B(7),DELPPS),(B(8),PS),(B(9),VLSL),
2(B(10),OPVDS),(B(11),CPIS),(B(12),OPBS),(B(13),ORCS),
3(B(14),OPPCS),(B(15),DOS),(B(16),CDOS),(B(17),DST),(B(18),SST),
4(B(19),CWSS),(B(20),CSTO),(B(21),CPST),(B(22),CACS),(B(23),XFGWS),
5(B(24),CFGWS),(B(25),XFGLS),(B(26),CEGLS),(B(27),XFLWS),
6(B(28),CFLWS),(B(29),RMS),(B(30),RCLS),(B(31),TFS),(B(32),XMWCS),
7(B(33),XKCS),(B(37),XMUCS),(B(41),CPCS),(B(45),HLCLS),
8(B(49),CPCLS),(B(53),XMUSV),(B(56),PSV),(B(58),CVAPS),
9(B(62),CKSV),(B(66),RFTVS),(B(70),XKVS),(B(74),XMUVS)
EQUIVALENCE (B(78),CPVS),(B(82),HVAPS),(B(86),XKLS),(B(90),XMULS),
1(B(94),BETLS),(B(98),CPLS1),(B(99),CPLS2),(B(100),CRLS1),
2(B(101),CRLS2),(B(102),VDLOS),(B(106),SSIG),(B(110),ALGS),
3(B(114),ZS),(B(118),DZSRDV),(B(122),HAS),(B(126),TAWS)
-----
C
WALL NEXT TO GAS
TT=(TGP +TPTG)/2.
DELTFX = ARSF(TGP -TPTG)
XF = XFGWP
CF = CFGWP
CALL HTSPT
QDGP = HF*SPTG*(TGP - TPTG)
CALL TABS(T,HAP,153)
CALL TABS(T,TAWP,157)
QDGP = CPTO*SPTG*HAP*(IPTG-TAWP)
-----
C
WALL NEXT TO LIQUID
TT = (TLP + TPTL)/2.
DELTFX = ABSE(TLP - TPTL)
CALL TABS(TT,XKLP,113)
CPLP = CPI,P1 + CPLP2*TT
CALL TABS(TT,XMULP,117)
RHOLP = CRLP1 + CRLP2*TT
CALL TABS(TT,BETLP,121)
HF=XKLP*CELWP/DPT*(DPT**3-RHOLD**3)/ACC*BETLB*DELTFX+CPLP*.03108/1
1XMULP*XKLP)**XFLWP
QDLWP = HF*SPTL*(TLP - TPTL)
QDLOP = CPTO*SPTL*HAP*(TPTL -TAWP)
-----
C
GAS TO LIQUID SURFACE
TT = (TGP + TLP)/2.
DELTFX = ABSE(TGP - TLP)
XF = XFLP
CF = CFLP
CALL HTSPT
CALL TABS(VGP,ALGP,141)
QDGLP = HF*ALGP*(TGP - TLP)
RETURN
END

```

```

C HEAT TRANSFER SUBROUTINE PRIMARY TANK
SURROUTINE HTSPT
COMMON A,C,F
DIMENSION A(1320),H(130),C(180)
EQUIVALENCE (A(1),RUNNO),(A(2),PLIQ),(A(3),TI),(A(4),VPT),(A(5),VG
1P),(A(6),PGP),(A(7),TGP),(A(8),TLP),(A(9),CPO),(A(10),PPL),(A(11),
2PPH),(A(12),VPL),(A(13),OPVDP),(A(14),OPTP),(A(15),OPHP),(A(16),O
3PTNK),(A(17),OPPCP),(A(18),DOP),(A(19),CDOP),(A(20),PRI),
4(A(21),TRP),(A(22),RHOR),(A(23),AV),(A(24),CDV),(A(25),CPR1),
5(A(26),CPR2),(A(27),DPT),(A(28),SPT),(A(29),CWSP),(A(30),CRTQ),
6(A(31),CPPT),(A(32),CACPI),(A(33),CHC),(A(34),CDT),(A(35),XFGWP),
7(A(36),CFGWP),(A(37),XFLP),(A(38),CFGLP),(A(39),XFLWP),
8(A(40),CFLWP),(A(41),RMP),(A(42),RCLP),(A(43),TFP),(A(44),TR),
9(A(45),XMWCP),(A(46),XKCP),(A(50),XMUCP),(A(54),CPCP)
EQUIVALENCE (A(58),HLCLP),(A(62),CPCLP),(A(56),XMWPV),(A(67),PPV),
1(A(71),CVAPP),(A(75),CKPV),(A(79),BEIVP),(A(83),XKVP),
2(A(87),XMUVP),(A(91),CPVP),(A(95),HVAPP),(A(99),XHW1),
3(A(103),XK1),(A(104),XMUI),(A(108),CPI),(A(112),XKLP),
4(A(116),XMULP),(A(120),BETLP),(A(124),CPLP1),(A(125),CPLP2),
5(A(126),CRLP1),(A(127),CRLP2),(A(128),ACC),(A(132),VDLUP),
6(A(136),SPTG),(A(140),ALGP),(A(144),ZP),(A(148),DZPBDV),
7(A(152),HAP),(A(156),TAWP)
EQUIVALENCE (C(1),CCP),(C(2),CF),(C(3),CPGFX),(C(4),CPGP),(C(5),CPG
1S),(C(6),CPLP),(C(7),CPLS),(C(8),CYC),(C(9),DMBDT),(C(10),DPBDT),
2(C(11),DTTBDT),(C(12),DVAR1),(C(13),DVRTT),(C(14),DWBBDT),(C(15),F
3P),(C(16),FIS),(C(17),FISFX),(C(18),FCP),(C(19),FCS),(C(20),FCSFX),
4,(C(21),FPVS),(C(22),FPVSFX),(C(23),FVP),(C(24),FVS),(C(25),FVSFX),
5,(C(26),FCPEFX),(C(27),FIFEX),(C(28),FVPEFX),(C(29),HCP),(C(30),HCS),
6,(C(31),HF),(C(32),HGS),(C(33),HGP),(C(34),HI),(C(35),HSCLP),(C(36
7),HSCLS),(C(37),HVPG),(C(38),HVSG),(C(39),XKGF), (C(41
8),XMGWP),(C(42),XMGEX),(C(43),XMGGS),(C(44),XMGGS2),(C(45),XMWVP),
9),(C(46),XMWVP),(C(47),XMWVP1),(C(48),XMWVS),(C(49),XMWVS1)
EQUIVALENCE (C(51),PIP),(C(52),PIS),(C(53),RHOLS),(C(
154),RTP),(C(55),PTS),(C(56),QDCLP),(C(57),QDCLS),(C(58),QDGLP),(C(
259),QDGLS),(C(60),QDGGCP),(C(61),QDGDOS),(C(62),QDGS),(C(63),QDGGWP),
3(C(64),QDGS1),(C(65),QDLOP),(C(66),QDLOS),(C(67),QDLPC),(C(68),QDL
4PR),(C(69),QDLSC),(C(70),QDLWP),(C(71),QDLWS),(C(72),QDPPR),(C(73)
5,QDPR),(C(74),QDRPR),(C(75),QDSPC),(C(76),QDSR),(C(77),QDSSC),(C(7
68),QDWP),(C(79),QDWS), (C(82),SPTL),(C(83
7),SSTL),(C(84),T),(C(85),TECP),(C(86),TECS),(C(87),TGS2),(C(88),TP
8TL),(C(89),TSTG),(C(90),TSTL),(C(91),TT),(C(92),VLP),(C(93),VLS),
9(C(94),VLP2),(C(95),VL52)
DEQUIVALENCE (C(96),WDHP),(C(97),WDHS),(C(98),WDCFX),(C(99),WDCPL),
1(C(100),WDCLS),(C(101),WDCP),(C(102),WCP2),(C(103),WDUS),(C(104),
2WCS2),(C(105),WGS),(C(106),WIP),(C(107),WIP2),(C(108),WIS),(C(1
39),WIS2),(C(110),WRVS2),(C(111),WDR),(C(112),WSTG2),(C(113),WVP),
4(C(114),WDVP),(C(115),WVP2),(C(116),WVS),(C(117),WDVS),(C(118),WVS
52),(C(119),WFCLP),(C(120),WFCLS),(C(121),WTCCF),(C(122),WTCLP),(C(
6123),WTCL6),(C(124),WTCP),(C(125),WTCS),(C(126),WTCEX),(C(127),WT
7R),(C(128),WTVCFX),(C(129),XF),(C(130),YCP),(C(131),YCS),(C(132),
8YIP),(C(133),YIS),(C(134),YPVS),(C(135),YVP),(C(136),YVS),(C(137),
9WETGFX),(C(138),GANGR),(C(139),GANGS)
DEQUIVALENCE (C(141),DELOGP),(C(142),DELOGS),(C(143),DELQLP),(C(144
1),DELQLS),(C(145),DELOWP),(C(146),DELOWS),(C(147),DELT),(C(148),DE
2LTFX),(C(149),DENCL6),(C(150),DELWVP),(C(151),DELWVS),(C(152),XNUG
3FX),(C(153),XMGUS),(C(154),RHOGFX),(C(155),PGS2),(C(156),RHOLP)
EQUIVALENCE (C(157),WCP),(C(158),WCS)
EQUIVALENCE (C(159),TPTG),(C(160),WGR),(C(161),CRD2)
EQUIVALENCE (B(1),SLIQ),(B(2),VST),(B(3),VGS),(B(4),PGS),
1(B(5),TGS),(B(6),TLS),(B(7),DELPPS),(B(8),PS),(B(9),VLSL),
2(B(10),OPVDS),(B(11),OPIS),(B(12),OPBS),(B(13),OPCS),
3(B(14),OPPCS),(B(15),DUS),(B(16),CDUS),(B(17),DST),(B(18),SST),
4(B(19),CWSS),(B(20),CSTO),(B(21),CPST),(B(22),CACS),(B(23),XFGWS),
5(B(24),CFGWS),(B(25),XFGLS),(B(26),CFGLS),(B(27),XFLWS),
6(B(28),CFLWS),(B(29),RMS),(B(30),RCLS),(B(31),TFS),(B(32),XMGCS),
7(B(33),XKCS),(B(37),XMUCS),(B(41),CPCS),(B(45),HLCLS),
8(B(49),CPLS),(B(53),XWVS),(B(54),PSV),(B(58),CVAPS),

```

```

9(B(62),CKSV),(B(66),BETVS),(B(70),XKVS),(B(74),XMUVS)
EQUIVALENCE(B(78),CPVS),(B(82),HVAPS),(B(86),XKLS),(B(90),XMULS),
1(B(94),BETLS),(B(98),CPLS1),(B(99),CPLS2),(B(100),CRLS1),
2(B(101),CRLS2),(B(102),VDLOS),(B(106),SSTG),(B(110),ALGS),
3(B(114),ZS),(B(118),DZSRDV),(B(122),HAS),(B(126),TAVS)
IF(YVP) 91,91,92
91 XMWVP1 = 0.
   BETVP = 0.
   GO TO 95
92 IF(OPVDP) 93,93,94
93 XMWVP1 = XMWPV
   BETVP = 1./TT
   GO TO 95
94 CALL TABS(ITT,CKPV,76)
   XMWVP1 = XMWPV/(1.+1./SQRT(1.+4.*CKPV*YVP*PGP))
   CALL TABS(ITT,BETVP,80)
95 XMWGFx = YVP*XMWVP1 + YIP*XMWI + YCP*XMWCP
   FVPEX = YVP*XMWVP1/XMWGFx
   FCPFX = YCP*XMWCP/XMWGFx
   FIPFX = 1. - FVPEX - FCPFX
   RHOGFX = RGR*XMWGFx/(10.73*TT)
   CALL TABS(ITT,CPVP,92)
   CALL TABS(ITT,CPI,109)
   CALL TABS(ITT,CPCP,55)
   CPGFX = FVPEX*CPVP + FCPFX*CPCP + FIPFX*CPI
   CALL TABS(ITT,XKVP,84)
   CALL TABS(ITT,XKI,101)
   CALL TABS(ITT,XKCP,47)
   XKGFx = YVP*XKVP + YCP*XKCP + YIP*XKI
   CALL TABS(ITT,XMUI,105)
   CALL TABS(ITT,XMUCP,51)
   XMUGFx = (YVP*XMUI*SQRT(XMWVP1) + YCP*XMUCP*SQRT(XMWCP) +
1YIP*XMUI*SQRT(XMWI))/(YVP*SQRT(XMWVP1) + YCP*SQRT(XMWCP) +
2YIP*SQRT(XMWI))
   BETGFX = YVP*BETVP + (YCP + YIP)/TT
   HF=XKGFx*CF/DPT*(DPT**3*RHOGFX**2*ACC*BETGFX*DELTFx*CPGFx*.03108/
1(XMUGFx*XKGFx))**XF
RETURN
END

```

```

C      EVAPORATION PRIMARY TANK
SURROUTINE EVPT
COMMON A,C,B
-----
DIMENSION A(1320),B(1130),C(180)
-----
EQUIVALENCE (A(1),RUNNO),(A(2),PLIQ),(A(3),TI),(A(4),VPT),(A(5),VVG
1P),(A(6),PGF),(A(7),TGP),(A(8),TLP),(A(9),CPU),(A(10),PPL),(A(11),
2RRH),(A(12),VPL),(A(13),OPVDP),(A(14),OPIP),(A(15),OPBP),(A(16),O
3PTNK),(A(17),OPPCP),(A(18),DOP),(A(19),CDOP),(A(20),PR),
4(A(21),TRP),(A(22),RHCR),(A(23),AV),(A(24),CDV),(A(25),CPR1),
5(A(26),CPR2),(A(27),DPT),(A(28),SPT),(A(29),CWSB),(A(30),CPTO),
6(A(31),CPPT),(A(32),CACPI),(A(33),CHC),(A(34),CNT),(A(35),XFGWP),
7(A(36),CFGWP),(A(37),XFGLP),(A(38),CFGLP),(A(39),XFLWP),
8(A(40),CFLWP),(A(41),RMP),(A(42),RCLP),(A(43),TEP),(A(44),TR),
9(A(45),XWUCP),(A(46),XKCP),(A(50),XMUCP),(A(54),CPCP)
EQUIVALENCE (A(58),HLCLP),(A(62),CPCLP),(A(66),XWVPV),(A(67),PPV),
1(A(71),CVAPP),(A(75),CKPVP),(A(79),BETVP),(A(83),XKVP),
2(A(87),XWVP),(A(91),CPVP),(A(95),HVAPP),(A(99),XWV),
3(A(103),XK), (A(104),XMUI),(A(108),CPI),(A(112),XKLP),
4(A(116),XWULP),(A(120),BTLPI),(A(124),CPLPI),(A(125),CPLP2),
5(A(126),CRLP1),(A(127),CRLP2),(A(128),ACC),(A(132),VDLUP),
6(A(136),SPTG),(A(140),ALGP),(A(144),ZP),(A(148),DZPRDV),
7(A(152),HAP),(A(156),TAMP)
EQUIVALENCE (C(1),CCP),(C(2),CF),(C(3),CPGFX),(C(4),CPG),(C(5),CPG
1S),(C(6),CPLP),(C(7),CPLS),(C(8),CYC),(C(9),DMHDT),(C(10),DPHDT),
2(C(11),DTTBDT),(C(12),DVAR),(C(13),DVBBDT),(C(14),DWBBDT),(C(15),F
3P),(C(16),FIS),(C(17),FISFX),(C(18),FCP),(C(19),FCS),(C(20),FCSFX)
4,(C(21),FPVS),(C(22),FPVSFX),(C(23),FVP),(C(24),FVS),(C(25),FVSFX)
5,(C(26),FCPEX),(C(27),FIPFX),(C(28),FVPEX),(C(29),HCP),(C(30),HCS)
6,(C(31),HF),(C(32),HGS),(C(33),HGP),(C(34),HI),(C(35),HSCLP),(C(36
7),HSCLS),(C(37),HVPG),(C(38),HVSG),(C(39),XKGF), (C(4
8),XWUGP),(C(42),XWUGFX),(C(43),XWUGS),(C(44),XWUGS2),(C(45),XWVPV)
9),(C(46),XWVVP),(C(47),XWVVP1),(C(48),XWVVS),(C(49),XWVVS1)
EQUIVALENCE (C(51),PIP),(C(52),PIS),(C(53),RHOLS),(C(
154),PTP),(C(55),PIS),(C(56),QDCLP),(C(57),QDCLS),(C(58),QDGLP),(C(
259),QDGLS),(C(60),QDGGP),(C(61),QDQOS),(C(62),QDGS),(C(63),QDQWP),
3(C(64),QDQWS),(C(65),QDLOP),(C(66),QDLOS),(C(67),QDLPC),(C(68),QDL
4RR),(C(69),QDLSC),(C(70),QDLWP),(C(71),QDLWS),(C(72),QDQGR),(C(73)
5,QDPR),(C(74),QDRRR),(C(75),QDSPC),(C(76),QDSR),(C(77),QDSSC),(C(7
68),QDWP),(C(79),QDWS), (C(82),SPTL),(C(83
7),SSTL),(C(84),T),(C(85),TFCP),(C(86),TFCS),(C(87),TGS2),(C(88),TP
8TL),(C(89),TSTG),(C(90),TSTL),(C(91),TT),(C(92),VLP),(C(93),VLS),
9(C(94),VLP2),(C(95),VLS2)
-----
EQUIVALENCE (C(96),WDRW),(C(97),WDDG),(C(98),WDCFX),(C(99),WDCLR),
1(C(100),WDCLS),(C(101),WDGP),(C(102),WCP2),(C(103),WDCS),(C(104),
2WCS2),(C(105),WGS),(C(106),WIP),(C(107),WIP2),(C(108),WIS),(C(1
39),WIS2),(C(110),WVVS2),(C(111),WDR),(C(112),WSTG2),(C(113),WVR),
4(C(114),WDVP),(C(115),WVR2),(C(116),WVS),(C(117),WDVS),(C(118),WVS
52),(C(119),WFCLP),(C(120),WFCLS),(C(121),WTCCF),(C(122),WTCLP),(C(
A123),WTCLS),(C(124),WTCP),(C(125),WTCS),(C(126),WTCEX),(C(127),WT
7R),(C(128),WTVCFX),(C(129),XF),(C(130),YCP),(C(131),YCS),(C(132),
8YIP),(C(133),YIS),(C(134),YPVS),(C(135),YVP),(C(136),YVS),(C(137),
9BETGFX),(C(138),GAMGP),(C(139),GAMGS)
-----
EQUIVALENCE (C(141),DELOGP),(C(142),DELOGS),(C(143),DELOLP),(C(144
1),DELOLS),(C(145),DELOWP),(C(146),DELOWS),(C(147),DELT),(C(148),DE
2LTFX),(C(149),DEWCLS),(C(150),DELWVP),(C(151),DELWVS),(C(152),XWUG
3FX),(C(153),XWUGS),(C(154),RHOGFX),(C(155),PGS2),(C(156),RHOLP)
EQUIVALENCE (C(157),WCP),(C(158),WCS)
EQUIVALENCE (C(159),TPTG),(C(160),WGP),(C(161),CPD2)
EQUIVALENCE (B(1),SLIQ),(B(2),VST),(B(3),VGS),(B(4),PGS),
1(B(5),TGS),(B(6),TLS),(B(7),DELPPS),(B(8),PS),(B(9),VLSL),
2(B(10),OPVDS),(B(11),CPI), (B(12),OPBS),(B(13),OPCS),
3(B(14),OPPCS),(B(15),CDS),(B(16),CDS), (B(17),DST),(B(18),SST),
4(B(19),CWS), (B(20),CSTO),(B(21),CPST),(B(22),CACS),(B(23),XFGWS),
5(B(24),CFGWS),(B(25),XFGS),(B(26),CFGLS),(B(27),XFLWS),
6(B(28),CFLWS),(B(29),RMS),(B(30),RCLS),(B(31),TFS),(B(32),XWVCS),
7(B(33),XKCS),(B(37),XMUCS),(B(41),CPCS),(B(45),HLCLS),
8(B(49),CPLS),(B(53),XWVSV),(B(54),PSV),(B(58),CVAPS),

```

```

9(B(62),CKSV),(B(66),RFTVS),(B(70),XKVS),(B(74),XMOV5)
EQUIVALENCE(B(78),CPVS),(B(82),HVAPS),(B(86),XKLS),(B(90),XMULS),
1(B(94),BETLS),(B(98),CPLS1),(B(99),CPLS2),(B(100),CRLS1),
2(B(101),CRLS2),(B(102),VDLOS),(B(106),SSTG),(B(110),ALGS),
3(B(114),ZS),(B(118),DZSBDV),(B(122),HAS),(B(126),TAW5)
IF(CVAPP) 1000,1000,1001
-----
1000 WDVP = 0.
      HVPG = 0.
      HVAPP = 0.
      GO TO 1099
-----
1001 WDVP = FVP*(WDBP + WDCFX) + XMWVP*VDLOP*YVP*PGP/(10.73*TGP)
      CALL INTG(TLP,TGP,TT,CPVP,92,HVPG,A)
-----
      TT = TLP
      CALL TABS(TT,HVAPP,96)
      TT = TGP
      CALL TABS(TT,CPVP,92)
1090 RETURN
      END

```

~~C COMBUSTION PRIMARY TANK~~
~~SUBROUTINE CRPT~~
~~COMMON A,C,B~~
~~DIMENSION A(1320),B(1130),C(180)~~
~~EQUIVALENCE (A(1),RUNNO),(A(2),PLIQ),(A(3),TI),(A(4),VPT),(A(5),VG~~
~~1P),(A(6),PGP),(A(7),TGP),(A(8),TLP),(A(9),CPU),(A(10),PPL),(A(11),~~
~~2PRR),(A(12),VPLP),(A(13),OPVDP),(A(14),OPIP),(A(15),OPBP),(A(16),O~~
~~3PTNK),(A(17),OPPCP),(A(18),DOP),(A(19),CDOP),(A(20),PR),~~
~~4(A(21),TRP),(A(22),RHCR),(A(23),AV),(A(24),CDV),(A(25),CPR1),~~
~~5(A(26),CPR2),(A(27),DPT),(A(28),SPT),(A(29),CWSPI),(A(30),CPTO),~~
~~6(A(31),CPPT),(A(32),CACP),(A(33),CHC),(A(34),CIDT),(A(35),XFGWP),~~
~~7(A(36),CFGWP),(A(37),XFGLP),(A(38),CFGLP),(A(39),XFLWP),~~
~~8(A(40),CFIWP),(A(41),RMP),(A(42),RCLP),(A(43),TFP),(A(44),TR),~~
~~9(A(45),XMWCP),(A(46),XKCP),(A(50),XMUCP),(A(54),CPCP)~~
~~EQUIVALENCE (A(58),HLCLP),(A(62),CPCLP),(A(66),XHWPV),(A(67),PPV),~~
~~1(A(71),CVAPP),(A(75),CKPV),(A(79),BETVP),(A(83),XKVP),~~
~~2(A(87),XMUVP),(A(91),CPVP),(A(95),HVAPP),(A(99),XMWI),~~
~~3(A(103),XKI),(A(104),XMUJ),(A(108),CPI),(A(112),XKLP),~~
~~4(A(116),XMULTP),(A(120),BETLP),(A(124),CPLP1),(A(125),CPLP2),~~
~~5(A(126),CRLP1),(A(127),CRLP2),(A(128),ACC),(A(132),VDLUP),~~
~~6(A(136),SPTG),(A(140),ALGP),(A(144),ZP),(A(148),DZMBDV),~~
~~7(A(152),HAP),(A(156),TAWP)~~
~~EQUIVALENCE (C(1),CCP),(C(2),CF),(C(3),CPGFX),(C(4),CPGP),(C(5),CPG~~
~~1S),(C(6),CPLP),(C(7),CPLS),(C(8),CYC),(C(9),DMHDT),(C(10),DPBDT),~~
~~2(C(11),DTHBDT),(C(12),DVAR1),(C(13),DVHDT),(C(14),DWBHDT),(C(15),FI~~
~~3P),(C(16),FIS),(C(17),FISFX),(C(18),FCP),(C(19),FCS),(C(20),FCSFX)~~
~~4(C(21),FPVS),(C(22),FPVSFX),(C(23),FVP),(C(24),FVS),(C(25),FVSFX)~~
~~5(C(26),FCPFX),(C(27),FIPFX),(C(28),FVFPX),(C(29),HCP),(C(30),HCS)~~
~~6(C(31),HF),(C(32),HGS),(C(33),HGP),(C(34),HI),(C(35),HSCLR),(C(36)~~
~~7),HSCLS),(C(37),HVP),(C(38),HVS),(C(39),XKGF), (C(4)~~
~~8),XMWGP),(C(42),XMWGFX),(C(43),XMWGS),(C(44),XMWGS2),(C(45),XMWVP)~~
~~9),(C(46),XMWVP),(C(47),XMWVP1),(C(48),XMWVS),(C(49),XMWVS1)~~
~~EQUIVALENCE (C(51),PIP),(C(52),PIS),(C(53),RHOLS),(C(~~
~~154),PTP),(C(55),PIS),(C(56),QDCLP),(C(57),QDCLS),(C(58),QDGLP),(C(~~
~~159),QDGLS),(C(60),QDGGP),(C(61),QDGDOS),(C(62),QDGS),(C(63),QDGGP),~~
~~3(C(64),QDGS),(C(65),QDLOP),(C(66),QDLOS),(C(67),QDLPC),(C(68),QDL~~
~~4PR),(C(69),QDLSC),(C(70),QDLWP),(C(71),QDLWS),(C(72),QDPGR),(C(73)~~
~~5),QDPR),(C(74),QDRPR),(C(75),QDSPC),(C(76),QDSR),(C(77),QDSSC),(C(7~~
~~68),QDWP),(C(79),QDWS), (C(82),SPTL),(C(83~~
~~7),SSTL),(C(84),T),(C(85),TECP),(C(86),TECS),(C(87),TGS2),(C(88),TP~~
~~8TL),(C(89),TSTG),(C(90),TSTL),(C(91),TT),(C(92),VLP),(C(93),VLS),~~
~~9(C(94),VLP2),(C(95),VLS2)~~
~~0EQUIVALENCE (C(96),WDHP),(C(97),WDBS),(C(98),WDCFX),(C(99),WDCLP),~~
~~1(C(100),WDCLS),(C(101),WDCP),(C(102),WCP2),(C(103),WDCS),(C(104),~~
~~2WCS2),(C(105),WGS),(C(106),WIP),(C(107),WIP2),(C(108),WIS),(C(1~~
~~39),WIS2),(C(110),WVVS2),(C(111),WDR),(C(112),WSTG2),(C(113),WVP),~~
~~4(C(114),WDVP),(C(115),WVP2),(C(116),WVS),(C(117),WDVS),(C(118),WVS~~
~~52),(C(119),WFCLP),(C(120),WFCLS),(C(121),WTCCF),(C(122),WTCLP),(C(~~
~~123),WTCLS),(C(124),WTCB),(C(125),WTCS),(C(126),WTICFX),(C(127),WT~~
~~7R),(C(128),WTVCFX),(C(129),XF),(C(130),YCP),(C(131),YCS),(C(132),~~
~~BYIP),(C(133),YIS),(C(134),YVVS),(C(135),YVP),(C(136),YVS),(C(137),~~
~~9BETGFX),(C(138),GANGP),(C(139),GANGS)~~
~~0EQUIVALENCE (C(141),DELOGP),(C(142),DELOGS),(C(143),DELOLP),(C(144~~
~~1),DELOLS),(C(145),DELOWP),(C(146),DELOWS),(C(147),DELT),(C(148),DE~~
~~2LTFX),(C(149),DEWCLS),(C(150),DEWVP),(C(151),DEWVS),(C(152),XWUG~~
~~3FX),(C(153),XWUGS),(C(154),RHOGFX),(C(155),PGS2),(C(156),RHOLP)~~
~~EQUIVALENCE (C(157),WCP),(C(158),WCS)~~
~~EQUIVALENCE (C(159),TPTG),(C(160),WGP),(C(161),CPO2)~~
~~EQUIVALENCE (B(1),SLIQ),(B(2),VST),(B(3),VGS),(B(4),PGS),~~
~~1(B(5),TGS),(B(6),TLS),(B(7),DELPPS),(B(8),PS),(B(9),VLSL),~~
~~2(B(10),ORVDS),(B(11),ORIS),(B(12),ORBS),(B(13),ORCS),~~
~~3(B(14),OPPCS),(B(15),COS),(B(16),CDOS),(B(17),DST),(B(18),SST),~~
~~4(B(19),CWS3),(B(20),CSTO),(B(21),CPST),(B(22),CACS),(B(23),XFGWS),~~

RTD-TDR-63-1123

```
5(B(24),CFGWS),(B(25),XFGLS),(B(26),CFGLS),(B(27),XFLWS),
6(B(28),CFLWS),(B(29),RMS),(B(30),RCLS),(B(31),TFS),(B(32),XMWCS),
7(B(33),XKCS),(B(37),XMUCS),(B(41),CPCS),(B(45),HLCLS),
8(B(49),CPLS1),(B(53),XMWSV),(B(54),PSV),(B(58),CVAPS),
9(B(62),CKSV),(B(66),BETVS),(B(70),XKVS),(B(74),XMUVS),
EQUIVALENCE(B(78),CPVS),(B(82),HVAPS),(B(86),XKLS),(B(90),XMULS),
11(B(94),BETLS),(B(98),CPLS1),(B(99),CPLS2),(B(100),CRLS1),
2(B(101),CRLS2),(B(102),VDLOS),(B(106),SSTG),(B(110),ALGS),
3(B(114),ZS),(B(118),DZSRDV),(B(122),HAS),(B(126),TAW5)
1F(CCP) 1101,1102,1102
1101 WDR = 0.
      WDCP = 0.
      WDCLP = 0.
      QDSPC = 0.
      QDCLP = 0.
      QDLPC = 0.
      GO TO 1199
1102 WD = (WDR * WDR/RMP)
      WDCP = WD*(1.-RCLP)
      WDCLP = WD*RCLP
      QDRPR = (CPR1 + CPR2*(TR + TRP)/2.)*WDR*(TRP-TR)
      QDLPR = (CPLR1 + CPLR2*(TR + TLR)/2.)*WDR/RMP*(TLR - TR)
      CALL INTG(TR,TFP,TT,CPCP,55,HCP,A)
      QDRR = (WDCP + WDCLP)*HCP + QDRPR + QDLPR
      TFCP = TR + QDRR*(TFCP - TR)/(HCP*(WDCP + WDCLP))
      CALL INTG(TR,TFCP,TT,CPCP,55,HCP,A)
      TFCP = TR + QDRR*(TFCP - TR)/(HCP*(WDCP + WDCLP))
      QDLPC = CACP*CHC*WDR*(1.-AT*(TECP - TLR))
      TT = TLR
      CALL TABS(TT,HLCLP,59)
      CALL INTG(TLR,TECP,TT,CCLP,63,HSCLP,A)
      QDCLP = (HLCLP + HSCLP)*WDCLP
      CALL INTG (TR,TGP,TT,CPCP,55,HCP,A)
      CALL INTG (TR,TLR,TT,CCLP,63,HSCLP,A)
      QDSPC=QDRR-WDCP*HCP+WDCLP*(HLCLP+HSCLP)
1199 RETURN
      END
```

TIME INCREMENT
 SURROUNDING TIME
 COMMON A,C,P
 DIMENSION A(1320),B(1130),C(180)
 EQUIVALENCE (A(1),RUPN), (A(2),PLIQ), (A(3),TI), (A(4),VPT), (A(5),VQ
 1P), (A(6),PSP), (A(7),TGP), (A(8),TLP), (A(9),CPV), (A(10),PPL), (A(11),
 2PPH), (A(12),VLPL), (A(13),QPVD), (A(14),CPIP), (A(15),QBP), (A(16),C
 3PTK), (A(17),OPPC), (A(18),COP), (A(19),CPOP), (A(20),PK),
 4(A(21),TRP), (A(22),RHUR), (A(23),AV), (A(24),CDV), (A(25),CPR1),
 5(A(26),CPR2), (A(27),DPT), (A(28),SPI), (A(29),CNSP), (A(30),CPTO),
 6(A(31),CPPT), (A(32),CAC), (A(33),CHC), (A(34),CRT), (A(35),XFCWP),
 7(A(36),CFGWP), (A(37),XFGLP), (A(38),CFGLP), (A(39),XFLWP),
 8(A(40),CFLWP), (A(41),RNP), (A(42),RCLP), (A(43),TFP), (A(44),TK),
 9(A(45),XMWCP), (A(46),XKCP), (A(50),XMLCP), (A(54),CPCP)
 EQUIVALENCE (A(58),HLCLP), (A(62),CPLLP), (A(66),XAMPV), (A(67),MPV),
 1(A(71),CVAPP), (A(75),CKPV), (A(79),SETVP), (A(83),XKVP),
 2(A(87),XMUVP), (A(91),CPVP), (A(95),IVAPP), (A(99),XKW),
 3(A(103),XK1), (A(104),XMU1), (A(108),CPI), (A(112),XKLP),
 4(A(116),XMULP), (A(120),BETLP), (A(124),CPLP1), (A(125),CPLP2),
 5(A(126),CRLP1), (A(127),CRLP2), (A(128),ACC), (A(132),WDLOP),
 6(A(136),SPTC), (A(140),ALGP), (A(144),ZP), (A(148),DZPRDV),
 7(A(152),HAP), (A(156),TAWP)
 EQUIVALENCE (C(1),CCP), (C(2),CF), (C(3),CPGFX), (C(4),CPGP), (C(5),CPG
 15), (C(6),CPLP), (C(7),CPLS), (C(8),CYC), (C(9),UMBDT), (C(10),DPRDT),
 2(C(11),DITBDT), (C(12),DVAR1), (C(13),DVBOT), (C(14),DWARDT), (C(15),E
 3P), (C(16),FIS), (C(17),FISFX), (C(18),FCP), (C(19),FCS), (C(20),FCSFX),
 4(C(21),FPVS), (C(22),FPV5FX), (C(23),FVP), (C(24),FVS), (C(25),FVSFX),
 5(C(26),FCPFX), (C(27),FIPFX), (C(28),FVFPX), (C(29),HCP), (C(30),HCS),
 6(C(31),HF), (C(32),HGS), (C(33),HGP), (C(34),HI), (C(35),HSCLP), (C(36
 7),HSCLS), (C(37),HVP), (C(38),HVS), (C(39),XKGF), (C(41
 8),XMWGR), (C(42),XMWGX), (C(43),XMWGS), (C(44),XMWGS2), (C(45),XMWV
 9), (C(46),XMWVP), (C(47),XMWVP1), (C(48),XMWVS), (C(49),XMWVS1)
 EQUIVALENCE (C(51),PIP), (C(52),PIS), (C(53),RHULS), (C
 154),PTP), (C(55),PTS), (C(56),QDCLP), (C(57),QDCLS), (C(58),QDGLP), (C
 259),QDGLS), (C(60),QDGP), (C(61),QDGS), (C(62),QDGS), (C(63),QDGW),
 3(C(64),QDGS), (C(65),QDLOP), (C(66),QDLOS), (C(67),QDLPC), (C(68),QDL
 4PR), (C(69),QDLSC), (C(70),QDLWP), (C(71),QDLWS), (C(72),QDPGR), (C(73)
 5,QDPR), (C(74),QDRPR), (C(75),QDSPC), (C(76),QDSR), (C(77),QDSSC), (C(7
 68),QDWP), (C(79),QDWS), (C(82),SPTL), (C(83
 7),SSTL), (C(84),T), (C(85),TECP), (C(86),TECS), (C(87),TGS2), (C(88),TP
 8TL), (C(89),TSTG), (C(90),TSTL), (C(91),TT), (C(92),VLP), (C(93),VLS),
 9(C(94),VLP2), (C(95),VLS2)
 EQUIVALENCE (C(96),WDR), (C(97),WDBS), (C(98),WV), (C(99),WDCLP),
 1(C(100),WDCLS), (C(101),WDCP), (C(102),WCP2), (C(103),WDCS), (C(104),
 2WCS2), (C(105),WGS), (C(106),WIP), (C(107),WIP2), (C(108),WIS), (C(1
 39),WIS2), (C(110),WVGS2), (C(111),WDR), (C(112),WSTG2), (C(113),WVR),
 4(C(114),WDVP), (C(115),WVP2), (C(116),WVS), (C(117),WDVS), (C(118),WVS
 52), (C(119),WFCLP), (C(120),WFCLS), (C(121),WTCCF), (C(122),WTCLP), (C
 6123),WTCLS), (C(124),WTCR), (C(125),WTCF), (C(126),WTCEX), (C(127),WT
 7R), (C(128),WTVCF), (C(129),XF), (C(130),YCP), (C(131),YCS), (C(132),
 8YIP), (C(133),YIS), (C(134),YPVS), (C(135),YVP), (C(136),YVS), (C(137),
 9BETGFX), (C(138),GANGP), (C(139),GANGS)
 EQUIVALENCE (C(141),DELOGP), (C(142),DELOGS), (C(143),DELOLP), (C(144
 1),DELOLS), (C(145),DELOWP), (C(146),DELOWS), (C(147),DELT), (C(148),DE
 2LTX), (C(149),DEWCLS), (C(150),DELWVP), (C(151),DELWVS), (C(152),XWUG
 3FX), (C(153),XMUGS), (C(154),RHOGFX), (C(155),PGS2), (C(156),RMULP)
 EQUIVALENCE (C(157),WCP), (C(158),WCS)
 EQUIVALENCE (C(159),TRTG), (C(160),WGR), (C(161),CRD2)
 EQUIVALENCE (B(1),SLIQ), (B(2),VST), (B(3),VGS), (B(4),PGS),
 1(B(5),TGS), (B(6),TLS), (B(7),DELPPS), (B(8),PS), (B(9),VLSL),
 2(B(10),ORVDS), (B(11),ORIS), (B(12),ORBS), (B(13),ORCS),
 3(B(14),OPPCS), (B(15),DOS), (B(16),CDOS), (B(17),DST), (B(18),SST),
 4(B(19),CWSS), (B(20),CSTO), (B(21),CPST), (B(22),CACS), (B(23),XFGWS),

```

5(B(24),CFGWS),(B(25),XFGLS),(B(26),CEGLS),(B(27),XFLWS),
6(B(28),CFLWS),(B(29),RMS),(B(30),RCLS),(B(31),TFS),(B(32),XMWCS),
7(B(33),XKCS),(B(37),XMUCS),(B(41),CPCS),(B(45),HLCLS),
8(B(49),CPCLS),(B(53),XMWSV),(B(54),PSV),(B(58),CVAPS),
9(B(62),CKSV),(B(66),HFTVS),(B(70),XKVS),(B(74),XMUVS)
EQUIVALENCE(B(78),CPVS),(B(82),HVAPS),(B(86),XKLS),(B(90),XMULS),
1(B(94),BETLS),(B(98),CPLS),(B(99),CPLS2),(B(100),CRLS),
2(B(101),CRLS2),(B(102),VDLOS),(B(106),SSTG),(B(110),ALGS),
3(B(114),ZS),(B(118),DZSBDV),(B(122),HAS),(B(126),TAWS)
IF(OPIP) 1201,1201,1202
1201 DELT = CDT
GO TO 1297
1202 IF(CCP) 1203, 1201, 1204
1203 PP = PPI
GO TO 1205
1204 PP = PPH
1205 CALL TABS(VGP,DZPBDV,149)
DWBDT = WDCP - WDHP - WDCFX
DVBDT = VDLOP + WDVP/RHOLP
WIP2 = WIP - FIP*(WDBP+WDCFX)
WCP2 = WCP - FCP*(WDRP+WDCFX) + WDCP
DMBDT = (WVP - WIP2 + WCP2)/(WVP/XMWVP + WIP2/XMWI + WCP2/XMWCP) - XMWGP
DTTBDT = (QDSPC - QDLPC - QDCLP - QDGWP - QDGLP - WDVP + HVPG - QUWP)/(WGP*CPGP)
DPHDT = DTTBDT*WGP*10.73/(VGP*XMWGP) + DWBDT*10.73*TGP/(VGP*XMWGP)
1 = DWBDT*WGP*10.73*TGP/(VGP*XMWGP) - DMBDT*WGP*10.73*TGP/(XMWGP**2
2*VGP)
DELT2 = (PP - PGP - ACC*RHOLP*ZP/4633.)/(DPBDT + DZPBDV + VDLOP + ACC*RHOLP/
14633.)
IF(OPVDR) 1206, 1206, 1207
1206 DELT = DELT2
GO TO 1214
1207 IF(DELT2) 1220,1218,12075
12075 RHOLP = CRLP1 + CRLP2*TLP
VLP2 = VLP - DELT3*(VDLOP + WDR/(RMP*RHOLP))
IF(CVAPP) 1208, 1208, 1209
1208 DELWVP = 0.
WVP2 = WVP - DELT2*FVP*(WDBP + WDCFX)
GO TO 1210
1209 WVP2 = CVAPP*PPV*(VPT - VLP2)*XMWVP/(10.73*TGP)
DELWVP = WVP2 - WVP + DELT2*FVP*(WDBP + WDCFX)
IF(DELWVP) 1208, 1208, 1210
1210 VLP2 = VLP2 - DELWVP/RHOLP
DELOWP = PGP2/(VLP - VLP2)*.185
VGP2 = VPT - VLP2
WIP2 = WIP - DELT2*FIP*(WDBP + WDCFX)
WCP2 = WCP - DELT2*FCP*(WDRP + WDCFX) + DELT2*WDCP
WGP = WVP2 + WIP2 + WCP2
DELQGP = DELT2*(QDSPC - QDLPC - QDCLP - QDGWP - QDGLP) - DELWVP + HVPG - DELOWP
HGP = WVP2*CBVP + WCP2*CBCP + WIP2*CB1
TGP2 = TGP + DELQGP/HGP
TT = TGP2
CALL TABS(TT, CKPV, 76)
XMWVP = XMWVP/(1. + 1./SQRT(1. + 4.*CKPV*YVP*PGP))
XMWGP = WGP/(WVP2/XMWVP + WIP2/XMWI + WCP2/XMWCP)
RGP2 = WGP*10.73*TGP2/(VGP2*XMWGP)
CALL TABS(VGP, ZP, 145)
PTP2 = PGP2 + ZP*RHOLP*ACC/4633.
DELT3 = DELT2*(PTP - PP)/(PTP - PTP2)
VLP2 = VLP - DELT3*(VDLOP + WDR/(RMP*RHOLP))
IF(CVAPP) 1211, 1211, 1212
1211 DELWVP = 0.
WVP2 = WVP - DELT3*FVP*(WDBP + WDCFX)
GO TO 1213

```

```

1212 WVP2 = CVAPP*PPV/(VPT - VLP2)*XWVWP/(10.73*TGP)
DELWVP = WVP2 - WVP + DELT3*FVP*(WDBP + WDCFX)
IF(DFLWVP) 1211,1211, 1213
1213 VLP2 = VLP2 - DELWVP/RHOLP
DELQWP = PGP*(VLP - VLP2)*.185
VGP2 = VPT - VLP2
WIP2 = WIP - DELT3*FIP*(WDBP + WDCFX)
WCP2 = WCP - DELT3*FCP*(WDBP + WDCFX) + DELT3*WDCP
WGP = WVP2 + WIP2 + WCP2
DELQGP = DELT3*(QD$PC = QDCLP = QDGLP = QDGLP) - DELWVP*HVPG - DELQWP
HGP = WVP2 *CPVP + WCP2*CPCP + WIP2*CPI
TGP2 = TGP + DELQGP/HGP
TT = TGP2
CALL TABS(TT, CKPV, 76)
XWVWP = XWVWP/(1. + 1./SQRT(1. + 4.*CKPV*YVP*PGP))
XWVGP = WGP/(WVP2/XWVWP + WIP2/XWVW1 + WCP2/XWVWCP)
PGP2 = WGP*10.73*TGP2/(VGP2*XWVGP)
CALL TABS(VGP, ZP, 145)
PTP3 = PGP2 + ZP*RHOLP*ACC/4633.
IF((PTP3-PP)*(PTP2-PP)) 1214, 1215, 1215
1214 DELT = DELT3 * (DEL2 - DELT3)*(PTP3-PP)/(PTP3-PTP2)
GO TO 1216
1215 DELT = DELT3*(PTP-PP)/(PTP-PTP3)
1216 IF(DEL.T) 1219,1218,1217
1218 DELT = 0.
K = K + 1
IF(K=4) 1299,1299,1219
1219 SENSE LIGHT 1
GO TO 1217
1220 IF(CCP) 1218,1201,1221
1221 IF(PGP) 12215,12215,1222
12215 DELT = 0.
GO TO 1219
1222 DELT = .5
1217 K = 0
1299 RETURN
END

```

C. NEW CONDITIONS PRIMARY TANK
 SUBROUTINE NCPT
 COMMON A,C,B
 DIMENSION A(1320),B(1130),C(180)
 EQUIVALENCE (A(1),RUNNG),(A(2),PLIQ),(A(3),TI),(A(4),VPT),(A(5),VG
 1P),(A(6),PGP),(A(7),TGP),(A(8),TLP),(A(9),CPU),(A(10),PPL),(A(11),
 2PPH),(A(12),VPL),(A(13),OPVDP),(A(14),OPIP),(A(15),OPBP),(A(16),O
 3PTNK),(A(17),OPPCP),(A(18),DOP),(A(19),CDOP),(A(20),PR),
 4(A(21),TRP),(A(22),RHCR),(A(23),AV),(A(24),CDV),(A(25),CPR1),
 5(A(26),CPR2),(A(27),DPT),(A(28),SPT),(A(29),CWSP),(A(30),CPTO),
 6(A(31),CPPT),(A(32),CACP),(A(33),CHC),(A(34),CDT),(A(35),XFGWP),
 7(A(36),CFGWF),(A(37),XFGLP),(A(38),CFGLP),(A(39),XFLWP),
 8(A(40),CELWP),(A(41),RMP),(A(42),RCLP),(A(43),TEP),(A(44),TR),
 9(A(45),XMWCP),(A(46),XKCP),(A(50),XMUCP),(A(54),CPCP)
 EQUIVALENCE(A(58),HLCLP),(A(62),CPCLP),(A(66),XMWVP),(A(67),PPV),
 1(A(71),CVAPP),(A(75),CKPV),(A(79),BETVP),(A(83),XKVP),
 2(A(87),XMUVV),(A(91),CPVP),(A(95),HIVAPP),(A(99),XMWI),
 3(A(100),XKI),(A(104),XMU),(A(108),CPI),(A(112),XKLP),
 4(A(116),XMULP),(A(120),BETLP),(A(124),CPLP),(A(125),CPLP2),
 5(A(126),CRLP1),(A(127),CRLP2),(A(128),ACC),(A(132),VDLUP),
 6(A(136),SPTG),(A(140),ALGP),(A(144),ZP),(A(148),DZPRDV),
 7(A(152),HAB),(A(156),TAWP)
 EQUIVALENCE(C(1),CCP),(C(2),CF),(C(3),CPGFX),(C(4),CPGP),(C(5),CPG
 1S),(C(6),CPLP),(C(7),CPLS),(C(8),CYC),(C(9),DMBDT),(C(10),DPBUT),
 2(C(11),DTTBDT),(C(12),DVART),(C(13),DVBDT),(C(14),DWBDT),(C(15),F
 3P),(C(16),FIS),(C(17),FISFX),(C(18),FCP),(C(19),FCS),(C(20),FCSFX),
 4(C(21),FPVS),(C(22),FPVSFX),(C(23),FVP),(C(24),FVS),(C(25),FVSFX),
 5(C(26),FCPFX),(C(27),FIPFX),(C(28),FVPEX),(C(29),HCP),(C(30),HCS),
 6(C(31),HF),(C(32),HGS),(C(33),HGP),(C(34),HI),(C(35),HSCLP),(C(36)
 7),HSCLS),(C(37),HVP),(C(38),HVS),(C(39),XKGF), (C(4)
 8),XMGWP),(C(42),XMGFX),(C(43),XMGWS),(C(44),XMGWS2),(C(45),XMWVP),
 9),(C(46),XMWVP),(C(47),XMWVP1),(C(48),XMWVS),(C(49),XMWVS1)
 EQUIVALENCE
 (C(51),PIP),(C(52),PIS),(C(53),RHOLS),(C(1
 154),PTP),(C(55),PTS),(C(56),QDCLP),(C(57),QDCLS),(C(58),WDGLP),(C(1
 259),QDGLS),(C(60),QDQWP),(C(61),QDQGS),(C(62),QDQS),(C(63),QDQWP),
 3(C(64),QDQYS),(C(65),QDLOP),(C(66),QDLOS),(C(67),QDLPC),(C(68),QDL
 4PR),(C(69),QDLSC),(C(70),QDLWP),(C(71),QDLWS),(C(72),QDQGR),(C(73)
 5,QDPR),(C(74),QDRPR),(C(75),QDSPC),(C(76),QDSR),(C(77),QDSSC),(C(17
 68),QDWP),(C(79),QDWS), (C(82),SPTL),(C(83
 7),SSTL),(C(84),T),(C(85),TFCP),(C(86),TFCFS),(C(87),TGS2),(C(88),TP
 8TL),(C(89),TSTG),(C(90),STL),(C(91),TT),(C(92),VLP),(C(93),VLS),
 9(C(94),VLP2),(C(95),VLS2)
 OEQUIVALENCE (C(96),WDBR),(C(97),WDBS),(C(98),WDFCX),(C(99),WDCLP),
 1(C(100),WDCLS),(C(101),WDCP),(C(102),WCP2),(C(103),WDCCS),(C(104),
 2WCS2),(C(105),WGS),(C(106),WIP),(C(107),WIP2),(C(108),WIS),(C(11
 30),WIS2),(C(110),WVGS2),(C(111),WDR),(C(112),WSTG2),(C(113),WVP),
 4(C(114),WDVP),(C(115),WVP2),(C(116),WVS),(C(117),WDVS),(C(118),WVS
 52),(C(119),WFCLP),(C(120),WFCLS),(C(121),WTCF),(C(122),WTCLP),(C(1
 6123),WTCLS),(C(124),WTCB),(C(125),WTCF),(C(126),WTCFX),(C(127),WT
 7R),(C(128),WTVCFX),(C(129),XF),(C(130),YCP),(C(131),YCS),(C(132),
 8YIP),(C(133),YIS),(C(134),YPVS),(C(135),YVP),(C(136),YVS),(C(137),
 9RETGF),(C(138),GANGP),(C(139),GANGS)
 OEQUIVALENCE (C(141),DELQGP),(C(142),DELQGS),(C(143),DELQLP),(C(144
 1),DELOLS),(C(145),DELQWP),(C(146),DELQWS),(C(147),DEL7),(C(148),DE
 2LTFX),(C(149),DEWCLS),(C(150),DEWVWP),(C(151),DEWVWS),(C(152),XMGU
 3FX),(C(153),XMGUS),(C(154),RHOGFX),(C(155),PGS2),(C(156),RHOLP)
 EQUIVALENCE (C(157),WCP),(C(158),WCS)
 EQUIVALENCE (C(159),TPTG),(C(160),WGP),(C(161),CP02)
 EQUIVALENCE (C(165),WPTG),(C(166),WSTG)
 EQUIVALENCE(B(1),SLIQ),(B(2),VST),(B(3),VGS),(B(4),PGS),
 1(B(5),TGS),(B(6),TIS),(B(7),DELPPS),(B(8),PS),(B(9),VLS),
 2(B(10),OPVDS),(B(11),OPIS),(B(12),OPBS),(B(13),OPCS),
 3(B(14),OPPCS),(B(15),DOS),(B(16),CDOS),(B(17),DST),(B(18),SST),
 4(B(19),CWSS),(B(20),CSTO),(B(21),CPST),(B(22),CACS),(B(23),XEGWS),
 5(B(24),CFGWS),(B(25),XFGLS),(B(26),CFGLS),(B(27),XFLWS),
 6(B(28),CFLIS),(B(29),RMS),(B(30),RCLS),(B(31),TFS),(B(32),XMWCS),
 7(B(33),XKCS),(B(37),XMUCS),(B(41),CPCS),(B(45),HLCLS)

```

8 (Z(49),CPCLS),(B(53),XMWV),(B(54),PSV),(B(58),CVAPS),
9 (B(62),CKSV),(B(66),PFTVS),(B(70),XKVS),(B(74),XMUVS)
EQUIVALENCE(B(78),CPVS),(B(82),HVAPS),(B(85),XKLS),(B(90),XMULS),
1 (B(94),BETLS),(B(98),CPLS1),(B(99),CPLS2),(B(100),CRLS1),
2 (B(101),CRLS2),(B(102),VDLOS),(B(106),SSTG),(B(110),ALGS),
3 (B(114),ZS),(B(118),DZSBDV),(B(122),HASS),(B(126),TAVS)
T = T + DELT
CYC = CYC + .5
TT = TLP
CALL TABS(TT,CVAPP,77)
RHOLP = CRLP1 + CRLP2*TLP
VLP2 = VLP - DELT*(VDLQP + WDR/(RMP*RHOLP))
IF(CVAPP) 1301,1301,1302
1301 DELWVP = 0.
WVP = WVP - DELT*FVP*(WDBP + WDCFX)
GO TO 1304
1302 WVP2 = CVAPP*PPV*(VPT - VLP2)*XMWVP/(10.73*TGP)
DELWVP = WVP2 - WVP + DELT*FVP*(WDBP + WDCFX)
IF(DELWVP) 1301,1301,1303
1303 WVP = WVP2
VLP2 = VLP2 - DELWVP/RHOLP
1304 DELQWP = PGP*(VLP - VLP2)*.185
WIP = VLP2
WLP = VLP/RHOLP
DELQLP = DELT*(QDCLP+QDLPC-QDLWP+QDGLP) - DELWVP*HVAPP
TLP = TLP + DELQLP/(WLP*(CPLP1 + CPLP2*TLP))
RHOLP = CRLP1 + CRLP2*TLP
VLP = WIP/RHOLP
VGP = VPT - VLP
TT = TLP
CALL TABS(TT,PPV,68)
WIP = WIP - DELT*FIP*(WDBP + WDCFX)
WCP = WCP - DELT*FCP*(WDBP + WDCFX) + DELT*WDCP
WGP = WVP + WIP + WCP
FVP = WVP/WGP
FCP = WCP/WGP
FIP = 1. - FVP - FCP
WFCLP = (WFCLP*WLP + DELT*WDCLP)/WLP
WTCLP = WTCLP + DELT*WDCLP
WTR = WTR + DELT*WDR
WTCP = WTCP + DELT*WDCP
CALL TABS(WGP,SPTG,137)
WPTG2 = WSP*SPTG
TPTG = (WPTC*TPTG + (WPTG2 - WPTG)*TPTL + DELT*(QDQWP - QDQUP)/CPPT)/
WPTG2
WPTG = WPTG2
SPTL = SPT - SPTG
TPTL = TPTL + DELT*(QDQWP - QDQUP)/(CPPT*WSP*SPTL)
DELOGP = DELT*(QDQPC-QDLPC-QDCLP-QDQWP-QDGLP) - DELWVP*HVGP - DELOGP
HGP = WVP*CPVP + WCP*CPCP + WIP*CPI
TGP = TGP + DELOGP/HGP
IF(FVP) 1305,1305,1306
1305 XMWVP = 1.
GO TO 1309
1306 IF(OPVDP) 1307,1307,1308
1307 XMWVP = XMWVPV
GO TO 1309
1308 TT = TGP
CALL TABS(TT,CKPV,76)
XMWVP = XMWVPV/(1. + (SPTL/(1. + SPTL*WAVVW*WDBP)))
1309 XMWGP = WGP/(WVP/XMWVP + WIP/XMWI + WCP/XMWCP)
CALL TABS(VGP,ZP,145)

```

CALL TABS (T.ACC.128)

YVP = FVP*XMWGP/XMWVP

YCP = FCP*XMWGP/XMWCP

YIP = 1, YVR = YCR

PGP = WGP*10.73*TGP/(VGP*XMWGP)

PTP = PGP + ZP*RHOLP*ACC/4633.

CCP = CCP

RETURN

END

```

C NEW CONDITIONS SECONDARY TANK
SUBROUTINE NCST
COMMON A,C,B
DIMENSION A(1320),R(1130),C(180)
EQUIVALENCE (A(1),RUNNO),(A(2),PLIQ),(A(3),TI),(A(4),VPT),(A(5),VG
1P),(A(6),PGP),(A(7),TGP),(A(8),TLP),(A(9),CPO),(A(10),PPL),(A(11),
2PPH),(A(12),VLR),(A(13),OPVDP),(A(14),QPIP),(A(15),OPBR),(A(16),O
3PTNK),(A(17),OPPCP),(A(18),DOP),(A(19),CDOP),(A(20),PR),
4(A(21),TRP),(A(22),RHUR),(A(23),AV),(A(24),CDV),(A(25),CPR1),
5(A(26),CPR2),(A(27),DPT),(A(28),SPT),(A(29),CWSPL),(A(30),CPTO),
6(A(31),CPPT),(A(32),CACP),(A(33),CHC),(A(34),CDT),(A(35),XFGWP),
7(A(36),CFGWP),(A(37),XFGLP),(A(38),CFGLP),(A(39),XFLWP),
8(A(40),CFLWP),(A(41),RMP),(A(42),RCLP),(A(43),TFP),(A(44),TR),
9(A(45),XMWCP),(A(46),XKCP),(A(50),XMUCP),(A(54),CPCP)
EQUIVALENCE (A(58),HCLP),(A(62),CPCLP),(A(66),XMWPV),(A(67),PPV),
1(A(71),CVAPP),(A(75),CKPV),(A(79),BETVP),(A(83),XKVP),
2(A(87),XMVVP),(A(91),CPVP),(A(95),HVAPP),(A(99),XMW1),
3(A(103),XKJ),(A(104),XMUI),(A(108),CPI),(A(112),XKLP),
4(A(116),XMULP),(A(120),BETLP),(A(124),CPLP),(A(128),CPLP2),
5(A(126),CRLP),(A(127),CRLP2),(A(128),ACC),(A(132),VDLOP),
6(A(136),SPTG),(A(140),ALGP),(A(144),ZP),(A(148),DZPBDV),
7(A(152),HAR),(A(156),TAWP)
EQUIVALENCE (C(1),CCP),(C(2),CF),(C(3),CPGFX),(C(4),CPGP),(C(5),CPG
1S),(C(6),CPLP),(C(7),CPLS),(C(8),CYC),(C(9),DMBDT),(C(10),DPBDT),
2(C(11),DTTBDT),(C(12),DVAR),(C(13),DVBDT),(C(14),DWBBDT),(C(15),F
3P),(C(16),FIS),(C(17),FISFX),(C(18),FCP),(C(19),FCS),(C(20),FCSFX)
4(C(21),FPVS),(C(22),FPVSFX),(C(23),FVP),(C(24),FVS),(C(25),FVSFX)
5(C(26),FCPEX),(C(27),FIPFX),(C(28),FVPEX),(C(29),HCP),(C(30),HCS)
6(C(31),HF),(C(32),HGS),(C(33),HGP),(C(34),HI),(C(35),HSCLP),(C(36
7),HSCLS),(C(37),HVP),(C(38),HVS),(C(39),XKGF),(C(40),XKGF)
8(XMWGP),(C(42),XMGFX),(C(43),XMGGS),(C(44),XMGGS2),(C(45),XMWVP)
9(C(46),XMWVP),(C(47),XMWVP),(C(48),XMWVS),(C(49),XMWVS)
EQUIVALENCE (C(51),PIP),(C(52),PIS),(C(53),RHOLS),(C(
154),PTP),(C(55),PTS),(C(56),QDCLP),(C(57),QDCLS),(C(58),QDGLP),(C(
259),QDGLS),(C(60),QDQCP),(C(61),QDQOS),(C(62),QDGS),(C(63),QDQWP),
3(C(64),QDQWS),(C(65),QDLUP),(C(66),QDLOS),(C(67),QDLPC),(C(68),QDL
4RR),(C(69),QDLSC),(C(70),QDLWR),(C(71),QDLWS),(C(72),QDRGH),(C(73)
5,QDPH),(C(74),QDRPR),(C(75),QDSPC),(C(76),QDSR),(C(77),QDSSC),(C(7
68),QDWP),(C(79),QDWS),
(C(82),SPTL),(C(83
7),SSTL),(C(84),TL),(C(85),TECP),(C(86),TECS),(C(87),TGS2),(C(88),TP
8TL),(C(89),TSTG),(C(90),TSTL),(C(91),TT),(C(92),VLP),(C(93),VLS),
9(C(94),VLP2),(C(95),VLS2)
EQUIVALENCE (C(98),WDR),(C(107),WDWS),(C(108),WDCKX),(C(109),WDCLP),
1(C(100),WDCLS),(C(101),WDCP),(C(102),WCP2),(C(103),WDCS),(C(104),
2WCS2),(C(105),WGS),(C(106),WIP),(C(107),WIP2),(C(108),WIS),(C(1
30),WFS),(C(110),WVFS),(C(111),WDR),(C(112),WSTG2),(C(113),WVP),
4(C(114),WDVP),(C(115),WVP2),(C(116),WVS),(C(117),WDVS),(C(118),WVS
52),(C(119),WFCLP),(C(120),WFCLS),(C(121),WTCCF),(C(122),WTCLP),(C(
6123),WTCLS),(C(124),WTCR),(C(125),WTCR),(C(126),WTCR),(C(127),WT
7R),(C(128),WTVCFX),(C(129),XF),(C(130),YCP),(C(131),YCS),(C(132),
8YIP),(C(133),YIS),(C(134),YVS),(C(135),YVP),(C(136),YVS),(C(137),
9RETGFX),(C(138),GANGP),(C(139),GANGS)
EQUIVALENCE (C(141),DELOGP),(C(142),DELOGS),(C(143),DELQLP),(C(144
1),DELQLS),(C(145),DELQWP),(C(146),DELQWS),(C(147),DELQ),(C(148),DE
2LTFX),(C(149),DEWCLS),(C(150),DELWVP),(C(151),DELWVS),(C(152),XMG
3FX),(C(153),XMGGS),(C(154),RHOGFX),(C(155),PGS2),(C(156),RHOLP)
EQUIVALENCE (C(157),WCP),(C(158),WCS)
EQUIVALENCE (C(159),TPTG),(C(160),WGR),(C(161),CPO2)
EQUIVALENCE (C(162),XWVS),(C(163),XWVVS),(C(164),WTCCFX)
EQUIVALENCE (C(165),WPTS),(C(166),WSTG)
EQUIVALENCE (B(1),S10),(B(2),VST),(B(3),VGS),(B(4),PGS),
1(B(5),TGS),(B(6),TLS),(C(7),DELPPS),(B(8),PS),(B(9),VLSL),
2(B(10),OPVDS),(B(11),OPIS),(B(12),OPRS),(B(13),OPCS),
3(B(14),OPPCS),(B(15),DOS),(B(16),CDOS),(B(17),DST),(B(18),SST),

```

RTD-TDR-63-1123

```
4(B(19),CWSS),(B(20),CS10),(B(21),CPST),(B(22),CAC5),(B(23),XFGWS),
5(B(24),CFGWS),(B(25),XFGLS),(B(26),CFGLS),(B(27),XFLWS),
6(B(28),CFLWS),(B(29),RMS),(B(30),RCLS),(B(31),TES),(B(32),XMWCS),
7(B(33),XKCS),(B(37),XMUCS),(B(41),CPCS),(B(45),HLCLS),
8(B(49),CPLS),(B(53),XMWSV),(B(54),PSV),(B(58),CVAPS),
9(B(62),CKSV),(B(66),BETVS),(B(70),XKVS),(B(74),XMUVS)
EQUIVALENCE(B(78),CPVS),(B(82),HVAPS),(B(86),XXLS),(B(90),XMULS),
1(B(94),BETLS),(B(98),CPLS1),(B(99),CPLS2),(B(100),CRLS1),
2(B(101),CRLS2),(B(102),VDLOS),(B(106),SSTG),(B(110),ALGS),
3(B(114),ZS),(B(118),DZSDV),(B(122),HAS),(B(126),TAWS)
TT = TLS
CALL TABS(TT,CVAPS,15*9)
RHOLS = CRLS1 + CRLS2*TLS
IF(CVAPS) 1401,1401,1406
1401 DELWVS = 0.
WVS = WVS - DELT*WDBS*FVS
IF(OPCS) 1402,1402,1404
1402 VLS2 = VLS - DELT*VDLCS
1403 WPVS = WPVS - DELT*(WDBS*FPVS + WDCFX*FVP)
GO TO 1416
1404 WPVS = 0.
1405 VLS2 = VLS - DELT*(VDLCS+WDCFX*(FVP + FCP)*RMS/RHOLS) - DELWVS/RHOLS
GO TO 1416
1406 VLS2 = VLS - DELT*VDLCS
WVS2 = CVAPS*PSV*(VST - VLS2)*XMWVS/(10.73*TG5)
IF(OPCS) 1407,1407,1409
1407 DELWVS = WVS2 - WVS + DELT*WDBS*FVS
IF(DELWVS) 1401,1401,1408
1408 WVS = WVS2
VLS2 = VLS - DELT*VDLOS - DELWVS/RHOLS
GO TO 1403
1409 WPVS = 0.
IF(OPIS) 1413,1413,1410
1410 DELWVS = WVS2 - WVS + DELT*WDBS*FVS
IF(DELWVS) 1411,1411,1412
1411 DELWVS = 0.
WVS = WVS - DELT*WDBS*FVS
GO TO 1405
1412 WVS = WVS2
GO TO 1405
1413 DELWVS = WVS2 - WVS + DELT*(WDBS*FVS + WDCFX*(FVP+FCP)*RMS)
IF(DELWVS) 1414,1414,1415
1414 DELWVS = 0.
WVS = WVS - DELT*(WDBS*FVS + WDCFX*(FVP + FCP)*RMS)
VLS2 = VLS - DELT*VDLOS
GO TO 1416
1415 WVS = WVS2
VLS2 = VLS - DELT*VDLCS - DELWVS/RHOLS
1416 DELOWS = PGS*(VLS - VLS2)*.185
VLS = VLS2
WLS = VLS/RHOLS
DELOLS = DELT*(WDCFX*ODCLS + WDCFX*.0.87*ODLSC - QDLWS + QDGLS)
1- DELWVS*HVAPS
TLS = TL + DELLOLS/(WLS*(CPLS1 + CRLS2*TLS))
RHOLS = CRLS1 + CRLS2*TLS
VLS = WLS/RHOLS
VGS = VST - VLS
CALL TABS(VGS,ZS,1615)
TT = TLS
CALL TABS(TT,PSV,15*5)
WIS = WIS - DELT*(WDBS*FIS - WDCFX*FIP)
WCS = WCS - DELT*(WDBS*FCS - WDCFX*WDCS)
```

```

-----
WGS = WVS + WPVS + WIS + WCS
FVS = WVS/WGS
FPVS = WPVS/WGS
FCS = WCS/WGS
-----
FIS = 1. - FVS - FPVS - FCS
DEWCLS = DELT*WDCFX*WDCLS
WECLS = (WECLS*WLS + DEWCLS)/WLS
-----
WTCLS = WTCLS + DEWCLS
WTCS = WTCS + DELT*WDCFX*WDCS
WTICFX = WTICFX + DELT*WDCFX*FIP
WTVCFX = WTVCFX + DELT*WDCFX*FVP
WTCCFX = WTCCFX + DELT*WDCFX*FCP
-----
CALL TABS(VGS,SSTG,1607)
WSTG2 = CWSS*SSTG
ISTG = (WSTC*ISTG + (WSTG2 - WSTG)*TSTL + DELT*(QDQWS-QDQUS)/CPST)/
1*WSTG2
WSTG = WSTG2
SSTL = SST - SSTG
TSTL = TSTL + DELT*(QDLWS - QDLQS)/(CPSTR*CWSS*SSTL)
DELOGS = DELT*(WDCFX*(QDQSC-QDQCL) - WDCFX**87*QDLSC-QDQUS-QDGLS)
1-DELWVS*HVSC-DELOGS
TT = TGS
-----
CALL TABS(TT,CPVP,92)
CALL TABS(TT,CPI,109)
HGS = WVS*CPVS + WPVS*CPVP + WCS*CPCS + WIS*CPI
TGS = TGS + DELOGS/HGS
IF(FVS) 1417,1417,1418
1417 XMWVS = 1.
GO TO 1421
1418 IF(OPVDS) 1419,1419,1420
1419 XMWVS = XMWSV
GO TO 1421
1420 TT = TGS
-----
CALL TABS(TT,CKSV,15621)
XMWVS = XMWSV/(1.+1./SQRT(1.+4.*CKSV*YVS*PGS))
1421 IF(FPVS) 1422,1422,1423
1422 XMWPVS = 1.
GO TO 1426
1423 IF(OPVDP) 1424,1424,1425
1424 XMWPVS = XMWPV
GO TO 1426
1425 TT = TGS
-----
CALL TABS(TT,CKPV,76)
XMWPVS = XMWPV/(1.+1./SQRT(1.+4.*CKPV*YPVS*PGS))
1426 XMWGS = WGS/(WVS/XMWVS + WPVS/XMWPVS + WCS/XMWCS + WIS/XMWI)
YVS = FVS*XMWGS/XMWVS
YPVS = FPVS*XMWGS/XMWPVS
YCS = FCS*XMWGS/XMWCS
YIS = 1. - YVS - YPVS - YCS
PGS = WGS*10.73*TGS/(VGS*XMWGS)
PTS = PGS + ZS*RHOLS*ACC/4633.
RETURN
END
-----

```

```

C      INTEGRATION SUBROUTINE
SUBROUTINE INTG(G,U,VAR,FUNC,I,SOLN,Y)
R = U-G
H = R/20
VAR = G
CALL TABS(VAR,FUNC,I,Y)
X = FUNC
DO 30 J = 1,9
VAR = VAR + H
CALL TABS(VAR,FUNC,I,Y)
X = X + 4.*FUNC
VAR = VAR + H
CALL TABS(VAR,FUNC,I,Y)
30  X = X + 2.*FUNC
VAR = VAR + H
CALL TABS(VAR,FUNC,I,Y)
X = X + 4.*FUNC
VAR = U
CALL TABS(VAR,FUNC,I,Y)
SOLN = (X + FUNC)*H/3
C      THIS SUBROUTINE USES THE GENERAL SIMPSON RULE WITH TWENTY
C      INTERVALS FOR THE EVALUATION OF A DEFINITE INTEGRAL. THE
C      CALLING SEQUENCE IS CALL INTG(G,U,VAR,FUNC,I,SOLN), WHERE
C      G = LOWER LIMIT, U = UPPER LIMIT, VAR = VARIABLE,
C      I = LOCATION OF A TABLE LOOKUP FOR TABS SUBROUTINE.
C      SOLN = SOLUTION, Y = A OR B FOR THE USE OF THE PRIMARY OR SECONDARY
C      TANK RESPECTIVELY.
RETURN
END

```

DISTRIBUTION

<u>Copies</u>	<u>To</u>
1 thru 20	Defense Documentation Center Cameron Station Alexandria, Virginia
21 thru 23	GPFA Applied Physics Laboratory Johns Hopkins University Silver Spring, Maryland
24	RTD (RTA) Wolling AFB Washington 25, D.C.
25 thru 34	Air Force Flight Test Center Edwards AFB, California Attn: FTOT
35	DCAS (DCIMT) AF Unit Post Office Los Angeles 45, California Attn: Mrs. Densmore
36 thru 45	Air Force Rocket Propulsion Laboratory Edwards AFB, California Attn: DGRPT/Mr. Allen
46	NASA Langley Research Center Langley Field, Virginia Attn: Library
47	NASA Lewis Research Center 21000 Brookpark Road Cleveland 35, Ohio Attn: Library
48	NASA Marshall Spaceflight Center Huntsville, Alabama

49 NASA
Manned Spacecraft Center
Houston, Texas

50 Commander
NOTS
China Lake, California
Attn: Code 753

51 Aerojet-General Corporation
P.O. Box 296
Azusa, California
Attn: Library

52 Aerojet-General Corporation
P.O. Box 1947
Sacramento 9, California
Attn: Technical Information Office

53 Aeroprojects, Inc
West Chester, Pennsylvania
Attn: W. Tarpley

54 and 55 Aerospace Corporation
P.O. Box 93081
Los Angeles 45, California

56 Armour Research Foundation
Illinois Institute of Technology
Chicago, Illinois
Attn: M. Klein

57 Atlantic Research Corporation
Edwall Rd and Shirley Hwy
Alexandria, Virginia

58 Beech Aircraft Corporation
P.O. Box 631
Boulder, Colorado

59 Bendix Aviation Corporation
Research Labs
Detroit, Michigan

60 Bell Aerosystems Company
P.O. Box 1
Buffalo 5, New York

61 Boeing Company
Aerospace Division
Seattle 24, Washington

62 Chance Vought Aircraft, Inc
P.O. Box 5907
Dallas, Texas

63 Chrysler Corporation
Missile Division
P.O. Box 1827
Detroit 31, Michigan

64 Curtiss-Wright Corporation
Research Division
Quehanna, Pennsylvania

65 and 66 Douglas Aircraft Corporation
Santa Monica, California
Attn: Library

67 Ford Motor Company
Aeronutronic Division
Ford Road
Newport Beach, California
Attn: Library

68 Garrett Corporation
AirResearch Division
Phoenix, Arizona

69 General Electric Company
3198 Chestnut St.
Philadelphia 1, Pennsylvania

70 B.F. Goodrich Company
Akron, Ohio
Attn: Library

71 Hughes Tool Company
Culver City, California
Attn: Library

72 Grumman Aircraft Engineering Corporation
Bethpage, L.I., New York

73 Jet Propulsion Laboratory
4800 Oak Grove Dr.
Pasadena 3, California
Attn: Reports Group

74 Walter Kidde and Company
Belleville 9, New Jersey

75 Lockheed-Georgia Company
Space Vehicle Dept
Marietta, Georgia

76 Lockheed-California Company
Missiles and Space Division
Sunnyvale, California

77 Marquardt Corporation
16555 Saticoy St.
Van Nuys, California

78 and 79 General Dynamics Corporation
Aeronautics Division
San Diego, California

80 and 81 Martin Company
Denver, Colorado 80201
Attn: Libraries Section

82 and 83 Martin Company
Baltimore 3, Maryland
Attn: Library

84 McDonnell Aircraft Corporation
St. Louis, Missouri

85 Minnesota Mining and Manufacturing Company
900 Bush Ave.
St. Paul, Minnesota
Attn: J. W. Millin

86 and 87 North American Aviation, Inc
Rocketdyne Division
Canoga Park, California
Attn: Library

88 and 89 North American Aviation, Inc
Space and Information Systems Division
Downey, California

90 Northrup Corporation
Hawthorne, California

91 Republic Aviation Corporation
Farmingdale, L.I., New York

92 Solar Aircraft Company
2200 Pacific Hwy
San Diego 12, California

93 Ryan Aeronautical Company
San Diego, California

94 and 95 Space Technology Laboratories
One Space Park
Redondo Beach, California

96 Sunstrand Corporation
13445 Glencreek Blvd
Pasadena, California
Attn: W. Unterberg

97 Thiokol Chemical Corporation
Reaction Motors Division
Denville, New Jersey

98 Thompson Ramo Wooldridge, Inc
2355 Kuehl Ave,
Cleveland, Ohio

99 United Aircraft Corporation
Missiles and Space Systems Div
East Hartford, Connecticut

100 United Technology Center
Bunnyvale, California

Agencies
Copies Martin Company
Denver Division
Denver 1, Colorado
Attn: Library